Understanding Aerospace Chemical Propulsion

Understanding Aerospace Chemical Propulsion

Prof. H. S. Mukunda
ABETS, CGPL, Department of Aerospace Engineering
Indian Institute of Science, Bangalore.

Interline Publishing
Bangalore Mumbai Kollam Kaula Lampur

About the Author

Professor H S Mukunda has been leading the group at the Combustion, Gasification and Propulsion Laboratory (CGPL), Department of Aerospace Engineering, Indian institute of Science, Bangalore, India. CGPL is involved in frontier work in Aerospace propulsion in addition to innovative research and development in the field of Energy from Bio-resource.

Professor Mukunda has made significant scientific contributions to solid, liquid and ramjet propulsion systems. He has chaired a number of critical reviews of solid and liquid propulsion systems as well as ramjets developed by defense and space establishments. He is currently providing advice on the development of scramjet engines. His fundamental contributions relate to the areas of modeling of combustion in hybrid rocket engines and solid propellants and ingredients; combustion of liquid droplets and instability in liquid rocket engines; of propagation of premixed flames with complex chemistry and diffusion; of reacting flows in nozzles and air inlets in aircraft and missiles; of combustion of wood in gasifiers and in stoves; of heat transfer in nuclear reactor system and large pressure vessels of petrochemical complex. Over the past thirty five years, he has taught post-graduate courses on rocket propulsion, mechanics and thermodynamics of aerospace propulsion, introduction to aerospace vehicles, mathematical techniques in reacting flows, and fundamentals of combustion.

He has been a Fellow of Indian Academy of Sciences from 1984, Fellow of the Indian National Academy of Engineering from 1994, and Fellow of Aeronautical society of India, 1993. He has been conferred the DRDO Academic Excellence Award 2002 for his valuable contribution in the field of missile propulsion and the Om Prakash Bhasin Award for contributions to Science and Technology in Energy in 1994 and Alumni award of Indian Institute of Science for excellence in Research in Engineering in 1994.

He has held several administrative positions at Indian Institute of Science: Convener, Space Technology Cell (1982–83); Convener, Joint Advanced Technology Programme (1983–87); Chairman, Centre for Scientific and Industrial Consultancy (1989–91); Chairman, Department of Aerospace Engineering (1995 – 2000); Chief Executive, Advanced Bioresidue Energy Technologies Society (1996– 2003).

Preface

With my involvement in combustion and propulsion for over thirty five years in teaching, research and in the development of propulsion systems for space vehicles as well as missiles, I have had to participate in many reviews as a member some times, chairman at other times to discuss the preliminary design of a vehicle or unclarified test results from which one would need to make some sense to suggest a considered future course of action. The meetings have left indelible mark in me and perhaps altered the traditional "academic" in me nearly completely. Real systems behave in ways that appear strange at first sight, but a careful examination, modeling of the system and analysis show a small but influential parameter that sets everything in the right place. Nature's inscrutable ways and the power of analysis to clarify them have been a source of amazement and joy many a time.

The current book titled "Understanding Aerospace Chemical Propulsion" has grown out of my many faceted activities over the last three and half decades.

There are many good books on propulsion. There is a need to see if a new book is needed at all, and if a new one is written, what will be new in it.

Many treat non-air breathing and air breathing engines separately. A few treat them in the same volume, but as separate topics. It is intended here that both be treated in the same book and comparisons drawn where possible. The development of many of the propulsion systems has reached maturity and changes if any, are made to meet specific needs of a class of clients. It is necessary to understand if the systems that have been developed follow the general principles of thermodynamics and if they fall short of expectations of thermodynamics what engineering limitations make them deviate from expectations. This book therefore draws upon the data on many propulsion systems both air breathing and non-air breathing far more extensively than any other book written till now and subjects the data to analysis to see a pattern and draw possible general conclusions. *Data from Indian developments have rarely been documented as a part of a book earlier. This book attempts to make amends for this lacuna.*

This book is limited to chemical propulsion. Many books on propulsion deal with other methods of propulsion, like electric and ion rockets. I have felt that the

subject of chemical propulsion itself is vast and deserves a more comprehensive treatment than is possible otherwise.

There are eleven chapters in the book. Chapter 1 is a detailed introduction to propulsion systems. All the systems discussed subsequently in the book are discussed at a level where a reading should give the reader an overview. Chapter 2 deals with the question of needs and specifications of the propulsion systems. This provides an appreciation of why so many varieties of propulsion systems have been developed and what requirements they fulfill.

Chapter 3 deals with efficiencies of propulsion systems. This is a classical subject that provides a backdrop for detailed system analysis. Chapter 4 lays further background with the necessary thermodynamic and gas dynamic fundamentals needed in any book that discusses propulsion system performance. Chapter 5 is concerned with the detailed cycle analysis of several propulsion systems - most airbreathing engines - in a format that helps capture the relationship between performance parameters (thrust per unit area, dimensionless thrust, normalized flow rate and specific impulse) on geometric, design and flight variables. Chapter 6 is concerned with a detailed discussion of all the components of an airbreathing engine including scramjets - air intake, compressor, combustion chamber, turbine and nozzle. This discussion is around the principles involved in the conceptualization of various design approaches and to understand the variety of systems.

Chapter 7 deals with fuels, propellants and their characterization. While the range of fuels used in airbreathing engines is not wide, the range prevalent in rocket engines is very wide and it is important to understand why so many of them have still are around. The principles involved in characterizing them for adiabatic flame temperature and composition are presented. The performance of rocket propellants - solid and liquid are discussed in some detail.

Chapters 8 is devoted to the principles of rocket combustion process - solid, liquid and hybrid. Emphasis is given to clearly delineating the process fundamentals in all the combustion processes and connecting them to the performance of the systems.

Chapter 9 is devoted to solid propulsion systems - propellant grain geometry, internal ballistics of solid rocket motors, ignition systems, nozzle thermal analysis and protection schemes, thrust vector control (including flex nozzles), and features of large size motors.

Chapter 10 is concerned with liquid rocket engines. Monopropellant rocket engines, zero-g propellant acquisition devices, thruster life management and related aspects occupy the first part. Bipropellant rocket engines with all the elements – injection systems, thrust chamber sizing and cooling aspects, feed systems – turbines and pumps, arrangement of feed system – thrust chambers for optimal performance are discussed in considerable detail.

Chapter 11 is devoted to combustion instability in solid and liquid rockets. The fundamental features of low frequency and high frequency instabilities, the causes for their occurrence and solutions dominate the discussion in this chapter.

Comparisons are sought between gas turbine combustion chambers and rocket engine combustion chambers, fundamental process commonalities between rocket engines and air breathing engines, turbines and compressors in air breathing engines and turbines and pumps in rocket engines.

Who do I think should read this book? Engineers beginning their career in the Aerospace industry who should have a good understanding of the underlying principles of propulsion systems can benefit considerably from reading this book. Engineers who have turned managers wanting to move up and shoulder greater responsibilities, overseeing more than one group should revisit the ideas on the commonalities between propulsion systems from which they would have alienated themselves for decade or more working hard at specific tasks. Their understanding would be considerably enhanced and they might even enjoy reading some sections since they have had practical insight into some systems in great detail.

I have benefitted from many in a critical analysis of propulsion systems that has provided insight into systems. A colleague, Prof. P. J. Paul has been a companion in many of these journeys towards getting insight. The graphics in this book has been the devoted and careful work of Mr. B. K. Ashwini Kumar. Grateful thanks to him for being patient with the demands for a better picture, a more wholesome depiction many a time. Review of the book towards its improvement has been received from several sources including Prof. A. G. Marathe, Prof. T. Sunderarajan, Dr. P. A. Ramakrishna, Dr. C. S. Bhaskar Dixit, Mr. Sudarshan Kumar and Mr. Binoy Phillip. Contribution to cover page design has come from Dr. N. K. S. Rajan and colleagues. Thanks to all of them. The personnel at the Combustion, Gasification and Propulsion Laboratory where I have spent twenty years have been very understanding and supportive. Grateful thanks to all of them. Finally, none of this would have been possible without the support of my family, especially my wife Indira, who has been an incredible source of encouragement.

$B = \rho_p \dot{r}/\rho u(c_f/2)$

Prof. H. S. Mukunda
ABETS, CGPL, Department of Aerospace Engineering,
Indian Institute of Science, Bangalore.
URL:http://cgpl.iisc.ernet.in

Contents

About the Author v

A Message from the President of India,
His Excellency Dr. A. P. J. Abdul Kalam vii

Preface xi

1 Introduction **1**

1.1 Piston Engine - Propeller 2

1.2 Turbojet 3

1.3 Thrust Augmentation in Turbojets 9

1.3.1 The Afterburner 9

1.3.2 Water – Methanol Injection 12

1.4 Two – Three Spool Engines 12

1.5 Turboprops 13

1.6 Turbofans 18

1.7 Ramjets 19

1.8 Pulsejet 23

1.9 Valveless Pulsejets 24

1.10 Scramjet 24

1.10.1 Scramjets vs. Other Vehicles 28

1.11 Starting Systems 29

1.12 The Non-Air-breathing Engines 30

1.13 Solid Propellant Rockets 31

1.14 Liquid Propulsion Systems 35

1.15 Hybrid Rocket Engines 41
1.16 Hybrid Engines 42
1.17 Summary 47

2 Needs, Specifications **49**
2.1 Introduction 49
2.2 The Needs of Airborne Vehicles 49
2.3 The Specifications 52
2.4 Life of Components 53
2.5 Noise Pollution 55
2.6 Exhaust Chemical Pollution 56
2.7 Performance Parameters and Their Importance 56
2.8 The Needs of Space and Military Systems 57
2.9 Specifications 61
2.10 Performance Parameters 61
2.11 Staging, TSTO and SSTO Concepts 65
2.12 Summary 68

3 The Efficiencies **71**
3.1 Introduction 71
3.2 Analysis 71
3.3 The Propulsive Efficiency 73
3.3.1 Air Breathing Engines 73
3.4 Further Analysis 74
3.4.1 Non-Air Breathing Engines (Rocket Engines) 75
3.5 Thermal and Overall Efficiency 76
3.5.1 Air Breathing Engines 77
3.5.2 Non-Air Breathing Engines 77
3.6 Analysis 78
3.7 Summary 79

4 Thermo-Gas Dynamics **81**

4.1 Introduction 81

4.2 Essentials of Nozzle Flows 82

4.2.1 The Conservation Equations 82

4.2.2 Acoustic Speed 82

4.2.3 The Laws of Thermodynamics 82

4.2.4 T – s Diagram 83

4.2.5 Stagnation Conditions 84

4.2.6 Nozzle Flow 85

4.2.7 Choked Nozzle and Mass Flow Rate 88

4.3 Relationship of $\mathbf{c^*}$ with $\mathbf{I_{sp}}$ 90

4.4 The Nozzle Shape 96

4.5 Thrust Generation Process and the Nozzle 98

4.6 The Gas Dynamics of the Exit Plume 102

4.6.1 Importance of $\mathbf{p_{c,t}}$ in Rocket Engines 105

4.6.2 The Rayleigh Process 105

4.7 Summary 110

5 Air Breathing Propulsion System Analysis **111**

5.1 The Ramjet 111

5.1.1 Results With 100 % Efficiency 115

5.1.2 Dependence on Ambient Pressure and Temperature 119

5.1.3 Mach Number for Positive Thrust 119

5.1.4 Summary 121

5.2 The Turbojet 122

5.2.1 Optimum Expansion 123

5.2.2 Choked Nozzle 128

5.2.3 Turbojet With an Afterburner 137

5.2.4 Thrust Augmentation by Liquid Injection 142

5.2.5 Performance of Turbojet With Inefficient Components 143

5.2.6 Step-by-step Procedure 147
5.3 The Turbofan 148
5.4 Gas Turbine Controls and Thrust vs. RPM 151
5.5 Summary 155

6 System Elements **157**
6.1 Air Intakes 157
6.1.1 Inlets for Subsonic Aircraft 159
6.1.2 Intake Geometries for Supersonic Flight 163
6.1.3 External, Internal and Mixed Compression Strategies 167
6.1.4 Starting Issues of Intakes 170
6.1.5 Off-Design Performance 171
6.1.6 Buzz and Other Instabilities 171
6.1.7 Summary 175
6.2 Compressors 176
6.2.1 Centrifugal Compressors 176
6.2.2 Axial Compressors 183
6.2.3 Uses of Centrifugal and Axial Compressors 191
6.2.4 Summary 191
6.3 Combustors 192
6.3.1 Typical Combustor Geometries 195
6.3.2 Fuel Injection Systems 199
6.3.3 Processes Inside the Combustor 201
6.3.4 Emission Performance of Combustors 209
6.3.5 Afterburner and Ramjet Combustion System 209
6.3.6 Scramjets 212
6.3.7 Summary 219
6.4 Turbines 221
6.4.1 Turbine vs Compressor 221
6.4.2 Degree of Reaction (R), Stage Loading (ψ) and Efficiency (η_t) . 224

6.4.3 Pressure Distribution Over the Blade 228
6.4.4 Three-Dimensional Viscous Flow Effects 230
6.4.5 Turbine Cooling 231
6.4.6 Choice of Geometric Features 232
6.4.7 Turbine Performance 233
6.4.8 Compressor-Turbine Matching 234
6.4.9 Summary 235
6.5 Gas Turbine Nozzles 237
6.6 Materials for Various Parts of an Aircraft Engine 241

7 Fuels and Propellants 243
7.1 Thermodynamic Requirements 243
7.2 Operational Requirements 244
7.3 Fuels for Piston Engines, Gas Turbines, and Ramjets 244
7.4 Equilibrium Performance 245
7.5 Fuels for Scramjets 251
7.6 Fuels and Oxidizers for Solid Rockets 252
7.6.1 Polymeric Fuels for Composite Propellants 258
7.6.2 Double base (DB) Propellant Manufacture 259
7.6.3 Composite Propellant (CP) Manufacture 260
7.6.4 Inhibition and Insulation 267
7.6.5 Non-Destructive Testing 269
7.6.6 Mechanical Properties 270
7.6.7 Thermochemical Performance 271
7.6.8 Linear Regression Rates or Burn Rates 273
7.6.9 Erosive Burning Effect 277
7.7 Ignition Composition 278
7.8 Fuels and Oxidizers for Liquid Rockets 280
7.8.1 Monopropellants 280
7.8.2 Bipropellants 282

7.9 Fuels and Oxidizers for Hybrid Rockets 288
7.10 Summary 288

8 Rocket Combustion Processes 291
8.1 General Combustion Features 291
8.1.1 Premixed Combustion 291
8.1.2 Diffusive Mode Combustion 294
8.2 Combustion Mechanism of Solid Propellants 297
8.2.1 DB Propellants 297
8.2.2 Composite and CMDB Propellants 299
8.3 Combustion Mechanism in Liquid Rockets 302
8.3.1 Monopropellants 302
8.3.2 Hypergolic and Other Propellants 303
8.4 Combustion Mechanism of Hybrid Rockets 306
8.5 Comparative Analysis of the Combustion Features 307
8.6 Summary 309

9 Solid Rocket Engine 311
9.1 General Features 311
9.1.1 Stability of Motor Operation 314
9.1.2 Transients 316
9.2 Geometric Aspects of Solid Propellants 318
9.2.1 Choice of Neutral and Other Configurations 324
9.3 Rocket Motor Operation 327
9.4 Ignition System and Process 330
9.5 Extinction and Thrust Termination 335
9.6 Thermal Protection Systems 336
9.6.1 Materials for Thermal Protection 339
9.7 Thrust Vector Control 342
9.8 Performance Losses 346
9.9 Features of Rocket Motors 348

9.10 Design of Solid Rockets 351
9.11 Summary 352

10 Liquid Rocket Engine **353**
10.1 Monopropellant Thruster 354
10.1.1 Propellant Acquisition 355
10.1.2 The Acquisition Device 358
10.1.3 System Schematic and Pulsing Performance 360
10.2 Bipropellant Engines 363
10.2.1 Injectors and Injection Head 367
10.2.2 Drop Size Distribution 374
10.2.3 Gas Generators for Turbo-Pumps 381
10.2.4 Pressurization Systems 384
10.2.5 Turbopumps in Feed Systems 385
10.2.6 Schematics of Turbopump-Gas Generator Systems 385
10.2.7 Choices of Turbines and Pumps 387
10.2.8 Cavitation and Inducers 396
10.3 Thrust Chamber Sizing 400
10.4 Thrust Chamber Cooling 403
10.4.1 Film Cooling 404
10.4.2 Heat Sink and Radiation Cooling 405
10.4.3 Ablative Cooling 407
10.4.4 Regenerative Cooling 407
10.4.5 The Heat Transfer Process 410
10.4.6 Analysis of the Heat Transfer Process 416
10.5 Comparison of Cooling Systems 417
10.6 Ignition System 419
10.7 Clustering Engines 419
10.8 Propulsion System Option Comparison 420
10.9 Comparison of Gas Turbines and Liquid Rocket Engines 422

10.10 Summary 424

11 Combustion Instability **425**

11.1 General 425

11.2 Low Frequency Instability in Liquid Engines 427

11.3 High Frequency Instability (HFI) 429

11.3.1 Solutions to HFI in Liquid Rocket Engines 436

11.4 Intermediate Frequency Instability (IFI) 441

11.4.1 Analytical Tools for Studying Instability 441

11.4.2 Stability Rating 442

11.5 POGO Instability 442

11.6 HFI in Solid Rocket Motors 444

11.6.1 Growth Rates and Response Function 444

11.7 Summary 447

A Atmospheric Data **449**

Chapter 1

Introduction

Aerospace propulsion has been achieved by several propulsive devices based on several principles. In this book we are concerned only with chemical propulsion. This implies that the energy for propulsion is derived from the energy in the bonds of chemical structure of species. There are other devices like electrical rockets, plasma jet, nuclear rockets which are not discussed herein. The propulsive devices based on chemical energy evolved over the last century can be classified as shown in Table 1.1.

In the first set, the air from the atmosphere is taken in and used as the oxidizer. In the second set, there is no restriction on the kind of chemical compounds that need to be used as an oxidizer. As such, solid/liquid oxidizers and fuels can be used. In the third set, the best elements of operation of both non-air breathing and air breathing engines are used to evolve efficient propulsion systems for specific applications.

In each of the above cases, the essential principles used are to (i) generate hot gases at high pressure and (ii) expand the gases to extract work. The thrust

Table 1.1: The various propulsion systems

Airbreathing engines	Non-airbreathing engines	Hybrid engines
* Piston engine- Propeller	+ Liquid rockets	* Integral ram-rockets
* Turbojet	+ Solid rockets	* Ducted rockets
* Turbojet-Propeller	+ Hybrid rockets	* Air-turbo rockets
* Turbo fan		
* Pulse jet		
* Ramjet		
* Scramjet		

producing element is directly related to expansion of gases in many cases. In some cases the thrust generating element is separate – like in the case of Piston engine – Propeller combination. Firstly we will examine the elements of each of the above systems and identify the above features in the systems.

1.1 Piston Engine - Propeller

Figure 1.1 shows the elements of a piston engine - propeller system. Several arrangements in a multi-cylinder configuration are shown in this figure – radial, V, inline and H. Others including X and Y arrangements are also possible. While the reciprocating engine is similar to the engines used in automobiles on the road, the flight version will need to be much lighter for the same power. During the early part of twentieth century, the water cooled engines developed by the Wright Brothers that powered the first heavier-than-air craft flights produced about 9 kW shaft power with engine mass of 90 kg (0.1 kW/kg). Subsequently, Manly developed an engine suitable for aircraft at a record of 0.57 kW/kg producing 40 kW of power with a water cooled radial design. While typically, the power to engine mass ratios were in the range of 0.4 to 0.6 kW/kg during the early forties, they have evolved to levels of 0.9 to 1.2 kW/kg in recent times (see Table 1.2 for data on some typical engines). Apart from the measure of power-to-engine mass ratio, one should also consider the power-to-volume ratio, because at large power levels, the reciprocating systems can turn out to be voluminous and this would affect the choice of the systems. Typical power-to-volume ratio of most reciprocating engines would be 0.3 to 0.5 kW/m^3.

The power output (P) from the reciprocating engine can be written as,

$$P = K\ N\ V_c\ \rho_{air}\ (1+f)\ Q_m\,(f)\ \eta_{ov} \tag{1.1}$$

where, K = constant = 1 or 0.5 depending on whether the engine is two stroke or four stroke, N = rpm of the engine, V_c = volume of the cylinder, ρ_{air} = density of air, f = fuel/air ratio of operation – typically stoichiometric, Q_m = heat released per unit mass of the mixture, η_{ov} = overall efficiency.

The above expression is otherwise stated as a product of mass flow rate of air ingested modified to include the fuel burnt in the engine, the heat released per unit mass of the mixture and the overall efficiency of conversion from heat to work. Typically overall efficiency of the engines varies between 20 – 25 %.

From the above expression it is clear that the power output is proportional to the ambient density. Since the ambient density decreases with increase in altitude, power output of the engine decreases with altitude. The power reduction rate can be offset by deploying a turbo-super-charger which is driven by the exhaust gases from the engine. The expression also indicates that power output

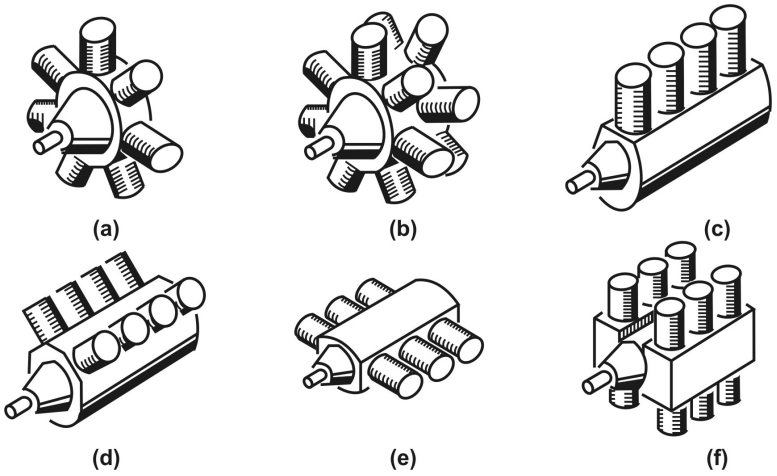

Figure 1.1: Various configurations of piston engine - propeller system (a) refers to single row radial arrangement, (b) refers to two-row arrangement allowing for more power with the same frontal area, (c) a typical four – cylinder in-line arrangement liquid or air cooled, (d) V – configuration usually liquid cooled, (e) a horizontally-opposed configuration, both air and liquid cooled alternatives used extensively, and (f) a H – configuration is effectively used for high power levels, drawn from [30]

increases with rpm. For fixed power, one can make the engine more compact by increasing the rpm.

The power generated by the engine is transmitted to the propeller whose rotation causes increase in the speed of the stream passing through the blades. This increased momentum flux generates the force. Thus, the thrust producing element is the propeller. While this device was the main stay of propulsion till the end of 1940's, subsequently, jet propulsion became a dominating system and the development of piston-engine propeller systems took a low profile. Even so, newer applications of piston engine-propeller are continuously being found and these engines still continue to be developed. For example, in recent times, low power, low mass, high efficiency engines are used in small single seater aircraft and unmanned aerial vehicles.

Advanced propeller concepts have been revitalized in the use of propeller driven devices primarily for reducing specific fuel consumption (sfc) .

1.2 Turbojet

Though turbojets were conceived a long time ago, practically realizable concepts were put together in Italy in 1936, in Germany in 1939, and in United Kingdom

Table 1.2: Data on aircraft piston engines (sfc = specific fuel consumption, * = kg/kWh)

Engine	Power P, kW	Mass M, kg	P/M kW/kg	Size m × m × m	sfc *	P/Vol MW/m^3
Sportavia-Limbach	50	74	0.69	$0.65 \times 0.80 \times 0.4$L	–	0.25
Al - 14 R, Poland	242	245	0.98	1 m dia x 1 L	0.36	0.31
AVCO-Lycoming	298	251	1.2	1.1x0.9 x0.5 L	–	0.58
Teledyne-Continental	324	290	1.1	1.4x0.9 x.66 m L	-	0.4

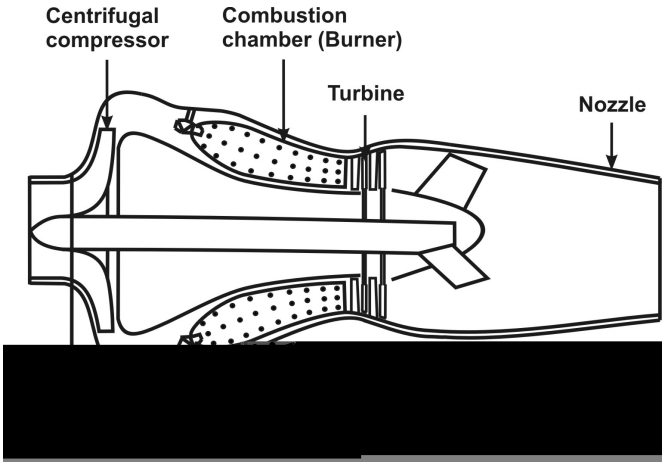

Figure 1.2: A simple Turbojet with Centrifugal compressor

in 1941 towards a working turbojet. Since then, the growth of turbojets or their variants for application to flight systems in aircrafts and missiles – has never been a matter of doubt. The last forty years have seen several significant performance improvements in terms of specific fuel consumption, compactness, engine mass, life of components, modularity of elements, pollution levels both in terms of noise and chemicals in the exhaust stream.

Turbojet aims at generating hot gases at pressures much higher than the ambient for expansion in a nozzle. The ambient air taken in (i) through a simple or complex air intake depending on the flight speed and the geometry of the aircraft is (ii) compressed in a centrifugal (Figure 1.2) or axial compressor (Figure 1.3), (iii)

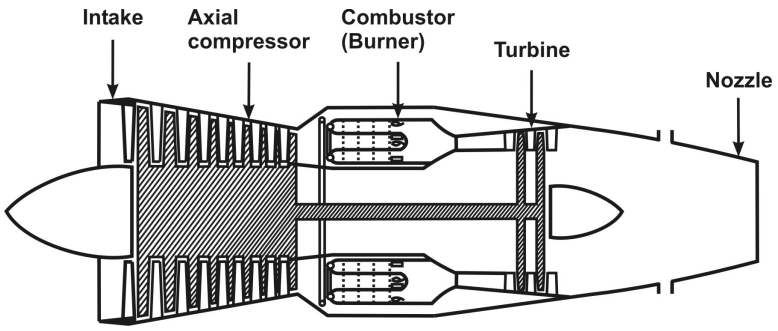

Figure 1.3: A simple Turbojet with Axial compressor

heat put in through combustion of a liquid fuel in the combustor, (iv) with a part of the energy used to run a turbine that provides power for running the compressor, and (v) the remaining energy of the fluid stream extracted by expansion in a nozzle to produce thrust.

Thus, *the intake – compressor – combustor – turbine forms a gas generating system and the nozzle that helps in generating the thrust*. The thrust generation from a turbojet is the integration of the pressures acting on the surfaces and all components contribute to it in differing proportions (see section 6.5) Figures 1.2 and 1.3 show the typical elements of a turbojet. In Figure 1.2, the compressor is of centrifugal type. This was the type developed by Sir Frank Whittle in the early forties. Figure 1.2 shows the engine with axial compressor, the original idea for which goes to German engineers as well as Griffith in the United Kingdom.

Typical pressure ratios in the case of centrifugal compressors vary up to 4 in a single stage. In recent times, single stage pressure ratios of 8 have been achieved in some compressors using supersonic compression. Axial compressors use many stages, each stage consisting of a stator and a rotor. The first stator is called inlet guide vane. In the rotor, the fluid is accelerated and in the stator the kinetic momentum is recovered in the form of enhanced pressure. Typical pressure ratios across a single stage vary from 1.4 – 1.6. But as a part of a multistage compressor, the pressure ratio across a single stage exceeded unity slightly in the design up to fifties. A six stage axial compressor produced pressure ratios of 4 – 5.5. In recent times, fluid flow aspects of turbo-machinery have been better understood and current designs achieve single stage pressure ratios of 1.1 – 1.3 in a multistage system. One of the features responsible for this situation is the use of multi-spool systems. This leads to better organization of the fluid flow that leads to better pressure ratio. Advanced engines develop a pressure ratio of 30 in 16 – 18 stages constituting the fan, low, intermediate and high pressure stages.

The gases entering the combustion chamber usually have temperatures vary-

ing between 400 – 750 K depending the flight altitude and compressor pressure ratio. Fuel, which is typically kerosene of suitable grade, is burned in the combustor to raise the temperature to about 950 – 1600 K depending on the design and technology used for the turbine blades. Though the flame temperatures which can be achieved go right up to 2300 K for stoichiometric mixture of fuel and air (f = fuel-to-air ratio = 0.067), the temperature is restricted to lower values because of the constraints of the turbine material. Due to high temperatures and rotational speed, the stresses caused in the material of the turbine may make it creep much before failure. The creep, if beyond a narrow range, causes rubbing against casing and so deterioration in the performance and reduction of life of the turbine segment. During the early periods of development the temperature was restricted to about 1000 K. Since the gains in the overall performance with increase in turbine inlet temperature are significant, considerable effort to raise it without any problems in the running of the turbine have been made. With efficient cooling techniques it has been raised to as much as 1600 K in engines presently being used on aircraft. Effort to raise it further are still being made at various aircraft industries like Rolls Royce (United Kingdom), Turbomeca and SNECMA (France), General Electric Company (USA), Pratt and Whitney Company (USA).

The hot gases pass through the stator and rotor stages of the turbine. In most modern turbines, the flow gets choked in the turbine blades (i.e. the pressure ratio across the turbine section is more than about 1.8). The gases at reduced pressure (1.5 to 2.5 atm) and temperature (550 – 850 K) flow through the jet pipe and are expanded in the nozzle which is usually of the convergent type. In most cases, the flow at the exit section gets choked; i.e., flow attains a speed equal to acoustic speed in the fluid ($M = u/a = 1$) at the appropriate static temperature. Following Newton's second law, the thrust developed in a turbojet can be written down as

$$F \;=\; \dot{m}_a[(1+f)\,V_e \;-V_a] \;+\; A_e\,(p_e \;-\; p_a) \tag{1.2}$$

where $\dot{m}_a$ = mass flow rate of air, f = fuel air ratio, V_e = exit speed of the fluid, V_a = aircraft forward speed, A_e = nozzle exit area, p_e = exit pressure, and p_a = ambient pressure.

In the above equation the first term on the right hand side constitutes the difference in convective momentum flux between the exit and the inflow. The second term constitutes the pressure thrust arising out of the difference in pressure between the exit plane and the ambient. It can be derived by integrating the pressures exerted on the inner wall throughout the propulsion unit (see for instance, Barrare et. al [12]). It can also be reconciled by looking upon the propulsion unit as a black box with appropriate inflow and exit plane fluxes.

There are conditions of the nozzle flow where p_e = p_a. In such cases the flow would have been completely expanded and this condition is called optimum expansion. It occurs if the stagnation pressure at the entry to the nozzle bears a

definite ratio with the ambient static pressure (typically of the order of 1.8). For all pressure ratios larger than this value, the exit plane pressure (p_e) is larger than the ambient pressure (a condition called under-expansion) and so the second term called pressure thrust term makes a non-zero contribution. One can show that the thrust is maximized when jet is expanded optimally.

If the engine is taking off or is on a fixed test bed on ground, the velocity V_a = 0 and we have

$$F \;=\; \dot{m}_a(1+f)\,V_e \;+\; A_e\,(p_e \;-\; p_a) \tag{1.3}$$

The fuel consumed in generating the thrust is expressed in terms of specific fuel consumption (sfc) or specific Impulse (I_{sp}) . While the first term is classically aeronautical, implying fuel consumption per unit time per unit thrust, the second term is taken from rocket engine literature. Both the quantities refer to the fuel efficiency of the propulsion system. In the case of air breathing engines, the propellant is only fuel. Thus,

$$\text{sfc} \;=\; \dot{m}_f g/F \;\; [\text{kg(fuel)/hr kg (thrust)}] \tag{1.4}$$

$$\;=\; \dot{m}_f \;/\; F \;[\text{kg/N s}] \;\; \text{in SI Units.} \tag{1.5}$$

Conventionally, sfc is denoted in terms of kg/hr kg. The more appropriate way of stating it is kg/N s. Recent literature (for instance, Janes All the World Aircraft Series) expresses it in both ways.

Specific impulse is defined as thrust per unit mass flow rate of the propellant. Hence, $I_{sp} = F/\dot{m}_f$ g, the units being kgf/(kg/s) or s. In SI units it should be N s/kg. The conversion from one to the other is, sfc in kg/kgf hr = 3600/I_{sp} (s).

Typical values of sfc for turbojets is 1.1 – 1.3 kg/hr kg (31 – 36 mg/N s) or in terms of $I_{sp} \sim$ 3270 – 2770 s (or more appropriately, 32090 – 27150 N s/kg) in the early periods of development and in recent times the sfc has dropped to about 0.9 – 1.0 kg/kgf hr (or specific impulse raised to 39200 – 35320 N s/kg).

The performance characteristics of turbojet engine are just not thrust and specific fuel consumption. They also include the compactness of the engine given by the thrust per unit air flow rate, (larger quantity implies smaller cross section for a given thrust and so smaller drag), thrust per unit dry mass (larger quantity implies lighter engine), life of components, modularity of design (implying quick change of elements and hence, a better turn around time), and exhaust pollution concentration etc.

The various alternatives for the elements of a turbojet are presented in the Table 1.3. Air intakes will be discussed in Chapter 6. The choice of the compressor between centrifugal or axial type is governed by the pressure ratio needed as discussed earlier. For pressure ratios up to 4, a single stage centrifugal compressor is satisfactory. For reduced frontal area, axial type is preferred. One uses a single shaft or single spool engine for pressure ratios of 4 or thereabouts. For higher

Table 1.3: The variants of the simple turbojet (F. = Fixed, V. = Variable, AB = Afterburner, C. = Convergent, TPC = Two position convergent, VGC = Variable geometry convergent, Geom = Geometry, CD = Convergent-Divergent.)

Air intake	Compressor	Combustor	Turbine	Jet Pipe	Nozzle
Subsonic	Centrifugal	Can	Axial	No AB	F. Geom.
Supersonic	Axial	Annular	Radial	AB	TPC
F. Geom.	Mixed	Can-annular			VGC
V. Geom.	1/2/3 spool	Reverse flow			CD

pressure ratios, usually one uses a two spool axial compressor system. Occasionally a three spool system has been used for high efficiency over the entire thrust range.

The combustion chamber can be of the four types as shown in Table 1.3. In recent times, the choice is somewhat divided between annular and can-annular. Only a few engines use reverse flow combustors. Most turbines are axial machines. Only small thrust engines use radial type. The demand for a large thrust on some specific occasions is met with by using an after burner. These are used mostly in engines for military aircraft. In engines for supersonic aircraft like Olympus for Concorde and Kuznetsov for Tupolev Tu 144 the engines run with a minimum amount of afterburning throughout the flight. The thrust contributed by afterburning varies from $10 - 30$ % in such cases. In some civil Aircraft like HS748, water methanol injection into combustor is used to augment the power under take off or critical conditions (see section1.3).

The nozzles are usually of fixed geometry and of convergent type. The engines with afterburning some times use a two position nozzle. In recent times, the engines use variable geometry nozzle. Till recently, exhausts had only circular cross section. Now engines with rectangular exhaust have been developed.

Table 1.4 shows the list of some turbojet engines around the world and some select features. An explanation of the contents of the table is in order. The first eight columns following the name of the engine are the dimensions and engine mass, thrust, specific fuel consumption, compressor pressure ratio, turbine inlet temperature (TIT), air flow rate where the data were available, and three non-dimensional quantities. These are the thrust normalized by the product of the air mass flow rate and the ambient acoustic speed, the turbine inlet temperature normalized by the ambient temperature (ISA), the thrust divided by the free stream static pressure and the engine diameter squared, and ratio of the thrust to the engine mass. Some of the non-dimensional quantities appear naturally in the cycle analysis (see chapter 4). The three engines Mamba, Lucas CT 3201 and TRS-

10-046 micro-turbo are all small engines with thrust less than 100 kgf (about 1.0 kN). The other engines have thrust as high as 50 kN without after burning and about 70 kN with after burning. Small engines run at high rpm – as much as 44000 for the micro-turbo engine. Larger engines run at lower rpm – like 8400 rpm for ATAR SNECMA. This is so because of the limits of peripheral speeds due to compressibility. The specific fuel consumption indicated are similar to the values described earlier. The compressor pressure ratio of small engines is less than 4 and for large engines which use axial compressors goes up to 12.0 or so. The turbine inlet temperatures are typically in the range of 1000 – 1300 K. The thrust per unit mass flow rate in the non-dimensional form indicated is about 1.5 – 2.0, the latter value being valid for large engines. It is almost directly related to the choice of pressure ratio. The thrust per unit dry engine mass is low for small thrust engines and about 71 (N/kg) or 7 (kgf/kg) for large engines. These are the typical values valid even in recent times. Jet engines are generally sleek, particularly with axial compressors. Typical thrust-to-volume values are 15 to 30 N/m^3, with the entire engine periphery taken into account.

1.3 Thrust Augmentation in Turbojets

While the turbojets are designed to produce a certain level of thrust for large range of operating conditions, there is need for excess thrust for short durations. These may arise (i) for turbojets or turboprop engines during take-off at high altitude and/or at unusually large ambient temperatures, (ii) when the pilot of an aircraft involved in a combat decides to get away from the scene of combat in a short duration, or (iii) when enemy strike aircraft need to be intercepted by quick climb at short notice. Though the scenario of combat is continuously changing with the advent of long distance radars, pilotless target aircraft and other related advances, the need for short duration excess thrust/power from the power plant remains.

Two devices which have been used extensively are the afterburner or reheat system and injection of water or water-methanol into the compressor or combustor.

1.3.1 The Afterburner

Afterburner is essentially a long pipe between the turbine exit and the nozzle entry as in Figure 1.4. It is firstly to be recognized that because of limitations of turbine, the main combustor does not utilize the full combustion capabilities of the air taken in. Whereas typically, one needs a fuel to air ratio (f) of 0.067 for obtaining peak temperature of 2300 K, one limits the fuel air ratio in the main combustor to 0.01 – 0.03 to restrict the temperatures to 1200 – 1600 K. This means that only about 20 – 45 % of the oxidizing capability would have been used. The rest can

Table 1.4: Turbojet engines (* = kg/kgf.hr, Noz. = Nozzle, C = Convergent, D = Divergent, AB = Afterburner, p_o = Atmospheric pressure, d_{en} = envolope diameter)

Name	d_{en} m	L m	Mass M, kg	F kN	sfc *	π_c	TIT K	$\dot{m}_a$ kg/s	$\frac{F}{\dot{m}_a a_o}$	θ_b	$\frac{F}{p_o d_{en}^2}$	F/M N/kg	Noz. C
Mamba	0.15	0.42	6.4	0.25		2.8	1043	0.5	1.44	3.62	0.11	38.3	C
				0.20									C
Lucas	0.3	0.58	18.6	0.51	1.31	3.5	1190	0.93	1.61	4.13	0.05	27.4	C
CT-3201				0.32									
TRS-18-046	0.34	0.65	32.0	0.90	1.27						0.08	28.0	C
TRI-60	0.31	0.88	45.0	3.43	1.25	3.9	1023	5.6	1.80		0.35		C
Teledyne 402	0.32	0.75	45v	2.94	1.2	5.8		4.35	1.98		0.29	65.0	C
RR-Viper	0.62	2.27	790	16.7	0.94	5.8		26.5	1.85		0.42	21.0	C
J 3-IHI-7C	0.63	1.90	430	13.5	1.05	4.5		25.4	1.56		0.34	31.4	C
J85-4,USA	0.45	1.03	188	13.1	0.98	7.0	1180	20.0	1.93	4.10	0.64	70.0	C
J85-21	0.51	2.86	310	15.6	1.0	8.3	1250	20	2.29	4.34	0.59		C
(AB)				22.2	2.13				3.26			71.0	
J79-7A,11A	1.00	5.30	1685	44.5	0.84	12.4	930	74.4	1.76		0.44		C
(AB)				70.3	2.07		1985		2.78			41.7	C
Atar 9K-50	1.02	5.94	1582	49.2	0.97	6.1		70.7	2.04				C
(AB)				70.6					2.96		0.67	44.6	
Orpheus 703	0.82	1.80	400	22.0	1.05								C
Olympus 593	1.20	4.02	3175	139.4	1.0	15.5	1560	186.0	2.20	4.3			CD
				169.2	1.4				2.67		1.16	53.2	

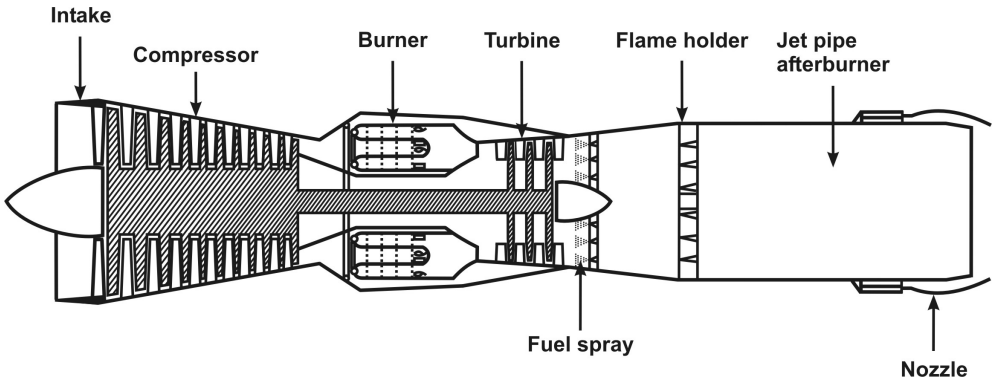

Figure 1.4: A Simple turbojet with afterburner (or reheat)

be put to use by burning the fuel in the afterburner at f up to 0.067 raising the temperature to 2300 K. The nozzle continues to be choked because the pressure ratio across the nozzle is not reduced. Since the inlet temperatures are higher, the nozzle exit temperatures also will be higher. The choking at higher temperatures implies higher exit velocity (equal to acoustic speed). This causes the enhanced thrust. Another important feature is that the density of the gas stream goes down because of enhanced temperature; this causes the mass flux ρu to decrease like $1/\sqrt{T}$ because $u = a$ (acoustic speed) varies like $\sqrt{T}$ and $\rho \sim$ 1/T. Thus, to accommodate the same mass flow (only slightly enhanced by additional fuel), the exit area has to be increased so as to keep the conditions ahead of the afterburner unaffected. Most afterburning turbojets use variable area nozzle. Only some use a two position system. The operation of the after burner also calls for care since inadvertent operation involving fixed nozzle area causes jet pipe pressures to shoot up. These cause pressure waves back into the compressor and compressor stall or surge occurs, destabilizing the engine operating point. Examination of Table 1.4 shows several large thrust engines like J 79 and ATAR-SNECMA 9K-50 have afterburners. Others like J 85, Orpheus 703 also have versions involving afterburners. As can be noted, the thrust augmentation is by as much as 40 – 60 % and specific fuel consumption goes up by more than 100 %.

Thus, the sfc increase is much larger than of thrust. This is the reason why this operational mode is used only under certain circumstances described earlier. It is also interesting to reason why combustion occurring in the main combustor leads to lower fuel consumption than after burner to produce the same thrust. The behavior is due to the fact that energy addition to fluid at high pressure is more efficient than that at lower pressure. This will be discussed in the chapter on cycle analysis (see section 5.2.3).

1.3.2 Water – Methanol Injection

The second method of thrust augmentation is by using water or water-methanol mixture. Water can be used in the combustion chamber or at the entry to the compressor. The injection of water into the combustion chamber causes an enhanced flow rate of hot gases. This enhancement is significant particularly because the turbine inlet temperature is a control variable and held constant. This calls for the increase in fuel flow rate, albeit a small fraction of the water flow rate. This is primarily because the evaporation of water calls for about 2.5 MJ/kg whereas the heat of combustion of kerosene is 42 MJ/kg. Use of methanol in water-methanol mixture is essentially to prevent water from freezing at the low temperatures which the liquid is subject to in flight conditions. If we note the fact that the flow across the turbine is usually choked, the enhanced mass injection upstream of turbine blades causes increase in combustor operating pressure. This implies compressor pressure ratio is increased. The pressure ratio gets set at a value which is determined by the compressor – turbine power balance. The use of the mixture of water and methanol partially offsets the loss of energy due to the use of water alone. Again, the sfc increases (not as much as with water alone) when the mixture is used. Both the above techniques have been analyzed for thrust augmentation and specific fuel consumption in chapter 5.

1.4 Two – Three Spool Engines

Amongst the engines designed in the last twenty years, many high thrust engines have two or three spools and variable stators. There are good reasons for such a development. To understand this, we must examine as to what happens in various regions of an axial compressor. As the fluid moves through the compressor pressure increases. The static temperature also increases. These are such that the density increases through the compressor (because, temperature rise is much smaller than pressure rise due to the isentropic relationship); acoustic speed increases as well. In order to account for these changes and maintain good performance at each stage, the cross section is decreased as we move towards the high pressure stages. One can do this by reducing the tip radius or increasing the hub radius or both.

While the the first feature was indeed the characteristic feature of some early designs, there is no special advantage in it. Increasing the hub radius alone can cause enhanced tip clearance losses in later stages, decreasing the tip radius implies reduction in blade tip Mach number and thus lowering the pressure ratio across the stage. It is possible to look for an optimum and make the above scheme satisfactory at one design point. At off-design conditions, because of the non-linear dependence between pressure, velocity and temperature across the stages, the

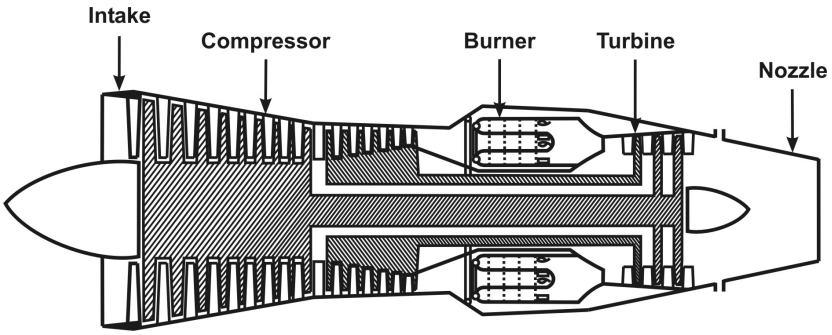

Figure 1.5: A two shaft axial compressor based turbojet

front stages and rear stages are affected differently; at lower speeds, the axial speeds in the front stages will be relatively lower than the tangential speed and so higher effective angles of attack. This causes greater tendencies of flow separation over the blades and so towards 'stall'. The rear axial stages will be poorly loaded and they would be "windmilling". These problems are indeed serious for all compressors beyond a pressure ratio of about 4.

One of the classical methods of overcoming the problem is to use two or three spools . Figure 1.5 shows the schematic of a two spool turbojet. The low pressure compressor is run by a low pressure turbine both being fixed on the same shaft. The intermediate pressure compressor is run by an intermediate pressure turbine, if such a stage is used. The high pressure stage running at higher speeds is run by the high pressure turbine, both mounted on the outer (or outermost) shaft.

The high pressure stage is run at higher speeds to take advantage of the higher static temperature in this region. It is this stage that is involved in the control circuit of the gas turbine. Depending on the strategy used for control, one needs to consider the turbine inlet temperature (TIT) and speed of the H.P. compressor along with fuel flow rate and nozzle exit area. Some engines run with fixed high pressure compressor rpm or corrected rpm, while not exceeding a fixed TIT.

It is the high pressure spool that is cranked up during the start-up of the engine. Because of the smaller overall moment of inertia, the starting systems turn out to be smaller and lighter.

1.5 Turboprops

We have already discussed piston engine-propeller combination and turbojets. In the first case, the thrust producing element is the propeller. In the second case, it is the jet. If one uses a gas turbine and couples propeller to a turbine such

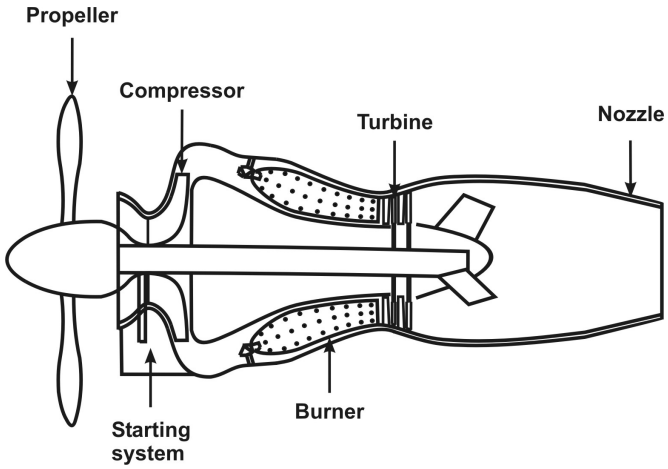

Figure 1.6: A Conventional Turbo Prop Engine

that most of the expansion takes place across the turbine with little left to the nozzle, one gets a turboprop. Of course, one has the freedom of splitting the power delivered partially to the propeller and partially through the jet.

The performance of turboprop is between that of a piston engine-propeller system and turbojet. It is far more fuel efficient compared to a turbojet and has a large range of altitude – speed envelope for its operation compared to piston engine. Its fuel efficiency in comparison to a turbojet emanates from the fact that it moves a larger mass of air through a smaller velocity increment to give the same thrust. This increases propulsive efficiency and so leads to reduced specific fuel consumption. (These are discussed in detail in chapter 3).

Turboprops are used for aircrafts and in one form as turboshaft units for helicopters. They fill in a range of speeds up to 500 – 550 km/hr and altitudes up to 5 – 8 km. The flight Mach numbers are restricted to about 0.7 because at this Mach number and beyond, shock waves are formed on the surface of the rotating propeller reducing the efficiency of the power conversion to useful propulsive power.

In a turboprop, it is possible to design a system such that the total power may be shared between the propeller and that through the jet in varying proportions. In fact an optimum sharing which depends on the flight speed can be determined and can be practically achieved through the use of variable pitch propellers to a reasonable extent. There are several variations in the turboprops. These are the conventional turboprops, the free turbine systems and turboshaft engines. Figures 1.6 and 1.7 show the elements of these engines all having centrifugal compressors. Figure 1.8 refers to axial compressor based engine. In a conventional turboprop

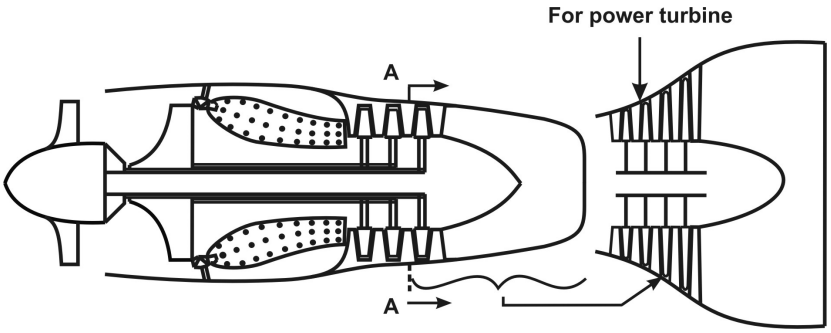

Figure 1.7: A Turbo Prop with Free Turbine (centrifugal compressor)

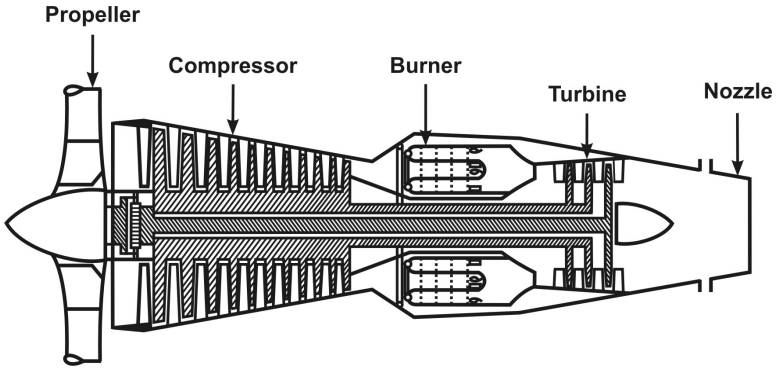

Figure 1.8: A single shaft Turboprop on a free turbine (axial compressor)

the propeller is connected through gearing to the shaft which drives the compressor. Typical examples are the Rolls Royce Dart and Tyne as seen from the Table 1.5.

In free turbine concept, the compressor – turbine system is decoupled from the shaft which connects the propeller to a turbine mounted on the same axis. This gives flexibility in the rotational speed of the compressor – turbine system governed by certain considerations and those of propeller – turbine system which are governed by other aspects. This feature is some what like the multi-spool system in turbojets/turbofans. In both of the above concepts, the power sharing between the propeller and jet can be different.

A turboshaft engine is one in which the expansion work of the hot, high pressure gases is entirely taken through a turbine so that all the energy is available in terms of shaft power. All that this means is that the expansion in the turbine must occur to comparatively lower pressures and so the the turbine blades for these stages have to be indeed large. Even so, they are lighter than the piston

Table 1.5: Turboprops (π_c = compressor pressure ratio, * = kg/kWh)

Name	Dia m	L m	Mass M, kg	Power kW	sfc *	π_c	TIT K	$\dot{m}_a$ kg/s
Allison 250	0.50	1.05	72	298	0.45	7.20	1083	1.6
Astazou XIV	0.55	0.20	206	597	0.55			
Turbomec B VI	0.55	1.90	322	595	0.58	5.83		4.5
R R Dart	0.96	2.50	608	1700	0.73	5.40		9.4
(6 km, M = 0.4)				975	0.65			
Allison T - 53A	0.58	1.20	250	1044	0.58	7.40		4.9
LT C 34	0.62	1.12	263	1976	0.62	8.20		12.2
R R Tyne	1.10	2.76	1034	4985	0.49	13.5		21.1

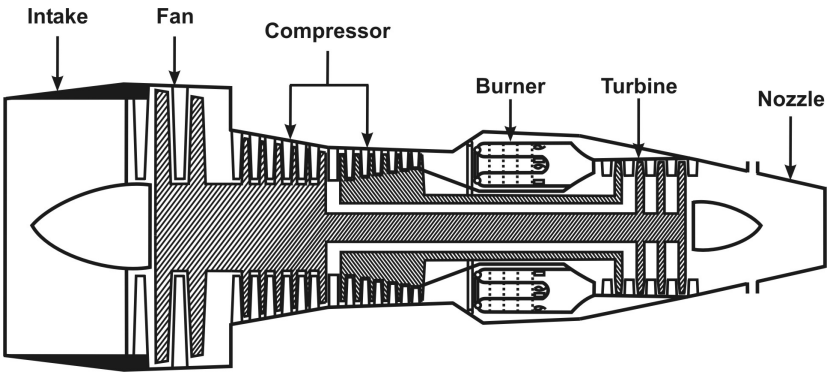

Figure 1.9: A two shaft (spool) Turbofan

engine propeller system for the same power.

Table 1.5 shows some of the turboprop systems over the world. Single engine power level is as much as 5000 kW with sfc of 0.4 – 0.6 kg/kW hr. The pressure ratios of engines vary from about 6 – 14. Some of the engines like Turbomeca Boston and Dart use water-methanol injection for obtaining enhanced power for short durations like during take-off. The power-to-engine mass ratio varies from 4 to 10 kW/kg, about two to ten times that of reciprocating engines and the power-to-volume ratio is 1 to 8 MW/m^3, *the maximum being eight to ten times that of reciprocating engines*. It is for these reasons that larger aircrafts use turboprops rather than reciprocating engine-propeller combinations.

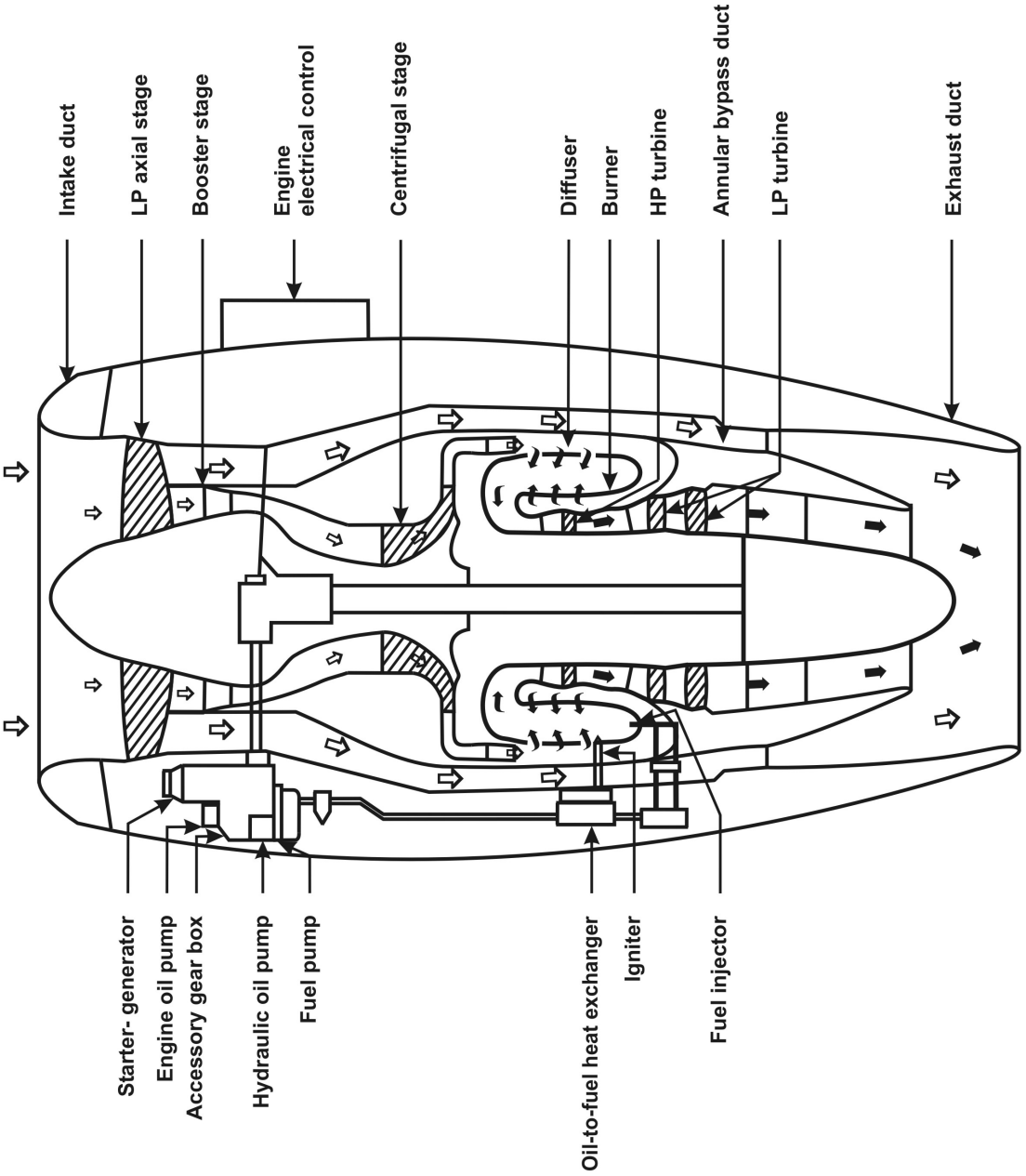

Figure 1.10: A Turbofan in section using a fan, a two stage axial-centrifugal compressor, a reversed flow combustor, and an axial turbine

1.6 Turbofans

Turbofans (see Figures 1.9 and 1.10) are a further evolution over the turboprops in terms of permitting extended range of flight speeds. If in front of the propeller and over it one adds a duct which acts as a diffuser, then it is possible to reduce the speeds in front of the propeller for a given flight speed and thus extend the range compared to turboprop. Further, if one shapes the annular space between the outer profile of the core engine and the outer duct such as to generate a convergent nozzle, one can expect to generate thrust from the system. These are the prominent differences between the two systems.

Thus, once one has a duct, the propeller becomes a fan which compresses the air. The compressed air is expanded and one obtains an enhanced velocity and so, thrust. Obviously the efficiency depends on the amount of the air handled via fan and its pressure ratio. The ratio of the air handled by the fan to that going through the core engine is called the bypass ratio, α. A straight turbojet has α = 0. Table 1.6 shows the details for several engines, civil and military. There are some basic features that govern the choice of the bypass ratios. The single most important performance criterion for a civil aircraft engine is the specific fuel consumption. Increase of α will help achieving the thrust demand by keeping the velocity increment (between the exhaust and intake) low. Typical bypass ratios of engines for civil aircraft go up to 6; there have been arguments about increasing it further. Inordinate increase will lead to a large frontal area. This leads to enhanced nacelle drag. It is argued that even though this large size is reasonable in large aircrafts where the the contribution of the drag from the engine is a small fraction of the total drag, it begins to have avoidable drag increase amongst other features – enhanced diameter of the engine and an increased separation of the engine from the ground implies larger and heavier landing gear. Even so, General Electric company has developed the GE 90 engine with a bypass ratio of 9. Engines of military aircraft that operate in supersonic range are usually buried in the fuselage. They need to be compact. They need also an afterburner to obtain burst of thrust for short durations. Low specific fuel consumption is not an important criterion. Hence, afterburning turbojets are one good choice. If the engines have a high enough turbine inlet temperature, there will not be enough of oxidizing ability available for obtaining desired enhancement of thrust. In such a case a low bypass ratio turbofan would provide enough bypass air for obtaining desired enhancement of thrust. Hence, military aircrafts use bypass ratios, typically between 0.3 to 1.0. Many western engines use single stage fan with pressure ratio of 1.4 – 1.6 with bypass ratios close to 1. It is also possible to design for very low bypass ratios, but higher pressure ratios with multi-stage arrangement. Russian engines use relatively low bypass ratios but a number of stages leading to pressure ratio of 2.5 – 3. This arrangement can provide for higher thrust-to-area ratio. The thrust-to-engine mass ratio is typically 30 to 40 N/kg and the thrust-to-volume is

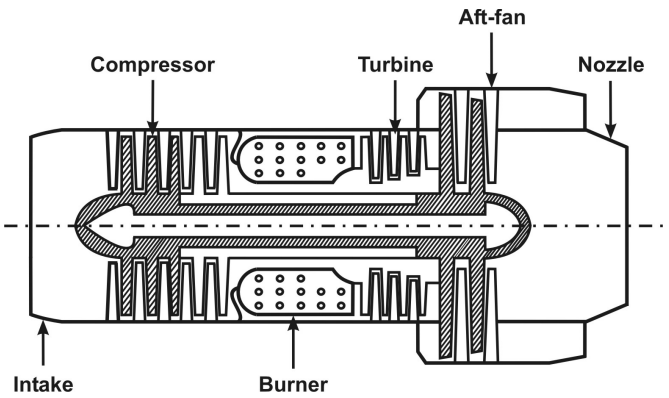

Figure 1.11: A two spool turbofan with an aft fan

30 to 50 N/m^3. These values are slightly lower than pure jet. For an afterburning turbofan however, the values will be much larger.

The power absorbed by the fan can be substantial as compression of large flow rates is involved. In order to provide for this, the compressor pressure ratio of the core engine usually has to be large – 8 to 30. By the arguments made earlier, to handle these pressure ratios, one needs multi-spool designs for compressor-turbine system. Thus, the evolution of a modern turbofan from the turbojet and turboprop seems natural in extending the flight envelope without sacrificing the desirable low specific fuel consumption.

The fan can be ahead of the core engine like in most engines or in the aft portion like in CFM 700. Figure 1.11 shows the elements of such a design.

An examination of Table 1.6 along with Table 1.4 shows that the sfc of turbofans is about 55 – 65 % of turbojets. The non-dimensional thrust per unit flow rate, $F/\dot{m}_a a_o$ is lower compared to that of turbojets. This would mean that the drag penalties on aircraft using such engines will be larger. The gains because of saving in sfc so outweigh the drag contribution from the reduced $F/\dot{m}_a a_o$ that most civil aircraft like the Boeing series use turbofans. The thrust-to-engine mass ratio goes up to 60 (N/kg) and the turbine inlet temperature goes as high as 1550 K. These have been achieved through the use of better materials and turbine cooling techniques.

1.7 Ramjets

Ramjets can be thought of as propulsive devices evolved out of turbojets. As flight Mach number increases say up to 2, the stagnation pressure of the stream is 12

Table 1.6: Turbofans (* = kg/kgh, π_c = compressor pressure ratio, π_f = fan pressure ratio, $\dot{m}_{core}$ = core mass flow rate, $\dot{m}_{fan}$ = mass flow rate through the fan, p_o = atmospheric pressure, (cont) = (continuous operation), to = Take off, ab = Afterburner

Engine	Dia d_{en},m	L m	Mass M, kg	F kN	sfc *	π_c	$\dot{m}_{core}$ kg/s	π_f	$\dot{m}_{fan}$, α kg/s, -	TIT K	F/M (N/kg)	$F/p_o d_{en}^2$
JT 15D-4	0.69	1.60	253	9.8	0.56	10	8	1.5	26.4, 3.3	1233	38.7	0.205
(cont)				9.3								
Ivchenko	0.85	2.00	290	to, 14.7	0.56	8		1.7	- , 2.0		50.6	0.2
(6 km, M = 0.6)				3.5	0.84							
Garret TFE 731-32	0.8	1.26	329	to, 16.4	0.52	14.6			54.6, 2.3	1283	45.6	0.19
(8 km, M = 0.8)				3.9	0.84							
GE CF 700	0.84	1.90	334	to, 20.0	0.65	7.0			40.0, 1.6		60.0	0.28
(cont)				18.3	0.64							
Garret RATF 3 6	0.85	2.30	431	to, 22.5	0.48	21	18.1		55.4, 2.8		52.0	0.30
(12 km, M = 0.8)				4.5	0.79							
Soloviev D 20P	0.98	3.30	1468	to, 53.0	0.72	13	113.0	2.4	113.0, 1.0		36.1	
11 km, M = 0.75					0.90							
SNECMA M53	1.05	4.85	1420	55.0	0.87	–	86.0	–	22.3, 0.35	–	58.7	0.49
				ab, 83.4								
GE F404	0.88	4.03	908	52.0	0.85	27.1	54.2	-	18.5, 0.34	1560	57.2	0.66
				ab, 81.0	1.9							
Pegasus 11	1.22	2.51	1404	95.6		14	196	2.3	, 1.4		68.1	
RR Allison TF 41	0.93	2.6	1370	66.7	0.65	20	67.0		52.0, 0.77		48.7	0.76

Table 1.6: Turbofans (continued.)

Engine	Dia d_{en}, m	L m	Mass M, kg	F kN	sfc *	π_c	$\dot{m}_{core}$ kg/s	π_f	$\dot{m}_{fan}$, α kg/s, -	TIT K	F/M (N/kg)	$F/p_0 d_{en}^2$
P&W F100	1.18	4.85	1371	64.0	0.68	23		2.57	, 0.6			
				ab, 106.0								
P&WF401	1.28		1655	73.0	0.62	26.9			, 0.6			
				ab, 125.0	2.45							
JT 8D-217	1.43	3.28	1896	84.5	0.65	18.0	80.5	1.4	142.5, 1.77		48.7	0.40
11 km, M = 0.8				26.3								
CFM - 56	1.81	2.28	1963	97.9	0.66	25.0	55.0		333.0, 6.0	1533	50.0	0.29
9 km, M = 0.8				25.5								
Kuznetsov	1.44	5.3	2400	99.1	0.78	10.8		2.15	-,1	1143	41.3	0.47
11 km, M= 0.85				27.0								
Soloviev D 30	1.56	5.7	2650	to, 108.0		20.0		2.4	269.0, 2.42	1395	40.8	0.44
11 km, M= 0.8				27.0								
P&W JT9D-70A	2.46	3.36	4153	to, 236.0	0.37	24.0	116.0	1.6	568.0, 4.9	1520	56.8	0.38
11km, M = 0.85				53.2								
GE CF 6 50M	2.2	4.65	5000	to, 247	0.38	32.4	121.0	1.6	532.0, 4.4	1563	49.4	0.50
10 km, M = 0.85				52.4	0.65							
RR RB 211 524	2.17	3.03	5980	to, 227	0.37	25.0	121.6		535.4, 4.4			
11 km, M = 0,85				50.0	0.66							
P&W TF30-P-100	1.24	6.14	1807	ab, 111.7	2.45			2.14	118.9, 0.34	1589		

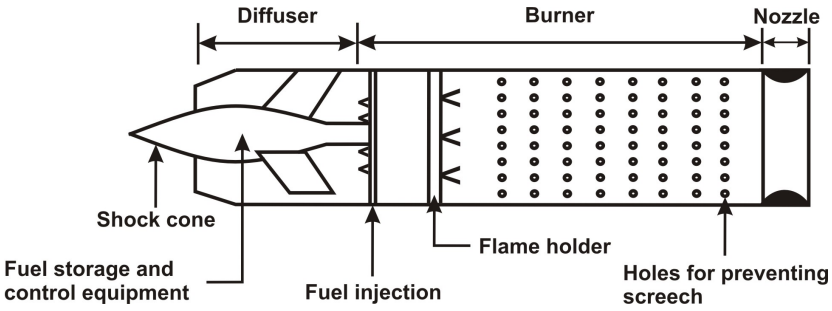

Figure 1.12: Schematic of a Ramjet

times the free stream static pressure. Taking the recovery of the stream stagnation pressure as 60 – 70 % as is usually the case in fixed geometry intakes, the free stream diffuser end pressure is seven times the static pressure. This pressure, as may be recognized is comparable to what one obtains at the end of a compressor of a turbojet. Thus, one can dispense with the compressor. Once the compressor is dispensed with, the turbine can also be dispensed with, since power need not be generated to run the compressor. One, therefore, has a diffuser, combustor and an exit nozzle. The stagnation pressures available at the end of the combustor will be several times the ambient pressure (at least 5 – 7 times). In order to extract the expansion work, one uses a convergent-divergent nozzle. Figure 1.12 shows the schematic details of a ramjet.

By the arguments made earlier, it is clear that ramjets operate well only at high speeds, typically between M = 2.0 and 4.0. The combustion mode being not very different from that of an afterburner, the specific fuel consumption is comparable to that of afterburner, namely 2 – 3 kg/ hr kgf. Because of the high speed at which they are efficient and yet simple in construction, they are used for missiles extensively.

The ramjet, unlike turbojet and turbofan does not produce any thrust at zero flight speed. Therefore ramjets need an auxiliary system which propels to a speed (or Mach number) range where they can work. In most missile systems, rocket engines boost the vehicle to a range where ramjets can begin functioning.

The data on ramjets are generally not easily available because ramjets are mostly contemplated for use in military applications. Some brief data on some systems are presented in Table 1.7. Two of the applications correspond to solid fuel ramjet (SFRJ) and Integral ram rockets (IRR). In the case of solid fuel ramjets, as the name indicates, the fuel is a solid block. Air flows through the port of the fuel block, combustion takes place at higher pressures created by the ram effect, and the hot gases pass through the nozzle producing thrust. In the case of integral ram rockets, the chamber which contains the rocket propellant is used as the ramjet

Table 1.7: Ramjets and Ram Rockets (* = kg/kgh, Appln. = Application, RJ = Ramjet, IRR = Integral Ram Rocket.)

System	Dia. (m)	L (m)	Wt. (kg)	Thrust (kN)	Speed (M)	sfc *	Appln.
Marquardt (MA 212-x AA)	0.38	2.1	35.2	6.05	2.5 (at 12 km)	2.3	RJ
SA-6, SFRJ	0.35	2.0	–	15.0	2.0	7.5	IRR
LVRJ	0.38	4.5	680.0	–	3.0	–	IRR
THOR (Blood Hound)	0.40	2.6	81.0	13.0	2.0 (at 6 km)	2.0	RJ

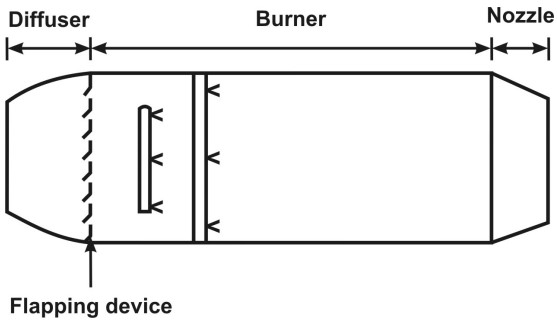

Figure 1.13: Schematic of a Pulsejet

combustion chamber after the rocket propellant is burnt up in the boost phase.

1.8 Pulsejet

Pulsejet is a constant volume combustion device (unlike ramjet which is a constant pressure device) which is quite efficient only at low speeds and uses unsteady combustion for its operation. Once the system is started, it works by taking in air and fuel and combusting them during a part of the cycle and exhausting it during the next part of the cycle (Figure 1.13). In order to promote and sustain the operation, a flapper device of metal or plastic, in recent times, is used in the front end. During the exhaust of the gases through the nozzle, the pressure falls down and it causes the flapper valve to open. This causes air to come in. At the same time fuel is injected and igniter spark is put on. This initiates combustion and pressure rises in the combustor. Due to this pressure rise the flapper valve closes. This whole operation repeats by itself and there will be net thrust developed during the cycle.

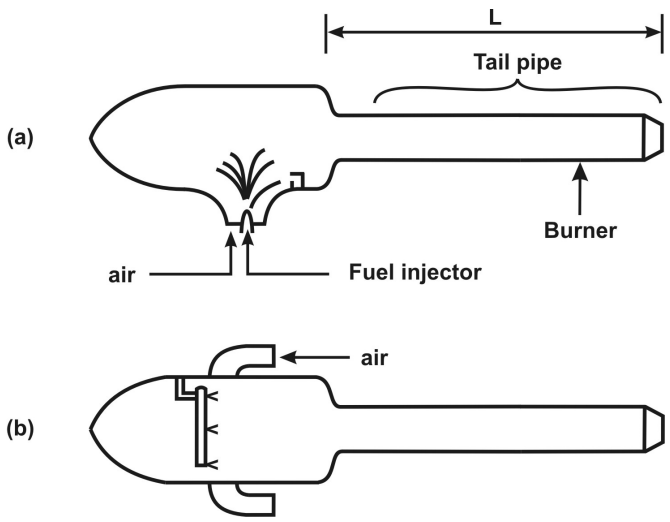

Figure 1.14: Valveless Pulsejets – air is inducted into the combustion chamber due to oscillatory combustion in which the pressure falls below ambient during a part of the cycle

In modern times, several new devices which work without valve (called valve-less pulsejets have been developed).

1.9 Valveless Pulsejets

Figure 1.14 shows two such devices. These devices use acoustic behavior of ducts for their operation. In these cases, the organ pipe longitudinal mode frequency is given by a_c /4L, where a_c is the speed of sound in the combustion chamber. For temperature of 1800 K, the acoustic speed is about 840 m/s and for L$\sim$ 1 m, f $\sim$ 210 Hz. At this frequency, combustion interacts with acoustics in such a manner that the fluctuations in the chemical heat release are in phase with that of the acoustic fluctuations and a continuous oscillatory combustion operation is set up. The fluctuations generate pressure waves so as to enable continuous self-induction of the air and the subsequent combustion. The hot gases exhausting through the nozzle produce thrust.

1.10 Scramjet

Flights at high Mach numbers are characterized by large stagnation temperatures and pressures. At the high temperatures experienced under stagnation conditions

Table 1.8: Properties of air at stagnation conditions at high Mach numbers calculated for ambient conditions of 243 K and 0.0058 atm (Note that all the composition is in terms of mole fraction. 3E-04 implies 3.0 $\times 10^{-4}$)

M_∞	T_{stag} K	N_2	O_2	NO	O	CO_2	Ar
4.0	980	0.7808	0.2095	4E-05	-	3E-04	0.00932
5.0	1355	0.7803	0.2087	0.001	-	3E-04	0.00932
6.0	1788	0.7780	0.2070	0.004	3E-04	3E-04	0.00932
7.0	2265	0.7730	0.2015	0.015	3E-04	3E-04	0.00932
8.0	2777	0.7630	0.1910	0.034	0.002	2.9E-04	0.00930
9.0	3293	0.7450	0.1700	0.072	0.010	2.5E-04	0.00930
10.0	3878	0.7275	0.1518	0.092	0.018	2.1E-04	0.00920

or even behind oblique shocks, it is possible that air will dissociate. Typical properties at Mach numbers from 4 to 10 are shown in Table 1.8. The results shown in the table assume equilibrium properties of air as a mixture of reactive species like oxygen, nitrogen, and carbon dioxide. Of these species, Nitrogen is very difficult to dissociate or react with (this is the reason for a stable life on earth). The equilibrium assumption implies that the chemical reaction times are small compared to flow times. But at high Mach numbers, while high temperatures favor faster reaction rates, lower static pressures reduce the rates and in addition, flow times reduce and could become comparable to reaction times. This will imply that chemistry controlled flow could be relevant at these conditions.

As Mach number increases, the stagnation temperature rises sharply and air normally thought as a fluid composed of Nitrogen and Oxygen for most gas dynamic applications below a Mach number of 4, begins to generate other species. Species like NO and O get generated. The fraction of oxygen in the dissociated stream comes down. At M = 10, oxygen fraction (including atomic oxygen) is about 16 % compared to 21 % at M = 4. Argon (Ar) is a monotonic species and is an inert. Its marginal change is reflective of changes in other species.

At M = 7, the stagnation temperature achieved is 2265 K, comparable to fuel-air combustion temperatures at ambient conditions. This implies that adding heat to fluids brought to rest from high Mach number conditions becomes marginal. This will imply that thrust generation potential becomes small. This happens largely because, most of the energy at high enthalpies goes into dissociating the species. Further, at M = 9, the stagnation temperature is 3293 K that is close to the maximum temperature that a chemical system can provide because, beyond this value, dissociation prevents energy input into translational mode. This is illustrated in Table 1.9 where the combustion properties of stoichiometric hydrogen–air mixture are presented. Clearly, the increment in the temperature from stag-

Table 1.9: Combustion properties of stoichiometric H_2 – air (The two sets of compositional data refer to higher (top) and lower pressures (bottom) at Mach numbers of 8, 9 and 10. All composition is in terms of mole fraction)

Sl. No.	M_∞	T_{stag} K	T_{adiab}, K at p_{stag}	T_{adiab}, K at lower p	N_2	O_2	NO	H_2O	OH	O	H
1	2	3	4	5	6	7	8	9	10	11	12
1.	4.0	980	2600	2560	0.626	0.009	0.005	0.295	0.016	0.002	0.007
			0.92 atm	0.46 atm							
2.	5.0	1355	2793	2747	0.623	0.009	0.007	0.288	0.019	0.003	0.008
			3.45 atm	1.73 atm							
3.	6.0	1788	3015	2921	0.618	0.010	0.010	0.295	0.023	0.003	0.010
			11.5 atm	3.43 atm							
4.	7.0	2265	3264	3114	0.612	0.011	0.013	0.265	0.029	0.004	0.012
			34.1 atm	6.83 atm							
5.	8.0	2777	3543	3287	0.605	0.011	0.017	0.250	0.035	0.005	0.015
			94.2 atm	9.42 atm	0.592	0.015	0.016	0.222	0.042	0.011	0.029
6.	9.0	3293	3842	3148	0.596	0.011	0.021	0.235	0.040	0.007	0.019
			235 atm	1.17 atm	0.570	0.019	0.018	0.190	0.049	0.018	0.040
7.	10.0	3878	4201	3600	0.586	0.011	0.027	0.215	0.048	0.009	0.024
			595 atm	11.9 atm	0.568	0.018	0.023	0.162	0.059	0.025	0.060

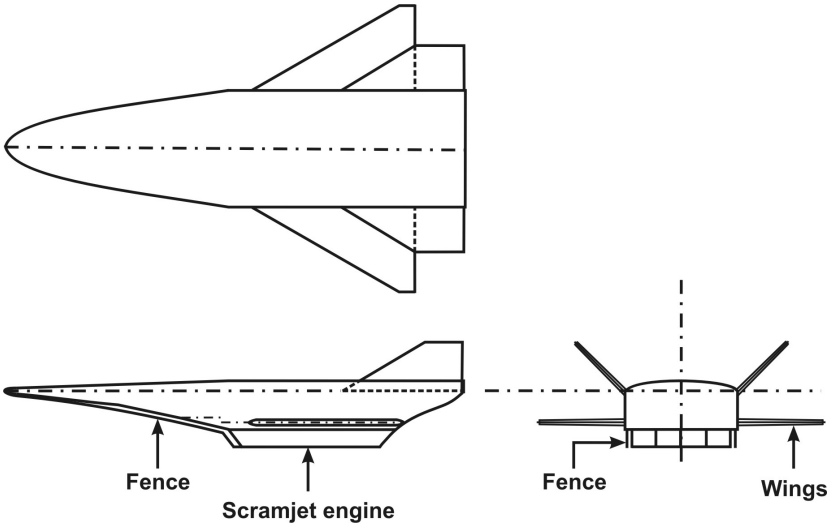

Figure 1.15: The schematic of a hypersonic vehicle

nation to the flame as seen in columns 3 and 4 goes down with the increase in Mach number. Assuming that the flow conditions are not brought down to subsonic state, but to a Mach number with associated stagnation pressure losses that occur in the intake, the results of column 5 when compared with column 3 again show that combustion process contributes to decrease in the flame temperature (at M = 9 and 10) from free stream stagnation conditions! This is simply because of the presence of easily dissociating species in the mixture (note that between oxygen and hydrogen, it is the hydrogen that dissociates more readily as can be noted from columns 11 and 12). The effects of dissociation are very dramatically displayed in the results of M = 8, 9, 10 where the two rows refer to the higher and lower pressures identified in columns 4 and 5. It is this dissociation that contributes to the reduction in the flame temperature at the stagnation pressure (column 4) and at a lower pressure (column 5). Hence, in a scramjet the flow is not decelerated to subsonic conditions like in the case of a ramjet, but is decelerated to about a third of the flight Mach number. Thus, at a flight Mach number of 8, the combustor Mach number is about 2.7. In this process, the static temperature in the combustor is maintained at about 1200 to 1400 K to enable smoother ignition of the fuel (hydrogen or a hydrocarbon fuel). The static pressure becomes as low as 0.5 to 1.0 atm. Since chemical reaction rates vary as the square of the static pressure, the reduction in static pressure reduces the reaction rates significantly.

1.10.1 Scramjets vs. Other Vehicles

Turbojet based aircrafts have been built to fly at Mach numbers close to 3 (MiG. 25 flies at M = 2.8). Ramjet based missiles fly at M = 2 to 3. These are generally cylindrically shaped and boosted to the required speed by a rocket, and subsequently, the ramjet works in a sustain or weak–acceleration mode. Scramjets have been conceived for meeting a part of the propulsion needs of a space launch vehicle – between Mach numbers of 4 to 10. But no systems have been built yet. The only well argued case for a scramjet has been a cruise missile to fly at Mach numbers between 6.5 to 8. In this case the missile needs to be boosted to the required Mach number and allowed to function in cruise mode for long time, typically 10 to 20 minutes. The ostensible reason for this mission is to have a "very fast" missile that cannot be chased and shot down by other missiles of the current generation that operate at a maximum Mach number of about 4. Since the missile has to function for a reasonable duration with some minimal payload, it has to carry substantive amount of fuel. It is optimal to consider a winged vehicle so that the demand on the propulsion can be brought down by using the better lift-to-drag features. The principal wing shape at high Mach numbers is a delta wing. This is aimed at reducing the drag penalties and common to nearly all of the supersonic aircraft. Because of the deep delta configuration, the aspect ratio (the ratio of the square of span to the wing area) of the wing will be small ($\sim$ 1.5 – 2) that one cannot expect a lift-to-drag ratio of more than 4. The engines are usually located at the bottom of the wing as shown in Figure 1.15.

Another feature of hypersonic flight condition is the very significant interaction between the engine and the rest of the vehicle. This is true even for other flying vehicles, but takes on increasingly important proportion as Mach number increases. Normally discussed under the title airframe-engine integration, it influences the design of interfaces and can be managed if there is demand for say, change of the engine profile within limits for most aircrafts. In the case of hyperplane, the entire plane has to be looked at together since the engine fore and aft-body are very closely connected. For instance, it should be understood that the 'airintake' starts from the nose of the vehicle with external compression in the entire bottom section ahead of the engine framework with possible additional compression inside the engine portion (see Chapter 6, intake section for further details of external and internal compression aspects). Hence, any change that occurs in the geometry far ahead of the engine can affect the pressure recovery and mass flow characteristics of the engine. Further, the drag, D written as $D = (\gamma p_o M_o^2/2) c_d A_w$ where, c_d is the drag coefficient and A_w is the wing area, indicates that the drag rises sharply with Mach number. Hence, the thrust produced must equal the large drag values for steady flight. The engine must have the ability to produce some excess thrust to enable control of the vehicle. Since this excess happens to be the difference between two large quantities, it is important to ensure that other geometric

or flow features do not affect the availability of this excess force. One fluid dynamic feature in hypersonic flow regime that remains inadequately understood is the flow transition process. Hypersonic boundary layer over a non-smooth heated surface with curvature is known to have extended transition regime that can affect the drag experienced by the vehicle and this uncertainty must be covered in the design margin.

The above features are special to hypersonic vehicle in comparison to supersonic aircrafts and ramjet based missiles.

The design of the combustion system is usually contemplated along the lines of can combustor in gas turbine engines. The basic idea is to build a module and use as many modules as needed to enable reduction in development costs. One of the classical modules contemplated is *not a circular geometry*, but a rectangular one. This is because, circular geometry does not provide any benefits due to complex shock structure in the flow field with struts, injectors and such other protrusions. More discussion on this subject is presented in section 6.3.6.

Scramjets are in developmental stage in different countries at this time. While, successful laboratory developments have been reported, autonomous hypersonic flight with supersonic combustion is yet to be demonstrated. The difficulties in the realisation of this objective lie in the discussion presented earlier.

1.11 Starting Systems

Most of the air breathing engines are not self-starting (as discussed earlier in the case of turbojet). The starting devices for turbojets, turboprops and turbofans are those needing to spin the rotating machinery up to a certain minimum speed (15 – 20 % rated speed). During this period, the air flow is taken in, pressurized and then passed through the combustor and turbine. When a minimum air flow rate is a achieved, fuel is injected, and ignited. The gases flow through the turbine and generate power to accelerate the compressor. Typical time required to achieve steady state varies between 30 – 80 s depending on the size of the engine, smaller engines taking smaller time to accelerate. All starting systems automatically disengage once the main system starts functioning.

Engine start-up is done by using (i) ground based compressed air, (ii) electric motor, and (iii) pyrotechnic operated systems. In (i), the compressed air jets impinge on the main turbine or an auxiliary turbine connected through the gearing to the main system until the speed crosses a minimum value. At this stage, the fuel injection sequence under the action of the control system begins to take over. The igniter is a high energy continuous spark source with an energy of about 2 J. This level of high ignition energy is not needed in the more benign circumstances of ground starting. However, it is provided so as to account for a far more criti-

cal condition that arises during an in-flight blow-out of the flame in the combustor during adverse conditions of high altitude, high angle of attack of flight, and heavy rain. Some engines have more than one spark source so that redundancy of ignition is provided for. In (ii), the auxiliary power source on board the aircraft is used to run the electric motor which runs the rotating machinery through a gearing system.

In (iii), an auxiliary turbine is started by using a small rocket motor fitted with a propellant which burns for 3 – 4 s. At the end of the combustion, the main rotating machinery would have accelerated. Some aircrafts like Canberra use such cartridge starters. Each engine has a maximum of three cartridges which can be used during a flight. The discharged cartridges are recharged at the end of each flight.

Ramjets and scramjets are not self-starting and begin to produce positive thrust only at relatively high speeds (M = 0.8 – 1.2) and (M = 4 – 5) respectively. Therefore, they need to be accelerated to their optimum speeds (of the order of M = 2 – 2.5 for Ramjets and around M = 6 for scramjets) before being allowed to operate. The acceleration is performed using rocket engines (mostly solid rockets operating for a short burn time of the order of a few seconds).

Pulse jets are not popular devices for use in many applications. The starting of pulse jets with flapper valves is initiated by causing combustion in an interrupted manner for a few operating cycles. For valveless pulse jets, the operation is automatic after the system has been heated up.

1.12 The Non-Air-breathing Engines

Non-air breathing engines came into being in an effort to provide large thrust for short or ultra short durations (like fractions of a second) for missile applications or flight outside the atmosphere. The only way of achieving this was to avoid dependence on the ambient air for the purposes of exothermic oxidation and use more exotic oxidizers of high density to facilitate obtaining high energy density. Rocket engines do this precisely. They dispense with air of the ambient atmosphere. As a result of this, they can provide thrust even in outer space devoid of air. They carry their own oxidizer and fuel. The argument that air compressed to, say a thousand atmospheres to achieve densities comparable to solids or liquids in favor of air is dispensed with by the consideration of two features. First, even the compressed air needs to be stored in a vessel. The weight of the vessel will indeed be significant because of the high pressures. Instead of this, one can use a solid or liquid so that storage does not call for a vessel with high pressure and hence, lesser weight. Second, Nitrogen in air does not contribute to energy, but absorbs whatever energy is released because of the reaction of oxidizer with fuel. Hence,

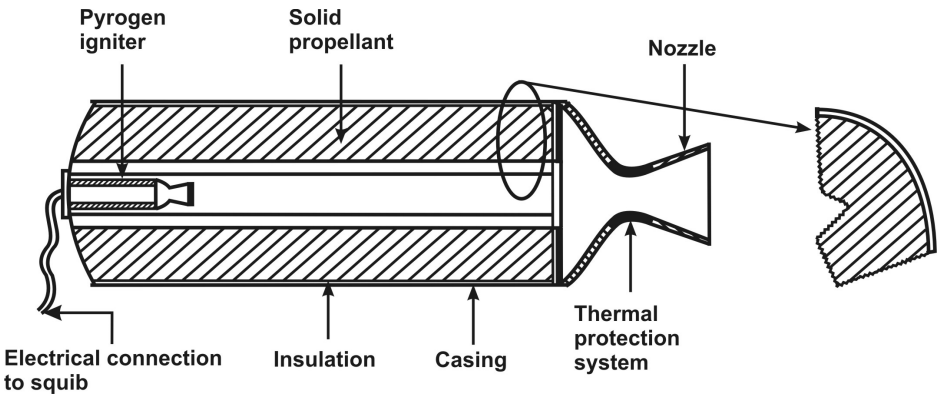

Figure 1.16: Elements of a Solid rocket engine

one can eliminate the molecular nitrogen in the oxidizer. Thus, one concludes that one could use for instance liquid oxygen. Indeed, it was the oxidizer thought of by early rocket pioneers; it has since been used extensively for boosters based on liquid rockets. One of the other features with rocket propellants is that many of them are compounds composed of both fuel and oxidizer elements. Depending on the relative extents of the fuel and oxidizer elements, the compound will express itself as fuel or oxidizer.

1.13 Solid Propellant Rockets

Solid rocket engines are traditionally called solid rocket motors. The rocket motors are classified based on the physical state of the constituents of the solid propellant used in these motors. A Homogeneous combination like nitrocellulose (fuel) and nitroglycerin (oxidizer) has been used as a solid propellant for a long time for military applications. As different from this kind, heterogeneous propellant (also, a composite propellant) that uses a solid oxidizer like Ammonium Percholorate and a polymeric fuel like polybutadiene, has been developed and extensively used in the last four decades because of much higher performance. The typical elements of a solid rocket engine are shown in Figure 1.16. The outer shell can be of metal or fibre reinforced composite material. Between the propellant and the wall is insulation. This has largely, thermal insulation quality. The face towards the nozzle end may have an inhibitor. Inhibitor is a polymeric material which is chemically bonded to the propellant so that the exposed surface does not burn. This feature uses the principle that the propellant burns along the local normal to any exposed surface. If the surface is covered with a ‘fuel’, then no combustion can take place in this zone. The nozzle is the element of convergent-divergent construction which expands the hot and high pressure gases to low pressures nearly equal to the am-

bient pressure. In this process gases acquire high velocity at the exit so that thrust is generated.

The thrust of a rocket motor is given by

$$F = \dot{m}V_e + A_e\,(p_e - p_a) \tag{1.6}$$

where $\dot{m}$ is the mass flow rate of gases (kg/s). V_e is the exit gas velocity (m/s), A_e is the exit cross sectional area (m^2) and $(p_e - p_a)$ is the pressure difference between the exit and the ambient (N/m^2). The above equation is different from the one for air-breathing engines in the sense that there is no inflow of air-stream and hence, the contribution of inflow momentum is zero.

The magnitude of the second term in equation (1.6) constitutes no more than a few percent of the first term in most well designed situations.

Typical values of exit speed are about 2 – 4 km/s, being more close to 2.5 km/s in solid rockets. This implies that one kg/s of flow rate gives a thrust of 2 – 4 kN. The single most important parameter characterizing the performance of rocket engines is the thrust per unit propellant mass flow rate or impulse per unit mass of the propellant, denoted as the specific impulse (I_{sp}). The exit speed is itself a measure of the performance. As discussed already, its units are N-s/kg in SI units and more conventionally as seconds when it is treated as thrust per unit weight flow rate. Thus, I_{sp} is V_e/g in these units.

The specific impulse, as will be shown later (see section 4.2.7) is dependent on two features: The energy of propellants as expressed through what is termed the characteristic velocity (c^*, m/s) and a quantity called thrust coefficient (c_F) describing the nozzle expansion process. The relationship between the three quantities is described by

$$I_{sp} = c^*\,c_F \tag{1.7}$$

where $c^* = \sqrt{RT_c/\mathscr{M}}\ /\ \Gamma(\gamma)$, R = Universal Gas Constant = 8314 m^2/s^2K (also J/kg-mole K), T_c = Temperature of gases in the combustion chamber (K) , $\mathscr{M}$ = Molecular weight of the gases. $\Gamma(\gamma)$ = 0.62 to 0.6 for γ variation between 1.15 to 1.25 covering most rocket engine operating conditions.

$$c_F = f(p_c/p_a,\ \ A_e/A_t,\ \ \gamma) \tag{1.8}$$

Where p_c and p_a are the chamber and ambient pressures. A_e/A_t is the nozzle exit to throat area ratio.

As I_{sp} depends on nozzle expansion process, any statement of its magnitude in a specific case must involve the explicit indication of the chamber and ambient pressure as well as A_e/A_t. If, however, the nozzle expands the gas to the ambient pressure, the area ratio need not be indicated as it gets fixed by the condition of complete (or optimum) expansion.

For solid rocket motors and liquid rocket engines in many instances, p_c = 1000 psi or 70 atm or 7.1 MPa, p_e = p_a = 0.1 MPa the case of optimum expansion.

In many cases where the engine operates in near–vacuum conditions at very high altitudes, a term known as vacuum specific impulse is used. In the case p_a = 0, one needs to know p_c as well as area ratio A_e/A_t for the interpretation of actual values.

Most solid rocket motors are single start systems. No controllability or restartability is possible. However, some systems like of Lockheeds (USA) do have restartability and different levels of thrust in pulse mode (see Janes All World Aircraft, 1977-78).

Another important element of a solid rocket motor is the igniter. Igniter can be a bag of pellets of a composition, usually, having higher metal loading (40 - -60 %). It has also an initiator and a squib which is essentially a nichrome or similar wire coated with a heat sensitive composition. On the application of a current of about one ampere, the wire becomes hot and the heat sensitive composition bursts into a flame. This then causes the main igniter composition to burst into flame. The products consisting of hot gaseous products as well as hot metal oxide particles impinge on the surface of the propellant and cause ignition of the main propellant. While small rockets work with igniters of the kind noted above, large rockets have smaller rockets with igniter composition to cause ignition. These are called Pyrogen igniters.

The ignition system of modern boost motors have safe arm devices and protection against electromagnetic interference (EMI). In some designs, the ignition current is not initiated until the current exceeds several hundred amperes essentially to protect against EMI.

Solid propellants have high density and good specific impulse. Double base or homogeneous propellants have a density of 1500 kg/m^3 and specific impulse of 2000 – 2250 N-s/kg and used in tactical military arsenal. Composite propellants have a density of 1700 – 1790 kg/m^3 and a specific impulse of 2400 – 2500 N s/kg. They are largely used in strategic military vehicles or launch vehicles for space applications.

Solid rockets have been built to produce thrust of no more than a few Newton's to as much as several hundred kilo Newton's. The burn time varies from a few milliseconds to as much as thousand seconds. The applications of solid propellant rockets vary from those required to cause impulse for structural response analysis (systems called Bonkers) through auxiliary power generating units in missiles to missile and launch vehicle propulsion systems. Table 1.10 illustrates a few of the engines across the world with some salient characteristics.

Table 1.10: Solid Rocket Engines (m_p = Propellant mass, p_c = Chamber Pressure, A_t = Throat cross sectional area, L = Length, EDB = Extruded Double Base, PB = Poly butadiene, AP = Ammonium Perchlorate, Al = Aluminum, PBAN = Poly Butyl Acrylo Nitrile PC = Polycarbutene, (v) = Vacuum)

Engine	Thrust $\times t_b$ kN $\times$ s	Propellant	m_p tonnes	p_c atm.	A_e/A_t	I_{sp} kN s/kg	Dimensions
SAM I, Stage I USSR	250–380 $\times$ 4.5–3.0	EDB	0.19	30-60	6.0	2.10 (SL)	0.53 m dia $\times$2.5 m L
Missile Target	1.5 $\times$ 180	EDB					
Rocket Dyne MK 60 Phoenix	8 kN $\times$ 60	PU-AP-Al	0.20	–	6.0	2.5	0.38 m dia $\times$ 1.78 m
Stop-start motor, Aerojet		PB-AP-Al	0.40				0.51 m dia $\times$ 2.21 m L
Minuteman Stage II	270 $\times$ –	PB-AP-Al	7.08	–	–	–	1.32 m dia $\times$ 4.01 m L
Lockheed LSM–156	13600 $\times$ 120 s	PC-AP-Al	317.50				3.96 m dia $\times$ 18 m L
SLV3 - SI India	450 $\times$ 49	15PBAN-70 AP -15Al	8.64	32	6.7	2.54	1 m dia $\times$ 9.7 L
SLV3 - SII India	211 $\times$ 40	15PBAN-70AP -15Al	3.78	38	14.6	2.69	0.8 m dia $\times$ 6.2 m L
SLV3 - SIV India	21.2 $\times$ 31.5	15 HTPB-70AP -15Al	0.26	23	31	2.74(v)	0.65 m dia $\times$ 1.6 m L
PS 1 (PSLV) India	4500 $\times$ 100	- same -	139.00	60	8	2.5	2.8 m dia 20 m L

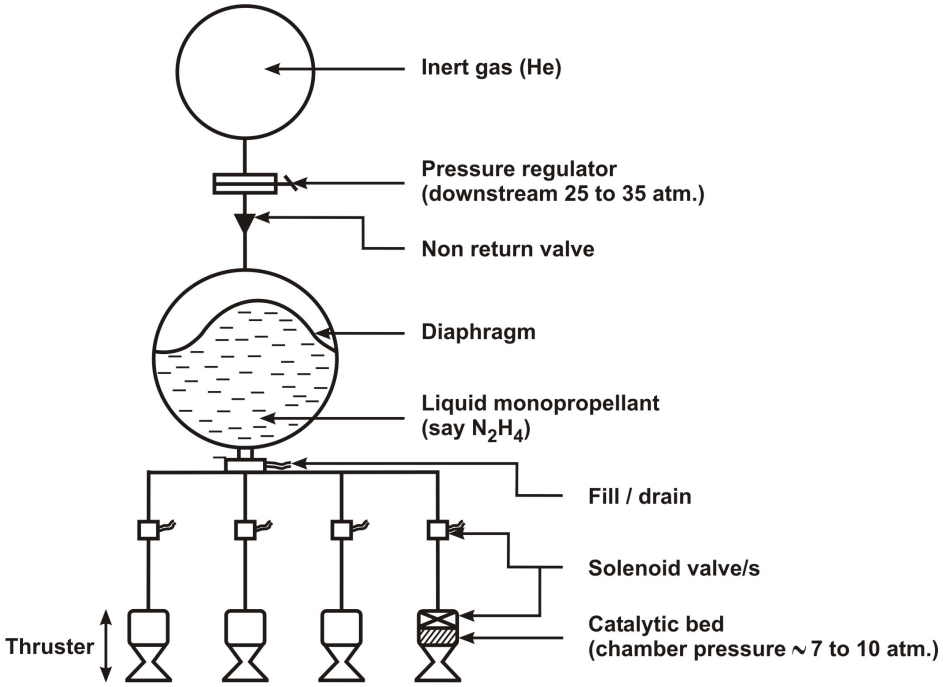

Figure 1.17: A Liquid Monopropellent Thruster System

1.14 Liquid Propulsion Systems

There are many types of liquid propulsion systems. They can be based on a single liquid which decomposes in the presence of a catalyst to hot gases which expand and produce thrust. These are called monopropellant thrusters. They are usually limited to low thrust and relatively small durations during each firing.

As different from them, there are bipropellant thrusters which use two liquids in which one is a fuel and the other oxidizer. These rockets vary in size from small to very large, many can be restarted and some are of variable thrust.

The bipropellant thrusters are further classified in two different ways. (i) Do they form a self-igniting or hypergolic combination or otherwise and (ii) Are they storable at ambient conditions or do they need special facilities for storage.

Many fuels like amines–aniline, xylidine, triethylamine and hydrazine and its derivatives like unsymmetrical dimethyl hydrazine and monomethyl–hydrazine are all hypergolic with white fuming nitric acid (having 4 – 6 % nitrogen tetroxide), red fuming nitric acid (having 10 – 14 % nitrogen tetroxide) or nitrogen tetroxide which are the oxidizers. All the above propellants are earth storable (storable under normal earth conditions without any special equipment). The fuel-

oxidizer combinations like liquid oxygen-liquid Hydrogen are non–hypergolic and cryogenic, i.e. they need carefully insulated low temperature storage vessels.

The not-so-used fuel–oxidizer combination like liquid fluorine–liquid hydrogen is hypergolic and cryogenic. The combination liquid oxygen–kerosene is non-hypergolic and semi–cryogenic in which liquid oxygen alone needs low temperature storage. Some unusual combinations like Ammonia–liquid oxygen have also been used in some rocket engines (X-15 Research Aircraft).

Every propulsion system has two elements – a feed system and thrust chamber. The feed system in relatively small impulse rockets are fed by using a high pressure inert gas source on board. Large impulse rockets are turbo pump fed. Most monopropellant rocket engines are pressure fed due to the additional need for reliability. Figure 1.17 shows the elements of a monopropellant rocket. The feed system consists firstly of high pressure inert gas storage. The inert gas can be either nitrogen or helium (to reduce the weight of the gas). The pressure at which the gas is stored is 300 – 350 atm (30.4 to 35.6 MPa) essentially to reduce the total weight of the feed system. The pressure is dropped to levels of 2 – 4 MPa (depending on the design) through a pressure regulator and the gas pressure is applied on the surface of the liquids in the container of the liquid propellant.

Since many monopropellant thrusters are used for space applications involving zero gravity, the feed systems involve positive expulsion devices. Bladders made of teflon or EPDM (Ethylene-Propylene Diene Monomer) over which gas pressure is imposed was a conventional technique. The liquid is expelled independent of the orientation of the vehicle or space craft. A more recently developed device is the surface tension acquisition device having high expulsion efficiency ($\sim$ 99 % or better).

The thrust chamber receives the liquid from the tank through a solenoid valve which serves the purpose of on or off. The thrust chamber has an injector which atomizes the liquid to fine droplets which impinge on a catalytic bed. The catalytic material is porous alumina pellets of 2 to 6 mm dia with a coating of noble metals like Iridium. The catalytic bed is packed between meshed screens. The exit of the screen becomes the entry to the convergent-divergent nozzle. The monopropellant thrusters have a thrust as low as 0.1 N to as much as 20 N. The duct carrying the liquid monopropellant in a 0.1 N thruster has a diameter of 200 μm. The diameter of the thruster is about 1.5 mm. The thruster is maintained at temperatures up to 300 $^{\circ}$C to ensure smooth start-up and long life.

To start the system all that one does is to open the solenoid valve which allows the liquid monopropellant to flow into the thrust chamber, decompose and pass through the nozzle to produce thrust. Shutting off the solenoid valve automatically cuts off the flow and causes thrust to decay to zero.

A pressure fed bipropellant engine is shown in Figure 1.18. Like in the pre-

vious description, the engine has a high pressure bottle, a regulator and a pyro-valve which separates the high pressure region from the downstream region till the system needs to be made operational for the first time. The line pressure is fed through non-return valves (used to prevent mixing of fuel and oxidizer vapors) to the tanks having fuel and oxidizer. The pressure of the propellant bottles varies from 10 – 40 atm. depending on the application. The gas pressure is delivered to the upper space in the liquid filled tanks. The space above the liquids inside the tank is called ullage. Providing for a minimum of this space fulfills the requirement of maintaining a small pressure variation in the tanks to ensure nominal liquid flow rates through the system. The tanks have also 'fill' and 'drain' systems. The downstream path takes two lines for fuel and oxidizer to the thrust chamber through electro-mechanical (or solenoid) valves or pyro-operated valves. The use of pyro-operated valves implies one shot 'on' operation. The thrust chamber has an injector with separate manifolds for oxidizer and fuel and injector plate with holes for fuel and oxidizer separately. The liquids on passing through the holes atomise by impinging on themselves (called like-impingement system) or on one-another (called unlike-impingement system). The combustion chamber is sized to complete the reaction between the fuel and oxidizer to final products at high temperature. The hot gases pass through the nozzle, producing thrust. Typical thrust chambers may have injection holes from about half a dozen for 50 – 500 N thrust engines to as many as several thousand for engines of thrust 100 – 8000 kN. In order to obtain thrust from the system, one needs to command the valves of fuel and oxidizer to open. The relative times of arrival of the fluids into the combustion chamber can be important in obtaining a smooth build up of thrust or otherwise a hard start or an explosion may result in the case of hypergolic fuel-oxidizer combination. It is usually the practice to allow the oxidizer arrive at the chamber about 50 – 200 ms earlier to the fuel in most rocket engines. Shutting off of the valves causes rapid decay of thrust depending on how much is trapped in the ducting. For LOX – LH_2 systems that operate on fuel rich mode, the shut-off sequence closes the oxidizer valve first and then the fuel valve to ensure that no transition through stoichiometric condition takes place. The amount of the propellant remaining trapped is usually very small for un-cooled pressure fed engines. For high thrust engines, the fact that the tanks need to have high pressure in pressure fed engines, will imply excessive weight of the feed system. For handling such situations, the tanks are maintained at relatively low pressure and the fluids pass though pumps which raise the pressure to as much as 80 – 450 atm. The high pressure fluids pass on then to the thrust chamber through valves operated hydraulically or pneumatically. Figure 1.19 shows the various elements of a turbo pump fed system. While the pressure fed system can start with the opening of valves, without any other system entering into picture, in the case of turbo-pump fed system, the pumps have to be spun by running the turbine. The source of power for running the turbine can be several. One of these is a separate monopropellant gas generator; a separately pressure fed tank supplies the liquid at the predesigned rate to a com-

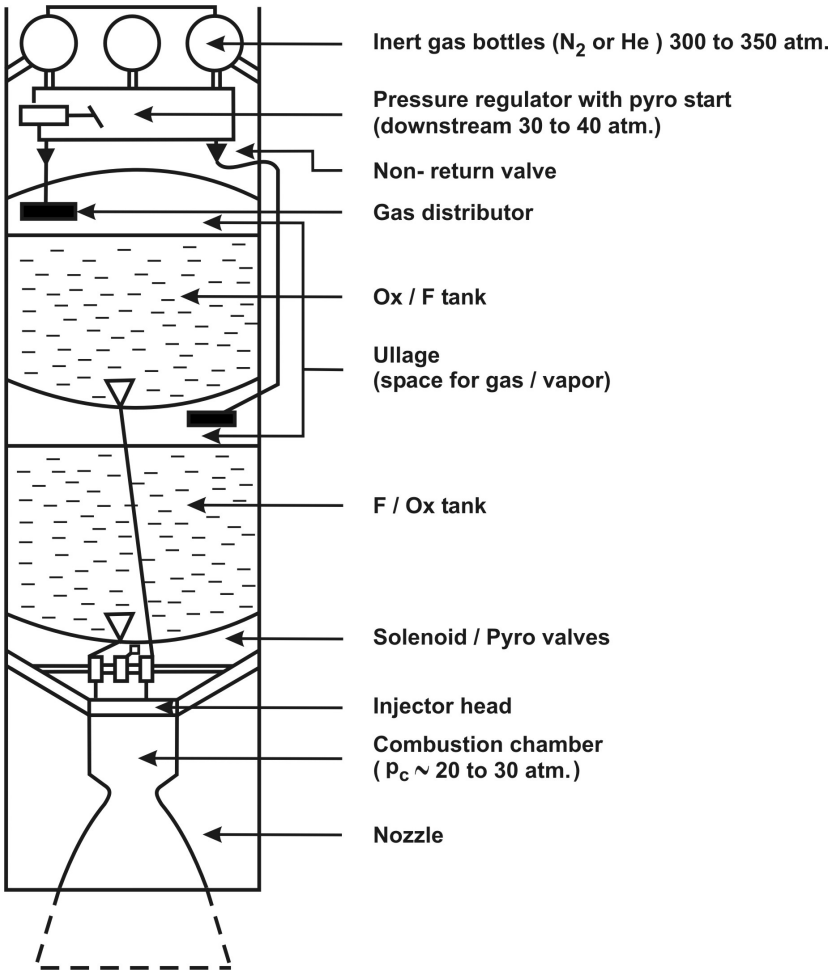

Figure 1.18: Schematic of Bipropellant pressure fed liquid rocket engine

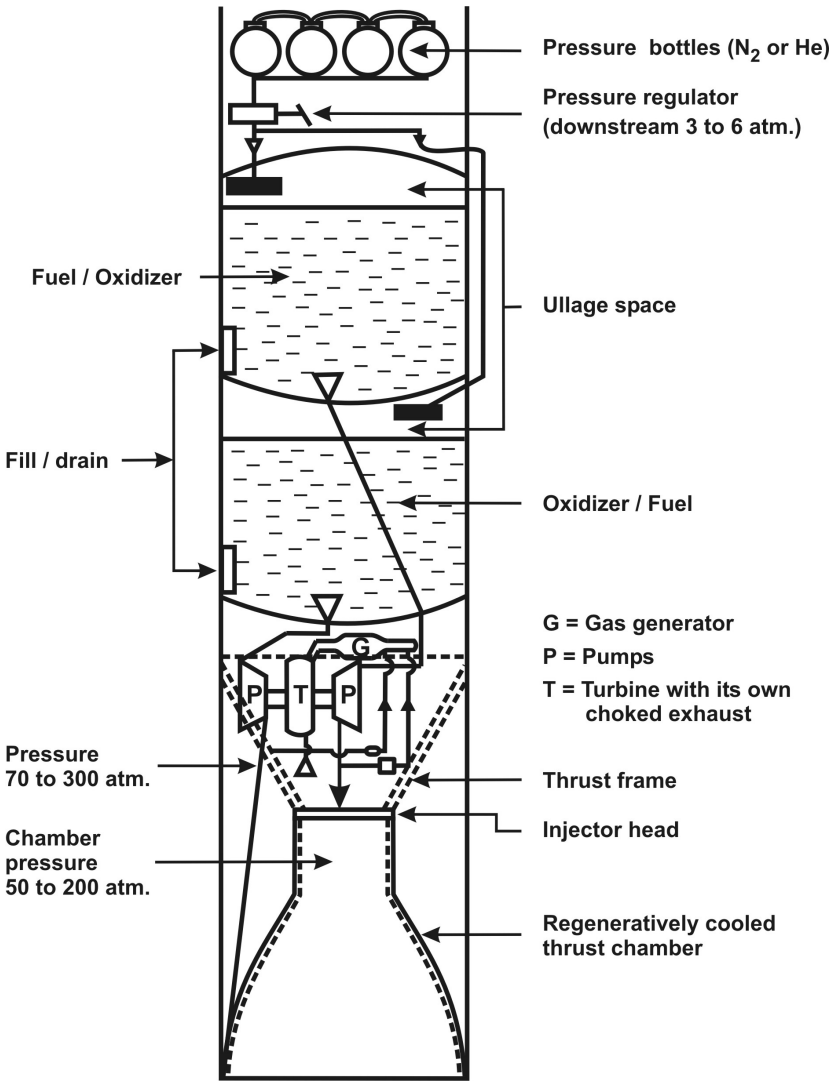

Figure 1.19: Schematic of a bipropellant turbo-pump fed liquid rocket engine

bustion chamber; the gases from the combustor at temperatures not exceeding 1200 – 1400 K at reasonably high pressures (30 – 40 atm) are led into the turbine for extraction of work. In another scheme that is more extensively used, the fluids from the outlet of the pumps are drawn-off in predesigned amounts and delivered to a combustion chamber usually termed gas generator. The oxidizer-to-fuel ratio used here is far off-stoichiometry to limit the temperatures to no more than 1400 K keeping the operation of the high speed turbine in view. The second system is called boot–strap system as it draws off the fluids from the main system itself.

There are two methods of starting of the turbo pump system. The conventional system is to spin the turbine with the hot gases from a separate small solid propellant cartridge that burns up in a few seconds. And once, the turbine has reached enough speed, a separate liquid monopropellant stream that gets injected into the gas generator decomposes exothermically and maintains the condition for steady operation. Alternately, one could derive a part of the fluids that are delivered by the pumps and introduce them into the gas generator for ignition and combustion leading to steady operation.

A second strategy is to allow the fluids to flow under the pressure of the storage vessel (maintained at 3 – 6 atm in the tanks) rotate the pumps as they flow into the combustion chamber. Subsequently a control system will keep metering amounts of fuel and oxidizer from the outlet of the pumps into a gas generator, the gases from which keep feeding power through the turbine into the pumps. In large thrust engines, this operation usually takes 2 – 4 s till the steady full thrust is achieved.

Liquid engine combustors and nozzles experience high temperatures and high flow rates and added to this, the high pressures of the combustion chamber contribute to high heat fluxes. The walls of the thrust chamber are therefore to be thermally protected. There are several techniques for keeping the walls of the thrust chamber relatively cool. By design, the mixture ratio near the outer periphery is arranged somewhat fuel rich so that temperatures are lower. In addition, fuel jets may be directed towards the wall to allow vaporization processes to occur to keep the wall zone cool. In some designs, one might have an ablative layer. In others, the outer portions of the nozzle may be coated with ceramic. In most high thrust engines one adopts what is known as regenerative cooling. In this technique, the fuel or the oxidizer with better cooling capacity is passed around the chamber at relatively high velocities with heat transfer occurring across thin walls. The liquid extracts the heat and later enters the combustion chamber. This technique is used in very long duration and high thrust engines and provides excellent performance.

Typical single chamber thrusts can go up 6.8 MN as in the case of F 1 engine used on the Apollo mission to moon. In the case of high pressure engines the

Table 1.11: Liquid Rocket Engines; * = kN s/kg, NTO = Nitrogen tetra oxide, N_2O_4; Hydzine = Hydrazine, N_2H_4, ETR = Exit-to-throat area ratio = A_e/A_t; Marqdt = Marquardt, Sustnr = Sustainer, Y = Yes

Engine	Vehicle Country	Thrust kN	Propellants	I_{sp} *	p_c atm.	Wt. kg	ETR	O/F	Pump fed?
HM7	Ariane	70.1	LOX/LH_2	4.25	35.0	145	48	5.1	Y
Marqdt R40A	Control USA	3.87	NTO -MMH	2.86	10.5	6.3	20	1.6	Pr.fed
RL 10	USA	66.7	LOX/LH_2	4.44	28.0		57	5.0	Y
Lunar Descent	USA Apollo	159	NTO -Aerozine	3.36	9.0				Pr.fed
J 2	Apollo	1045.0	LOX/LH_2		55.0	1578	27	5.0	Y
F 1	Apollo	6860.0	LOX/RP1	2.61	76.3	8353	16	2.3	Y
LM25R2	SLV-3 India	0.25	Hydzine	2.10	15.0	2.9	20		Pr.fed
LB250A	SLV-3 India	2.5	IRFNA -Hydzine	2.90	10.0	15.0	14	1.5	Pr.fed
LB600 E	PSLV India	6.0	NTO -MMH	2.70	10.0	15.0	8	1.6	Pr.fed
Sustnr	India	30.0	IRFNA -UDMH	2.13	53.0	45	9	3.3	Y
Vikas	PSLV India	735.0	NTO -UDMH	2.95	54.0	775	31	1.9	Y

chamber pressure goes up to 200 atm. like in the case of Space Shuttle Main Engine (SSME). The burn times of the booster rockets go up to 120 – 160 s. In special cases, they can be extended up to several minutes mostly limited by the volume of the propellants in the tankage. Table 1.11 summarizes details of some of the liquid rocket engines of the world.

1.15 Hybrid Rocket Engines

Hybrid rocket engines are those which use liquid oxidizer and a solid fuel. The other possibility namely, solid oxidizer and liquid fuel is not common because the solid oxidizer, usually is a crystalline powder and cannot be produced in a mechanically acceptable form. The liquid oxidizers used are nitric acid in the white fuming or red fuming variety, nitrogen tetroxide, hydrogen peroxide or liquid oxygen. The solid fuels which are hypergolic with nitric acid or nitrogen tetroxide are

not easy to make and not well known. Even so, solid fuels based on acetone and furfural as well as Aniline and formaldehyde hypergolic with RFNA have been developed. Liquid oxygen with polymeric fuels have been used to develop semi-cryogenic hybrid rocket engines. Figure 1.20 shows the typical elements. The liquid oxidizer is atomized and sprayed over the fuel block. In hypergolic systems, some condensed phase reactions take place and in non-hypergolic systems, only gas phase reactions occur. The oxidizer content of the hot product gases decreases along the port and the length of the grain. Two of the issues in this combustion process are (i) mixing of the oxidizer rich and fuel rich gases across the diffusion flame occurs much later than the length of the fuel grain and (ii) fuel regression rate is small. The first issue is resolved by adding mixing devices and the second issue is solved by adding a certain amount of oxidizer into the fuel. Hybrid rocket engines retain the advantage of controllability like liquid rockets because of the fluid line and are simpler compared to liquid rockets because of a single fluid line. Specific impulse comparable to liquid and solid rocket engines have been achieved. While most of the current developments have been devoted to sounding rockets, ideas about their benefits for launch vehicle applications keep appearing in literature. Table 1.12 shows the hybrid rocket engines built in various countries. The development of hybrid rocket engines has not attracted the attention of major propulsion system designers essentially because both solid and liquid rockets were in an advanced stage of development by the time the combustion behavior in hybrid rocket engines that affects the performance was understood. The higher safety of the hybrid rocket engine in comparison to solid or liquid rocket engine is due to the fact that the fuel is solid and the oxidiser that is held separated from the fuel. The most powerful oxidizer, liquid oxygen that may be contemplated for use due to performance benefits is handled in many commonly known industrial uses and hence, is understood much better for safe handling. The added safety is an attraction for use of hybrid rockets in situations calling for safety similar to civil aircraft operations. There may be possibilities for their use in single stage-to-orbit vehicles providing low cost access to space.

1.16 Hybrid Engines

These engines are those obtained as a combination of air-breathing and non-air breathing engines. For military applications, one uses rockets to obtain a quick boost. Then for sustaining the flight within the atmosphere, one uses air-breathing engine. One can use a ramjet or a turbojet depending on the application. Use of ramjets and rockets separately is not uncommon (like in Blood Hound missile of United Kingdom). Use of turbojets for cruise missiles which fly long distances (1000–1500 km) at tree top heights carrying nuclear warheads is another common feature (like Tomohawk of USA).

Table 1.12: Hybrid Rocket Engines (SF/Ox = Solid fuel/Oxidizer, t_b = Burn time, L = Length, OD = Outer Diameter, a = TAGAFORM, b = Metatoulene diamine in 4 % Nylon, c = 30 % p-toludine + 70 % p - Aminophenol, d = 10 – 20 % AP in polyester, e = Polydutadiene + PMMA, f = Li + LiH + Polyethylene)

Engine	Country	Thrust kN	SF/Ox	Dimensions L x OD (m)	t_b sec
HR -4	Sweden	0.34	a/RFNA	1.05 x 0.1	6 – 10
SR-1	Sweden	14.4	a/RFNA	3.15 x 0.25	20
–	France	10.8	b/RFNA	0.95 x 0.16	6 - 24
Sounding rocket	Germany	0.39	c/HNO_3	–	18
Demo. of R-D motor	Israel	2.25	d/RFNA	–	
Target drone	USA	–	e/RFNA	3.4 x 0.33	–
Upper stage	USA	53.3	f/FLOX	3.7 x 1.20	–

Ducted rockets, Ejector rocket-ramjets and Integral ram rockets are concepts considered for use in missiles. Figure 1.21 shows the schematic of ducted rockets and integral ram rockets. In the case of ducted rockets, usually, the fuel rich exhaust of solid rocket passes through a convergent–divergent nozzle at high speed. By a suitable arrangement of geometry and pressures, the exhausting hot gases are made to entrain atmospheric air. The fuel rich gases react with air and the higher temperature product stream exhausts out of a nozzle located subsequently. While at start-up and low velocity conditions, there will be drag due to ejector action, however, there will be enhancement of the specific impulse from the ejector action after a certain flight condition. In ejector-rocket-ramjets, the first portion of the flight involves the ejector and rocket. After the attainment of sufficiently high speed (say, M = 2+), the ramjet mode of operation can sustain the flight.

Integral ram rockets are a further variant of the above concepts. They use a solid rocket to boost the vehicle. At the burnout of the solid propellant, the nozzle corresponding to the rocket is ejected. The blockage at the exit of the air inlets and inlet to the combustion chamber will break open and simultaneously the hot fuel rich gases from a primary rocket motor come into the combustion chamber. Unlike ducted rocket, no ejector action takes place, but the air from the air inlet and the hot fuel rich gases get mixed in the dump region. The reaction between the two raises the temperature of the mixture as well as the pressure and the gases exit from a convergent–divergent nozzle meant for the purpose.

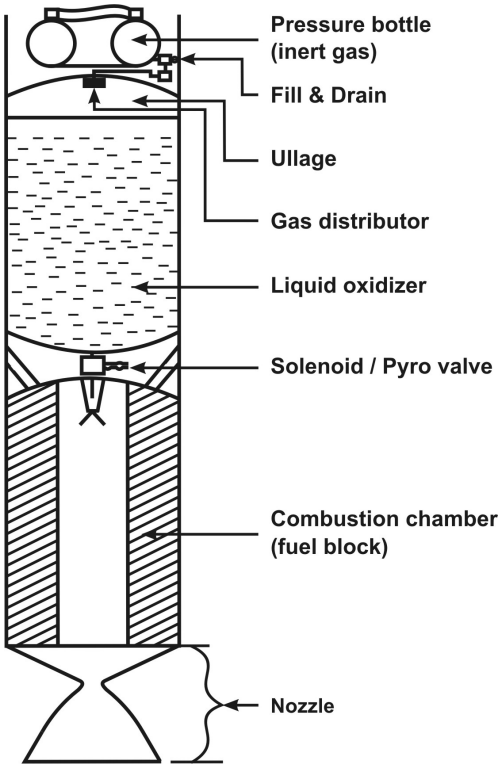

Figure 1.20: Schematic of Hybrid rocket with a solid fuel and a liquid oxidizer

One can conceive the use of liquid fuels or solid fuel rich propellant for the ramjet phase. Figure 1.22 shows the sizes of different vehicles to achieve a fixed mission (drawn from the interesting work of Marguet et al, [55]). For relatively short duration missions ($\sim$ 50 s or less), the vehicle performance will be affected by the volume required to store the propellant. The specific impulse of liquid propellants will be higher ($\sim$ 10 kN s/kg) and the density lower (like kerosene will be about 800 kg/m^3) compared to those of fuel rich solid propellant based ramjets with values of I_{sp} = 6 kN s/kg and a density of 1700 kg/m^3. In terms of comparison of weights of the systems at launch, the ratio of fully solid propellant : rocket-liquid ramjet : rocket-solid fuel ramjet systems is 1 : 0.6 : 0.5 for the operational duration of 50 s or less.

Air–Turbo rockets are hybrid engines which have been built for demonstration in smaller sizes but have not been used or deployed. A monopropellant rocket engine operating at relatively high pressures exhausts the gases through a turbine. The power of the turbine drives a compressor which delivers required amount of air for combustion with the products of decomposition of the monopropellant. The resulting products exhaust through a nozzle. The advantage of air–turbo rocket in

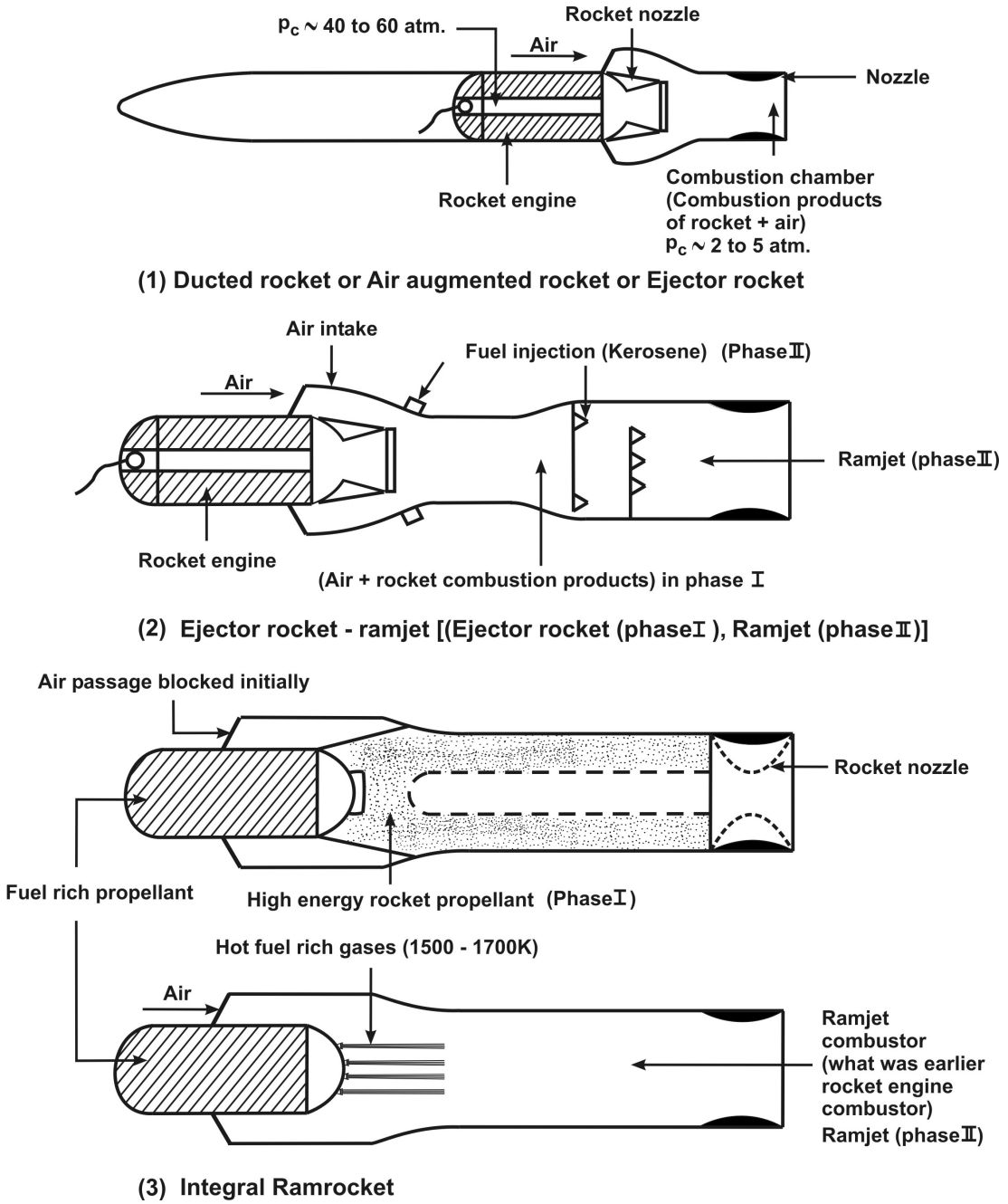

Figure 1.21: Schematic of ducted rocket, ejector rocket-ramjet and integral ram rocket

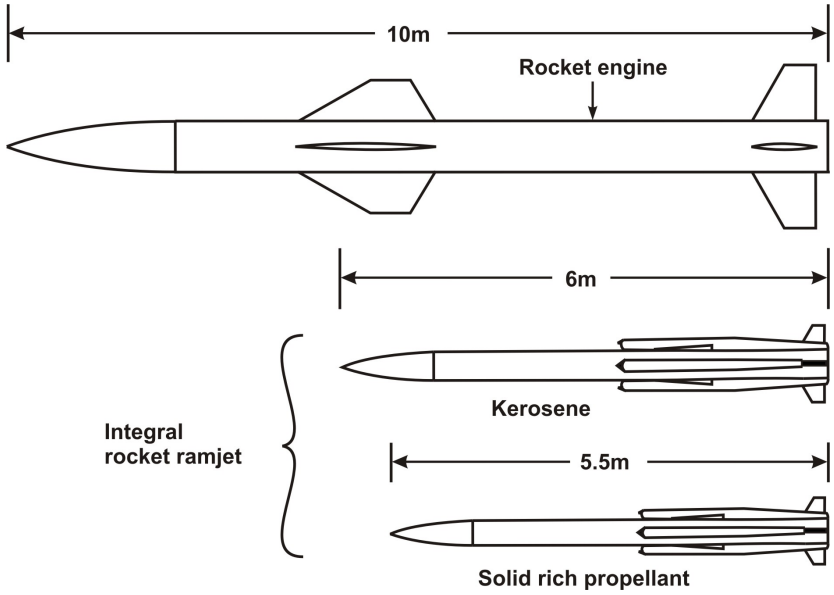

Figure 1.22: Options for a missile to achieve a mission drawn from ref. [55]

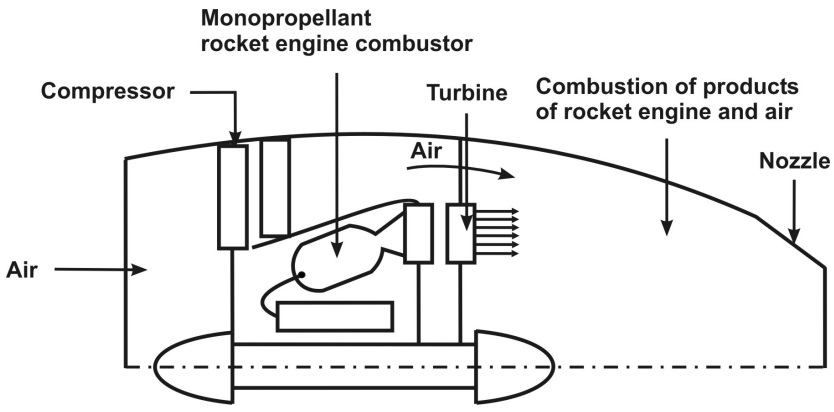

Figure 1.23: The schematic of an air-turbo rocket; Hydrazine could be a typical fuel whose decomposition and passage through a nozzle producing high velocity stream drives the turbine. The decomposition products burn with the compressed air downstream and generate thrust after passing through a nozzle.

comparison to a normal turbojet is that one can make the system a little more compact by using high pressure monopropellant engine for obtaining large expansion work. Figure 1.23 shows these schematically.

1.17 Summary

In this chapter, the various propulsive devices in current existence have been described. Their evolution, from devices first built – namely propeller driven devices has been brought out. Piston engine-propeller systems were the first set of propulsion systems built and they met the needs of flying at low altitudes at speeds less than about 400 km/hr. The requirement to fly at higher speeds and altitudes has been fulfilled by turbojets. The speeds of M = 3 and altitudes of 20 km can be reached by using turbojets. Fuel efficiency for low subsonic transport compelled the adoption of the more compact tuboprops (compared to piston engines). Achieving speeds as high as possible under subsonic conditions, typically M = 0.85 has been met with by the development of turbofans. Obtaining higher fuel efficiency in turbofans has driven the design to the choice of bypass ratios as high as 9 for civil transport. Turbofans with small bypass ratios (less than 1) have been developed to combine the need for compactness with higher thrust augmentation. Flying for short durations at speeds of M = 2 – 3 has resulted in the development of ramjets (for missiles). Flying at higher speeds (M $>$ 6) has resulted in the quest for propulsion systems where the combustion process has to be handled under supersonic conditions because deceleration to subsonic conditions prevents additional heat being put in from the fuel and no net thrust can be generated. This technology is currently under development even though research and development has continued for over forty years. The key point is that the process is highly sensitive to geometry and flow conditions. Flying within the atmosphere for short durations with high accelerations as demanded from military defense systems calls for the use of rocket engines. Those of such systems designed for tactical operations (like anti-tank missile, air-to-air and surface-to-air missiles of short range – up to 50 km, say) demand that the principal propulsion system be as compact as possible. These are fulfilled by the option of solid rockets better. Control demands are taken care of by aerodynamic means where ever possible. If these are inadequate, one needs to use liquid propellant based control thrusters.

Flying outside the atmosphere (> 30 km, say) calls for the use of rocket engines for all vehicles. Space vehicles depend only on rocket engines that need to carry their own fuel and oxidizer. Solid rocket motors are largely used for single burn applications. Solid propellants have very high density and reasonable specific impulse. Liquid propulsion systems have a range of specific impulse from about 60 % to 180 %, but much lower density – from 60 % to as low as 20 % compared to solid propulsion systems. Hence, the choice between solid rockets and liquid

rockets needs additional features to be considered. Liquid rocket engines are capable of restart, variable thrust (that can be decided during the flight) and pulsing, features that are beyond the realm of solid rockets. Different class of liquid propellants and systems are used for these applications. Monopropellant systems are used in satellites for station keeping and related operations using some times, the pulse mode of firing the thrusters. Getting a satellite from transfer orbit to the designated orbit (that is typically a geo-synchronous orbit) is usually performed by a bipropellant liquid rocket engine that allows multiple burns and adopts hypergolic storable combinations. Booster propulsion is performed by solid rockets as well as liquid rockets and the choice is many times on the consideration of costs. Semi-cryogenic liquid propellants are perhaps the cheapest of the propellant combinations and provide specific impulse comparable to solid rockets but lower density impulse. Since the density impulse is not an important criterion for the choice of propellants for large boosters (though it is an important criterion for tactical propulsion systems), semi-cryo systems are very good candidates for booster propulsion systems. Satellite launch vehicles are sized for a predesignated trajectory to the orbit; control is exercised by using flexible nozzles with solid rockets and with thrust chamber gimballing with liquid rockets. Finer attitude control is also possible by mounting liquid bipropellant thrusters on the vehicle and operating them depending on the need. Thrust modulation as a part of launch sequence is not demanded. Obtaining high specific impulse even at the cost of low density is usually required of upper stages and this is met with by the use of full cryogenic propulsion system. Strategic missile propulsion needs thrust termination scheme to be available to enable a single missile capable of being used on targets with different ranges.

The variety of propulsion systems built over the last hundred years (with a majority in the last fifty years) has met most of the needs. The familiarity with the various kinds of engines in this chapter provides the back drop for further analysis and discussion of the performance of the engines. Many parts of the subject covered in this chapter are found in many text books on propulsion [34, 4, 10, 11, 7, 31, 12, 16, 25, 14]. The proceedings of ISABE (International Society of Air Breathing Engines) conference are another source of scientific and technological material for study. The books by Janes All the World Aircraft provides rich source of data and insight when one reads them carefully. A set of papers published in the November – December 2003 issue of Journal of Propulsion and Power ([45]) provides a broad summary of the technological developments in aerospace propulsion.

Chapter 2

The Needs, Specifications and Performance Parameters

2.1 Introduction

What do we need propulsion system for? The simplest answer in the context of aerospace propulsion would be "to fly". But then, which kind of flying?

In the early nineties, the objective was to first have sustained flight of heavier-than-air craft. This called for engines with power to weight ratio being as large as possible (typically, 2). When this was achieved and as time progressed, the objectives became more extended and constraints, more severe. The propulsive devices began to be used for several requirements. And depending on the requirements, the specifications became different in details and so the "propulsive devices" became different "species". Today, there are just so many varieties, the question of what kind of engine will be appropriate for meeting a specific requirement becomes very important and relevant.

Let us first see what requirements are needed to be met with by the propulsion system.

2.2 The Needs of Airborne Vehicles

The various modes of utilization of aircrafts and rotorcrafts are shown in Tables 2.1 and 2.2. These tables show the characteristics of civilian aircrafts and military aircrafts separately. The first four rows in Table 2.1 refer to transportation of passengers or freight. In most cases, the maximum speed possible and expected from the aircraft, is usually limited to a value close to drag rise Mach

Table 2.1: Civilian Applications–Features with Impact on Engines (P + B = Passengers + Baggage, Tns = tonnes, LOp. cost = Low operational cost, d. = desirable, n.i = not important, i = important, n.v.i = not very important, v. i = very important, v.v.i = very very important)

Application	Range km	Payload	Speed M	Fuel used	LOp. cost?	Low Noise
Executive Trans.	2000	10 P + B	$<$0.7	n.v.i.	d.	i.
Frieght/Cargo Trans.	$\sim$6000	10–500 Tns	0.85	i	i.	n.i
Short haul passenger Trans.	$\sim$2000	50–200 P + B	0.75	v.i.	i	v.i
Medium/Long Range Pass. Trans.	$\sim$6000	250–600 P + B	0.85	v.v.i	i	v.i
Agricultural & other applns.	$\sim$400	$\sim$20 P + B or payload	$<$ 0.4	i	n.i	n.i
Supersonic Trans.	$\sim$6000	$\sim$100 P + B	2+	v.v.i	i	v.v.i
Helicopters (VTOL)	$\sim$200	$\sim$20 P + B	0.4	i	i	n.v.i

number or critical Mach number (both these refer to increase in drag due to compressibility effects that appear around M = 1), because the penalties in terms of drag will rise very steeply beyond this speed. Since the dynamic pressure ($\rho\, V^2/2$) decreases with increase in altitude ($\sim$ p M^2) one would like to fly as high as possible in order that the drag force is kept lower, so much so the fuel consumption decreases. In the case of piston engines this altitude is typically 5 – 6 km. In the case of turbofans/turbojets it is typically 10 – 11 km. Beyond these altitudes there will be no benefits in flying higher (because temperature does not decrease further but pressure decreases) and so, most civilian aircraft based on turbofans operate in this altitude range and with speeds close to M = 0.85, which is the maximum drag rise Mach number that one can design for.

In respect of agricultural aircraft, piston engine-propeller combination is almost universally used because the speeds and altitudes are low and fuel consumption can be kept low by using these engines.

Supersonic transport has been attempted successfully by only two countries – (France + UK) and USSR. The project by the USA has been shelved. The Anglo–French Concorde uses Olympus engine which is essentially a turbojet. The aircraft Tupolev Tu-144 uses Kuznetsov NK-144 low bypass turbofan with an afterburner. The common feature of these engines is that both run with the afterburner at 17 – 35 % of the maximum additional thrust throughout the flight which occurs at M $\sim$ 2.0 and 2.3 at altitudes of 15 – 18 km. The commercial operations of Concorde

Table 2.2: Military Applications–Features with Impact on Engines (nominal range a few hundred km; nom. = nominal; nominal speed high subsonic; Low altitude 100 m; High altitude 25 km; Multiple role aircraft = combinations of 1 to 6 ; * = attack on non-strategic targets deep in the enemy hold.)

	Combat role	Range	Speed	Altitude	Payload
1.	Air superiority fighter	nom.	high	high	nom.
2.	Interceptor	nom.	v.high	high	nom.
3.	Close Air support	high	nom.	low	low
4.	Deep penetration Strike	v.high	nom.	low	v.high
5.	Interdictor*	high	nom.	low	v.high
6.	Bomber	v.high	nom.	high	v.high
7.	Reconnaissance (ECM)	v.high	nom. - high	low - high	nom.
8.	Cruise missile	v.high	nom.	v.low	nom.

have been closed in early 2004.

Most of the aircraft engines do need a statement of the noise level during take off and landing. The ICAO standards call for noise levels not exceeding certain values. These came up essentially to minimize the noise pollution to communities located in close proximity of airports. There are also specifications on the pollutant concentrations in the exhaust of the engines. These refer to CO, NO_x and HC (unburnt hydrocarbons). The engine development in the last ten years has been significantly affected by these specifications on the environmental pollution.

For all vertical take-off applications, helicopters serve the purpose very well (excepting certain military applications for which one builds V/STOL aircraft). Most present day helicopters utilize turbo–shaft engines. Even for helicopters, there are specifications on the noise level. The specifications on the chemical emissions are covered by those on engines.

The development of engines has, like other systems (avionics, for instance) had the benefit of military applications. There are a wide variety of applications, most of them being listed and characterized in the Table 2.2. While fighters and bombers were some what 'classical' in the development scenario, several new roles like DPSA (Deep Penetration Strike Aircraft), CAS (Close Air Support) have been added in the last twenty years. In the second world war (1939–1945) superiority of one fighting unit over the other was characterized by speed. It was during this period that high subsonic speeds were being attempted. Once the sound barrier was crossed several military aircrafts going up to M = 2 were built. The succeeding wars fought in other theaters of the world with the weaponry of a few nations showed that the development of missiles and electronic detection systems called for changes in the desired characteristics of military aircraft. In order to prevent

detection, low flying tactics became more used. This led to the development of DPSA.

The combat scene showed that combat invariably occurred at low Mach numbers (0.5 – 0.8) and get away called for supersonic dash. Thus, the aircraft needed to spend in low or high subsonic speeds most of the time with relatively short durations of supersonic speeds. This did affect the engine system features. For instance, the intake would be of pitot type without any variable geometry features unlike those for supersonic speeds. The engine itself could be a low bypass fan or a turbojet. The low bypass fan with a mixed exhaust with after burning capability is used to get greater thrust ratio and a relatively low thrust for subsonic flight. Many of the military aircraft built in recent times do use turbofans with low bypass ratio (Adour, Allison RRTF-41, Kuznetsov NK-8-4).

The aircrafts for reconnaissance usually do not need unusual features. Those flying at altitudes below 10 km can work with turboprops. Those which work at very high altitudes like 20 km and above invariably use turbojets.

Remotely Piloted Vehicles (RPV's) or unmanned aerial vehicles (UAV's) have evolved tremendously over the last twenty years. Those for battle field reconnaissance or harassment use piston engine-propeller systems. Those meant for strike purposes could use modification of existing aircraft. Most of these have advanced avionics of various kinds. The propulsion systems vary from piston engine-propeller systems to turbojets. The various engine types along with the examples are presented for both civil and military aircraft in Table 2.3.

While Table 2.3 shows the classification around aircraft/rotorcraft and the kinds of engines that can be used in such applications, the engines that have been used in various classes of aircraft/rotorcraft are presented in Table 2.4. It covers a wide range of applications for which aircraft engines have been deployed in different countries.

2.3 The Specifications

The specifications are evolved out of the needs stated. Some of the specifications, of course, are not related to needs but to complete the technical description of the various elements. A typical specification for CF6-50M turbofan (used on AIRBUS-A-300 flying in Indian skies) would read as below (see Table 2.5).

The thrust to weight ratio is seen to be about 10. The bypass ratio is 4.4, a relatively large value consistent with the observed low sfc of 0.65 kg/kgh compared to classical turbojet value of 0.9–1 kg/kgh.

Table 2.3: Aircraft Engine Types

Application	Engine	Example	Comments
Business Aircraft	a. Piston Engine -Prop	Cessna 180 Beechcraft Bonanza (USA)	Most applications covered by (a) & (b), some may need (c). Some use Turbofans also for long range executive transport, to reduce sfc.
	b. Turboprop	Beechcraft King C-90 (USA)	
	c. Turbojet	GE CJ610 (USA)	
Freight/ cargo Transport	a. Turboprop	AN–24, (USSR)	
	b. Turbofan	C–5, USA	
Short haul Passenger Transport	a. Turboprop	HS748 (India)	Though Turbofans are the most used engines, future aircraft may have advanced turboprops
	b. Turbo fan	Boeing737 (USA)	
Medium/ long range Transport	a. Turbo fan	Airbus A300 - A340	Most transports use Turbo fans. Only some use Turboprops
	b. Turboprop	Illyushin II - 18 D (USSR)	
Agricultural and others	Piston Engine-Prop	HPT 32 (India)	
VTOL	Helicopters	Altoutte -	

2.4 Life of Components

While user expectations are that the engine components must function without replacement for as long as is possible, the statement on the life of components is not a specification given by the user, but a statement of performance given by the manufacturer. Once engines of certain life cycles of components are available, the future ones will inevitably have to better these. In this sense, these values become specifications. In the early development of the engines, the life was indicated for the entire engine. The engine after this period was discarded from active use. It became clear that life of the engine was governed by that of a specific component like turbine blades. The ordering of the components in terms of life would then be the turbine blades, the combustor and the compressor. With the understanding that the life of different components can be different and replacing the most critical of them alone is sufficient to prolong the life of the total system without any compromise on the performance, the concept of modularity of engine got introduced. Apart from the extension of life through the use of the concept of modularity, the life of the engine has been enhanced by improved mechanical design of the compo-

Table 2.4: Engines and aircrafts using them with the country and the engine type (C = Civil Transport, M = Military, T = Training, BJ = Business Jet, MR = Multiple role, MT = Military Transport,HT = Heavy Transport, RPV = Remotely piloted Vehicle, AB = After Burner, 1S = Single shaft, 2S = Two-shaft, TJ = Turbojet, TS = Turboshaft, TP = Turboprop, TF = Turbofan, Fr = free turbine, TVC = Thrust Vector Control

Name	Aircraft/Rotorcraft	Country	Engine type
Lucas CT-3201	RPV	UK	TJ, 1S
TRS-18-046	RPV	France	TJ, 1S
TRI-60	RPV	France	TJ, 1S
RR Viper 601	M, Civil, Training	UK	TJ, 1S
P&W JT-15D	M. Cessna	Canada	TF, 2S
J3-IHI-7C	M, F 4 (USA)	Japan	TJ, 1S
GE J85-21	M, F 5E	USA	TJ, 1S, AB
GE J79-7A	M, F 106, F4	USA	TJ, 1S, AB
SNECMA-M53	M, Mirage 2000	France	TF, 1S, AB
RB199 - 34R-2	M (MR), Tornedo	UK, FRG, Italy	TF, 3S, AB
Adour Mk. 102	M (Tact.), Jaguar	UK, France	TF, 2S, AB
Pegasus 11	V/STOL, Sea Harrier	UK	TF, 2S, TVC
P&W F 100	M, F15, F16	USA	TF, 2S, AB
F 404 (GE)	M, F18, LCA (India)	USA	TF, 1S, AB
Allison 250-C-20B	Heavy Transport	USA	TS, 1S, Fr
Ivchenko AI-24	Heavy Transport,	USSR	TP, 1S
Astazou XIV	Helicopters	France	TS, 1S
Lycoming LTC1-L13	Bell Helicopter	USA	TS, 1S, Fr
Lycoming LTCAR - 1	Chinook Helicopter	USA	TS, 1S, Fr
Garret TFE.731-3	Business Jet	USA	TF, 2S
Garret ATF3-6	Business Jet	USA	TF, 3S
Turbo meca Baston	C	France	TP, 1S
RR Dart	C	UK	TP, 1S
Olympus 593	C, Concorde	UK, France	TJ, 2S, AB
Soloviev D-20P	C, Tu 124	USSR	TF, 2S
P&W JT 8D	C, B 727, B 737	USA	TF, 2S
P&W JT 9D	C, B 747, A 300	USA	TF, 2S
CFM 56	C, B 737, A 340	USA, France	TF, 2S
Soleviev D-30kU	C, Tu 154, I l62	USSR	TF, 2S
GE CF6-50M	C, B 747, A 300	USA	TF, 2S
RB-211; 524B	C, B 747, A 300	UK	TF, 3S
GE 90-B4	C, B 777	USA	TF, 2S

Table 2.5: Specifications of CF6–50M turbofan, TET = Turbine Exit Temperature

Take-of Thrust (flat rated to 25° C), kN	247
Bypass ratio	4.4
Fan tip diameter, m	2.2
Max. Width cold, m	2.39
Max height, m	2.675
Length, m	4.64
sfc at take off, kg/kgfh (mg/Ns)	0.381 (10.8)
or Take-off I_{sp}, kN s/ kg	92
Weight : dry basic engine, kg	4983
, With fan & turbine reverser, kg	5067
Acceleration time, s	6.0
TET margin, ° C	60

Table 2.6: Life of components of CF - 6 engine (H.P = High pressure)

Part	Hrs	Cycles
Fan rotor		25,000
H.P Compressor rotor		39,000
Combustor	4000	8,000
H.P Turbine static parts		12,000
H.P.Turbine blades		8,000

nents to nearly twice to thrice as much as in the fifties. Typical values for the life of the components of a CF6 class of engine is shown in Table 2.6.

2.5 Noise Pollution

The noise generating elements in an aircraft are: from the body of the aircraft caused by the pressure fluctuations in the turbulent boundary layer and from the engine with the contributions from the rotating parts that virtually chop the flow of the fluid between the rotor and the stator and from the exhaust jet. Attempts are made to absorb the noise through acoustic liners that can dampen several acoustic frequencies. For instance, the use of a perforated sheet causes sympathetic compression of the fluid in the perforations by the acoustic fluctuations that leads to absorption of the energy. The standards of noise level are set for take-off, overflying and landing. A side line acoustic level is also specified to account for the fact that habitation is located on both sides of the airstrip, many a time. The limits

are a function of the weight of the aircraft and the number of engines. The actual magnitude varies between 95 to 110 dB. Typical values are 90 dB for take-off, 101 dB for approach, and 95 dB for the side line (along the sides of the airstrip).

2.6 Exhaust Chemical Pollution

Amongst the chemical pollutants, carbon monoxide and unburnt hydrocarbons are significant at low power that occurs at ground idling conditions and the oxides of nitrogen, a mixture of NO and NO_2, denoted by NO_x is significant at high power of the combustor that occurs at take-off and cruise conditions. The presence of these chemical pollutants causes the production of smog and toxicity in the environment. NO_x is considered particularly harmful for acid rain and reduction of ozone layer in the upper atmosphere. Meeting these requirements calls for conflicting approaches. Increased flame temperature helps reducing CO, but increases NO_x. Hence, the temperature corridor that must be traversed in the design of the combustor is very small. The reduction of the pollutants is effected through the design changes in combustor. Meeting these specifications with the fuel with increasing carbon content as is happening world over in recent times, has led to more new designs of the combustor. Typical standards for the pollutant emissions are assessed as a mass per unit thrust measured over an ICAO (International Civil Aviation Organization) flight cycle consisting of take-off at 100 % thrust for 0.7 minutes, climb at 85 % thrust for 2.2 minutes, approach at 30 % thrust for 4 minutes, and ground idle at 7 % thrust for 26 minutes. The values are 120 g/kN thrust for CO and unburnt hydrocarbons and (40 + 2 $\times$ compressor pressure ratio) for NO_x. For a modern engine with a compressor pressure ratio of 30, this translates to a limit of 100 g/kN for NO_x.

2.7 Performance Parameters and Their Importance

The performance parameters are essentially evolved out of the need to meet the specifications. Typically, the specific fuel consumption, thrust per unit front cross section, thrust to weight (dry) ratio at sea level static conditions or cruise are the important specifications as well as performance parameters. The features along with cycle analysis form a part of any computer aided design for an aircraft currently planned based on the engine or to evolve a better aircraft with improved characteristics desired from the engine. This two way interaction is the basis of the continuous progress achieved in the field of engine development.

The importance of the specific fuel consumption (sfc), can be recognized from the statement "In the case of medium range air-plane a 14% increase in the engine price or a 16% increase in maintenance cost can be offset by a 1% reduction in

fuel consumption when fuel costs US$ 1.5 per gallon " ($\sim$ 5 Rs./liter as per 1990 currency conversion rates)" [49]. Further, the same paper illustrates that a 1% reduction in sfc reduces the direct operation cost (DOC) by at least 0.3%. This amount can be substantial for large fleet operations.

The thrust to weight ratio of the engine has a significant influence on the total weight of the aircraft. Typical values of F/W have increased from about 30 N/kg in the early fifties to about 70 N/kg in recent times. They are expected to go up to 85 N/kg. In the case of short haul civil aircraft as well as combat aircraft, the rise of F/W from 40 to 80 decreases the DOC by 0.15 %.

For military aircraft, the sfc is a sufficiently important, but not overriding parameter. The time of acceleration from one speed to another is an important feature. Typical times to accelerate from M = 0.8 to 1.6 is about 80 s. With the reduced weight of the rotational inertia of compressor-turbine systems of modern engines (of high thrust-to-weight ratio), the acceleration times are expected to be reduced to as much as 50 s with no other loss in performance.

The first cost of aircraft and of operation of an aircraft are known to be important for civil aircraft; but thought to be secondary for military aircraft. This is not indeed so in recent times. The cost factor is introduced into the design right at inception and it produces quite often total systems at substantially low cost. One of the recent examples is F16. Its cost is about one third of an aircraft of comparable capabilities developed in the USA or other countries.

2.8 The Needs of Space and Military Systems

Table 2.7 shows a dozen applications of non-air breathing engine systems. We shall briefly discuss the various applications and their relevance to the choice of the propulsion systems. The Rocket Assisted Take Off (RATO) is used in aircraft to obtain smaller take off runs on short runways or runways at high altitudes or high ambient temperatures or both. Generally solid rocket is preferred for RATO as it is a relatively small system and the total aircraft weight will be smaller with a solid rocket.

Sounding rockets are used to obtain information on atmospheric characteristics like temperature, pressure, concentration of specific species, magnetic and other characteristics. They are used for altitudes up to 200 km; most use is limited to an altitude of 20-25 km. These carry the payload of instrumentation. They can be sent up with rockets of one or two stages. The first stage usually is a solid rocket burning for relatively small duration like 5 – 6 s. The second stage is a long burning, relatively low thrust system. It can be based on solids or liquids. In the last ten years or so, hybrid rocket engines have been built to meet the requirements, specially of sustainer or second stage. The advantage is that it is

Table 2.7: Rocket Engine Propelled Vehicles (CS = Composite Solid, DBS = Double base solid propellant, SFRJ = Solid fuel ramjet, PAM = Perigee-Apogee Module, AKM = Apogee Kick Module, L = Liquid, NTO = Nitrogen Tetroxide, IRFNA-UDMH = Inhibited Red fuming nitric acid and unsymmetrical dimethyl hydrazine, TEA Triethylamine, Xy = Xylidine)

System and Vehicle	No. Stages and Propellants
Sounding rocket (India) RH 125	1 CS
Sounding rocket (India) RH 560	2 CS + CS
Rocket assisted Takeoff (USA),	1 CS
Air-Air M (USA), AIM 5c Phoenix	1 CS
Air-Air missile (USA), AGM 65	1 DBS
Air-Air missile (France), Matra	1 DBS
Surface-air missile (USSR), SAM2	2 DBS + L (IRFNA + TEA/Xy)
Surface-air missile (USSR), SA6	IRR with SFRJ
Air-Surface missile (UK), Sea Cat	2 DBS + DBS
Surface-surface missile (UK), Vigilant	1 DBS
Tactical missile (USA), LANCE	1 L (IRFNA-UDMH)
Strategic SS IRBM (USA), Thor	3 [1, L (LOX–Kerosene) + 2,3 (IRFNA–UDMH)]
Strategic SS ICBM (USA), Polaris	2 CS + CS
Satellite launch vehicle (India), SLV3	4 (all CS motors)
Polar Satellite Launch Vehicle, PSLV (India)	4 [1CS +(4 CS strap-ons) + 2L + 3CS + 4L] [2L - NTO–UDMH, 4LS-NTO–MMH]
PAM for INSAT (India)	L (N_2O_4–MMH)
AKM for APPLE Satellite (India)	CS of stage IV of SLV 3

less complex compared to liquids and yet retains the flexibility of controllability of thrust.

Air–to–air missiles are generally small in size compared to other kinds of missiles. This is because the missiles already have an initial velocity given by the aircraft on which they are carried. They are generally based on solid rockets because of the volume limitedness of the application. This is because solid propellants have higher density and the propulsion system based on them have higher mass ratio compared to liquids (rather, you can pack more propellant mass in the same volume).

Surface–to–air missiles and surface-to-surface missiles of the smaller range use two stages usually. The first is called Boost and the second Sustain. Since gravity loss is reduced by traversing the distance in a small duration (ideally zero), most such missiles which anyway operate for short durations, do so with large initial acceleration. Once having reached a required speed, they will overcome the drag loss by the sustainer firing whose thrust is much smaller than of boost.

Typical sustain to boost thrust ratios will be 1:5 to 1:10. Typical burn times of the sustainer vary from 10-30 s for smaller systems and up to 100 s for larger systems.

IRBM (Intermediate Range Ballistic Missiles) and ICBM (Inter–Continental Ballistic Missiles) belong to the class of surface-to-surface missiles but of long range and partial ballistic nature of the trajectory. All that the propulsion system does is to deposit the payload (which is invariably nuclear) at a location in space with a velocity of the order of 3-5 km/s (correct to 0.01 % or better) so that the payload will take the ballistic trajectory from then on, go up as much as 400-600 km above earth, reenter the earth and reach the target with in 0.5 - 1 km of the target (CEP is Circular Error Probability of this distance) even though it is launched from a distance of 3000-6000 km from the target. The propulsion systems for IRBM / ICBM can be either solid or liquid. Because the systems are large, the restrictions associated with small ones do not apply. Many considerations like reliability, simplicity, and availability have played part in the choice of the systems. There are solid based systems like Polaris and Minuteman and liquid based systems like Atlas and Titan.

The launch vehicles for satellites are based on the stages that would have been developed for military applications. In many cases, both civilian and military applications have the same propulsion stages. While all the stages can either be solids or liquids, most high performance satellite launch vehicles use liquids for upper stages. The launch vehicles use the fully cryogenic (LOX/ LH_2) upper stage due to the very high specific impulse that can be achieved with this combination (for upper stages maximizing the specific impulse is the most important criterion as will be seen subsequently).

The Apogee Kick Module (AKM) and Perigee-Apogee Module (PAM) are the units which go along with satellites. The present day concept of satellite launching is that launch vehicles like Ariane (France) or Space Shuttle (USA) take a number of satellites and leave them in what is known as parking orbit which may be a circular orbit at an altitude of 150–300 km. From this orbit the propulsion system with the satellite is used to get to the geosynchronous orbit in stages. The satellite first gets into an orbit with apogee at 36000 km (the geosynchronous altitude) and perigee at 150-300 km. At a time when the satellite is at its apogee, it is given thrust so that the satellite circularizes at geo-synchronous altitude.

The choice of the propulsion system for this application is dependent on the mission. If the corrections to the flight path are required to be done over a period of time, liquid engine is preferred (like in INSAT series of satellites). If the trajectory is well defined with a need for a single burst of impulse, then the choice is for solids. Most of the liquid engines for this application use self–igniting storable propellant combinations.

Control rockets and orbital manoeuvring systems are low thrust systems operating largely in pulse mode. Typical values of thrust vary from 1 N to 2000 N, a large number of them in the 10-100 N range. They are used for correcting vehicle trajectory in launch vehicles or for performing station keeping operations in polar and geosynchronous satellites. Many thrusters are mounted on the satellites to give desired force in various directions as needed for correction. Though the launch vehicle control rocket needs to have a life of no more than a few hours or a few days, those meant for satellite station keeping need to have long life, as much as 5-7 years. This requirement calls for a careful design as well as selection of materials for long term compatibility with the propellants.

The integral ram rockets use a solid propellant for boost and either liquid or fuel rich solid for the ramjet. Those meant for cruise applications with range of 50-100 km can still benefit from ramjets. But with range exceeding this value, it is replaced with a turbojet; the rocket may or may not be used for boost, for, the vehicle can be air-launched to provide the initial boost.

Table 2.7 shows the engines used for various applications. As can be seen from the table, the air-to-air and air-to-surface missiles are of single stage and usually solids; The tactical surface-to-air as well as surface-to-surface missiles can be either of single or two stages, either of solids or liquids. The strategic missiles of IRBM/ICBM class are of two or three stages. There are missiles like ATLAS which are stated to be one and half stages. In this system, the propellant tanks are the same for booster as well as sustainer. The booster engines fall off at the end of the booster burn-out and the sustainer engine continues to fire for its additional duration of burn. Since this system of operation is different from the conventional operation of stages in which the complete hardware of different stages get completely separated, the ATLAS is designated to have one and a half stages. The engines which have been developed and qualified for military application are also used for space applications. As such, the engines for many launch vehicles like Atlas–Centaur, Thor–Delta are derived from the Atlas–ICBM, Thor–IRBM. The launch vehicles for earth satellites and polar satellites listed in the Table 2.7 are from the Indian space effort. While the SLV-3 launch vehicle is based entirely on solids, that for polar satellite launch application, two stages are liquids and the first stage Booster is solid motor with six SLV S-1 class strap- ons with canted nozzle. This design is similar to Thor Delta vehicle.

The AKM and PAM systems again are from the Indian context. The Indian built Apple communication satellite used the SLV-3 IV stage for the AKM. The orbital manoeuvring systems or launch vehicle control systems use monopropellant or bipropellant thrusters of thrust ranging from a few to a few kilo newtons.

The Integral ram rocket invariably uses a solid boost and liquid/solid sustainer which is a ramjet. Some vehicles like SA 6 use solid fuel ramjet. Others use liquid ramjet.

Table 2.8: Specifications of VIKAS Engine

Thrust, kN	735
Burn duration, s	180
Propellants, Ox & Fuel	N_2O_4 & UDMH
Mixture ratio	1.866 ($\pm$ 2 %)
Feed system	Turbo pump
Thrust chamber	Film cooled
Nozzle	Contour, 2-axes gimballing
Engine Envolope, Ht. and dia, m	3.5, 1.7
I_{sp}, kN s/kg	2.95 ± 0.02
Dry weight, kg	900
Thrust rise time to 90 % thrust, s	2.8
Thrust decay time (5 % thrust), s	4.0

2.9 Specifications

The specifications for a rocket engine are similar to those of air-breathing engines. A typical specification for a liquid rocket engine will read as shown in Table 2.8.

The specification for a Catalytic Hydrazine thruster meant for control applications is as in Table 2.9.

The two examples given above for liquid engines are typical of the specifications. While the primary specifications refer to thrust, propellants, burn time, specific impulse achieved, weight and volume required, the other features like transient times are important from the point of view of interfaces as well as operation. The specification on qualification requirements will affect the mechanical and thermal design to varying extents. There will be variations on the qualification requirements depending on the mission for which the engine is needed.

In the case of solid rocket engines, the specifications involve the items noted above. In so far as the propellant itself is concerned, it is characterized by its ballistic and mechanical properties. A typical specification of a solid propellant would read as in Table 2.10 and the mechanical properties as in Table 2.11.

2.10 Performance Parameters

The performance parameters are again, the ones imbedded in the specifications. There are some important performance parameters that dictate the choice of the propulsion system (solid/liquid/hybrid) as well as the propellants. These, in the

Table 2.9: Specifications of a Monopropellant Thruster

Thruster, N	1.5
Propellant	Hydrazine
Catalyst	Shell 405A
Chamber pressure, atm.	11.0
Thrust repeatability, N	$\pm$ 0.1
Steady state I_{sp}, kN s/kg	$>$ 2.1
I_{sp} degradation, %	$<$ 8
Minimum impulse bit, N.s	0.035
Impulse bit repeatability, %	$\pm$ 10
Rise time to 90 % thrust, ms	$<$ 50 (steady mode) $<$ 30 (pulse mode)
Decay to 10 % thrust	$<$ 100 (steady mode) $<$ 70 (pulse mode)
Roughness, %	$<\pm$ 15
Life, million hot pulses, time (s)	0.15, 10,000 (steady)
Space life	5 years
Vibration, Freq (Hz), Amp (mm)	10-25 Hz, 12.5 mm DA
sinusoidal	25-35 Hz, 15g 35-100 Hz, 20 g 100-200 Hz, 20 g
Random Vibration Freq, Sweep rate	20-2000 Hz, 2 octaves/min at 0.2 g/Hz for 2min/axis
Shock (as half sine wave)	100 g for 5 $\pm$ 0.1 ms
No. of shocks per axis	3
Steady g for 3 axes	$\pm$ 18 g/ min each axis

Table 2.10: Specification of a Solid propellant : PBAN–Al–AP

Ammonium Perchlorate, %	67.75
Aluminium, %	17.75
Total solids, %	85.5
PBAN + Curatives, %	14
Burn rate modifier (copper chromite), %	0.5
Average density, kg/m^3	1790
Vacuum I_{sp} (Area ratio 10), kN-s / kg	2.58 $\pm$ 0.02
Burn rate ($\dot{r}$) at 308K and 60.0 atm, mm/s	10 $\pm$ 0.2
Burn rate index between 30 - 70 atm.	0.35 $\pm$ 0.02
Temperature sensitivity of $\dot{r}$, % / K	0.2

Table 2.11: Mechanical Properties

Tensile strength, MPa	0.441 - 0.637
Hardness shore A	70 ± 5
Elongation (minimum %)	25
Initial modulus, MPa (max)	3.43

case of rocket engines, are (i) the specific Impulse and (ii) the average density of the propellant combination. The velocity increment caused by a propulsion system can be derived from simple considerations. The momentum balance can be drawn by expecting the momentum caused by a certain gas packet Δm going out of the nozzle at the velocity V_e to be equal to the increase the velocity of the vehicle by ΔV at an instantaneous mass m. Thus,

$$m\Delta V = V_e \Delta m \tag{2.1}$$

If we now divide both the differences by Δt and take a limit to express it in terms of differentials, and also note that $dm/dt = \dot{m}$, we get

$$m\frac{dV}{dt} = V_e \dot{m} \tag{2.2}$$

This is the same classical expression,

$$m\frac{dV}{dt} = F = I_{sp}\dot{m} \tag{2.3}$$

where the velocity V_e is replaced by I_{sp}. Equation (2.3) is more general in the sense that the contribution of the pressure thrust term is included through the use of the specific impulse. If we integrate the above equation expressed as $dV = I_{sp}dm/m$

$$\Delta V = I_{sp} ln(m_{at\ ign}/m_{bo}) = -I_{sp} ln(1 - m_p/m_{at\ ign}) = I_{sp} ln[1/(1-\xi)] \tag{2.4}$$

Where ΔV is the velocity increment imparted to the propulsion system and $m_{at\ ign}$ is the mass of the stage at ignition and m_{bo} is the mass at burn out composed of inert structural mass and unutilized propellants. This mass has to be kept to a minimum. The ratio $m_p/m_{at\ ign}$ between the propellant and initial masses is called the propellant mass ratio denoted by ξ. It plays an important role in the design of aerospace vehicles propelled by rocket engines. For efficient large systems, the mass ratio varies from 0.85 - 0.9. For small systems, the propellant mass ratio is lower. If we write

$$\frac{m_{at\ ign}}{m_{bo}} = \frac{m_{bo} + m_{prop}}{m_{bo}} = 1 + \frac{\rho_p V_p}{m_{bo}} \tag{2.5}$$

for cases where $\rho_p V_p >> m_{bo}$, which is true for large systems, the increment in velocity is governed largely by the specific impulse, I_{sp}. For cases where $\rho_p V_p <<$

m_{bo} as is the case with tactical systems, one can write by using the first term of the Taylor series expansion as

$$\Delta V \sim I_{sp} \frac{\rho_p V_p}{m_{bo}} \tag{2.6}$$

In these cases, the increment in velocity is governed by $\rho_p I_{sp}$, the density impulse as it is called. Thus, in volume (size) limited applications, the density impulse needs to be high. This is why solid propulsion systems with high/higher density impulse are preferred for tactical application where the operational duration is about a few seconds or thereabouts. For large rockets where the total propellant load is much more than structural weight (typically in Atlas, the propellant weight is nine times the structural and inert weight), the need for higher specific impulse permits the choice between liquids and solids. In the early stages of development it was thought the performance of liquids is superior to that of solids; however, as time passed, better and better solid propellants have been made available and the choice between the two is less clear. In the upper stages where the importance of specific impulse to the mission is very critical, the fully cryogenic stages whose specific impulse is significantly higher (of the order of 4600 N s/kg for LOX–LH_2 system vacuum I_{sp} compared to 2900 – 3200 N s /kg for solids or storable liquids), become a natural choice. Saturn V and Ariane are the examples of vehicles using full cryogenic upper stages.

It should be noted that the equation for velocity increment as in (2.4) is obtained with no gravitational effects and atmospheric drag effects. The equation of motion of a mass point in a gravitational field within the atmosphere is given by

$$\frac{dV}{dt} = \frac{F}{m} - gsin\theta - \frac{c_D \rho V^2 A}{2m} \tag{2.7}$$

where c_D is the drag coefficient and θ is the flight path angle with the horizontal. This can be integrated expressing the velocity increment of the vehicle as

$$\Delta V = I_{sp} ln[1/(1-\xi)] - gt_b sin\theta - \text{Drag loss} \tag{2.8}$$

One would like to optimize the velocity increment of the vehicle. This calls for reducing the gravity loss as well as drag loss. For satellite launch vehicles that are designed to launch satellites in orbits of 1000 km altitude for remote sensing applications, the velocity increment required is about 8.5 km/s and for geosynchronous satellites, the velocity increment required is about 8 km/s. For such applications, the satellite traverses through the atmosphere vertically in less than 50 to 70 s. Hence, the drag losses will get minimized. Though shaping the trajectory can help reduce the gravity loss, there is an irreducible minimum that would need to be accepted. For short range missiles flying at Mach numbers up to 4, the drag losses are significant and can be reduced by designing a vehicle with the smallest diameter. Gravity losses will vary depending on the trajectory that the missile takes to reach the target.

2.11 Staging, TSTO and SSTO Concepts

Strategic missiles are expected to have a range of 1000 to 10,000 km. These vehicles have a ballistic trajectory that takes parts of the vehicle and the payload to high altitudes - 400 to 600 km above the surface of the earth and then the payload re-enters the atmosphere. Satellite launch vehicles traverse the atmosphere through a vertical path and then parts of the vehicle including the satellite take a curved path to reach a specific orbit - circular or elliptic and in some cases escape the earth's gravity towards moon, a satellite of earth or other planets of the solar system. In order to understand the number of stages needed, it is first necessary to obtain the velocities required for escaping earth's gravity and getting to a circular orbit. It is necessary to recognize that the acceleration due to gravity decreases with distance from earth as

$$g_h = g[R_e/(R_e + h)]^2 \tag{2.9}$$

where h is the altitude, g_h is the acceleration due to gravity at any height h and R_e is the radius of the earth at the equator = 6378.4 km and g = 9.81 m/s^2. The escape velocity is obtained by equating the kinetic energy of the mass to the work needed to overcome gravity. This leads to

$$\frac{1}{2}mV_{es}^2 = m\int_0^h gdR \tag{2.10}$$

where R is the coordinate measured from the center of the earth. Integration leads to

$$V_{es} = R_e\sqrt{\frac{2g}{(R_e + h)}} \tag{2.11}$$

For obtaining the velocity of a satellite at any orbit of radius R, we equate the centrifugal force to gravitational pull. We get

$$\frac{mV^2}{R} = mg \tag{2.12}$$

This gives

$$V_{orb} = R_e\sqrt{\frac{g}{(R_e + h)}} \tag{2.13}$$

This orbit velocity, V_{orb} is less than escape velocity by a factor of $\sqrt{2}$. The period of rotation around the earth, P is given by $2\pi(R_e + h)/V_{orb}$. Typical values for these parameters for several applications are set out in Table 2.12 for space vehicles and 2.13 for missiles. The interesting feature to notice is that the escape velocity shown in Table 2.12 decreases with height. This is simply because the gravitational pull is decreasing with height. At an altitude of 36000 km, the acceleration

Table 2.12: The velocity increment and orbit related data, LEO = Low earth orbit, SSO = Sunsynchronous orbit, GSO = Geosynchronous orbit achieved by a geosunchronous launch vehicle, $^+$ = The incremental velocity that propulsion system should provide including gravity and drag losses, P = period of rotation around the earth

Vehicle /application	h km	g m/s^2	ΔV^+ km/s	V_{es} km/s	V_{orb} km/s	P hours
	0	9.81		11.2	7.92	1.40
Sounding rocket	20	9.81	< 5	-	-	-
LEO	100	9.51	8.5	11.1	7.85	1.44
SSO (PSLV)	1000	7.33	9.0	10.4	7.35	1.75
GSO (GSLV)	36000	3.04	10.0	4.3	3.04	24.28

Table 2.13: The velocity increment and vehicle related data; G = Total vehicle mass/payload mass

Vehicle /application	Range $\times$ 1000 km	Max. h km	ΔV km/s	No. stages	Payload kg	G
Atlas (ICBM)	9 - 14	800 - 1000	6.7	$1\frac{1}{2}$	1350	85
Titan (ICBM)	9 - 12	700 - 900	7.5	2	2270	44
Minuteman	> 6	1000	> 7	2	500	80
Polaris	> 2	600	> 4	2	500	28

due to gravity is as low as 3 m/s^2. The period of rotation at a height of 36000 km is 24.3 hours, close to a day. The satellite will rotate along with the earth and that is why the satellite is termed "geostationary or geosynchronous satellite". In satellite launch operations, the process of arranging the satellite to reach its home is delicate and is handled slowly. The orbit rising maneuvers are performed over a two week period to ensure smooth approach to the correct orbit. We can estimate the dependence of the orbit velocity on height around the geostationary altitude as

$$\frac{dV}{V} = -\frac{1}{2(1 + R_o/h)}\frac{dh}{h} \tag{2.14}$$

One important question that needs to be dealt with staging is: Why is staging required at all? We examine the results of equation (2.4) by using some typical values as in Table 2.14. Even with a low structural factor of 0.13, it is difficult to provide for the ΔV indicated in Tables 2.12 and 2.13 in a single stage using storable or semi-cryo systems. Full cryogenic systems demand a higher structural fraction and even in these cases reaching the orbit with a single-stage-to-orbit vehicle (SSTO) is barely possible. This is the primary reason for going in for multi-stage vehicles. Equation (2.4) can be used to add the velocity increment from

Table 2.14: Velocity increments from propulsion systems, (ξ = propellant mass ratio)

ξ	Inert fraction	I_{sp} N s /kg	ΔV km/s	Remarks
0.85	0.15	2600	4.93	Sea level operation
0.87	0.13	2600	5.30	storable/semi-cryo
0.85	0.15	3000	5.69	Space operation;
0.87	0.13	3000	6.12	storable system
0.85	0.15	4600	8.72	Full cryogenic
0.87	0.13	4600	9.38	system

several stages. Thus,

$$\Delta V = \sum_{1}^{n} \Delta V_i = I_{sp_i} ln[1/(1-\xi_i)] \tag{2.15}$$

Thus, it can be seen that with the addition of different velocity increments, one can obtain the desired total velocity increment. In the early developments (1960 - 1970), the vehicle structural fractions were not so low and propulsion system specific impulse values were close to 2500 N s/kg; therefore, 4-stage vehicles were designed and produced. The details of PSLV vehicle are presented in Table 2.15. There are interesting features in this table. The structural fraction varies between 0.11 to 0.24. Several other vehicles are able to control the structural fraction to better levels - to as low as 0.07 by material quality control, better design practices and most importantly, improved fabricational techniques. The velocity increment in each of the stages is about 3 km/s. The gravity loss is less than 1 km/s in each of the stages.

Developments, both on structural efficiency and propellant energetics, over years allowed 3-stage systems to be deployed for satellite launch vehicles. The upper stage in these 3-stage vehicles would invariably be a full cryogenic stage. Long range missiles used two-stage arrangement because the payload has shrunk also due to the use of higher energy explosives or better nuclear warhead technology. The one-and-a-half stage design implies that some of the booster thrust chambers will fall off, but the tankage and the sustainer engine will continue to function. Staging need not always be linear. The first stage can have starp-ons. All the propulsion systems can be ignited on ground to ensure higher reliability and the strap on systems can be discarded after burn-out before or simultaneously with the core stage. It could also be a piggy back arrangement as in space shuttle. Thus, a variety of schematics have been used in the design of the vehicles.

Space shuttle is an example of the effort that went in to produce reusable launch vehicles. This vehicle was designed as partially reusable. The solid boost-

ers would be jettisoned into sea from where they would be recovered and refurbished before use. The liquid tankage would fall off at an altitude that it would be burnt up. In actuality, the changes that were required to be done to various components of the liquid engine and to the vehicle itself were such that the feature of reusability was compromised significantly. This has retained the cost of delivery of payload in a 200 km orbit at 10000 USD per kg. The fact is that a well conceived vehicle like the space shuttle itself has not been able to bring down the cost of delivering a payload substantially, and other concepts to reduce the cost of access to space to about 1000 to 3000 USD per kg are being considered by several researchers. The key point in this conceptualization is that one should adopt aircraft modes of operation. It is important to recognize that in an aircraft operation, the only expendable is the fuel; the checkout time is typically 15 to 30 minutes at an airport - in fact less than the time it takes to take on the passengers and the baggage on board. The checkout in a space craft launch occurs through a launch campaign that takes upwards of two weeks, typically two months for a major vehicle. An aircraft can do so because, the vehicle used is the same, the operational health is monitored during the flight and does not need to be elaborately rechecked ab-initio before take-off. It is therefore suggested that spacecraft launch vehicle design must proceed from concepts in aircraft design and operation. The ΔV requirement of 9 km/s is split into two parts, one part related to aircraft operations that take the vehicle to M $\sim$ 3 (1 km/s) and the rest using rocket like operations beyond the atmosphere using a rocket engine that must be considered safe. While a reliably operating LOX - kerosene class engine offers a good choice, the design becomes very critical at structural factors even of 0.13. LOX-LH_2 engines might be inevitable. Whether such engines with propellant storage on-board are considered safe is a serious question. One of the other options considered seriously in design is an aerial transfer of some propellants classically used in aircraft operations (like the aircraft KC 135 used for aerial refuelling). It is also possible to conceive of a hydrogen-solid hydrocarbon-oxygen combination to combine high performance with safety. These are possible future developments. These constitute the efforts on a single-stage-to-orbit (SSTO) class of vehicle. With the possibility that this might be difficult to achieve at a stage when the structural factors are sufficiently not low enough for the realization of an efficient SSTO vehicle, many studies have been advocating a two stage-to-orbit (TSTO) vehicles as possibilities to reduce the cost of access to space.

2.12 Summary

In this chapter we have examined the various applications in the aerospace scenario, both of air breathing and non-air breathing kind. We have also seen the nature of the propulsion units used to power these vehicles. These are civilian or

Table 2.15: The stage parameters of PSLV vehicle (India); s-ons = strap-ons, all mass in t = tonnes, PL = Payload, St. str. fraction = Stage structural fraction, $\sum \Delta V_{th}$ = ideal velocity increment; $\sum \Delta V_a$ = Actual velocity increment, the difference is due to drag and gravity loss in the first stage and gravity loss in the later stages, * = The calculation is less than rigorous because the strap-ons are operated between the start-up and burn-out of the core engine, ** = coasting between stage III and IV reduces ΔV by 0.36 km/s

Property	I stage+s-ons	II stage	III stage	IV stage	PL
Stage Mass, t	236.00	45.75	8.60	3.37	1.0
$m_{at\ ign}$, t	293.72	57.72	12.97	4.37	
Propellant	Solid	Liquid	Solid	Liquid	
m_p, t	138.0, 6 x 53.5	37.5	7.22	1.16	
Inert mass, t	44.5	5.25	0.96	0.81	
St. str. fraction	0.188	0.115	0.112	0.24	
m_{bo}, t	102.2	18.2	5.33	1.81	
t_b, s	108.8, 48.7	160.0	109.4	555.0	
I_{sp}, kN s/kg	2.64, 2.57	2.90	2.93	3.01	
F, kN	4673, 640	725	246	2 x 7.35	
$F/m_{at\ ign}$, N/kg	15.9	12.6	20.5	3.3	
$m_{bo}/m_{at\ ign}$	0.348	0.307	0.411	0.414	
ΔV, km/s	2.78	3.42	2.61	2.66	
$\sum \Delta V_{th}$, km/s	2.78 (*)	6.20	8.81	11.47	
$\sum \Delta V_a$, km/s	2.23	5.19	7.78 (**)	10.0	

scientific and military applications. The military applications have quite often led the technology growth in most cases excepting perhaps in the civilian long range passenger transport sector. One of the most important parameters affecting the performance of engines is the specific fuel consumption or specific impulse. There are other parameters like the density of the propellants in the case of rocket engines as well as thrust to weight, life, mean time between failures, turn around time for operations and others in the case of air breathing engines which are also important. The developments in aircrafts and rocket based vehicles have reached a stage that one can expect only incremental advances in them individually. Hybrid propulsion systems that use airbreathing engines within the atmosphere and rocket engines outside the atmosphere in a manner that take-off weight can be reduced and true safety ensured in a manner that accounts for public perception of safety is the possible direction of developments in future.

Several books provide an understanding of the relationship of the choice of the engines to applications. [1, 5, 7, 8, 11]

Chapter 3

The Efficiencies of Propulsion Systems

3.1 Introduction

In this chapter we treat the propulsive, thermal and overall efficiencies of propulsion systems. As different from these, there are efficiencies related to components like diffuser, compressor, combustor, turbine and nozzle which will be discussed subsequently. The use of propulsive and related efficiencies is limited to obtaining an appreciation of the speed range in which a given propulsion system is most efficient. It must be understood that these efficiencies alone do not dominate the choice of a system in a specific speed range and other aspects of the mission are very important. In fact, specific aspects of the mission are so over-riding that these efficiencies (propulsive or overall) become irrelevant. Nevertheless, much can be learnt about the efficiency or inefficiency of an operating system by examining it in the light of these definitions.

3.2 Analysis

In the analysis to follow, the propulsive system is treated as a black box that enhances the exit momentum flow in relation to that of the inlet by introducing energy generated by combustion. Figures 3.1, a and b show the specific features of such a system for air breathing and non-air breathing engines.

The important distinction between the air breathing and non-air breathing engines is that while air is ingested in the case of air breathing engines, no free stream flow is ingested into the engine in the case of non-air breathing engines. The expression for thrust for an air breathing engine can be written following

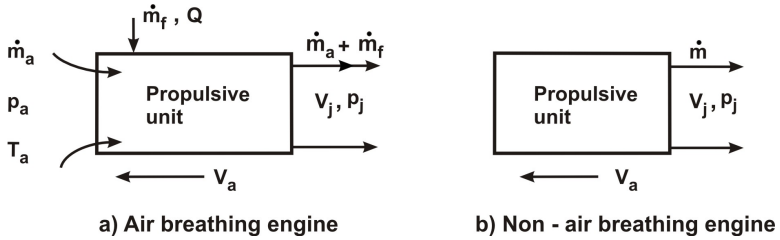

Figure 3.1: The Block diagrams of Propulsion system

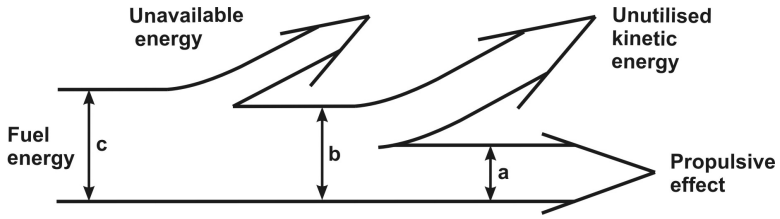

Figure 3.2: The energy balance of a propulsion system

Newton's II law as

$$F = [\dot{m}_a + \dot{m}_f] V_e - \dot{m}_a V_a + A_e (p_e - p_a) \tag{3.1}$$

where the first term on the right hand side is due to the velocity change and the second due to the difference in pressure between the exit and the ambient. A_e refers to the cross sectional area of the nozzle exit.

In the case of a non-airbreathing engine (a rocket engine), the expression for thrust is

$$F = \dot{m} V_e + A_e (p_e - p_a) \tag{3.2}$$

One of the classical design conditions for the rocket nozzle is $p_e = p_a$, since this ensures complete expansion. For an operational rocket, the change in altitude during the flight affects the second term. However, the second term is very small or negligible as compared to the first term. In fact, in the worst operating off-design conditions, the magnitude of the second term does not exceed 10 % in the case of rocket engines. This is not true in the case of air breathing engines always. In the analysis to follow, the second term will be ignored for simplicity for rocket engines.

Efficiencies can be defined as output/ (output + losses) or output / input. It must be understood that these two definitions have indeed different implications. Both these definitions will be used below. The losses can be several. Transmission and other mechanical losses are ignored for the present. The losses accounted for

are essentially those due to unutilized kinetic energy in the exhaust stream and the unavailable energy fundamental to thermodynamics. The diagram in Fig. 3.2 illustrates the energy balance.

3.3 The Propulsive Efficiency

In evolving this definition, input fuel energy is not considered. The output which is the propulsive effect is divided by the output plus the unutilized kinetic energy of the exhaust stream. (This is defined in terms of power). The power due to the propulsive effect is FV_a, where V_a is the flight speed of the vehicle carrying the propulsive unit. The losses in the jet are estimated to be $\dot{m}_a(V_e - V_a)^2 / 2$ since V_e is the velocity of the jet relative to the propulsive unit, and $(V_e - V_a)^2 / 2$ the kinetic energy per unit mass flow rate of the jet. Thus,

$$\text{Thrust Power} = F\ V_a \tag{3.3}$$

$$\text{Power lost in the jet} = \dot{m}_a(V_e - V_a)^2 / 2 \tag{3.4}$$

3.3.1 Air Breathing Engines

The expression for the power lost can also be written as $F\,(V_e - V_a) / 2$, if we note that $F = \dot{m}_a(V_e - V_a)$; thus, the propulsive efficiency (η_p) can be written down as

$$\eta_p = \frac{FV_a}{FV_a + F(V_e - V_a)/2} = \frac{2V_a}{V_a + V_e} = \frac{2r}{1+r} \tag{3.5}$$

where $r = V_a/V_e$. The above expression for propulsive efficiency is valid for all air breathing engines with $\dot{m}_f / \dot{m}_a = f << 1$. Typical values of f for turbojets, turboprop and turbofans will be around 0.005 – 0.02. Only in the case of a ramjet or an after-burning turbojet, f is about 0.067, the stoichiometric value for a kerosene-air system. Even in this case the above expression is approximately valid. The expression that allows for non-zero f can be obtained as

$$\eta_p = \frac{2r(1+f-r)}{1-r^2 + f(1+r^2)} \tag{3.6}$$

It is useful to obtain the order of magnitude of the power usefully spent and lost. For a typical operating condition like F = 70 kN, V_a = 800 km/hr (222 m/s), V_e = 522 m/s,

$$\text{Useful power} = FV_a = 15.5MW \tag{3.7}$$

$$\text{Power lost} = F(V_e - V_a)/2 = 10.5MW \tag{3.8}$$

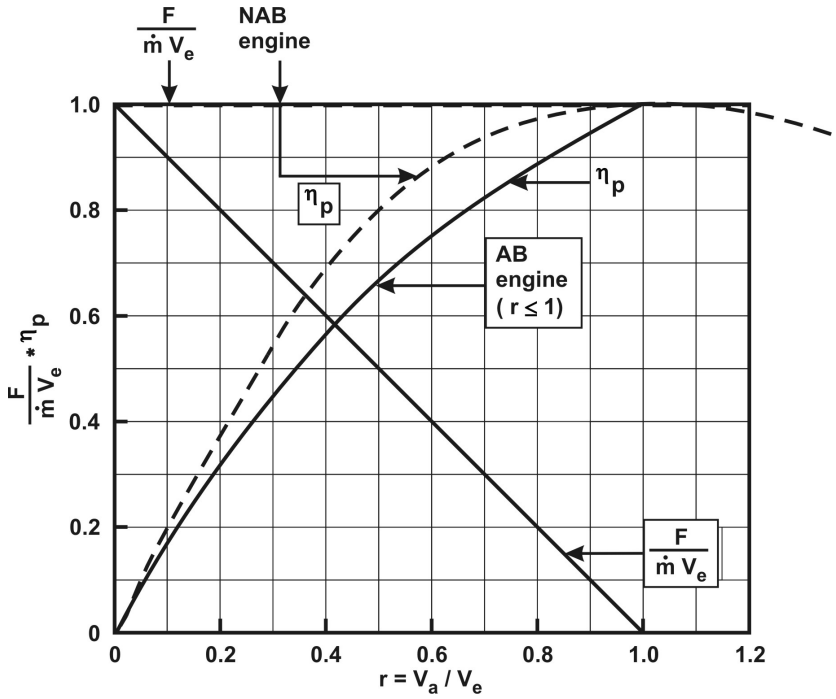

Figure 3.3: Plot of F/mV_j and η_p with velocity ratio for air breathing and non-airbreathing engines

$$\text{Propulsive efficiency} = 15.5/(15.5 + 10.5) = 59.6\% \tag{3.9}$$

Thus, the enormous power of the propulsion system and also that lost in the jet can be noted. Propulsive efficiencies of the order of 60 % are considered reasonable from an overall operation point of view. If we put the expressions for thrust and propulsive efficiency together we obtain,

$$F = \dot{m}_a V_e(1 - r) \tag{3.10}$$

$$\eta_p = 2r/(1 + r), \quad f << 1 \tag{3.11}$$

3.4 Further Analysis

Figure 3.3 shows a plot of both $F/(\dot{m}_a V_e)$ and η_p with r. If $r > 1$, the developed thrust is negative. Thus, for an air breathing engine $r < 1$. The maximum efficiency is obtained at r = 1, at which η_p = 1 and F = 0. Apparently, the propulsive units are most efficient when they do no work!. How do we interpret this situation in actual practice? In order to obtain a non-zero thrust and have a high propulsive

efficiency, we should let r be less than 1, i.e. the jet speed be only a little larger than the flight speed, so that one can obtain the desired thrust by increasing the flow rate, $\dot{m}_a$. For the fixed flight speed, increased flow rates are obtained by increasing the area of cross section of the flow. This is precisely what happens in a propeller where a large air flow is given a small velocity increment to obtain the desired thrust at high propulsive efficiency ($\sim$ 95 %). We raise the next question: If propeller devices are so efficient, how come other devices like turbojets are also in existence?

The answer lies in the fluid mechanics associated with propellers. The flow over the airfoil cross sections of the propeller blades is governed by the vector combination of the flight speed and the local peripheral velocity of the rotating blade (2π R N, R = local radius, N = rotational speed of the propeller). At flight speeds of 450 km/hr (125 m/s), rotational speeds of 4500 rpm (75 rps), radius of about 0.5 m, the peripheral speed amounts to 235 m/s. Vector velocity over the blades amounts to 266 m/s. Expressed in terms of Mach numbers (the ratio of flow velocity to the speed of sound), the local Mach number is 0.8, approaching a condition which leads to drastic reduction in the efficiency of the propeller, due to the formation of strong acoustic waves (weak shock waves) on the surface of the propeller. As such, propeller devices are not used for flight speeds beyond 450 – 500 km/hr. Hence, other devices like turbojets have evolved. Also devices like turbojets have a much higher thrust per unit cross section and thus, enable better packaging.

3.4.1 Non-Air Breathing Engines (Rocket Engines)

In the case of rocket engines, the definition for propulsive efficiency leads to

$$\eta_p \;=\; \frac{F\,V_a}{F\,V_a \;+\; \frac{\dot{m}\,(V_e - V_a)^2}{2}} \;=\; \frac{2\,V_a\,V_e}{2\,V_a\,V_e \;+\; (V_e \;-\; V_a)^2} \;=\; \frac{2\,r}{1 \;+\; r^2} \tag{3.12}$$

Again, if we set the expression for thrust and propulsive efficiency together we obtain,

$$F \;=\; \dot{m}V_e \quad and \quad \eta_p \;=\; 2\,r/\,(1 \;+\; r^2) \tag{3.13}$$

It can be seen that the thrust of the rocket is independent of flight speed (otherwise an elementary fact). The propulsive efficiency is maximum (100 %) at r = 1 (see Figure 3.3). One feature different from that of air breathing engines is that r can be greater than unity i.e. the flight speed does not always have to be less than jet speed. This derives from the fact that the rocket engine generates its own hot gases, exhausting them through the nozzle to produce thrust.

At the same r, the propulsive efficiency of a rocket engine is larger than that of an airbreathing engine. At r = 0.425 (= 222/522.0), from the previous example, η_p

for air breathing engines is 59.6 % and for rocket engine, 78.9 %. Though this has no deep physical interpretation, it is pertinent to point out that the propulsive efficiency applied to a rocket engine is devoid of serious application because a rocket works mostly in an acceleration mode. Typically, r varies from 0 or 0.1 to values up to 2 or more.

One of the dramatic uses of the concept of propulsive efficiency occurs in the case of underwater propulsion systems. Though this falls outside the scope of aerospace propulsion systems, it is worth considering them. A typical underwater propulsive application is for vehicle speeds of 60 – 80 km/hr (16.6 – 22.2 m/s). The choice of propulsion system is between a rocket engine or a gas generator running a turbine or a piston engine which runs a propeller at speeds of 1000 – 2000 rpm. An existing system using gas generator-piston engine-propeller seems to produce a power of 355 kW and an equivalent thrust of 16 kN at 80 km/hr. This is performed by the gas generator whose flow rates are about 0.7 kg/s. If one were to use a rocket engine at 0.7 kg/s, the maximum thrust that could be extracted is $\dot{m} I_{sp}$ = 0.7 kg/s $\times$ 2300 N-s/kg = 1.6 kN, about one tenth of that obtained by using the propeller. The reason for this is that $r = V_a/V_e$ = 22.2 / 2300 = 0.01 (and η_p = 0.02) being so small. Most of the energy generated in combustion is lost in the exhaust jet such that *very little* is used in propulsion. The choice of propeller as the thrust producing element is clear in this case. Newer underwater propulsion systems using supercavitating vehicles (torpedoes) moving at 250 to 300 km/hr may benefit from rocket engines.

3.5 Thermal and Overall Efficiency

Referring to Fig. 3.2, the input is treated as the fuel energy. The output is kinetic energy imparted to the jet taken as the sum of useful power plus the loss of kinetic energy in the jet. Thus, the input or (output + losses) of the expression for the propulsive efficiency is the output in the present expression.

$$\text{Output Power} = F\,V_a + \dot{m}\,(V_e - V_a)^2/\,2 = F\,(V_a + V_e)/2 \tag{3.14}$$

$$\text{Input Power} = \dot{m}_f Q \tag{3.15}$$

$$\text{Thermal Efficiency} = \eta_{th} = \frac{\text{Output Power}}{\text{Input Power}} = \frac{F\,(V_e + V_a)/\,2}{\dot{m}_f Q} \tag{3.16}$$

It is seen appropriate to include the power required to carry the fuel ($\dot{m}_f V_a^2$ / 2) in the definition of input. The expression for thermal efficiency will then become

$$\eta_{th} = \frac{F\,(V_e + V_a)/\,2}{\dot{m}_f(Q + \dot{V_a}^2/2)} \tag{3.17}$$

The above expression is valid both for air breathing and non-air breathing engines, the term m_f is treated as fuel flow rate in the former case and propellant flow rate in the latter.

The overall efficiency (η_{ov}) is defined as the ratio of useful output power to the input power.

$$\text{Overall Efficiency} \;=\; \eta_{ov} \;=\; \frac{F\,V_a}{\dot{m}_f Q \;+\; \dot{m}_f\,V_a^2\,/\,2} \tag{3.18}$$

$$\eta_{ov} \;=\; \frac{F\,V_a}{F\,V_a \;+\; \dot{m}\,(V_e \;-\; V_a)^2/\,2} \times \frac{F\,V_a \;+\; \dot{m}\,(V_e \;-\; V_a)^2/\,2}{\dot{m}_f Q \;+\; \dot{m}_f V_a^2\,/\,2} \tag{3.19}$$

$$\eta_{ov} \;=\; \eta_p \times \eta_{th} \tag{3.20}$$

3.5.1 Air Breathing Engines

Introducing the expression for thrust we get the expression for the overall efficiency as

$$\eta_{ov} \;=\; \frac{\dot{m}_a(V_e \;-\; V_a)\,V_a}{\dot{m}_f Q \;+\; \dot{m}\,V_a^2\,/\,2} \;=\; \frac{2\,r\,(1 \;-\; r)}{2\,f\,Q\,/\,V_e^2 \;+\; f\,r^2} \tag{3.21}$$

Defining $E = fQ/(V_e^2/2)$, we write

$$\eta_{ov} \;=\; \frac{2\,r\,(1 \;-\; r)}{E \;+\; f\,r^2} \tag{3.22}$$

The typical value of E is between 4 – 10. The second term in the denominator is about 0.01 – 0.04. As such,

$$\eta_{ov} \;=\; 2\,r\,(1 \;-\; r)\,/\,E \tag{3.23}$$

The maximum overall efficiency is obtained at r = 0.5 as ($\eta_{ov,max} \;=\; 1/2E$). For typical situations, the maximum overall efficiency is about 12 %. The propulsive efficiency at r = 0.5 is 66 %. One, therefore notices that the velocity ratio for optimum propulsive efficiency is different from that for overall efficiency. This feature causes a conflict and the usual choice is to look for an optimum in the overall efficiency.

3.5.2 Non-Air Breathing Engines

The expression for η_{ov} can be written as

$$\eta_{ov} \;=\; \frac{\dot{m}\,V_e\,V_a}{\dot{m}\,(Q \;+\; V_a^2\,/\,2)} \tag{3.24}$$

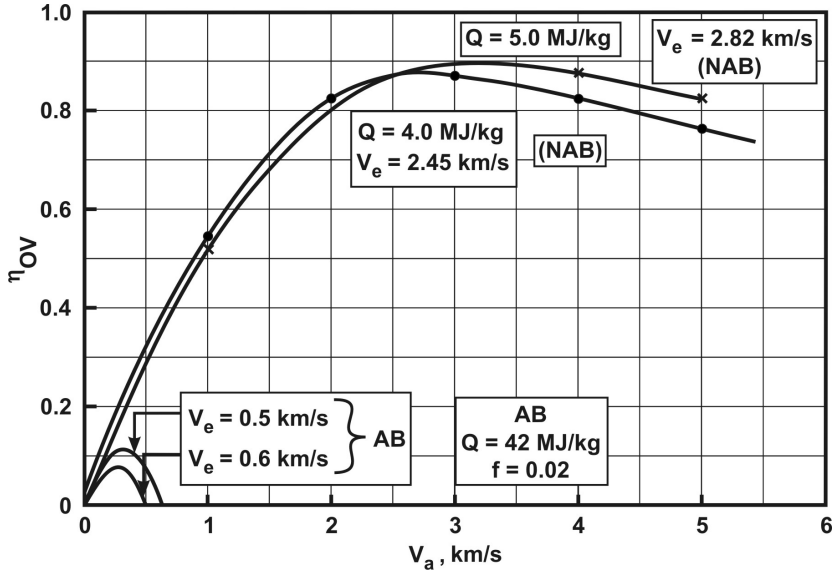

Figure 3.4: The plot of overall efficiency (η_{op}) with flight speed at various jet speeds

The subscript f or a on $\dot{m}$ has been dropped to indicate the total flow of propellant passing through the nozzle. The expression then reduces to

$$\eta_{ov} \;=\; 2\,r \;/\; (\,2\,Q\,/V_e^2 \;+\; r^2) \tag{3.25}$$

Defining $E_r = 2Q/V_e^2$, we get

$$\eta_{ov} = 2r/(E_r + r^2) \tag{3.26}$$

It is also possible to write $V_e^2/2 \sim Q - Q_e$, where Q is the heat of combustion of the propellant and Q_e is the heat in the exit stream. Because of this, $E_r \;> 1$ and $\eta_{ov} \;< 1$.

The optimum (maximum) with respect to r is obtained at $r = \sqrt{E_r}$ and its value is $\eta_{ov} = 1/\sqrt{E_r}$.

The typical values of Q is about 4.2 – 6 MJ / kg (notice it is about a tenth of the heat of combustion of kerosene-air because of oxidizer weight being included in the propellant) and V_e = 2 – 3 km/s. These lead to E_r = 1.5 – 3 and so overall efficiency is about 60 – 80 %.

3.6 Analysis

Figure 3.4 shows the variation of η_{ov} of airbreathing and non-airbreathing engines with speed for some typical parameters. It is clear from the figure that air

Table 3.1: Summary of the results ($r = V_a/V_e$, $E = 2fQ/V_e^2$, $E_r = 2Q/V_e^2$)

Efficiency	Propeller, Turbo-jet, fan	Rocket
η_p	$2r/(1+r)$	$2r/(1+r^2)$
η_{ov}	$2r(1-r)/E$	$2r/(E_r+r^2)$
Maximum η_{ov}	$1/2E$ at $r = 0.5$	$1/\sqrt{E_r}$ at $r = \sqrt{E_r}$

breathing engines work with much less overall efficiencies as compared to non-airbreathing engines.

This implies that the energy of combustion is better utilized in rocket engines. It is not unlikely that one may conclude that non-airbreathing engines can therefore be used for most applications. And why not?

One of the important measures of performance, not considered directly in the above analysis, is the fuel/propellant consumed to obtain a certain total impulse. The fuel/propellant flow rate required to obtain a desired thrust or thrust power needs to be as small as possible. This helps reducing the amount of fuel/propellant taken on board.

Viewed from this angle, it can be seen that an airbreathing engine takes in oxidizer about 50 – 100 times the fuel, from the atmosphere. Since the rocket engine has to take on board all the oxidizer (about 3 – 5 times the weight of the fuel instead of 50 – 100 partly because no N_2 is carried and one works near stoichiometry or on the fuel rich side) and to do the same task, the weight of expendables is much more in a rocket engine compared to an air breathing engine. For doing work indefinitely (hundreds of hours) one uses an air breathing engine and to put in a certain impulse (high thrust for a small time of the order of seconds or minutes) one uses non-air breathing engines. Thus, mission characteristics dictate the choice of the system irrespective of efficiencies identified above. These features have been brought out in some detail in Chapters 1 and 2.

3.7 Summary

This chapter is devoted to an analysis of the propulsive and overall efficiencies of propulsion systems. Table 3.1 summarizes the final results.

The choice of propeller devices as efficient devices at relatively low speeds is justified by the high propulsive efficiency. The choice of turbojets, ramjets and rockets become meaningful at high flight speeds through a similar logic. Factors other than the above mentioned efficiencies, like specific fuel consumption (fuel

consumption per unit thrust or power) are important in the choice of propulsion systems. For flights within the atmosphere where one needs "work" for long durations of time air breathing engines are an appropriate choice. For flights beyond the atmosphere or when one needs Impulse for short durations, non-air breathing engines are the appropriate choice. The book by Shepherd [34] has a brief and clear presentation of the importance of the efficiencies.

Chapter 4

Thermodynamics and Gas Dynamics

4.1 Introduction

In the design and analysis of propulsion systems, questions like – How much is the specific fuel consumption lower for a turbofan in relation to turbojet? Is turbine efficiency less important compared to compressor efficiency? For getting a fixed thrust, how much is the size of the engine reduced if one adopts a higher turbine inlet temperature or a higher compressor pressure ratio? – are raised often and it is necessary to provide answers to them. How is this done? The basic elements of the engine are modeled thermodynamically and the overall performance in terms of thrust produced, fuel consumed can then be calculated. The thermodynamic behavior can be enunciated at several levels of complexity. In the first instance the losses in the system can be ignored and the ideal behavior evaluated. The overall system is split into elements – like a turbojet into air intake, compressor, combustor, turbine, and nozzle. Each of these is treated as a black box with certain input–output characteristics. The relationships between pressure, temperature and velocity are established depending on the process in each element and the exit conditions obtained for given inlet conditions. This is what is attempted presently.

The flow is assumed one-dimensional. This assumption is not satisfactory if the flow through individual elements is concerned, but is good in so far as overall performance estimation is concerned. The influences of non-one dimensionality and losses can be brought in through the use of efficiencies. If the loss through an element is frictional, it amounts only to a stagnation pressure loss. The ratio of downstream to upstream stagnation pressure is taken as an efficiency of the element. The analysis also benefits from the choice of a single constant specific heat and molecular weight of the products. The simplicity gained by these assumptions

leads to simple expressions for a number of results and a quick appreciation of parametric dependence is possible. It is also important to note that more careful consideration of properties changes only the actual values but not the qualitative picture.

4.2 Essentials of Nozzle Flows

4.2.1 The Conservation Equations

The conservation equations for a one dimensional steady inviscid flow are:

$$\text{Mass conservation} : \quad \rho A V = \dot{m} = \text{constant} \tag{4.1}$$

$$\text{Momentum conservation} : dp/\rho + V dV = 0 \tag{4.2}$$

$$\text{Energy conservation} : c_p T + \frac{V^2}{2} = \text{constant} \tag{4.3}$$

$$\text{Equation of state} : p = \rho R T \quad or \quad pv = mRT \tag{4.4}$$

As can be noticed, the momentum equation is written in a differential form while the others are in an integrated form. This is because the density varies in a compressible flow field that we need to consider here. The differential forms of the conservation equations for mass and energy lend themselves to integration and hence, they are written down in the integrated form.

4.2.2 Acoustic Speed

The speed of propagation of a small disturbance in a fluid is derived as

$$a^2 \; = \; \left[\frac{\partial p}{\partial \rho}\right]_{s \, = \, constant} \tag{4.5}$$

This equation states that the change of pressure with density under isentropic conditions gives the square of the acoustic speed.

4.2.3 The Laws of Thermodynamics

The laws of thermodynamics give us

$$T \, ds \; = \; c_v \, dT \; + \; p \, dv \tag{4.6}$$

where v = specific volume, s = specific entropy and c_v = specific heat at constant volume. The equation is written in terms of quantities per unit mass. Under

isentropic conditions the left hand side is zero and the use of equation of state on the right hand side gives,

$$c_v\, dT \;+\; RT\,\frac{dv}{v} \;=\; 0 \tag{4.7}$$

Integration yields

$$Tv^{R/c_v} = \text{constant} \tag{4.8}$$

$$Tv^{(\gamma-1)} = \text{constant} \tag{4.9}$$

$$pv^{\gamma} = \text{constant} \;\; or \;\; T\,p^{-\frac{\gamma-1}{\gamma}} \;=\; \text{constant} \tag{4.10}$$

$$p\rho^{-\gamma} = \text{constant} \tag{4.11}$$

The various forms of the above equations in terms of T and v, p and v, T and p are obtained by using the equation of state appropriately.

Use of equation (4.11) in the relation for the acoustic speed equation (4.5) gives,

$$a^2 \;=\; \gamma\, p\,/\,\rho \;\text{ and so } a \;=\; \sqrt{\gamma\, R\, T} \tag{4.12}$$

The R in the above equation is the specific gas constant and is related to the universal gas constant $\mathscr{R}$ by

$$R = \mathscr{R}\;/\;\mathscr{M} \tag{4.13}$$

where $\mathscr{M}$, is the average molecular weight of the gaseous species. The value of $\mathscr{R}$ in different units is as below.

$\mathscr{R}$ = 1.986 cal/g-mole K = 8.314 kJ/kg mole K = 8314 m^2/s^2 K

For γ = 1.4, $\mathscr{M}$ = 28.96 for air, T = 288 K, the acoustic speed is

a = $\sqrt{1.4 \times (8314/28.96) \times 288}$ = 340.2 m/s

4.2.4 T – s Diagram

The eqn. (4.6) can be recast as

$$T\,ds = c_v dT + R\,dT - vdp \;=\; c_p\,dT \;-\; R\,T\frac{dp}{p} \tag{4.14}$$

At constant pressure, the second term on the right hand side drops off and we get on integration

$$T = T_{ref}\; exp\left[\frac{s - s_{ref}}{c_p}\right] \tag{4.15}$$

Thus, on a $T - s$ plot, constant pressure lines appear as exponential curves and the slope of these curves is given by

$$\left[\frac{d\,T}{d\,s}\right]_{p=constant} = \frac{T}{c_p} \tag{4.16}$$

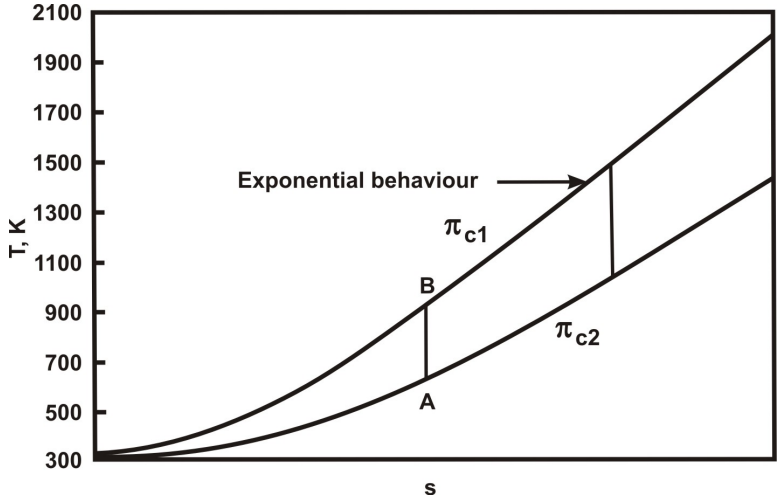

Figure 4.1: A typical Temperature – Entropy diagram

This expression can be used to show that constant pressure curves on a $T--s$ plot will be diverging with increasing entropy. Figure 4.1 shows schematically a $T--s$ plot. The values of constant pressure for the curves increase as we move towards the higher temperature region; if we conceive an isentropic compression process, then pressure and temperature have to increase along a vertical line. On a vertical constant entropy line like AB, the value of dT/ds must increase because temperature increases. This implies that each of the curves at higher pressure will have higher local slope. Therefore the curves diverge as seen in the figure.

4.2.5 Stagnation Conditions

Stagnation conditions of a flowing fluid are defined as those which are attained when the flow is isentropically brought to rest. The stagnation quantities are defined for temperature, pressure and density. For temperature, one obtains

$$c_p T_t = c_p T + \frac{V^2}{2} \tag{4.17}$$

where T_t is the stagnation temperature.

One defines a Mach number = M = ratio of speed of the fluid to the speed of sound in the fluid. It reflects the effects of compressibility. For a fluid moving at the speed of the sound, no signals can move upstream. Thus, the changes downstream will not be known upstream. This feature produces changes in flow which are significant. The single parameter characterizing the gas dynamics of flow at high speeds is the Mach number. It can also be understood as the ratio of the kinetic

energy of the fluid to the energy in the random motion of molecules. [$M^2 = V^2/a^2 \sim V^2/RT$]. When a fluid decelerates from high speed to low speed, the kinetic energy of mean motion gets converted to energy of random motion of molecules thus, raising the temperature of the fluid.

We can rewrite equation (4.17) by dividing both sides by c_pT and noting that $c_p = \gamma R/(\gamma - 1)$,

$$\frac{T_t}{T} = 1 + \frac{\gamma - 1}{2} M^2 \tag{4.18}$$

For pressure and density, one can use isentropic relations and get

$$\frac{p_t}{p} = \left[1 + \frac{\gamma - 1}{2} M^2\right]^{\frac{\gamma}{\gamma - 1}} \tag{4.19}$$

$$\frac{\rho_t}{\rho} = \left[1 + \frac{\gamma - 1}{2} M^2\right]^{\frac{1}{\gamma - 1}} \tag{4.20}$$

At M = 1,

$$\frac{T_t}{T} = \frac{\gamma + 1}{2} \tag{4.21}$$

$$\frac{p_t}{p} = \left[\frac{\gamma + 1}{2}\right]^{\frac{\gamma}{\gamma - 1}} \tag{4.22}$$

$$\frac{\rho_t}{\rho} = \left[\frac{\gamma + 1}{2}\right]^{\frac{1}{\gamma - 1}} \tag{4.23}$$

For γ = 1.4, T_t/T = 1.2, p_t/p = 1.892, ρ_t/ρ = 1.577

For γ = 1.2, T_t/T = 1.1, p_t/p = 1.77, ρ_t/ρ = 1.61

The significance of these results will be made explicit in the sections to follow.

4.2.6 Nozzle Flow

Logarithmic differentiation of equation (4.1) gives,

$$\frac{d\,\rho}{\rho} + \frac{d\,A}{A} + \frac{d\,V}{V} = 0 \tag{4.24}$$

Substituting equation (4.5) in equation (4.2), we get

$$a^2\,\frac{d\,\rho}{\rho} + V d\,V = 0 \tag{4.25}$$

$$\frac{d\,\rho}{\rho} = -\frac{V^2}{a^2}\frac{d\,V}{V} = -\,M^2\frac{d\,V}{V} \tag{4.26}$$

Equations (4.24) and (4.26) give

$$\frac{d\,V}{V} = \frac{d\,A\,/\,A}{M^2 - 1} \tag{4.27}$$

Equation (4.27) forms the basis of the design of nozzles.

If a subsonic flow ($M < 1$) is to be accelerated and so expanded from higher to lower pressure, the area of cross section has to decrease ($dA < 0$); equivalently, this means that one should use a convergent passage.

If $M = 1$ gets attained, dA should be zero so that dV does not become infinitely large. Further, it can be shown that at this condition, $d^2A > 0$ indicating that A attains a minimum (also called the throat) at $M = 1$. It is important to note that equation (4.27) does not indicate that if $dA = 0$, M should be unity. In fact M can acquire any value at $dA = 0$. This means that the flow through a throat can be supersonic. This condition can be realized only where the inlet flow is supersonic.

If supersonic flow ($M > 1$) is to be further accelerated, one has to increase the area of section ($dA > 0$) or one has to use a divergent passage. The various conditions of nozzle flow are shown in Figure 4.2.

In case (a), the flow through the convergent is entirely subsonic. In case (b), the flow at the end of the convergent (or throat) has attained sonic conditions.

In case (c), the choice of inlet stagnation pressure is such that at the throat the static pressure is greater than the ambient. As such the flow is under expanded. The Mach number at the throat continues to be unity. To enable complete expansion, a divergent section is to be provided. As shown in Figure 4.2 (d), the expansion takes place such that the exit plane pressure equals atmospheric pressure and at this condition, the exit Mach number will be greater than 1. If the chamber pressure is raised substantially, the exit-to-throat area ratio has to be raised substantially to extract the momentum present in the gas stream. Case (e) shows the situation when the chamber pressure is raised by a factor of ten compared to case (d). In case (f) the exit plane pressure is brought down corresponding to high altitude application. The nozzle can be designed to have optimum expansion at this condition. If the rocket engine flies at much higher altitudes, the ambient pressure becomes very small and the nozzle experiences under-expansion. *This condition is inevitable for all space applications*.

All rocket engine nozzles use convergent-divergent (C–D, or de-Laval) nozzles since the stagnation pressures at the entry to the nozzle are high (1-20 MPa). Ramjet engine nozzles are also convergent-divergent since the nozzle inlet stagnation pressures are about 3–5 times the ambient pressure. Most aircraft (gas turbine) engine nozzles are convergent and many include area variation because the nozzle inlet stagnation pressures are between 1.5 - 3 times the ambient pressure. The additional performance at higher pressure end is sacrificed in favor of simpler geometric and operational convenience. However, engines used on supersonic aircraft

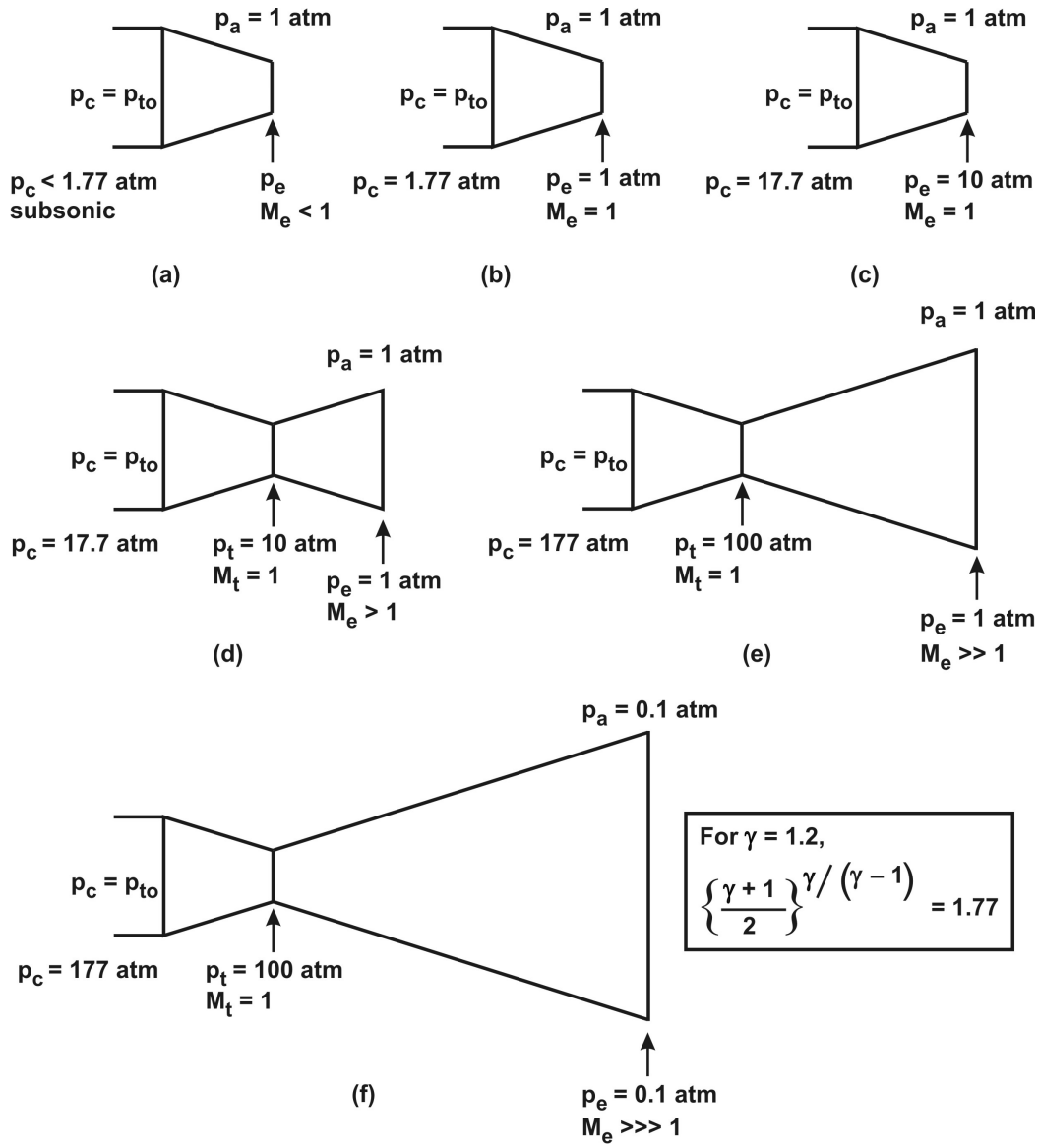

Figure 4.2: The different regimes of nozzle flow ($p_c = p_{t0}$, total pressure at entry level to the nozzle p_e, p_{th}, p_a, static pressure at exit, throat and ambient respectively)

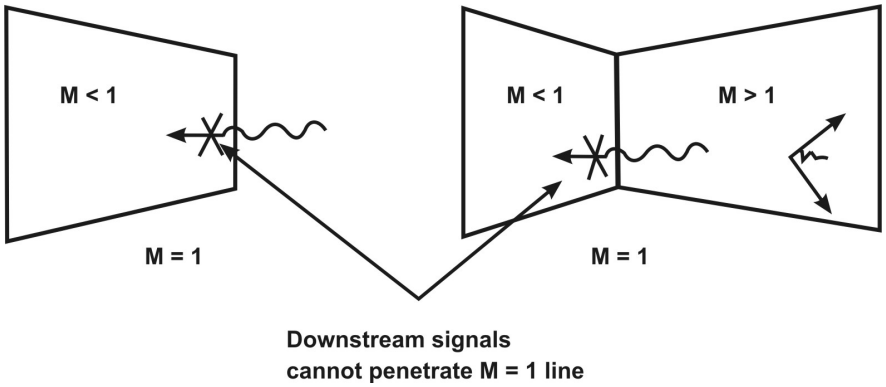

Figure 4.3: The Choked nozzle (the flow cannot be altered by changing the downstream conditions but can be altered by altering the upstream pressure)

generally deploy C–D nozzles, some with variable geometry to ensure adequate and appropriate performance, particularly under combat conditions. Most of the other engines designed in recent times also attempt to use C–D nozzles to ensure high performance.

4.2.7 Choked Nozzle and Mass Flow Rate

A nozzle is said to be choked if the flow rate through the nozzle cannot be increased by altering the downstream conditions. Once a nozzle is choked, the Mach number at the throat attains a value of unity. Once the Mach number at the throat is unity, no downstream signals propagating at the local acoustic speed can cross the throat section and move upstream. Consequently, the demands at a downstream section are not felt upstream. The flow up to the throat remains unaltered thus. The flow rate then depends on the upstream stagnation pressure, stagnation temperature and the throat area. Figure 4.3 illustrates these concepts.

The dependence of the mass flow rate through a choked nozzle on various parameters is an important aspect of understanding the flow process through a nozzle. Flow through (a) stators and rotors of turbine section, (b) nozzles of supersonic aircraft, (c) ramjets and scramjets, and (d) all rocket engines will be choked. The mass flow rate is related to the stagnation conditions ahead of the nozzle entry section and thermodynamic properties of the fluid.

In analyzing the flow through the nozzle, it is recognized that the flow is one in which pressure decreases from the nozzle entry section to the exit and therefore the flow experiences favorable pressure gradient. This implies that viscous effects expressing through the formation of boundary layer are small and a very good approximation to the predictions can be obtained by assuming the flow to be inviscid.

The short residence time of the fluid in the nozzle (compared to conduction time or better, heat transfer time through the nozzle hardware) allows the wall heat transfer effects to be ignored. The assumption of one-dimensional flow will also be invoked as already indicated. Two dimensional effects are important in (a) rectangular nozzles used sparingly in aircraft engines and (b) large area and large area ratio axisymmetric nozzles used in booster class rocket engines operating at high altitudes; yet the results of one-dimensional approximation offer a fairly accurate representation of overall results. The flow through the nozzle is therefore taken as isentropic and one-dimensional.

The mass flow rate is expressed by $\dot{m} = \rho_{th} A_{th} V_{th}$ where the subscript th refers to throat, ρ, A, V refer to the density, throat area and velocity of the fluid at the throat. The throat area is the geometric minimum cross section along the fluid path. In most cases where an axisymmetric or two dimensional geometry is used, the minimum cross section normal to the axis is the appropriate value. In some cases, there will be a central plug that is axisymmetric that controls the effective throat area. In this case, the flow undergoes a turn and the "aerodynamic throat" may not be the same as the "geometric throat". This will lead to differences that need to be kept in mind while reconciling the experimental data with theoretical results. The above expression for the mass flow is written as

$$\dot{m} = (\rho_t/\rho_{th,t})\rho_{th,t} A_{th} (V_{th}/a_{th}) \sqrt{\gamma R (T_{th}/T_{th,t})} \sqrt{T_{th,t}} \tag{4.28}$$

In the above equation, the density is normalized by the stagnation density, and the velocity by the local acoustic speed with the acoustic speed expressed in terms of temperature (see equation 4.12) that is again normalized by stagnation temperature. The stagnation temperature and pressure are constant through the nozzle due to isentropicity of the flow. The stagnation pressure is usually obtained after measuring the wall static pressure at the inlet region that has low Mach number. For this reason, the stagnation conditions are referred to as "chamber" conditions - conditions just ahead of the nozzle entry. The word "chamber" is appropriate only in the case of rocket nozzle, as the region upstream of the nozzle is the chamber carrying solid or hybrid fuel in the port ducts of which combustion takes place or is directly the combustion chamber as in liquid rockets. Thus

$$\dot{m} = (\rho_{th}/\rho_{c,t})\rho_{c,t} A_{th} (V_{th}/a_{th}) \sqrt{\gamma R (T_{th}/T_{c,t})} \sqrt{T_{c,t}} \tag{4.29}$$

where the subscript c refers to chamber conditions. We recognize that V_{th}/a_{th} is M_{th} = 1 because the throat is choked. We can now invoke the isentropic relations between the static and stagnation conditions (see section 4.2.5) and obtain after some algebra,

$$\dot{m} = A_{th}\rho_{c,t}\sqrt{\gamma R}\sqrt{T_{c,t}}\left[\frac{\gamma+1}{2}\right]^{-\frac{1}{\gamma-1}}\left[\frac{\gamma+1}{2}\right]^{-\frac{1}{2}} \tag{4.30}$$

We invoke the equation of state $\rho_{c,t} = p_{c,t}/RT_{c,t}$ in the above equation and write

$$\dot{m} = \frac{p_{c,t}A_{th}}{c^*} \tag{4.31}$$

with

$$c^* = \sqrt{RT_{c,t}}/\Gamma(\gamma) = \sqrt{\frac{\mathscr{R}T_{c,t}}{\mathscr{M}}}/\Gamma(\gamma) \tag{4.32}$$

where

$$\Gamma(\gamma) = \gamma^{\frac{1}{2}}\left[\frac{2}{(\gamma+1)}\right]^{(\gamma+1)/2(\gamma-1)} \tag{4.33}$$

In the equation (4.32), c^* is called the characteristic velocity in rocket engine literature. The variation of $\Gamma(\gamma)$ is as follows: 0.628 (at γ = 1.1), 0.6485 (at γ = 1.2), and 0.6735 (at γ = 1.3), 0.6862 (at γ = 1.4), and 0.7164 (at γ = 1.6). The values of $\Gamma(\gamma)$ can be simply correlated to a high degree of accuracy as $\Gamma = 0.61+0.177(\gamma-1)$. It is appropriate to recognize the range of the values of γ in different situations. The value of γ in the turbine section is 1.3 to 1.35, at the entry to the nozzle of an afterburning turbojet, 1.2 to 1.25, at the entry to a rocket nozzle, 1.15 to 1.2. This is simply due to the range of temperatures experienced in these cases. In rocket engines, the chemical components of the fluid also influence the value of γ.

The equation for mass flow rate is usually expressed as $\dot{m} = p_c A_t/c^*$ in traditional rocket engine literature with the usual understanding that p_c as the stagnation pressure at the entry to the nozzle and A_t as the throat area.

4.3 Relationship of c^* with I_{sp}

For a rocket engine, the thrust equation is given by equation (1.6) as $F = \dot{m}V_e + A_e(p_e - p_a)$. Since $I_{sp} = F/\dot{m}$, one gets $I_{sp} = V_e + A_e(p_e - p_a)/\dot{m}$. If we now use the expression for $\dot{m}$ from equation (4.31), we can rewrite the equation for I_{sp} as

$$I_{sp} = V_e + c^*\frac{A_e}{A_t}\left[\frac{p_e}{p_{c,t}} - \frac{p_a}{p_{c,t}}\right] \tag{4.34}$$

In the above equation, the last term changes if the vehicle flies into the atmosphere and the ambient pressure keeps decreasing. The term $p_e/p_{c,t}$ will decrease with increase in A_e/A_{th} since this increase allows greater expansion of the fluid. It is possible to choose A_e/A_{th} such that $p_e = p_a$. In such a case, one obtains optimum

expansion. If the flight occurs in space with hard vacuum, the expansion of the fluid is limited to that allowed by the chosen A_e/A_{th}. Thus, we now need to obtain a relationship for V_e and A_e/A_{th}. The exit velocity, V_e is obtained from the energy equation as

$$V_e^2 = c_p(T_{c,t} - T_e) \tag{4.35}$$

The above equation assumes constant specific heat (the right hand side is to be replaced by $(h_{c,t} - h_e)$ for variable properties). Using isentropic relations, the temperatures can be connected to pressures. This leads to

$$V_e = \sqrt{\frac{c_p}{R} R T_{c,t} \left[1 - (p_e/p_{c,t})^{\gamma/(\gamma-1)}\right]} \tag{4.36}$$

which can be further written as

$$V_e = c^* \Gamma(\gamma) \left[\frac{\gamma}{(\gamma-1)}\right]^{1/2} \sqrt{\left[1 - (p_e/p_{c,t})^{\gamma/(\gamma-1)}\right]} \tag{4.37}$$

If we now set $\dot{m} = p_{c,t} A_{th}/c^* = \rho_e A_e V_e$ as required by one-dimensional mass conservation relation, and perform some algebra, we get

$$\frac{A_e}{A_{th}} = \frac{(p_{c,t}/p_e)^{1/\gamma}}{\left[\frac{\gamma}{(\gamma-1)}\right]^{1/2} \sqrt{\left[1 - (p_e/p_{c,t})^{\gamma/(\gamma-1)}\right]}} \tag{4.38}$$

The above equation can be used to obtain the exit-to-throat area ratio if the ratio of exit pressure to chamber pressure is known or vice-versa. For optimum expansion, p_e is set equal to p_a and the area ratio is obtained from the above equation. Or if the area ratio is fixed, one obtains the pressure ratio by an iterative calculation.

By combining equations (4.34) and (4.37) we can write I_{sp} = $c^* c_F$, where c_F is called the thrust coefficient expressed by

$$c_F = \Gamma(\gamma) \left[\frac{\gamma}{(\gamma-1)}\right]^{1/2} \sqrt{\left[1 - (p_e/p_{c,t})^{\gamma/(\gamma-1)}\right]} + \frac{A_e}{A_{th}} \left[\frac{p_e}{p_{c,t}} - \frac{p_a}{p_{c,t}}\right] \tag{4.39}$$

In the above equation, the second term on the right hand side can be obtained using the equation (4.38). For the case of $p_e = p_a$, the second term in the equation (4.39) drops off and the value of c_F is denoted by c_F^0.

By invoking the expression for $\dot{m}$ from equation 4.31, the equation $F = \dot{m} V_e + A_e(p_e - p_a)$ can be rewritten as

$$F = p_{c,t} A_{th} [(V_e/c^*) + (A_e/A_{th})(p_e - p_a)/p_{c,t}] \tag{4.40}$$

The quantities in the square brackets on the right hand side are non-dimensional. The quantity A_e/A_{th} is related to $p_e/p_{c,t}$ and decided by the designer based on the maximum value to be allowed or obtaining optimum expansion whichever is critical for the mission. Hence, one can write $F = c_F p_{c,t} A_{th}$ or in classical rocket engine terminology $F = c_F p_c A_t$, where c_F is given by equation (4.39). Since c_F connects thrust to a force $p_{c,t}A_{th}$, it is called a thrust coefficient. The three major equations of nozzle flow very important for rocket engines are

$$\dot{m} = F/I_{sp} \tag{4.41}$$
$$\dot{m} = p_{c,t}A_{th}/c^* \tag{4.42}$$
$$F = c_F p_{c,t} A_{th} \tag{4.43}$$
$$I_{sp} = c^* c_F \tag{4.44}$$

We can now discuss the significance of the quantities in the above equations.

If one is designing a rocket engine for a given thrust, one can reduce the mass flow rate by increasing the specific impulse. This conclusion interpreted for air breathing engines is - increased I_{sp} implies reduced sfc, indicating reduced propellant flow rate for the same thrust.

To pass a fixed flow rate through a given nozzle, enhanced c^* allows the choice of higher stagnation pressure that implies realization of larger c_F as can be inferred from equation (4.39). This implies higher I_{sp}.

The expression for specific impulse is composed of two terms – $c^* \sim \sqrt{\mathscr{R}T_{c,t}/\mathscr{M}}$ (from equation (4.32)) and c_F. It is important to note that the characteristic velocity varies as the square root of the ratio of the adiabatic flame temperature to the average molecular weight of the gases and depends on the propellant characteristics largely. Both these quantities vary depending on the propellant combination. Some typical data are presented in Table 4.1. Larger values of c^* are obtained by raising the combustion temperature or by reducing the molecular weight of gases. While in the case of solid propellants, the former method is used, in the case of cryogenic liquid oxygen - liquid hydrogen system, reduction in molecular weight is responsible for the enhancement; in fact the largest values of c^* are obtained for this system.

The second factor that influences the specific impulse is the thrust coefficient. It is dependent very significantly on the nozzle characteristics - the area ratio and the geometry (this is not clear from the equation (4.39) since two-dimensional effects not covered in this equation come into play) and the connection to the propellant is through γ. For this reason, specific impulse is understood to be a function of the propellant (through c^*) and the nozzle (through c_F). This principal decomposition of influence helps understanding and design of the propulsion system. When

Table 4.1: Flame temperature and Molecular weight of gases

Propellant	$T_{c,t}$ K	$\mathscr{M}$ g/mole	c^* km/s
Double Base Solid	2400 - 2700	23 - 26	1.5 - 1.6
Composite Solid	3300 - 3600	24 - 26	1.7 - 1.8
Hydrazine Liquid monopropellant	1000 - 1300	12 - 15	1.2 - 1.4
Storable Liquid bipropellant	3000 - 3400	22 - 24	1.7 - 1.9
LOX - LH_2 Cryo-liquid system	3000 - 3400	12 - 15	2.3 - 2.5
Turbojet afterburner	1900 - 2100	28 - 29	1.2 - 1.3

the specific impulse of a propellant is spoken about, it is usually understood that the thrust coefficient is held constant through the choice of p_e and $p_{c,t}$. By requiring that the flow be optimally expanded, $p_e = p_a$, and values for p_a = 1 atm. and a chosen value of $p_{c,t}$ (typically, 70 atm.), the values quoted for I_{sp} will be virtually dependent only on the propellant. The value so obtained will be useful for assessing rocket engines operating within the atmosphere - lower stages of launch vehicles/strategic missiles and tactical missiles. As apart from this, for rocket engines and thrusters working in space, the ambient pressure can be taken as 0 and the equation for thrust becomes $F(vac) = \dot{m}V_e + A_e p_e$ that can be translated to $I_{sp,vac} = V_e + c^*(A_e/A_{th})(p_e/p_{c,t})$. Since the choice of A_e and A_{th} are made in the design, and use of equation (4.38) gives $p_e/p_{c,t}$, one can obtain the specific impulse at space operating conditions. This is termed vacuum specific impulse. Its value is about 10 to 15 % higher than sea level specific impulse.

The dependence of c_F on A_e/A_{th} and $p_a/p_{c,t}$ is presented in Figures 4.4 and 4.5. These are instructive. It can be noted from Figure 4.4 that the value of optimum c_F increases from 1.2 at area ratios of 2 and pressure ratios of 10, to 2.0 at area ratios of 200, pressure ratios of 10,000 for γ = 1.2. The influence of γ is substantial. In reality, the flow through the nozzle has varying composition since pressures and temperatures keep decreasing allowing the equilibrium to keep shifting; typically γ can change by 3 to 5 % while flowing through the nozzle. For this reason, nozzle performance is obtained by using a rigorous approach in which these variations are taken into account. Figure 4.5 shows the results for expansion that could be also non-optimal. For any given pressure ratio, the thrust coefficient has a peak at one area ratio. For instance for γ = 1.2, and $p_a/p_{c,t}$ = 50, c_F takes on a maximum value of 1.56 at A_e/A_{th} = 7. At this condition, the expansion is optimal, i.e. p_e = p_a. On either side of this area ratio, c_F drops off. Larger area ratio implies higher expansion and lower exit plane pressure (p_e). For the same p_a, this implies over-expansion. Similarly for nozzles shorter than for optimal condition, the exit plane pressure is higher than the ambient pressure and and hence, one obtains

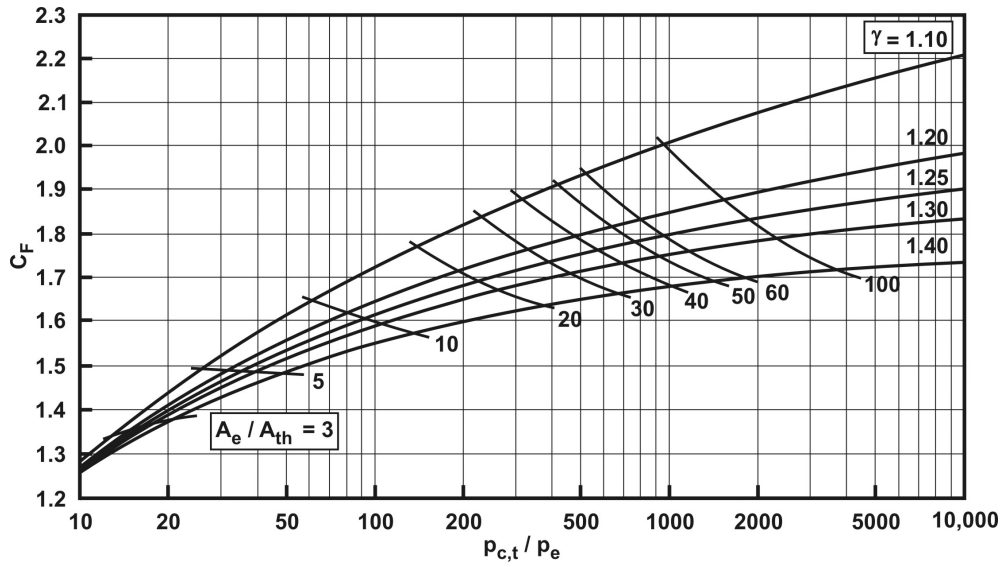

Figure 4.4: Thrust coefficient as a function of various parameters for optimum expansion, $p_e = p_a$

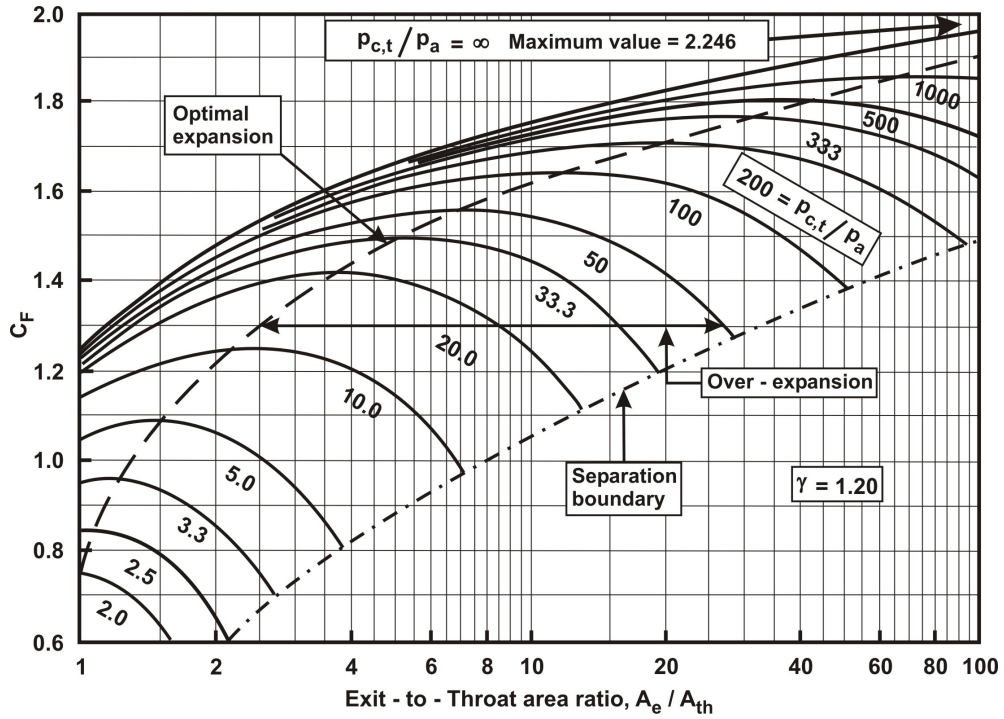

Figure 4.5: Thrust coefficient as a function of the ratio of exit-to-throat area for γ = 1.2

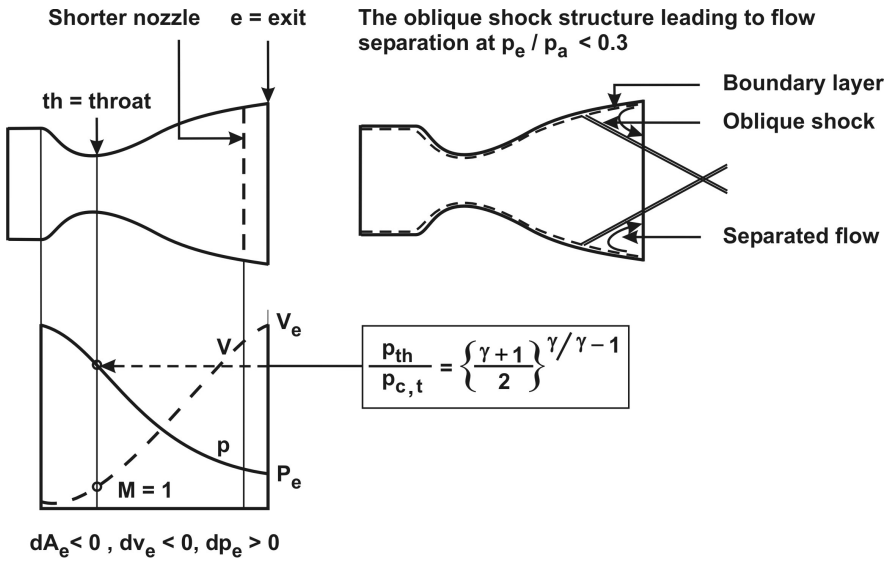

Figure 4.6: Wall static pressure distribution along the nozzle and the behavior at large over-expansion

under-expansion. Thus, the left side of the dotted curve for optimal expansion constitutes under-expansion and right side constitutes over-expansion. There is a limit to over-expansion as indicated by the lower dotted line. To appreciate this, we need to examine the flow through the nozzle. Figure 4.6 shows the distribution of wall static pressure through the nozzle.

The static pressure decreases from the chamber to the exit plane monotonically (in actuality, there could be a small kink (increase in pressure) at the throat resulting from waves near the entry to the throat converging to a zone just aft of the throat) and the velocity increases similarly. The exit plane pressure can be greater than, equal to or lower than the ambient pressure. If the nozzle is shortened, the exit plane pressure is larger, velocity smaller. This is indicated by the inequalities in the figure. If the exit plane pressure is smaller than the ambient pressure, a shock wave is located at the edge of the nozzle to cause a pressure rise to the ambient value. The wall boundary layer then has to negotiate the pressure gradient caused by the shock. Until a certain pressure ratio, the flow will remain smooth. However, below a certain pressure ratio, typically p_e/p_a < 0.3, the flow cannot withstand the pressure rise and it breaks down as shown in Figure 4.6. The separation region within the nozzle leads to very unsteady pressure distribution over the nozzle. This is an undesirable operating condition for the nozzle and is avoided.

The interesting feature of the curve that optimum thrust is generated for $p_e = p_a$ can be demonstrated very simply as follows. Using the momentum equation

$dp/\rho + VdV = 0$ can be set out as $Adp + \rho AVdV = 0$ after multiplying by A, the local cross sectional area. The mass conservation relation $\dot{m} = \rho AV$ is used to rewrite the momentum equation as

$$Adp + \dot{m}dV = 0 \tag{4.45}$$

We have $F = \dot{m}V_e + A_e(p_e - p_a)$. We now take a differential of this equation and equate it to 0 to obtain the optimal condition. This gives

$$dF = 0 = d(\dot{m})V_e + \dot{m}dV_e + (dA_e)(p_e - p_a) + A_e[d(p_e) - d(p_a)] \tag{4.46}$$

Now, we recognize that

$$d(\dot{m}) = d(p_a) = 0 \tag{4.47}$$

as both $\dot{m}$ and p_a are constants. When A_e increases, p_e decreases and V_e increases, according to the momentum equation just noted above. Invoking it by subscripting the quantities by e as

$$A_e dp_e + \dot{m}dV_e = 0 \tag{4.48}$$

we get

$$dF = 0 = dA_e(p_e - p_a) \tag{4.49}$$

Since $dA_e \neq 0$, $p_e = p_a$ for optimal condition. If we take the second derivative to determine if the optimum is a maximum, we get

$$d^2F = d^2A_e(p_e - p_a) + dA_e dp_e = dA_e dp_e \quad \text{at} \;\; p_e = p_a \tag{4.50}$$

Since $dA_e > 0$ implies $dp_e < 0$, it follows that $dA_e dp_e$ is always < 0. *Hence, the optimal condition $p_e = p_a$ leads to a maximum in thrust.*

4.4 The Nozzle Shape

Two classical shapes that have been used are: (a) conical and (b) contour. The conical nozzle is simple to conceive and manufacture. The conical angle that is used is limited by the losses involved in the divergence. The flow stream lines are conical in nature and the fluid has a velocity component normal to the axis. The maximum normal velocity is for the stream lines along the wall. Since what contributes to the thrust of the engine is the axial component of the momentum and the normal momentum gets canceled due to symmetry, the divergence loss is a function of the divergence angle. This is estimated as follows.

If we extend the conical section backwards to a center from which we draw the part of a sphere to go through the edge of the nozzle, we can a take a cylindrical segment at an angle ϕ which varies from 0 to α, the semi-cone angle of the nozzle, we can write

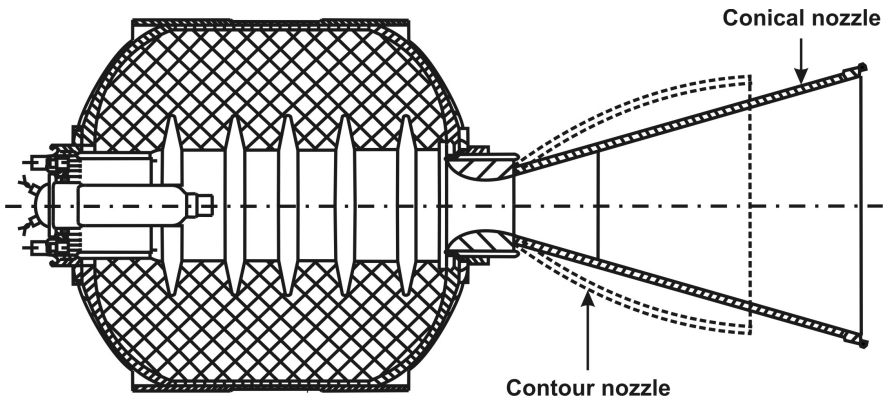

Figure 4.7: The nozzle shapes - conical and contour shapes located on a rocket motor

$$d\dot{m} = \rho_e V_e (2\pi R sin\phi)(Rd\phi) \tag{4.51}$$

This gives

$$\dot{m} = 2\pi R^2 \rho_e V_e \int_0^{\alpha} sin\phi d\phi \tag{4.52}$$

The thrust is obtained as

$$F = 2\pi R^2 \rho_e V_e^2 \int_0^{\alpha} sin\phi cos\phi d\phi \tag{4.53}$$

By combining the above two equations we get,

$$F = \dot{m} V_e \frac{(1 + cos\alpha)}{2} \tag{4.54}$$

For a typical value of $\alpha = 15^{\circ}$, the reduction of thrust due to divergence is 1.7 %. Though this appears like a small value, in view of any clear benefit to be taken advantage of, attention is paid to it. Contour nozzles shown in Figure 4.7 provide for reduced exit angles and hence, reduced divergence losses. The principal features of a contour nozzle are that: (a) provide for a large expansion near the throat (to the extent of 40°), (b) smoothen this contour into a bell shape with continued decrease of the exit angle, (c) the actual shape arranged in such a manner that expansion waves generated from the sharp expansion in the early stage cancel the weak compression waves from the downstream bell shaped zone so that the non-isentropic effects are brought down. Typical nozzle divergence angles are 5 - 7°. The advantage of such a shape, even more important than the increased performance, is the reduction in the nozzle length. It is typically 70 to 75 % of a conical nozzle for the same area ratio (A_e/A_{th}). This reduces the weight of the nozzle, a factor that is very important for upper stages of launch vehicles or strategic missiles. The special emphasis on upper stages is derived from the result that in a

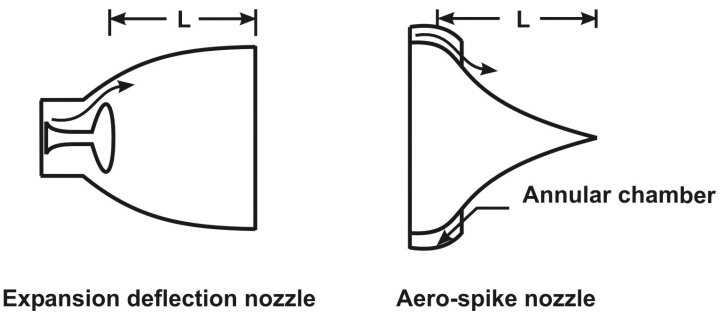

Figure 4.8: The expansion deflection and aero-spike or plug nozzle

multi-stage vehicle, any performance improvement in the first stage onwards will have increasingly larger influence on the payload capability of the vehicle. Hence, the use of contour nozzles may be debatable for the lower stages, but considered mandatory for upper stages. As different from the above two classical shapes used very extensively in most engines built till now, two more concepts considered important are the expansion deflection and aero-spike designs. The shapes of these nozzles are shown in Figure 4.8. In both these cases, the flow through the nozzle occurs in annular zone. They are considered useful as they adapt to variation in altitude better than the earlier designs. Much research has been conducted and their use in actual vehicles is yet to be seen.

4.5 Thrust Generation Process and the Nozzle

In all propulsion systems, it is understood that the nozzle is responsible for producing the thrust. Its role is simple to appreciate in the case of a rocket engine; it becomes subtler as we move towards a ramjet and turbojet. It is also clear that all propulsion systems create an exit jet speed higher than the flight speed leading to a positive momentum flux across the engine and hence, generate a force termed thrust. Another way of interpreting the thrust generation process is that it is the integral of the difference in pressure across the wall of the engine. This way of understanding the thrust generation process is insightful and is presented now for rocket engines first, ramjet next and a turbojet engine.

Figure 4.9 presents the pressure distribution in a typical rocket engine. The thrust can be obtained as the sum of (a) the positive force over the back wall, AB - difference between the chamber pressure and the ambient times the cross sectional area bounded by AB, (b) the negative force integrated over CD – the difference between the local pressure and the ambient multiplied by the difference in cross sectional area between the chamber and the throat, and (c) the positive

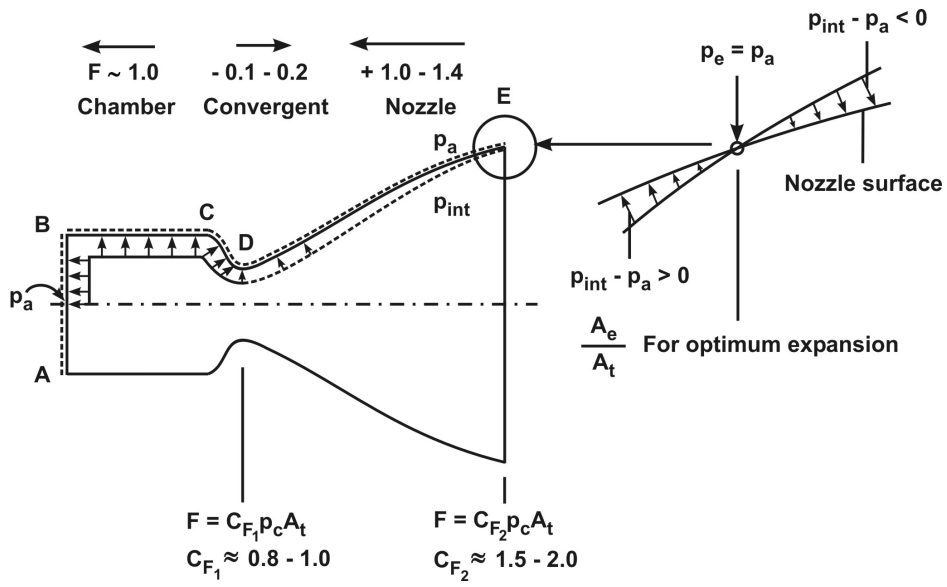

Figure 4.9: Thrust generation process in a rocket thrust chamber. Notice that the back wall and the divergent contribute to positive force and the convergent to negative force. The net is positive. Notice that the thrust up the throat region is also positive; but larger contribution comes from the divergent section due to expansion from relatively large pressures even at the throat section.

force obtained from integrating the the difference between the inner wall pressure and the ambient over the divergent surface of the nozzle. In the case of (b), it must be understood that the wall pressure keeps falling from $p_c = p_{c,stag}$ to a value 52 to 56 % (1/1.892 to 1/1.77 depending on γ between 1.4 and 1.2) from the chamber to the throat and this variation is helpful in reducing the negative contribution. In the case of (c), the wall pressure keeps reducing and can be slightly higher, equal to or less than the ambient pressure depending on the exit area chosen. As shown in the top corner of Figure 4.9, the condition $p_e = p_a$ refers to optimum expansion. Shorter nozzle leads to under-expansion and longer one over-expansion. Using under-expansion implies that additional force is remaining unused and over-expansion can be noted as beginning to contribute negatively to thrust generation. The magnitude of the different components in a well designed rocket nozzle is presented as arrows with the magnitude of the components of forces. The chamber and the divergent contribute about equal amounts and the convergent segment contributes negatively about 5 to 10 %.

We can now consider a ramjet engine. Figure 4.10 shows two cases of the flow and pressures – (i) without and (ii) with combustion.

The flow is considered inviscid. In case (i), the flow decelerates in the intake,

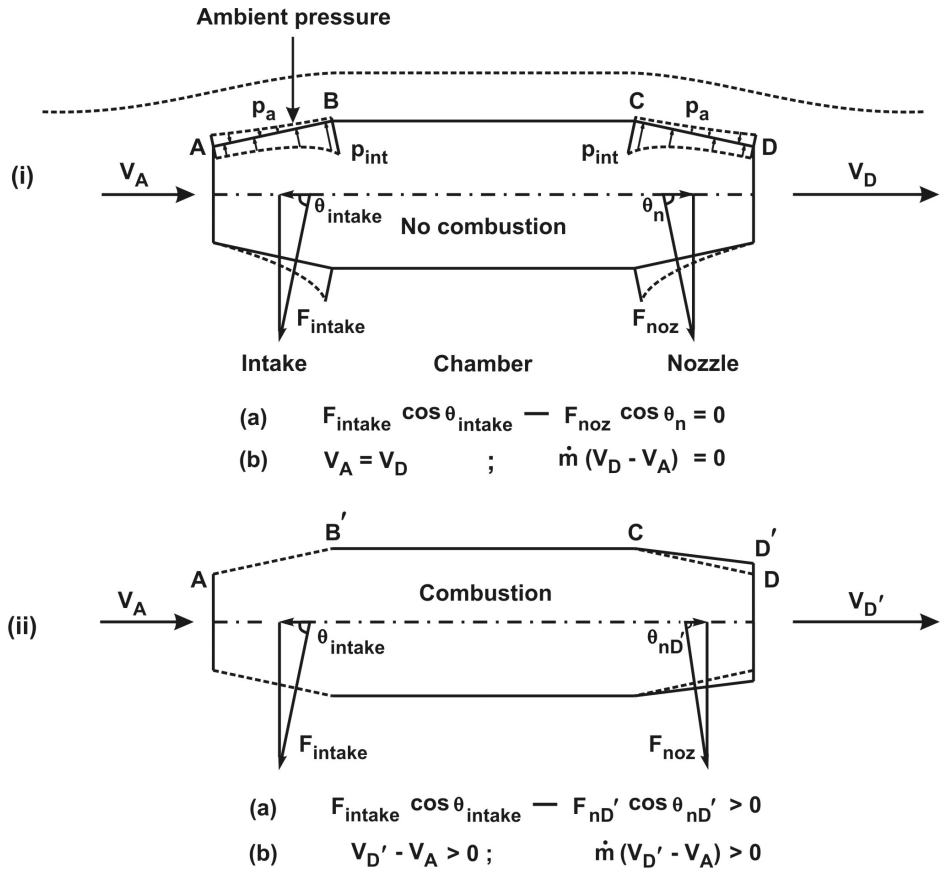

Figure 4.10: The thrust generation process in a ramjet. Section (i) without combustion has equal forces generated by the intake section and the nozzle in the ideal case. The nozzle insection (ii) with combustion generates lesser negative force and hence, contributes to thrust(!)

flows through the chamber without combustion and accelerates through the nozzle section before coming out of the nozzle. The inflow and exit velocities are V_A and V_D and in the ideal case $V_D = V_A$. We now examine the wall pressures. The flow outside the air intake is accelerating and hence, the wall static pressure drops over the intake (along AB). The reverse happens on the outer surface of the nozzle (along CD). The flow inside the diffuser decelerates the flow and the local pressure will be

$$p_{local} = p_a + \rho_a V_A^2/2 - \dot{m}_a^2/2\rho A^2 \tag{4.55}$$

where p_{local} and p_a are the local and ambient pressures and ρ_a is the density, V_A = flight speed, $\dot{m}_a$ = mass flow rate of the air, A_l = local cross sectional area. The wall pressure increases as the diffuser cross section increases (note the steep dependence due to the square of the area term). At the nozzle end, similar behavior is repeated. The difference between the inner and outer wall pressures is shown the lower part of the figure for case (i). The integrated force is represented as F_{intake} and F_{noz} acting normal to the surface. The horizontal components are $F_{intake}cos\theta_{intake}$ and $F_{noz}cos\theta_n$. The chamber does not contribute to any force in the axial direction (because of ideal flow). The net force is therefore $F_{intake}cos\theta_{intake}$ - $F_{noz}cos\theta_n$ = 0 due to symmetry. Now let us take the case with combustion - case (ii). In this case, due to combustion, the stream temperature through the nozzle will be higher and stream density will be lower ($\rho_{exit} < \rho_a$). To maintain the same pressure balance through the exit region as well (a requirement that is imposed to ensure that upstream flow remains the same with or without combustion), the exit area is to be increased such that $\rho_{exit}A_l^2$ is maintained the same, as can be inferred from the equation (4.55). This implies that $A_l \sim 1/\sqrt{\rho_{exit}}$. To pass the same flow through the system (assuming that the fuel fraction is very small, as is true in reality), $V_{D'} \sim 1/\sqrt{\rho_{exit}}$. This leads to $V_{D'} > V_A$.

Now, we examine the forces on the surfaces. Even assuming that the wall pressures are the same, the fact that the nozzle is opened up leads to a shallower nozzle shape compared to the intake shape. This leads to $\theta_{nD'} > \theta_n$, and so $F_{intake}cos\theta_{intake}$ - $F_{noz}cos\theta_{nD'} > 0$. Thus, the nozzle area change because of combustion reduces the negative force created by the nozzle and this causes a forward thrust.

There are departures from the above analysis in reality. The frictional force over the surfaces both inside and outside the duct will create drag, an additional negative force. Thus, the geometry in Figure 4.10 results in drag - one needs to move it with additional force to maintain the condition indicated in the figure. Further, the pressure at the end of the combustion process will be affected by heat addition. This will reduce the mass flow through the system and therefore the thrust generated.

One might argue that we can introduce objects like flame holder inside the combustion chamber and these will reduce the pressures downstream over the

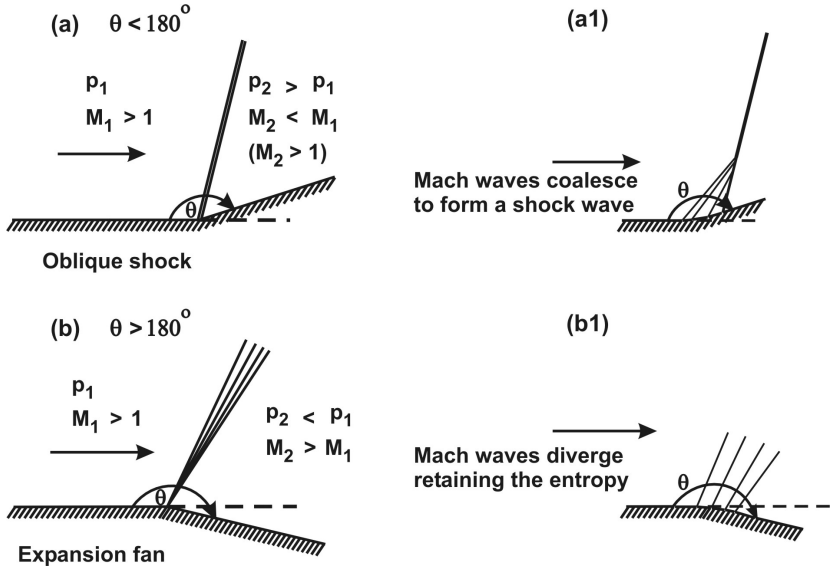

Figure 4.11: The flow structure at a compression corner and an expansion corner

nozzle and hence, reduce the negative force. Two important departures occur. The drag on the flame holder will need to be added to the negative force. The reduced stagnation pressure downstream of the flame holder will reduce the flow rate through the system and hence, thrust generated.

In the case of a gas turbine engine, the approach to clearly delineate the zones where the axial forces are created is far more complex since the forces are created due to surfaces including those of stationary and rotating blades. What is clear is that the nozzle segment produces a negative force like in the earlier case. The turbine produces a negative force as well. It is the compressor that generates a large positive force; Combustor can also produce a significant positive force. It is this combination that overcomes the negative components of the nozzle and the turbine leading to a net positive thrust. The relative distribution of forces depends strongly on the design of the gas turbine engine, but the principal elements contributing to the positive and negative forces are the ones described above.

4.6 The Gas Dynamics of the Exit Plume

The pressure in the combustion chamber of a rocket engine increases to the full value in 100 ms to a few seconds depending on the size of the engine. In all rocket motors whose start-up occurs within the atmosphere, the ratio of chamber-to-ambient pressure increases from unity to a large value (50 – 200). This implies

that p_e/p_a increases from very low values to the design value. In the early stages the nozzle will experience over-expansion; this is true of every rocket engine. The question is for how long and with what impact. In most cases, the transition is over in 30 ms for small tactical engines and about 0.5 s for large engines. Hence, the impact is little. Engines designed and built for high altitudes have to be tested at the sea level altitude conditions. In this case, the engine will experience unacceptably low p_e/p_a. To deal with this problem, high altitude test chamber with adequate preparation to ensure low enough pressure at the nozzle exit or relatively simple ejector based test facility is created.

As the rocket engine accelerates to higher altitudes, the ambient pressure keeps falling. Depending on the design condition considered, the engine may start with over-expansion, move through complete expansion to under-expansion. If the vehicle has clustered engines, the jet plumes can interact and (a) modify the base pressure and alter the drag on the vehicle, and/or (b) affect the heat transfer in the base section. If the engine were to be a thruster for a satellite, it will always experience under-expansion and under these conditions, the jet expansion can occur to an extent of being normal to the jet axis in the initial stage. Hence, it is useful to understand the behavior of the jet plume. To do this, we examine Figures 4.11 (a) and (b) that show the behavior of a stream meeting a corner taking a turn less and more than 180° respectively. In the first case, the flow is compressed. An oblique shock is located at the corner downstream of which the *Mach number is lower and static pressure higher*. This is understood by examining the behavior of the flow at the corner. We split the change in direction to a large number of small changes, as shown in the Figure 4.11 (a1). Each small change of direction causes a small wave to be created. These waves coalesce because of the change in the direction of the wall and form a strong compression wave or a shock. As different from this, for the case where the flow turns beyond 180°, the flow expands. In this case, as shown in Figure 4.11 (b1), the waves do not meet. Hence, each wave with small change remains isentropic and the flow expands to *higher Mach number and lower static pressure* unlike in the previous case.

Figure 4.12 shows the behavior of the jet after it leaves the nozzle exit plane for both under-expansion as well as over-expansion. Let us first consider the case of under-expansion - Figure 4.12 (a). It can be noticed that since the exit plane pressure is higher than the ambient pressure, an expansion fan will result. The turn that the flow will undergo is set by requiring that the pressure in section (ii) be equal to the ambient pressure since there can be no pressure difference across a free jet. Since the jet is axisymmetric, the expansion fan follows a conical path and the flow undergoes additional expansion as shown in the Figure 4.12, section (iii). Because this diamond looking section experiences a pressure lower than the ambient, there will be a pressure rise through an oblique shock to the extent that the static pressure in section (iv) is the ambient. From this point onwards, the flow structure will repeat. Fluid viscous effects will cause additional deceleration. Nev-

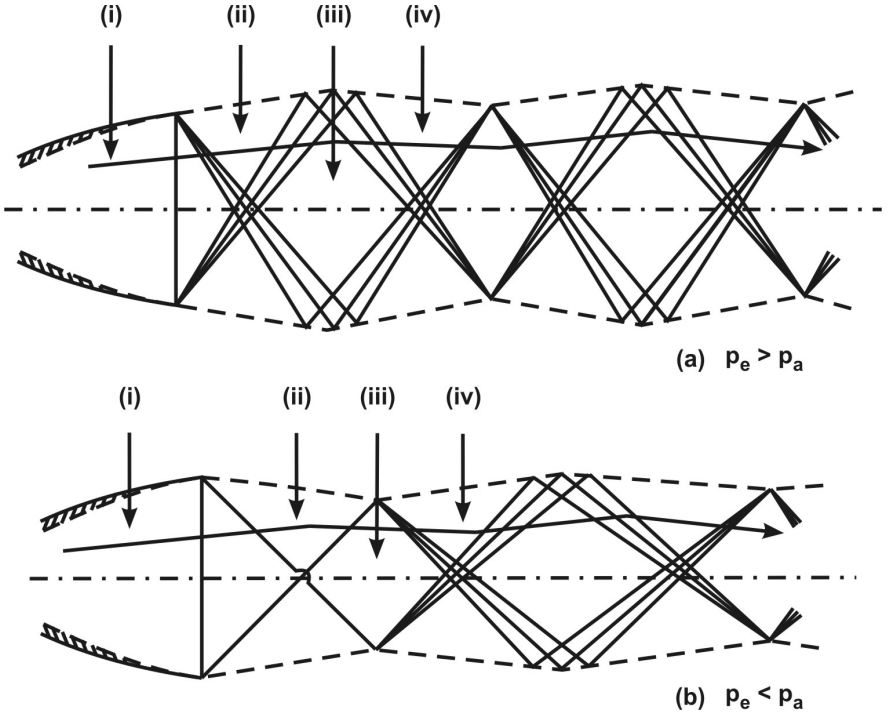

Figure 4.12: The flow structures from a nozzle exit - (a) under-expansion and (b) over-expansion

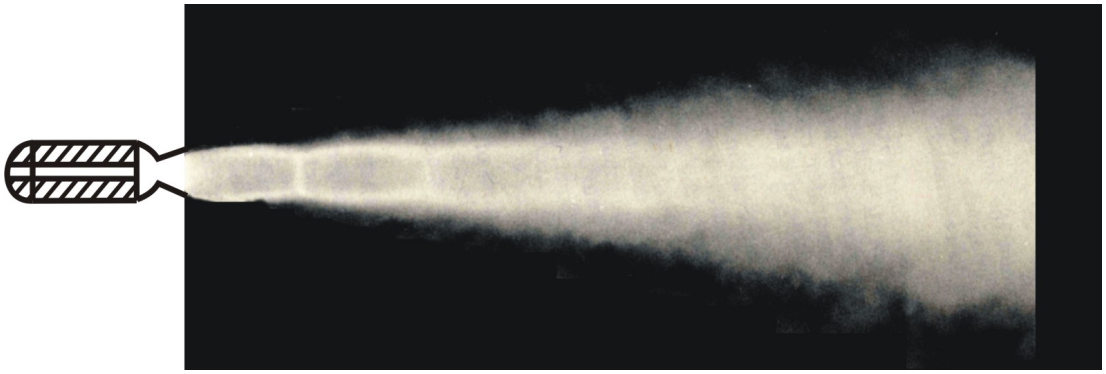

Figure 4.13: A photograph of a nozzle exhaust plume indicating the periodic shock diamonds

ertheless, the zones where shocks are present will present themselves as higher temperature zones and one will be able to notice the shock diamonds as they are called; they can be seen in the photograph [Figure 4.13]. The flow structure will remain supersonic till a point when a normal shock occurs along the flow and the subsequent flow will be subsonic.

In the case of over-expansion, the first set of waves would be oblique shocks and the subsequent flow behavior after this event can be argued along the lines noted earlier. These flows can be captured through computational fluid dynamic tools.

4.6.1 Importance of $\mathrm{p_{c,t}}$ in Rocket Engines

The relationship $F = c_F p_{c,t} A_{th}$ can be used to derive significant conclusions on the importance of the choice of $p_{c,t}$. The choice affects the solid and liquid rocket engines differently. In the case of solid rocket engine, the motor size is related to the amount of propellant to be loaded, its volumetric loading being decided by the design and the burn time. Its size is substantive in most applications. In comparison to the motor size, the nozzle could look small or smaller than the chamber carrying the propellant. In the case of liquid engine, the storage of propellants is separated from the thrust chamber which is a combination of the combustion chamber and the nozzle. The nozzle may look larger than the combustion chamber. Increased value of $p_{c,t}$ increases the solid rocket motor casing thickness and weight. In the case of liquid engine, it can reduce the dimension of the thrust chamber substantially. The size of the nozzle is determined from $A_{th} = F/c_F p_{c,t}$. Increase of $p_{c,t}$ by a factor of four (say from 50 atm., as is classically used, to 200 atm. as in the case of space shuttle main engine) decreases the throat diameter by a factor of 2. This reduces the size of the combustion chamber also similarly. A typical comparison presented in Figure 4.14 shows the two geometries. The reduced sizes at high pressure will decrease the cooling area substantially and even though heat transfer problem becomes more acute at higher pressure, the degree is smaller than the benefit obtained by the reduction in cooling area (the total peripheral area). This effect is not so significant for solid rocket engine since the rocket casing that is substantive in volume in large thrust – long burn motors; the reduction in the nozzle size could be offset by the increase in motor casing weight. Typical solid rocket thrust chambers operate at pressures of 50 to 60 atm. High performance liquid engines could have combustion chamber pressures of as high as 200 atm.

4.6.2 The Rayleigh Process

Energy addition into a duct (of constant area, for instance) causes drop in stagnation pressure essentially because of reduction in the density which leads to in-

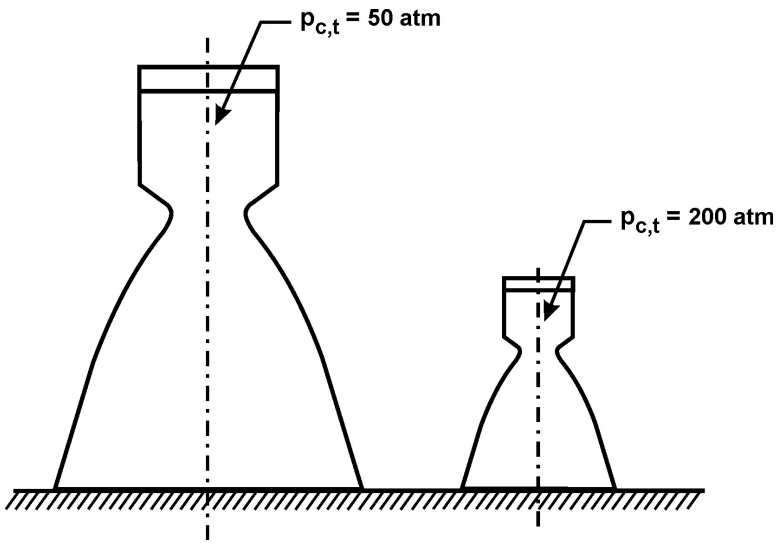

Figure 4.14: Schematic of two liquid rocket thrust chambers (combustion chamber + nozzle) at chamber pressures of 50 atm. and 200 atm. Notice the reduction in size at high pressures

crease in velocity which further leads to increase in momentum due to the kinetic component. Momentum conservation then leads to loss in stagnation pressure. This loss can be high at high levels of energy addition, typical of ramjets and less so in the case of turbojets. It is an ideal phenomenon in the sense that its origin does not involve viscous and heat conduction phenomena usually responsible for loss in stagnation pressure. Its analysis is based on the conservation equations $4.1-4.3$ with the energy equation written down to take account of energy addition.

If stations 3 and 4 are taken to represent inlet and exit of a combustor (where energy addition takes place), the equations are

$$\rho_3 V_3 \;=\; \rho_4 V_4 \tag{4.56}$$

$$p_3 \;+\; \rho_3 V_3^2 \;=\; p_4 \;+\; \rho_4 V_4^2 \tag{4.57}$$

$$c_p T_{t3} \;+\; Q_f \;=\; c_p T_{t4} \tag{4.58}$$

$$p \;=\; \rho\, R\, T \tag{4.59}$$

Use of relations (4.57) in (4.59) and recasting equations in terms of Mach number gives

$$p_3(1 \;+\; \gamma\, M_3^2) \;=\; p_4(1 \;+\; \gamma\, M_4^2) \tag{4.60}$$

Thus,

$$\frac{p_4}{p_3} \;=\; \frac{(1 \;+\; \gamma\, M_3^2)}{(1 \;+\; \gamma\, M_4^2)} \tag{4.61}$$

from equation (4.58)

$$\frac{T_{t4}}{T_{t3}} = 1 + \frac{Q_f}{c_p T_{t3}} \tag{4.62}$$

But,

$$\frac{T_{t4}}{T_{t3}} = \frac{T_4}{T_3}\frac{T_{t4}}{T_4}\frac{T_3}{T_{t3}} = \frac{T_4}{T_3}\frac{(1+\frac{\gamma-1}{2}{M_4}^2)}{(1+\frac{\gamma-1}{2}{M_3}^2)} \tag{4.63}$$

In obtaining the above relations, equation (4.18) is used. Equation (4.56) can be cast in terms of pressure, temperature and Mach numbers as

$$\begin{aligned} \rho_3 V_3 &= \frac{p_3}{RT_3} M_3 \sqrt{\gamma R\, T_3} \\ &= p_3 M_3 \sqrt{\frac{\gamma}{R\, T_3}} \\ &= p_4 M_4 \sqrt{\frac{\gamma}{R\, T_4}} \end{aligned} \tag{4.64}$$

Therefore,

$$\frac{p_3 M_3}{\sqrt{T_3}} = \frac{p_4 M_4}{\sqrt{T_4}} \tag{4.65}$$

$$\frac{T_4}{T_3} = \left(\frac{p_4 M_4}{p_3 M_3}\right)^2 \tag{4.66}$$

From equations (4.66),(4.63) and (4.61)

$$\begin{aligned} \frac{T_{t4}}{T_{t3}} &= \frac{M_4^2}{M_3^2}\frac{(1+\gamma M_3^2)^2}{(1+\gamma M_4^2)^2}\frac{(1+\frac{(\gamma-1)}{2}M_4^2)}{(1+\frac{(\gamma-1)}{2}M_3^2)} \\ &= [1 + \frac{Q_f}{c_p T_{t3}}] \end{aligned} \tag{4.67}$$

Given M_3, T_{t3} and Q_f, one can obtain M_4 from equation (4.68). Then p_4 / p_3 can be obtained from equation. (4.61). Using isentropic relation (4.22) for stations 3 and 4, one can get p_{t4} / p_{t3}. Figure 4.15 shows the variation of p_{t4} / p_{t3} and T_{t4} / T_{t3} as a function of M_4 for different values of M_3.

The maximum Mach number to which a subsonic stream can be accelerated by heat addition in a straight duct is unity.

For a gas turbine combustor $Q_f/c_p T_{t3}$ = (0.02 $\times$ 42 MJ/ kg)/(1 kJ/ kgK) $\times$ (600 K) = 1.4. Therefore, T_{t4} / T_{t3} = 2.4, M_3 = 0.20, M_4 = .34 and p_{t4}/p_{t3} = 0.96.

For a ramjet combustor $Q_f/c_p T_{t3}$ = (0.06 $\times$ 42 MJ/kg)/(1 kJ/ kg K) $\times$ (600 K) = 4.2, and therefore, M_3 = 0.20, M_4 = .7, and p_{t4}/p_{t3} = 0.855.

One can, thus, see the influence of Rayleigh loss being significant for ramjets and being less significant for turbojets. An important feature that should be recognized from Fig. 4.15 is that if substantial energy is to be introduced into the

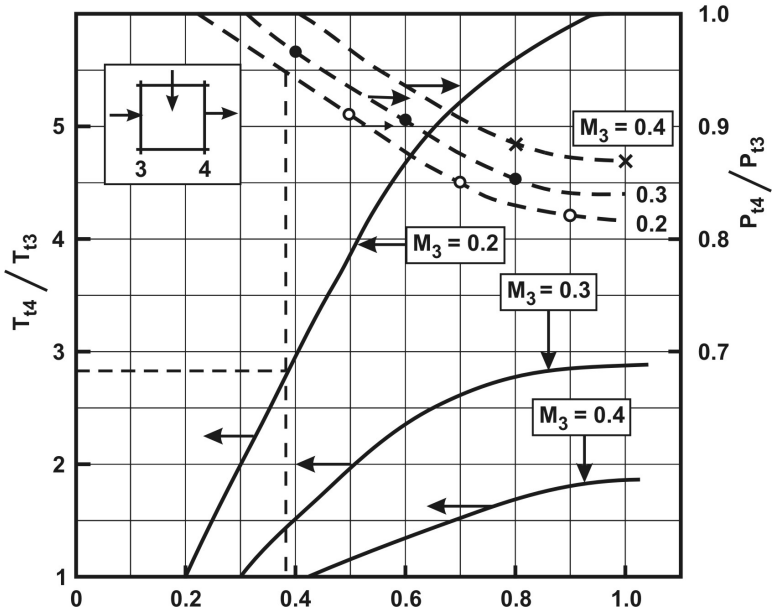

Figure 4.15: The stagnation temperature and pressure ratios across the combustor as a function of inflow and outflow Mach numbers

stream without much loss in the stagnation pressure, one has to bring the stream to low Mach numbers. Even at M = 0.3, it is not possible to raise the heat input beyond producing thrice the inlet stagnation temperature. More understanding can be gained if the results are plotted by setting the Mach number M_4 = 1. The plots of static and stagnation pressure and temperature ratios as a function of Mach number are shown in Fig. 4.16. The way to utilize this figure is to set F_4 / F_3 as (F_4 / F*)/(F_3 / F*) where F is any quantity and move from one point to another and read off change in the properties. Typically increase in heat input is reflected through change in stagnation temperature, say from A to B in the subsonic flow or from E to D in the supersonic flow. The results of the heat input are summarized in Table 4.2.

Thus, heat addition to a subsonic stream accelerates it and that to a supersonic stream decelerates it. This makes the peak Mach number to be reached for a subsonic stream under heat addition as unity. There are other interesting features like heat addition to a subsonic stream at Mach numbers between $1/\sqrt{\gamma}$ and unity cause decrease in static temperature. This is related to the way energy is shared between random and stream wise motion dictated by the conservation equations.

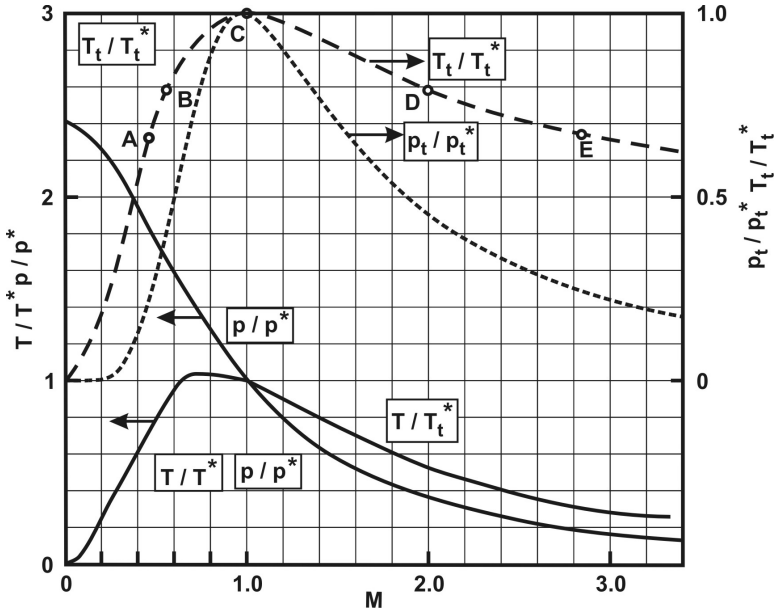

Figure 4.16: The variation of thermodynamic properties with Mach number (γ = 1.4, subscript t refers to stagnation quantities and starred quantities are at M=1)

Table 4.2: Summary of the effects of heat input into a flow

Quantity	A $\rightarrow$ B M_{inlet} < 1	E $\rightarrow$ D M_{inlet} > 1
Heat input	Increases	Increases
Stagnation Pressure	Decreases	Decreases
Static Pressure	Increases	Increases
Static Temperature	Increases, ($M < 1/\sqrt{\gamma}$) Decreases ($M > 1/\sqrt{\gamma}$)	Increases

4.7 Summary

This chapter is devoted to the considerations of thermodynamics and gas dynamics in propulsion systems. All propulsion systems work by raising the pressure of the working fluid, add heat and expand it to ambient pressure to extract the work. In this process, flow through the nozzle is one of the key elements in thrust generation. It is therefore important to understand the behavior of the fluid flow through a nozzle. Both air breathing and non-air breathing engines have different considerations in respect of nozzle design and associated gas dynamic issues. Many aircraft engines use convergent nozzles – some of fixed design and several of variable area. The temperatures involved are not high (typically less than 1000 K except for short durations during after burner operation) and one can therefore adopt metals as material for nozzles. For rocket engines, the pressures used are high and the nozzle is a significant component (even physically) and thermal protection system is mandatory. One needs to determine the heat flux distribution over the nozzle inner surface. This calls for the knowledge of pressures and temperatures inside the nozzle as a function of axial location. These are derived from the gas dynamic relations derived in this chapter. Flows in combustion chambers of gas turbine engines as well rocket engines involve heat addition and associated stagnation pressure loss. This is obtained from the above analysis. In liquid rocket engines, stagnation pressure losses between the head end (which is the injector end) to the nozzle entrance the magnitude of which becomes increasingly significant with lower chamber-to-throat dimensions. These are obtained from the analysis in this chapter.

Chapter 5

Cycle Analysis

5.1 The Ramjet

Ramjet is considered first for analysis since it is thermodynamically the simplest. The analysis aims at obtaining mathematical expressions for thrust, mass flow rate through the engine and the specific impulse as a function of flight Mach number, altitude (or ambient pressure and temperature each as independent variables) and design parameters (combustor temperature and exit diameter). The assumption of one-dimensional flow made in the earlier chapter will continue here as well. One can derive from such an analysis answers to several generic questions like: At what condition will the design of a ramjet be most compact? Does the thrust for a given engine attain peak with flight Mach number at the same condition? How does thrust depend on ambient temperature? etc.

A schematic of the various units and the various points on a T – s diagram are shown in Fig. 5.1. The operation 0 – 2 is isentropic compression, 2 – 3 isobaric combustion, 3 – 4 isentropic expansion. Since the chamber pressures are typically 3 to 5 atm., the nozzle chosen is usually of convergent-divergent type. This leads to exit pressure being close to atmospheric pressure. Hence, the nozzle is treated as undergoing optimum expansion i.e. $p_4 = p_o$. Thrust, F is defined by

$$F = \dot{m}_a[(1+f)V_4 - V_o] \; + \; A_4(p_4 - p_o) \tag{5.1}$$

Since many ramjet applications use convergent divergent nozzle, optimal nozzle expansion condition, p_4 = p_o would be appropriate and is invoked here. The above equation is written as

$$F = \dot{m}_a V_o[(1+f)\frac{V_4}{V_o} - 1] \tag{5.2}$$

We write V_4/V_o = $M_4 a_4/M_o a_o$ and use the expression for acoustic speed in terms of

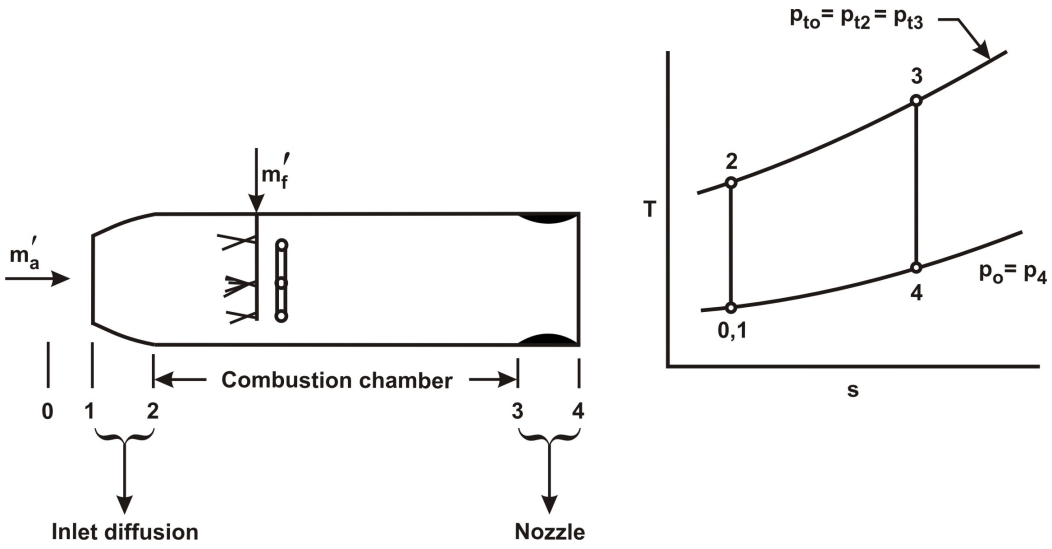

Figure 5.1: The Schematic of ramjet and the operating points on a T–s diagram.

temperature to rewrite the equation as

$$F = \dot{m}_a a_o M_o \left[(1+f)\frac{M_4}{M_o}\sqrt{\frac{T_4}{T_o}} - 1 \right] \tag{5.3}$$

In order to obtain M_4/M_o and T_4/T_o, we perform a cascading of stagnation temperatures and pressures. We express T_4/T_o as below.

$$\frac{T_4}{T_o} = \frac{T_4}{T_{t4}} . \frac{T_{t4}}{T_{t3}} . \frac{T_{t3}}{T_{t2}} . \frac{T_{t2}}{T_{t1}} . \frac{T_{t1}}{T_{to}} . \frac{T_{to}}{T_o} \tag{5.4}$$

$$\frac{T_4}{T_o} = \frac{1}{\left(1 + \frac{(\gamma-1)}{2} M_4^2\right)} .1.\tau_b.1.1.\theta_o \tag{5.5}$$

One can interpret the various fractions on the right hand side of equation (5.4). The first term is the relationship between local stagnation and static temperatures. The second term is an expression of the fact that the nozzle flow is isoenergetic, though there could be loss in stagnation pressure. The third term $\tau_b = T_{t3}/T_{t2}$ is the ratio of stagnation temperatures across the combustor or burner. The flow through the diffuser and intake are also taken isoenergetic. The last term in the equation (5.5), θ_o is expressed as follows.

$$\theta_o = T_{to}/T_o = (1 + \frac{\gamma - 1}{2} M_o^2) \tag{5.6}$$

The quantity θ_o can be interpreted as representative of free stream Mach number. It is used extensively in the analysis of all air breathing engines. Equation (5.5)

can be written now as

$$\frac{T_4}{T_o} = \frac{\theta_o.\tau_b}{(1 + \frac{\gamma-1}{2}M_4^2)} \tag{5.7}$$

τ_b is expressed often in a different manner.

$$\tau_b = \frac{T_{t3}}{T_{t2}} = \frac{T_{t3}}{T_o}.\frac{T_o}{T_{t2}} = \frac{\theta_b}{\theta_o} \tag{5.8}$$

where $\theta_b = T_{t3}/T_o$. Casting the term in this way is important because the combustor outlet temperature T_{t3} is a control variable. It can be varied by the amount of fuel injected into the combustor. In practice, it is controlled by the temperature that the outer wall of the combustor can withstand. With the use of ceramic materials and a relatively cool stream of air near the boundaries, one can go up to stoichiometric mixture of fuel-air with gas temperature of 2200 – 2400 K.

With the definition of τ_b in terms of θ_b as in equation (5.8), the equation (5.7) becomes,

$$\frac{T_4}{T_o} = \frac{\theta_b}{1 + \frac{\gamma-1}{2}M_4^2} \tag{5.9}$$

Similarly, cascading the static pressures through stagnation pressures leads to

$$\frac{p_4}{p_o} = \frac{p_4}{p_{t4}}.\frac{p_{t4}}{p_{t3}}.\frac{p_{t3}}{p_{t2}}.\frac{p_{t2}}{p_{to}}.\frac{p_{to}}{p_o} \tag{5.10}$$

We denote the stagnation pressure ratios across the nozzle, the combustor (or burner, as denoted here) and the air intake by efficiencies - $p_{t4}/p_{t3} = \eta'_n$, $p_{t3}/p_{t2} = \eta'_b$, and $p_{t2}/p_{to} = \eta'_d$. We know that for optimum expansion, $p_4 = p_o$, and therefore, we write,

$$1 = \frac{1}{(1 + \frac{\gamma-1}{2}M_4^2)^{\gamma/(\gamma-1)}}\ \eta'_n\ \eta'_b\eta'_d.(1 + \frac{\gamma-1}{2}M_o^2)^{\gamma/(\gamma-1)} \tag{5.11}$$

Like in the case of temperature ratios, the first term on the right hand side is the ratio of static to stagnation pressures; the second term, the nozzle efficiency denoting the decrease in stagnation pressure across the nozzle due to friction; the third term is due to loss in stagnation pressure in the burner because of heat addition and friction; the fourth term is due to intake and diffuser losses due to possible wave losses for supersonic flows and friction. We can recast equation (5.11) by raising all the terms to the power $(\gamma-1)/\gamma$ and denoting by η the efficiency terms given by the following expression.

$$\eta = [\eta'_n\eta'_b\eta'_d]^{(\gamma-1)/\gamma} \tag{5.12}$$

The nozzle efficiency, η'_n is typically 0.96 to 0.98, the burner efficiency, η'_b is about 0.94 to 0.96, and the diffuser efficiency η'_d is 0.6 to 0.95 depending on the Mach number. These values lead to η of 0.86 to 0.92. Recasting equation (5.11) gives

$$\left(1 + \frac{\gamma-1}{2}M_4^2\right)\ =\ \eta\left(1 + \frac{\gamma-1}{2}M_o^2\right) \tag{5.13}$$

This equation can be used to express M_4 in terms of θ_o (M_o) by

$$M_4 = \sqrt{\frac{2}{(\gamma-1)}(\eta\theta_o - 1)} \tag{5.14}$$

Flight Mach number, M_o can be expressed in terms of θ_o by

$$M_o = \sqrt{\frac{2}{(\gamma-1)}(\theta_o - 1)} \tag{5.15}$$

The ratio of the Mach numbers can be expressed by

$$\frac{M_4}{M_o} = \sqrt{\frac{(\eta\theta_o - 1)}{(\theta_o - 1)}} \tag{5.16}$$

The expression for thrust can be written in non–dimensional terms as

$$\frac{F}{\dot{m}_a a_o} \;=\; M_o \left[(1+f)\sqrt{\frac{\theta_b}{\eta\theta_o}\frac{(\eta\theta_o - 1)}{(\theta_o - 1)}} - 1 \right] \tag{5.17}$$

where $F/\dot{m}_a a_o$ is the thrust per unit flow rate. The mass flow rate $\dot{m}_a$ is then to be estimated. It is determined from the flow going through the nozzle. The flow rate is expressed by

$$(1+f)\dot{m}_a \;=\; \rho_4 V_4 A_4 \;=\; \frac{p_4}{RT_4}.M_4.\sqrt{\gamma RT_4}.A_4$$

Noting $p_4 = p_o$ and ignoring f in comparison to unity, we can write

$$\dot{m}_a = p_o A_4 \left\{ M_4 \sqrt{\frac{\gamma}{RT_4}} \right\}$$

Multiplying the right hand side by $\sqrt{\gamma RT_o}/a_o$ (=1, because numerator and denominator are equal), we get

$$\dot{m}_a = \gamma p_o A_4 M_o \sqrt{\frac{T_o}{T_4}} \cdot \frac{M_4}{M_o}\frac{1}{a_o}$$

This can be recast in non–dimensional terms as

$$\frac{\dot{m}_a a_o}{p_o A_4} \;=\; \gamma M_o \sqrt{\frac{\eta\theta_o}{\theta_b}\frac{(\eta\theta_o - 1)}{(\theta_o - 1)}} \tag{5.18}$$

Introducing this into equation (5.17) we get the non–dimensional thrust as,

$$\frac{F}{p_o A_4} = \gamma M_o^2 \left[(1+f)\frac{(\eta\theta_o - 1)}{(\theta_o - 1)} - \sqrt{\frac{\eta\theta_o(\eta\theta_o - 1)}{\theta_b(\theta_o - 1)}} \right] \tag{5.19}$$

The specific impulse defined as thrust per unit mass flow rate of the fuel is obtained as

$$I_{sp} \;=\; \frac{F}{\dot{m}_a a_o} \,.\, a_o \,.\, \frac{1}{f} \tag{5.20}$$

f can be obtained by striking energy balance across the combustor as

$$\dot{m}_f Q = \dot{m}_a[(1+f)\, c_p T_{t3} \;-\; c_p T_{t2}]$$

Since $f \ll 1$, we shall ignore it on the right hand side. After some algebra, one gets

$$\frac{1}{f} \;=\; \frac{Q}{c_p T_o}\, \frac{1}{(\theta_b - \theta_o)}$$

If we use these, we get,

$$\frac{I_{sp}}{a_o} \;=\; M_o\, \frac{F}{\dot{m}_a a_o} \frac{Q}{c_p T_o}\, \frac{1}{(\theta_b - \theta_o)} \tag{5.21}$$

As such the variation of I_{sp} is the same as of $(F/\dot{m}_a a_o)$. In terms of the various parameters, specific impulse is described by,

$$\frac{I_{sp}}{a_o} \;=\; M_o \left[\sqrt{\frac{\theta_b}{\eta\theta_o} \frac{(\eta\theta_o - 1)}{(\theta_o - 1)}} - 1\right] \frac{Q}{c_p T_o}\, \frac{1}{(\theta_b - \theta_o)} \tag{5.22}$$

5.1.1 Results With 100 % Efficiency

The first important result concerns the relationship between M_4 and M_o. For η = 1, equation (5.13) leads to $M_4 = M_o$. Thus, under ideal conditions, the exit Mach number equals the flight Mach number. Since the exit temperatures will be higher by 500 to 1000 K (when compared with the ambient temperature), the exit acoustic speed will be much larger and hence, the exit speed will be much larger than the flight speed. Thus, one gets positive thrust.

The expression for thrust per unit flow rate (for $\eta = 1$) is given by

$$\frac{F}{\dot{m}_a a_o} \;=\; M_o \left[(1+f)\sqrt{\frac{\theta_b}{\theta_o}} - 1\right] \tag{5.23}$$

The expression for mass flow rate (for $\eta = 1$) is obtained as

$$\frac{m_a a_o}{p_o A_4} = \gamma M_o \sqrt{\frac{\theta_o}{\theta_b}} \tag{5.24}$$

Therefore, the expression for non-dimensional thrust is obtained as

$$\frac{F}{p_o A_4} = \gamma M_o^2 \left[(1+f) - \sqrt{\frac{\theta_o}{\theta_b}}\right] \tag{5.25}$$

The equation for specific impulse is the same as equation 5.21.

The quantity $F/(\dot{m}_a a_o)$ represents the thrust per unit air flow rate. Larger this value, smaller will be the diameter of the combustor. This will imply lesser drag penalty on the vehicle and so the overall performance of the vehicle will be superior. An examination of the equation for $F/(\dot{m}_a a_o)$ indicates two features: the dependence on the burner outlet temperature through θ_b shows that increase in this value contributes to increase in thrust per unit flow rate and thus, allowing for a reduction in the size of the ramjet for the same thrust. In respect of dependence on the flight Mach number, $F/(\dot{m}_a a_o)$ has two terms depending on M_o. The first term increases linearly with M_o. The term $1/\sqrt{\theta_o}$ inside the brackets decreases with M_o. Hence, there appears to be a possibility for thrust per unit flow rate to have an optimum. This will be pursued later.

The equation for thrust indicates that as M_o approaches zero, thrust tends to zero. This simply confirms a known result that ramjet has zero static thrust. Also, when θ_o approaches θ_b, thrust tends to zero (f = 0 is assumed here). In this limit, the flight Mach number is very large. For $\gamma = 1.4$ and $\theta_b = 10.0$, M_o = 6.7. At this condition, the free stream stagnation temperature is equal to the burner outlet stagnation temperature and no heat addition through fuel injection is possible (see the discussion on scramjets - section 1.10). Therefore no thrust can be produced. Because thrust will be zero at Mach numbers of zero and a non-zero high value, one can expect it to have a maximum at some intermediate Mach number.

Before we proceed with more analysis, we should examine the order of magnitude of various quantities.

Typically for flights at altitude, $p_o \sim$ 0.05 MPa, T_o = 250 K, and $M_o = 2.0$ (θ_o = 1.8). One can take $T_{t3} \approx 2000\ K$, Q = 42000 kJ/kg, $\gamma = 1.4$, c_p = 1.0 kJ/kg K. The exit area is taken as A_4 = 0.2 m^2.

We get $\theta_b = T_{t3}/T_o$ = 8.0 and $Q/c_p T_o$ = 168.0.

For these parameters we get,

$$\frac{F}{\dot{m}_a a_o} = 2.0\left\{1.067\sqrt{8/1.8} - 1\right\} = 2.5$$

$$\frac{\dot{m}_a a_o}{p_o A_4} = 1.4 \times 2.0\sqrt{1.88} = 1.33$$

$$\frac{F}{p_o A_4} = 1.4 \times 2.0^2\left\{1.067\ -\ \sqrt{1.88}\right\} = 3.32$$

This further leads to

$$F \;=\; 0.05 \times 10^6 \frac{N}{m^2} \times 0.2m^2 \times 3.32 = 33.2kN$$

Further, $a_o \;=\; 340\sqrt{\frac{250}{288}} \;=\; 316$ m/s and

I_{sp} = 316 m/s $\times 2.0 \times 168 \times 2.5 \times \frac{1}{(8-1.8)} \;\simeq\; 42.8$ kN.s/kg.

The specific fuel consumption works out to 36000/I_{sp} = 0.84 kg/hr kg thrust. These values are appropriate for an ideal ramjet.

Optimum thrust per unit airflow rate

Now it is useful to examine if $F/(\dot{m}_a a_o)$ has a maximum with respect to M_o. Taking the derivative of this quantity with M_o gives

$$\frac{dF/\dot{m}_a a_o}{dM_o} \;=\; 1.\left[(1+f)\sqrt{\frac{\theta_b}{\theta_o}} - 1\right] \;-\; \frac{1}{2}\, M_o(1+f)\, \frac{\sqrt{\theta_b}}{\theta_o^{3/2}}\, (\gamma-1)\, M_o$$

$$= \;(1+f)\sqrt{\frac{\theta_b}{\theta_o}} \;-1 \;-\; \frac{(\theta_o - 1)}{\theta_o}\sqrt{\frac{\theta_b}{\theta_o}}\,(1+f) \;=\; 0$$

This gives the condition for maximum thrust per unit flow rate as,

$$\theta_o \;=\; \theta_b^{1/3}\,(1+f)^{2/3} \tag{5.26}$$

For $\theta_b \approx 10$, $f = 0$ and $f \sim 0.067$, one gets, $\theta_o \sim$ 2.15 and 2.25 and $M_o \simeq$ 2.4 and 2.5 respectively.

Thus, the propulsive unit of maximum compactness is obtained by making a choice of Mach number as indicated above. This is the reason why ramjets are used in the range of Mach numbers from 2.5 – 3.0.

For $\eta < 1$, $f \simeq 0$, the maximization of thrust per unit flow rate can be shown to occur at

$$\theta_b \;=\; \frac{\eta^2\theta_o^3\,(\theta_o - \frac{1}{\eta})}{(\theta_o - 1)} \tag{5.27}$$

which reduces to the previous result at $\eta = 1$ for $f = 0$. This result is implicit in θ_o. The equation can be recast as

$$\theta_o^3 - \frac{\theta_b}{\eta^2} = \frac{\theta_b}{\eta^2}\frac{(1-\eta)}{(\eta\theta_o - 1)}$$

By approximating θ_o on right hand side by $\theta_o = (\theta_b/\eta^2)^{1/3}$, a result which is close to the result for η = 1, we obtain a good approximation to θ_o as

$$\theta_o = \left[\frac{\theta_b}{\eta^2}\right]^{1/3} \left[1 - \frac{1-\eta}{(\eta\theta_b)^{1/3} - 1}\right]^{1/3} \tag{5.28}$$

For $\theta_b = 10, f = 0.0, \eta = 0.86$ one gets θ_o = 2.27, M_o = 2.52. Thus, inefficiencies will increase the optimum Mach number compared to the ideal case.

Optimum non–dimensional thrust

The equation for non–dimensional thrust (5.25) can be recast as

$$\frac{F}{p_o A_4} = \frac{2\gamma}{(\gamma-1)}(\theta_o - 1)\left[(1+f) - \sqrt{\frac{\theta_o}{\theta_b}}\right] \tag{5.29}$$

It can be recognized that the linear term in θ_o contributes to the increase of thrust and the term under square root within the parenthesis contributes to decrease of thrust. Hence, one can expect an optimum. Differentiating the equation with respect to θ_o and equating it to 0, one can extract the condition for optimum thrust. This implies

$$\frac{d}{d\theta_o}(\theta_o - 1)[(1+f) - \sqrt{\frac{\theta_o}{\theta_b}}] = 0 \tag{5.30}$$

that leads to

$$\sqrt{\theta_o} = \frac{1}{3}\left[(1+f)\sqrt{\theta_b} + \sqrt{(1+f)^2\theta_b + 3}\right] \tag{5.31}$$

It can be seen from equations (5.28) and (5.31) that the free stream conditions scale as $\theta_o \sim \theta_b^{(1/3)}$ for maximum thrust per unit flow rate and $\theta_o \sim \theta_b$ for maximum thrust. This implies that the Mach number for maximum thrust per unit flow rate is lower than for maximum thrust. Typically, the Mach number for maximum thrust per unit flow rate is between 2 to 2.5 and for maximum thrust, 3.6 to 5. Even though it is tempting to consider a design for maximum thrust, one should recognize that any acceleration implies providing a force that is the difference between thrust and drag, increased size to get the same thrust that results from maximum thrust design will cause greater drag and perhaps there will be reduced net performance. Hence, the design choice is around one that gives maximum thrust per unit flow rate.

5.1.2 Dependence on Ambient Pressure and Temperature

It can be seen from the thrust equation that the dependence of thrust on ambient pressure (equation 5.19) is linear. The dependence on ambient temperature arises from the term $\theta_b = T_{t3}/T_o$ in which there is requirement to keep T_{t3} constant below a fixed value due to material limitations and T_o varies due to altitude variation. This dependence can be extracted by taking differentials and expressing in terms of fractional changes by obtaining dF/dT_o and dividing by F/T_o. This leads to

$$\frac{dF}{F} \;=\; -\frac{1}{2(\sqrt{\theta_b} - \sqrt{\theta_o})}\frac{dT_o}{T_o} \tag{5.32}$$

For a reduction in ambient temperature from 260 K to 240 K at a mean of 250 K (implying a fractional change of 8 % in temperature), for θ_o = 1.8 and θ_b = 10, one gets thrust increase of 2.2 %.

5.1.3 Mach Number for Positive Thrust

An examination of equation (5.19) shows that for $\eta < 1$, thrust at M_o = 0 is negative. This implies that unless a minimum flight Mach number is reached, positive thrust cannot be obtained. Therefore, we ask the question: at what Mach number will the system give positive thrust?

For $\eta < 1$, one has to compute θ_o for which

$$(1+f)^2\frac{(\eta\theta_o - 1)}{(\theta_o - 1)} \;>\; \frac{\eta\theta_o}{\theta_b} \tag{5.33}$$

An approximate treatment with η not very different from unity leads to

$$[M_o]_{min} \;\sim\; \sqrt{\frac{2(\frac{1}{\eta} - 1)(1+f)^2\theta_b}{(\gamma-1)[\theta_b(1+f)^2 - 1]}} \tag{5.34}$$

At the efficiency of 0.86 for η, and $\theta_b = 10.0$, f = 0.06, we get $M_{o\,min} \sim 0.95$. For higher efficiency, the Mach number for positive thrust will be lower. As can be seen, the efficiency of the components has a significant effect on the engine. Also one can see why subsonic ramjets are rarely adopted.

Figures 5.2 and 5.3 show plots of $F/\dot{m}_a a_o$ and I_{sp} as a function of M_o and θ_b. This figure has several features. Decrease in efficiency to 86% (defined above) causes decrease in the thrust per unit flow rate by 10%. The Mach number for maximum thrust shifts towards higher values with reduced efficiencies of components. The use of higher burner temperature increases the thrust per unit flow rate significantly.

$$\frac{d(F/\dot{m}_a a_o)_{max}}{d\,\theta_b} \;\simeq\; \frac{2.41 - 1.3}{10 - 6} \;\simeq\; 0.2$$

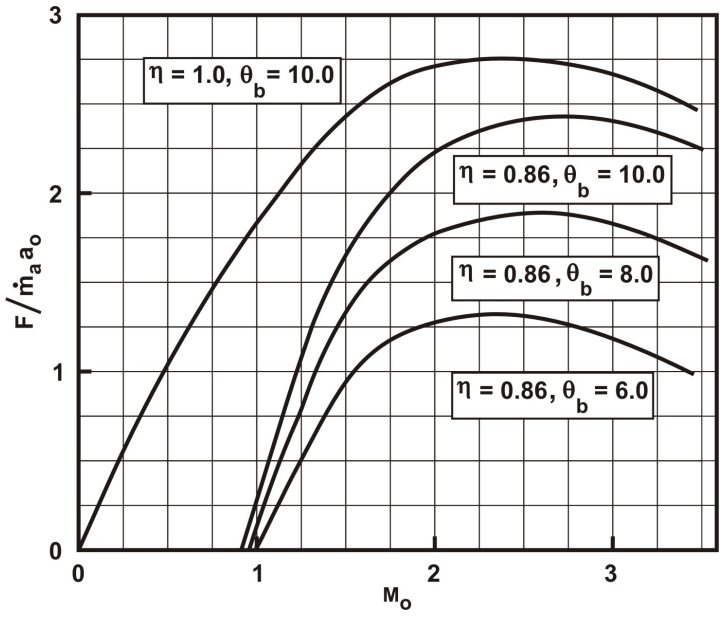

Figure 5.2: Plot of $F/\dot{m}_a a_o$ for a ramjet with flight Mach number as a function of burner temperature and efficiency.

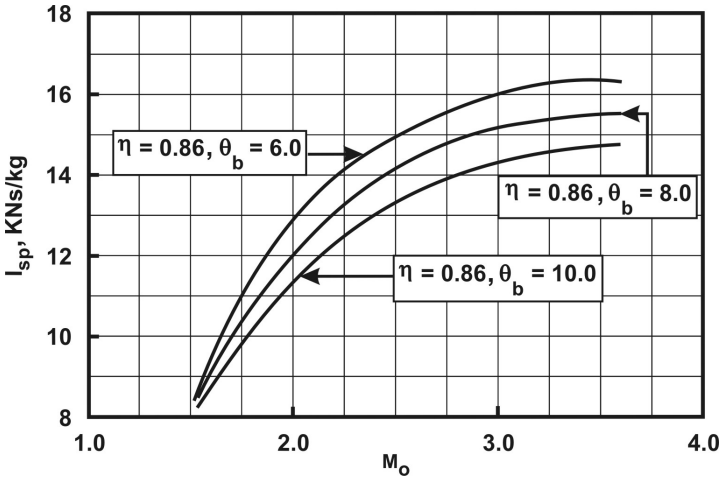

Figure 5.3: The plot of Specific Impulse with Mach number for various burner temperatures.

The change of $F/\dot{m}_a a_o$ from 1.3 to 2.41 when burner temperature varies from 1500 K (at T_o = 250 K) to 2500 K implies that air flow rate required to produce the same thrust is less by the corresponding amount, namely 45%. This causes a decrease in diameter by about 22 %. The corresponding decrease in drag would further add to the increase in performance. These benefits need to be tempered with the fact that increased burner temperature calls for higher fuel consumption and so the specific impulse drops. It drops by about 12% as can be seen from Figure 5.3.

5.1.4 Summary

This section has been devoted to a thermodynamic analysis of a ramjet. It has explicitly brought out the dependence of thrust and specific impulse on flight parameters (Mach number, ambient pressure and temperature) and design variables (θ_b and A_4). The importance of enhancing the burner outlet temperature for making the ramjet more compact at the expense of larger fuel consumption is also shown. The role of inefficiency in limiting the lower end of the flight Mach number for positive thrust is also brought out.

5.2 The Turbojet

In the discussion to follow, a simple turbojet is first considered. It is followed by the treatment of the case with afterburner. The methodology to handle choked nozzle is also discussed. The aspects concerning inefficiency of components will be dealt with in some detail. Figure 5.4 shows the schematic of a simple turbojet and the corresponding features on a T–s diagram. In the diagrams, 0 represents the free stream, 1 represents the intake, 2 the end of the intake and the inlet to the compressor, 3 the end of the compressor, 4 the end of the combustor, 5 the end of the turbine, 6 the end of the jet pipe entry and 7 the end of the nozzle. The design parameters of the engine are the compressor pressure ratio, $\pi_c = p_{t3}/p_{t2}$, and the burner outlet temperature equal to the turbine inlet temperature, T_{t4}. The operating parameters are the flight Mach number, M_o, the ambient conditions involving temperature and pressure. Of the above, the turbine pressure ratio = $\pi_t = p_{t5}/p_{t4}$ is decided by the power required by the compressor.

The following definitions are needed in the analysis to follow:

$$\pi_c = p_{t3}/p_{t2}\ ; \qquad \tau_c = T_{t3}/T_{t2} = (\pi_c)^{\frac{\gamma-1}{\gamma}}$$

$$\pi_t = p_{t5}/p_{t4}\ ; \qquad \tau_t = T_{t5}/T_{t4} = (\pi_t)^{\frac{\gamma-1}{\gamma}}$$

$$\theta_o = \frac{T_{to}}{T_o} = (1 + \frac{\gamma-1}{2} M_o^2) \tag{5.35}$$

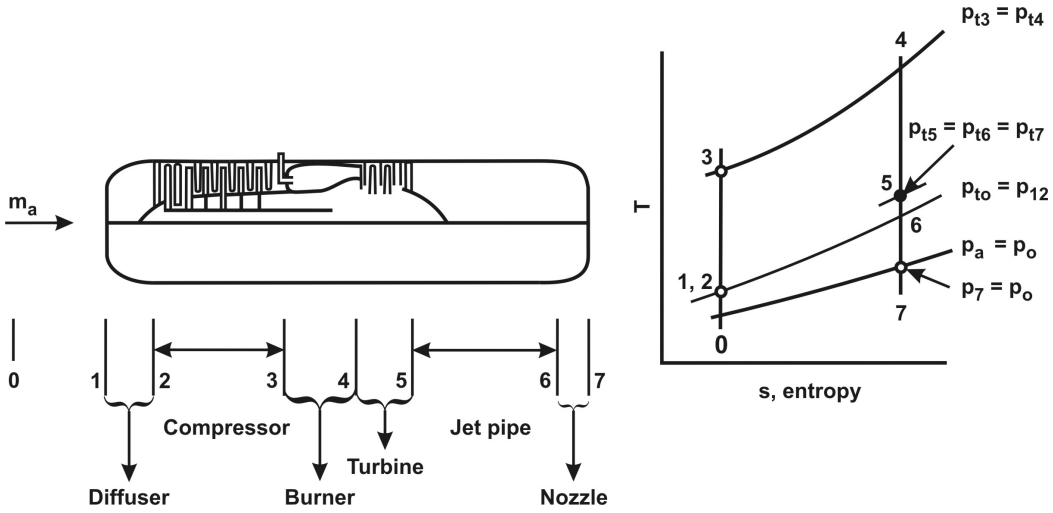

Figure 5.4: Schematic of a Turbojet and the corresponding features on a T–s diagram.

or

$$M_o = \sqrt{\frac{2}{\gamma - 1}(\theta_o - 1)} \tag{5.36}$$

$$\theta_b = \frac{T_{t4}}{T_o} = \frac{T_{t4}}{T_{t3}} \times \frac{T_{t3}}{T_{t2}} \times \frac{T_{t2}}{T_o} = \tau_b.\tau_c.\theta_o \tag{5.37}$$

Thus, τ_b = Burner stagnation temperature ratio will be given by

$$\tau_b = \frac{\theta_b}{\tau_c \theta_o} \tag{5.38}$$

The expression for thrust is given by

$$F = \dot{m}_a[V_7(1+f) - V_o] + A_7(p_7 - p_o) \tag{5.39}$$

5.2.1 Optimum Expansion

The first part of the analysis assumes that the nozzle has optimum expansion implying $p_7 = p_o$. Therefore, the second term drops off. It is also assumed that $f \ll 1$ and is therefore ignored in the above expression. We get therefore,

$$F \;=\; \dot{m}(V_7 - V_o)$$

$$F = \dot{m}_a a_o M_o \left[\frac{V_7}{V_o} - 1\right] \;=\; (\dot{m}_a a_o).M_o \left[\frac{M_7}{M_o}\sqrt{\frac{T_7}{T_o}} - 1\right] \tag{5.40}$$

In obtaining equation 5.40, it is assumed that $a_7 = \sqrt{\gamma R T_7}$, $a_o = \sqrt{\gamma R T_o}$, the properties γR are the same. This assumption in particular, is reasonably accurate. Therefore

$$\frac{F}{\dot{m}_a a_o} = M_o \left[\frac{M_7}{M_o}\sqrt{\frac{T_7}{T_o}} - 1\right] \tag{5.41}$$

In order to obtain M_7/M_o and T_7/T_o, we perform cascading of the stagnation temperature and pressures through the system.

$$\frac{T_7}{T_o} = \frac{T_7}{T_{t7}}.\frac{T_{t7}}{T_{t6}}.\frac{T_{t6}}{T_{t5}}.\frac{T_{t5}}{T_{t4}}.\frac{T_{t4}}{T_{t3}}.\frac{T_{t3}}{T_{t2}}.\frac{T_{t2}}{T_{t1}}.\frac{T_{t1}}{T_{to}}.\frac{T_{to}}{T_o} \tag{5.42}$$

$$= noz.jp.turb.bur.comp.diffuser \tag{5.43}$$

$$= \frac{1}{(1 + \frac{\gamma-1}{2}M_7^2}).1.1.\tau_t.\tau_b.\tau_c.1.1.(1 + \frac{\gamma - 1}{2}M_o^2) \tag{5.44}$$

where the symbols in the middle row of the above set of equations refer to nozzle, jet pipe, turbine, burner, compressor and diffuser respectively. From this equation we get,

$$\frac{T_7}{T_o} = \frac{(1 + \frac{\gamma-1}{2} M_o^2)}{(1 + \frac{\gamma-1}{2} M_7^2)} \cdot \tau_t \tau_b \tau_c \tag{5.45}$$

Using equation (5.38) one can rewrite the above equation as

$$\frac{T_7}{T_o} = \frac{\theta_b \tau_t}{(1 + \frac{\gamma-1}{2} M_7^2)} \tag{5.46}$$

Cascading of pressures gives,

$$\frac{p_7}{p_o} = 1 = \frac{p_7}{p_{t7}} . \frac{p_{t7}}{p_{t6}} . \frac{p_{t6}}{p_{t5}} . \frac{p_{t5}}{p_{t4}} . \frac{p_{t4}}{p_{t3}} . \frac{p_{t3}}{p_{t2}} . \frac{p_{t2}}{p_{to}} . \frac{p_{to}}{p_o}$$

$$= \frac{1}{(1 + \frac{\gamma-1}{2} M_7^2)^{\gamma/\gamma-1}} .1. \pi_t . \pi_b . \pi_c .1. \left(1 + \frac{\gamma - 1}{2} M_o^2\right)^{\gamma/\gamma-1}$$

The component efficiencies, having been taken as unity (also π_b = 1) leads to

$$\begin{aligned} \left(1 + \frac{\gamma - 1}{2} M_7^2\right) &= (\pi_t \pi_c)^{\gamma-1/\gamma} \cdot \left(1 + \frac{\gamma - 1}{2} M_o^2\right) \\ &= \tau_c \tau_t \theta_o \end{aligned} \tag{5.47}$$

Thus,

$$M_7 = \sqrt{(\tau_c \tau_t \theta_o - 1) \frac{2}{\gamma - 1}} \tag{5.48}$$

Equations (5.36) and (5.48) give

$$\frac{M_7}{M_o} = \sqrt{\frac{(\tau_c \tau_t \theta_o - 1)}{(\theta_o - 1)}} \tag{5.49}$$

Equation (5.46) with (5.47) yields,

$$\frac{T_7}{T_o} = \frac{\theta_b \tau_t}{\tau_c \tau_t \theta_o} = \frac{\theta_b}{\tau_c \theta_o} \tag{5.50}$$

Thus

$$\frac{F}{\dot{m}_a a_o} = M_o \left[\sqrt{\frac{\theta_b (\tau_c \tau_t \theta_o - 1)}{\tau_c \theta_o (\theta_o - 1)}} - 1 \right] \tag{5.51}$$

We now have the task of relating τ_t to other parameters. If we make a compressor-turbine power balance we have

$$\dot{m}_a c_p (T_{t3} - T_{t2}) = \dot{m}_a (1 + f) c_p (T_{t4} - T_{t5}) \tag{5.52}$$

In the above expression, the specific heats are assumed constant and equal. Ignoring f in the expression, we get

$$(T_{t3} - T_{t2}) \;=\; (T_{t4} - T_{t5}) \tag{5.53}$$

Dividing by T_o and simplifying we get

$$\theta_o\,(\tau_c - 1) \;=\; \theta_b\,(1 - \tau_t)$$

Thus

$$\tau_t \;=\; 1 - \frac{\theta_o}{\theta_b}(\tau_c - 1) \tag{5.54}$$

The term $[\theta_b/(\tau_c\theta_o)][\tau_c\tau_t\theta_o - 1]$ of equation (5.51) becomes $[\theta_b\tau_t - \theta_b/\tau_c\theta_o)]$ which in conjunction with equation (5.54) becomes $[\theta_b - \theta_o\,(\tau_c - 1) - \theta_b/(\tau_c\theta_o)]$.

Thus, the expression for thrust per unit flow rate becomes,

$$\frac{F}{\dot{m}_a a_o} \;=\; M_o\left[\sqrt{\frac{\theta_b - \theta_o\tau_c + \theta_o - \theta_b/(\tau_c\theta_o)}{(\theta_o - 1)}} - 1\right] \tag{5.55}$$

The result for ramjet is obtained by setting τ_c = 1. It is

$$\left(\frac{F}{\dot{m}_a a_o}\right)_{ramjet} \;=\; M_o\left[\sqrt{\frac{\theta_b}{\theta_o}} - 1\right]$$

which is the same as equation (5.23). The thrust at $M_o = 0$ called *static thrust* is obtained by recognizing that $\theta_o - 1 = [(\gamma-1)/2]M_o^2$ and so, $M_o/\sqrt{\theta_o - 1} = \sqrt{2/(\gamma - 1)}$. We get,

$$\frac{F}{\dot{m}_a a_o} \;=\; \sqrt{\frac{2}{\gamma - 1}(\theta_b - \tau_c + 1 - \frac{\theta_b}{\tau_c})} \tag{5.56}$$

This equation can be recast as

$$\frac{F}{\dot{m}_a a_o} \;=\; \sqrt{\frac{2}{\gamma - 1}(\tau_c - 1)(\frac{\theta_b}{\tau_c} - 1)} \tag{5.57}$$

The specific impulse is obtained as (see equation 5.20)

$$\frac{I_{sp}}{a_o} \;=\; \frac{1}{f}.\frac{F}{\dot{m}_a a_o}$$

The fuel fraction f used is obtained by striking energy balance across the burner. We have

$$\dot{m}_f Q \;\simeq\; \dot{m}_a c_p\,(T_{t4} - T_{t3}) \tag{5.58}$$

Therefore,

$$\frac{1}{f} \;=\; \frac{Q}{c_p T_o}\cdot\frac{1}{(\theta_b - \tau_c\theta_o)} \tag{5.59}$$

Then,

$$\frac{I_{sp}}{a_o} = \frac{Q}{c_p T_o}.\frac{F}{\dot{m}_a a_o}.\frac{1}{(\theta_b - \tau_c \theta_o)} \tag{5.60}$$

$$\frac{I_{sp}}{a_o} \cdot \frac{c_p T_o}{Q} = \frac{M_o}{(\theta_b - \tau_c \theta_o)} \left[\sqrt{\frac{\left(\theta_b - \theta_o \tau_c + \theta_o - \frac{\theta_b}{\tau_c \theta_o}\right)}{(\theta_o - 1)}} - 1 \right]$$

The mass flow rate ingested is obtained from

$$\dot{m}_a(1+f) = \rho_7 V_7 A_7 = \frac{p_7}{RT_7}.M_7.\sqrt{\gamma R T_7}.A_7 \tag{5.61}$$

Using $f \ll 1$, $p_7 = p_o$ and $T_7 = \frac{T_7}{T_o}.T_o$, we get

$$\dot{m}_a a_o \simeq \gamma P_o A_7.M_7.\sqrt{\frac{T_o}{T_7}} \tag{5.62}$$

Using expressions from (5.48), (5.46) and (5.54), we get

$$\dot{m}_a a_o = \gamma p_o A_7.\frac{\tau_c \theta_o}{\theta_b}\sqrt{\frac{2}{(\gamma-1)}\left(\theta_b - \tau_c \theta_o + \theta_o - \frac{\theta_b}{\tau_c \theta_o}\right)} \tag{5.63}$$

Using the above result (5.63) in equation (5.55) one can obtain the dimensionless thrust, $F/p_o A_7$ stated in functional form as

$$\frac{F}{p_o A_7} = F\left(\tau_c \text{ or } \pi_c,\ M_o \text{ or } \theta_o,\ \theta_b = \frac{T_{t4}}{T_o}\right) \tag{5.64}$$

Thus, the dimensionless thrust is dependent on compressor pressure ratio, flight Mach number and ratio of turbine inlet temperature to ambient temperature. It must be remembered that all these variables vary independently and affect the performance significantly.

The static thrust can be expressed as

$$\frac{F}{p_0 A_7} = \frac{2\gamma}{(\gamma-1)}(\tau_c - 1)(1 - \frac{\tau_c}{\theta_b}) \tag{5.65}$$

The implication of thrust per unit flow rate is that larger this value is, the more compact the engine is. Typical values of $(F/\dot{m}_a a_o)$ vary from 1.8–3.2. We should now estimate the values of thrust per unit flow rate and specific impulse for specific values of parameters. Two conditions generally used to indicate the performance parameters are those at sea level for ISA conditions, T_o = 288.15 K, p_o = 101.3 kN/m^2 and at cruise conditions of M_o = 0.8, altitude of 11 km (for ISA conditions, T_o = 226.15 K, p_o = 22.6 kN/m^2) indicating the start of tropopause. These are

Table 5.1: Results for nozzle with optimum expansion

Condition	$\frac{F}{\dot{m}_a a_o}$	$\frac{\dot{m}_a a_o}{p_o A_7}$	$\frac{F}{p_o A_7}$	V_7 m/s	V_o m/s	$\frac{F}{A_7}$ kN/m^2	$\frac{I_{sp}, kNs/kg}{\text{sfc,kg/kg hr}}$
$M_o = 0$							44.9
S.l, ISA	1.8	1.08	1.94	612	0	197	0.8
$M_o = 0.8$							34.0
11km, ISA	1.76	1.30	2.28	756	235	51.6	1.06

relevant in the case of civil aircraft. For military aircraft, the conditions depend on the requirements.

Two sets of parameters, one for take-off and one for cruise conditions are considered as follows.

Set I: $p_o = 101.3kPa$, T_o = 288.15 K, M_o = 0, π_c = 4.0 (τ_c = 1.484), T_{t4} = 1000 K, (θ_b = 1000/288.15 = 3.4), Q = 42.0 MJ/kg, c_p= 1.0 kJ/kg K, (Q/c_pT_o = 145.7),

Set II: $p_o = 22.6kPa$, T_o = 216.15 K, M_o = 0.8, π_c = 4.0 (τ_c = 1.484), T_{t4} = 1000 K, (θ_b = 1000/216.15 = 4.63), Q = 42.0 MJ/kg, c_p = 1.0 kJ/kg K, (Q/c_pT_o = 194.3).

The results of the first four columns in Table 5.1 are dependent on Mach number and ambient temperature through defining of θ_b and the ambient pressure enters in absolute terms only in the evaluation of thrust.

It can be noted that the thrust per unit flow rate decreases (though marginally here) and mass flow rate ratio increases. This happens largely because Mach number has increased. The velocity difference ($V_7 - -V_o$) decreases with flight speed as can be seen from the Table 5.1. Part of the reduction in thrust noted in the table is due to the reduction in velocity increment through the turbojet. It is a known observation that increase in flight speed leads to increase in mass flow rate inducted, but decrease in the velocity increment through the system, thus, keeping the variation in thrust to a minimum. The dominant effect of the ambient pressure in decreasing the thrust to about a quarter of that at the sea level is clearly seen in the results of the sixth column.

Another interesting feature of the results is the fact that the specific impulse is lower for cruise conditions than for take-off. This feature could be noted from the tables where the data of various engines have been given (see the data on turbojet J85-4 in Table 1.4, or turbofans GE CF 6 50M or RB 211 in Table 1.6 for instance). The reason why this occurs is that the turbine inlet temperature (TIT, for short) being nearly fixed, the fuel required to raise the fluid to this temperature is larger at high altitudes where the ambient temperature is lower. In some instances, this could be different; it depends on the the engine operational scheme. If the control

system drops TIT due to other constraints, the performance at altitude could be better than that at ambient temperature. This situation arises in a natural way in actual flight operations. A four engine aircraft is required to function even if one engine fails completely. This means that three engines would be required to deliver the thrust required of four engines under normal flight conditions. This implies that each engine in a four-engine configuration produces 75 % of the thrust that it is expected to be produced in a three-engine configuration. Thus, each engine works at a lower thrust level in a nominal four-engine configuration; this is achieved by operating the combustor at a lower f. Typically, the temperature gets dropped by 60 to 75°C in the process. This will enhance the life of engines significantly. When the engine-out condition gets created, the engine can generate the required thrust only with higher mass flow rate derived from higher density that can be obtained by reducing the altitude of operation.

It is interesting to calculate the power needed by the compressor for the above case. At an air flow rate of 25.4 kg/s (for instance, for J 3 IHI-7C Japanese engine, see Table 1.4), with parameters of set I, Compressor power is 25.4 $kg/s\times$ 1.0 kJ/kgK $\times(427.7 - -288.2)K$ = 3541 kW or 3.54 MW. This engine produces about 13.7 kN of thrust and can be considered to be in the range of small engines. For Olympus engine used on Concorde aircraft, the compressor power works out to 63 MW. These values indicate to one aspect of the testing problems of compressors and turbines – for providing power to test the compressors and arrangements for absorbing the power for turbines.

5.2.2 Choked Nozzle

Both turbojet and turbofans (core engine) operate under conditions of nozzle being choked. Under these conditions, the pressure at the minimum cross section of the convergent end will be larger than the ambient pressure. The contribution by the pressure thrust can be as much as 20 – 25 %. The loss in thrust due to under-expansion rarely exceeds a few percent. The analysis for the case of choked nozzle is as follows. As different from the earlier analysis where we got M_7 from $p_7 = p_o$, we get p_7 from $M_7 = 1$. We have

$$F = \dot{m}_a\ (V_7 - V_o)\ +\ A_7\ (p_7 - p_o) \tag{5.66}$$

We can write,

$$\frac{F}{p_o A_7}\ =\ \frac{\dot{m}_a a_o}{p_o A_7}\left[\sqrt{\frac{T_7}{T_o}} - M_o\right]\ +\ \left(\frac{p_7}{p_o} - 1\right) \tag{5.67}$$

We get from equation (5.46) and (5.54)

$$\frac{T_7}{T_o}\ =\ \frac{2\theta_b\tau_t}{(\gamma+1)}\ =\ \frac{2\{\theta_b - \theta_o(\tau_c - 1)\}}{(\gamma+1)} \tag{5.68}$$

Further,

$$\frac{p_7}{p_o} = \left[\frac{2\tau_c\theta_o}{(\gamma+1)}\left\{1-\frac{\theta_o}{\theta_b}(\tau_c-1)\right\}\right]^{\gamma/(\gamma-1)} \tag{5.69}$$

and

$$\frac{\dot{m}_a a_o}{p_o A_7} = \gamma\,\frac{p_7}{p_o}\sqrt{\frac{T_o}{T_7}} \tag{5.70}$$

We can rewrite F/p_oA_7 as,

$$\frac{F}{p_oA_7} = \gamma\frac{p_7}{p_o}\left[1-\sqrt{\frac{T_7}{T_o}}M_o\right]+\frac{p_7}{p_o}-1 \tag{5.71}$$

$(F/\dot{m}_a a_o)$ can be written as

$$\frac{F}{\dot{m}_a a_o} = \left[\sqrt{\frac{T_7}{T_o}}-M_o\right]+\frac{p_oA_7}{\dot{m}_a a_o}\left[\frac{p_7}{p_o}-1\right] \tag{5.72}$$

which can be expressed as

$$\frac{F}{\dot{m}_a a_o} = \left[\sqrt{\frac{T_7}{T_o}}-M_o\right]+\frac{1}{\gamma}\sqrt{\frac{T_7}{T_o}}\left[1-\frac{p_o}{p_7}\right] \tag{5.73}$$

For static conditions M_o= 0 (θ_o= 1), one can write out the expressions as,

$$\frac{F}{p_0A_7} = (\gamma+1)\left[\frac{2}{(\gamma+1)}\left\{\tau_c-\frac{\tau_c(\tau_c-1)}{\theta_b}\right\}\right]^{\frac{\gamma}{(\gamma-1)}}-1 \tag{5.74}$$

and

$$\frac{F}{\dot{m}_a a_o} = \frac{\sqrt{2(\gamma+1)(1+\theta_b-\tau_c)}}{\gamma}\left[1-\frac{1}{(\gamma+1)}\left\{\frac{2\tau_c}{\gamma+1}\left(1-\frac{(\tau_c-1)}{\theta_b}\right)\right\}^{-\frac{\gamma}{(\gamma-1)}}\right] \tag{5.75}$$

The expression for specific impulse remains the same as equation (5.60). The above expression for $(F/\dot{m}_a a_o)$ can be introduced into equation (5.60) to get the specific impulse. We will now present the calculations of the mass flow rate, thrust per unit flow rate and specific impulse for typical engine and flight parameters set out below for take-off and cruise conditions respectively. The principal difference between these data sets and the earlier ones is that the compressor pressure ratio is much higher in the case to be discussed presently.

Set III: M_o = 0 (θ_o = 1), p_o = 101.3 kN/m^2, T_o = 288.15 K, π_c = 12 (τ_c= 2.03), T_{t4} = 1200 K, c_p = 1.0 $kJ/kg\ K$, a_o = 340 m/s, θ_b = 4.16, Q/c_pT_o = 145.7.

Computation with these data leads to

Table 5.2: Results of calculation for choked nozzle, * = kN s/kg, ** kg/kg h

Condition	$\frac{F}{\dot{m}_a a_o}$	$\frac{\dot{m}_a a_o}{p_o A_7}$	$\frac{F}{p_o A_7}$	$\frac{p_7}{p_o}$	V_7 m/s	V_o m/s	$\frac{F}{A_7}$ kN/m^2	$I_{sp}, *$ sfc,**
$M_o = 0$	1.61+0.66							52.8
S.l, ISA	= 2.27	2.02	4.58	2.32	550	0	464	0.67
$M_o = 0.8$	1.11+1.04							37.7
Altitude	= 2.15	3.09	6.65	4.22	563	236	150	0.94
11 km, ISA								

p_7/p_o = 2.326, T_7/T_o = 2.607, $\dot{m}_a a_o$ / $p_o A_7$ = 2.017, $F/\dot{m}_a a_o$ = 1.614 + 0.657 = 2.271, $F/p_o A_7$ = 3.25 + 1.44 = 4.58, and I_{sp}/a_o = 155.2. This leads to I_{sp} = 52.8 $kN.s/kg$ or sfc = 0.668 $kg/kg\ hr$

With Set IV: M_o = 0.8 (θ_o = 1.128), p_o = 22.6 kN/m^2, T_o = 216.15 K, a_o = 294 m/s, V_o = 848 km/hr, π_c = 12 (τ_c = 2.03), T_{t4} = 1200 K, θ_b = 5.55, $Q/c_p T_o$ = 194.4, we get

p_7/p_o = 4.22, T_7/T_o = 3.66, $\dot{m}_a a_o/p_o A_7$= 3.09, $F/\dot{m}_a a_o$ = 1.11 + 1.04 = 2.15, $F/p_o A_7$ = 3.43 + 3.22 = 6.65, and I_{sp}/a_o= 128.3. This leads to I_{sp} = 37.7 $kN.s/kg$ or sfc = 0.935 $kg/kg\ hr$. These results can be set out in a tabular form as shown in Table 5.2.

The results noted above are similar to those discussed earlier for the case of optimum expansion. The results on p_7/p_o show that for the case of take-off, the choice of a convergent nozzle is just about satisfactory. However, for the case of cruise, the under-expansion is so large that performance optimization needs a C–D nozzle in this case. Of course, one should note that the results presented above are for an ideal cycle and if pressure drops through the system are taken into account, the pressure ratio will not be as high as indicated.

Having known the orders of magnitude, we should like to ask several questions regarding the performance.

One question concerns the choice of compressor pressure ratio (π_c). Is there an optimum or not? In order to answer this question, we should first be clear which parameters to hold constant. The turbine inlet temperature, flight and engine speeds are held constant. Thus, we ask if the thrust per unit flow rate can be maximized with the choice of π_c or τ_c.

For the case of optimum expansion, equation (5.51) needs examination. Maximum of $F/m_a a_o$ for fixed M_o (and so θ_o) and θ_o is obtained by maximizing $[-\theta_c \tau_c - \theta_b/(\tau_c \theta_o)]$

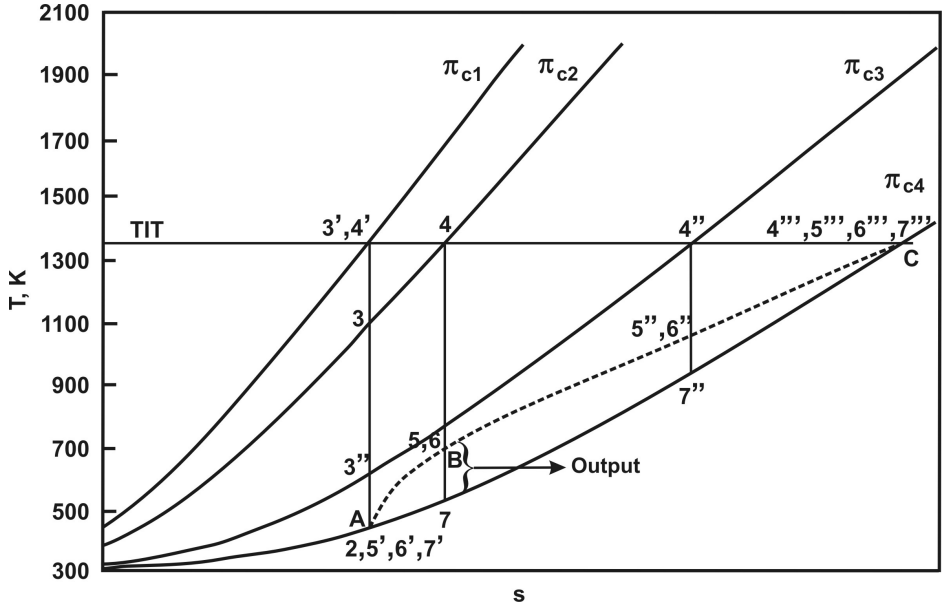

Figure 5.5: T-s diagram for a turbojet to explain the optimum τ_c with $\theta_b(\pi_c)$. The dotted line shows the net output from the turbojet for different compressor pressure ratios

This leads to

$$-\theta_o + \frac{\theta_b}{\tau_c^2 \theta_o} \quad \Rightarrow \quad \tau_c = \frac{\sqrt{\theta_b}}{\theta_o} \tag{5.76}$$

One can further show that this condition leads to maximizing $F/m_a a_o$. This can be explained by using the cycle diagram for various pressure ratios as in Figure 5.5. One can notice from this figure the nominal cycles, the cycles with much higher pressure ratio and lower pressure ratio. The work available for expansion in the nozzle is the enthalpy difference between 6 and 7. At the extreme case of very high pressure ratio such that the exit temperature of the compressor equals the turbine inlet temperature, the situation calls for no fuel input and the turbine uses all the energy available to run the compressor (under ideal conditions) and thus, leaves nothing for expansion (path A3′4′A). Hence, no thrust is developed in this condition. At the other end of small pressure ratio, very little enthalpy is left for expansion, understandably because small pressure ratio allows for small enthalpies only (A4‴5‴6‴C for which $\pi_{c,4}$ = 1). Hence, there must be a maximum in between (A34B7). The net output follows the difference between the curve ABC and constant pressure line passing through C (the segment B7). The result is a consequence of a fixed turbine inlet temperature, a feature which is physically realistic. We shall subsequently explore the result for engine with inefficient components.

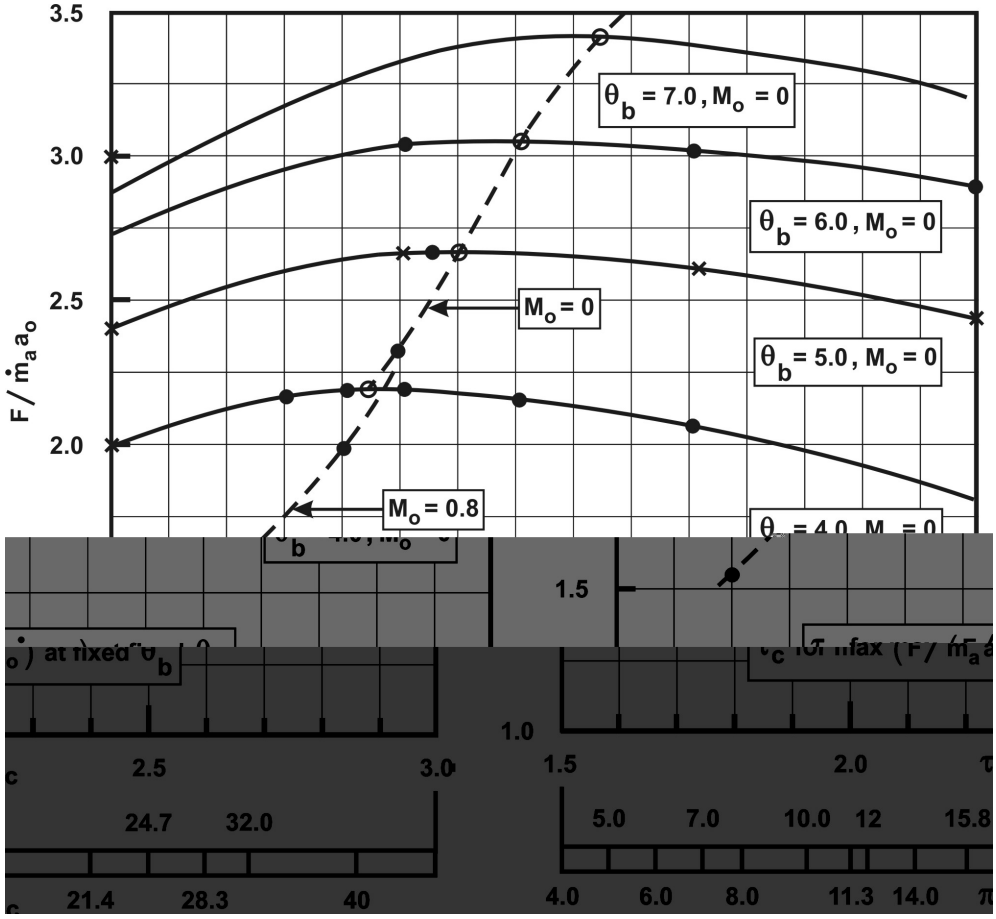

Figure 5.6: Variation of $F/m_a a_0$ with $\tau_c(\pi_c)$ and θ_b for a choked nozzle. Note that the dotted lines correspond to the peak in $F/m_a a_0$

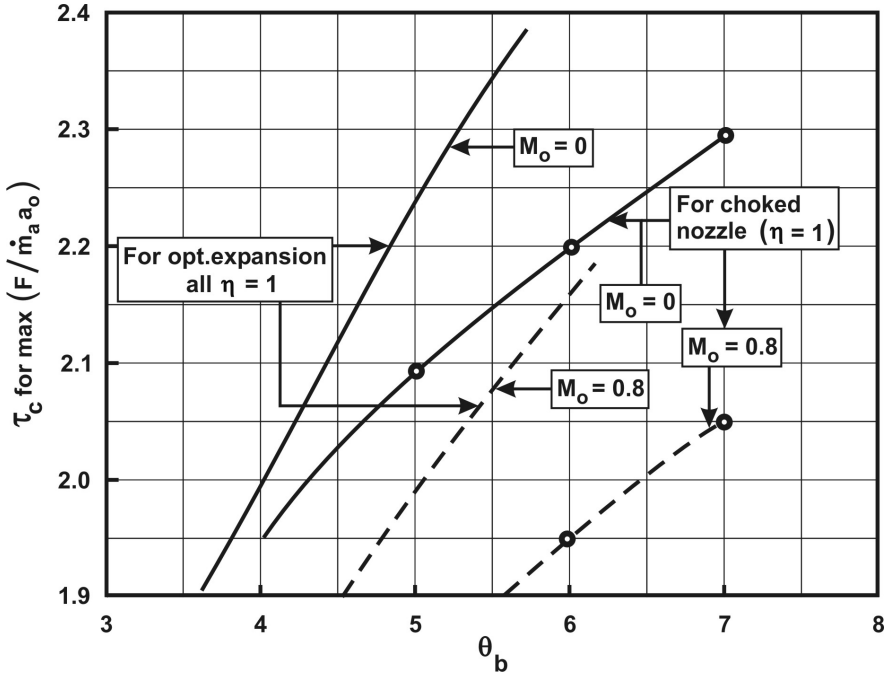

Figure 5.7: Variation of optimum τ_c with $\theta_b(\pi_c)$ for different conditions

There is no optimum for I_{sp} with variation of π_c (τ_c). Increase of τ_c increases I_{sp} monotonically till $\tau_c = \theta_b/\theta_o$. At this condition, $I_{sp} \rightarrow \infty$ because fuel input is zero. At this condition, $F \rightarrow 0$. This is the condition which corresponds to maximum propulsive efficiency, a feature which we have already discussed in chapter 3. Thus, a choice of larger π_c is helpful increasing I_{sp} beyond the one which gives maximum $(F/\dot{m}_a a_o)$.

Since many turbojets work with choked nozzle, we must also examine the results of choked nozzle. Since it is algebraically messy to deal with this case, the equation (5.73), has been used for making plots of $(F/\dot{m}_a a_o)$with τ_c for θ_b = 4 to 7 for M_o = 0 and M_o = 0.8. These are shown in Fig 5.6. The detailed plots for M_o = 0.8 are not shown for the sake of clarity. As can be seen from the curves, the thrust per unit flow rate has a maximum with compressor temperature (pressure) ratio and also increases with θ_b. The variation of the optimum compressor temperature ratio with θ_b is shown in Fig 5.7. On this figure, the results of optimum expansion (which can be obtained analytically) and those for choked condition are shown. Though the nature of the curves is similar, the optimum values given by the two are different. For instance, for M_o = 0.8 and θ_b = 5, the optimum pressure ratio is 11 for optimum expansion and 8.6 for choked flow. It must be further noted that these results are for the engine with 100 % efficiency. Thus, the broad conclusion that can be drawn from these calculations is that there is an optimum compres-

sor pressure ratio which increases with the ratio of burner outlet temperature to ambient temperature, but decreases with Mach Number like $1/\theta_o$.

The variation of $(F/\dot{m}_a a_o)$with θ_b has other implications. For clarifying these, the results of Fig. 5.7 are re-plotted in Fig. 5.8 for fixed τ_c values. The slope of the curves can be used to estimate percentage variations in $(F/\dot{m}_a a_o)$with similar variations in θ_b (or TIT = T_{t4}/T_o). As can be noted from Fig. 5.8,

$$\frac{\Delta(F/\dot{m}_a a_o)}{(F/\dot{m}_a a_o)} \simeq b\frac{\Delta\theta_b}{\theta_b} \simeq b\left(\frac{\Delta T_{t4}}{T_{t4}}\right)_{T_o=Const}$$

where b can be estimated from the figure to be 0.6 – 0.8. The static thrust is given by

$$F = \frac{2\gamma}{(\gamma-1)}p_o A_7 \frac{\tau_c}{\theta_b}(\theta_b - \tau_c + 1 - \frac{\theta_b}{\tau_c}) \tag{5.77}$$

This can be rewritten as

$$F = \frac{2\gamma}{(\gamma-1)}p_o A_7(\tau_c - 1)(1 - \tau_c/\theta_b) \tag{5.78}$$

The dependence on the ambient temperature comes through T_o. For fixed T_{t4},

$$\frac{dF}{F} = -\frac{1}{[(\theta_b/\tau_c) - 1]}\frac{dT_o}{T_o} = -(0.4 \text{ to } 0.6)\frac{dT_o}{T_o} \tag{5.79}$$

Since in most engines the choice of τ_c and θ_b are interlinked by optimum considerations discussed earlier, the broad band shown in Figure 5.8 indicates this trend. In such a case, change in turbine inlet temperature (TIT) from 1100 to 1400 K (θ_b from 3.8 to 4.86 for ISA conditions) causes the dimensionless thrust per unit flow rate to move from 1.7 to 2.5, a near fifty percent increase. This increase results in the corresponding decrease of air flow needed to produce the same thrust. The air flow rate being proportional to exit area, the decrease in diameter will be by 25 %. Thus, the engine becomes more compact with the choice of higher θ_b and τ_c or higher TIT and compressor pressure ratio. Figure 5.8 shows two engines whose data seem to roughly plot on the trends shown.

While the dimensionless thrust per unit flow rate increases with increase in the burner inlet temperature, the specific impulse decreases in the range of parameters of practical interest. Table 5.3 shows the typical values. In obtaining the results of Table 5.3, the compressor pressure ratio is chosen as optimum for choked nozzle flow. As can be seen, the specific impulse decreases significantly with the increase in turbine inlet temperature.

Figures 5.6 - 5.8 can be used to obtain the dependence of thrust on the ambient temperature, T_o. Figure 5.9 brings out the results explicitly. The results are

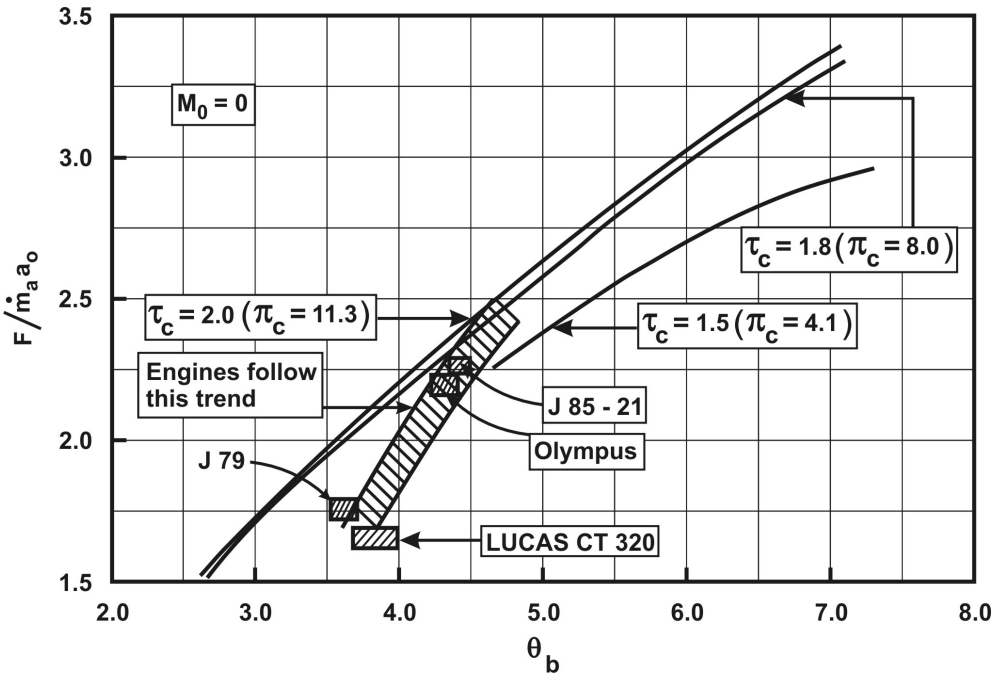

Figure 5.8: Variation of thrust per unit flow rate per with burner outlet temperature

Table 5.3: Dependence of Specific impulse on Turbine Inlet temperature (* From Fig. 5.6 for choked nozzle; M_o = 0; $(Q/c_pT_o)a_o$ = 49.5 kN s/kg)

θ_b	τ_c	$F/\dot{m}_a a_o$	I_{sp} kNs/kg	sfc kg/kg.hr
4	1.95*	2.18	52.7	0.67
5	2.1	2.68	45.8	0.77
6	2.2	3.05	39.7	0.89

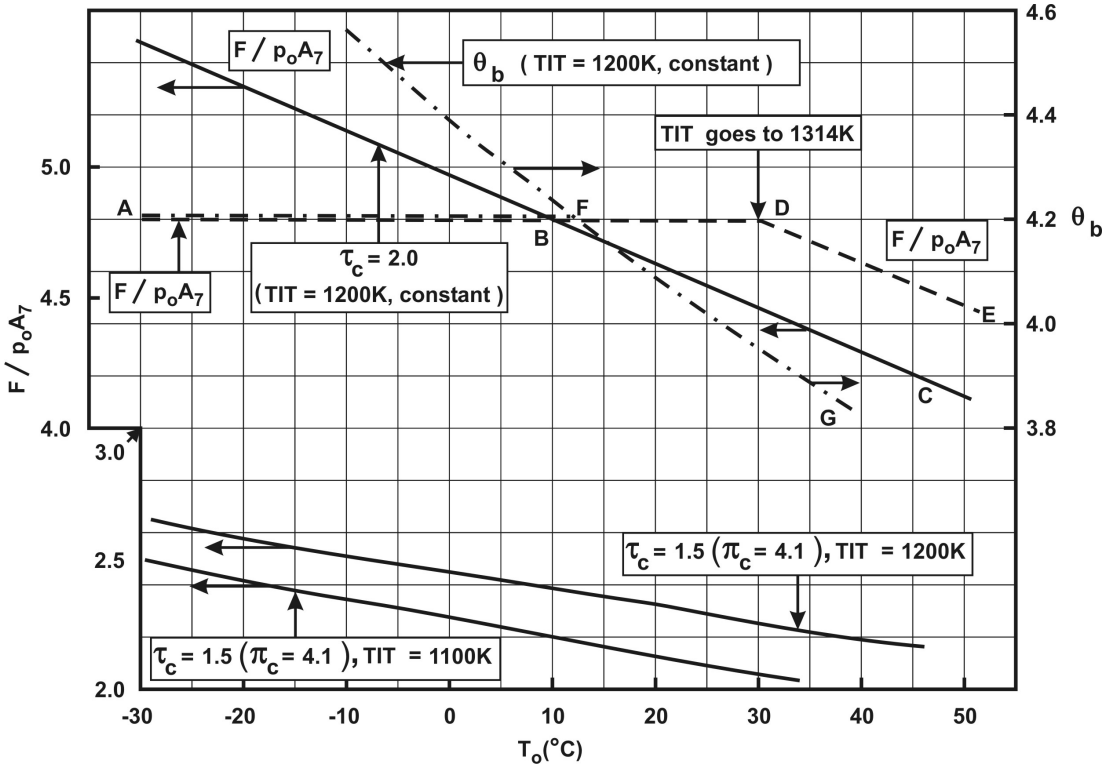

Figure 5.9: Variation of F/$p_0 A_7$ with T_0 the ambient temperature.

shown to provide dependence of thrust on ambient temperature with compressor pressure ratio and turbine inlet temperature as parameters. The variation of θ_b for a TIT = 1200 K is also shown. The dependence of thrust on ambient temperature is of considerable concern to operation in tropical climates. A rise in ambient temperature of 10^oC causes a decrease on thrust by about 2 – 4 % depending on whether the engine is of low pressure ratio or high pressure ratio. If the peak thrust demanded is for an ambient temperature of 12^oC, then, the control system maintains the same θ_b and generates a fixed thrust as indicated by the line AF in Figure 5.9. The loss in thrust at higher ambient temperatures common in Tropical countries can be particularly inconvenient at take-off conditions. In order to alleviate the problems of reduced thrust in tropical countries, a feature known as “flat rating” is performed. If the nominal thrust variation is along ABC, performing flat rating curve leads to the thrust variation along ABDE. The enhanced thrust between B and D in comparison to BC is obtained essentially by allowing combustor temperatures to exceed normal maximum temperature. In Figure 5.9, the TIT increases from 1200 K up to 1314 K at 30^oC. Such a modification is caused some times by better materials for combustor and turbine, bur more often by a re-

Table 5.4: Influence of parameters on performance of a turbojet

Parameter (increase in)	Thrust per unit flow rate $((F/\dot{m}_a a_o))$	Thrust F/A_7	Specific Impulse	Comment
Pr. ratio (π_c)	increases	increases	increases	
TIT (T_{t4})	increases	increases	decreases	Optimum considerations need use of higher TIT with higher π_c
Ambient pressure	increases	increases	increases	
Ambient temp.	linearly decreases	linearly decreases	linearly –	
Altitude	–	decreases	–	

evaluation and re-definition of the life of the components as well as limits to the use of the engine in the range BD. If the engine were to reside in the range BD for more than a few minutes the life of combustor and turbine will possibly be reduced by a few percent.

An *ab initio* design can take care of the thrust demand with ambient temperature with little difficulty.

Thus, in the above discussion we have covered the dependence of thrust & fuel consumption parameters, namely, pressure ratio, turbine inlet temperature and ambient temperature which in some combination can reflect the effect of altitude. Table 5.4 summarizes many of these features.

5.2.3 Turbojet With an Afterburner

The present analysis, like in the earlier cases, is meant to determine the specific thrust, thrust and the specific fuel consumption. Figure 5.10 shows the path of the fluid on a cycle diagram. The fluid will take the path 5-6 which is a constant pressure heat addition in the jet pipe and raises the fluid to high temperatures characteristic of afterburners. Most afterburners function with the exit nozzle choked. Also, as explained earlier, the exit nozzle area is to be increased to accommodate the marginally enhanced mass flow of reduced density. The present analysis uses the same notation for the various stations like in the earlier case of a simple turbojet. The only point to notice is that station 6 refers to the exit

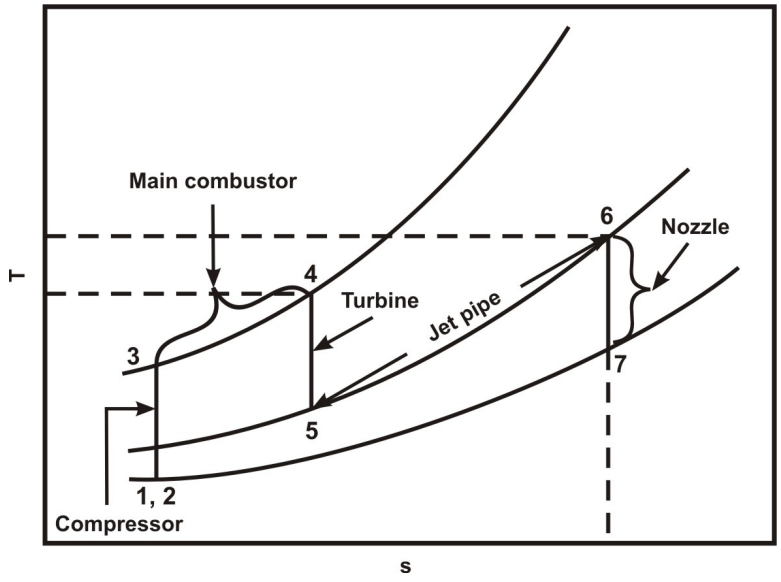

Figure 5.10: The Temperature-entropy plot for a turbojet with an afterburner

of the afterburner and station 5, inlet of the afterburner. The afterburner exit temperature (T_{t6}) is a control variable and the ratio (T_{t6}/T_o) is denoted by θ_{ab}.

$$\frac{F}{m_a a_o} = M_o \left[(1 + f + f_{ab}) \frac{M_7}{M_o} \sqrt{\frac{T_7}{T_o}} - 1 \right] + A_7 (p_7 - p_o)$$

Where f_{ab} is the afterburner fuel mass fraction = $\dot{m}_{f,ab}/\dot{m}_a$. We present the analysis for optimum expansion and also for choked nozzle.

Noting that all efficiencies are treated as unity, specific heats as constant and equal, specific heat ratio is the same both for compressor and turbine sections and $T_{t2} = T_{to}$, $T_{t7} = T_{t6}$, we obtain $T_{t7} = T_7(1 + \frac{\gamma-1}{2} M_7^{/} 2) = \theta_{ab} T_o$

$$\text{Therefore, } \frac{T_7}{T_o} = \left(\frac{\theta_{ab}}{1 + \frac{\gamma-1}{2} M_7^2} \right) \tag{5.80}$$

$$\text{Similarly, } p_{t7} = p_7 \left(1 + \frac{\gamma - 1}{2} M_7^2 \right)^{\gamma/\gamma-1} = \pi_c \pi_t \theta_o^{\gamma/(\gamma-1)} p_o \tag{5.81}$$

Since, p_7 = p_o for optimum expansion, and π_c, $\pi_t \equiv \tau_c^{\gamma/\gamma-1}$, $\tau_t^{\gamma/\gamma-1}$, we have $1 + \frac{\gamma-1}{2} M_7^2 = \tau_t \tau_c \theta_o$.

$$\text{Thus, } M_7 = \sqrt{\frac{2}{\gamma - 1}(\tau_t \tau_c \theta_o - 1)} \tag{5.82}$$

And, $M_o = \sqrt{\frac{2}{\gamma-1}(\theta_o - 1)}$, by definition compressor – turbine power balance gives $\tau_t = 1 - \theta_o(\tau_c - 1)/\theta_b$

Putting together the results from the above equations we get,

$$\frac{F}{\dot{m}_a a_o} = M_o \left[(1 + f + f_{ab}) \sqrt{\frac{\theta_{ab}}{\theta_o - 1} \{1 - \frac{1}{\tau_t \tau_c \theta_o}\}} - 1 \right] \tag{5.83}$$

The mass flow rate, $\dot{m}_a$ is given by, $\dot{m}_a = \rho_7 A_7 V_7/(1 + f + f_{ab})$

It can also be written as

$$\dot{m}_a a_o = \gamma p_o A_7 \times M_7 \frac{p_7}{p_o} \sqrt{\frac{T_o}{T_7}} \times \frac{1}{(1 + f + f_{ab})} \tag{5.84}$$

In the above case,

$$\frac{\dot{m}_a a_o}{p_o A_7} = \frac{\gamma}{(1 + f + f_{ab})} \sqrt{\frac{2}{\gamma - 1}(\tau_c \tau_t + \theta_o - 1)}.1.\sqrt{\frac{\tau_c \tau_t \theta_o}{\theta_{ab}}} \tag{5.85}$$

$$\frac{\dot{m}_a a_o}{p_o A_7} = \frac{\gamma}{(1 + f + f_{ab})} \sqrt{\frac{2\tau_c \tau_t \theta_o (\tau_c \tau_t + \theta_o - 1)}{(\gamma - 1)\theta_{ab}}} \tag{5.86}$$

In the above equations $f + f_{ab} \simeq$ 0.05 -0.067.

Specific impulse can be expressed as

$$I_{sp} = \frac{1}{f + f_{ab}} . \frac{F}{\dot{m}_a a_o} . a_o \tag{5.87}$$

The energy balance across the combustion chamber and afterburner is

$$(\dot{m}_f + \dot{m}_{f_{ab}})Q = \dot{m}_a c_p (T_{t4} - T_{t3}) + \dot{m}_a c_p (T_{t6} - T_{t5}) \tag{5.88}$$

In the terms on the right hand side, both f and f_{ab} are ignored. This gives

$$(f + f_{ab})Q = c_p (T_{t4} - T_{t3}) + c_p (T_{t6} - T_{t5}) \tag{5.89}$$

It is possible to rearrange the terms in the above equation such that

$$T_{t6} - T_{t5} + T_{t4} - T_{t3} = T_{t6} - (T_{t5} - T_{t4}) - (T_{t3} - T_{t2}) - (T_{t2} - T_{to}) - T_{to} \tag{5.90}$$

If we note that $T_{t5} - T_{t4} = T_{t3} - T_{t2}$ from compressor turbine work balance, and $T_{t2} = T_{to}$, we get

$$(f + f_{ab})Q = c_p(T_{t6} - T_{to}) \tag{5.91}$$

If we divide both sides by c_pT_o and rearrange the terms, we get

$$\frac{1}{(f + f_{ab})} = \frac{Q}{c_pT_o}.\frac{1}{(\theta_{ab} - \theta_o)} \tag{5.92}$$

Using the above expression in equation (5.87), we get

$$I_{sp} = a_o.\frac{Q}{(c_pT_o)} \times \frac{F}{\dot{m}_a a_o} \times \frac{1}{(\theta_{ab} - \theta_o)} \tag{5.93}$$

Since we already have $(F/\dot{m}_a a_o)$, we can compute I_{sp}.

In the case of a choked nozzle, $M_7 = 1$ and p_7 is to be obtained from the stagnation pressure relationship. Firstly, using $M_7 = 1$ in equation (5.80) and (5.81) we get,

$$\frac{T_7}{T_o} = \frac{2\theta_{ab}}{(\gamma - 1)} \tag{5.94}$$

and

$$\frac{p_7}{p_0} = \left[\frac{2\tau_c\tau_t\theta_0}{(\gamma + 1)}\right]^{\gamma/(\gamma-1)} \tag{5.95}$$

The mass flow rate can be obtained from equation (5.84) as,

$$\dot{m}_a a_o = \frac{\gamma p_o A_7}{(1 + f + f_{ab})}\sqrt{\frac{(\gamma + 1)}{2\theta_a b}}.\left\{\frac{2\tau_c\tau_t\theta_0}{(\gamma + 1)}\right\}^{\gamma/(\gamma-1)} \tag{5.96}$$

The thrust for unit flow rate expression becomes

$$\frac{F}{\dot{m}_a a_o} = M_0\left[(1 + f + f_{ab})\left\{\sqrt{\frac{\theta_{ab}}{\theta_0 - 1}} - 1\right\}\right] + \frac{p_0 A_7}{\dot{m}_a a_o}\left[\frac{p_7}{p_0} - 1\right] \tag{5.97}$$

The expression for thrust is

$$\frac{F}{p_0 A_7} = M_0\frac{\dot{m}_a a_o}{p_o A_7}\left[(1 + f + f_{ab})\left\{\sqrt{\frac{\theta_{ab}}{\theta_0 - 1}} - 1\right\}\right] + \left(\frac{p_7}{p_o} - 1\right) \tag{5.98}$$

It is useful now to look at the order of magnitude of various quantities. For the two set of parameters for take-off and at altitude already discussed, calculations can

Table 5.5: Comparison of results for turbojet without and with afterburner (TO + Take-off, Alt. = Altitude, Condn. = Condition; AB = Afterburner, * = kN s/kg, ** = kg/kg h)

Set	Condn.	$\frac{T_7}{T_o}$	$\frac{p_7}{p_o}$	$\frac{\dot{m}_a a_o}{p_o A_7}$	$\frac{F}{\dot{m}_a a_o}$	I_{sp} *	sfc **	$\frac{F}{\dot{m}_a a_o}$ ratio	sfc ratio
III	No AB	2.61	2.32	2.02	2.27	53.9	0.67	1.62	1.79
2-8 (TO)	with AB	6.07	2.32	1.24	3.67	29.5	1.2		
IV	No AB	3.66	4.22	3.09	2.15	37.7	0.94	1.79	1.46
2-8 (Alt.)	with AB	8.08	4.22	1.96	3.85	26.1	1.37		

be made for the case without and with afterburner. The data used and summary of results are as below.

For the case without afterburner, set III and IV are used. The only additional parameter needed is the afterburner exit temperature. It is taken as $T_{t6} = 2100\ K$. For take off and cruise conditions, the values of θ and θ_{ab} will be 4.16, 7.28 and 5.55, 9.7 respectively. Calculations lead to results presented in Table 5.5.

As can be seen from the table, the thrust ratio between the afterburner case and that without is 1.62 and 1.79 at take off and at altitude. The ratio of $(F/\dot{m}_a a_o)$ can also be interpreted as thrust ratio because $\dot{m}_a a_o$ remains about the same with or without afterburner. The change in mass flow rate is due to enhanced fuel flow into the afterburner. This constitutes an additional 3 to 4 % of the flow rate. However, the ratio $\dot{m}_a a_o / p_o A_7$ decreases with afterburner on. As discussed in chapter 1, the increase in exit area is needed to maintain the flow rate. This increase is proportional to the square root of the ratio between the jet pipe exit temperatures with and without afterburner. This increase is substantial by as much as 50 – 60 %. The increase in thrust is obtained at the expense of sfc which also increases by 50 – 80 %. If one examines the results of set IV, one might be tempted to conclude that the condition of afterburner-on could be a normal design operating point since sfc's of 1.37 kg/kghr are acceptable. However, the benefit of large $(F/\dot{m}_a a_o)$ with afterburner is only one component in the total vehicle design. One would normally like to get larger $(F/\dot{m}_a a_o)$ with only marginal changes in sfc, something which can be achieved by increasing TIT. In such a case, 60 % increase is $(F/\dot{m}_a a_o)$ can be obtained at an increase in sfc of 30 – 40 %, whereas for an increase in $(F/\dot{m}_a a_o)$ with afterburner would call for an increase in sfc of 70 – 80 %. This is because *the energy addition occurs at much higher pressure in the main combustor and hence,*

is far more efficient thermodynamically.

5.2.4 Thrust Augmentation by Liquid Injection

As has been discussed in chapter 1, thrust augmentation can be obtained by injecting water or water-methanol mixture into compressor inlet or into the combustion chamber. In the former case, the compressor work is decreased because of the lower inlet temperature. Further, at the same TIT, turbine work available will be larger because of larger flow through it. Consequently, the pressure ratio obtained will be higher and so one gets higher jet pressure and so higher thrust.

In the second case, of the two causes identified above, only the second is valid. The analysis is now carried out to indicate how thrust augmentation and specific impulse deterioration takes place in liquid injection into the combustion chamber.

If f_w is the fraction of water injected into the combustion chamber, the expression for thrust becomes

$$\frac{F}{\dot{m}_a a_o} = M_o \left[(1 + f + f_w) \frac{M_7}{M_o} \sqrt{\frac{T_7}{T_o}} - 1 \right] + \frac{A_7 p_o}{\dot{m}_a a_o} \left(\frac{p_7}{p_o} - 1 \right) \tag{5.99}$$

where $f = \dot{m}_f / \dot{m}_a$ and $f_w = \dot{m}_w / \dot{m}_a$.

We will now treat the case of optimum expansion ($p_7 = p_0$).

Using the procedure of cascading of ratios of total temperature and pressure gives,

$$\frac{M_7}{M_o} = \sqrt{\frac{(\tau_t \tau_c \theta_o - 1)}{(\theta_o - 1}} \tag{5.100}$$

and

$$\frac{T_7}{T_o} = \frac{\theta_b}{\tau_c \theta_o} \tag{5.101}$$

The compressor–turbine power balance gives,

$$\dot{m}_a c_p (T_{t3} - T_{t2}) = \dot{m}_a (1 + f + f_w) c_p (T_{t4} - T_{t5}) \tag{5.102}$$

The pressure in the combustion chamber is altered because of the increase in mass flow downstream. If turbine nozzles are taken as choked as is usually the case, the pressure in the combustion chamber can be taken to be proportional to mass flow rate for constant TIT considered here. Thus, any increase in the flow rate will cause a proportional increase in pressure at the compressor outlet or combustion chamber. This gives

Table 5.6: Nondimensional thrust and specific impulse with different water injection fractions (f_w), * = kN s/kg, θ_b = 5.55, τ_c^o = 2.03, M_o = 0.8, θ_o = 1.128, f = 0.03, a_o = 294 m/s

f_w	τ_c (π_c)	τ_t	$F/m_a a_o$	I_{sp}, *
0.0	2.03 (12)	0.80	2.46	41.8
0.1	2.08 (13)	0.80	2.87	36.9
0.2	2.14 (14.3)	0.81	3.28	34.0
0.3	2.18 (15.3)	0.82	3.70	31.8

$$\frac{p_{t3}}{p_{t2}} = \pi_c = \pi_c^o \frac{(1+f+f_w)}{(1+f)} \tag{5.103}$$

where π_c^o is the nominal pressure ratio.

Equation (5.102) can be reduced to

$$\tau_t = 1 - \frac{\theta_o}{\theta_b} \frac{(\tau_c - 1)}{(1+f+f_w)} = 1 - \frac{\theta_o}{\theta_b} \frac{\tau_c^o \left\{\frac{1+f+f_w}{1+f}\right\}^{\frac{\gamma-1}{\gamma}} - 1}{(1+f+f_w)} \tag{5.104}$$

The expression for $\dot{m}_a$ can be obtained from equation (5.84) by replacing f_{ab} by f_w. We get

$$\dot{m}_a a_o \;=\; \gamma p_o A_7 \times M_7 \frac{p_7}{p_o} \sqrt{\frac{T_o}{T_7}} \frac{1}{(1+f+f_w)} \tag{5.105}$$

The use of equations (5.100) and (5.101) in the above equation gives $\dot{m}_a a_o$. The expression for specific impulse can be obtained after some algebra, as

$$\frac{I_{sp}}{a_o} = \frac{Q}{c_p T_o} \frac{1}{(1+f+f_w)(\theta_b - \tau_c \theta_o) + \mathscr{L}' f_w} \frac{F}{\dot{m}_a a_o} \tag{5.106}$$

In the above equation $\mathscr{L}' = \mathscr{L}/c_p T_o$ with $\mathscr{L}$ representing the heat absorbed by water from a liquid at T_o to a gas at T_{t3}. Typical value of $\mathscr{L}'$ is 8.33. Calculations made with a few values of f_w are illustrated in Table 5.6.

At f_w = 0.3, the increase in thrust due to water injection is by 50 % and the degradation in specific impulse, 20 %. The increase in pressure ratio is by as much as 30 % for f_w = 0.3.

5.2.5 Performance of Turbojet With Inefficient Components

We will describe the efficiencies of various components as follows:

1. Diffuser: The efficiency of the diffuser denoted by η_d' (where the supercript $\prime$ is used to refer to ratio of pressures) is characterized by the ratio of stagnation pressure downstream to upstream. The value is close to 100% ($\sim$ 98 – 99%) for subsonic Mach numbers and decreases to values as low as 15% at high supersonic Mach numbers because of losses across shocks. These are presented in Table 6.1.

2. Compressor: The efficiency of the compressor is defined in terms of total enthalpies (or stagnation temperatures) as

$$\eta_c = \frac{T_{t3} - T_{t2}}{T_{t3'} - T_{t2}} \tag{5.107}$$

where $T_{t3'}$ is the stagnation temperature achieved at the end of compression of pressure ratio π_c due to real gas effects (viscous effects). The expression can be cast as

$$T_{t3'} = T_{t2} + T_{t2}\frac{(\tau_c - 1)}{\eta_c}\ ,\ \tau_c = \pi_c^{\frac{\gamma-1}{\gamma}}$$

Typical values of η_c are 0.80 – 0.87. Larger values of η_c are difficult to achieve because the flow is one of adverse pressure gradient. Recent designs based on insight obtained through computational fluid dynamics have reached the upper end of η_c indicated above.

3. Combustor: The efficiency of the combustor (also termed burner) is related to the loss in stagnation pressure that occurs because of two reasons – frictional loss and thermodynamic effect due to heat addition. It is defined as

$$\eta_c' = p_{t4}'/p_{t3} = p\prime_{t4}/p_{t4} \tag{5.108}$$

Typical values of η_c' are 0.93 – 0.95 for modern combustors.

There is also another efficiency related to combustor – combustion or burner efficiency (η_b). This quantity relates to the complete release of chemical enthalpy into sensible enthalpy. Most combustors are designed to operate with combustion efficiencies of 99 % or better for most operating conditions. Its value is chosen as 100 % for the present analysis. Its influence is felt in the current analysis in the specific impulse through higher fuel consumption as fuel is regulated to meet the specified TIT. More about η_b can be found in section 6.3.3

4. Turbine: The efficiency of the turbine is expressed like in the case of compressor by

$$\eta_t = \frac{T_{t4} - T_{t5'}}{T_{t4} - T_{t5}} \tag{5.109}$$

where $T_{t5'}$ is the actual stagnation temperature downstream of the turbine. It can be re-expressed as

$$T_{t5'} = T_{t4} \; - \; \eta_t(T_{t4} - T_{t5})$$

$$= T_{t4} - \eta_t \, . \, T_{t4}(1 - \tau_t) \; ; \; \tau_t = \pi_t^{\frac{(\gamma-1)}{\gamma}}$$

Typical values of η_t are close to 90–93 $\%$. It is easier to achieve higher efficiencies across the turbine since the flow is accelerating (favorable pressure gradient)

5. Jet Pipe: The losses in the jet pipe are frictional for the flow without afterburning and involve thermodynamic effects for flow with after burning. The losses are described by

$$\eta'_{jp} = p'_{t6}/p_{t5} = p'_{t6}/p_{t6}$$

Typical value of $\eta'_{jp} \simeq 0.95 - 0.97$.

6. Nozzle: The loss in stagnation pressure across the nozzle constitutes the reason for inefficiency in the nozzle.

$$\eta'_n = p'_{t7}/p_{t6} = p'_{t7}/p_{t7}$$

Typically $\eta'_n \simeq 0.95 - 0.97$

If we need to take into account these in the analysis of simple turbojet, we need to examine the equations – the cascading of stagnation pressure.

$$\frac{p_7}{p_0} = \frac{1}{\left(1 + \frac{\gamma-1}{2} M_7^2\right)^{\gamma} (\gamma - 1)} \quad \eta'_n \, \eta'_{jp} \, \pi_t \, \eta'_c \, \pi_c \, \eta'_d \, . \, \theta_o^{\frac{\gamma}{\gamma-1}}$$

we can define

$$\eta = (\eta'_n \, \eta'_{jp} \, \eta'_c \, \eta'_d)^{\frac{\gamma-1}{\gamma}} \tag{5.110}$$

and note $p_7 = p_0$ for the case of optimum expansion to write

$$\left(1 + \frac{\gamma - 1}{2} M_7^2\right) = \eta \, . \, \tau_t \, \tau_c \, \theta_o \tag{5.111}$$

This gives $\frac{M_7}{M_0} = \sqrt{(\eta \, \tau_t \, \tau_c \, \theta_o - 1)}(\theta_o - 1)$ and

$$\frac{T_7}{T_0} = \frac{\theta_b \tau_t}{\left(1 + \frac{\gamma-1}{2} M_7^2\right)} = \frac{\theta_b \tau_t}{\eta\, \tau_t\, \tau_c\, \theta_o} = \frac{\theta_b}{\eta \tau_c \theta_o}$$

Compressor – Turbine power balance gives

$$\dot{m}_a c_p (T'_{t3} - T_{t2}) = \dot{m}_a (1+f) c_p (T_{t4} - T_{t5'}) \tag{5.112}$$

If we invoke the definitions of compressor and turbine efficiencies, we get for $f \ll 1$

$$\theta_o \frac{(\tau_c - 1)}{\eta_c} = \eta_t (\tau_t - 1)\theta_b \tag{5.113}$$

and therefore,

$$\tau_t = 1 - \frac{\theta_o}{\theta_b} \quad \frac{(\tau_c - 1)}{\eta_c \eta_t} \tag{5.114}$$

Thus,

$$\frac{F}{\dot{m}_a a_o} = M_o \left[\sqrt{\frac{(\eta \tau_t \tau_c \theta_o - 1)}{(\theta_o - 1)} \frac{\theta_b}{\eta \tau_c \theta_o}} - 1 \right] \tag{5.115}$$

with τ_t given as above. One can independently examine the influence of η, η_c, η_t from the above equations. Similarly, the mass flow rate and specific impulse relations can be written as

$$\frac{\dot{m}_a a_o}{p_o A_7} = \gamma \; M_o \; \frac{M_7}{M_0} \sqrt{\frac{T_0}{T_7}} = \gamma \; M_o \; \sqrt{\frac{(\eta \tau_t \tau_c \theta_o - 1)}{(\theta_o - 1)}} \cdot \sqrt{\frac{\eta \tau_c \theta_o}{\theta_b}} \tag{5.116}$$

$$\frac{I_{sp}}{a_o} = \frac{F}{\dot{m}_a a_o} \cdot \frac{1}{f}$$

At this stage f can be obtained by striking a thermal power balance across the burner.

$$\dot{m}_f Q \simeq \dot{m}_a c_p (T_{t4} - T_{t3'})$$

It must be noted that since $T_{t3'}$ is larger than T_{t3}, one benefit of non-isentropic behavior of the compressor, therefore, is a reduced demand from fuel injection to raise the fluid to T_{t4}. The usual treatment gives

$$f \cdot \frac{Q}{c_p T_o} = \left[\theta_b - \theta_o \left(1 + \frac{\tau_c - 1}{\eta_c}\right)\right]$$

Thus,

$$\frac{I_{sp}}{a_o} = \frac{F}{\dot{m}_a a_o} \cdot \frac{Q}{c_p T_o} \cdot \frac{1}{\theta_b - \theta_o \left(1 + \frac{\tau_c - 1}{\eta_c}\right)} \tag{5.117}$$

5.2.6 Step-by-step Procedure

While it is not easy to draw general conclusions for several conditions under which a gas turbine engine has to function – like air bleed from a certain stage of the compressor coupled with inefficiencies addressed above, it is important to be able to compute and obtain an idea of the influence. This can be done by a step-by-step procedure described below.

Known information: $p_o, T_o, M_o, \pi_c, TIT, A_7, \eta_i$.

To be calculated: $F, I_{sp}, F/\dot{m}_a a_o, F/p_o A_7, I_{sp}/a_o$

Thermodynamic data required: Compressor, burner and turbine section specific heats at constant pressure and Heat of combustion of the fuel, ratio of specific heats ($c_{p,comp}, c_{p,comb}, c_{p,tur}$, Q and γ)

Step 1: $\theta_o = 1 + \frac{(\gamma+1)}{2} M_o^2$, $T_{to} = T_o \theta_o$, $p_{to} = \theta_o^{\gamma/(\gamma-1)}$. This step gives p_{to} and T_{to}.

Step 2: $p_{t2} = \eta_d \times p_{to}$, $\tau_c = \pi_c^{(\gamma-1)/\gamma}$, $p_{t3} = \pi_c p_{t2}$, $T_{t3'} = T_{t2} + T_{t2} \frac{(\tau_c - 1)}{\eta_c}$. This step gives p_{t3}, $T_{t3'}$.

Step 3: $p_{t4} = \eta_b \times p_{t3}$, $T_{t4} = TIT$. This step gives p_{t4} and T_{t4}.

Step 4: $T_{t5\prime} = T_{t4} - (T_{t3'} - T_{t2})(c_{p,comp}/c_{p,tur})/(1 + f)$, $T_{t5} = T_{t4} - (T_{t4} - T_{t5'})/\eta_t$, $p_{t5} = p_{t4} \times (T_{t5}/T_{t4})^{\gamma/(\gamma-1)}$. This step gives p_{t5}.

Step 5: $p_{t6} = \eta_{jp} \times p_{t5},\ T_{t6} = T_{t5}$.

Step 6: $p_{t7} = \eta_n \times p_{t6},\ T_{t7} = T_{t6}$.

Step 7: If $p_{t7}/p_o < [(\gamma+1)/2]^{\gamma/(\gamma-1)}$ and a convergent nozzle is used or if $p_{t7}/p_o > [(\gamma+1)/2]^{\gamma/(\gamma-1)}$, and a C-D nozzle is used, we take $p_7 = p_o$ and calculate quantities below:

$$M_7 = \sqrt{(2/(\gamma - 1)) \times (p_{t7}/p_7)^{\gamma/(\gamma-1)} - 1}. \tag{5.118}$$

Then, $T_7 = T_{t7}/(1 + (\gamma + 1)/2\ M_7^2)$, $a_7 = \sqrt{\gamma R T_7}$, $V_7 = a_7 \times M_7$, $\rho_7 = p_7/RT_7$, $\dot{m}_a = \rho_7 A_7 V_7$.

If $p_{t7}/p_o > [(\gamma+1)/2]^{\gamma/(\gamma-1)}$, and only a convergent nozzle is used, then the following quantities are to be calculated. $M_7 = 1,\ T_7 = 2 \times T_{t7}/(\gamma+1),\ p_7 = p_{t7}/[(\gamma+1)/2]^{\gamma/(\gamma-1)}$, $a_7 = \sqrt{\gamma R T_7},\ V_7 = a_7$, $\rho_7 = p_7/RT_7,\ \dot{m}_a = \rho_7 A_7 V_7$.

Step 8: $F = \dot{m}_a(V_7 - V_o) + A_7(p_7 - p_o)$, $\dot{m}_f = \dot{m}_a c_{p,comb}(T_{t4} - T_{t3})/Q$

Step 9: One can obtain the non-dimensional quantities from the above values.

The above method needs modifications if a certain amount of flow from the compressor at one of the stages is diverted for other functional purposes. They relate to the energy balance between the compressor and turbine to account for a reduced flow through part of the stages of the compressor and the power derived from it.

The influence of the efficiencies is discussed subsequently for the case of a turbofan.

5.3 The Turbofan

Figure 5.11 shows the elements of a turbofan. The circuit 0-1-2-3-4-5-6-7 constitutes the core engine. The circuit 0-1-2-8-9 constitutes the fan. The mass flow rate through the core engine is $\dot{m}_a$. The mass flow rate through the fan is $\alpha\dot{m}_a$, where $\alpha =$ bypass ratio. The notation for various stations is identified as follows. 0 – free stream; 1– engine front face; 2 – compressor entry; 3 – Compressor exit or burner entry; 4 – burner outlet or turbine inlet; 5 – turbine outlet or get entry; 6 – pipe exit or nozzle entry; 7 – nozzle exit

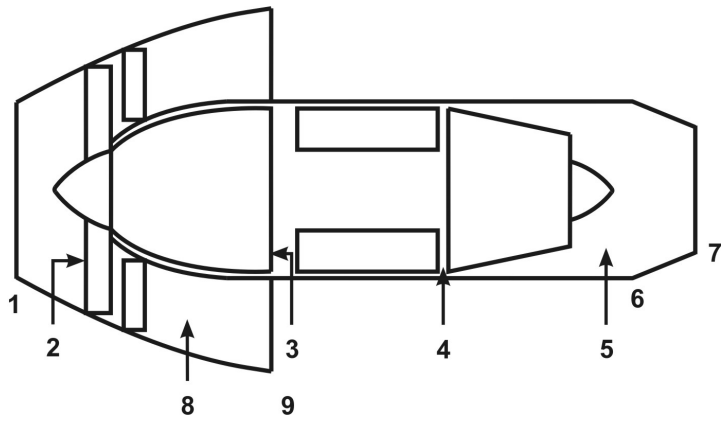

Figure 5.11: The Turbofan with the elements identified for analysis

The thrust equation is given by

$$F = \dot{m}_a \left[(1+f)V_7 - V_0\right] + \alpha \dot{m}_a [V_9 - V_0] + A_7(p_7 - p_0) + A_9(p_9 - p_0)$$

Therefore,

$$\frac{F}{\dot{m}_a a_o} = M_o \left[(1+f)\frac{V_7}{V_o} - 1\right] + \alpha M_o \left[\frac{V_9}{V_o} - 1\right] + \frac{A_7(p_7 - p_0) + A_9(p_9 - p_0)}{\dot{m}_a a_0}$$

Like in the case of turbojet, the ratio of velocities can be expressed in terms of Mach number and temperature ratio as

$$\frac{V_7}{V_0} = \frac{M_7}{M_0}\sqrt{\frac{T_7}{T_0}} \qquad and \qquad \frac{V_9}{V_0} = \frac{M_9}{M_0}\sqrt{\frac{T_9}{T_0}}$$

The Mach number and temperature ratio can be obtained in terms of various parameters like in the case of turbojet. For the case of optimum expansion, which is more realistic for the operation of turbofan, one can write

$$\frac{T_7}{T_0} = \frac{\theta_b \tau_t}{(1 + \frac{\gamma-1}{2}M_7^2)} \qquad and \qquad \left(\frac{p_7}{p_0}\right)^{\frac{\gamma-1}{\gamma}} = 1 = \frac{\tau_t \tau_c \theta_o}{\left(1 + \frac{\gamma-1}{2}\right)M_7^2}$$

And therefore

$$\frac{M_7}{M_0} = \sqrt{\frac{(\theta_0 \tau_t \tau_c - 1)}{(\theta_0 - 1)}} \quad ; \quad \frac{T_7}{T_0} = \frac{\theta_b}{\tau_c \theta_0}$$

For the case of the fan section,

$$\left(\frac{p_9}{p_0}\right)^{\frac{\gamma-1}{\gamma}} = 1 = \frac{\tau_f \theta_o}{1 + \frac{\gamma-1}{2}M_9^2} \quad ; \quad \frac{T_9}{T_0} = \frac{\tau_f \theta_0}{(1 + \frac{\gamma-1}{2}M_9^2)}$$

Since $1 + [(\gamma-1)/2]M_9^2 = \tau_f \theta_0$, $T_9/T_0 = 1$, $M_9/M_0 = \sqrt{(\tau_f \theta_0 - 1)/(\theta_0 - 1)}$

Now, to determine τ_t, one has to set out the compressor – turbine power balance. This should account for power to be delivered to the fan. This is stated as

$$\dot{m}_a(1+f)c_p(T_{t4} - T_{t5}) = \dot{m}_a c_p(T_{t3} - T_{t2}) + \alpha \dot{m}_a c_p(T_{t8} - T_{t2}) \tag{5.119}$$

Non-dimensionalising by $c_p T_o$, taking $f \ll 1$, and performing some simplifications, we get

$$\tau_t = 1 - \frac{\theta_o}{\theta_b}(\tau_c - 1) - \alpha\frac{\theta_o}{\theta_b}(\tau_f - 1) \tag{5.120}$$

The expression for thrust per unit flow rate becomes

$$\frac{F}{\dot{m}_a a_o} = M_o\left[(1+f)\sqrt{\frac{(\tau_t\tau_c\theta_o - 1)}{(\theta_o - 1)}\frac{\theta_b}{\tau_c\theta_o}} - 1\right] + \alpha M_o\left[\sqrt{\frac{\tau_f\theta_o - 1}{\theta_o - 1}} - 1\right] \tag{5.121}$$

along with the equation for τ_t as stated above.

Specific impulse can be obtained from $I_{sp}/a_o = F/\dot{m}_a a_o . 1/f$ where f is obtained in a manner identical to that for turbo jet as

$$\frac{1}{f} = \frac{Q}{c_p T_o} \cdot \frac{1}{(\theta_b - \tau_c\theta_o)}$$

Therefore,

$$\frac{I_{sp}}{a_o} = \frac{Q}{c_p T_o} \cdot \frac{F}{\dot{m}_a a_o}\frac{1}{(\theta_b - \tau_c\theta_o)} \tag{5.122}$$

The expression for $\dot{m}_a/p_o A_7$ is identical to that for turbojet.

One can notice from the thrust equation that $F/\dot{m}_a a_o$ will be much more for turbo jet because of the term involving α. This leads to much higher I_{sp} as can be seen from the equation for I_{sp}. However, $F/(1+\alpha)\dot{m}_a a_o$ constituting the thrust per unit total flow rate will decrease with increasing α and this is a drawback of the turbofan. As discussed earlier in Chapter 1, at large values of α (~ 6.0) like with civil aircraft engines, the larger frontal area is not an issue since the additive drag will be overweighed by the benefits in terms of reduced specific fuel consumption. Typical calculations made with the above equations for a set of parameters $M_o = 0$, $\tau_c = 3.0$ ($\pi_c = 46.8$), $\theta_b = 5.5$, $T_0 = 288.16K$, $Q = 42MJ/kg$, $c_p = 1.0kJ/kgK$ leads to results presented in Table 5.7 for different values of α.

The results presented in Table 5.7 confirm the conclusions stated above.

To determine the influence of the various efficiencies, the following parameters of an engine are chosen. $\pi_c = 25$, $T_{t4} = 1560\ K$, $c_{p,tur} = 1.2$, $\gamma_{tur} = 1.2$. The bypass ratio, α is fixed at 4.5. Table 5.8 presents the results.

An observation of the table shows that the loss in performance due to inefficiency is both in terms of specific thrust and specific impulse, both to the extent of 6 to 8 %. The loss in performance due to compressor is more severe than due to turbine. The inefficiency due to components (passive) other than compressor and turbine is not severe.

Table 5.7: Influence of Bypass ratio on the performance of a Turbofan, * = kN s/kg

α	$\left(\frac{F}{\dot{m}_a a_o}\right)_1$	$\left(\frac{F}{\dot{m}_a a_o}\right)_2$	$\frac{F}{\dot{m}_a a_o}$	$\frac{F}{(1+\alpha)\dot{m}_a a_o}$	I_{sp}, *	$\frac{(4)}{(4)\alpha=0}$	$\frac{(5)}{(5)\alpha=0}$
	1	2	3	4	5	6	7
0.0	3.11	–	3.11	3.11	43.8	1.00	1.00
1.0	3.03	0.72	3.75	1.87	52.9	0.60	1.21
2.0	3.02	1.48	4.50	1.50	62.3	0.48	1.42
4.0	2.72	2.97	5.69	1.20	80.9	0.38	1.85
6.0	3.74	4.30	7.04	1.01	100.1	0.32	2.28

Table 5.8: Influence of efficiencies on the performance of a turbofan, η as defined in equation (5.110)

η_c, %	η_t, %	η, %	$\left(\frac{F}{\dot{m}_a a_o}\right)$	$\frac{F}{(1+\alpha)\dot{m}_a a_o}$	I_{sp}, $kN.s/kg$
100.0	100.0	100.0	7.81	1.42	106.5
85.0	100.0	100.0	7.60	1.38	104.1
100.0	90.0	100.0	7.66	1.39	104.0
100.0	100.0	97.0	7.72	1.40	104.8
85.0	90.0	97.0	7.22	1.31	100.6

5.4 Gas Turbine Controls and Thrust vs. RPM

Gas turbine engine operation needs control for steady operation and acceleration from the point of view of obtaining the desired demand on power as well as safety. The elements that can be controlled are (a) fuel flow rate and its rate of increase or decrease, (b) bleed valve settings, (c) nozzle area variation with engines having variable area design, (d) compressor inlet guide vane area and angle, (e) turbine stator guide vanes, both area and angle, and (f) afterburner fuel flow rate. Not all the engines have the need for all these features. Typical high bypass ratio engines on civil aircraft have no afterburner. Several engines do not have variable inlet guide vanes and some have a fixed nozzle area. But most engines have the features (a) and (b) noted above.

Consequent upon the choice of the pilot setting of power/thrust level, the inputs for implementing the control are derived from several sensors - (i) engine inlet total temperature, T_{t0}, (ii) engine inlet total pressure, p_{t0}, (iii) the rotor spool speeds, N (fan), N(LP), N(HP), (iv) Combustor inlet total pressure, p_{t3}, (v) Jet pipe temperature and pressure, T_{t5} and p_{t5}. While these are adequate for most conventional

control, some recent advances in measurement techniques have included turbine blade temperature using infrared techniques. New advances in sensor technology are being conceived for closer health monitoring of the engine components.

The acceleration of the engine either from start or from one power/thrust setting to another is an important specification. To move from one setting to another, one needs to ramp the fuel flow rate so that the difference in power generated by the turbine and the power drawn by the compressor is able to increase the rotational speed to induct more air flow and equilibrate to the new speed and power/thrust. The power balance is expressed by

$$J\omega\frac{d\omega}{dt} = \dot{m}_a c_p T_o[\theta_b(1-\tau_t) - \theta_o(\tau_c - 1)] \tag{5.123}$$

where J, ω are the angular moment of inertia and $\omega = 2\pi$N, the angular velocity.

The time for acceleration, t_{acc} can be set out from the above equation as

$$t_{acc} = J4\pi^2 N\Delta N/\dot{m}_a c_p T_o EP \tag{5.124}$$

where ΔN is the increment in the speed of the rotor to go to the new equilibrium state and EP is representative of the non-dimensional enthalpy potential available for causing the acceleration, the quantity in parenthesis of equation (5.123). For a typical large turbofan engine with $J \sim 200kgm^2$, T_o = 288 K, $\dot{m}_a \sim 600$ kg/s, c_p = 1000 J/kg K, EP = 0.05 to 0.1, N = 100 rps, ΔN = 10 rps, t_{acc} = 2 s. If the change required is from idle to full speed, ΔN will increase perhaps to 20 rps, and EP will also increase. The data for CF-6 engine shown in Table 2.5 indicates the acceleration time as 6 s, a value comparable to the value derived from the equation (5.124). Another important factor that emerges from the above equation is that for the same engine, the acceleration time increases with increase in altitude; typically, the mass flow rate decreases by a factor of 2 and static temperature by 25 % increasing the acceleration time by an additional factor more than 2.

We now examine the dependence of the thrust developed by a turbojet/turbofan on the rotational speed (revolutions per minute, rpm) of the engine. It is generally known that the thrust producing capability of the engine is in high ranges of speed (typically more than 70 % of the nominal speed). The equations indicated in the earlier sections provide expressions for thrust in terms of compressor pressure ratio. Since compressor ratio depends on the speed of the rotor assembly, one should expect a strong dependence of thrust on rpm. In fact, the display of engine parameters in the cockpit of an aircraft usually includes % rpm as an indication of the thrust level of the engine. It will be interesting to extract this dependence from the equations described till now. The enthalpy rise in the compressor is related to the tangential velocity of the compressor blades and can be expressed in a

compressor as

$$\frac{(T_{t3} - T_{t2})}{T_{t2}} = (\alpha N^2) \tag{5.125}$$

where α is a constant. The above equation can be rewritten as

$$\tau_c = 1 + \alpha(N/N_o)^2 \tag{5.126}$$

If we assume that the efficiencies do not affect the above relationship, we get

$$\tau_c = 1 + (\tau_c^o - 1)\left(\frac{N}{N_o}\right)^2 \tag{5.127}$$

where τ_c^o refers to the compressor temperature ratio at the rated speed.

We now couple this with the equation of static thrust (equation 5.56)

$$\frac{F}{p_o A_7} = \frac{2\gamma}{\gamma - 1}\ (\tau_c - 1)\left(1 - \frac{\tau_c}{\theta_b}\right) \tag{5.128}$$

for 100 % efficiencies and

$$\frac{F}{p_o A_7} = \frac{2\gamma}{\gamma - 1}\left[\eta\tau_c(1 - \frac{\tau_c}{\eta_c\eta_t\theta_b}) - (1 - \frac{\eta\tau_c}{\eta_c\eta_t\theta_b})\right] \tag{5.129}$$

for non-ideal condition with η_c, η_t, η referring to the efficiencies defined earlier to obtain the thrust of the engine at any rotor assembly speed.

At this stage, one needs to determine the dependence of θ_b on the speed. At speeds lower than the rated speed, the compressor pressure ratio and the flow rate will be lower. The turbine enthalpy drop required to meet the demand of the compressor will be lower. Hence if θ_b is held constant, the jet pipe stagnation temperature will be higher. Going by this logic, it turns out that jet pipe temperature will continue to increase as the speed gets smaller and smaller. Since this cannot be allowed to happen, the engine control system will limit the jet pipe temperature. There are several strategies for doing this. One of these can be that the jet pipe temperature is held constant for any power/thrust level. Alternately, an approach that is simple to examine – keeping τ_t constant throughout the power/thrust range of interest can be accepted. In an actual engine, the strategies may be complex and will usually be handled by FADEC (Full Authority Digital Electronic Control) systems developed for this purpose.

If the jet pipe temperature (defined by θ_{jp} = T_{t5}/T_o) is held constant, then the turbine inlet temperature will vary with compressor pressure ratio that itself varies with the shaft speed as in equation(5.127) and this can be used to obtain

$$\frac{\theta_b}{\theta_b^o} = \frac{\theta_{jp}^o}{\theta_b^o} + (1 - \frac{\theta_{jp}^o}{\theta_b^o})(\frac{N}{N^o})^2 \tag{5.130}$$

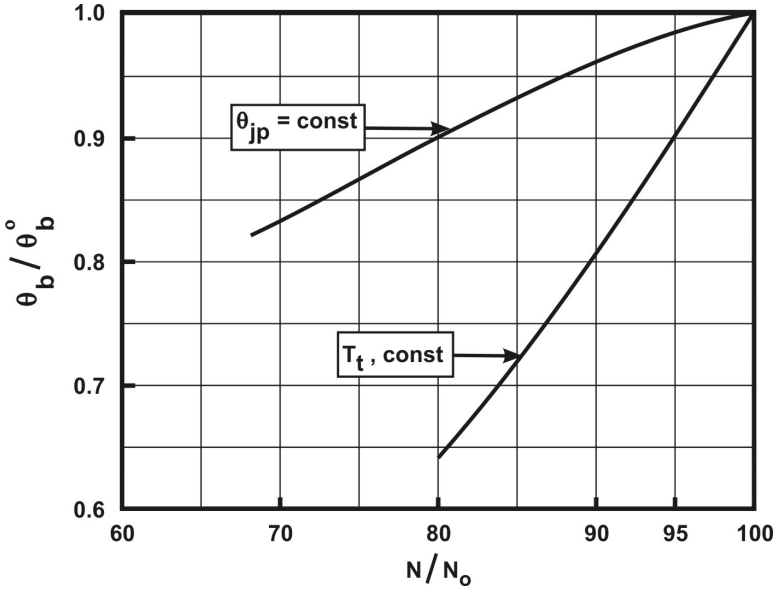

Figure 5.12: The variation of normalized turbine inlet temperature with shaft speed

where θ_b^o and θ_{jp}^o are the values of turbine inlet and jet pipe stagnation temperature ratios at 100 % rpm condition.

If τ_t is taken constant, then it is simple to show that θ_b varies in the same manner as $(\tau_c - 1)$ with the shaft speed. This leads to

$$\theta_b/\theta_b^o = (\tau_c - 1)/(\tau_c^o - 1) = (N/N^o)^2 \tag{5.131}$$

The variation in the normalized TIT with rpm is presented in Figure 5.12. It is clear that the assumption of τ_t = constant causes much lower turbine inlet temperatures at reduced rpm conditions compared to the case of constant jet pipe temperature. It is also to be noted that there is no compelling reason to keep the jet pipe temperature constant with changes in rpm. Hence, the fuel scheduling can be done with changes in rpm to suit the demand of idle or taxiing condition in relation to the 100 % rpm condition. The variation in thrust obtained with τ_t = constant assumption for one specific case using equation (5.129) is shown in Table 5.9 for a turbojet with the assumptions of τ_c^o = 2.4, θ_b^o = 5.0, $\eta_c\eta_t$ = 0.765, η = 0.9. It can be seen that that the drop in thrust with rpm is very significant. The minimum speed at which the gas turbine will have sustained operation is above 70 % rated rpm in this case.

A similar calculation can be made for a turbofan using typical RB 211 data set to compare the estimates made here (using τ_t = constant hypothesis) with actual values. The calculations are made with the thrust equation

Table 5.9: Variation in thrust with speed

N/N_o	τ_c	θ_b	$\frac{F}{p_o A_7}$	$\frac{F}{F_o}$
1.0	2.40	5.00	2.59	1.00
0.9	2.13	4.05	1.53	0.59
0.8	1.90	3.20	0.57	0.22
0.7	1.56	2.45	-ve	-ve

$$F/p_o A_7 = \gamma M_o^2[(S_0 - \sqrt{S_0 S_1}) + \alpha\sqrt{S_0 S_1}(S_2 - 1)] \tag{5.132}$$

where $S_0 = (\eta\tau_t\tau_c\theta_o - 1)/(\theta_o - 1)$, $S_1 = \eta\tau_c\theta_o/\theta_b$, $S_2 = (\eta_f\tau_f\theta_o - 1)/(\theta_o - 1)$, and data as π_c = 25, π_f = 1.5, α = 4.4, TIT = 1530 K, T_o = 288 K, θ_b = 5.31, η_c = 0.90, η_t = 0.9, and η = 0.95. Taking 100 % rpm as reference, the results for thrust for 95 % rpm and 90 % rpm from the above equation are 70 % and 43 % whereas the actual data on the engine show 71 % and 48 %. This comparison is good considering the approximations made.

5.5 Summary

This chapter has been devoted to performance analysis of several propulsion systems – more aimed at understanding the influence of atmospheric, flight and design parameters. In several cases, one can obtain simple expressions which delineate the role of the specific parameter. One system that has been left without analysis is the turboprop. The reason for skipping this is that it is virtually operated in a manner where the thrust power is entirely obtained from the excess power in the turbine with little left to the jet. Hence, the many conclusions of a turbojet would still be valid for this case.

There are several variants of the systems that can be analyzed by the methods outlined above. For instance, an air-turbo rocket based on hydrazine fuel is amenable for analysis of the above kind. These are not discussed here as no general conclusions can be drawn from such analysis. There are several books that deal with cycle analysis - Zucrow [36] in earlier times, Mattingly [7] and Kerrebrock [5] in recent times. The treatment presented here is much along the lines of Kerrebrock [5] since it helps understanding the complex behavior in simple terms.

Chapter 6

Air breathing Engine System Elements

6.1 Air Intakes

Air intake is an essential part of an air breathing engine. Air breathing engines provide power/thrust to aircrafts, ramjet based missiles as well as cruise missiles. The air intake is located upstream of the engine components. In its function, it is the inverse of the nozzle. It helps in decelerating a fluid to conditions acceptable to the compressor of the engine, while the nozzle helps in accelerating the fluid from low speeds to as high a speed as appropriate. It is always understood that decelerating a fluid with little loss is a more complex process compared to accelerating the fluid. Thus, while nozzles can be designed based on isentropic flow assumption quite accurately, it is almost impossible to do this for intakes. On a theoretical basis, for one-point flow optimization, it is possible to conceive of isentropic flow deceleration. However, it is rarely adopted since in actual operation it is not so robust – when changes like angle of attack and Mach number occur, the performance fall-off is so much more than with other design options.

The design of the intake in terms of location, shape, size and internal construction depends on the aspects related to the aircraft/missile and the operational regime – Mach number being the most important parameter, the design acquiring complexity with increasing flight Mach number. One of the design factors that influences the choice amongst competing designs would be the weight of the intake component. One can obtain 20 to 30 % reduction in weight for a performance loss of no more than a percent or so. In such instances, the choice will be governed by the overall mission performance.

Every intake has to function so that it provides a certain mass flow to the de-

vice downstream - a gas turbine like engine or a combustor in a ramjet. In doing this, it must recover as much of free stream stagnation pressure as possible (this is defined in terms of pressure recovery – η_d' – the ratio of downstream stagnation pressure to the free stream stagnation pressure). The air intake design should also ensure the reduction in flow distortion if and where possible (particularly when good angle-of-attack performance is needed). The key parameters controlling the operation of an intake are the geometry upstream of a throat section, the throat area, and the back pressure in the downstream section. For supersonic flight, the operation of the air intake is classified into sub-critical, critical and super-critical. For the critical operation, the terminal normal shock is located at the throat section so that stagnation pressure loss across the terminal normal shock occurs at the lowest possible Mach number, namely unity. Also, if we trace back the stream lines entering the intake to the upstream section, the area of the stream tube that enters the intake will be the same as the air intake front cross section – the ratio of the free stream capture area to the air intake flow cross section will be 1. For subcritical operation, the upstream capture area will be lower than the intake flow cross section and hence there will be spillage – a part of the flow through the same cross section as the intake cross section will flow out of the intake. This might cause additional drag, though not always. In fact, at slightly subcritical conditions, the pressure recovery may turn out to be slightly better than at critical conditions. Under super-critical conditions, the free stream capture area will be the same as the intake cross section, but the terminal shock will get shifted to a section downstream of the throat. In such a case, the flow up to the terminal shock will be supersonic (remember the equation: $dA/A = (dV/V)(M^2-1)$ for one dimensional flow through variable cross sectional configuration like nozzles/air intakes, that indicates that if $M = 1$, $dA = 0$, but if $dA = 0$, M can be > 1) and the stagnation pressure drop across the terminal shock will be higher since the upstream Mach number is higher.

For a gas turbine engine air intake, the "back pressure" is the pressure ahead of the compressor. This pressure is transformed through the compressor-combustor-turbine into the jet pipe pressure (and a temperature controlled by the combustor) that dictates the thrust through the nozzle in a straight turbojet (in a turbo-prop, the very similar process provides the power for operating the propeller). The "back pressure" is used to control the variable geometry of the intake to ensure that the pressure does not change abruptly as this might cause compressor malfunction due to transients.

When the air intake operates in missile propulsion system, air drawn through the air intake gets delivered to the combustor. The combustion process reduces the stagnation pressure somewhat (because heat addition is a non-isentropic process) before the gas goes through a nozzle to produce the thrust. Since the missile path is variable depending on the target being pursued, the drag and the thrust are strongly path dependent. To preserve the performance of the air intake in terms

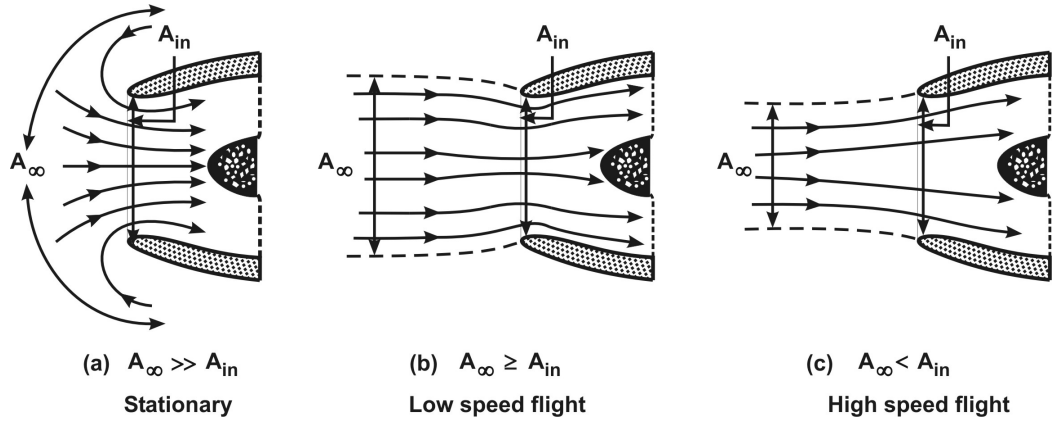

Figure 6.1: Flow through a subsonic intake under different conditions. (a) Flow at take-off or taxying conditions, (b) Flow at speeds lower than the nominal speed, (c) Flow at speeds higher than the nominal speed

of mass flow ingested, it would be necessary to operate the intake in critical/supercritical mode. The flow through the ramjet nozzle that effectively controls the pressure is adjusted by controlling the fuel flow rate so that the heat released due to combustion is altered. This pressure is maintained such that the air intake does not go subcritical (for reasons of instability like buzz that may set in – see later discussion).

6.1.1 Inlets for Subsonic Aircraft

At very low speeds, a simple smooth contoured cylindrical duct - the contouring particularly important at front region – can meet the requirements. The smoothing of the contours in the entry area is important because the stream has to flow from all over the space into the engine at start-up and taxying conditions. As speed increases and goes up to the most preferred operating subsonic Mach number, typically 0.85 in a jet airliner, bringing down the Mach number to about 0.4 to 0.6 at the compressor face through a diverging duct configuration, completes the air intake at subsonic conditions. Figure 6.1 shows the fluid flow behavior through the system. The flow into the air intake depends on the thrust demanded by the aircraft from the engine. This depends on the total weight of the aircraft (that means the payload) and the flight conditions – take-off and the altitude at take-off or steady flight or landing. During take-off, the thrust demanded is very large and hence the air flow demanded also will be large. Since the free stream speeds (air flow with reference to the aircraft) are low, the area from which the flow is drawn will be large and some flow from the sections aft of the intake also will be drawn in (as shown in Figure 6.1 a). Under these conditions, the flow is acceler-

ated significantly and deep turning is involved. This may cause flow separation at the entry area. This should be avoided to the extent the overall design allows for. When flying at speeds lower than the design speeds, the flow will be drawn from a cross section only slightly larger than the intake cross section. In this case the flow accelerates moderately up to the intake at which location, flow deceleration will begin. When flying at speeds larger than the design speed (subsonic), flow will be drawn from a cross section smaller than the intake cross section. In this case, the flow deceleration will be occurring in the free flow before air intake is encountered. A question arises as to what the intake cross section should be? If take-off condition is considered the design point, then the cross section will be too large. This will entail larger drag penalty in several ways. If cruise condition is considered the design point, then the area may be so small that larger flow deceleration inside the air intake duct with accompanying frictional losses will become the limiting condition for the design. In view of the conflicting features, normally, the air intake is sized such that the flow will accelerate moderately outside the intake at the nominal flight condition.

There are issues concerning the non-uniformity of the flow (distortions in the flow structure) when the aircraft is flying at an angle of attack in pitch or lateral modes. The flow through the duct carrying air from the intake to the compressor can undergo reduction or enhancement in the distortion. Also, there is need to ensure that compressor design is robust to avoid stall or surge. This is partly accomplished by providing surge margin that prevents the best point performance at all conditions from being obtained. One of the other roles of the intake is minimizing the loss in stagnation pressure through the intake system. This feature is not a major issue at subsonic conditions. Typical stagnation pressure recovery in subsonic aircraft would be around 97 to 99 % (the ratio of local to free stream stagnation pressure). When speed crosses $M = 1$, the presence of shock waves ahead of the intake poses issues of pressure loss through the intake system. There are supersonic military aircrafts that operate at subsonic conditions or low supersonic conditions ($M \sim 1.5$, say) over a significant part of the flight regime except under getaway conditions during combat. For such aircraft, the design is limited to accepting a normal shock at the intake (and consequent subsonic flow downstream). Such a design is called Pitot intake (similar to pitot static tube front area). The loss in stagnation pressure is accepted as a part of overall simplicity in design in the background that the loss occurs over a small part of the overall flight regime. This situation can be improved by ensuring the presence of surfaces that may create oblique shocks before the flow becomes subsonic. The geometry, of course, will be fixed. Such intakes where the compression takes place outside the ducting are called external compression intakes. As different from this geometry, compression can also be arranged in the internal part of the ducting. These are internal compression intakes. There are also intakes that perform part of the compression inside and part outside. Such intakes are mixed compression intakes.

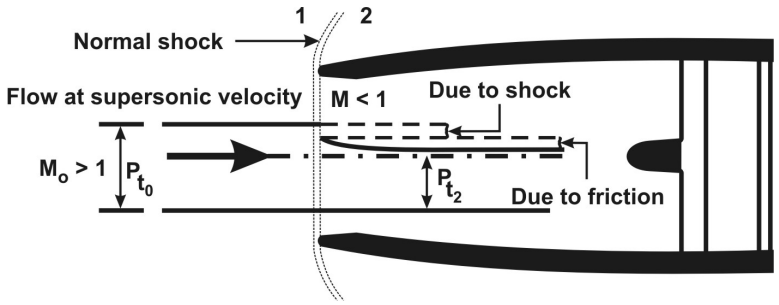

Figure 6.2: A pitot intake

Table 6.1: Pressure recovery (stagnation pressure ratio) across a normal shock, and oblique shocks (N-sh = Normal shock, 1os-1n, 2os-1n = single and two-oblique shock followed by 1 terminal normal shock; δ = Wedge or cone angle; In columns 7 and 9, the two angles denote the wedge angle/cone angles of the two-oblique shock configurations, R = Pressure recovery = η_d')

M_0	N-sh	1os-1n Wedge		1os-1n Cone		2os-1n Wedge		2os-1n Cone	
	R	δ	R	δ	R	δ	R	δ	R
1.5	0.92	8	0.97	20	0.99	-	-	-	-
2.0	0.72	17	0.90	27	0.92	14, 10	0.96	24, 10	0.97
2.5	0.49	21	0.74	30	0.77	14, 15	0.87	25, 15	0.88
3.0	0.32	23	0.58	31	0.60	16, 18	0.75	25, 19	0.77
3.5	0.21	-	-	-	-	16, 20	0.62	25, 21	0.63
4.0	0.13	-	-	-	-	16, 22	0.48	25, 22	0.50

Figure 6.2 shows the pitot intake. A normal shock is located at the intake lip when the flow crosses M = 1. The stagnation pressure drops across the shock. For a normal shock, the stagnation pressure recovery (η_d') is as shown in the Table 6.1.

One can enhance the performance of the intake by providing a surface ahead of the intake duct - a rectangular opening with a wedge at one or more of the walls, a conical object at the center of a circular duct (see the top of the Figure 6.3), a cone with two angles, a semi-conical object ahead of a semi-conical intake located normally on the sides of the fuselage of an aircraft (see the middle of the Figure 6.3), a splitter plate located ahead of the air intake to create an oblique shock (see the bottom of the Figure 6.3), or simply locating the air intake on the aft location on the body where the flow has been partly decelerated by the fore body. The enhanced recovery from these modifications are illustrated in Table 6.1.

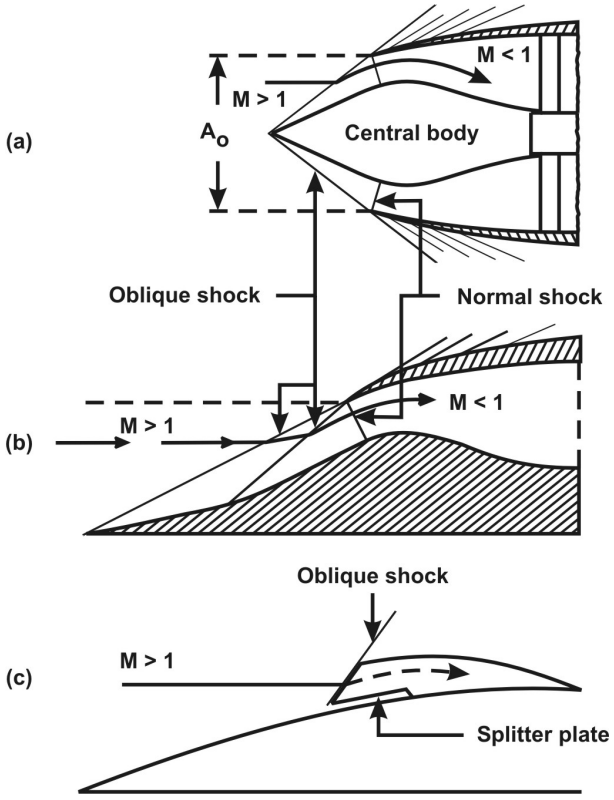

Figure 6.3: The center cone and other intakes. Top: A single cone ahead of the inlet, can be moved back and forth if necessary; Middle: Two cone body ahead of the inlet, with similar features if necessary; Bottom: A splitter plate performing dual functions – diverting the boundary layer and creating an oblique shock ahead of the inlet

At any fixed Mach number, if one reads off the data, one can see that use of a single oblique shock and a terminal normal shock will lead to an increment of 0.05 to 0.26 depending on the Mach number. This magnitude is enhanced in a cone which has a three dimensional flow feature by another 0.02. Use of two-oblique shock wedge or cone will extend the range of Mach numbers at which reasonable recovery can be expected. For Mach numbers up to 2, one uses a single oblique shock and a terminal normal shock arrangement (1os - 1n) and for Mach numbers beyond 3, one has to change over to a configuration consisting of two-oblique shock wedge or cone followed by a terminal normal shock (2os -1n). In the above cases, it is possible to incorporate variable geometry if needed. The center cone can be moved back and forth depending on the flight Mach number. The splitter plate is usually of a fixed geometry design.

By calculations of system performance, it has been determined that every one percent in the loss of stagnation pressure leads to a loss in engine thrust of about

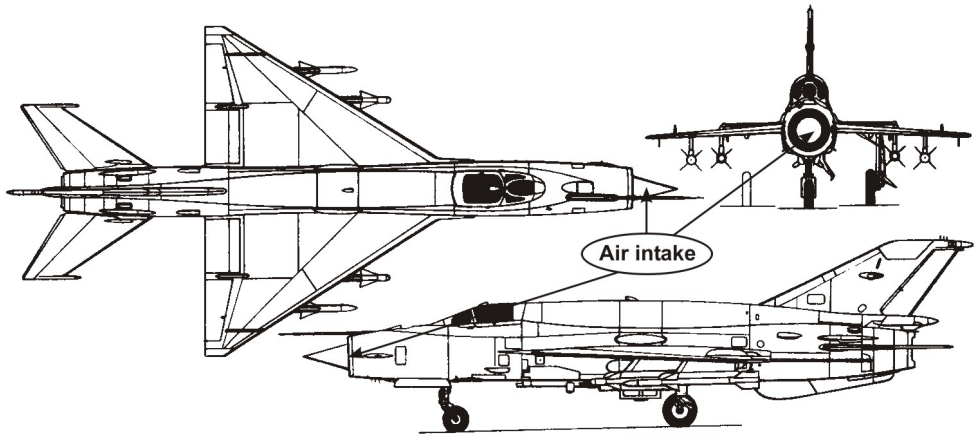

Figure 6.4: Views of a Mig-21 aircraft showing the nose intake geometry, adapted from ref. [29]

1.5 %. Thus, at a free stream Mach number of about 1.3, the loss in thrust will be about 3 %. One might argue that this is significant. The fact that one needs to provide a more complex geometry whose performance at angles of attack may lead to poorer performance has led designers to derive more comfort with a pitot intake. Even with some aircraft whose maximum flight Mach number is much higher, one tends to ask a question as to what proportion of time will the aircraft need to reside at higher Mach number and how important is it to the mission profile. If these are not so important, one tends to stay with simpler pitot intake and accept the lower performance from the intake for specific mission durations. It is clear that if the flight Mach number exceeds 2, one needs to go in for multiple oblique shock structure so that the Mach number at the entry to the terminal normal shock is about 1.4.

6.1.2 Intake Geometries for Supersonic Flight

Typical intake geometries used in aircrafts and missiles are shown in Figures 6.4, 6.5 and 6.6. Figure 6.4 shows the intake in the nose region of the aircraft; Mig-21 and Su-20 (Sukhoi 20) have such an intake. These are variable geometry intakes in which center cone can be moved back and forth to enable higher pressure recovery resulting from locating the terminal normal shock at a low supersonic Mach number. Figure 6.5 shows the intake located on the sides of the aircraft ahead of the wings. Several modern high performance aircrafts have used two-dimensional air intakes (see Table 6.2). Several of them are of variable geometry. This is because of the need for high pressure recovery over a range of Mach numbers and angles of attack. Figure 6.6 shows the intake of the F-16 aircraft at the bottom of

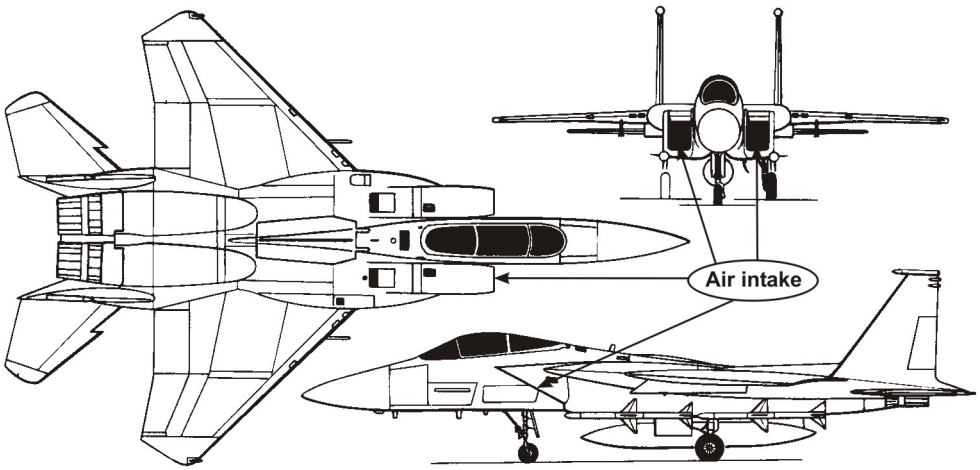

Figure 6.5: Views of a F-15A aircraft showing the side air intakes, adapted from ref. [29]

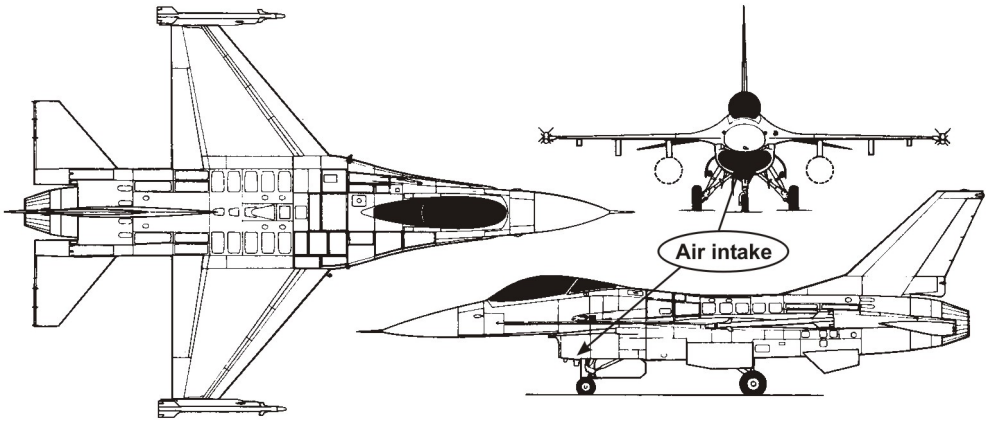

Figure 6.6: Views of a F-16 aircraft showing the bottom shielded air intakes, adapted from ref. [29]

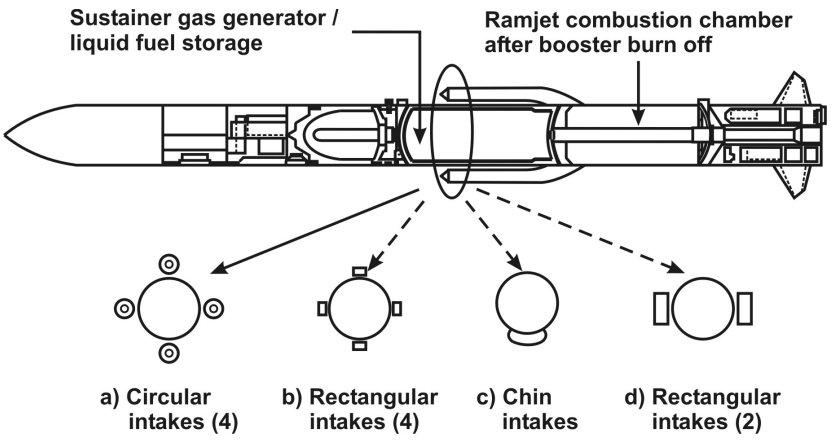

Figure 6.7: Missile intake geometries

the fuselage. This intake is shielded by the fore body significantly. Part of the pressure recovery occurs because of the oblique shock over the fore body. In the case of Concorde aircraft as well, the whole air intake – engine system is located at the bottom aft region of the aircraft. Such designs that benefit from fore body shielding almost always have to have boundary layer diverter so as to avoid additional unsteady flow problems arising out of shockwave – boundary layer interactions. It is also possible to use the boundary layer diverter to cause an oblique shock that allows a part pressure recovery. This is the design used in LCA aircraft (India, see Figure 6.3).

Air breathing missile air intakes are shown in Figure 6.7. One can have two or four circular or rectangular intakes around the core cylindrical body. These carry the air into a combustion chamber for combustion with liquid fuels as it happens in a liquid fuel based ramjet or hot gases from a fuel rich solid propellant based hot gas generator as it happens in a solid fuel based ramjet. In some cases, the ramjet combustion chamber would be the same space that carried a solid rocket propellant used in the initial boost stage. One of the designs is a chin air intake. Even though the choice of any of these intakes is related to the performance parameters, many choices can still meet the requirement even if all the criteria are to be met with. Several designs are still being practiced since it turns out that the approach taken by the development group at an early stage of development becomes the basis for modifications since ab-initio selection of a new concept implies much larger development time and cost.

Table 6.2: Intake features of several aircrafts and some missiles; Comp. = Nature of compression; Ext. = External

Aircraft	Geometry	Location	Comp.	Special features
Mirage 2000	Semicircular	Side	Ext.	Semi-conical movable center body
Jaguar	Rectangular	Side	Mixed	Fixed geometry aft of cockpit
F-14	Rectangular and 2-d	Side	Ext.	A double hinged ramp variable geometry
F-15A	2-d Rectangular	Side	Ext.	Air inlet controlled by actuators
F-16	curved	Bottom	Mixed	Fixed Geometry
F-18	Rectangular	Side		Reduced radar cross section by suitable alignment with wings
Mig-21	Axisymmetric Circular	Nose	Ext.	Center body can take three positions
Mig-23	2-d	Side	Mixed	
Mig-25	Rectangular with wedges	Side	Mixed	Has hinged panels with electronic area control
Mig-27	Rectangular	Side	Mixed	Engine ducts canted at 9^o with sweep back of 35^o
Mig-29	Wedge	Bottom	Mixed	Inner walls are curved and has hinged panels for area control
EuFighter		Bottom	Mixed	Twin boxes with wedge and ramp and variable cowl lip
TU-26	Rectangular	Side	Mixed	Variable geom. Ramp and a large splitter plate
TU-28	Semi-circular	Side	Ext.	M_o = 1.6 (maximum)
SA6	Circular	Side	Ext.	Air-to-air missile, M_o = 2
ASMP	Rectangular	Side	Ext.	Air-to-Surface missile, M_o = 2
ANS	Rectangular	Side	Ext.	4 intakes (M_o = 2 - 2.5)

6.1.3 External, Internal and Mixed Compression Strategies

As the names indicate, the various classes of inlets achieve the compression in a region largely external to the inflow duct, internal to the duct or a combination of both. External compression intakes in the simplest possible approach, use a pitot intake (Figure 6.2) or in a more refined version, an oblique shock from a splitter plate that separates the boundary layer fluid from the mainstream (see Figure 6.3 c). More usually, a cone with a single change of direction or two conical shapes (with two oblique shocks as in Figure 6.3 a) can also be used. The basis of using oblique shocks is as follows:

As the flight Mach number, M_o, increases, the shock angle (the angle between the shock and the flow central line) will be smaller so much so that the effective terminal Mach number (normal to the shock) – $M_o sin\theta_{sh}$ will remain about same – even at Mach 3, it will be less than 1.4 for a choice of total turning angle of 10°. This implies that the the final effective Mach number before normal shock will be less than 1.4. Thus a combination of multiple oblique shocks with a final normal shock should be adequate to decelerate the fluid with minimum loss of stagnation pressure. In the case of external compression inlets, the outer duct profile must be designed to align itself with the shock emanating from the apex of the cone as can be seen in Figures 6.3 and 6.8. The segment that has curvature will impose drag penalties because of the expansion of the flow over the outer curvature on the intake. With increasing flight Mach number, the flow turning will increase and the curvature of the outer profile also increases, leading to larger drag penalties. Also, the internal flow that has been turned to steep angles must be turned back towards the axis. At large Mach numbers these imply longer and stouter intakes undesirable from weight and drag view points. Hence, external compression approach is usually limited to a Mach number of about 2.5. In the external compression inlets, a possibility of using unfocussed shocks (not focussed to the intake cowl) exists. This approach also leads to larger spillage at critical operation, longer, stouter and heavier intake and hence, is usually not recommended. Beyond M_o = 2.5, internal compression concepts need to be invoked in the design.

Figure 6.8 (a) – (d) shows various intakes for a Mach number of 2.2. In the case of Figure 6.8 (a) that represents an internal compression intake, the oblique shock system required to bring down the Mach number to subsonic conditions is inside the body of the intake. For symmetric flow condition, the shocks occur in a manner that the terminal normal shock is close to the throat of the intake. Subsequent divergence reduces the Mach number to reasonable levels ($\sim$ 0.4). One of the issues in these intakes is that since the wall boundary layers grow through the geometry, avoidance of shock-boundary layer interactions calls for applying boundary layer suction particularly near the throat region. One can combine external and internal compression to meet the objectives of minimizing cowl drag due to external compression geometry and also dealing with shock-boundary layer issues of

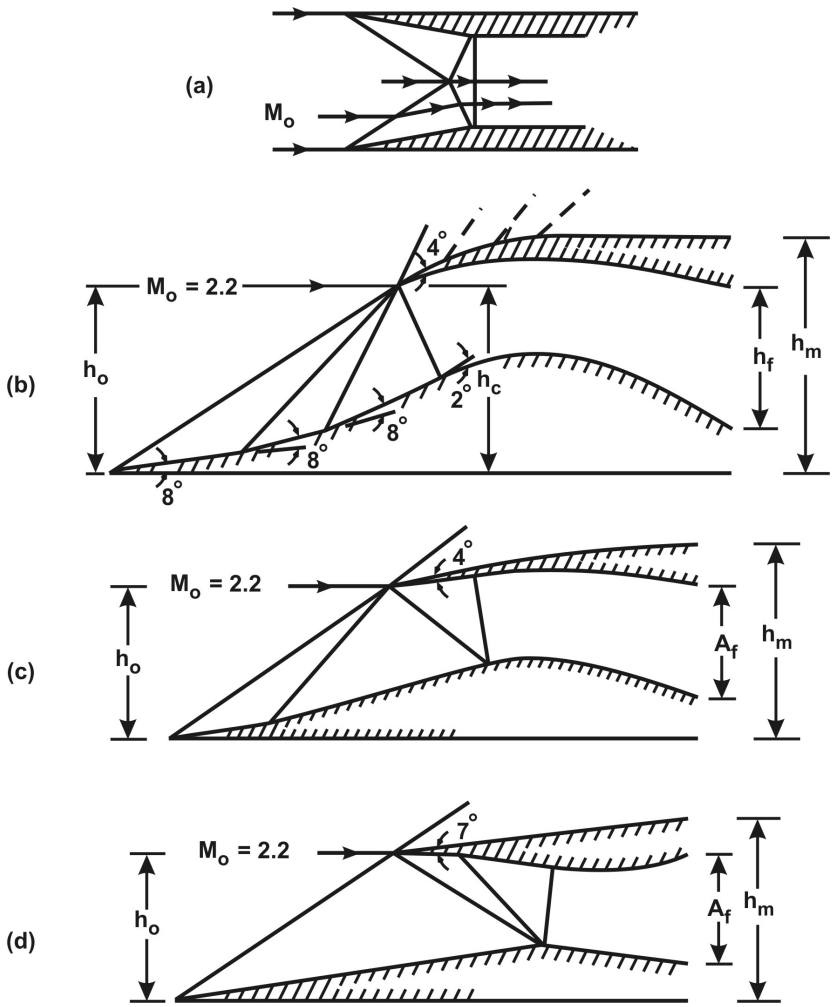

Figure 6.8: Schematic of an internal compression intake (a), external compression intake (b), mixed compression intake with 50 % pressure rise in the internal segment (c), mixed compression intake with 75 % compression in the internal segment (d), all designed for $M_0 = 2.2$

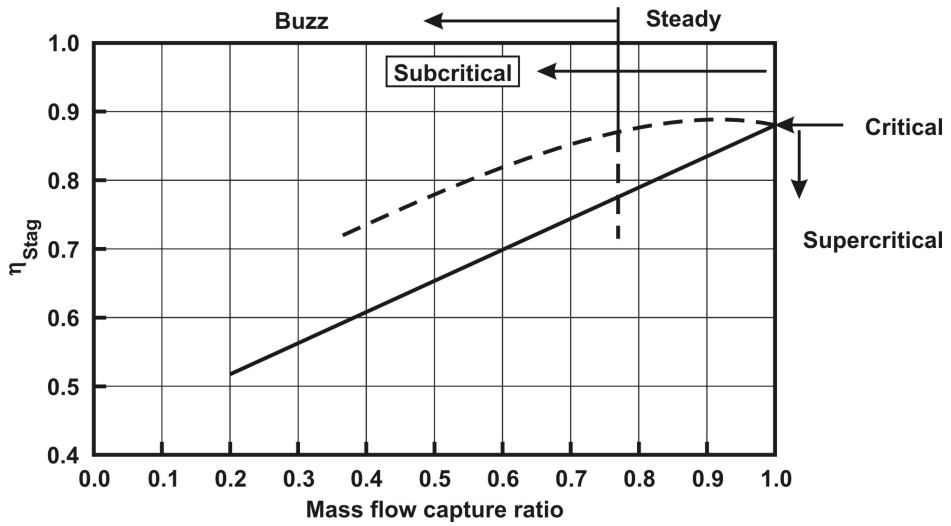

Figure 6.9: Pressure recovery – η_{stag} with mass capture ratio. Subcritical zone occurs to the left side; the critical operation occurs at one point; the supercritical operation occurs at fixed mass capture ratio equal to the value at critical conditions; the upper and lower curves are different intake designs

internal compression intakes.

Figures 6.8 (b) – (d) taken from Seddon and Goldsmith [33] show how a given requirement can be met with by both external and mixed compression strategies. In Figure 6.8 b, the flow at a Mach number of 2.2 is being decelerated through three oblique shocks and one terminal normal shock. The significant change in direction discussed earlier is seen in the figure. By allowing a part of the compression to occur inside the body as in Figure 6.8 c, the flow turning can be reduced. One can enhance the contribution of internal compression as in Figure 6.8 d. The magnitudes of internal compression in the previous two cases are 50 % and 75 %. In all the cases, the total pressure recovery is about the same. However, there are other subtle, but substantial differences. In some cases where the extent of surface that experiences supersonic flow is large, the net forces on the intake can be so substantive that the weight of the intake can be very large and strategies need to be evolved to reduce these loads. Of course, boundary layer effects have to be handled through appropriate bleed. The cowl drag too can be very different between the extent of external and internal compression. These can, in fact, decide the choice between the systems.

One of the important performance plots of an air intake is the relationship between the pressure recovery and the capture ratio (the ratio between the stream tube far upstream and the air intake section. Figure 6.9 shows the typical plot of the relationship. In the sub-critical zone, the pressure recovery improves with

capture ratio with a peak in slightly sub-critical zone till the critical operating condition is reached. This occurs because at slight sub-critical condition, the flow rate through the intake reduces and hence the losses through the system. Beyond the critical point, the capture ratio is unity but the pressure recovery drops because the terminal shock will become stronger with greater super-criticality.

6.1.4 Starting Issues of Intakes

One of the problems that intakes face not encountered by nozzles is the starting problem at supersonic Mach flight Mach numbers. The problem may be posed thus: Suppose, one wants to take an aircraft or a missile to a given Mach number at which the air intake must function at a nominal operating condition – a certain mass flow and a pressure recovery that is optimized, such a condition obtained when the terminal shock is located at the throat. Can one do this by accelerating to the desired condition in a direct path? Since the air intake has to pass through a whole range of Mach numbers from sonic conditions, the front of the air intake will experience a shock system that is obtained at lower-than-nominal flight Mach numbers. These shocks will be normal shocks or oblique shocks of higher strength and hence the pressure recovery will be lower than optimal value. This implies with the throat area that is set for nominal operation, the nominal mass flow will not be ingested. Thus, both pressure recovery and mass flow will be lower than at nominal condition.

The solution to this problem is obtained by one or both of the following methods – over-speeding and increase in throat area. In the former case, the increase in Mach number beyond the nominal value will provide enough stagnation pressure to ingest the flow. During this operation, the terminal shock will move into the intake and locate itself in a stable position downstream of the throat. Decrease in the speed to the nominal value will then bring the terminal shock to the throat and nominal operating condition is established. Equally well, if the throat area is increased when the aircraft is at nominal speed, the effect of reduced stagnation pressure due to the shock structure ahead of the intake will be compensated by the enhanced throat area and the mass flow ingested will approach the nominal value. This process causes "shock swallowing" that can be readjusted by reducing the throat to the original condition to ensure the terminal shock to be at the throat. In variable geometry intakes adopted by aircraft, the control system will position the cone or vary the wall positions automatically to match the requirements of high pressure recovery. If additional mass flow demand is made by the engine, a separate set of surfaces will open out allowing the atmospheric air to be drawn in. Under conditions of deceleration of the aircraft, the control system will position itself to match the requirement. Sharp transients are handled by opening additional surfaces between the air intake and the engine into the atmosphere so that pressure build up is avoided. Thus, a modern aircraft intake may have

Table 6.3: Pressure recovery in intakes of different aircrafts

Aircraft	Mach number range	Pressure recovery
F-14	0.7, 1.0, 1.2	0.98, 0.97, 0.96
F-15A	0, 0.5, 1.0	0.88, 0.97, 0.97
	1.5, 2, 2.5	0.96, 0.92, 0.82
F-16	1.0, 1.5, 1.8	0.97, 0.90, 0.80

many separately controlled elements put together managed to ensure that the engine gets its mass flow with the best possible pressure recovery. Table 6.3 shows the pressure recovery at different Mach numbers for some aircraft (from reference [33]).

For missile intakes, fixed geometry intakes are usually preferred since the range of Mach numbers is not large – typically, say from 2.0 to 2.5 and in some cases up to 3.0. The performance would be optimized for one condition and the intake is designed to run super-critical if fuel flow rate cannot be managed (along all trajectories that the missile may take during pursuit) as it happens with solid fuel based ramjets. Liquid fuel ramjets can be designed to run at near-critical conditions by controlling the fuel flow rate so that the terminal shock is close to the throat.

6.1.5 Off-Design Performance

When fixed geometry intakes are required to operate at Mach numbers different from the nominal condition and at angles of attack, the flow features that affect the performance are the shock losses and spillage. While usually, spillage has the connotation of loss of mass flow, the term spillage drag is also used to indicate the deleterious effects of the pressure distribution over the body that occurs when conditions of spillage (of mass flow) get created. One of the requirements of a good design is to account for spillage effects in the mission domain and optimize the design to minimize the effects of spillage.

6.1.6 Buzz and Other Instabilities

Buzz is a low frequency instability that is found to occur at flow rate lower than the rated flow. It can occur at low flow rates (up to 40 % nominal value) and at high flow rates (of about 70 to 80 % nominal value). The frequency of oscillations is about 200 to 300 Hz with low amplitudes at high flow rates and significant amplitudes at low flow rates. In the low flow rate regime, the flow structure can

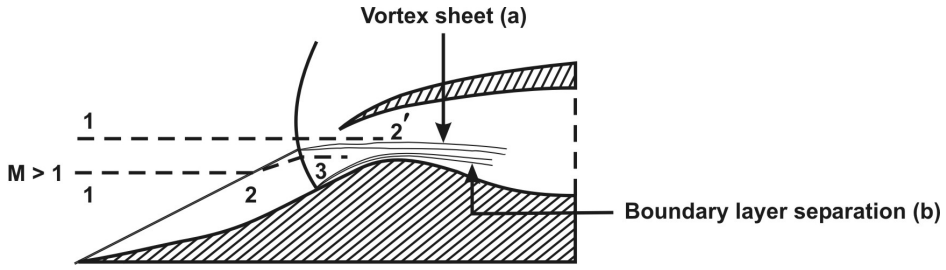

Figure 6.10: Mechanisms of the cause for Buzz. Notice the two undesirable fluid dynamic features that can cause flow foul up – vortex sheet from the two shock impingement region and a shock boundary layer interaction related flow separation on the cowl

oscillate between two possible steady conditions and lead to possible compressor surge that is dreaded in any flight operation.

Buzz is a problem associated with fixed geometry intakes and with external compression concept. Two elements of the explanation are (a) shock-shock interaction that can lead to a vortex sheet that further leads to flow breakdown in the intake section and (b) a separation of the flow from the cowl lip that can occur due to a large pressure gradient along with subsonic flow at the cowl region. These are illustrated in Figure 6.10. As indicated in the figure, the flow going through $1 \rightarrow 2 \rightarrow 3$ will have a velocity different from that which goes along $1 \rightarrow 2'$, since, in the former case, the flow is processed by an oblique shock and a near-normal shock and in the latter case, it is processed by only a normal shock. This leads to a shear layer that causes a vortex sheet. Depending on the magnitude of the velocity difference, the vortex structure in interaction with wall boundary layer can cause further flow breakdown. As indicated in Figure 6.10, it may turn out that flow separation starts from the cowl itself. In such conditions not accounted for in the nominal design, it has been found that more than one solution can be possible. These are found to be unstable. The flow then can shift from one to the other.

Buzz is not a problem with variable geometry intakes and those with good boundary layer bleed, since flow dumping without affecting the normal flow into the intake is possible. Buzz avoidance in fixed geometry intakes requires careful design accounting for possible difficult regimes of operation revealed through early testing, occasionally combining with boundary layer treatment (both suction and blowing) and in some cases, with flow dumping surfaces.

The design of any intake for a complex operational regime in a supersonic transport aircraft requires many elements. Figures 6.11 and 6.12 illustrate the details for Concorde aircraft that uses Olympus engine and two-dimensional variable geometry intake. One can clearly see how the requirements for varying flight conditions like take-off, transonic acceleration and cruise are managed by chang-

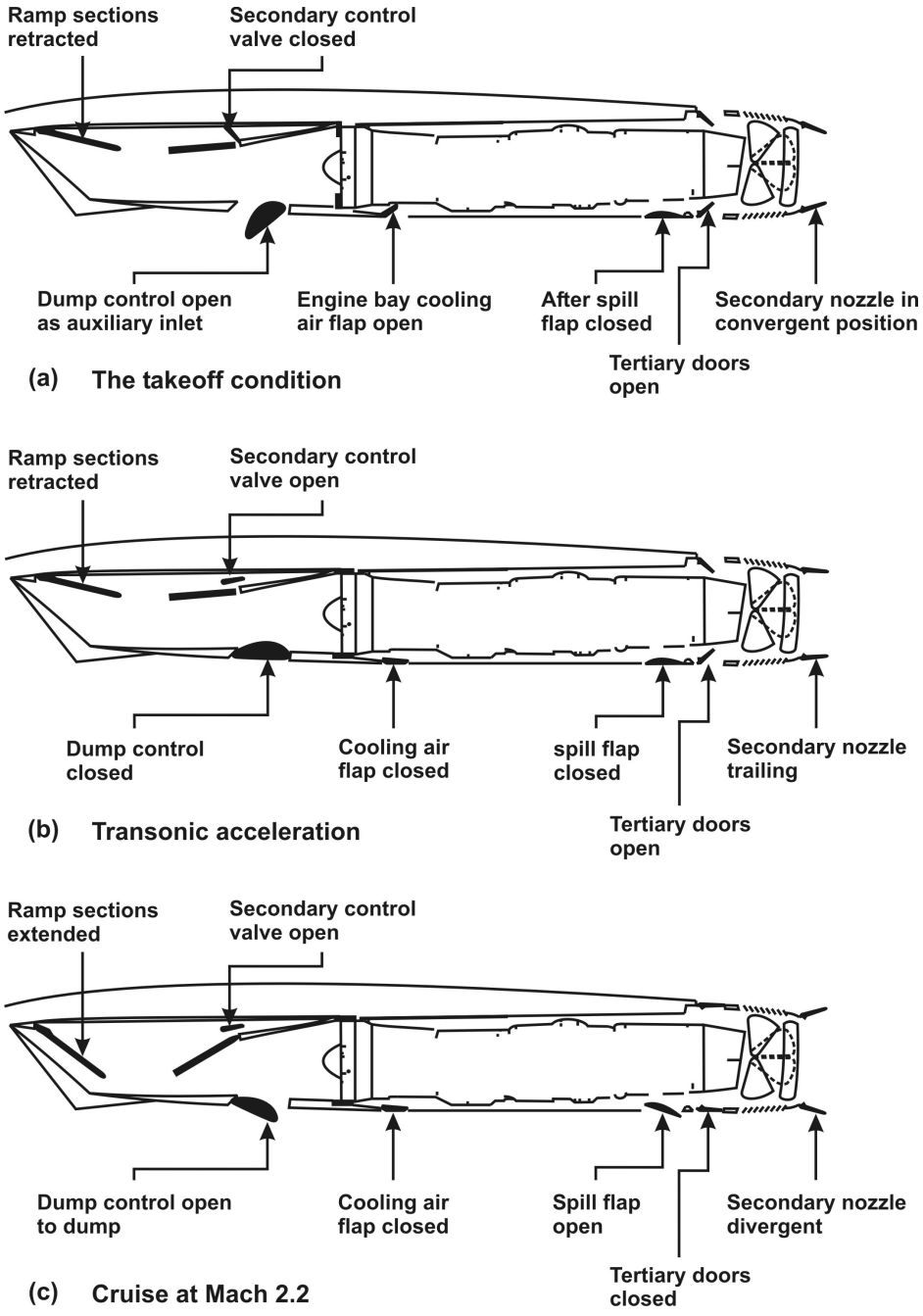

Figure 6.11: Modes of operation of Concord intake and nozzle system for take-off, transonic acceleration and cruise drawn from reference [33]

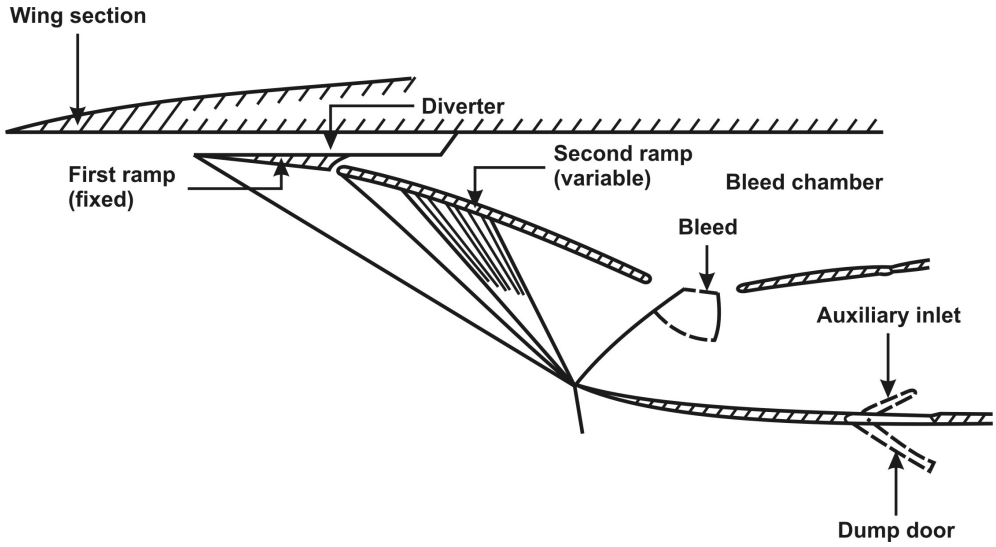

Figure 6.12: Front region of the Concorde intake, adapted from ref. [7]

ing the ramp section (as in Figure 6.12), opening and closing the dump doors, and allowing boundary layer bleed to be drawn away (by opening the secondary control valve as in the figure). Once it is agreed that the performance of the aircraft is best handled through the use of variable geometry intake, one can design the system for varying operational regimes as demonstrated in Figure 6.13. The most interesting part of the design is that one can operate the intake to act as an external compression system or a mixed compression system with suitable adjustment for spillage as well.

6.1.7 Summary

Intakes are a subject of substantial importance, but not as well or widely understood as nozzles. This section has dealt with the basic features of the intakes and their deployment in aircraft. It is the fixed geometry intakes that pose greater challenge since a minimum flow quality has to be preserved under a number of adverse conditions. Since successful designs have been generated, it would indicate that several complex issues have been substantively understood. The book "Intake Aerodynamics" by Seddon and Goldsmith [33] is excellent to understand the subject of air intakes. Most of the development discussed in the book relates to developments largely in the pre-eighties period and has taken place through extensive testing and simple analysis; it is only in recent times that newer tools of computational fluid dynamics are making incursion into the field through providing the details of the flow behavior under a variety of operating conditions, and

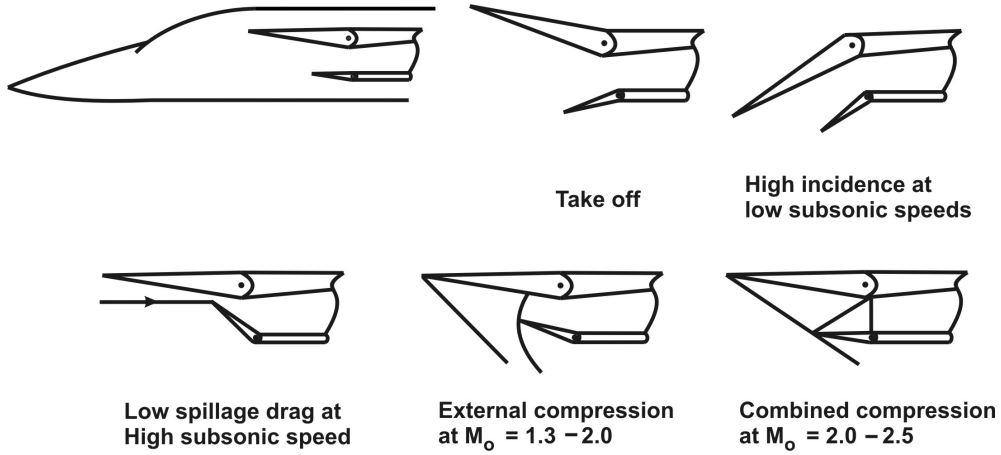

Figure 6.13: Various geometric conditions of a variable geometry air intake adapted from ref. [33]

changes of geometry to enable better appreciation of design and performance of the intakes. These tools play a pivotal role in the design of air intakes for hypersonic vehicles since the entire vehicle has to be treated as a single unit with very strongly interacting components; any "small" change may turn to be very harsh on the performance of the vehicle. These are the new areas that will become important in the coming times. While no special new phenomena will possibly be uncovered, it is in the degree of emphasis of one concept or the other (how much of external compression for instance), that will be found to have profound influence on the design of the vehicle.

6.2 Compressors

The compressor is an element in a gas turbine engine which provides for the possibility of extracting work from fluids. It either draws in or takes in atmospheric air and raises the pressure (and associated temperature) to enable heat addition and work extraction from the turbine subsequently. There are two means of performing compression – centrifugal and axial. In the former, the fluid moves radially through an impeller which imparts it radial velocity. After this section, the fluid is decelerated in a diffuser to convert the kinetic energy into potential energy. This builds the pressure of the fluid. A typical centrifugal compressor raises the pressure by a factor of 3 to 4. Special designs for pressure ratios of 8 are possible using designs that have half vanes. These require that the fluid be raised to supersonic speeds through the impeller. A typical design of a radial compressor with half vanes is shown in Fig.6.14. Since the amount of energy that can be imparted to the fluid depends of radial motion, centrifugal compressors need a combination of a high rotational speed and a reasonably large diameter and therefore, frontal area for typical pressure ratios of 4. If much larger pressure ratios like 8 to 30 are needed, one needs to go in for axial compressors. In these systems, a number of stages, each one having a stator and rotor is used. Typical pressure ratios across each of the stages is about 1.15 to 1.25, averaging to 1.2. Thus, a pressure ratio of 30 can be obtained by a compressor with n stages, 1.2^n = 30 leading to $n = 19$. Keeping a large number of stages on a shaft and running at high speeds is one mechanical problem; there are aerodynamic and thermodynamic issues as well causing decay in performance. These issues have led to solutions which have given rise to designs with (a) twin/three spools, (b) inlet guide vanes, and (c) air off-take at some stage of compression in the design of the compressors. The aim of the present discussion is to understand the principles behind the design variants of the systems, in particular, the centrifugal and the axial compressors.

6.2.1 Centrifugal Compressors

These require that the fluid be raised to supersonic speeds through the impeller.

Figure 6.14 shows the schematic of the centrifugal compressor and several features. It has a rotor, a vane-less space and a diffuser section before the air is discharged at the exit. The entire assembly is enclosed with controlled spacing between the rotor assembly and the outer shroud. To ensure that the moving rotor will impart momentum to the fluid coming in, adequate number of vanes is deployed. Typically, the number of vanes is set between 19 to 21. As the fluid is drawn axially and moved radially outwards, its velocity and static pressure will rise largely due to centrifugal action. The fluid after departing from the rotor will move to diffuser for the conversion of kinetic head to pressure head. The shape of

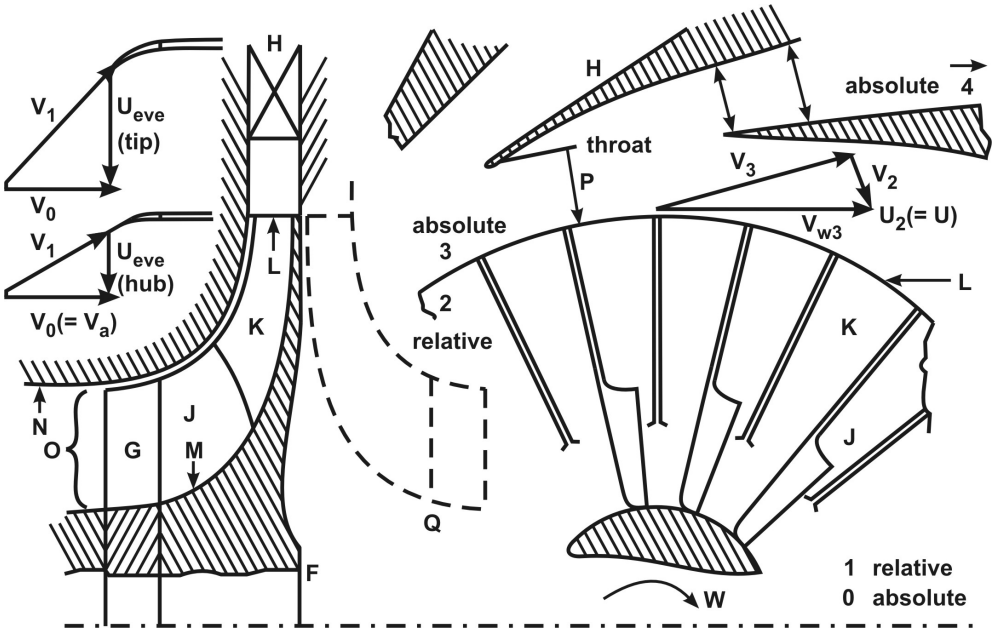

Figure 6.14: Details of a single sided compressor with channel-type diffuser. (G is the inducer with rotating guide vanes, H is the diffuser, J is the impeller vane, K is a half vane, L is the impeller outer limit, M is the impeller hub, N is the shroud, O is the impeller eye, P is the vane-less gap. Notice the twist in the vane close to the hub as also seen in the velocity diagram at the top left)

the vanes shown in Figure 6.14 indicates a twist in the impeller suction area. This is because, the fluid entering axially has to be drawn into the rotating impeller at the correct angle – essentially to account for the peripheral velocity of the vanes as a function of radius. By accounting for the work done on the fluid by the impeller, one can write

$$T_{02} - T_{01} = c_0 U^2 / c_p \tag{6.1}$$

where T_{02} and T_{01} are the stagnation temperatures of the fluid after and before the compressor, U is the mean velocity of the impeller at the outer edge, c_p, the constant pressure specific heat, c_0, a constant which is the product of two factors, power input factor and slip factor. The power input factor accounts for frictional heat aiding the rise in temperature, typically between 1.035 to 1.04. The slip factor the ratio of the exit tangential velocity of the fluid (from the impeller) to the impeller tangential velocity. This factor is less than unity and depends prominently on the number of vanes, larger number leading to smaller departure from unity. However, larger number of vanes implies greater frictional loss and smaller fluid flow area. Typically, c_0 is about 0.9. The conversion of the stagnation temperature

rise to stagnation pressure rise is controlled by the overall isentropic efficiency denoted by η_c. One can now write,

$$\frac{p_{02}}{p_{01}} = \pi_c = \left[1 + \frac{\eta_c(T_{02} - T_{01})}{T_{01}}\right]^{\gamma/(\gamma-1)} = \left[1 + \frac{\eta_c c_0 U^2}{c_p T_{01}}\right]^{\gamma/(\gamma-1)} \tag{6.2}$$

Typical value of η_c varies from 0.8 to 0.85.

The above equation is very revealing. It expresses the influence of various parameters on the performance of the compressor. We will now examine these around some typical nominal values. For $U \sim 450$ m/s, $c_p \sim 1$ kJ/kg K, $T_{01} \sim 300$ K, $\eta_c \sim 0.8$, $c_0 \sim 0.95$, γ = 1.4, the nominal value of the quantity in the parenthesis sign on the right hand side is 1.513. This leads to π_c = 4.26. The impeller speed is proportional to the rpm of the impeller. One can ask a question: if the rpm is 90 % of the nominal, what would be the pressure ratio. The pressure ratio falls to 3.13. At 80 % of the nominal speed, the pressure ratio is 2.7. Thus, a 10 and 20 % fall in rpm leads to a pressure ratio reduction of 26.5 and 36.6 % respectively. These imply that performance degradation at speeds below nominal are very significant; therefore, one must achieve speeds as close to rated value as possible to realize the performance of the compressor. A 10 % reduction in any of the efficiencies is equivalent to 5 % reduction in rpm and will amount to 12 % reduction in realized pressure ratio. This again implies that one should try to achieve efficiencies as high as possible. The loss in performance due to less than careful attention to detail will turn out to be severe.

In order to appreciate the criticality of the above features, one should know the flow behavior. The flow aspects are described in Fig. 6.15. The lateral flow occurs because the impeller drags the fluid at the hub region and the flow turns around within the cavity of the vane as in the left extreme figure of Fig. 6.15. The radial flow combines with the lateral flow leading to the distribution of velocity and pressure as shown. The forward part of the compartment experiences lesser stagnation pressure compared to part behind at the same radial location. This implies that each vane experiences higher pressure on one side compared to its back face. This creates the possibility of flow spilling over the vanes in a direction opposite to the rotational direction. In order to restrict such a flow, the spacing between the rotating vane edge and the stationary outer shroud is kept low. Typically, the spacing is about 0.5 to 1 mm in large machines with impeller outer diameter of 0.6 to 1 m and 200 μm in the case of smaller engines (1 kN thrust class). This will call for careful balancing of the rotating part. As the flow moves outwards, it acquires higher static pressure due to centrifugal action and also higher velocities. Thus, there is a radial static pressure gradient in addition to lateral pressure gradient described earlier. The flow is, therefore, very non-uniform with pressure gradients all over the compartment between the vanes. Since the entry of the flow into the compartment occurs over the rotating vanes, the angle of attack at which the flow

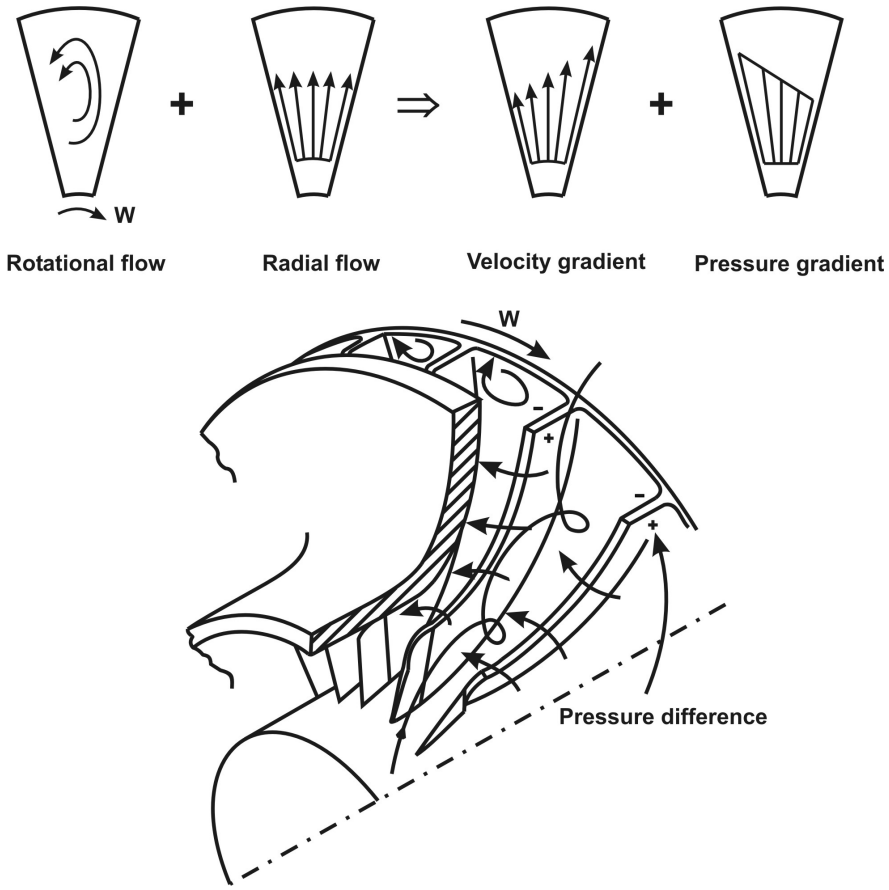

Figure 6.15: Fluid flow patterns in the vane of a centrifugal compressor. The rotational component of the fluid is due to the rotation of the impeller and the fluid being dragged by the hub region and consequent effects. Combined with the radial velocity, a distorted velocity distribution and a consistent pressure distribution are generated as shown. The difference in pressures on the two sides of the vanes leads to a flow across the edge through the tip clearance region as seen in the right most figure. The combination of radial and lateral flow leads to helical fluid flow path, taken from ref. [4].

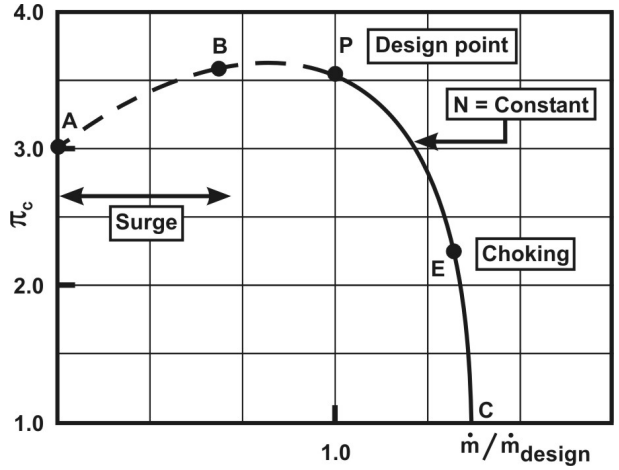

Figure 6.16: Overall characteristics of a centrifugal compressor at a fixed speed of rotation (P is the design point around which the operation is stable; The region AB at low flow rates experiences surge)

enters is determined by the ratio of the axial to the rotational speed at any fixed radius (see Figure 6.14). Since the tangential speed increases with radius, one would expect a twist in the vane to ensure correct angles of attack. If the axial entry velocity is small as might happen during start up (at low rotational speeds) or conditions of reduced flow through the system at a fixed rotational speed, it may turn out that the angle of attack departs from design significantly and this can induce separation. This separation process causes a phenomenon called surge in compressors – fluctuation of mass flow and pressure ratio across the compressor. The phenomenon of surge in compressors is a function of two major parameters – speed and flow rate. Flow rate is an independent variable in most cases because usually compressor delivers to other devices – combustion chamber, turbine and an exit nozzle, another stage / set of stages of compressor whose cross sectional dimensions must permit the flow delivered by this stage, or a downstream device which needs variable flow. A typical plot of pressure ratio delivered by a compressor as a function of flow rate at one fixed speed of rotation is shown in Fig. 6.16.

The parabolic shape has two segments (ABP and PEC). The portion in which the pressure ratio increases with flow rate (ABP) and another in which pressure ratio decreases with flow rate (PEC). With increase in rpm, the same behavior of the curve with increased peak pressure ratio will result. The portion to the left of the peak is set in dotted lines. This is the segment in which both unsteady flow, and flow separation lead to rotating stall and surge. The portion of the curve to the right of the peak in which pressure ratio increases with decrease in flow

rate is argued to be stable. Any decrease in flow due to additional resistance in the delivery leads to increased pressure, thus, helping restore the equilibrium point. Such a behavior is not obtained for any operating point on the left side. Any tendency towards decrease in flow implies reduction in pressure developed thus, leading to further decrease in flow rate. This condition leads to flow separation at some condition and then one obtains a highly unsteady flow behavior. One contributing factor has been diagnosed to be the diffuser section. If the diffuser is arranged as a large number of sections comparable in number to the number of vanes, the flow from more than one set of vanes may try and pass through one diffuser section, starving the neighbor of the flow, thus, leading to reversal of flows in the diffuser segments. This reduces the instantaneous local flow even though the total flow is passed through due to averaging of the flow over the unsteady period. A simple way to delay the occurrence is to reduce the number of diffuser sections. One can obtain steady operating points to a part of the left portion of the peak pressure point (PB). Even so, the segment AB is beset with surge, a condition of unsteady operation with large pressure fluctuations. One cannot let the compressor get into this operating mode. Compressor operation is designed to have surge margin – a boundary zone away from surge line so that under any operational mode, one has safe steady mass flow rate - pressure behavior. One less stringent operating condition that is experienced is called rotating stall. In this condition, the flow through one compartment becomes less due to separation on the suction surface and this gets loaded on to one neighboring compartment and flow separation conditions are created in another neighbor. When the flow separates in this neighbor, the stall moves on by rotating counter to the impeller rotation. High frequency vibrations and material fatigue are the consequences which are to be avoided in design and operation.

Compressor Performance Maps

Compressor performance maps are set out in terms of what are known as corrected parameters that are a replacement for dimensionless parameters. The performance of a compressor described in terms of stagnation pressure ratio as a function of the mass flow rate, the rotational speed, the impeller diameter and related geometric variables. If one wishes to generate appropriate dimensionless quantities, with respect to peripheral speed, one can render them dimensionless by using the acoustic speed. This is consistent with the thinking that the peripheral Mach number is one controlling parameter. The mass flow rate can be normalized by a quantity derived out of the inlet stagnation pressure and temperature (by noting that $\dot{m} \sim p_t A_r/\sqrt{RT_t}$). In these relations, the subscripts t refer to reference stagnation conditions, and p, A, T refer to pressure, area and temperature. Since these quantities will involve geometric parameters like disc diameter or an area and in any case, the performance of the compressor is strongly dependent on the ge-

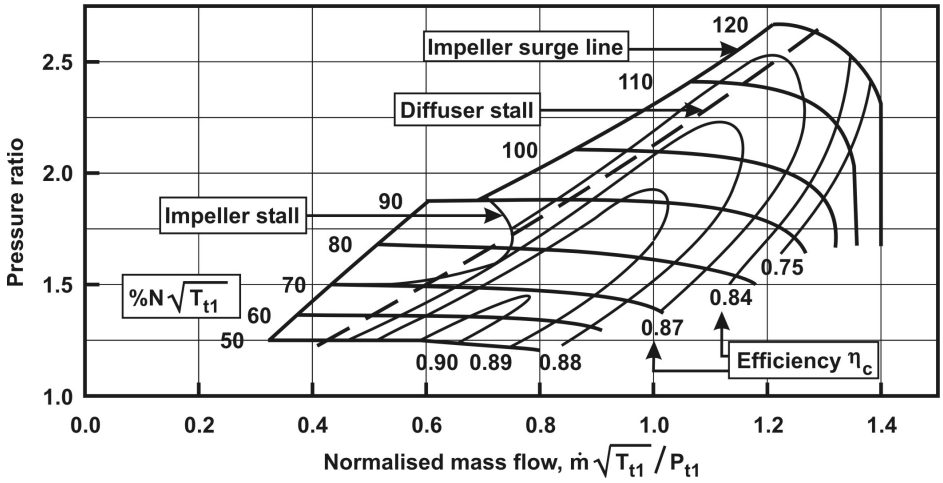

Figure 6.17: Overall characteristics of centrifugal compressor showing flow limits and efficiency

ometry, one constructs normalized parameters by ignoring geometric parameters and other constants. Thus, $N/\sqrt{T_t}$ where N is the rotational speed and T_t is the stagnation temperature at the upstream condition constitutes the corrected speed parameter. The quantity $\dot{m}\sqrt{T_t}/p_t$ is the corrected mass flow parameter. The performance is, therefore, described by a plot of stagnation pressure ratio vs corrected mass flow parameter at different corrected speed parameters. Another quantity which describes the performance of a compressor is the isentropic efficiency which is the ratio of the ideal stagnation enthalpy rise required to the actual rise for a given pressure ratio. It is a function of the corrected parameters discussed above. Its typical value varies from 80 to 85 %.

Figure 6.17 shows the performance map of a typical compressor. This summarizes all the features discussed earlier. As can be seen, diffuser stall occurs earlier to impeller surge. Diffuser section is the most difficult region to negotiate since this region has a large unfavorable pressure gradient. Hence, if problems occur at all, they will begin to occur in the diffuser section first. One would try to operate the system such that the region is avoided. The avoidance of this region also ensures that impeller stall will not occur. At low enough flow rates, the large incidence at the intake region causes impeller stall. The distinction between impeller stall and impeller surge is that in the former case, the cause is the inlet region directly and in the latter case, it is the flow region between the vanes. The peak performance points correspond closely to near peak pressure ratios obtained at any fixed corrected speed.

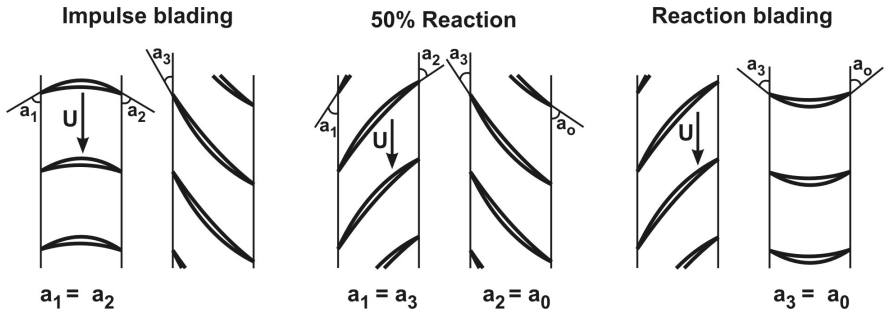

Figure 6.18: Blading angles for different degrees of reaction

Computational Fluid Dynamic Approach

In the evolution of designs for centrifugal compressors, most of the early work was performed by extensive testing. In the last two decades, the development of computational tools and the availability of fast computing machines has made it possible to understand the flow physics and reduce the demand on experimental tests by narrowing down the number of geometries to be tested or evaluated. These developments are very important for high speed compressors where even small changes in geometry can cause substantial deviations in performance. The perturbational effects can be evaluated from these calculations to help reduce the time and cost on experiments. Because of the availability of detailed flow behavior, it has been possible to optimize the single point performance to an extent that one can get single stage compressors with pressure ratios of 8. In such compressors, flow becomes supersonic in some regions.

6.2.2 Axial Compressors

Several aspects discussed in the earlier sections on centrifugal compressors are valid even in the case of axial compressors. These are: one has rotor-stator assembly in the present case similar to impeller-diffuser assembly in the case of centrifugal machines. The flow from the stator is directed to the rotor after accounting for its rotation in both cases. Flows between blades are three dimensional, affected by rotation and tip clearance flows; however, the principal direction of flow is radial in the earlier case and axial in the present one. Since the amount of energy that can be imparted in the impeller section is substantial in the case of centrifugal machine, the pressure rise per stage is very significant (typically 4, maximum of 8). In the case of axial machine, because of the limited energy transport to the fluid in the rotor, the pressure rise per stage (rotor + stator) also gets limited to about 1.3. As different from centrifugal machines, the amount of kinetic energy and pressure rise shared between rotor and stator can be controlled in design. This is called

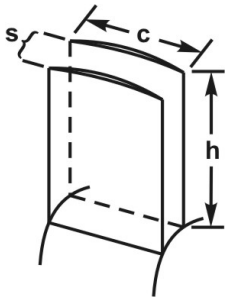

Figure 6.19: The geometric parameters of axial compressor blades

the degree of reaction. If all the pressure drop occurs only in the stator, the machine is an impulse machine – in the rotor, only velocity direction changes occur at constant mean pressure. A reaction machine is one in which pressure drop occurs in the rotor and velocity direction changes in the stator. Most compressors adopt 50 % reaction (also implying 50 % impulse) approach essentially aimed at obtaining better diffusion through the stage. It is also important to recognize that even though a representative value for the degree of reaction is provided, it will vary over the span of the blade, generally impulse at the hub and reaction at the tip with a mean value around 50 %. Under nominal conditions of design, this implies symmetrical blading profiles. Figure 6.18 shows the shapes of the profiles for the three cases of degree of reaction.

Geometric features of an axial compressor

The dimensions of a typical compressor blade are shown in Fig. 6.19. The spacing is denoted by s, chord by c, height or span, h. The height of the blade in the first stage is chosen along with the hub radius to allow the required mass flow rate. An additional feature that influences this choice indirectly is the rotational speed of the system. The non-dimensional quantities which dictate the choice are the Mach numbers of the axial and tangential flow (ratio of the rotor tip speed to the local acoustic speed). The former influences the flow rate and the latter, the pressure rise. Typical tip speeds of modern machines in which some of the stages are transonic – implying blade relative speed (with Mach number, M > 1 at the tip and < 1 at the hub) is about 250 to 450 m/s (leading to relative Mach number $\sim$ 0.9 to 1.4). The axial fluid velocity is chosen at values between 150 to 200 m/s (Mach number $\sim$ 0.4 to 0.6). The dimensions in the subsequent stages are chosen to ensure the passage of the total flow with appropriate pressure rise. The changes in Mach number in the later stages are affected by the rise in static temperature which helps reduce the Mach number. Typical fluid Mach numbers at the compressor will be about 0.2 to 0.3.

The blades have a twist over the height. This arises out of increasing peripheral velocities over the span of the blade from hub to the tip, much larger in the case of blades of large span as will happen for the initial stages of a multistage compressor. For uniform entry flow, blade twist is needed to maintain near constant angle of entry of the flow into the blade. This twist is larger for blades with larger span than for short blades found in the later stages of a multistage compressor. In practical design the so called "half vortex" design is used; it uses the arithmetical mean of the tangential speeds for free vortex ("tangential velocity $\times$ radius = constant" design) and constant reaction. This leads to compressor rotor and stator blades with moderate twist and variation of reaction from hub to tip.

Blades are chosen with an aspect ratio (blade area to square of chord or h/c for uniform cross section) between 1 and 2 as a compromise between better performance – higher lift-to-drag ratio with larger aspect ratio implying better transfer of momentum from the blades to the fluid and mechanical integrity obtained with lower aspect ratio – reduced vibration problems due to aerodynamic flutter. Also larger chord associated with this choice will imply lesser number of blades (at a fixed blade spacing to chord ratio)and lower costs on the blades. The fan blades use fairly high aspect ratio of about 4 to 5 and vibration problems are tackled by providing shroud rings or additional strips on the blade.

The spacing to chord ratio, s/c, is an important controlling variable. Smaller spacing implies greater frictional losses and larger spacing leads to inadequate transfer of momentum from the blades to the fluid, non-uniform exit flow angle distribution, and a tendency towards separation due to flow deceleration in the downstream segment of the blades; optimum value of s/c decided through experimentation is around unity.

The hub-to-tip radius ratio (r_h/r_t) is another important variable. Smaller values imply smaller outer diameter for a given mass flow; it also implies increased blade height and for chosen aspect ratio, increase in chord with attendant higher frictional losses. Typical values of r_h/r_t are about 0.5 increasing to 0.8 with increase in stage for core engines and about 0.3 for front stage high bypass ratio fans. The reduction in the passage height in the later stages arises from increasing density due to increased pressure (even though temperature increase works the other way; use of isentropic relation shows much smaller changes in temperature compared to pressure). *The increased density with the need to maintain similar velocities calls for reduction in cross sectional dimensions*. The mean radius over the height of the blade can increase/decrease/remain constant along the engine. Figure 6.20 illustrates this feature. The first figure corresponds to constant outer diameter (increasing mean radius), the second constant mean radius and the third decreasing mean radius. In the last two cases, the outer casing decreases in diameter. All the three designs are in vogue. The first geometry allows for shorter last stage blade compared to the third option and should be used for smaller num-

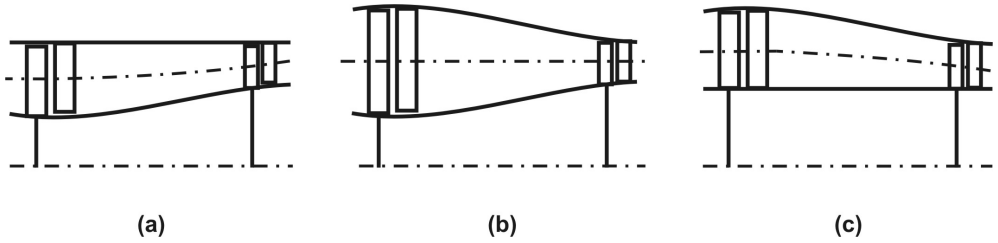

Figure 6.20: Various types of compressor flow geometry. Note the variation of the mean radius of the blades along the engine axis in the three figures – (a) the mean radius increases along the flow path, (b) the mean radius is constant and (c) the mean radius decreases. The mean speed of the fluid varies likewise

ber of stages also implying moderate pressure ratios, say less than about 12. The third option is capable of high pressure ratio (even as large as 40), but the pressure ratio per stage is limited by the tip speed. The middle option (constant mean radius) fills in the intermediate range of pressures. The qualitative features are to be moderated by the possibility of using multiple spools in which the freedom to use different speeds of rotation for different spools is allowed.

Fluid flow through the compressor

Flow enters axially into the compressor. While passing through the stator blades, it acquires the direction and some increase in pressure. It enters the rotor at the appropriate angle of attack and flows through the channel between the blades. In doing so, the fluid which is close to the rotor hub gets carried by the rotor because of the no-slip character of the flow. The fluid flowing through the space between the blades causes pressure on the following section of the blade and suction on the blade surface which is ahead as shown in Figure 6.21 and this causes a lateral pressure gradient. Towards the tip of each blade, the fact that the blade has a pressure and suction surface implies that there will be a flow from the pressure surface to the suction side through the tip clearance.

This leads to a vortical structure in the lateral direction in a direction opposite to the direction of rotation. This feature coupled with the lateral flow near the hub leads to two contra-rotating vortices. In addition, the mean axial flow will develop boundary layers on the wall. Thus, the flow that comes off a row of blades will have swirling regions with lower velocity wake sections as well. Such a flow will be processed by the next set of stator blades to be presented to the next set of rotor blades. The momentum transfer processes in the succeeding set of stator-rotor sections will, therefore, be complicated by the deteriorating flow profiles. In fact, the rather uniform velocity distribution will become parabolic with large asymme-

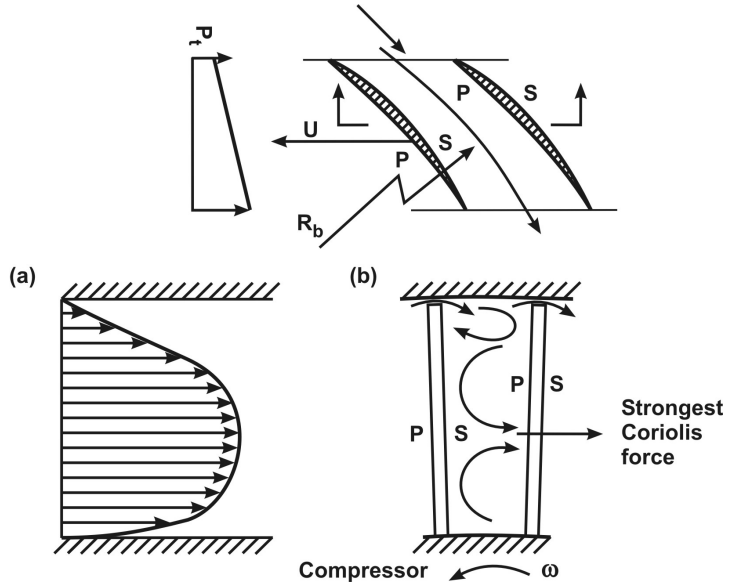

Figure 6.21: Radial variation of axial velocity across annulus, with variations of Coriolis force that generate secondary spiraling flows, and the effects of leakage at the blade tips, P = Pressure surface, S = Suction surface

try after several stages as shown in Figure 6.21. Such a profile in comparison to uniform distribution implies lesser work output per stage. In an axial compressor of pressure ratio, say 11 with 13 stages, for an ambient pressure of 1 atm., the pressure at the end of the first stage is 1.2 atm., at the end of 2nd stage 1.44 atm., at the end of third stage, 1.7 atm., at the end of fourth stage, 2.1 atm, etc till it is 9 atm. at the end of 12th stage and 11 atm. at the end of 13th stage. The change in pressure across the first stage is 0.2 atm. and across the last stage is 2 atm. This means that the adverse pressure gradient to be overcome by the fluid in the last stage is much larger compared to the first stage. Greater adverse pressure gradient implies greater possibility of undesirable viscous effects including separation. It is this feature which makes it difficult to build compressors with large pressure ratios.

Multi-spool compressors

The need for a multi-spool compressor can be realized if we appreciate the conditions of an operating single spool compressor. Taking note of the fact that the blades have to function under the action of axial and tangential velocities and that therefore, there is need to observe the correct angle of attack for each stage of blading, it is assumed that such a correct relationship has been obtained at the

Table 6.4: Nature of Compressors used on various engines; 1F = One fan; 5A = five axial stages; 1C = one centrifugal stage; (c) = core; 1 s = 1 spool or shaft; VIGV = Variable inlet guide vanes

Name	Stage/Axial Centrifugal	Pressure ratio	$\dot{m}_a$ kg/s
Mamba	1C	2.8	2.0
Lucas CT-3201	1C	3.5	0.93
TRS-18-046	1C		
TRI-60	8A	4.0	5.60
RR Viper 601	8A	5.8	26.5
J3-IHI-7C	8A	4.5	25.40
J85-21	8A	8.3	20.0
J79-7A	17A	12.9	76.5
ATAR-SNECMA 58	8A	6.15	70.7
Pegasus 11	8A	14.0	81.6
Olympus 593	14A	15.5	186.0
Allison 250-C-20B	6A +1C	7.2	1.56
Astazor XIV	2A +1C		2.5
Turbo meca Baston	2A +1C	6.68	5.9
RR Dart	2C	5.62	10.7
Lycoming LTC1-L13	5A+1C	7.4	4.85
Lycoming LTC4-L7B	7A+1C	8.2	12.25
P&W JT-15D	1F+1A+1C	10.0	8.0 (c)
Ivechenko AI-25	3F+8A	8.0	
Garret TFE.731-3	1F+4A+1C	14.6	19.20 (c)
Garret ATF3-6	1F+5A+1C	21.0	18.1 (c)
Soleviev D-20P	3F + 8A	13.0	113.0 (c)
SNECMA-M53	3F+5A	8.5	84.0
P&W JT 8D	2F+6A+7A	18.0	79.0 (c)
P&W JT 9D	1F+3A+11A	24.0	115.0 (f)
CFM 56	3F+12A	25.0	53.7 (c)
F 404 (GE)	3F + 7A	25.0	47.0 (c)
Soleviev D-30kU	4F+10A	17.4	78.0
GE CF6-50M	1F+16A	31.4	150.0 (c)
RB-211; 524B	1F+7A+6A	25.0	145.0 (c)
GE 90-76B	1F+3A + 10A	40.0	136.0 (c)

nominal speed. If the speed is increased beyond the nominal, mass flow rate can increase to such an extent that the flow may get choked in the inlet; in all the later stages, enhanced pressure and hence density (temperature effect is not dominant) allows the flow to pass through. When the speed falls below the nominal value, three conditions can arise : (a) the flow rates can be much lower and therefore, the axial velocity in the early stages will be lower. This creates angles of attack much higher than nominal and therefore, there is a tendency to stall. (b) in the later stages, the lower pressure ratio that is achieved can lower the density compared to the nominal to a degree more than compensated by the reduction in temperature rise, since changes in pressure and temperature are governed by isentropic relationship. This causes increased axial velocity in the later stages leading to choking of the flow in the limit. (c) Slight reduction in mass flow rates in the later stages can create angles of attack that may be close to stall. Such conditions are a possibility despite the mass flow being close to the limit because the dependence of the pressure ratio on the mass flow is steep in some zones of operation (see Fig. 6.22 for details)

The performance of the compressor is governed by the combination of these features. The general behavior namely that in a multistage compressor, the flow in the later stages will tend to windmill (angle of attack leading to zero or negative lift) while the early stages are loaded (angle of attack higher) at off-design conditions, has limited the achievable pressure ratio to about 5. For larger pressure ratios, solution to the above problem must be found. It has been tackled by one of the three techniques (or a combination). One solution to this behavior would be to provide a compressor bleed which gets activated once the appropriate off-design conditions are sensed. This permits the axial velocity in the later stages to be brought down to acceptable levels. The second technique is to provide variable inlet guide vanes (variable stator blades) which will control the flow and the vector to provide the right velocity triangles at off-design conditions. This is particularly provided for in the first few stages. The third technique is to split the stages into two/three sets and mount them on different shafts so that they can rotate at different speeds. In a two shaft system, the blades on the second shaft can rotate at a higher speed to allow for the higher axial velocity so that the velocity triangles are closer to design. When compressor pressure ratios demanded from the compressor are very large – 25 to 40, three shaft system is adopted. While it is true that the mechanical engineering of these systems becomes complicated, the extraordinary performance that these systems provide has led to their realization and use.

There are other set of important reasons for the choice of multi-spool compressors at higher pressure ratios. Use of higher pressure ratios in turbojets was considered appropriate in early long range jet transports because of lower specific fuel consumption (sfc). The increase in weight due to the choice of higher compressor pressure ratio was compensated by the reduced fuel load due to lower sfc. Otherwise, higher pressure ratios are used only in turbofans, be it for military or

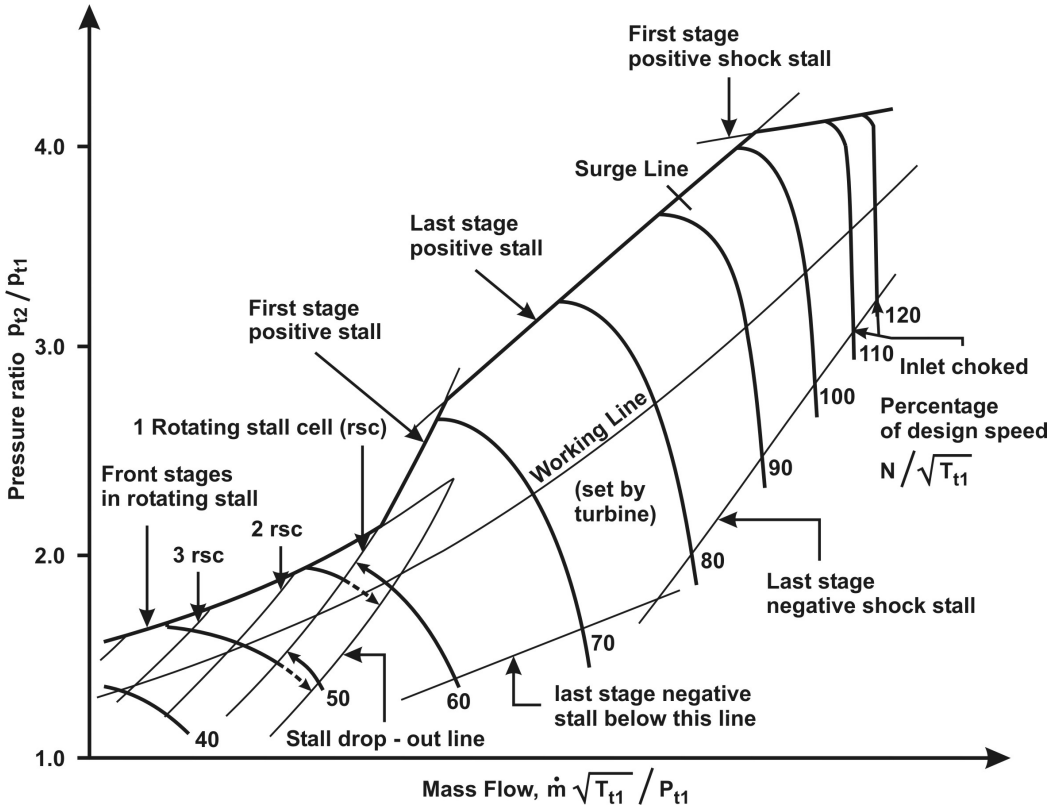

Figure 6.22: Over-all characteristics of an axial compressor showing various operational limitations applicable at different speeds, drawn from ref. [4]

civil applications. In the case of military engines, the bypass ratio used is typically 0.5 to 1.5; in the case of civil applications, it is between 4 to 6. At these bypass ratios, the fan has to process large flow rates. The fan diameters are large and rpm is low to maintain the limiting tip speeds of 400 – 450 m/s. If the low pressure (LP) stage of the core compressor runs at the same rpm as the fan (that is usually the case), the performance of the LP compressor is inadequate. This calls for another stage, normally the high pressure stage running at higher rpm to meet the performance demand. When very high pressure ratios are used (as is the case, for obtaining better sfc's) it would be necessary to adopt three spools with the low pressure stage combined with the fan and the two other stages contributing to the compressor performance significantly. Once multi-spool arrangement is adopted, the flow related problems identified earlier are overcome. Even so, a compressor designer may need to adopt a combination of strategies to ensure surge free performance in the operational regime of the aircraft using the engine.

6.2.3 Uses of Centrifugal and Axial Compressors

Centrifugal compressors are used when the flows to be handled are not large; this will reduce the demands on the frontal area. By and large, small thrust turbojets, turbo-shaft engines for helicopters where the engine is not exposed as in turbo-prop based aircraft, and land based power generation systems in which cost plays an important role, use centrifugal compressors. High thrust or power engines which need to handle large mass flows (typically 50 to 1300 kg/s) invariably use axial flow compressors. Table 6.4 shows a list of engines adopting centrifugal and axial machines.

Very small engines used on micro-air vehicles and pilotless target drones use centrifugal compressors since the pressure ratio is limited to less than 4. Many intermediate size systems use axial compressors in single spool mode. One of the largest engines with a mass flow of 186 kg/s using a 14 stage single spool compressor is the Olympus engine used on Concorde aircraft. One of the unusual features of the engines – Teledyne, Allison, Lycoming and Garret – is that a centrifugal stage follows several axial stages. One would expect that such developments have come about because at the point of time when the specific system design was needed, the lowest cost option to meet the product design objectives would be to modify an existing system with suitable add-ons. One can notice in the large engines – Pratt and Whitney JT 9D, General Electric CF-6, Rolls Royce RB 211 and General Electric GE 90, the mass flow rates handled are very large – of the order of 600 to 1300 kg/s. The power required by the compressors also would be stupendous – 50 to 70 MW. That is why any optimization in design would add to the efficiency in the gas turbine operation. Over several decades, the isentropic efficiency of the compressor has increased from 75 % to today's 87 %.

6.2.4 Summary

This part of the chapter has been devoted to compressors. The aim of the discussion was to present the essential fluid mechanics that governs the performance of compressors. The power put into the rotating machinery is transferred to the flowing fluid by enhancing its momentum. This momentum that is initially in the form of kinetic energy is transformed into potential energy by diffusion. Relatively simple considerations are adequate to understand the nature of compressors used in various engines. Experiments formed the foundation of the development through the eighties. It is only in the nineties that computational tools have had an impact on the design of high performance systems.

6.3 Combustors – Gas Turbines, Ramjets and Scramjets

When one imagines the development of a combustion chamber, it begins in isolation given the overall specifications. This is true in so far as the designs of gas turbine and ramjet combustors are concerned. There are a few points of interaction with the vehicles, but these are secondary. In the case of scramjets, the development of the combustor has to proceed along with that of the overall vehicle, since, any small engine performance variation has a significant effect on the mission. We shall discuss the gas turbine, ramjet and scramjet combustors in this sequence. We shall look at geometric and performance aspects, the essentials of the combustion process and design, and the role of computational tools in the process of development.

Gas Turbine Combustors

One would expect the combustor to meet the following requirements.

1. Good ignitability.
   $\Longrightarrow$ includes altitude relight capability up to 10 km.

2. Good (Broad) flame stability.
   $\Longrightarrow$ Over a range of air-to-fuel ratios up to 200 (13 times the stoichiometric value).

3. High combustion efficiency.
   $\Longrightarrow$ More than 99 % at all principal operational points (like take-off and cruise)

4. Low pressure loss.
   $\Longrightarrow$ Not more than 6 %

5. Good temperature traverse quality, γ_T = (T_{max} – T_{mean})/(T_{mean} – T_{comp}).
   $\Longrightarrow < 25$ %

6. Low exhaust emissions.
   $\Longrightarrow$ Must follow EPA standards on HC, NO_x, CO and smoke.

7. Low volume and weight.

8. Relative ease of maintainability.

9. Long life.

Each of these points has an important bearing on the design and an examination of engine combustion system shows that significant improvements have taken place on each of these over the last sixty years. Both combustor volume and weight have reduced to half their values in sixties. Modularity of design concept has improved maintainability.

Use of a high compressor pressure ratio has reduced the volume (and increased energy density), improved combustion efficiency at high altitudes and reduced the problems of relighting at higher altitudes and hence, improved the stability of operation. Extensive testing and analysis have produced several configurations which have low distortion in the temperature profile of hot gases exiting from the combustors. Thus, through a scheme of experiments, inventive approach, conclusions based on simple analysis, extensive testing, and computational reactive fluid dynamics, many kinds of designs have been evolved.

The inputs to a combustor designer are the pressure, mass flow rate and temperatures at the inlet and the outlet. Use of thermochemistry leads to the fuel flow rate required. In the early engines, the compressor pressure ratios were 8 – 12, main combustor inlet temperature about 450 – 500 K and exit temperatures 1000 – 1100 K. In recent times, engine pressure ratios have gone up to 25 – 40, main combustor inlet temperatures of 650 – 700 K and exit temperatures of 1400–1600 K or even more. If one considers the after–burner of a turbo jet engine of a ramjet, the inlet temperatures are in the range of 600 – 800 K and exit temperatures are close to 2000 – 2200 K. These values are close to stoichiometric combustion conditions. For kerosene class of fuels used in air breathing engines, the air-to-fuel ratio at stoichiometry is about 15 and adiabatic flame temperature 2300 K. The air-to-fuel ratio required to produce lower temperatures of 1000 – 1600 K are between 100–50. This means that the mixture is very lean. There are problems of burning ultra-lean mixtures. Fuel air mixtures have what are known as flammability limits. These are the air-to-fuel ratios within which the fuel-air mixture can ignite and burn and outside of which they do not burn. There are two limits – the lean and rich limits for each fuel-air mixture. The lean limit for kerosene – air mixture under the slightly turbulent conditions is about 30–35. This implies that circumstances in a gas turbine combustor in terms of overall mixture ratio can be beyond the lean flammability limit over a portion of the operational range. This problem is accentuated in an actual gas turbine combustor under the relatively high turbulence conditions. This is one of the central issues in the design of a gas turbine combustor – to ensure ignition and combustion at mixture ratios that are very lean and outside the flammability limit.

This problem is resolved by allowing about 25–35 % of the normal air flow to react with the fuel so that the mixture in the combustion zone is near-stoichiometric and adding the remaining air in stages to reach the desired dilution. Another important effect that is created to help combustion stability is a recirculation zone

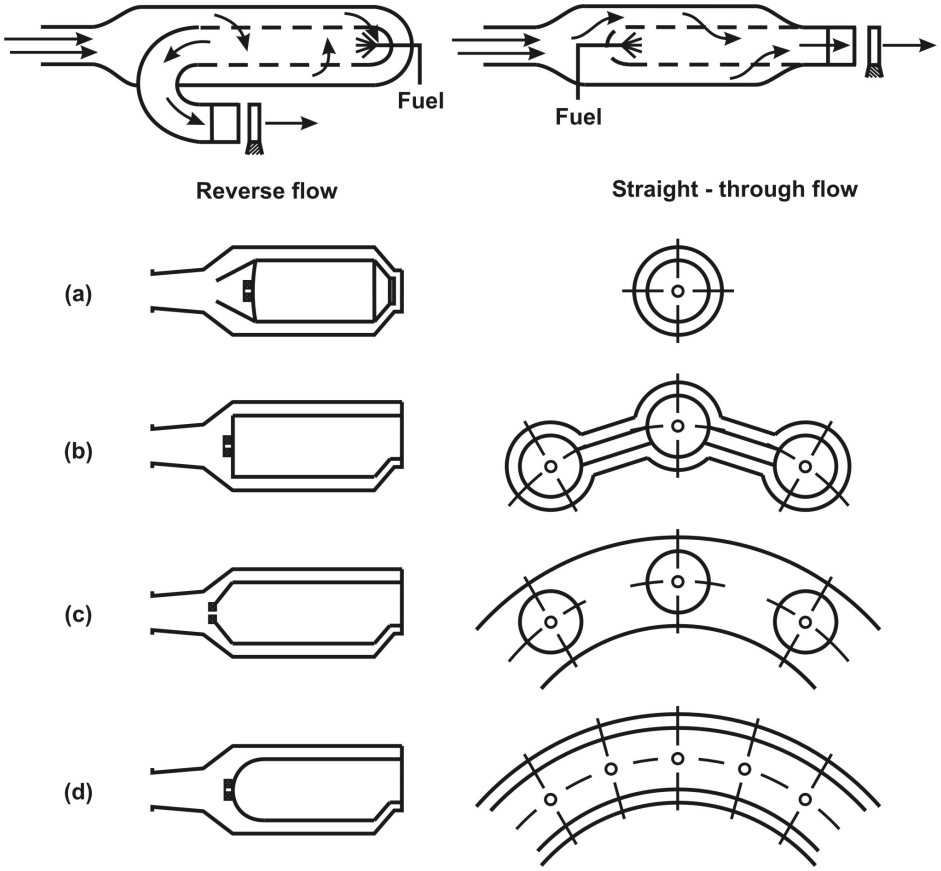

Figure 6.23: The cross section of the various combustors (above). The longitudinal sections of reverse flow (left) and straight flow can combustors (right) are seen at the top. Below are seen the cross sections of single can (a), multiple cans (b), can-annular (c) and annular combustors (d)

through the use of swirling air around the fuel injection zone. The recirculation zone provides greater residence time for the flow to permit completion of reactions. The rest of the air is mixed downstream so that combustion stability remains unaffected. This fact does not mean that flame will be stable at all pressures (lower than sea level) because of another limit which will affect the flame structure. As pressure becomes lower, the flame zone becomes extended into subsequent segments of air addition and the cooling effect of the air entering the downstream region will cause extinction or blow out of the flame. One has to keep the operational region of the combustor such that these limits are not reached.

6.3.1 Typical Combustor Geometries

Combustor geometries are either straight-through or reverse flow as shown in Figure 6.23. The straight flow combustors are most commonly used configurations particularly for high thrust axial flow systems. Reverse flow combustors are used more commonly with radial flow systems and they produce a more compact design. It was considered useful to limit the shaft length to reduce vibration problems despite the larger frontal area of the system. Recent technologies have overcome the limitations on shaft length and straight flow combustors have become the more acceptable configuration.

In either the straight or reverse flow designs, there are other variants with regard to the arrangement of the combustors. The relatively easy development cycle involved in can combustors (see Figure 6.23 third from the top) led the early engines to deploy these designs. The number of cans per engine varied from 8–16. Though maintenance and inspection were relatively simple, the poor utility of the space allocated to the combustor motivated the development of other designs. The other major design is the annular combustor which has several advantages namely, better space utility and hence, lower volume, lower weight, lower pressure drop, and relatively uniform circumferential distribution of properties. One of the problems is the development cycle of the combustor that occurs with the choice of a sector of the combustor considered representative of the overall system. The structural problems of the flame tube that is thin but large in diameter and hence, more difficult to repair and maintain are its other minor defects.

An intermediate between the can and the annular designs is the can-annular design (see Figure 6.23 c) that has a number of flame tubes in an annular zone through which air will flow. Though many recent engines have deployed this design, the favorite design is the annular one.

Some of the engines using these designs are as indicated in Table 6.5. The most common design is the annular configuration. Small engines built in early times were built around can or can-annular designs. Engines using centrifugal compressor stages (as in Lycoming and Garett series) find enough frontal area to use the reverse flow annular combustor design.

The details of the combustion system are shown in Figure 6.24. The air from the compressor enters through an inlet diffuser. The air from the compressor at a speed of 120 to 180 m/s needs to be slowed down to about 30 to 60 m/s. This can be done by techniques shown in Figure 6.25 – (a) that shows a curved wall diffuser that will take a substantial length to prevent flow separation typical of flows with sharp divergence. To reduce the length, one can use a dump diffuser where the separation point is located at the edge of the ducting opening up into the combustion chamber. In this case, (b), the separation point is fixed whatever be the flow rate. In recent times, a Coanda effect based inlet is being considered

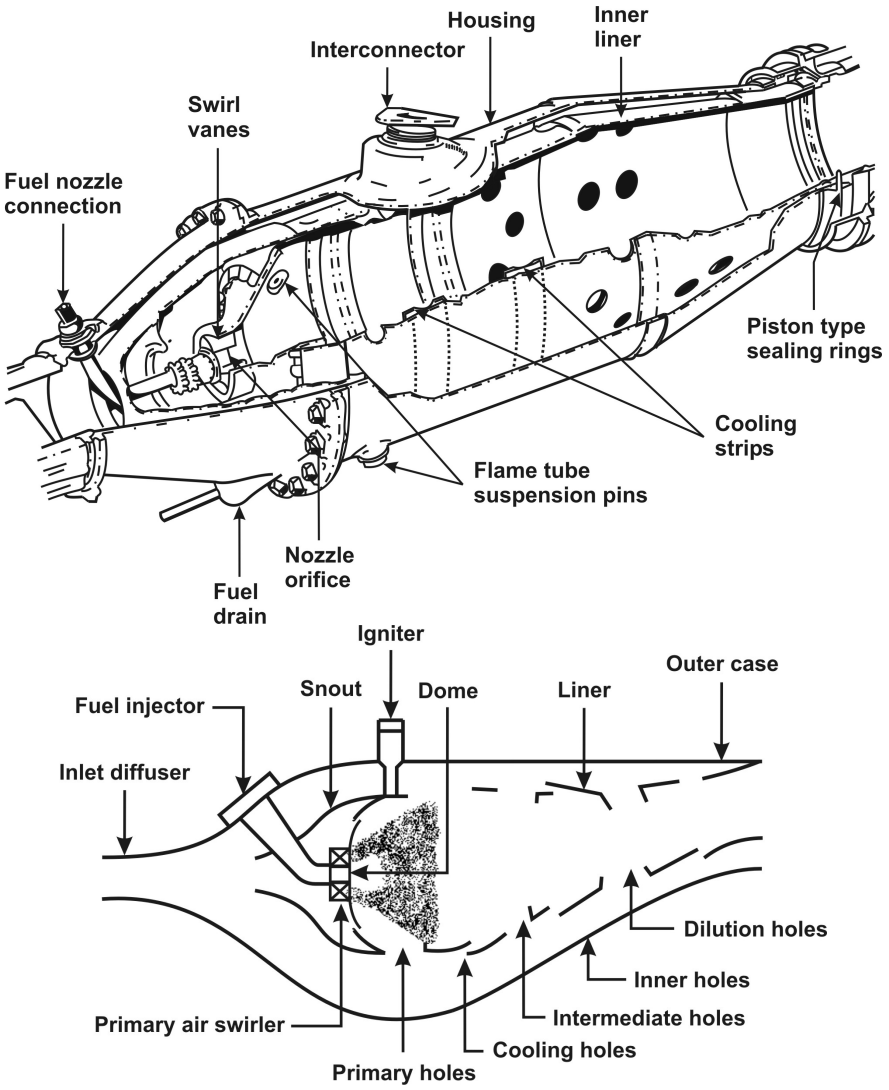

Figure 6.24: Details of the combustion system – top shows the can combustor and bottom shows the annular combustor adapted from ref. [7]

Table 6.5: Nature of Combustors used on various engines

Name	Nature	Features	$\dot{m}_a$, kg/s
Lucas CT-3201	Reverse, annular		0.93
TRS-18-046	Annular		
TRI-60	Annular		5.60
RR Viper 601	Annular	24 burners	26.5
J3-IHI-7C	Annular		25.40
J85-21	Annular	12 burners	
J79-7A	Can-annular	10 cans	76.5
ATAR-SNECMA 58	Annular		70.7
SNECMA-M53	Annular		84.0
Allison 250-C-20B	Single can		1.56
Ivachenko AI-25	Annular	12 burners	
Lycoming LTC1-L13	Reverse, Annular	22 burners	4.85
Lycoming LTC4-L7B	Reverse, Annular		12.25
Garret TFE.731-3	Reverse, Annular		19.20 (c)
Garret ATF3-6	Reverse, Annular		18.1 (c)
Astazou XIV	Single can		2.5
Turbomeca Baston	Annular		5.9
RR Dart	7 cans	Ign. (3, 7 cans)	10.7
P&W JT-15D	Reverse, Annular		8.0 (c)
Olympus 593	Annular	16 vap. burners	186.0
Soleview-D20P	Can-annular	12 cans	113.0 (c)
P&W JT 8D	Can-annular	9 cans	79.0 (c)
P&W JT 9D	Annular		115.0 (c)
CFM 56	Annular		53.7 (c)
F 404 (GE)	Annular		47.0 (c)
Soleview D-30kU	Can-annular	12 cans	78.0
GE CF6-50M	Annular	30 burners	150.0 (c)
RB-211; 524B	Annular	18 burners	145.0 (c)
GE 90-76B	Annular		136.0 (c)

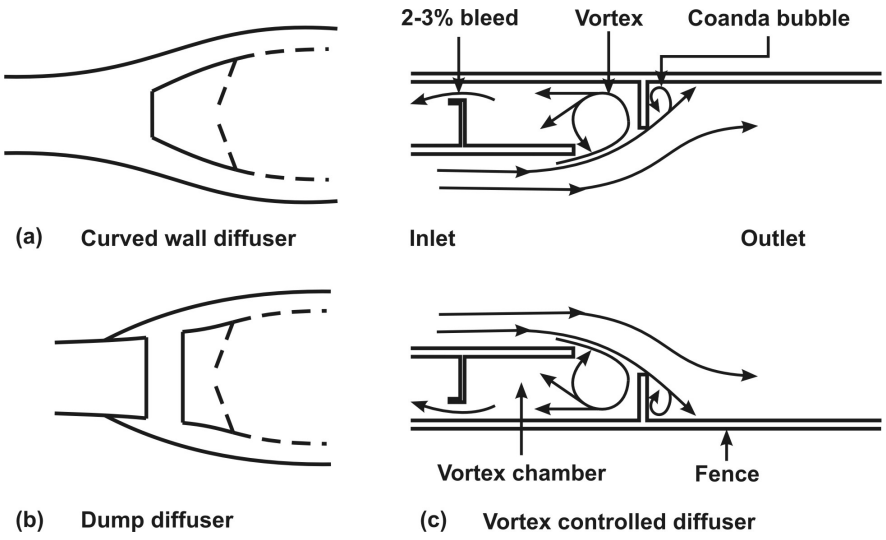

Figure 6.25: Diffuser section between the compressor and the combustor adapted from ref. [4]

as in (c). A small amount of flow – between 2 to 3 % is drawn away and the vortex stabilizes the flow diverging from the inlet zone. Air flows through the annular space and enters the combustion system from several locations. About 30 % of the air is arranged to flow along the central zone via a swirl path, the fuel injector being at the center (see Figure 6.24). This will provide an air-to-fuel ratio (A/F) close to stoichiometry in the primary zone. Earlier designs used to maintain the A/F near stoichiometry; but the demand to widen the lean operating zone (up to A/F of 200) has required that the primary zone is to be operated under fuel lean conditions – with equivalence ratios of 0.4 to 0.8. The remaining air flows around the annulus and enters the combustor through holes to provide dilution air and also cool the walls. While the combustors of an earlier era (with turbine inlet temperatures of 1200 K) used fractions of air for primary zone, dilution and liner cooling as 30 to 35 % in each segment, modern day combustors (with TIT $\sim$ 1600 K) use 45 to 55 %, 2 to 5 %, and 45 to 50 % respectively. Thus, very little air goes into dilution in modern day systems. Liner cooling takes up an important segment because it decides the life of the combustor. The design of the combustor to provide the distribution of air has evolved over times. Figure 6.26 shows the evolution of these strategies. Part of the developments is attributable to the choice of increased combustor pressures, with increased pressures leading to increased heat flux to the wall from the combustion zone.

There are several cooling designs. Some of the more recent designs are shown in Figure 6.26. In the early designs, the flow simply entered through punched holes with the holes projecting slightly into the combustor. In later designs, sec-

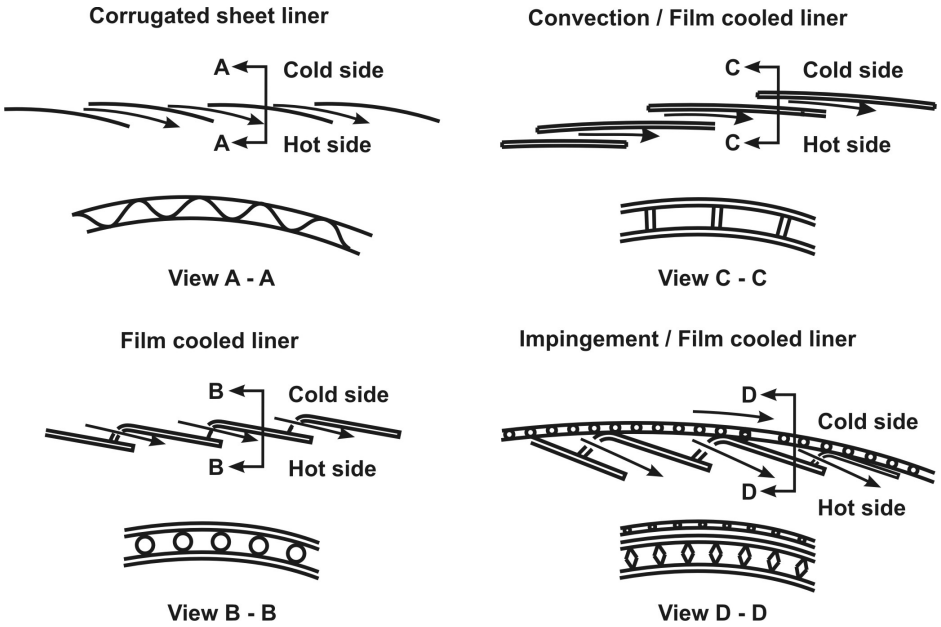

Figure 6.26: Combustor Liner cooling designs

tions of the combustor are connected by corrugated sheets as in A-A, other support structures as in B-B, C-C, and D-D (see Fig. 6.26).

6.3.2 Fuel Injection Systems

Liquid fuels are to be injected into the combustion chamber in a form in which the liquid is atomized into fine droplets. This is done by creating a thin sheet of the liquid and injecting it into a fluid stream at high velocity, typically 25 to 50 m/s. The thin sheet will break down to ligaments and droplets as the shear between the external flow and the thin sheet enhances the inherent instability of the fluid sheet. The droplets that are formed have a distribution over a range of sizes. The objective of the process of atomization is to obtain as small a peak drop size (as well as mean drop size as indicated by the Sauter Mean Diameter, SMD which is the mean diameter that gives the same total area as the actual distribution). There are two known approaches for atomization. These are pressure atomizers and air blast atomizers. Typical geometric details are shown in Figure 6.27. Pressure atomizers (see top part of the figure) utilize high pressures ($\sim$100 atm) to force the liquid through a set of tangential orifices into a swirl chamber. The liquid is finally forced out of the exit orifice. The high tangential velocity is amplified by the reduction of the diameter from the chamber to the exit so that a thin sheet comes out of the exit orifice with a large tangential velocity. The central part of

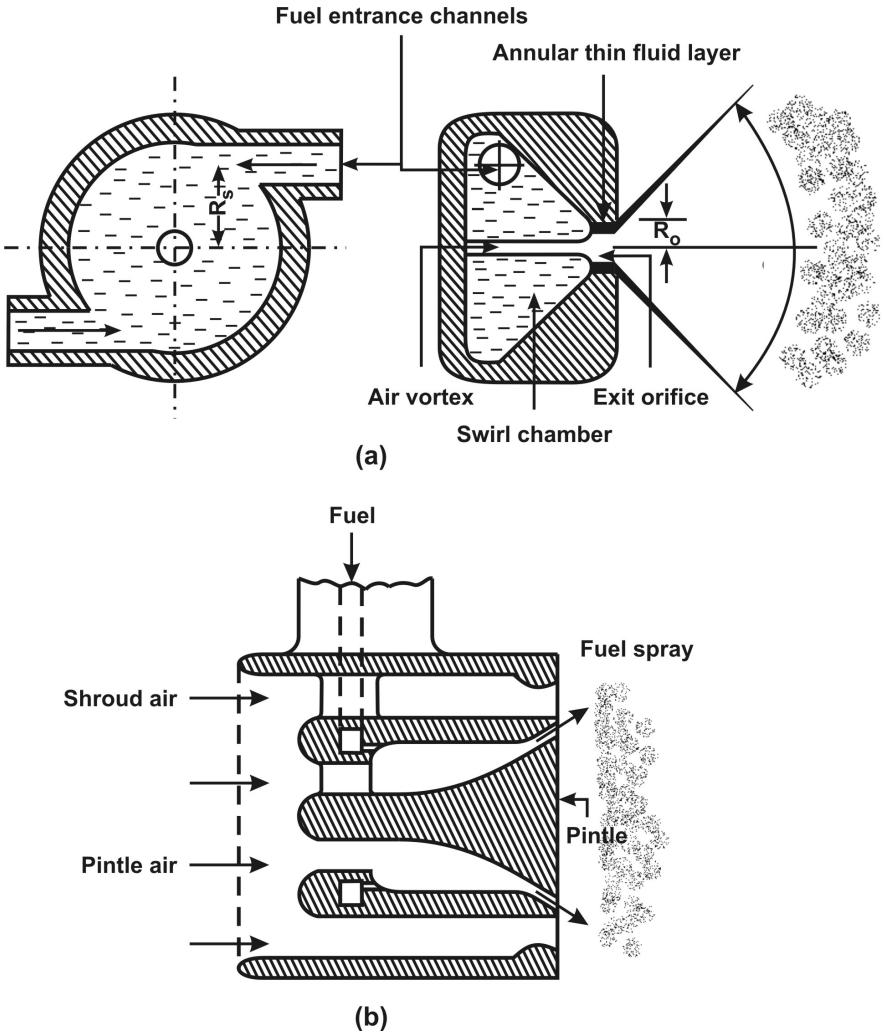

Figure 6.27: Two atomizer geometries - (a) Swirl atomizer (also called Pressure atomizer) and (b) Air blast atomizer

the swirl chamber experiences low pressure and an air core gets created. The thin sheet breaks down to ligaments and then droplets.

The air blast atomizer (see lower part of the Figure 6.27) uses much lower pressures for injecting the liquid and the air stream flows over it in a narrow annular passage until it comes out of the injector. The thin sheet that becomes thinner as it moves at high velocity and breaks down into fine droplets. The shear between the flowing air stream next to the thin sheet provides the aerodynamic force to break the fluid into ligaments and subsequently to droplets. Pressure atomizers have been in use for a long time. Their performance is a strong function

of throughput that depends on the power of the engine. The power to be delivered by a gas turbine engine varies significantly from about 30 % at idling to 100 % at full power. At low power levels, the fuel flow rate has to be lowered. Since $\dot{m} \sim \sqrt{\Delta p}$, a factor of three reduction in flow rate implies a factor nine reduction in pressure drop. This implies that at lower power level, the pressure drop will be very much smaller than at full power. Since the atomization characteristics are strongly dependent on pressure drop across the injector, it can be expected that the drop size distribution will be coarser at lower power levels. It is this feature that has provided the motivation for adopting the air blast atomizer in most gas turbine engines designed in the last thirty years. Other methods of resolving the poor atomization at low flow rates have been evolved. A typical high thrust engine with an annular combustor has a number of atomizers – 30 to 40 all around the periphery. If the flow rate to be passed is say, quarter the maximum value, then only a select group of atomizers will spray the fuel into the combustor. These could be arranged as a set of three each 120° around the periphery so that the fuel flows through nine atomizers.

6.3.3 Processes Inside the Combustor

In many combustors, the fuel is introduced through an injector at relatively high pressures. In some, the fuel is vaporized and mixed with air before the fuel is allowed to combust. In liquid fuel injected systems, the processes taking place are liquid vaporization, mixing with air and chemical reaction leading to heat release. The times taken for these processes are set out as

$$t_t = t_v + t_m + t_r \tag{6.3}$$

where t_t = total time, t_v = vaporization time, t_m = mixing time, t_r = chemical reaction times.

The time for vaporization is characterized by

$$t_v = d_0^2 / K_c \tag{6.4}$$

where K_c is the vaporization constant for combustion defined by

$$K_c = 8 \frac{k_g}{c_p} \frac{1}{\rho_l} \ln(1 + B_c) \tag{6.5}$$

where B_c called the transfer number, is given by $B_c = [c_p(T_g - T_s)]/[c_p(T_s - T_0) + L]$, where T_g = gas phase temperature, T_s and T_0 are the surface and initial temperature of the droplet, L = latent heat of phase change, c_p is the constant pressure specific heat of the gases, B_c, the transfer number defined by the expression above is the ratio of the gas phase heat transfer potential to the heat required to vaporize

the liquid, typically about 4, and d_0, the diameter of the droplet depends on the atomization technique and varies between 20–60 μm for most injection techniques adopted. The above result needs to be modified to take into account the flow effects inside the combustor. Typical correlations for flow effects can be stated as $t_v/t_{v,Re=0} = 1 + 0.33Re^{0.5}$, where the Reynolds number is based on the drop diameter and the difference in velocity between the droplet and the gas as

$$Re = \rho d_0 |u(drop) - u(gas)|/\mu \tag{6.6}$$

It is generally understood that the vaporization rate is not seriously affected by forced convection since the droplets reside in the recirculation zone with relatively low velocities. To obtain an idea of typical numbers, for kerosene, measurements show that a 45 μm droplet takes about a millisecond to burn up. A 20 μm diameter droplet, therefore, takes about 0.2 ms and a 60 μm droplet takes 1.8 ms or so. Thus, $t_v \sim 0.2 - 2$ ms. Fuel injection atomizers generate a range of droplets and the distribution is characterized in terms of a Sauter Mean Diameter (SMD). Since vaporization rate is proportional to the surface area (or the square of the diameter), SMD is an indication of the size of the spray for purposes of estimating the vaporization rate. Most modern day engines have atomizers with SMD between 20 to 40 μm and therefore the range of t_v is about 0.2 to 0.8 ms.

The time for mixing is to be estimated from the turbulent mixing $t_m \sim L/u'$ where L is the size of the energy carrying eddy and u' the turbulent fluctuation intensity. An estimate of u' is obtained by scaling with pressure drop through the combustor; i.e., $u' \sim C'\sqrt{\Delta p} \sim CU$ where C is a constant depending on the geometry and possibly Reynolds number and U, the mean flow velocity. L, itself scales like C_1, hole size or spacing between holes in the primary zone region of the perforated sheet. These give then,

$$t_m \sim \frac{C_1 d_h}{CU} \sim C_2 d_h/U \tag{6.7}$$

where d_h is the size of the hole or spacing which ever is higher. For $C_2 \sim 0.5 - 1$, $d_h \sim 10 - 20$ mm, $U \sim 20 - 50$ m/s, $t_m \sim 0.1 - 1$ ms.

The third term, t_c represents the time for the completion of chemical reactions. It varies typically as,

$$t_r \sim \frac{\bar{\rho}}{\overline{\dot{\omega}'''}} \sim \frac{1}{Ap^{n-1} exp(-E/RT_f) F(\phi)} \tag{6.8}$$

where $\overline{\dot{\omega}'''}$ is the average reaction rate, p = pressure, n = pressure exponent of the reaction, E = activation energy, T_f = flame temperature, which is a function of ϕ = equivalence ratio and F(ϕ) is a function (of equivalence ratio) depicting the dependence on the composition. The reaction rate peaks around ϕ = 1 and drops to low values on either side. This comes both from T_f peaking around ϕ = 1, E/R

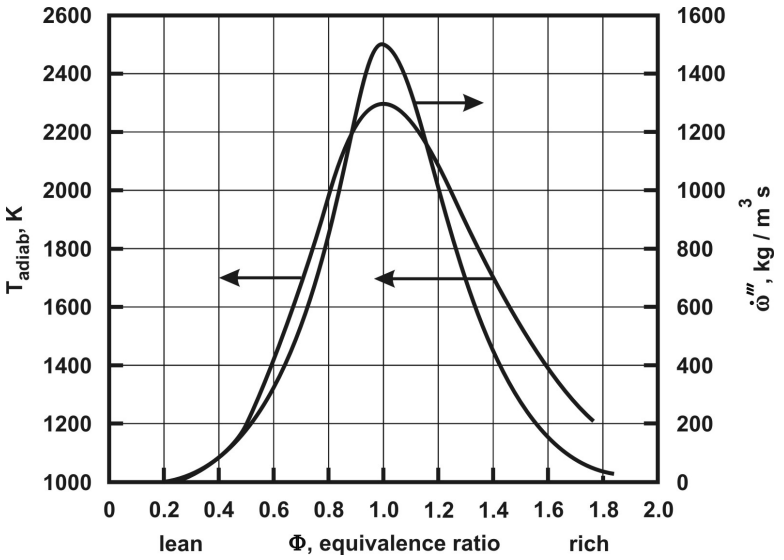

Figure 6.28: Flame temperature and reaction rate with equivalence ratio for natural gas/kerosene class fuels

being large around 15000 – 20000 K, and $F(\phi)$ due to composition. The effective value of t_r increases with altitude because of decrease in pressure $[n - 1 \sim 0.8 - 1]$ and an effect due to ϕ which occurs because of the significant influence of the secondary zone in reducing the mean temperature and equivalence ratio.

The mean reaction rate also has a peak around ϕ = 1 (stoichiometry). A simple way of estimating the mean reaction rate is to relate it to the one-dimensional flame burning velocity. A simple analysis will show that $\overline{\dot{\omega}'''} \sim \rho_u S_u (\overline{k/c_p})$ where ρ_u is the density of the premixed mixture, S_u is the burning velocity of the mixture $(\overline{k/c_p})$, the average of the ratio of conductivity to specific heat of the mixture. Measurements show that burning velocity is very weakly dependent on pressure. Therefore, the mass consumption rate ($\rho_u S_u$) increases with pressure. Figure 6.28 shows the typical plot of T_f and $\overline{\dot{\omega}'''}$ with ϕ. At a mean equivalence ratio of 0.3, the achieved values are about 20 $kg/m^3 s$ of the mixture and about 1 $kg/m^3 s$ of fuel consumption rate. At a calorific value of 42 MJ/kg, this amounts to 40 MW/m^3 of heat release rate. At higher pressures, the consumption rate and the corresponding heat release rate would go up due to the dependence of reaction rate on pressure.

The typical range of values of t_r is 0.5 – 5 ms. This variation is due to widely varying pressures at which the combustor operates. A typical pressure ratio of 10 implies a ratio of 8 in terms of time scale.

Thus, the total time for combustion can be set out as,

$$t_t = \frac{d_0^2}{K_c} + C_2 \frac{d_h}{U} + \frac{exp(E/RT_f)}{Ap^{n-1} f(\phi)} \tag{6.9}$$

Typical values can be set out as

$$t_t \sim (0.2 - 0.8)\text{s} + (0.1 - 1)\text{ms} + (0.05 - 5)\text{ms} \tag{6.10}$$

The first two terms are nearly constant and can be brought down to about 0.2 – 0.3 ms, through better atomization and flow distribution. It is the last term that appears to have a wide variation. In some combustors, the drops are atomized to such a fine degree ($\sim$ 20 μm or less) that time for vaporization and mixing are small and chemical conversion time is large. In such cases the rate limiting step is the chemical reaction. This situation is a better approximation at high altitudes where the combustor pressure is less, and reaction rates are lower. One compares this time scale, t_t with the residence time in the combustor defined as,

$$t_{res} \sim C_3 L/U \tag{6.11}$$

where t_{res} = residence time, L = length of the combustor, U = mean speed through the combustor, C_3 is a factor greater than unity which accounts for recirculation of the fluids in the primary zone. For $L \sim 200$ mm, $U \sim 50$ m/s, $C_3 \sim 1$, we have $t_{res} \sim 4$ ms. This is satisfactory for the combustor operating at sea level. At higher altitudes, the two times, t_t and t_{res} are comparable and hence, one finds difficulty in achieving the performance desired.

One forms a non-dimensional quantity called the first Damkohler number which is the ratio of fluid residence time to the total conversion/combustion time.

$$D_1 = t_{res}/t_t \tag{6.12}$$

For reactions to be complete one expects D_1 to be large. Combustion theory explains the extinction or blow out or stability limits on the basis of a critical lower value of D_1. It can also explain the behavior of combustion efficiency with altitude or operating conditions.

$$t_t = C_t . t_{res} \tag{6.13}$$

$$C_3 \frac{L}{U} = C_4 \left[\frac{d_0^2}{K_c} + C_2 \frac{d_h}{U} + \frac{exp(E/RT_f)}{Ap^{n-1} F(\phi)} \right] \tag{6.14}$$

If chemistry alone is rate limiting as it happens near extinction,

$$C_3 \frac{LA}{\rho U A} \sim \frac{exp(E/RT_f)}{Ap^{n-1} F(\phi)} \tag{6.15}$$

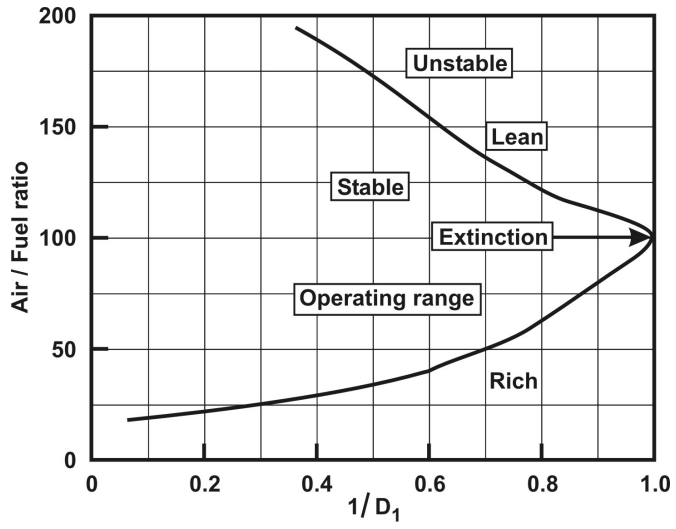

Figure 6.29: The stability plot on A/F vs. Inverse Damkohler number (proportional to the mass flow rate through the combustor)

which can be set as

$$\dot{m} = \mathscr{V} p^n exp(-E/RT_f) F(\phi) \tag{6.16}$$

Note that in the above expression $\mathscr{V}$ = Volume of the Combustor. The equation can also be written as

$$\frac{\dot{m}}{\mathscr{V} p^n} = exp(-E/RT_f) F(\phi) \tag{6.17}$$

The left hand side quantity is called the loading parameter of the combustor.

Earlier arguments have shown that F(ϕ)$exp(-E/RT_f)$ which is proportional to the mean reaction rate ($\overline{\dot{\omega}'''}$) has a maximum at ϕ = 1 and drops on both sides. Figure 6.29 depicts the stability plot of the combustor. The shift in A/F for peak loading is due to the involvement of the dilution air. This is the reason that the bell shaped distribution is shifted from stoichiometry to larger A/F (100 here).

One can now examine the dependence of combustion efficiency, η_b on various parameters. Combustion efficiency is defined as the ratio of the rate of heat release to the expected heat release rate. This can be set out as,

$$\eta_b = \frac{Q\overline{\dot{\omega}'''}\mathscr{V}}{\dot{m} c_p (T_f - T_0)} \tag{6.18}$$

where Q is the heat of combustion. Hence

$$\eta_b = \frac{\overline{\dot{\omega}'''}\mathscr{V}}{\dot{m}\ f}, f = \frac{\dot{m}_f}{\dot{m}_a} \tag{6.19}$$

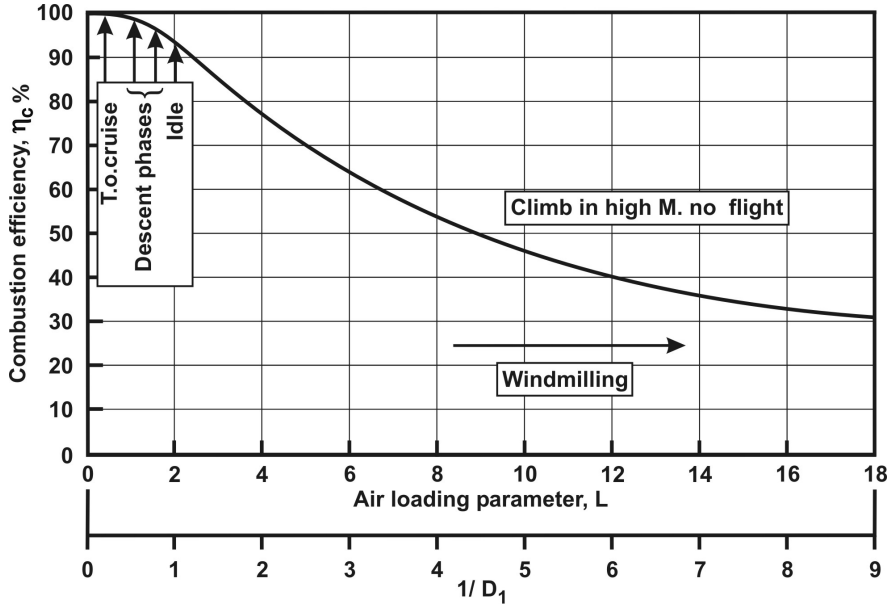

Figure 6.30: Combustion efficiency vs loading parameter and Damkohler number drawn from ref. [3]

Thus, one can expect the combustion efficiency also to scale with the loading parameter $\dot{m}/\mathcal{V}\overline{\dot{\omega}'''}$. This parameter is essentially same as the previous one expecting that p^n is replaced by $\overline{\dot{\omega}'''}$. In usual practice one uses p^n, since, it is not possible to measure reaction rates. Some studies have used the loading parameter as $\dot{m}/p^n T_t$, by dropping the volume from the expression and including the temperature term as the entry stagnation temperature. These variations still preserve the overall behavior since, it is controlled strongly by the flow rate through the combustor.

The data (drawn from ref. [9], see Figure 6.30) show that the efficiency varies with the loading parameter expressed as,

$$L = \dot{m}/[p^{1.8} T_{comb\ inlet}] \tag{6.20}$$

As can be noticed from the figure, the operation of the combustor at varying flight conditions occurs such that the combustion efficiency exceeds 99 % for the most critical operating conditions.

Typical combustion efficiencies go up to 99 % at near sea level operating conditions. At high altitudes it can drop to as much as 30 – 40 %. This used to be the case in the earlier generation engines (1960–1970) when compressor pressure ratio was not too large (up to 15). In recent times, the pressure ratio is as high as 25 – 30 and one expects the reduction in combustion efficiency by no more than 5 –

6 % over the flight envelope. The choice pressure ratio has a significant impact on altitude relighting problems as well. To perform relighting after a flame blow out, one needs to have a high heat release rate to initiate reactions. Partly augmented by an igniter of fairly high energy (2 J) and providing the right mixture ratio near the ignition spark, one expects the flame to catch on. But the heat release rate of the mixture is limited by pressure in the chamber. Higher this is, better is the chance of quick and stable combustion.

An examination of the data from two engines – Olympus 593 (on Concorde) and JT - 9D (similar to CF 6 engine) has been considered instructive. Table 6.6 shows the details of these engines. Some of the details have been obtained from standard sources including reference [3] and Janes All the World Aircraft [29] and others estimated. The results are revealing. The heat release rates are very large – 500 to 800 MW/m^3. This is a consequence of high operating combustor pressures and suitable design of the combustor by limiting the primary and dilution zones. The mass flow parameter at take-off and altitude differs by less than 15 %. This variation is accommodated by suitable changes of the operating corrected speed (rpm/ $\sqrt{T_{stag}/T_{static}}$) of about the same order. The quantity L is the loading parameter in which the choice of combustor inlet temperature in the denominator is based on common use in this form. Its behavior between cruise and take-off conditions merits examination. In the case of Olympus engine, θ is lower at higher altitude and in the case of JT - 9D, the value is higher at cruise conditions. Since the magnitude of this parameter is relative (as used in practice) and it is possible to conceive that the design accounts for the cruise conditions more favorably than others, and the relative difference implies that the system is operating at conditions far into the safe regime of design. It is possible to estimate the residence time as well as process time and hence, the Damkohler number, D_1. These are shown in the Table 6.6. While the estimate of residence time is straight forward, the estimate of process time requires assumptions. It is assumed that the Sauter Mean Diameter is less than 25 μ m so that the droplet vaporization time is about 0.3 ms, mixing time of 0.2 to 0.3 ms (due to differing flow rates between the two operating conditions), and chemical time of 0.8 to 1.2 ms derived from an estimate of the chemical heat release rates of stirred reactor of 2.3 $\times 10^6$ kg/m^3 s at a mean operating pressure of 10 atms. It can be noted that the Damkohler numbers are between 1.5 to 7 and the design of Olympus combustor is more compact compared to JT - 9D system and hence, more critical. Other turbofan engines that are used for short haul aircraft wherein the engine resides for much larger fraction of time in climb and descent compared to cruise, one needs to design the combustor with margins such that the Damkohler number is large at all critical points of flight profile.

Table 6.6: Combustor performance for Olympus and JT 9D engines (The normalized quantities have been calculated with the units for primary quantities shown below)

Parameter	Olympus 593	JT 9 D
Combustor volume, m^3	0.08	0.19
Comp. Pr. ratio	15.5	25.5
Sea level Take-off		
Thrust, kN	167.0	240.0
$\dot{m}_{air}$, kg/s	186.0	118.0 (core)
$\dot{m}_{fuel}$, kg/s	1.5	2.4
$p_{ambient}$, atm	1.01	1.01
$T_{ambient}$, K	288.0	288.0
T_{stag}, K	288.0	288.0
p_{comb}, atm	15.5	25.5
T_{comb}, K	627.0	722.0
Heat release rate, MW/m^3	787.5	530.5
$\dot{m}\sqrt{T_{stag}}/p_{stag}$	3125.2	2502.0
$L = \dot{m}/p_{comb}^{1.8}T_{comb} \times 10^4$	21.5	4.9
t_r, ms	2.5	9.5
t_t, ms	1.4 to 1.6	1.3 - 1.5
D_1	1.6 - 1.8	6.3 - 7.3
Cruise		
Flight altitude, km	16.0	11.0
Flight M	2.0	0.85
$T_{ambient}$, K	216.0	216.0
$p_{ambient}$, atm	0.101	0.226
T_{stag} @ ISA + 5, K	398.0	253.0
p_{stag}, atm	0.79	0.362
$\dot{m}_{air}$, kg/s	105.0	52.0 (core)
$\dot{m}_{fuel}$, kg/s	1.5	0.864
p_{comb}, atm	12.25	9.23
T_{comb}, K	867.0	635.0
$\dot{m}\sqrt{T_{stag}}/p_{stag}$	2651.6	2284.8
$L = \dot{m}/p_{comb}^{1.8}T_{comb}$ x 10^4	13.4	14.9
t_r, ms	2.33	5.1
t_t, ms	1.4 - 1.6	1.4 - 1.6
D_1	1.5 - 1.7	3.2 - 3.7

6.3.4 Emission Performance of Combustors

Emissions of concern are deposits of carbon/soot inside the combustor, unburnt hydrocarbons (UHC), Carbon monoxide (CO), and Oxides of nitrogen (denoted by NO_x, in actuality, a mixture of NO and NO_2 largely). It is useful to understand the mechanism of the generation of these undesirable components. Some of these components are the product of rich zones of combustion, low residence times in high temperature zone, and others, larger residence times in high temperature and oxidizer rich zones. Some are problematic under idling conditions and others problematic at high throughput. Reducing all of them will call for creating conflicting thermochemical environment and in a single combustion system one can look only for a compromise.

Depending on the distribution of air in the combustion chamber and the spray, it is possible that zones of fuel richness could get created. These will generate soot and some unburnt hydrocarbons. If the passage of the gases through the downstream zone quenches the possible oxidation, then the exhaust from the system will carry UHC. Thus, any reduction of UHC needs the consideration of the distribution of air in the primary and the secondary zones. Carbon monoxide is created as an intermediary product in the process of oxidation of carbon. The oxidation of carbon monoxide requires larger residence time in the high temperature zone and the presence of oxygen. Oxides of nitrogen are generated by a mechanism called extended Zeldovich mechanism that involves N, O, N_2, O_2 and OH. NO_x is formed in the presence of oxygen and high temperature with adequate residence time. Thus, conducting slightly rich combustion and raising the temperature and mixing it with air in graded amounts with a short residence time allows reducing NO_x in the combustion chamber. Such a reduction in residence time goes against the possibility of reducing CO. Therefore, one needs to strike a compromise between the emission of CO and NO_x. It is in this endeavour of lowering the emissions that computational tools would be helpful in mapping the fuel rich and lean zones for any given configuration and managing them by altering the configuration and arranging air flow patterns.

6.3.5 Afterburner and Ramjet Combustion System

In the case of gas turbines, afterburners are used to augment the thrust for short durations of time by burning more fuel in the jet pipe before entry to the nozzle. There are two major issues of combustion in the jet pipe, namely, ignition and flame stabilization. These come about for the following reasons. Typical velocities in the jet pipe are about 100 to 150 m/s before fuel is introduced. The length of the jet pipe is typically 1.5–2 m. The residence time in the jet pipe is therefore about 1 to 2 ms. To worsen the problem, the lowering of density due to combustion when it occurs, leads to a fluid residence time of 0.5 to 1 ms. In contrast to the main com-

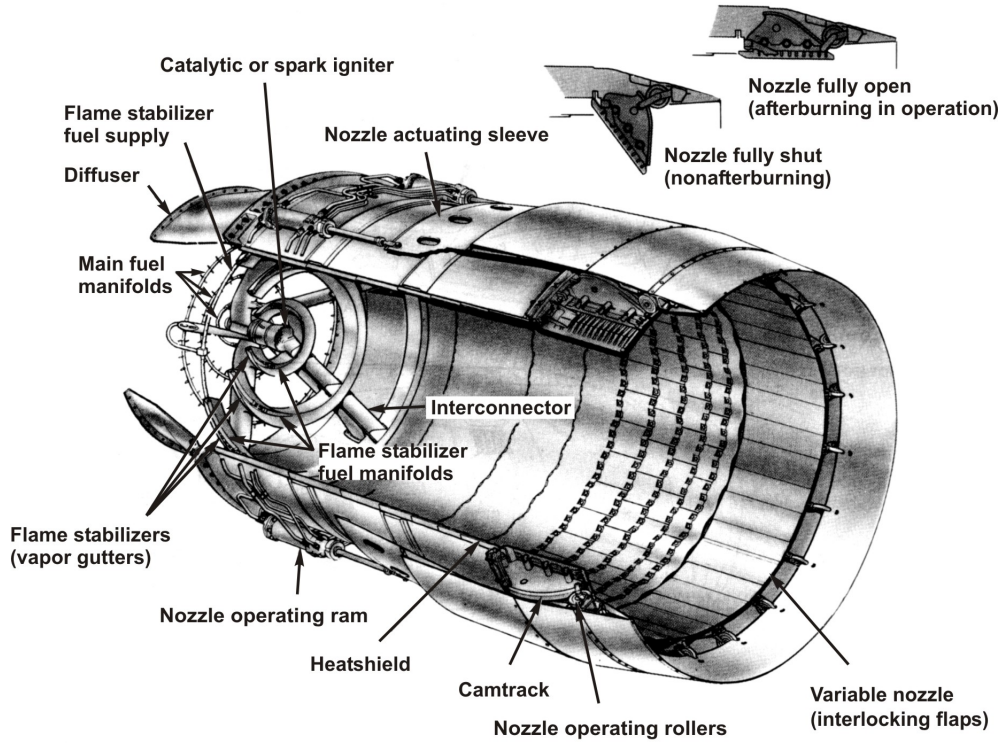

Figure 6.31: Elements of an afterburner, adapted from [6]

bustor, the reactions in the jet pipe occur at much lower pressures, typically 0.5 – 2 atm (the pressure ratio between the jet pipe and ambient is typically 3 to 5). A favorable factor is that the entry temperature of the gas is higher by 100–200 K compared to that at the entry of the main combustor. All in all, the situation is less favorable for the completion of the reactions in comparison to the main combustor of a gas turbine engine. As such the flame will not stabilize inside the high speed stream and auto-ignition of the fuel in the stream is difficult, particularly at higher altitudes when the pressures in the jet pipe could be as low as 0.5 atm. As such, there is a need to provide a scheme for enhancing the residence time without lengthening the chamber and if possible, improve the flame stabilization characteristics. Usually, an additional ignition system has to be provided.

Figure 6.31 shows the sketch of a typical after-burner with all the elements in it. The flame holder is the device to cause the flame stabilization. Its working is depicted in Fig. 6.32. When the flow goes over the flame holder which is a bluff body with the cross section of V or cylinder, there will be separation at the outer edge. The separation causes a recirculation zone. The flow consisting of droplets of fuel and hot air or gas enters this zone. Because of the recirculation

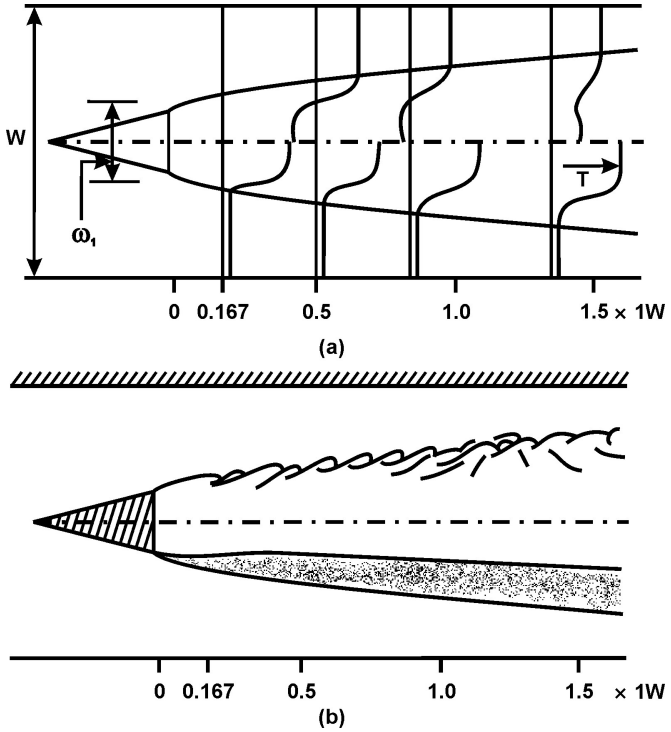

Figure 6.32: The flame stabilization process: The flame holder, the velocity and temperature profiles, and the flame brush; typical growth rate occurs at 5 to 7° to the mean flow direction, adapted from [10]

the residence time increases and hence, reactions of the mixture can indeed get completed with the flame being held in this zone. The flame occurs as a set of thin sheets emanating from the flame holder and any flow that passes through the flame gets combusted and permits the propagation of the flame. Two of the important questions concerning the design are the size of the bluff body (in the shape of a V-gutter as identified in traditional literature) and the gutter spacing inside the combustor. The ability of the gutter to provide stability depends on the size of the recirculation zone. The volume of the recirculation zone (proportional to the cross sectional area of the gutter and length of the recirculation zone) divided by the volumetric flow rate engulfed in the recirculation zone, gives the time of residence. Thus,

$$\tau_r = \bar{\rho} A_\gamma L_\gamma / f_\gamma \dot{m} \tag{6.21}$$

where ρ is the mean density,A_γ is the gutter cross section, $L_\gamma$the recirculation zone, f_γ is the fraction of main stream which is recirculated and $\dot{m}$ is the mass flow rate.

The time taken for reaction is given by

$$\tau_\gamma = \frac{\overline{\rho}}{\overline{\dot{\omega}'''}} = \frac{\overline{\rho}}{Ap^n exp(-E/RT_f)F(\phi)} \tag{6.22}$$

A condition for blow-off is that, τ_r/τ_γ = a critical value.

This relation gives,

$$\frac{\dot{m}}{L_\gamma p^n exp(-E/RT_f)} = CF(\phi) \tag{6.23}$$

L_γ from experiments behaves as D^m where D is the frontal size of the gutter, $m \sim$ 0.5 – 0.85. Thus,

$$\frac{\dot{m}}{D^m p^n exp(-E/RT_f)} = C_3 F(\phi) \tag{6.24}$$

It can be noted that the above relationship is similar to the one for the main combustor, equation 6.17. The angle of flame speed from the gutter is between 5 – 7° for high Reynolds number flows and cannot be changed by most manipulations. Consequently, if the entire cross section of the flow is to be combusted, one needs to provide more than one ring if the length of the jet pipe is to be reduced. Increase in the number of rings increases the pressure drop across the flame holder. Thus, one must design the flame holder such that within the flight envelope, flame is stable but the pressure drop is minimal.

Most after-burners need an ignition device as also the liquid fuel ramjets. This is because the gases coming out of the turbine have a temperature not exceeding 850 K. Auto–ignition calls for a temperature more than 1000 K. In some instances, ignition concepts that are employed are: catalytic ignition using platinum or noble metal inner surfaces or using hydrazine catalyzed combustion. Figure 6.31 indicates both possibilities.

6.3.6 Scramjets

The central problem of the design of supersonic combustor is the achieving of combustion in a short residence time with minimum stagnation pressure loss. While the two aspects – short residence time and minimum stagnation pressure loss are relevant for any combustor, supersonic combustors are special in demanding short residence time since, the combustor would otherwise be too long (or voluminous) with the high speeds of flow. To appreciate the problem in comparison with other combustors, the operating conditions of combustors of aeronautical and aerospace applications are set out in Table 6.7. In this table, solid rockets are not included since, the residence time is usually much larger than reaction time. This is because, the chamber holds the rocket propellant inside with its port that has a

large free volume and the combustion process is limited to a small zone near the propellant surface.

In the case of gas turbine combustors (GT Combustor), the pressure can become low at high altitudes and relatively low compressor pressure ratios. Typically, a pressure ratio of 8 and flight altitude of 10 km implies a combustor pressure of 2 atms. Higher compressor pressure ratio engines will have higher chamber pressures. In the case of a scramjet, the flight will be at high altitudes ($\sim$ 25 to 35 km), and therefore, the atmospheric pressure will be between 0.025 to 0.006 atm and rise in static pressure (when the Mach number of the flow gets reduced from say 6.5 to 2.5) through both external and internal compression processes will be about 0.5 to 1.5 atm. Achieving even this kind of static pressure rise would call for careful design of the forebody and the intake geometry. Achieving as high a static pressure as possible is desirable, since otherwise the volume required for combustion would be larger than allowable. An alternate way of expressing this feature is that as pressures decrease, the reaction rates that vary as the square of static pressure become very small and hence, reactions will not be completed within the combustor. A favorable feature of scramjet combustor compared to other air breathing engine combustors is that the minimum temperature is much higher and this is favorable for faster reaction. The net effect though is that one should aim to keep the static pressures close to 0.5 to 0.7 atm. and temperatures between 1200 to 1500 K.

The static temperature also decides the ease of ignition. At combustor Mach numbers of 2, hydrogen and kerosene need a minimum of 1200 K and 1500 K as static stream temperatures for auto-ignition to occur. For these cases, the fuel temperature is taken at 300 K. With higher fuel temperatures, at least for hydrogen (that is used as a coolant and one can expect it to enter the combustion chamber at 800 to 1000 K), ignition might occur even if the free stream temperature is around 1000 K. In the case of kerosene, it would be difficult to allow fuel temperature to exceed much beyond the boiling point ($\sim$ 500 K) even if it is used as a coolant, since, it has a tendency to pyrolise and produce carbon deposits. New research is to be undertaken to modify the fuel or the fuel passages to ensure that such pyrolisis is not problematic. It is appropriate to note new research being currently undertaken to develop "endothermic" fuels – fuels that decompose into "safe" non-depositing products by absorbing substantial energy in the decomposition process (see section 7.5).

Since the structure of compounds in kerosene is complex with a number of carbon and hydrogen atoms in any given molecule, the reaction process with kerosene is more complex than hydrogen. This is because the number of bonds to be broken or made as the chemical system moves from reactants to products is large. Inevitably, the activation energy (the energy barrier to be crossed along the reaction path) is large and reaction rate will be lower for kerosene – air system

Table 6.7: Comparison of various combustion devices; GT MC = Gas turbine main combustor, AB = Afterburner, RJ = ramjet, LR = Liquid Rocket

Type	GT MC	AB/ RJ	LR	Scramjet
Pressure, atm.	2 – 40	2 – 5	20 – 200	0.5 – 1.5
Temperature, K	500 – 750	600 – 2000	2500 – 3500	1200 – 1500
Mach number	0.2 – 0.4	0.3 – 0.5	0.5 – 0.7	1.5 – 3.5
Mean velocity, m/s	150 – 300	200 – 350	800 – 1000	700 – 1500
Reaction time, ms	0.3 – 1	3 – 4	1 – 2	1 – 1.5
Residence time, ms	3.5 – 5	4 – 5	2 – 3	0.7 – 1.0
Damkohler number	1 – 5	1 – 2	1 – 3	0.5 – 1.0
Pressure loss, %	6 – 8	4 – 5	5 – 20	15 – 25

compared to hydrogen–air system. This leads to higher reaction time and hence, a longer combustor to complete the combustion process. One way of combining the advantages of the ease of ignition and combustion of hydrogen fuel with the high density of kerosene would to use both of them in a manner in which hydrogen gas is injected along with kerosene. This will help better atomization of kerosene and ignition and flame stabilization helped by the presence of hydrogen. Typical residence times for various systems are in the range of 1 to 5 ms, the lowest amongst them being for scramjet. The Damkohler number (the ratio of the residence time to reaction time) is also the lowest for the scramjet. This poses a challenge for the design of the scramjet.

Achieving supersonic combustion has been a research objective for over forty years. In the early sixties many studies were conducted on supersonic combustion, particularly in the USA. Subsequent attention was paid to rocket engine based space vehicles and missiles and hypersonic vehicle development went into background. Again, in the late eighties, the subject was taken up with the ambition of developing a vehicle that flies at M_o of 21 and takes passengers between New York and Tokyo in three-and-a-half hours. This development effort lasted five years and got closed. In the second phase, several research studies were undertaken. One such study by Papamoschou and Roshko [59] revealed that the two-dimensional mixing layer thickness (δ) between two streams flowing parallel to each other as a ratio with its incompressible counterpart (δ_0) decreases with increase of a parameter called convective Mach number (M_c). M_c is the ratio of the difference between the velocity of the two streams and the average acoustic speed of the fluids. Beyond M_c = 0.5, there will be a drop in the ratio, δ/δ_0. This mixing problem was taken as a serious impediment to the development of scramjets. While most studies of the kind discussed above are relevant to mixing layers, in actuality, fuel is injected as jets through fine holes (0.4 to 1 mm dia.) drilled into struts/pylons as objects located inside the combustor much like in a

turbojet afterburner or a ramjet combustor. The essential difference is that one cannot afford to place larger blockages in the flow since, the stagnation pressure loss will be substantial. Hence, one should be careful in extrapolating the mixing problems brought out by mixing layer studies into jet interactions. There are also fundamental considerations that favor early mixing that need greater recognition. Marble and colleagues (1990, 1991) [54] showed that the presence of Baroclinique torque (the vector cross product of density and pressure, $\nabla(1/\rho) \times \nabla p$ term) in the momentum equation implies that if a shock intersects a hydrogen jet flowing into high speed streams, additional vorticity caused at the interface between the fuel and air leads to better mixing (this is because there is a pressure gradient normal to the density gradient). The suggestion arising out of this study is that the fuel jet path can be arranged such as to intersect shocks from surfaces ahead of the fuel injection zone. In a supersonic combustor of any design, it is difficult to avoid shocks bouncing from protuberances or edges in a confined supersonic flow. Therefore, the inevitable conclusion is that mixing related issues would not be a problem since, whatever method one might use to inject the fuel, the fuel jets would invariably intersect the compression waves and mixing will get enhanced. This suggestion and solution are valid for hydrogen as the fuel. For kerosene fuel, after the combustion gets initiated, one can expect to obtain high temperature zones separated from low temperature zones and these will provide the necessary density gradient. When these zones are intersected by shock waves, one can expect the "Marble effect" to take over and create enhanced mixing. Thus, one finds enhanced mixing mechanisms naturally prevalent in the combustor and it appears that no additional loss producing mixing devices other than those used for introducing the fuel need be introduced. Ingenuity lies in the design of fuel injection system to provide enough penetration of jets into the stream so that flame holding and residence time requirements are accounted for with minimal blockage to the main flow.

Typical strut and pylon injection systems are shown in Figure 6.33. The fluid can be introduced axially or into a recirculation zone or in a transverse direction into the main stream as seen in the above figures (see A, B, C in Figure 6.33). If the fluid is introduced from a centrally placed strut axially, there will be no possibility of creating even small recirculation zones for flame holding and hence, mixing issues will be significant. If introduced into the recirculation zone of the backward facing step, there will be low velocity zones and possibility of flame holding. If it is introduced in a transverse direction, there will be a bow shock ahead of the injected stream and the fuel velocity vector has to change from lateral to axial direction. This will enhance the mixing process. There will be inevitable pressure losses.

The issues related to mixing, ignition and combustion should be discussed for hydrogen and kerosene separately. Hydrogen fuel jets are injected at sonic conditions, say axially, typically at 1200 to 1300 m/s. The air stream speed is typically

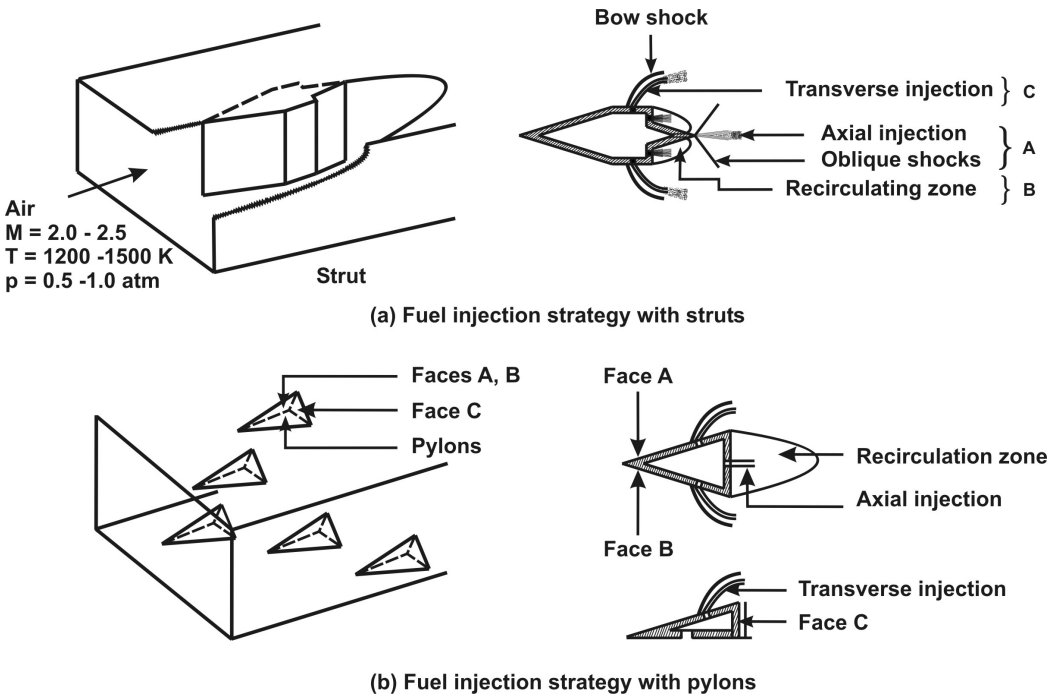

Figure 6.33: Two fuel injection systems for a scramjet - struts and pylons

1400 to 1600 m/s. The difference in speed between the streams is typically 100 to 300 m/s. At the average acoustic speed of 800 m/s, the convective Mach number is 0.2 to 0.4. If the hydrogen stream is injected normal to the stream, a bow shockwave gets located ahead of the jet, and the subsequent dynamics is related to mixing layer behavior in a more complex manner. In the case of liquid kerosene injection, there will be droplet cloud (of 20 to 30 microns size, typically), and questions of the above nature do not apply directly. By the time drop vaporization occurs, the stream speeds would have come down due to slow heat release. Hence, it is not obvious if the reduction in growth rates discussed with reference to planar mixing layers has any serious relevance to the design of scramjet combustors.

In any case, it is desirable to contemplate the strategy for injection to achieve early combustion. One of the key requirements in a hypersonic combustor is to ensure that the coupling between the air intake and the combustor must only be forward; otherwise, there will be breakdown of the flow structure. Transverse injection favors early heat release and axial injection, slow heat release. A combination of both may be required to moderate the heat release in the combustor without creating coupling problems noted above. By a suitable choice of the diameter of injection orifices, their spacing and the ratio of flow between the transverse and axial injection, one can obtain the desired heat release pattern. The com-

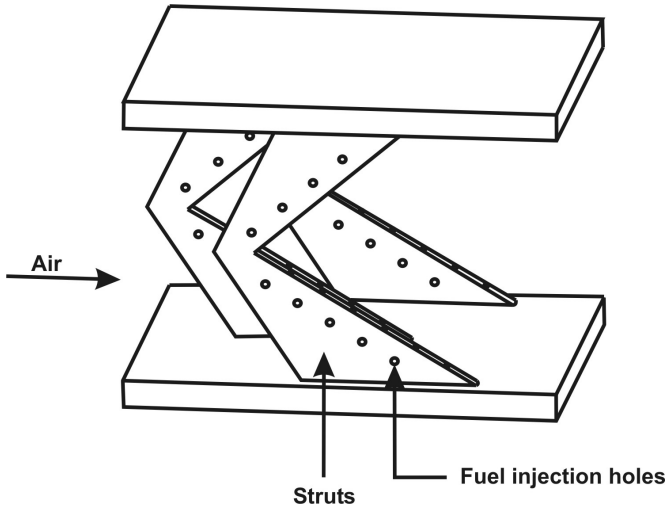

Figure 6.34: The strut injector used in the scram jet tests by Marquardt Company

plex interaction of the flow with reaction and the three-dimensionality imply that meaningful solutions can be obtained only through calibrated reacting flow computational fluid dynamic calculations.

It is also important to recognize that many successful developments of supersonic combustion even with liquid fuels took place even before the issue of mixing got highlighted (see for instance, Payne, [61]). Since one needs to have some device to inject the fuel either gaseous or liquid with the least intrusion unlike subsonic flows, one can use struts or pylons. Use of three-dimensional geometries – like sweptback pylons or struts, and injecting at several axial locations instead of one (as in Figure 6.33 b) and injection from several faces (A, B and C) will help create the desired axial heat release profile so that the inlet-combustor coupling problems will be reduced or eliminated. Further, issues of flame holding are addressed through the choice of the zone just aft of the struts or pylons for creating the necessary flame holding. The work of Marquardt Company (see Figures 6.34 and 6.35) in 1962 – 64 who performed a very valuable study with hydrogen as a fuel on a model combustor that has lessons to be learnt even now. More recent work of Avrashkov et al [46] with kerosene as the fuel, ia another example of successful attempt to obtain supersonic combustion at combustor Mach number of 2. There have been a number of studies on supersonic combustion and they are summarized in Table 6.8.

As can be noted, supersonic combustion has been attempted over a range of flow Mach numbers (1.6 to 3.6), stagnation temperatures (850 to 1811 K), static pressures (0.5 to 1.0 atm.), equivalence ratios up to 1 and the results show a combustor length of less than 0.65 m for hydrogen fueled systems and up to 1 m for

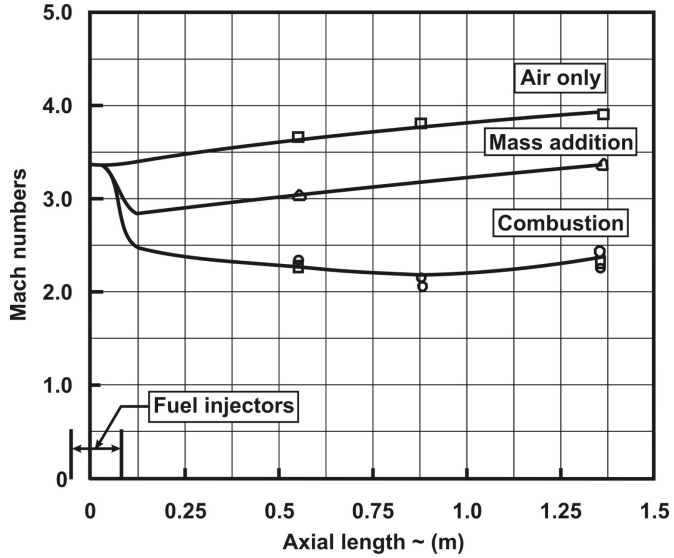

Figure 6.35: The Mach number distribution through a model scramjet tested by Marquardt Company

Table 6.8: A summary of the results of supersonic combustion; the fuel used is gaseous hydrogen in all cases excepting for Yu et al, '01; T_{fu} = Fuel temperature, T_a = Air temperature, sg = stagnation and sa = static, ϕ = fuel equivalence ratio

Author	T_{fu} K	T_a K	M	p_{sa} atm	$\dot{m}_a$,$\dot{m}_f$ kg/s	ϕ	L m
Marquardt [37]	550	1280	3.6	0.8	6, 0.15	0.90	0.80
Kanda et al [53]	150	1550 (sg)			6, 0.14	0.94	
Mitani et al [56]	280	1550 (sg)	2.0	0.6	4.8, 0.14	1.00	0.30
Gruenig et al [51]	150	760 (sa)	2.1	1.0	0.33, 0.003	0.34	0.65
Owens et al [58]	-	850 (sg)	1.6			0.71	
Tomioka et al [67]	300	1550 (sg)	2.5	0.5		0.90	0.60
Yu et al [68]	300	1811	2.5	1.0	1.5	0.78	1.00

kerosene fueled combustors.

Combustors of Integral ram rockets

Integral ram rockets are those in which the volume occupied by the booster propellant is used as the combustion chamber for the ramjet (see Figure 1.21). The combustor inner wall will usually be hot $\sim$ 2500 K at the time when the rocket stops functioning. In some integral ram rockets the fuel used is another fuel rich solid propellant. This propellant is ignited just about the time the booster stops functioning. The gases from the fuel rich propellant exit out of holes set into the plate covering the propellant container at Mach number of unity or more. The air coming from side ducts impinge on the hot jet (see Figure 1.21) and mixing and combustion processes begin from this zone. Because the air is hot (450–500 K) and the fuel rich hot gases are at 1600–1700 K, the combustion process will start without any need for separate ignition. The configuration produces a recirculation zone near the wall, just after the air entry region. Experiments on model combustors do not indicate that this plays a major role in the stability of the flame. In such cases where the 'fuel' and 'oxidizer' are reasonably hot and well prepared, the total time for combustion is essentially limited by the time for mixing. Mixing studies indicate that the combustor length provided is usually adequate for mixing to be complete (because in many such situations, the booster volume is significantly large in comparison to the demands of the ramjet).

Most other arguments on combustion follow the principles outlined above.

6.3.7 Summary

The discussion presented above is largely on the principles involved in the design of combustors for air breathing engines including gas turbines, ramjets and scramjets. All these use liquid fuels largely kerosene. The key issue in the design relates to ensuring adequate residence time for the processes of atomization, vaporization and combustion to occur. Of these processes, the rate limiting process is the vaporization. To help this happen in as short a duration of time as possible, drop atomization should occur to a fine degree. Attainment of high temperatures in the combustion zone causes higher emissions of nitric oxides. Reduction of oxides of nitrogen can be achieved by reducing the residence time. This reduction causes enhancement of emissions of carbon monoxide because the oxidation of carbon monoxide is a very slow process. Thus, managing low emissions with high combustion efficiency under the most critical operating condition calls for a careful design of the fluid flow path in the combustor. Coupled with this, are the facts that the flow is turbulent and has zones of recirculation. It is in this effort that computational techniques offer a powerful solution to the design of the combustion system.

In the early sixties and seventies, most of the design and development took place when the computational techniques were rudimentary. It is, therefore, correct to recognize that most successful early developments took place because of ingenuity and extensive testing. The mathematical modeling of these complex flow situations has attained some degree of maturity only in recent times and therefore, the design process has changed in the last fifteen years. The use of computational reactive fluid dynamic tools has reduced both the cycle time of design and cost. The principal direction taken is to calibrate the computational tools against extensive experimental data obtained carefully in test rigs, in addition to some long term overall data from operations. Once the calculation tool is calibrated, new designs are performed using this tool. Sensitivity studies are performed and critically examined for their veracity. The hardware is then produced against these designs and tested. Any changes in observations are used to correct the model features in the code for computations suitably. Refinements made in this way while being sensitive to the complex effects of reactive fluid flows has paid rich dividends to engine manufacturers. Conception-to-realization times have been cut by a factor of three over the last two decades. One can now realize the engine from conception in 18 to 24 months. This has been possible only because of the advances in computational tools apart from other advances in materials and manufacturing.

6.4 Turbines

Turbines are designed so that compressor power demand is firstly taken care of. The excess energy/power is used in various forms. In a turbojet, the pressure in the jet pipe generates thrust when the hot gas passes through the nozzle. Hence, in this case it is advantageous to maintain as high jet pipe pressure as possible (consistent with the need of the compressor) In a turboprop, the aim would be to expand the gas through another turbine stage to generate power that can be used by the propeller. Since this energy conversion process contributes to higher propulsive efficiency, it is the preferred route. In a turbofan, one has options. In military turbofans with low bypass ratio (typically less than 1), with significant need for excess afterburner thrust, the combined airflow from the fan and the core engine (as is the usual arrangement) passes through the nozzle to generate the thrust. In this case, the demand on the system between the afterburner thrust and no-afterburner thrust will decide the turbine expansion that is required as a part of the power that goes to drive the fan. In turbofans that aim to meet civil transport requirements with primary consideration for fuel efficiency, the energy in the hot gas is best used by expanding the gas through the turbine that can drive the fan that contributes to higher propulsive efficiency and consequent fuel efficiency. The above considerations can be used to understand the number of stages that are used in any given gas turbine engine as discussed below.

6.4.1 Turbine vs Compressor

Turbine differs from compressor in several ways.

(a) Turbine deals with a flow that has favorable pressure gradient (pressure decreases along the flow path) in contrast to a compressor (where pressure increases along the flow path). The dreaded flow separation that affects the design of a compressor is of much less concern in the case of turbine. This is not to discount the flow related issues in a turbine. The steep favorable pressure gradient sought to be imposed on the flow for better performance can cause reverse transition towards laminar condition to an extent that a fair segment of the flow could be in the transition regime. This is considered undesirable since the flow could be sensitive to disturbances in this regime and the final behavior becomes difficult to predict.

(b) The flow behavior is taken advantage of by allowing for larger pressure drops across each turbine stage compared to a compressor stage. Typically, one can go to sonic conditions by providing for the lowest cross section at the rotor trailing edge. Thus, one axial turbine can go up to a pressure ratio of 2 and in some instances up to 2.5 whereas an axial compressor stage may permit pressure ratios of only about 1.25 to 1.3 (in a multistage system). When pressure ratio higher than 2 across the turbine (like say, 3) is to be dealt with, one has to use

two stages. Thus, to achieve the same pressure ratio, in a turbine, one needs between one-quarter to one-half the number of compressor stages. In the design of a gas turbine for one has a conflict of choice – two to three stages of an axial system or a single centrifugal system. This conflict becomes much less in the case of turbine stages. Since one can use a single axial stage for much larger pressure ratio, axial turbines become a more favored arrangement in most applications. This is illustrated in Table 6.9 where, amongst others, the choice and the number of stages of turbine for a large number of existing engines is listed. As can be noted from the table, excepting the first two systems (Mamba and Lucas CT - 3201) all others use axial stages for the turbine.

(c) One needs to account for tip clearance flows in a compressor. These issues now become magnified in a turbine stage since the pressure ratios through a turbine stage are larger and consequently, the pressure difference between the pressure and suction side of the turbine blade. To overcome this problem, most turbines use shrouded blades.

(d) Turbines need to operate with high temperature gas. Small turbines restricted the TIT to about 1200 K. Larger engines have been designed for operations at 1600 K. In recent years, TIT has gone up to 1900 K (even though no commercial engines are operating at this level). Engines with TIT larger than 1200 K work with cooled blades. The demand on cooling requirements will become severe as operating temperatures are larger. The cooling air has to be put back into the stream. This is done through several holes, but principally through the trailing edge region. This leads to thicker trailing edges and hence the turbine blades show up generally thicker than the uncooled turbine blades or compressor blades.

(e) The fact that turbine blades have to (i) maintain structural integrity while working at high temperatures for large durations of time, (ii) experience thermal transients during the engine startup and shutdown and (iii) maintain small tip clearances during the engine operation over the load range with thermal creep that imposes serious demands on the choice of the geometric design, the choice of the material, and the fabrication procedures. On all these fronts significant developments have taken place over the last twenty years.

Table 6.9 shows the details of the nature of turbines and the number of stages along with other relevant parameters for various engines. We can examine the data of the engines and determine if the choice of the number of stages is appropriate.

For this purpose, we rewrite equation (5.120) to express the turbine temperature ratio ($\tau_t = T_{t5}/T_{t4}$), in terms of compressor temperature ratio (τ_c), and turbine inlet temperature (θ_b) for the case of efficiencies less than 100 %, then we get,

Table 6.9: Nature of Compressors and Turbines used on various engines; 1F = One fan; 5A = five axial stages; 1C = one centrifugal stage; f, c = fan, core engine; 1 s = 1 spool or shaft; 1R = One stage radial; Fr = Free turbine

Name	Compressor Axial/C	π_c	$\dot{m}_a$ f,c (kg/s)	α	Turbine
Mamba	1C	2.8	-, 2.0	-	1R
Lucas CT-3201	1C	3.5	-, 0.9	-	1R
TRS-18-046	1C			-	1A
TRI-60	8A	4.0	-, 5.6	-	1A
RR Viper 601	8A	5.8	-, 26.5	-	2A
J3-IHI-7C	8A	4.5	-, 25.4	-	1A
J85-21	8A	8.3		-	2A
J79-7A	17A	12.9	-, 76.5	-	3A
ATAR-SNECMA 50	9A	6.2	-, 70.7	-	2A
SNECMA-M53	3F+5A	8.5	22, 63	0.35	2A
RB199 - 34R-2	3F +3A + 6A	20.0	37, 33	1.1	1A + 2A
Adour Mk. 102	2F + 5A	11.0	19, 25	0.76	1A + 1A
Pegasus 11	3F + 8A	14.0	81.7	1.4	2A + 2A
P&W F 100	3F + 10A	23.0		0.6	2A + 2A
GE F 404	3F + 7A	25.0	16, 47	0.34	1A + 1A
Allison 250-C-20B	6A+1C	7.2	-, 1.6	-	2A + 2Fr
Ivchenko AI-25	3F+8A	8.0		2.0	1A + 2A
Astazou XIV	2A		-, 2.5	-	3A
Lycoming LTC1-L13	5A+1C	7.4	-, 4.85	-	4A
Lycoming LTC4-L7B	7A+1C	8.2	-, 12.25	-	1A + 2Fr
Garret TFE.731-3	1F+4A+1C	14.6	39, 14	2.8	1A + 3A
Garret ATF3-6	1F+5A+1C	21.0	54, 19	2.8	1A + 3A + 2A
Turbo meca Baston	2A+1C	6.7	5.9	-	3A
RR Dart	2C	5.6	10.7	-	2A
P&W JT-15D	1F+1A+1C	10.0	26, 8	3.3	1A + 2A
Olympus 593	14A	15.5	186.0	-	1A + 1A
Soloviev-D20P	3F + 8A	13.0	56,56	1.0	1A + 2A
P&W JT 8D	2F+6A+7A	18.0	133, 80	1.68	1A + 3A
P&W JT 9D	1F+3A+11A	24.0	568, 116	4.9	2A + 4A
CFM 56	1F+2A + 9A	25.0	322, 54	6.0	1A + 4A
Soloviev D-30kU	4F+10A	17.4	191, 78	2.42	2A + 4A
GE CF6-50M	1F+16A	31.4	533, 121	4.4	2A + 4A
RB-211; 524B	1F+7A+6A	25.0	536, 122	4.4	1A + 1A + 3A
GE 90-76B	1F+3A + 10A	40.0	1225, 136	9.0	2A + 6A

Table 6.10: Turbine features of turbojet and turbofan engines (π_c = Compressor pressure ratio, θ_b = Normalized turbine inlet temperature, $1\pi_t$ = Turbine pressure ratio, St+ty = No. stages and type, A = Axial)

Engine	π_c	π_f	α	θ_b	$1/\pi_t$	Turbine St+ty	Jet pipe pr, atm.
TRI - 60	3.90	-	-	3.55	2.05	1A	1.70
Atar 9K 50	6.15	-	-	4.20	2.29	2A	2.68
J - 85 - 21	8.30	-	-	4.10	3.00	2A	2.75
J - 79 - 7A	12.40	-	-	3.22	7.35	3A	1.68
Olympus 593	15.5	-	-	5.41	3.26	2A	4.75
JT 9D 70A	24.0	1.60	4.90	5.41	13,8	2A + 4A	1.74
CF 6 50M	32.4	1.56	4.40	5.41	13.1	2A + 4A	2.44
Soleviev D 30	20	2.40	2.42	4.84	16.5	2A + 4A	1.21
GE 90	40	1.53	9.0	5.73	38.5	2A + 6A	1.05

$$\tau_t = 1 - \frac{\theta_o}{\theta_b \eta_c \eta_t}[(\tau_c - 1) + \alpha(\tau_f - 1)] \tag{6.25}$$

For a choice of parameters obtained from actual engines (from Tables 1.4, 1.5 and 1.6), and a choice of efficiencies η_c = 0.85, and η_t = 0.9, the above equation has been used to obtain the turbine pressure ratio ($1/\pi_t$ = p_{t4}/p_{t5}). These are presented in Table 6.10. Using the rule of thumb noted in item (b) of section 6.4.1, the number of stages for the turbine can be predicted. These match completely with the actual choice as seen in Table 6.9.

6.4.2 Degree of Reaction (R), Stage Loading (ψ) and Efficiency (η_t)

Just as in the case of compressors, turbines can be designed with a certain degree of reaction - 0 reaction, implying 100 % impulse operation, or a certain degree of reaction. In a multi-stage system, one can design different stages with different degrees of reaction. The choice of the degree of reaction affects the number of stages required to expand over a certain pressure ratio with the exit flow with a certain amount of swirl. The degree of reaction is the ratio of the static enthalpy drop across the rotor (Δh_r) to the sum of the drops across the stator (Δh_s) and the rotor expressed as

$$R = \Delta h_r / (\Delta h_s + \Delta h_r) \tag{6.26}$$

It can also be expressed as the ratio of the kinetic energy drop across the rotor to the sum of the drops across the stator and the rotor. Thus, if all the enthalpy

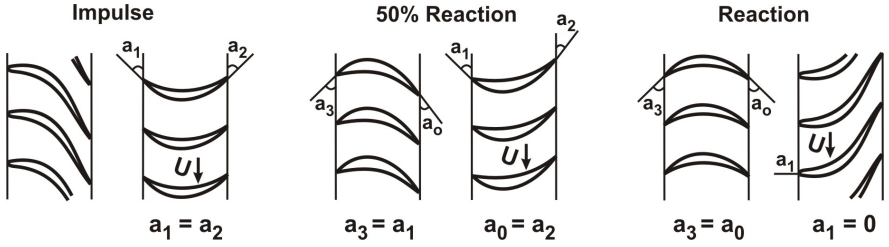

Figure 6.36: Turbine stator and rotor blade profiles for different degrees of reaction adapted from ref. [4]

drop occurs across the stator implying that the velocity change occurs across the stator, the degree of reaction, R = 0. This is an impulse turbine. The stator is also called the nozzle since all the expansion takes place in this segment. An additional requirement for the stator is to change the velocity vector so that momentum of the fluid is transferred to the rotor assembly. Since the pressure and velocity do not change in the rotor, the shape of the rotor is like a hemispherical bucket (classically used like this in high-head hydraulic turbines – Pelton wheel). Equally well, if R = 1, the stator would look like a bucket and all the expansion and enthalpy absorption occurs in the rotor. Given the fact that any rotating blade has different velocity of rotation at the hub and the tip, the angle of attack at which the flow will enter the blade will vary with the blade height. If the blade height is small compared to the mean radius of the rotating blade, one can expect the variation over the blade height to be small. However, if the blades are "long" (by the above definition), the blades will need to be given a twist to maintain the same conditions over the blade height. Alternately, the blade twist can be used as a parameter to control the degree of reaction. Figure 6.36 shows the blade cross sections for the stator and rotor combination for 0, 50 and 100 % reaction. As can be noted that the stator blade for 0 % reaction is the similar to the rotor blade for 100 % reaction. In both cases, all the enthalpy drop occurs only through them.

Stage loading (ψ) is the ratio of the enthalpy drop across the rotor, ΔH_r to the square of the turbine speed (U).

$$\psi = \frac{\Delta H_r}{U^2} \tag{6.27}$$

Its implication is that if it is larger, the enthalpy absorbed during expansion is higher or the pressure ratio across the rotor is higher for a fixed turbine speed. It is almost directly related to the pressure differential between the pressure and suction side of the blade. Large stage loading implies that the number of stages for a given pressure ratio will be smaller. This has implications on the degree of reaction as will be discussed now.

Figure 6.37 shows the velocity vector diagrams for 0 and 50 % reaction stages.

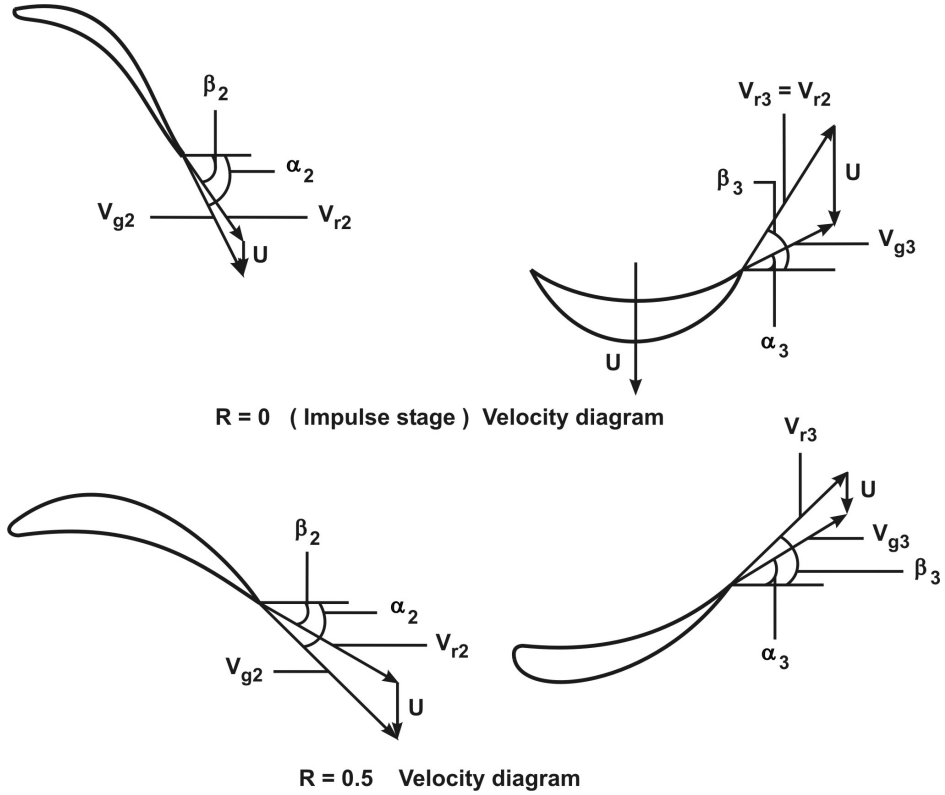

Figure 6.37: Velocity diagrams for 0 and 50 % reaction blading adapted from ref. [7]

Here, V_{g2} and V_{g3} refer to absolute velocities of the gas at the outlet of the stator and outlet of the rotor. The inlet to the rotor is taken the same as the outlet of the stator, and any difference between the two accounted for as losses. U is the mean speed of the rotor and V_{r2} and V_{r3} refer to the velocity of the gas with respect to the rotor. As the velocity diagrams indicate, the vector sum of the relative velocity and the velocity of the rotor gives the absolute velocity. The angles α_2 and α_3 refer to the angles between the absolute velocity vector and the rotational axis. Similarly, β_2 and β_3 refer to the angles between the relative velocity vector and the rotational axis. $V_{g2}sin\alpha_2$ and $V_{g3}sin\alpha_3$ refer to the tangential velocity of the gas at the entry and the exit of the rotor. The power of the turbine is given by

$$P = \dot{m}U[V_{g2}sin\alpha_2 - V_{g3}sin\alpha_3] \tag{6.28}$$

In the above equation, the change in the tangential velocity of the gas as it passes through the turbine multiplied by flow rate is the tangential momentum imparted to the rotor. This is the torque applied by the fluid on the rotor. Hence, power is the torque multiplied by the rotor speed. The turbine work per unit mass is also

Table 6.11: Typical Flow coefficient Φ_f, Stage loading coefficient ψ, and efficiencies

Φ_f	ψ	Leakage, %	Efficiency, %
0.6	1.0 – 1.5	2 – 5	94 – 90
0.8	1.5 – 2.0	1 – 3	92 – 88
1.0	1.5 – 3.0	1 – 3	90 – 86

expressed as the power per unit flow rate $P/\dot{m}$ and can also be expressed as the enthalpy drop across the stage. Using constant specific heat approximation, this can be written as

$$\text{Work per unit mass} = \mathrm{c_p}(\mathrm{T_{t2}} - \mathrm{T_{t3}}) = \mathrm{U}[\mathrm{V_{g2}sin}\alpha_2 - \mathrm{V_{g3}sin}\alpha_3] \tag{6.29}$$

The stage loading ψ is defined as the work per unit mass divided by the square of the rotor speed. This will reduce to,

$$\psi = \frac{[V_{g2}sin\alpha_2 - V_{g3}sin\alpha_3]}{U} \tag{6.30}$$

Now we consider the velocity diagram for R = 0. Since all the enthalpy drop occurs across the stator (or nozzle), and no change in enthalpy occurs across the rotor, the rotor blade simply changes the direction of the velocity vector without any change in magnitude. If the axial velocity is maintained constant through the stage, then, β_2 = - β_3. From a further analysis of the velocity diagrams, one can get

$$\psi = 2[\Phi_f \, tan\alpha_2 - 1] \tag{6.31}$$

In the equation 6.31, Φ_f is the ratio of axial gas velocity to the rotor speed defined as $\Phi_f = V_{axial}/U$ and is also called the flow coefficient. If we wish to maximize the energy absorbed per stage, one has to increase the nozzle exit angle α. Increased α leads to large absolute and relative velocities in the stage. This will imply larger fluid dynamic losses. Compromise between demand for higher stage loading and limiting the losses has led in practice to the choice of α_2 of about 70°. The exhaust angle also is large implying large swirl. For a fixed mass flow, greater swirl implies larger frictional loss. Demanding larger ψ for larger Φ_f implies larger losses and hence the reduction in efficiency. The efficiency discussed here is the same as discussed in section 4.11. Typical values of the expected performance are presented in Table 6.11.

In the above table, the list of parameters includes leakage as well. The running clearance between the rotor tip and the outer casing is typically 1 – 5 % of the blade span. And every percent clearance implies a loss in turbine efficiency of 1.5 %. Shrouding the turbine blade and designing for minimum clearances

by excellence in engineering are the methods to reduce this loss. It is generally true to state that achieving higher adiabatic efficiency in turbine is simpler than in compressor where the flow physics is the more unfavorable. However, getting good efficiencies from turbine is also controlled by a good mechanical design and a choice of materials with little creep.

If it is insisted that the exit velocity be axial, as may be desired of the first stage in a multi-stage turbine, one can use the velocity triangles to relate the stage loading to the degree of reaction as $\psi = 2(1 - R)$. From this equation, it is clear that an impulse stage ($R = 0$) has twice the loading of a 50 % reaction stage. *Use of impulse stage helps reducing the number of stages and hence the weight of the engine*. And if it is required that the exit velocity have little swirl, one would need to use a 50 % reaction blade with exit angle arranged to have the exit velocity aligned to axial direction.

Turbine designs in the earlier era (like JT 3D) had a loading coefficient of 1.44 in the low pressure stages, the engines in a later era (like JT 9D) were designed with a loading coefficient of 2.47. The last value can be estimated from equation 6.31 using α_2 = 70° and Φ_f = 0.89. This condition implies a significant swirl at the exit. One can manage this condition by providing a stator-anti-swirler at the exit of the turbine stage.

6.4.3 Pressure Distribution Over the Blade

Figure 6.38 shows the variation of the static pressure over one of the blades in a cascade. The variation over the pressure surface is denoted by p and the variation over the suction surface is denoted by s. The value of the Mach number presented in the figure is the mean exit flow Mach number. In the curves denoted by p, one can see a dip and recovery. This is due to the large acceleration of the flow over the curved surface at the leading edge and its sharp deceleration. While for the case of exit Mach number of 0.7, the flow is subsonic everywhere, the flow has a long curved Mach line (M = 1 line) when the pressure ratio across the stage increases beyond the choking condition. For pressure ratios larger than this, the flow distribution remains the same. If the geometry in the aft end of the turbine is designed with increasing area, supersonic flow can result, like the cases M = 1.2 and 1.4 indicated in Fig. 6.38. In these cases, one has shocks proceeding from the trailing edge as shown. These shocks impinge on the suction surface leading to a pressure rise and hence an adverse pressure gradient. The boundary layer over the suction surface will be subject to this pressure gradient. Depending on the intensity of interaction coupled with the three-dimensional flow (discussed below), one might have separation bubbles. The difference in pressure between the pressure and suction side exerts a force on the blade. One would expect to design the system so that such flow structures occupy minimal volume, if at all.

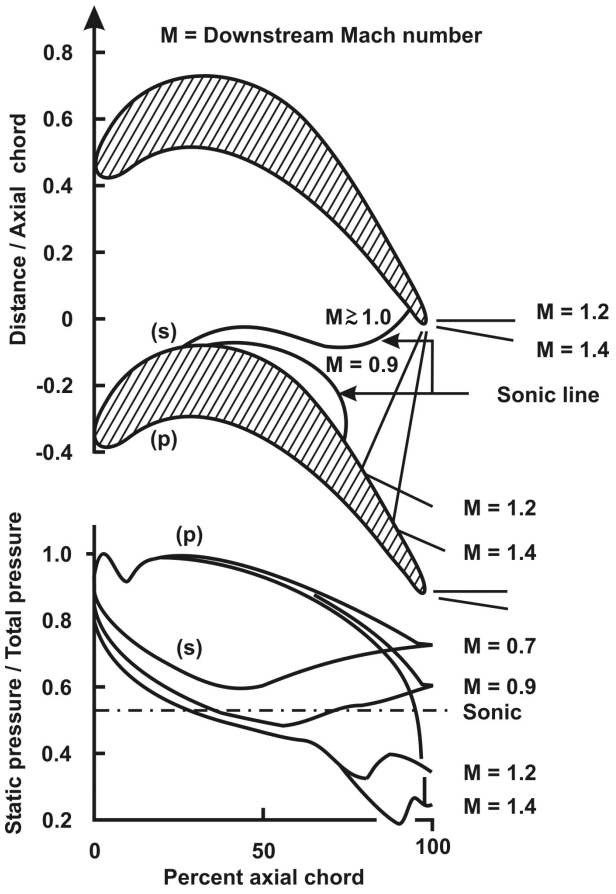

Figure 6.38: A typical turbine blade and static pressure distribution at different flow conditions. (p) refers to pessure surface and (s) refers to suction surface. Adapted from ref. [10]

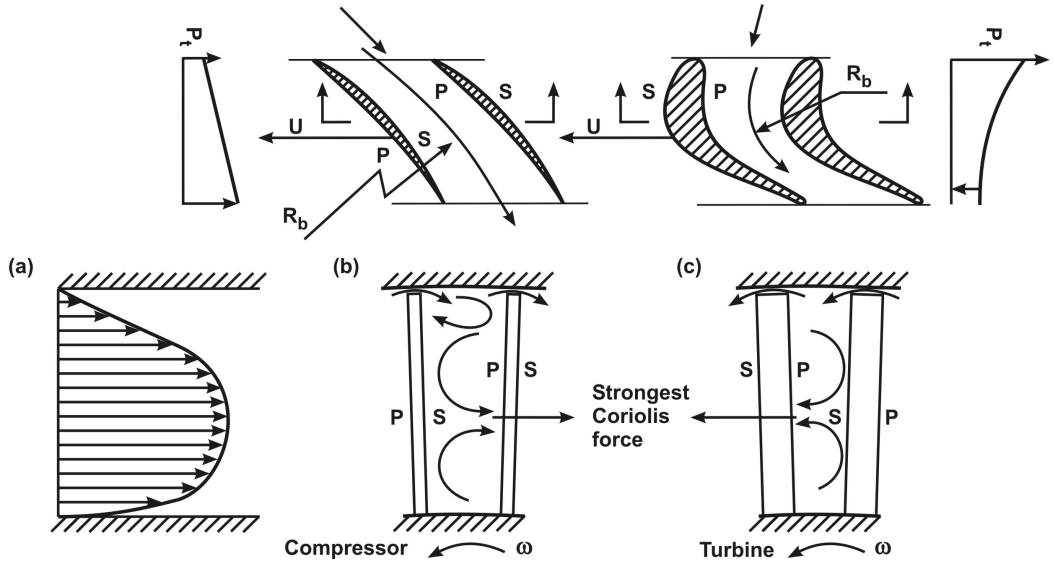

Figure 6.39: Viscous flow and secondary flows through compressor and turbine blades adapted from ref. [4]

The component of the force in the tangential direction (and largely, it will be in this direction) is the one responsible for sustaining the rotor torque.

6.4.4 Three-Dimensional Viscous Flow Effects

It must be recognized that the discussion presented so far does not explicitly bring out the viscous effects that affect the turbine flow behavior. In fact, it is somewhat loosely thought that viscous effects are very vital for compressors and inviscid approach is adequate for assessing the turbine flow behavior. This thinking process may be adequate when the expectations from turbine performance are modest, something true in the early designs. But after initial development, it was clear that bettering the performance of each component of a gas turbine adds to the performance and if something could be done to the turbine, it better be done. From this view point, taking into account three dimensional features that are also influenced strongly by viscous effects in confined flows was thought important.

Figure 6.39 shows the aspects connected with viscous flows. For the benefit of understanding, both compressor and turbine blades are shown side-by-side. In the figures, P and S refer to pressure and suction side. While in the case of compressor it is the blades that exert forces on the fluid, in the case of turbine, it is the flow that exerts pressure forces on the blades. The stagnation pressure increases through the blade for the compressor and it decreases in the case of turbine. The

inflow velocity profile that emerges from the stator into the rotor will have a broad peaky profile as shown on the left side. This effect and the pressure variation along the flow influence the secondary flow structure through the blade. Since the fluid turns around due to curved blade passages, the fluid will experience a Coriolis force of $2\ V_{axial}^2/R_l$, where R_l is the local radius from the axis of rotation. Since axial velocity is the largest around the mid-span, Coriolis forces are the largest around this zone. These create flow structures as shown in the figure. In addition, there are leakage flows across the blade tips due to the pressure difference between the pressure and suction side, a problem that is more serious for a turbine in comparison to compressor because of the relative value of pressures. It is precisely to avoid this problem that one uses *shrouded blades* in the case of turbine.

To add to these issues, there will be variations over the blade height, particularly in cases where the hub-to-tip radius ratio is small. Inevitably, there will be twist provided to the blade. Thus, the flow structure due to the combined effects will be complex and only computational fluid dynamic tools with appropriate physics put into the equations can hope to unravel the flow behavior. While computing the flows may by itself be accomplished without any serious problem, the issues of modeling are serious with the reverse transition that may occur with a turbulent flow subject to sharp favorable pressure gradient on the pressure side of the blade (see Fig. 6.38) or complex flows in the regions of shock boundary layer interaction or the secondary flows with disparate scales of variation compared to the main stream flow.

6.4.5 Turbine Cooling

It was brought out earlier that turbines handle gases at temperatures between 1200 to 1700 K. While the flows with lower temperature range can be handled without cooling, high performance turbines built in the last thirty years have had to use cooling to make the turbines survive the hostile thermal and mechanical environment. Figure 6.40 shows the schematic of the details of the cooling arrangements as well as the gas sealing arrangement. The hot air drawn from an appropriate stage of the compressor is passed through the stator and the rotor with suitable connections to plenums created for this purpose. Air will move from the central zone through the rotor holes and air from the top region will flow over the inner casing. In the un-shrouded design, turbine blades are provided with a recessed region so that relatively non-critical edges may occasionally rub against the casing. Several internal cooling techniques, like convection, impingement, film, and transpiration are adopted usually in combination of two/three of the techniques. For instance, in the leading edge zone, the flow may pass through a passage and exit at the top zone. In the middle zones, the cooling air may make a two pass before exiting through side holes. Towards the trailing edge, the flow may

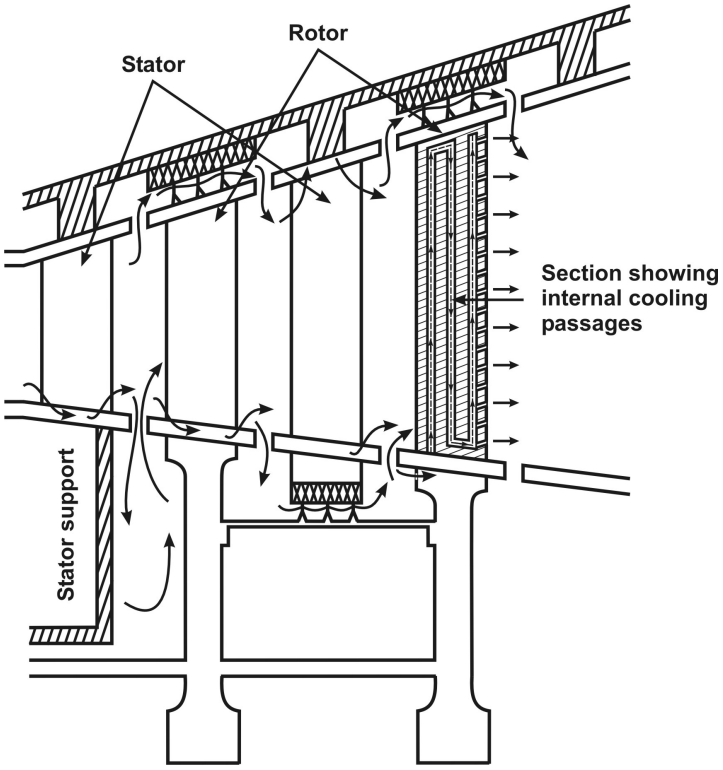

Figure 6.40: Schematic arrangement for turbine cooling and sealing, adapted from ref. [10]

impinge on the surfaces before exiting through the trailing edge itself (as shown in Figure 6.40). The internal cooling heat transfer processes involve both free and forced convection regimes.

6.4.6 Choice of Geometric Features

Like in the case of a compressor (see section 6.2.2), the geometric parameters that matter are thickness of the blade, t, chord, c, spacing, s, height, h and twist of the blade. One of issues concerns the hub-to-tip radius ratio that can also be reflected as the blade height-to-mean radius ratio, h/r_m. In high pressure turbine stages, h/r_m is small, typically 0.15. Any further decrease will imply substantive tip clearance and end wall frictional losses. These short blades can be designed without a twist and mean flow calculations are generally adequate for the design.

For the low pressure stages, h/r_m can be as large as 0.35. For such blades, there is a requirement for providing twist to the blade to ensure correct angle of attack over the height of the blade and smooth flow. Increase in h/r_m beyond the

above value is related to the degree of reaction for which the stage is designed. If the stage is designed for 50 % reaction at the mean, the hub may experience a condition of negative reaction – that is, the flow that has been expanded in the stator/nozzle will get re-compressed in a part of the rotor, thus reducing the performance in a manner totally unintended for the function of turbine.

The blade thickness-to-chord ratio (t/c) is larger than for compressors as already discussed – the need to accommodate internal cooling demand in turbine blades. Typical values are 0.15 to 0.25 (whereas for compressors it is 0.1 to 0.15).

The limits on spacing-to-chord ratio, s/c are caused by the following considerations. Small spacing implies larger fluid-to-surface contact with inevitable frictional losses. Larger spacing implies demand of higher loading on each of the blades with inevitable flow related issues – reverse transition on the pressure surface and shock-boundary layer transition related separation issues on the suction side. Between these considerations, an optimum is between s/c = 0.4 to 0.6 for impulse blades and 0.9 to 1.0 for reaction blades. The smaller spacing for the impulse stage is dictated by the need to limit the loading on each blade.

Finally, the h/c of high pressure blades is typically from 1 – 3 for high pressure stages and 3 – 6 for low pressure stages.

The precise values are chosen in an iterative detailed design that includes structural analysis as well. In a typical structural analysis of the blade as well as the disc supporting the blade, centrifugal stresses are primordial. Bending stresses are also caused by the force on the blade due to pressure difference between the pressure and suction side. Even though centrifugal stresses are much larger than the bending stresses, the importance of bending stresses to the rigidity at the root is about the same. In addition, the thermal stresses caused by the differences in temperature over the blade matter. To minimize the thermal stresses, it is important to keep the temperature differences as small as possible. It is for this reason that the specification of temperature traverse quality factor (TTQF) is imposed on the combustion chamber design.

6.4.7 Turbine Performance

As in the case of the compressor, the stagnation pressure ratio across the turbine can be related to the non-dimensional mass flow rate and the non-dimensional speed since both of these can be controlled independently (it is only the solution to the matching problem between the compressor and the turbine that couples them). Like in the case of compressor, one uses corrected parameters for the mass flow rate as $\dot{m}\sqrt{T_{t4}}/p_{t4}$ (note that the non-dimensional mass flow parameter is $\dot{m}\sqrt{R_g T_{t4}}/p_{04}A_t$ where R_g = Gas constant, subscript $t4$ refer to the turbine inlet condition and A_t is the flow cross section of the turbine) and for speed as $N/\sqrt{T_{t4}}$

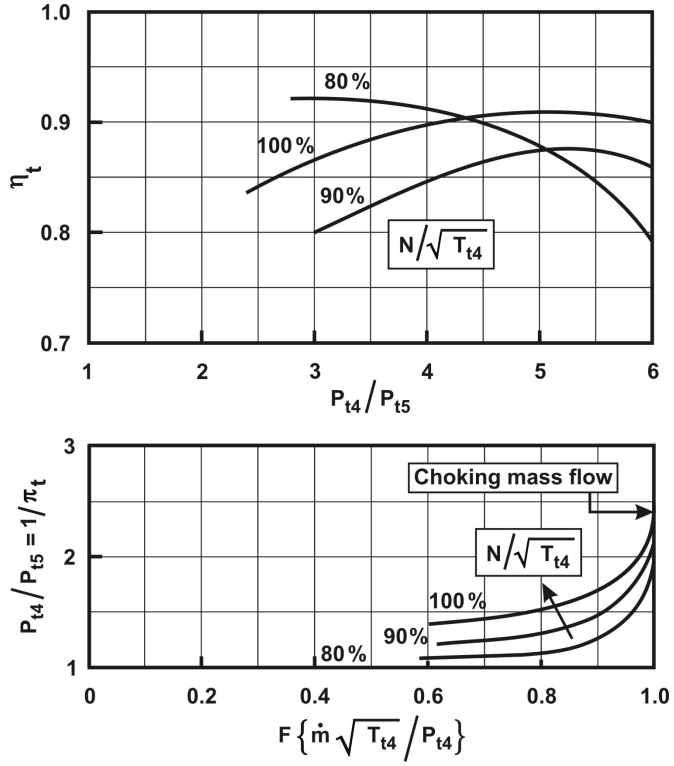

Figure 6.41: Typical pressure ratio and efficiency vs corrected mass flow rate and speed plot for an axial turbine

(note that the non-dimensional speed parameter is $ND/\sqrt{R_g T_{t4}}$) along with pressure ratio to present the performance of the turbine. Figure 6.41 shows the performance of the turbine in terms of the pressure ratio and efficiency as a function of corrected speed and mass flow rate. One can see that as the speed increases, the pressure ratio increases for a fixed mass flow rate and the mass flow parameter reaches a limit due to choking condition being reached. Another plot also includes efficiencies with rpm and mass flow. The degradation of efficiency for off-design speeds is clear from the figure.

6.4.8 Compressor-Turbine Matching

The essence of compressor-turbine matching is to find a speed at which the turbine will run delivering power to the compressor and permit excess power in the form of adequate jet pressure for expansion through the nozzle or additional turbine stages from which power can be derived to run a propeller or helicopter rotor. The step-by-step procedure outlined in section 5.2.6 can be used along with compressor

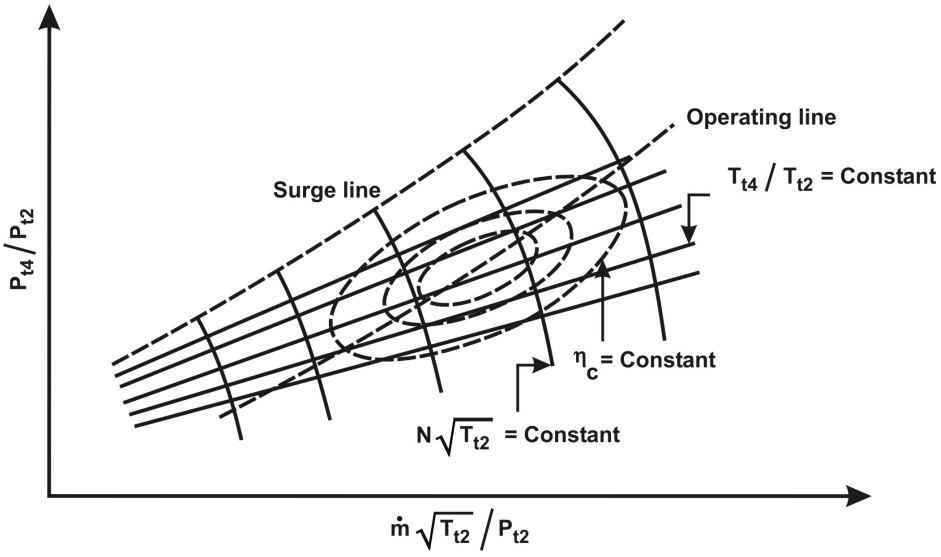

Figure 6.42: The operating line of a gas turbine on a compressor map

and turbine performance maps outlined in Figures 6.17 or 6.22 (for radial or axial compressors) and 6.41 to connect the data of pressure ratio and mass flow rate with the speed of the compressor-turbine assembly. In the case of multi-spool machine, the equations outlined in section 5.2.6 have to be set out sequentially for each of the spools along with air bleed from any appropriate stage from which it takes place.

After assuming a rotational speed and a condition of operation (say for take-off), one assumes the pressure ratio of the compressor and obtains the mass flow rate from the compressor map. These data are used to obtain the pressure drop required of the turbine. It is then verified if the turbine characteristics allow the flow rate through it at the appropriate pressure drop. If not, a choice of a new pressure ratio is made and an iteration process of calculation is made to obtain a steady operating point. Further on, the hot gas has to pass through a nozzle to produce the thrust. If the exit nozzle area is fixed, then one can calculate the thrust that is obtained from this system. The final result is an operating line on a compressor map of the kind depicted in Figure 6.42.

6.4.9 Summary

This section on turbines has brought out many features of aircraft gas turbines. It is first brought out that radial turbines are used in very small machines and the more common power extraction device is an axial turbine. Turbines differ from

compressors in several ways, principal amongst them are that they handle high temperature fluid and the flow is expanding. Mechanical and structural design are intimately related to aerodynamic design. High centrifugal stresses, coupled with thermal stresses and bending stresses can sometimes dictate the choice of geometric parameters like blade height, hub radius and degree of twist. Amongst all the components of a gas turbine engine, turbine usually has the least life (see Table 2.6) as it is the most stressed part. It is precisely for this reason, the idea of modularity has gained value in the manufacture, operation and economy of operation (allowing change of individual elements with different life cycles, but retaining other elements as they are).

6.5 Gas Turbine Nozzles

The elements of a gas turbine engine preceding the nozzles, namely, the intake, compressor, combustor and turbine constitute what is known by the term "gas generator". The implication is that these elements in combination generate high pressure hot gas that remains to be utilized for power/thrust generation. When it comes to power generation, the gas passes through a few more stator-rotor stages for the extraction of rotary power. When the intent is to generate thrust, the gas passes through a nozzle. Nozzles for aircraft engines are characterized by the fact they may have variable area and when they have convergent-divergent construction, the area ratio is not usually more than 1.5 as distinct from those for rocket engines where area ratios vary from 5 to 150. The primary reason for this condition is that the jet pipe stagnation pressure is relatively low - typically not exceeding 4 atm, where as the nozzle entry stagnation pressure in the case of rocket engines is 20 to 200 atm.

Aircraft engine nozzles can be convergent (C), variable convergent or CD with variable geometry, the variation in geometry being used to thrust vectoring as well. Civil aircraft engines are also equipped with thrust reversers to reduce the landing run. Hence, the variety in designs is large and the issues of design are related to mechanical construction that minimizes leakages and keeps the thermal environment in a manner that promotes long life. Table 6.12 indicates the nature of the nozzles used on various engines - civil and military. High bypass ratio turbofans that are used in civil aircraft applications extract all the power into the fan and hence, the thrust generated by the nozzle is not primary. It would suffice if a convergent nozzle is adopted. Only military turbojets and low bypass ratio turbofans with afterburner, have a reasonably large jet pipe pressure and benefit by using convergent-divergent nozzles. They also are variable area type and are operated in an asymmetric mode to obtain thrust vectoring. These have been adopted in RD 41 and Soyuz R - 79 engines. Figure 6.43 shows the schematic of a variable area convergent nozzle. The nozzle is constructed of petals put together

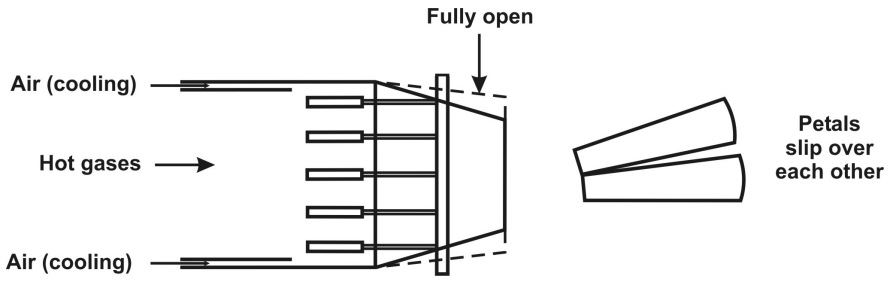

Figure 6.43: A variable area convergent nozzle adapted from [10, 11]

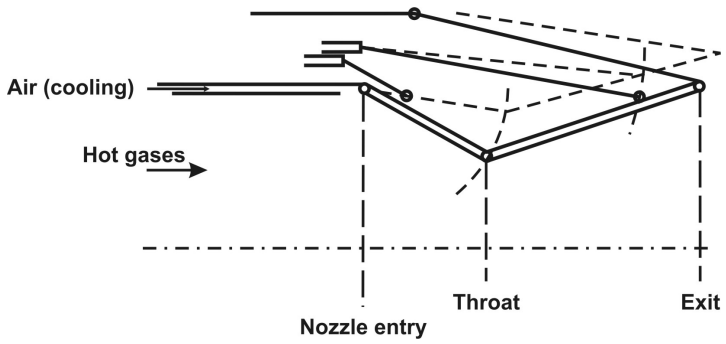

Figure 6.44: A variable area convergent-divergent nozzle adapted from [10, 11]

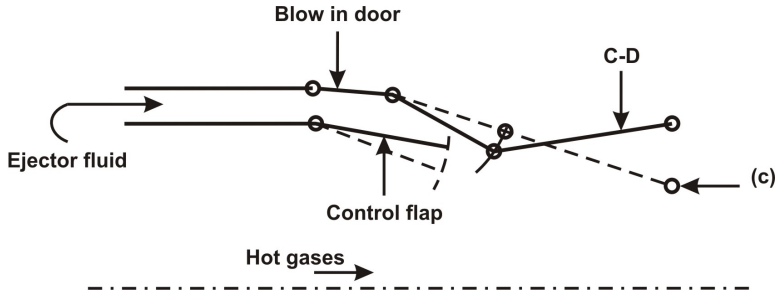

Figure 6.45: Convergent/convergent-divergent ejector nozzle

in manner that they slide past each other to the extent required. They are connected to a hydraulic actuator, the command to which will open the petals to the extent required. This construction is used in afterburning turbojets / low bypass turbofans used in military applications. The schematic of a convergent-divergent nozzle is shown in Figure 6.44. Here again, flaps/petals for the convergent and the divergent are constructed and controlled in a manner that the control command is converted into articulated movements for the given geometry. In both of the above cases, a fraction of the air bled from one of the stages of the compressor is allowed to pass along the wall and also close to the nozzle surfaces to permit film cooling. There will be leaks from the system into the outer regions at several joints. There could be leaks into the system at below nominal operating conditions since the jet pipe pressure will be below the nominal value and under some conditions, the flow separation that may occur in the divergent section might hamper thrust generation seriously. To overcome such problems, it would be useful to include a blow-in door ahead of the nozzle so flow could be inducted from outside and prevent flow separation problems. Figure 6.45 shows the ejector type CD nozzle in which the cooling air could be substantive and use of a control flap along with the controls on the CD nozzle could generate a convergent nozzle, with blow-in door open when

Table 6.12: Nozzle types on various aircraft jet engines (C = Convergent; CD = Convergent - Divergent; Ejctr = Ejector nozzle, AB = Afterburner, F. A = Fixed Area, V. = Variable)

Engine	Type	AB?	F. A?	Thrust reverser / vectoring
CFM 56	C	No	Yes	No
Ivchenko A120 DM	C	No	Yes	No
Ivchenko AI 25	C	No	Yes	No
Soloveiv D 30	C	No	Yes	No
P &W F 100	CD	Yes	V.	No
GE 100 F 101	CD	Yes	V.	No
P & W F 119	2D-CD	No	V.	No
P & W JTF 10 A	Ejctr	Yes	V.	No
Kuznetsov NK 144	CD	Yes	V.	No
Adour Mk 102	CD	Yes	V.	No
CF 6 80C2	CD	Yes	V.	Reverser (Side + clam shell)
P & W JT 3D	C	No	Yes	Reverser
Garrett TFE 731	C	No	Yes	Fan Reverser
RB 199	C	Yes	V.	Reverser (Clam shell)
Pegasus 11	C	No	Yes	Vectoring 0 - 90$\circ$
Soyuz R 79	CD	Yes	V.	Vectoring 0 - 95°
RD 41	C	Yes	V.	Vectoring by $\pm$ 12.5°

necessary and enhance the mixing inside the nozzle could add to the performance (by 1 to 2 %).

Figure 6.46 shows the thrust reverser used in civil aircraft. Two clam shaped shell structures are held with struts and the flow passes through the nozzle. In the Figure 6.46 (a), the engine is shown in normal thrust mode. The Figure 6.46 (b) shows the reverser in position. The gases go out through the louvers indicated in the figure and reverse thrust is generated. Figure 6.47 (a) and (b) show the thrust reverser elements on a JT-3D engine with the deployment of elements for both forward and reverse thrust conditions depicted in the figure. As is clear, the flows from the core jet as well as the fan, are used to generate the reverse thrust. In some engines like RB 211, only bypass flow (that is large) is used in reverse thrust mode.

The flow streams in turbofans used in military aircraft from the hot core and the surrounding bypass air stream are mixed before they pass through the nozzle. Figure 6.49 shows a typical mixing device used on such exhaust systems. The convoluted surface around the circumference provides large surface area that allows

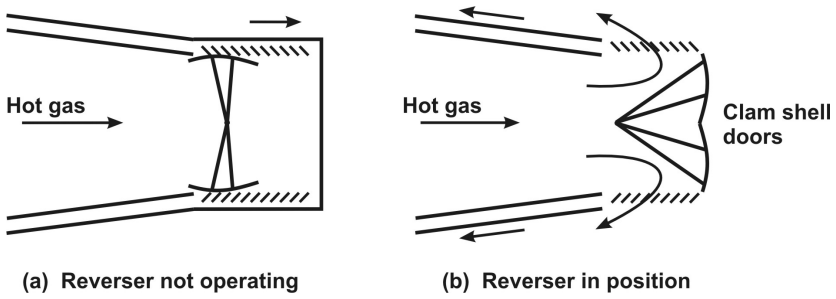

Figure 6.46: Clam-shell based thrust reverser

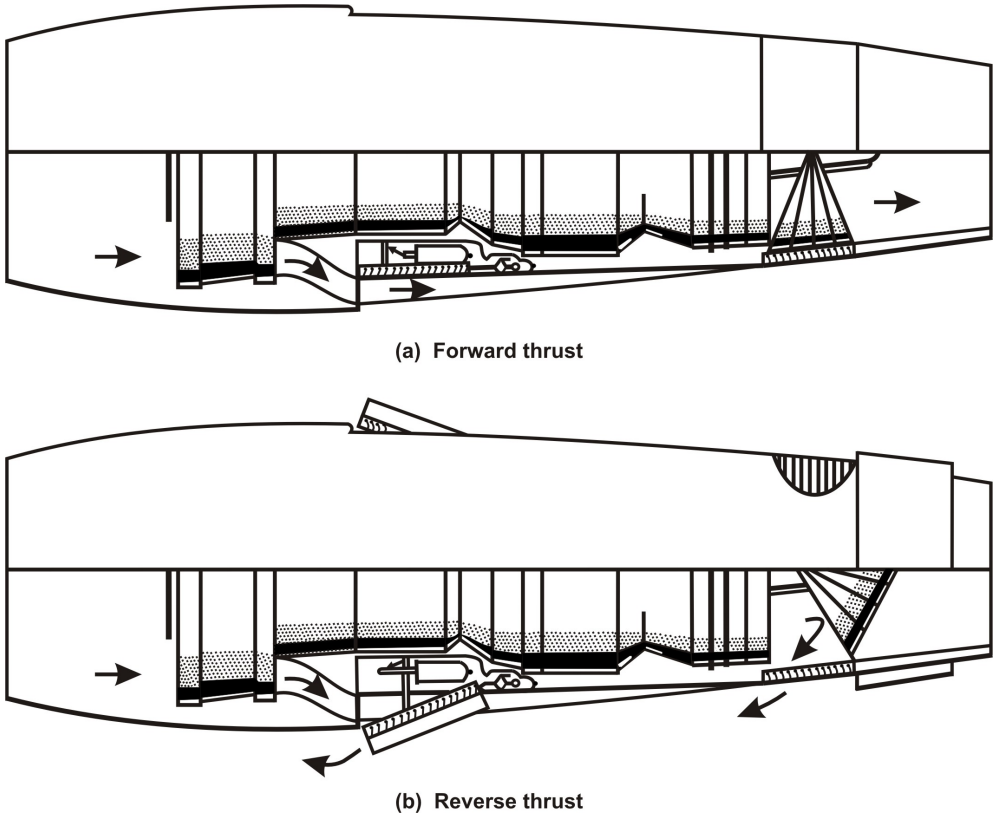

Figure 6.47: The elements of thrust reverser in a turbofan engine (JT-3D, here), adapted from ref.[6]

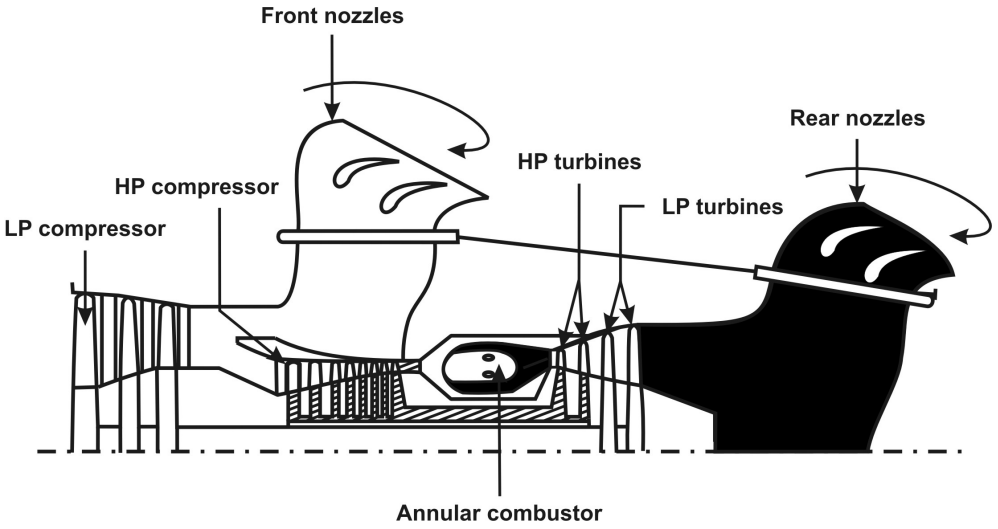

Figure 6.48: Thrust vectoring in Pegasus engine, adapted from ref.[2]

the generation of stream-wise vortices between the outer cold flow and the inner hot flow. Such a device called hyper-mixer provides very high mixing rate and mixing is completed in a short distance and it provides better propulsive efficiency in the case of turbofans (two jets - the core hot jet and the outer cold jet going out of the nozzle unmixed provide lesser mean exit momentum flux compared to the mixed jet out of the nozzle).

In some aircraft like F-117 stealth fighter and B2 stealth bomber, the design has to preserve features of stealth apart from other considerations. In such cases, one needs to reduce the thermal signatures of the engine exhaust. This is achieved by mixing the exhaust with ambient air in a very short distance by using a two-dimensional analog of hyper-mixers of the kind discussed above. In such aircraft, hyper-mixing is followed by an approach in which the jet flows over an extended surface - the trailing edge region of the wing to prevent access of hotter parts of the jet pipe and the engine to ground tracking.

6.6 Materials for Various Parts of an Aircraft Engine

Table 6.13 shows the materials used for various components of a gas turbine engine. The list is not complete and newer materials are continuously being introduced at component levels to enhance the properties and life. All these take place since failures that may occur after millons of hours of operation are used to incorporate new materials where needed. The table is self-explanatory.

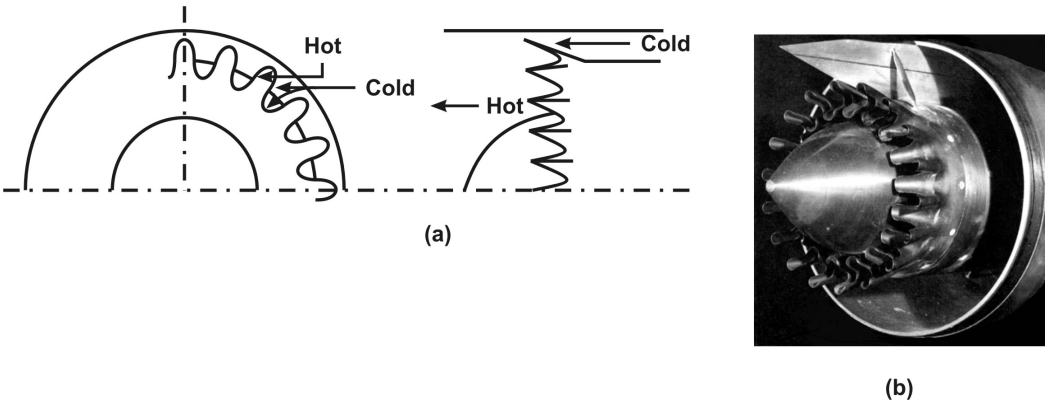

Figure 6.49: Hyper-mixers used to mix the hot core flow with the colder fan flow to improve the efficiency and reduce the thermal signature of the exhaust

Table 6.13: Nature of materials used in different components of various engines

Name	Fan/Compressor	Combustor	Turbine
J79-7A	403SS/321SS	Hastealloy	V57/A 286
Turbomeca Baston	Ti/Al. alloy	-	-
Lycoming LTC1-L13	SS blade Al. alloy disc	-	-
P&W JT-15D	Ti	SS outer, Ni. Alloy tube	-
P&W JT 9D	Ti. alloy/Ti		-
GE CF6-50M	Ti	Hastealloy liner HS 18-8 flame tube	X -40, Rene 80 -
RB 211	Ti Alloy/Ti	Nimonic, Ni. Alloy	-

Chapter 7

Fuels and Propellants

7.1 Thermodynamic Requirements

In the case of air breathing engines – piston engines, gas turbine engines, ramjets and scramjets, the oxidizer is atmospheric air. For flights outside the atmosphere, one has to carry the oxidizer and the fuel along with the vehicle and hence, one has a choice. The choice of fuels for air-breathing and rocket engines is also wide. The choice is made to optimize the performance requirements. For air-breathing engines, the fuel chosen should reduce the cost of payload transportation without hurting the environment. This is mandatory for civil transportation. The cost of payload transportation is directly linked to the cost of fuel energy, a fuel of high energy that has remained cheap for the last seventy years of air transportation (even though the cost of fuel has been rising over this period due to many factors including geopolitical considerations) is the one derived from petroleum sources. Aviation gasoline (Avgas) for reciprocating engines and aviation kerosene for turbine engines (ATF – Aviation Turbine Fuel) have become the standard fuels for use. Low compression ratio reciprocating engines can accept high octane rated petroleum derivatives and gasoline qualifies for this purpose. Several other properties that dictate the choice of the aviation fuel are discussed subsequently. In so far as energy is concerned, gasoline, kerosene or diesel and other derivatives have a calorific value that decreases by 5 % with the increase in density by 20 % all around 42 MJ/kg. Because the difference between the two extreme fuels is in the C:H ratio, gasolines have higher calorific value compared to diesels.

In so far as rocket engines are concerned, one has to make a choice of the fuel and the oxidizer. Key features that decide the choice of the fuel/oxidizer combination would be the specific impulse and density impulse. Others, like cost are important when it concerns large boosters, but not so for missile systems.

7.2 Operational Requirements

Aircrafts based on turbine engines fly at high Mach numbers and also at high altitudes. When flights occur at medium speeds, but high altitudes, the fuel in the tank equilibrates to low temperatures and could experience enhanced viscosity causing difficulties for the flow and in the extreme, lead to freezing. Many a time, water gets into the fuel in very small amounts and could cause difficulties in operation. For flights at high Mach numbers, the fuel tank could experience high heat load and this can lead to evaporation of some fluid that could further lead to vapor lock.

7.3 Fuels for Piston Engines, Gas Turbines, and Ramjets

Table 7.1 provides the details of the properties of some classical fuels for aircraft engines. It is to be recognized that kerosene is a mixture of aliphatic (straight chain) and aromatic (ring structured) compounds produced from the distillation of petroleum crude, and it is possible to control the mixture to obtain a minimum of freezing point and a certain boiling range. Thus, obtaining various "cuts", it is possible to meet the needs for different applications. In the development of fuels, JP - 1 was developed in the early stages and is now outdated; JP - 2 was an experimental fuel; JP - 3 was wide range fuel available extensively. Its excessive vapor loss at altitudes prevented its use.

The currently popular compositions are JP - 4 and JP - 8 used for select military and civil aircrafts respectively. RP - 1 is a close "cut" fraction used for rocket engines. JP - 7 is a fuel under development for new applications involving hypersonic vehicles. With regard to diesel, there are recent developments for reciprocating engines primarily to enhance the efficiency by using compression ignition engines with higher compression ratio. Many properties shown in the table are internally consistent. Avgas and JP - 4 have lighter fractions and consequently have low flash points in comparison to fuels boiling at higher temperature. They also have lower viscosity compared to other fuels. The calorific value of the fuels is between 42.7 to 44.2 MJ/kg with lighter fuels having better calorific value.

Combusting the fuels for higher efficiency is less of an issue compared to limiting the emissions. Lower H/C ratio noticed in JP - 8 class fuels implies that emissions could be higher compared to JP - 4 class. By the same token, if an aircraft engine is adopted for ground power generation application that can use natural gas instead of a kerosene, the emission performance can be expected to be far superior.

Table 7.1: Properties of some standard fuels (μ = viscosity in CP = CentiPoise, RCE = Reciprocating engines, Mil. = Military, HE = Hypersonic engines, Spl = Special)

Property	Avgas	JP - 4	JP - 7	JP - 5	JP - 8	RP - 1	Diesel
Aromatics, % v	33	10	3	19	18	3	20
Naphthenes, % v	15	29	32	34	20	58	40
Paraffins, % v	52	59	65	45	60	39	38
Olefins, % v	-	2	-	2			
Sulphur, % total	0.05	0.03	0.006	0.05	0.05	0.002	0.3
H/C, molar	1.98	2.00	2.07	1.92	1.91	1.98	1.89
Distillation range							
Initial BP, °C	55	60	180	187	165	176	202
50 %, °C	97	156	197	210	190	195	277
End point, °C	162	241	250	257	265	273	358
Density, kg/m^3	700	777	808	810	795	810	857
Freezing Pt, °C	- 50	- 50	- 50	- 40	-40	- 40	- 23
Flash Pt, °C	-29	-25	25	63	52	56	65
Cal. value, MJ/kg	44.2	43.6	43.9	43.2	43.2	43.5	42.7
μ, CP (15°C)	0.5	0.7	1.7	1.8	1.4	1.9	2.0
Application	RCE	Mil	HE	Navy	Civil	Rocket	Spl

Hydrogen has been tried as a fuel for aircraft engines – B 57 bomber aircraft ran one of the two engines on hydrogen and Tupolev 154 aircraft ran one of the three engines on hydrogen and therefore, it is appropriate to conclude that it is possible to operate a hydrogen fueled aircraft. However, safety issues in operating fleets of aircraft out of busy airports remain to be addressed. There are other issues of producing hydrogen at affordable costs that make hydrogen fuel as a future fuel for aircraft.

7.4 Equilibrium Performance

A key aspect of assessing the performance of propulsion systems is the determination of the properties of combustion of fuel-oxidizer mixtures and in some cases, single compounds containing fuel-oxidizer elements (like nitrocellulose or nitroglycerine or a combination) or simply in an unstable thermodynamic state (for example, monopropellants like hydrazine as a liquid) that they can decompose exothermically into products. This problem, simply stated is: given the initial reactants (fuel + oxidizer) and the initial temperature, to determine the adiabatic flame temperature and the equilibrium composition at a fixed pressure or at constant volume. The former case approximates the combustion process of gas turbine and rocket engines whereas the latter approximates the combustion in a recipro-

cating engine. In a gas turbine engine main combustion chamber, the fuel-air ratio is very lean. In such a case, the maximum temperatures achieved are such that no dissociation of products will occur. The principal products will be CO_2 and H_2O apart from N_2 that is an inert. One can compute the final temperature quite simply by equating the initial total enthalpy (consisting of sensible and chemical enthalpies) to the final enthalpy of the products at the final temperature. With the increase in fuel-air ratio, the final temperature will cross 2000 K (as will happen for the afterburner of a gas turbine or a ramjet), effects of dissociation will become important. Many compounds will not remain in the most stable form - H_2 will decompose to H, O_2 to O, other reactions will lead to the formation of the hydroxyl radical (OH), carbon monoxide (CO), and oxides of nitrogen like NO, and NO_2. These are valid for a C-H-N-O system. If other elements like Cl, Al and Mg are involved, several other compounds get generated. One will need to determine their composition as the adiabatic flame temperature is closely linked to the composition. Thus, for rocket engines - solid or liquid - having not been limited to C-H-N-O elements, one can choose more reactive chemicals as one usually will and the peak temperatures that will be achieved will be between 2500 - 3600 K. At these temperatures, there will be significant formation of compounds noted above.

Calculation of composition and adiabatic flame temperature can be conceived to be carried out in two steps. The first step is to calculate the composition of a given set of reactants at a fixed pressure and at any selected temperature. For this purpose what matters is the count of elements. For instance, (H_2 + O_2/2) or H_2O both have (2 H + 1 O) atoms and are *identical* for computing the composition of a reactive mixture at say, 3000 K. There will be formation of H, O and OH as additional species whose mole fraction needs to be determined along with those of H_2, O_2, H_2O. This is done by invoking two principal features - elemental balance and equilibrium reactive condition. Of the six mole fractions that need to be determined, two elements - H and O need to be preserved no matter in which form they exhibit themselves - as some OH, or H_2O. Thus, two relations relate to element balance (same as mass balance). The remaining four relations relate to equilibrium reaction statements and thermodynamic consistency. These lead to a minimum independent set. In the present case of H_2 + O_2 reactions, they could consist of $H_2 \leftrightarrow 2H$, $O_2 \leftrightarrow 2O$, $H_2 + O_2 \leftrightarrow OH$, and $2H_2$ + $O_2 \leftrightarrow 2H_2O$. One can derive from chemical thermodynamics, an expression $K_p(T) = {p_H}^2/p_{H_2}$ for the first reaction and similar expressions for others. In these expressions, the left hand side is known from the basic thermochemical data of the individual compounds/elements. Typical data for several gas phase reactions are presented in Table 7.2. These are shown only for select H_2 - O_2 reactions.

If we take note of the definition of various equilibrium constants and the values indicated in Table 7.2, we can infer several useful results. At 300 K, the values of all the constants are very small excepting $K_{p,4}$. In these cases, it can be inferred that the denominator is much larger than the numerator. Since the de-

Table 7.2: Equilibrium constants for several reactions - $K_{p,1} = p_O/p_{O_2}^{1/2}$, $K_{p,2} = p_H/p_{H_2}^{1/2}$, $K_{p,3} = p_{OH}/p_{H_2}^{1/2}p_{O_2}^{1/2}$, $K_{p,4} = p_{H_2O}/p_{H_2}p_{O_2}^{1/2}$, $K_{p,5} = p_N/p_{N_2}^{1/2}$, E-41 = $\times 10^{-41}$

T, K	$K_{p,1}$	$K_{p,2}$	$K_{p,3}$	$K_{p,4}$	$K_{p,5}$
300	9.01E-41	4.25E-36	3.13E-07	6.12E+39	4.65E-60
500	1.71E-29	7.00E-21	2.70E-04	7.69E+22	4.33E-35
1000	1.90E-10	2.27E-09	4.13E-02	1.15E+10	2.87E-16
1500	4.60E-06	1.76E-05	2.13E-01	5.25E+05	5.94E-10
2000	7.33E-04	1.62E-03	0.477	3390.0	8.85E-07
2500	0.00155	0.00251	0.767	161.0	7.21E-05
3000	0.120	0.158	1.048	20.10	1.35E-03
3500	0.518	0.590	1.305	4.930	0.0113
4000	1.553	1.593	1.531	1.662	0.0554
4500	3.652	3.460	1.732	0.703	0.1913
5000	7.240	6.451	1.907	0.355	0.5187

nominator contains partial pressures of stable species, the inference is that very little dissociation to atomic species or radicals takes place at low temperatures. As temperature increases, the values of equilibrium constants increase. This shows that the possibility of dissociation is higher at higher temperatures. In the case of $K_{p,4} = p_{H_2O}/p_{H_2}p_{O_2}^{1/2}$, the numerator is more stable product that would result from the reaction between the species indicated in the denominator. Hence, one would expect that the equilibrium favors the presence of the species in the numerator more than those in the denominator at lower temperatures. As temperature rises, values come down indicating significant presence of all the species at higher temperatures. The pathway for the production of water vapor in actual reaction would be through a number of other reactions like H + H + O $\rightarrow$ H_2O and H_2 + O + M $\rightarrow$ H_2O + M (where M is any species) amongst others. In these cases, it can be more easily seen that at low temperatures, the reaction is centered around H_2O and high temperatures, all may be present. In the case of K_{p_5}, the value of the equilibrium constant is low even at 3500 K, much lower than values for the dissociative equilibrium of H_2 and O_2. This implies very little dissociation of nitrogen even at high temperatures. Thus, most air breathing engines where the temperature is limited to 2300 K, nitrogen can be treated as an inert. The dissociation of O_2 and H_2 cannot be ignored (the effects of the presence of even small amounts of O and H could change the enthalpy balance significantly).

Reverting back to the calculation of equilibrium composition, for a H_2 - O_2 set with the species being H_2, O_2, H_2O, OH, H, and O, one has two element conservation equations and four equilibrium relations $K_{p,i}$, $i = 1, 4$ as in Table 7.2. The six non-linear algebraic equations can be solved to determine the six partial pres-

sures and one can then derive the mole fractions ($X_i = p_i/p$) and mass fractions ($\mathscr{M} = \sum X_i \mathscr{M}_i$ and $Y_i = X_i \mathscr{M}_i/\mathscr{M}$, where $\mathscr{M}$ refers to the molecular weight of the gases). Thus, one can determine the composition of the reactive mixture at any given temperature. Such a composition is a function of pressure as well. If we take the simple case of hydrogen dissociation, we have $H_2 \leftrightarrow 2H$. The equilibrium relation is

$$p_H/p_{H_2}^{1/2} = K_{p,1} \tag{7.1}$$

$$p = p_{H_2} + p_H \tag{7.2}$$

the second equation being the Dalton's law of partial pressures. This replaces the mass conservation relation in the present case. When more than one element is present, one can form a set of equations from them and reduce them to a set one less than the number of element equations and complement them by the Dalton's law. Manipulating the above equations, one gets

$$p_{H_2} + K_{p,1} p_{H_2}^{1/2} - p = 0 \tag{7.3}$$

whose solution is

$$p_{H_2}^{1/2} = \frac{-K_{p,1} + \sqrt{K_{p,1}^2 + 4p}}{2} \tag{7.4}$$

For large $K_{p,1}$ and relatively small p, one can simplify by expanding the terms under the quadratic to lead to

$$p_{H_2} \sim p^2/K_{p,1}^2 \tag{7.5}$$

This equation indicates that *as pressure increases*, p_{H_2} *increases* implying *reduced dissociation*. *Increased temperature* implies increase in $K_{p,1}$ and hence, lesser p_{H_2} and *therefore, more dissociation*. These features are very general and can be used to draw inferences in several situations.

After obtaining the composition at any fixed pressure and assumed temperature for combustion of products, the second step can be performed. The enthalpy difference between the reactants and the final products (obtained at a chosen temperature) can be obtained. If this difference is zero, then it implies that the conversion process between the reactants and the products is adiabatic. However, since the initial choice of temperature is arbitrary, it may turn out that the difference is negative. This implies that the chosen temperature is larger. If the difference is positive, the chosen temperature will be lower. Thus, by a suitable iterative scheme, one can obtain the estimate of adiabatic flame temperature to the desired accuracy. The enthalpy of species is composed of two aspects - the heat of formation and the sensible enthalpy. The heat of formation (denoted by $\Delta H_{f,i}^0$) is the heat of reaction in a reaction in which the species concerned alone is the product and the elements that compose of it at standard state are the only reactants. The

Table 7.3: Heats of formation for selected species, * = kJ/g-mole; (g) = gas; (l) = liquid; s= solid; no symbol usually implies gas

Species	$\Delta H^0_{f,i}$ *	Species	$\Delta H^0_{f,i}$ *
H_2	0.0	H	218.1
O_2	0.0	O	249.5
OH	39.5	H_2O (g)	- 242.0
H_2O (l)	- 160.4	H_2O_2 (l)	- 187.8
C (graphite)	0.0	CO	- 112.0
CO_2	- 393.7	N_2	0.0
N	473.0	NO	90.3
Cl_2	0.0	Cl	121.1
HCl	- 92.3	Al (s)	0.0
Al_2O_3 (s)	- 1670.2		

standard state is chosen as T = 298.16 K and p = 1 atm. The definition requires a statement of the heat of formation of the "elements" at standard state. Species like H_2, O_2, C, Cl_2, N_2 are taken to have zero heat of formation. Other products like H_2O, CO_2, and CO all have non-zero heats of formation. Table 7.3 provides the data for a select set of compounds that appear in the products at high temperature. Those species that have positive heat of formation at standard conditions may be thought of as unstable and would combine with other species to form stable species.

In the process of computation of the composition, it is possible that some of the products could condense into liquids or even solids particularly when the gas is expanding through a nozzle. This will happen if metals like Aluminum are a part of the reactive mixture (as the case will be for a solid propellant). In such a case, the pressure exerted by the species will be equal to the equilibrium vapor pressure. In such a case, a recalculation needs to be done by assuming the partial pressure as equal to the vapor pressure at the specified temperature.

The procedure outlined above is one strategy for obtaining the composition. Since it involves the solution of nonlinear algebraic equations of "stiff" nature, convergence problems are severe. An alternate strategy that has been adopted in CEC 71 program published in NASA SP 273 (Gordon and McBride, [50]) is very elegant and this computer code is perhaps the most universally used one to determine the performance of high temperature reacting systems. The essential strategy is to minimize a function subject to given constraints. The functions considered are: Gibbs free energy minimization for constant pressure and temperature constraint, Helmholtz free energy minimization for constant volume and temper-

ature constraint and modified equations for constant enthalpy and pressure (as required for scramjet application, see section 1.10) or in special cases, entropy and pressure as constraints. The solution scheme uses a Lagrangian multiplier technique and starts with a simple estimate of the composition and progresses through iteration that invokes a relaxation scheme to ensure that undesirable overshoots/undershoots do not occur. It uses standard thermodynamic data for over 400 species that are likely to be present in an equilibrium condition (not all in a given case) that are curve-fitted and are used automatically in the program. In addition to obtaining equilibrium composition, it provides adiabatic flame temperature and equilibrium composition, rocket engine performance for frozen and equilibrium nozzle operating conditions, Chapman-Jouget detonations, and shock tube parameter calculations.

The calculation of the performance of a rocket engine involves first, the calculation of the adiabatic flame temperature and equilibrium composition at chamber conditions (typically at a pressure of 10 atm to 200 atm). As the flow goes through the nozzle, the static temperature and pressure keep decreasing. Since the reaction rates are a strong function of both these parameters ($\dot{w}''' \sim p^2 exp(-E/RT)$) the reaction rates keep dropping. This happens in a way that beyond a certain area ratio downstream of the throat, the composition does not change. The reaction path through the nozzle can be covered by computing the reactive flow through it and is complex. A simpler procedure would be to determine the performance in the two limits - equilibrium and frozen. The former implies that the composition achieved at each location along the nozzle would be that corresponding to equilibrium at the local pressure and temperature. This is also called "shifting equilibrium" since the equilibrium is reached at different pressures and temperatures as expansion takes place. The latter implies that the composition remains unchanged through the nozzle. As already indicated, the actual result is between the two. What is done therefore is that the code determines and presents the performance under options of (a) equilibrium operation and (b) frozen operation. The essence of this procedure is to invoke the isentropic condition between the combustion chamber and the exit of the nozzle. The entropy of a mixture of gases at a given pressure and temperature is given by

$$s = \frac{n}{\mathscr{R}} \left[\sum X_i \frac{S_i^0(T)}{\mathscr{R}} - \ln\ p - \sum X_i\ \ln\ X_i \right] \tag{7.6}$$

where n is the total number of moles of gas, $X_i = n_i/n$ is the mole fraction, S_i^0 is the entropy at 1 atm and a function of temperature and the summation is taken over all the species. The last term on the right hand side arises due to mixing of the various species. Setting $s_c = s_e$ one can get T_e given a value of p_e. This process requires iteration with the equilibrium assumption since a choice of T_e needs to be made for a fixed p_e and the composition obtained at these values of p_e and T_e

and the isentropic condition checked out. If the equality is violated, T_e needs to be corrected and the process repeated. For the case of frozen composition, the above equation simplifies to

$$s_c = \left[\sum X_i \frac{S_i^0(T_c)}{\mathscr{R}} - \ln\ p_c\right] = s_e = \left[\sum X_i \frac{S_i^0(T_e)}{\mathscr{R}} - \ln\ p_e\right] \tag{7.7}$$

From the above equation, T_e can be obtained by solving for it directly without the calculation of composition. If we take note of the relationship $S_i^0 = c_{p,i}\ \ln\ T$ for constant specific heat, the above relationship becomes

$$\frac{p_c}{p_e} = \left[\frac{T_c}{T_e}\right]^{\gamma/(\gamma-1)} \tag{7.8}$$

a result that is well known and is the basis of the simple isentropic nozzle analysis discussed in chapter 4.

Once the limiting conditions of equilibrium and frozen flow have been explored, an estimate of the actual theoretical performance is obtained by a simple relation $I_{sp,act} = 0.7I_{sp,eqm} + 0.3I_{sp,frozen}$. The code can be used to get a better estimate by allowing equilibrium expansion until an area ratio at which the temperature falls below 2000 K and allowing the composition to be frozen beyond this stage.

7.5 Fuels for Scramjets

It has been pointed out (see Table 6.7) that despite the high static temperature at the combustor inlet of a scramjet (1200 to 1400 K), the relative low pressures (of the order of 0.5 to 1.0 atm), and high speeds (of 1.0 – 1.5 km/s) allow a very small residence time (of about 1 ms). Hence, ignition and combustion need to be completed in this duration. Also because, the hypersonic vehicle propelled by the scramjet experiences high aero-thermal load, cooling requirements need to be managed by the fuel to the extent possible. Unlike rocket engines where the flow rates are substantial, the fuel flow rates in air-breathing engines will be small and it will not be easy to meet with the cooling requirements at hyper-velocity conditions.

Hydrogen is a simply structured, easily igniting, fast burning fuel with high heat absorbing capacity (compare c_p of 14 kJ/kg K for H_2 with 2.3 kJ/kg K for JP class fuels). It is, therefore, a preferred fuel for scramjets. The weakest point about hydrogen is its low density even in liquid form under cryogenic conditions (70 kg/m^3). In a vehicle design that has to optimize the space for hyper-velocity flight conditions, kerosene or its derivatives offer a much better choice with densities of 800 to 1000 kg/m^3. Three directions that have been pursued are: (a)

designing a fuel that possesses useful properties – cooling capability through decomposition without generating condensible solids that could clog the injector orifices, (b) explore the use of an existing compound not identified yet as a fuel, and (c) use a combination of fuels, namely hydrogen and kerosene through suitably designed injectors so as to make available a fine spray of kerosene and a fast reacting hydrogen in the combustion chamber. All the three approaches are being pursued. Amongst kerosene – like fuels, JP - 7 is considered a good candidate. It is heavily refined (low aromatics $\sim$ 3 %) fuel developed specially for high performance, high Mach number aircraft, SR 71. Its thermal stability limit is about 560 K that implies a flight corridor with a maximum M $\sim$ 5. For hypersonic flights between 6.5 or better, there is need to enhance the cooling capability of the fuel. This is achieved by requiring it to be an endothermic fuel. This means that the fuel has to decompose and the absorption of energy in this process constitutes the endothermicity. The expectation is that at a typical temperature of 1000 K, the energy absorbed is about twice the sensible enthalpy. At Mach numbers of 7 – 8, the fuel heat sink required is about 2.5 – 3.0 MJ/kg and this can be met with at 1000 K with the magnitude of decomposition energy noted earlier. Methylcyclohexane (C_7H_{14}) decomposing to toulene (C_7H_8) and hydrogen absorbing about 2.1 MJ/kg of fuel reacted, n-heptane (C_7H_{16}) decomposing to toulene and hydrogen absorbing about 2.3 MJ/kg, methyl alcohol (CH_3OH) decomposing to CO and H_2 absorbing in the dehydrogenation process as high as 4 MJ/kg are some examples. The disadvantage of methyl alcohol is that its heat of combustion is about half of JP class fuels. This can be overcome by using higher alcohols (like butyl alcohol, etc) so that the benefits of calorific value are retained while achieving better heat sink capability. These are the current areas of research.

Russians have very actively pursued high speed combustion technology using gaseous hydrogen and kerosene in a mode called barbotaging in which kerosene mixed with hydrogen bubbles is forced out of the fuel injection orifices leading to fine atomization of kerosene. This is also called aeration in other literature.

7.6 Fuels and Oxidizers for Solid Rockets

Section 1.13 has provided a description of a solid rocket engine and the propellants. Solid propellants are classified into homogeneous and heterogeneous systems. Homogeneous propellants are such that it is not possible to distinguish between the components after the propellant is made – the components will have integrated into each other at a molecular level and are indistiguishable. In the case of heterogeneous propellants, the oxidizer, and fuel components remain separated but in close physical proximity in a manner that the propellant itself is a structurally sound solid. It would be possible to separate them, if necessary.

Homogeneous propellants were the first set of propellants to be made. They are based on nitrocellulose, NC (solid) and nitroglycerine, NG (liquid) both of which have fuel and oxidizer elements in their molecular structure. NC is slightly fuel rich and NG is slightly oxidizer rich. The stoichiometric condition that provides high performance occurs at a NG:NC ratio (typically, 6.5) that will be a slurry, since NG that is in large proportion is a liquid. To ensure that the propellant obtained is a rigid solid, one needs to reduce the proportion of nitroglycerin substantially. Typical NG:NC ratio will be 0.8 to 1. Hence, a homogeneous solid propellant is always fuel rich. These propellants are also called double base (DB) propellants.

Propellant making requires other ingredients as well for the following reasons. (i) Since both propellant ingredients are reactive compounds, they tend to react slowly and degrade after the propellant is made and stored even at ambient temperature. To reduce the degradation rate, it is necessary to add other compounds as stabilizers. (ii) The propellant so made must burn at a specified rate (linear burn rate, $\dot{r}$) that is a function of pressure, ambient temperature and lateral velocity of gases. If the burn rate of a propellant that has been engineered does not meet the requirements, then burn rate modifiers need to be included in the mix. (iii) The propellant made of NC-NG combination can be transparent. This leads to unusual problem of radiative heat absorption in depth from the intense flame when the propellant is burning. This leads to "bore holing" implying, undesirable subsurface burning. To reduce this problem, one needs to add an opacification agent – could be carbon black. In military applications, one wishes to have an exhaust that cannot be easily tracked particularly in the case of short range tactical missiles. This can be encouraged by adding certain chemicals in small quantities. Thus, propellant engineering involves incorporation of several ingredients all of which will have effect on the performance and this process is built on a foundation of extensive careful experimentation.

Heterogeneous propellants use a solid oxidizer, typically powdered ammonium perchlorate, AP ($\mathrm{NH_4ClO_4}$) with a polymeric binder. To enhance the performance, finely ground aluminum powder is also added. Typical solids fraction in a solid propellant is 87 % (AP $\sim$ 70 % and Al $\sim$ 17 %) and the solid powder needs to be mixed with the liquid polymeric binder till one gets a slurry that has to be cured to obtain a structurally satisfactory solid. Typical heterogeneity is caused by AP particle size that varies between 20 to 500 μm and could be multi-modal distribution; it is also caused by aluminum that varies in size between 20 to 50 μm.

Typical ingredients include curing agents that are solids or liquids ($\sim$ 2 % or less), and burn rate modifiers ($\sim$ 0.25 to 0.5 %) apart from the oxidizer, metal powder and binder. These propellants are also fuel rich since the peak performance obtained at near stoichiometry occurs at 92 % solid fraction, a level that cannot be achieved because the material does not have enough binding capacity to lead to a

structurally satisfactory solid. In fact, even to produce the propellant at 87 % solid loading is tough and needs the use of small but important wetting agents to ensure the formation of a uniformly mixed slurry. These propellants are called Composite propellants (CP). The combustion of these propellants leads to a highly visible flame and secondary smoke resulting from the products of combustion (like HCl) condensing with moisture in the atmosphere. While this issue is quite unimportant for space launches, and not-so-important for the launch of strategic missiles, it is important for short range tactical missiles. To avoid this, it is desirable to look for other high energy solids to replace AP. This effort has led to the use of compounds like RDX (cyclo trimethylene trinitramine) or HMX (cyclo tetramethylene tetra nitramine) that are otherwise used more extensively in the preparation of explosives. These are high energy compounds that are slightly fuel rich and produce high flame temperature on combustion and molecules with lower molecular weight. They can be mixed into double base propellant to enhance the performance (specific impulse) and reduce the signature of the exhaust. Such propellants are called composite modified double base propellants (CMDB). Ammonium perchlorate being an oxidizer can also be mixed into double base propellant to create a high energy CMDB when it is unnecessary to suppress exhaust gas signature.

Typical list of ingredients in DB, CP and CMDB is shown in Table 7.4. The list is by no means exhaustive. Several other compounds are used as equivalents for those indicated in this table.

Fuels and oxidizers in the context of rocket propellants could be composed of oxidizing elements (like O, Cl, typically) and reducing or fuel elements (like C, H, Al, Mg, etc) in a proportion that could make a single compound burn by itself at ambient pressure or higher pressures (more certainly), and yet reflect an overall "fuel" or "oxidizing" character. To appreciate this, it is necessary to examine the elemental composition of various compounds listed above. The chemical composition of the compounds is presented in Table 7.5 and the properties of active ingredients – those that burn by themselves by being in a state ready for exothermic decomposition on initiation – are presented in the Table 7.6. Both these tables are very instructive. The list of ingredients presented here are some of the most active compounds used for propellant making all over the world. There are a few other compounds that have been used sparingly for specific applications. These are TMETN (Trimethyl Olethane Trinitrate), TEGDN (TriEthylene Glycol DiNitrate) and DEGDN (Di Ethylene Glycol DiNitrate). These are not disussed here.

Nitrocellulose is prepared by nitration to varying extents with Nitrogen even up to 14 %. Propellant grade nitrocellulose is restricted to 13 % nitrogen due to possible explosive sensitivity beyond this value. Nitroglycerine is a liquid and an explosive and is to be handled very carefully. Compounds listed in Table 7.5 other than NC are compounds with a fixed structure. The third column contains the nature of the compound (fuel/oxidizer) and the fraction. All the compounds have

Table 7.4: Ingredients of Double base (DB), composite (CP) and composite-modified double base (CMDB) propellants

Nature	For DB	For CP	For CMDB
"Fuel"	NC	PU, PBAN, PBAA CTPB, HTPB	NC + HMX or RDX
"Oxidiser"	NG	AP, AN	NG
Stabiliser	EC, 2NDPA	-	EC, 2NDPA
Plasticiser	DEP, TA	DOP, DOA, IDP	DEP, TA
Burn rate modifier	PbSa, LiF Pb2EH CuSt, PbSt	IDP, Fe_2O_3 nBF, CuCH DnBF, LiF	Like for DB
Metal Fuel	Al, Mg	Al, Mg, B	Al, Mg
Curing agent	-	TDI, MAPO, IPDI	-
Wetting agent	-	Lecithin	Lecithin
Stability additive	Metal	Metal	Metal

PU = Polyurethane, PBAN = Poly Butyl Acrylo Nitrile, PBAA = Poly Butyl Acrylic Acid CTPB = Carboxy Terminated Poly Butadiene, HTPB = Hydroxy terminated Poly Butadiene, EC = Ethyl centralite, 2NDPA = 2 Nitro Di Phenyl Amine, AN = Ammonium Nitrate, DEP = Di Ethyl Phtalate, TA = Tri Acitin, DOP = Di Octyl Phtalate, DOA = Di Octyl Adipate, IDP = Iso Decyl Penargonate, PbSa = lead Salicilate, LiF = Lithium Fluoride, Pb2EH = Lead 2-Ethyl Hexoate, nBF = n-Butyl Ferrocene, CuCH = Copper Chromite, DnBF = Di-n-Butyl Ferrocene, TDI = Toulene-2, 4-Di-Isocyanate, MAPO = Tris (l-(2-Methyl) Aziridinyl) Phosphine Oxide, IDPI = Isophorone Di-Isocyanate

elements that are intrinsically fuel and oxidizer. In terms of oxidizers, oxygen is a more powerful oxidizer compared to chlorine (actually, fluorine is an even more powerful oxidizer, but is not used in practice due to its very corrosive and toxic nature). In terms of fuels, hydrogen is more easily oxidized compared to carbon. And aluminum requires much higher temperatures for oxidation to be complete (oxidation of aluminum powder causes a coating of aluminum oxide that requires high temperatures to melt and allow the interior to react). When these elements react, the oxidation process will proceed such that all the hydrogen will get oxidized to water first and the remaining oxygen oxidizes carbon to CO first and if more oxygen remains, CO_2 will get produced.

To estimate the net "fuel" value, all the O is consumed in converting H to H_2O and C to CO_2. The additional carbon that remains is taken as the residual fuel value and is presented as a ratio with the mass of the fuel. If oxygen is in excess, all H is converted to H_2O and C to CO_2 and the remaining oxygen is taken as a proportion of the mass of the oxidizer. In the case of AP, since chlorine competes with oxygen for oxidizing the fuels, more readily H, it is taken that a part (half) of

Table 7.5: Composition and properties of active ingredients, NC = NC (12.6 %N), ΔH_f = Heat of formation at 298.16 K

Ingredient	Chemical formula	F or Ox , %	State (300 K)	ρ_p kg/m^3	ΔH_f kJ/mole
NC	$C_6H_{7.55}O_5(NO_2)_{2.45}$	F, 12.9	Solid	1660	- 670.6
NG	$C_3H_5O_3(NO_2)_3$	Ox, 0.04	Liquid	1660	- 400.6
AP	NH_4ClO_4	Ox, 31.0	Solid	1950	-296.1
AN	NH_4NO_3	Ox, 20.0	Solid	1730	-327.6
RDX	$C_3H_6N_3(NO_2)_3$	F, 20.0	Solid	1820	+61.5
HMX	$C_4H_8N_4(NO_2)_4$	F, 20.0	Solid	1900	+75.0

H will be converted to HCl and the remaining H to H_2O. This is a simple approximate scheme for assessing the nature of the compound. There are, however, more rational methods of describing the fuel value based on valency considerations (see Williams, Barrere and Huang, [27]) but it is sufficient to understand the principles stated here as in any case, these are indicative in nature and the actual composition at high temperatures is governed by a large number of other reactions and the formation of other species.

NC and NG whose compositions are shown in Table 7.5 are mildly fuel rich and oxidizer rich as brought out earlier. Ammonium Perchorate is a solid that has a higher oxidizing value compared to others. RDX and HMX have similar elemental ratios and the difference is in the number of groups involved. Consequently, several properties are identical and some (like density and heat of formation) are close to each other. The column on density shows that all the solids have high density, the highest being AP (another good reason for choosing it as an oxidizer). The last column shows the heat of formation. The values of heats of formation are also interesting. Large positive values indicate structural instability leading to easy ignition and strong exothermic decomposition. Of the various values indicated, RDX and HMX show positive heats of formation and they can be expected to yield high degree of exothermicity. Amongst these compounds, all except AP will burn (or technically called self-deflagrate) at ambient pressure in an atmosphere of their own products of combustion (in reality, one provides an initial inert atmosphere and subsequent combustion will generate products of combustion). AP requires, however, a minimum pressure of 20 atms before self-deflagration can occur. This condition is called Low pressure deflagration limit (LPDL). This property is an interesting combustion behavior that has implications in understanding and modeling of propellant combustion.

One uses the elemental composition and the heat of formation provided in Table 7.5 in the code of Gordon and McBride [50] as discussed in section 7.4, to get

Table 7.6: Equilibrium combustion features of active ingredients, X_i = Mole fraction, * = kN s/kg, $\mathscr{M}$ = Average molecular weight of the gases, ** = g/mole

Species	NC	NG	AP	AN	RDX	HMX
T_c, K	2590	3289	1405	1247	3286	3278
X_i						
O_2		0.069	0.287	0.143	-	-
H_2O	0.225	0.280	0.377	0.571	0.226	0.227
CO	0.417	0.107	-	-	0.246	0.246
CO_2	0.128	0.275	-	-	0.082	0.082
H_2	0.116	0.014	-	-	0.089	0.089
N_2	0.111	0.181	0.119	0.286	0.326	0.326
HCl	-	-	0.197	-	-	-
Cl_2	-	-	0.020	-	-	-
OH	-	0.041	-	-	0.013	0.013
H	-	-	-	-	0.013	0.012
NO	-	0.018	-	-	-	-
$\mathscr{M}$, **	24.7	28.9	27.9	22.9	24.3	24.3
I_{sp}, *	2.30	2.44	1.57	1.61	2.66	2.66

the adiabatic flame temperature, equilibrium composition, and specific impulse that can be derived from a rocket engine working at a fixed chamber pressure and expanding to a certain condition (say, from 70 atms with optimal expansion to 1 atm). These are presented in Table 7.6. Even though these ingredients are not usually used in isolation, the results are very instructive. NG is a more reactive substance compared to NC. The oxidizer richness expresses itself in terms of 6.9 % oxygen (by volume) for NG, 28.7 % for AP and 14.3 % for AN. Others are all fuel rich. Even though it was stated that the way reaction takes place consumes H first and C later, due to equilibrium considerations, one finds that certain fractions of H_2 and CO are present in the case of NC, RDX and HMX because at high temperatures H_2O and CO_2 will decompose to smaller fragments – H_2 and CO. Nitric oxide, NO is present in small fractions in NG, RDX and HMX decomposition products, simply due to enhanced reactivity at high temperature. Another important parameter to be taken note of is the molecular weight of the products of combustion. While the lowest value is obtained for AN, it is not of much consequence since AN is not a very reactive oxidizer – its flame temperature is the lowest. It must be noticed that RDX and HMX show low molecular weights and high flame temperature.

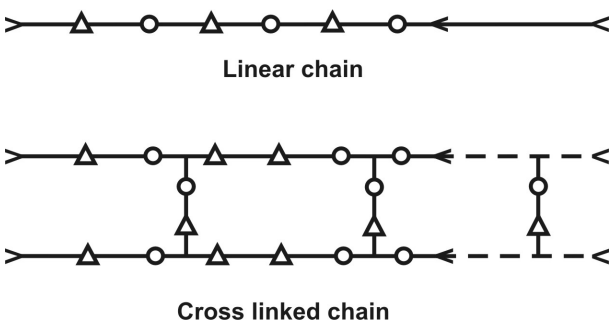

Figure 7.1: Polymer chain process upper part shows a linear chain and the lower part shows cross linked chain. The unfilled circles and triangles represent molecular segments

7.6.1 Polymeric Fuels for Composite Propellants

The fuels for composite propellants must be chosen such that they are in liquid form to begin with; they should enable mixing with solid powder of oxidizer and metal at as high a level of solid loading as possible leading to a flowing dough that can be cast into a mould before the "solidification" process begins. To ensure that the starting "stuff" is a liquid that becomes later a solid, the choice of liquid is a liquid prepolymer. Towards the end of mixing process, a chemical is added to start off the polymerization reaction so that a structurally acceptable solid is obtained. The rate of the expected reaction should be slow enough so that when added and mixed in the mixing device, no significant reaction takes place, and the chemical is uniformly mixed into the propellant mass before polymerization process becomes significant. The time between the addition of this chemical, called curing agent and the point at which the material is well mixed to enable it to be transported to the casting section is called "pot life". The chosen combination should provide enough pot life for productive functioning.

The mechanical properties are controlled by the curing process. Polymeric fuels can form linear chains that help allow large extension at break. As different from this, one can connect up the chains at intermediate points by cross linking them (both these are shown in Figure 7.1) so that the material becomes tough – extension per unit load is small. Further, the polymeric material is a visco-elastic material. This means that the properties are a function of time at the same loading. One simple feature of such materials is "slumping" – a large solid stored for several months might acquire distortions due to self weight even at ambient temperature.

Propellants loaded into the rocket motors experience a wide range of ambient temperatures, because the motors are stored in open ground for operational reasons. Tactical systems experience the harshest environment with ambient tem-

peratures varying from - 30 to + 50 °C. The structural integrity of the propellant is to be maintained over this wide range. At low temperatures, most polymeric materials become brittle. This is characterized by a quantity called "glass transition temperature". The glass transition temperatures must be lower than the lowest temperature at which the propellant is expected to function. Higher temperatures cause softening of polymeric material and hence, reduction in mechanical properties.

Thus, the choice of the fuel for producing a propellant is made on the basis of (a) high solid loading to obtain as high a c^* as possible, (b) adequate mechanical properties at all system operating temperatures, and (c) ease in terms of handling and facilitation of the mixing process.

Over years, many polymers have been developed. These are Poly Vinyl Chloride (PVC), Poly Sulfide (PS), Poly Urethane (PU), Poly Butyl Acrylic Acid (PBAA), Poly Butyl Acrylo Nitrile (PBAN), Carboxy Terminated Poly Butadiene (CTPB), Lactone Terminated Poly Butadiene (LTPB), and Hydroxy Terminated Poly Butadiene (HTPB). The improved properties with the polymers developed over three decades has led to the choice of HTPB for most of the propellants at present.

7.6.2 Double base (DB) Propellant Manufacture

The two primary approaches to making double base propellants are (i) casting and (ii) extrusion. Casting process allows very large size grains (as they are called) to be made with the same ease as small grains and the shapes could also be more complex. Usually, large size grains are cast into the rocket motor casing. Such grains are called “case bonded grains”. The extrusion process allows propellant grains of very good mechanical properties to be made, but grain size is limited. This process can be used for small tactical rocket motors or what are known as "free standing grains". This implies that the rocket motor may be composed of several grains all of them identical and produced by the extrusion process.

The manufacture by extrusion process can be made solvent-less. For the casting process, the preparation of a casting powder is considered the first step. This is usually done by a solvent process. The solvent used is typically acetone or alcohol.

The process involves making first a casting powder from nitrocellulose with stabilizers and other ingredients listed earlier, typically with 75 % NC, 20 – 30 % NG, 4 to 5 % DMP/DEP/DOP, carbon black, burn rate modifier in small fractions for double base casting powder and *without any NG* for a single base casting powder. The solid ingredients are all ground and sieved before use. All the ingredients are put into an incorporator with the solvent and operated at a temperature of 35°C for several hours to allow the formation of a coherent dough. After this, the dough is processed into sausages and extruded into a cord of 0.8 to 1 mm diameter

and cut into pieces of about 1 mm. The fines pieces are then dried to eliminate the solvent completely. Further processing demands finely cut pieces of similar size as it has been found that the liquid dispersion through the solid matrix will be better if attention is paid to the manufacture of the "powder" to ensure sharply cut well dimensioned material. The powder so obtained is dried to reduce the volatile content to less than a percent. In parallel, a casting liquid consisting of NG with some plasticizer (60 to 70 % NG and the rest Triacetin or Di-Ethyl Pthalate) would be needed for further processing. The solid powder is introduced into a mould with a mandrel required to produce the necessary hollow portion called the port. The casting liquid is allowed to be drawn into the container held under vacuum. Drawing off any gases is important to ensure structural integrity with no gas inclusions. The process of curing consists of inter-diffusion of the molecules of NG into NC and formation of bonds between them. The diffusion process is an activation barrier based phenomenon unlike molecular diffusion in gases. The process if facilitated by raising the temperature to about 60 °C and maintaining it for fifty to a few hundred hours depending on the size of the system.

In the case of solvent-less extrusion process, a slurry of NC with water is agitated along with periodic additions of NG till a NC-NG paste is produced. After the moisture is brought down to about 30 % by removing it by suction, it is mixed with all the other ingredients for a reasonable time (6 to 10 hours) to ensure uniformity, checked for the composition and then dried to < 0.5 %. Then it is passed through hot rollers till the thin sheets are transformed into carpet rolls suitable for use in an extrusion press through a die to obtain the appropriately sized propellant grains. The process described here may be treated as generic and several variants of the process are developed depending on the experience gained in the establishments. The reproducibility of the propellant properties – structural and ballistic are very strongly dependent on the quality control of the ingredients with the presence of metals or metal oxides at a very minute level being monitored and controlled as well as the process scheme used.

At all stages in the processing various classes of tests on the composition and its uniformity, dilatomeric evaluation to determine volume changes and others are performed to determine if the process has gone on as intended, for otherwise, one might loose the whole mix. Steinberger and Drechel [23] describe the propellant making process in more detail.

7.6.3 Composite Propellant (CP) Manufacture

The ingredients used in making a composite propellant are set out in the Table 7.4. The preparation for the manufacture of the propellants is to have ground and classified oxidizer. One normally uses a bi-model distribution in making the propellant. This helps better packing of the particles and obtain a higher solid

loading. The process of grinding generally produces all sizes of particles. It is considered sufficient if a few size ranges of importance are verified before use as a quality assurance measure. Typical particle sizes chosen are coarse of 200 – 300 μm (70 %) and fine at 50 – 100 μm (30 %). The fraction between the coarse and fine is varied to obtain burn rate changes as well. Metal powder, say of aluminum is also an ingredient in a high energy propellant. Its particle size is typically less than 40 μm. Aluminum does not affect the burn rate except as an inert (see section 8.2). The burn rate modifier is also to be processed by grinding and assessed for its purity, since its presence in very small quantities ($\sim$ 0.5 %) can affect the burn rate significantly ($\sim$ 5 to 20 %). Different batches of the compound may have ppm level impurities that can alter the burn rate by a few percent.

The actual process of making the propellant involves (a) mixing, (b) casting and (c) curing. Propellants are made in small sizes as well as very large sizes. A few tonnes per batch would be common in large sizes. There are processes that are also continuous. The mixing and casting processes require active control and care. The curing process needs no critical manual intervention and is amenable to automation more simply. The mixers consist of two contra–rotating sigma bladed arrangement to continuously bring in the materials for mixing. They can be horizontal or vertical. The process starts with the liquid ingredients – pre-polymers (with molecular weight of 2000 – 3000, viscosity of 40 – 50 poise) being mixed with the ingredients that have the largest influence – the burn rate modifiers. Batch addition of the oxidizer and the metal powder with mixing for a few hours will be repeated till the entire ingredients have gone through the mixing process for several hours. The composition is checked at various locations of the mix to determine the uniformity of the mix. It is to be ensured that the viscosity of the mix is within limits so that the visco-elastic material can flow smoothly, albiet slowly. The curative agent is added at this point and the mixing operation is performed so that the curing agent is uniformly dispersed throughout the mix. At this stage the material is ready for transportation to the casting section. The final mixing operation is performed with vacuum applied so that any air bubble trapped in the dough will get expelled during the mixing operation.

The largest amount of use of composite propellants is for moderate to large sized rocket motors. In these cases, the propellant is cast directly into the motor – to produce case bonded propellant system. The rocket motor is prepared by doing the necessary internal cleaning and introducing the insulation system. Typical insulator that has been used in large motors in India is called "Rocasin" rubber. These sheets are bonded to the inner motor casing. The casing for large motors is of metal and for upper stage motors, Kevlar fiber reinforced plastic. The motor is located below a device that will allow slow flow of the material in a manner that prevents gaseous inclusions. To help this, the entire casting with the motor and the mandrel arrangement is put under vacuum. The slurry is allowed to move down from a container by gravity (in one arrangement that is commonly used

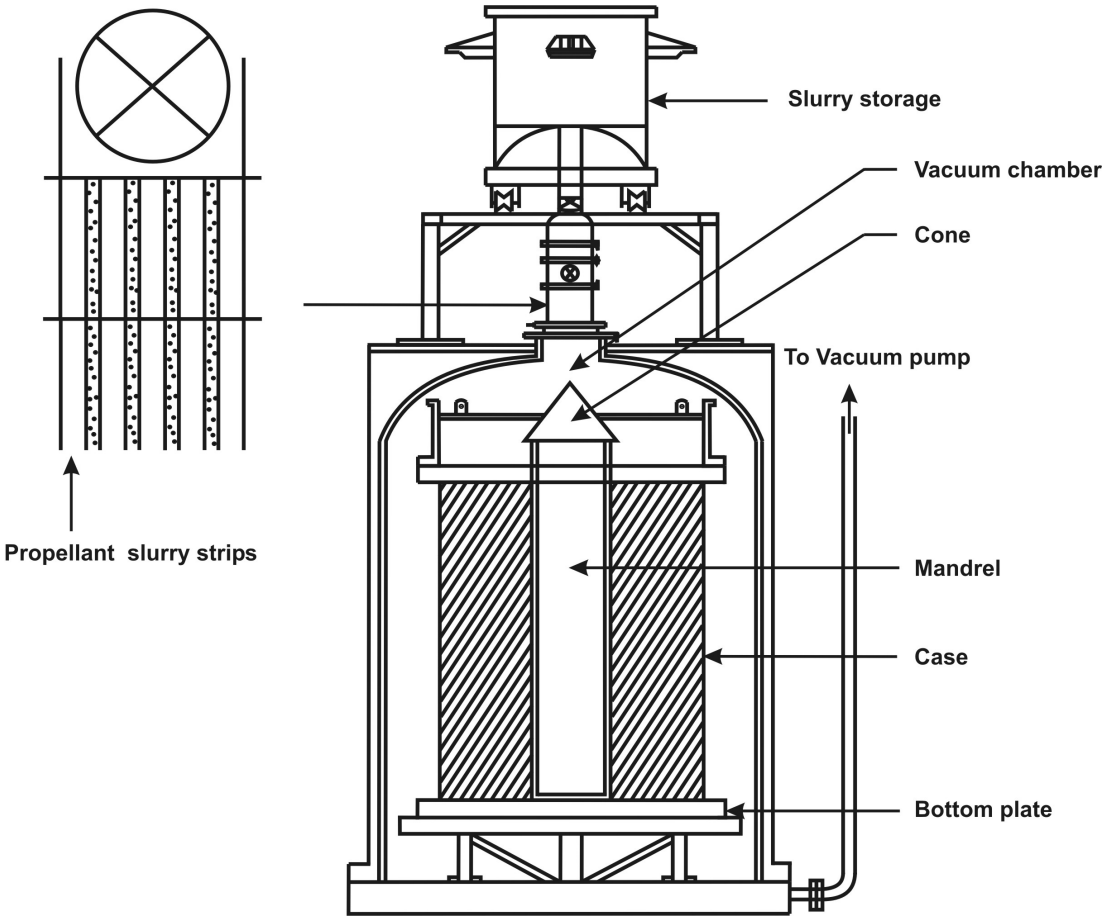

Figure 7.2: The vacuum casting system, adapted from [15]

in the manufacturing facilities for propellants for space vehicles) as thin strips as shown in Figure 7.2. While the material is falling into the mould, any gas inclusions will get expelled. There are also other methods of casting called Bayonet casting and Bottom casting used in propellant making industry [15]. After the casting process is completed, the hardware containing the propellant and the mandrel is moved into separate curing chambers that are maintained at suitable temperatures using hot air blowers. Typical temperatures for curing are between 50 to 65 °C. The curing process needs to be designed carefully. During the curing process, the low molecular weight polymer will begin to polymerize further – the molecular chains are built longer and if any cross linking process initiator is present, the cross linking also will occur. This process of addition of molecules to the chain is exothermic. Hence, the local temperatures will increase. The outer stream of hot air is expected to keep the temperature rise within limits. Since in reasonable size motors, the thickness of the propellant between the mandrel and the outer casing, called the web, is sufficiently large (up to 1 m) and the propellant material has a low thermal conductivity, heat build up in the core regions (mid-web regions) will be large. Thus, the thermal design of the curing process should account for the heat generated locally and its weak dissipation at the boundaries to ensure that temperature limits are not exceeded. If the limits are exceeded, de-polymerization will take place locally degrading the property of the propellant. Hence, curing trials are made in motors with lower propellant mass but simulating the web and other conditions properly and thermal field of the curing propellant is mapped. This is then simulated mathematically by solving the conduction equation with additional heat release term that would depend on the chemistry of polymerization and the uncertain parameters related to chemistry calibrated against the measured temperature profile. When these are known, the full scale curing process is simulated to determine the correct temperature for curing and the flux of hot air required to maintain the thermal profile within limits. In some motors of intermediate size (of the order of a meter in length and diameter), pressure is applied on the propellant during the curing process. In such an arrangement, the casing-propellant bond is improved providing better structural integrity.

After the curing process that may take half a day for small motors and about two to three weeks for large size motors (for instance, a 2 m dia motor with 0.6 m web is considered large), the motor is moved out of the curing section, allowed to cool down before removing the mandrel and the edges are trimmed suitably. In order to obtain an estimate of the ballistic properties of the propellant, smaller size motors called ballistic evaluation motors (BEM) are also cast in a standard configuration chosen for them. These are test fired subsequently to derive and confirm the projected ballistic parameters – burn rate dependence on pressure and ambient temperature. The procedures outlined for DB and CP propellants are also used for making composite modified double base (CMDB) propellants.

Typical compositions achieved for both DB, Composite and CMDB propellants

Table 7.7: Propellant compositions (wt. %)

Propellant	NC	NG	DEP	EC	AP	Al	HTPB	HMX
DB1	44.0	43.0	11.0	2.0				
DB2	55.6	40.4	4.0					
DB3	50.4	36.6	13.0					
CP1					80.0		20.0	
CP2					68.0	18.0	14.0	
CP3							20.0	80.0
CMDB1	30.8	30.1	7.7	1.4	30.0			
CMDB2	30.8	30.1	7.7	1.4				30.0
CMDB3	26.0	30.0	8.0		21.0	15.0		

with some performance data are shown in Table 7.7 and 7.8.

The results of the Table 7.8 are interesting. In understanding the performance of the propellants, it should be borne in mind that $I_{sp} \sim \sqrt{T_f/\mathscr{M}}$. One can notice that higher temperatures are also accompanied by increase in molecular weight. It is the relative variations that dictate the performance. The pattern is discernible for all the cases. Oxygen is absent in the product gas consistent with the fuel rich nature of all propellant compositions. The four compounds that influence the performance are CO, CO_2, H_2 and H_2O. The relative fractions decide the molecular weight and the temperature. The realized values of specific impulse in actual conditions would be about 92 to 94 % of the equilibrium value. From Table 7.8, it is clear that CP2, DB2, and CMDB3 constitute practical compositions of high performance. Other compositions are model compositions with illustrative value. Further insight can be gained by examining how the properties vary through the nozzle under equilibrium operating conditions. These are shown in Table 7.9 for p_c = 70 atm. with optimum expansion to 1 atm.

As the flow passes through the nozzle, pressure and temperature decrease. The way all the variables change is presented in Table 7.9. The thrust coefficient increases as one proceeds towards the exit of the nozzle with more thermal (or random) energy extracted to accelerate the fluid. This also implies that the specific impulse achieved will keep increasing till optimum expansion is achieved. The vacuum specific impulse is larger than the value obtained at any expansion; since the negative term due to p_a is absent. The composition is seen to vary as one goes through the nozzle. While the mole fractions of the major species change only slowly, there is rapid change of several radicals and the condensible species. It can be noted that aluminum oxide is in liquid phase in the chamber, but condenses to

Table 7.8: Performance of solid propellants as in Table 7.7, optimum expansion from 70 atm to 1 atm, X_i = Mole fraction, 1*, 2*, 3* = CMDB1, CMDB2, CMDB3, LAlOx* = Liquid Al_2O_3, $\mathscr{M}$ in g/mole, $I_{sp,e}$ and $I_{sp,f}$ are the specific impulse values for equilibrium and frozen conditions in kN.s/kg

Species	DB1	DB2	DB3	CP1	CP2	CP3	1*	2*	3*
T_c, K	2602	3009	2500	1785	3403	3005	3091	2835	3623
X_i									
CO	0.424	0.342	0.446	0.382	0.249	0.074	0.229	0.372	0.350
H_2O	0.210	0.267	0.195	0.003	0.088	0.336	0.315	0.219	0.151
H_2	0.139	0.074	0.158	0.360	0.320	0.012	0.054	0.122	0.163
CO_2	0.100	0.169	0.090	0.001	0.009	0.289	0.181	0.095	0.039
N_2	0.124	0.133	0.109	0.191	0.078	0.159	0.130	0.185	0.111
HCl	-	-	-	-	0.126	0.067	0.063	-	0.041
Cl	-	-	-	-	0.008	0.008	-	-	0.006
OH	0.001	0.006	-	-	0.004	0.020	0.012	0.002	0.017
H	0.002	0.005	0.001	-	0.030	0.002	0.006	0.004	0.036
NO	-	-	-	-	-	0.008	0.002	-	0.002
CH_4	-	-	-	0.008	-	-	-	-	-
C (s)	-	-	-	0.052	-	-	-	-	-
LAlOx*	-	-	-	-	0.079	-	-	-	0.075
AlCl	-	-	-	-	0.007	-	-	-	0.001
$AlCl_2$	-	-	-	-	0.002	-	-	-	-
$\mathscr{M}$	23.8	25.9	23.4	18.7	27.7	29.4	26.6	24.0	30.1
$I_{sp,e}$	2.29	2.41	2.26	2.16	2.59	2.38	2.44	2.39	2.58
$I_{sp,f}$	2.28	2.38	2.24	2.06	2.45	2.27	2.39	2.37	2.46

Table 7.9: Properties of gases through a nozzle for propellant CP2; $I_{sp,e}$ and $I_{sp,ev}$ are the specific impulse for equilibrium and vacuum conditions in N.s/kg

A_e/A_t		1.0	5.4	8.3	10.6	13.8
p_{stat}, atm	70	40.9	2.36	1.42	1.01	0.7
T_{stat}, K	3403	3204	2327	2254	2143	2026
c_F		0.657	1.500	1.590	1.640	1.692
$I_{sp,e}$		1041	2375	2515	2600	2821
$I_{sp,ev}$		1955	2660	2776	2839	2901
X_i						
CO	0.249	0.252	0.252	0.252	0.251	0.251
H_2	0.320	0.328	0.344	0.344	0.346	0.347
H_2O	0.088	0.085	0.076	0.076	0.075	0.074
CO_2	0.009	0.009	0.010	0.010	0.011	0.011
HCl	0.126	0.134	0.149	0.149	0.151	0.151
N_2	0.078	0.076	0.076	0.076	0.076	0.076
Al_2O_3 (l)	0.079	0.082	0.048	-	-	-
Al_2O_3 (s)	-	-	0.040	0.087	0.087	0.087
H	0.030	0.024	0.004	0.004	0.003	0.003
OH	0.004	0.003	-	-	-	-
Cl	0.008	0.007	0.001	0.002	-	-
ALCl	0.007	0.005	-	-	-	-
$AlCl_2$	0.002	-	-	-	-	-

Table 7.10: Effects of chamber pressure on the overall performance

p_c atm.	A_e/A_t	c^* m/s	$c_{F,opt}$	$I_{sp,eo}$ N s/kg	$I_{sp,ev}$ N s/kg
30.0	5.5	1578	1.50	2367	2654
50.0	8.3	1582	1.59	2513	2774
70.0	10.6	1585	1.64	2600	2839
100.0	13.8	1588	1.69	2683	2902

Table 7.11: Effects of chamber pressure on the mixture properties at the chamber and exit, temperature, ratio of specific heats, γ, average molecular weight of gases, $\mathscr{M}$

p_c atm.	T_c K	T_e K	γ_c	γ_e	$\mathscr{M}_c$ g/mole	$\mathscr{M}_e$ g/mole
30.0	3336	2327	1.134	0.998	27.6	28.5
50.0	3378	2252	1.137	1.177	27.7	28.5
70.0	3403	2142	1.138	1.185	27.8	28.6
100.0	3429	2024	1.140	1.192	27.9	28.6

solid through the nozzle. The enthalpy changes that occur due to these effects are significant.

In order to understand the role of chamber pressure, the results for different chamber pressures but expanding to ambient pressure optimally are presented in Table 7.10. It is clear from the table that the change in the characteristic velocity is only about 0.6 % and the change in the optimum thrust coefficient is about 12 % over the pressure range of 30 to 100 atm. and it is the latter that contributes largely to the change in specific impulse. Further insight can be gained by examining all other thermodynamic and transport properties at the chamber and the nozzle exit in Tables 7.11 and 7.12. The values of γ and $\mathscr{M}$ vary through the nozzle; the variation of γ being very significant, more particularly because terms like $\gamma/(\gamma-1)$ in the relationships between the pressure and temperature can exert large influence. It is also significant to note that the Prandtl number under these conditions is quite low (about half of the value at ambient conditions).

7.6.4 Inhibition and Insulation

Two aspects relevant to grain manufacture are (a) inhibition and (b) insulation.

Inhibition implies arrangement of the geometry such that it will not burn normal to inhibited surfaces. Inhibition is achieved by bonding a polymeric fuel sheet

Table 7.12: Effects of chamber pressure on the mixture properties at the chamber (subscript, c) and exit (subscript, e), constant pressure specific heat, viscosity and Prandtl number

p_c atm.	$c_{p,c}$ kJ/kg K	$c_{p,e}$ kJ/kg K	μ_c cP	μ_e cP	Pr_c	Pr_e
30.0	4.01	2.56	0.093	0.073	0.32	0.39
50.0	3.71	2.40	0.094	0.071	0.33	0.41
70.0	3.54	2.22	0.095	0.069	0.34	0.44
100.0	3.379	2.09	0.095	0.066	0.35	0.46

physically well, chemically also where possible. Such a binding prevents pealing of the sheathing and burn up of the treated surfaces. To ensure better bonding, the choice of the material is from the same family as the binder in the propellant. The criticality of the role of inhibition is recognized if we note that it has to function at high combustion chamber pressures and in some occasions high temperatures as well – particularly in cigarette like burning motors (see chapter 9) where the cylindrical grain will burn from the nozzle end for tens of seconds to minutes during which period the heat is transferred from the hot gases by conduction through insulation and metal wall to heat up the inhibition. Any small separation between the inhibition and the propellant grain will allow hot gases at high pressure to enter in and ignite segments not expected to burn at that stage. Such a condition is usually prevented if there is a chemical bond between the inhibitor sheathing and the propellant surface. Typical inhibitor material is poly vinyl cellulose for DB propellants and could be HTPB based material for HTPB based CPs.

Insulation is related to a material of low thermal conductivity that can be wrapped around the grain or set as a next-to-wall sheathing into which the propellant is cast or inserted. If the propellant is cast into a motor as in case bonded grains the outer most layer will be of insulation. If the propellant is free standing, it could burn from the outer side as well and this will need a thicker insulation layer next to the metal wall to prevent heat transfer to the outer casing of metal or fibre-reinforced plastic material. Figure 7.3 describes these features. The manufacture of the insulating material is in many ways similar to the propellant making. The insulating material will need to be flexible and for this purpose, synthetic rubbers are used. To make them thermally resistent, they are filled with ceramic fillers like precipitated silica. Recent trend is in favor of using inorganic elastomers like poly dimethyl siloxane reinforced with fibres of polyaramide. Flame retardants like Antimony trioxide or phosphates are commonly used. Curatives use sulfur compounds or peroxides. Principal properties of the material helpful in the operations are the density, conductivity and ablation rate (rate at which the material is consumed with the impingement or the flow of hot gases), all of which

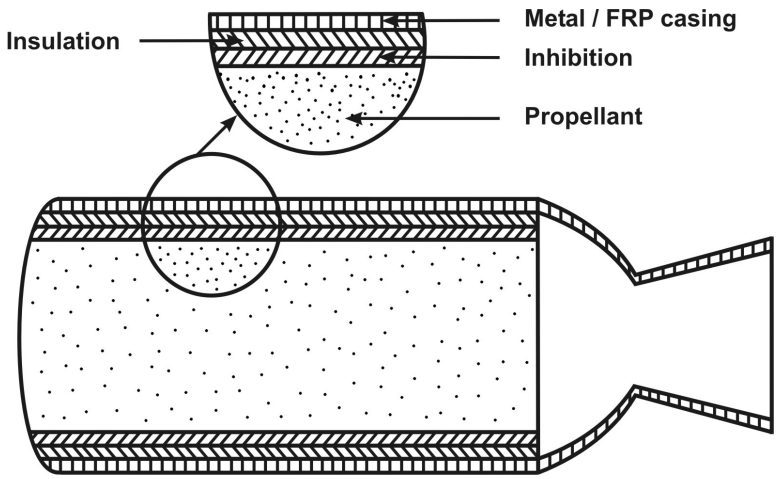

Figure 7.3: Schematic of a solid rocket with an end burning grain showing inhibition and insulation

must be as low as realizable. Typically, the material has a density of 800 to 1000 kg/m^3, specific heat of 2 kJ/kg K, a conductivity of 0.2 W/m K and an ablation rate of 0.05 to 0.15 mm/s. In recent times, developments of ceramic based throats have brought down the erosion rates by a factor of 20 compared to these rates (see US patent 6510694 B2 by Lockheed Martin, 2003).

In order to ensure that the insulation is reasonably well bonded to the propellant, a thin interface liner material of 100 to 200 μm thickness is introduced. In view of better compatibility, the liner material is chosen from the same binder system (as in the propellant) and will have fillers, plasticisers and curatives. In the application process, the insulation sheets are bonded to the inner wall with appropriate adhesives, and the liner sheet is then pasted before the motor is taken to the casting bay for introducing the propellant.

7.6.5 Non-Destructive Testing

The propellants, DB or CP so produced have to be examined for the presence of blow holes, inclusions, and de-bond between the inhibition or insulation and the parent propellant grain. These examinations are done using X–ray, Gamma ray or neutron radiography, infrared imaging and computerized tomography. Other new optical techniques have been brought into the field in recent times. All voluminar defects like the ones noted above can be detected with reasonable certainty with classical X–ray radiography. One of the more recent advances relates to real time radiography in which the information on radiography is acquired through the use of photodiode arrays or charge coupled devices and processed in a computer to

obtain the information in appropriate forms to help interpretation and analysis.

In X–ray radiography, the processed pictures can have various shades. Lighter shades belong to metals like steel and lead that absorb much more energy, and darker shades belong to solid propellant grain, rubber and other resinous materials.

Neutron beams are attenuated very little by high density materials, but are absorbed significantly by plastic materials. Neutron beam radiography is considered eminently suited to inspect pyro-technic devices related to ignition, separation, cable cutting, and others. It would be necessary to determine (a) the quality of assembly inside the pyro-device, (b) any possible discontinuity in the explosive train, (c) possible voids in the internal charge, (d) positioning of sealing devices, (e) moisture ingression and others.

The infrared imaging technique has become well used in the last ten years due to improved sensitivity with which the pictures can be interpreted. In this technique, a thermal profile is established by heating the object for some time with a small temperature difference, say 5 – 10°C. The infrared image taken at this time reveals many features like de-bonds.

Large motors like the ones for launch vehicles are cleared after 100 % radiographic study. All aspects that create suspicion are reviewed and cleared for operation or specific repair. Blow holes and cavities located close to the port that are easily accessible are opened up, filled with resin so that it will bond with the material of the propellant.

While the above discussion is largely concerned with propellants, the hardware also undergoes inspection by various methods – visual, die penetrant test, acoustic emission test are adopted at various stages in clearing the hardware – generally before the casting process.

7.6.6 Mechanical Properties

Propellants are viscoelastic materials. This implies that they carry properties of liquids as well as solids. Like liquids, the stress is proportional to strain rate and like solids, stress is proportional to strain (all taken in the small deformation linear range). Thus, the behavior of a solid propellant is a combination of the above limits. This has some simple implications. A material stressed, say in tension and allowed to remain in that condition, will retain the same deformation and stress for all times in the elastic range. If it also possesses "viscous" behavior, there will be slow deformation with time since the stress already applied leads to a strain rate. The complexity for rocket application arises from the fact that stress and strain rates tend to be large more particularly during ignition phase at which time pressure build up rate is the highest. This will lead to large stresses and the

Table 7.13: Mechanical properties of solid propellants, CL = cartridge loaded; NMNE (E) = Nitramine Extruded; CAB = Compression at break; CB = Case Bonded, Hrdnss = Hardness

Material	E_m MPa	% EB	UTS MPa	UCS MPa	CAB %	Hrdnss Shore A
DB (Cast)	200 – 300	2 – 4	6 – 10	-	-	70 – 90
DB (Ext.)	500 – 800	10 – 15	10 – 15	38 – 40	30 – 40	90 – 120
CP (CL)	30 – 40	6 – 25	1.0 – 2.0	4 – 5	30 – 35	60 – 80
CP (CB)	3 – 6	30 – 45	0.5 – 1.0	-	-	60 – 80
NMNE(E)	-	12 – 20	10 – 12	30 – 35	30 – 35	50 – 70
CMDB	20 – 30	15 – 25	1.5 – 2.0	12 – 14	35 – 40	40 – 60

combined visco-elastic effects must not have deleterious effect over the short burn duration. Since characterizing the propellant as an elastic solid provides input of value, these are used to characterize the propellant. The mechanical properties demanded from the propellant depend on the physical configuration used and the loads experienced. Case bonded grain (bonded to the motor casing) needs to have greater elongation features compared to UTS, the ultimate tensile strength. Free standing grain needs to have high UTS, but low elongation can be acceptable. The demand for high UTS and large elongation at break should be moderated by the consideration that what are being contemplated are composite materials based on a class of polymers and limitations arise from the consideration that enhancing the strength by cross linking leads to lower elongation and vice versa.

Typical mechanical properties of a propellant are the Initial modulus, E_m (slope of the stress-strain curve at strain = 0), UTS and % elongation at break (EB), and hardness as measured usually by Shore hardness apparatus. For various propellants considered here, typical values are presented in Table 7.13. As clear from the tables, extruded DB propellant is tough and cast DB propellant follows it; Composite propellant is flexible. Tactical motors using free standing grains adopt EDB propellants and case bonded propellants adopt composite propellants generally. There are exceptions. In these cases special effort would have been made to tailor-make the mechanical properties.

7.6.7 Thermochemical Performance

Figures 7.4, 7.5, and 7.6 show the variation of the flame temperature, average molecular weight of the gases and the specific impulse of double base and composite propellants. The peak in I_{sp} for double base propellants occurs in a range where the mix will not cure into a solid. Hence, practical propellants limit the amount of

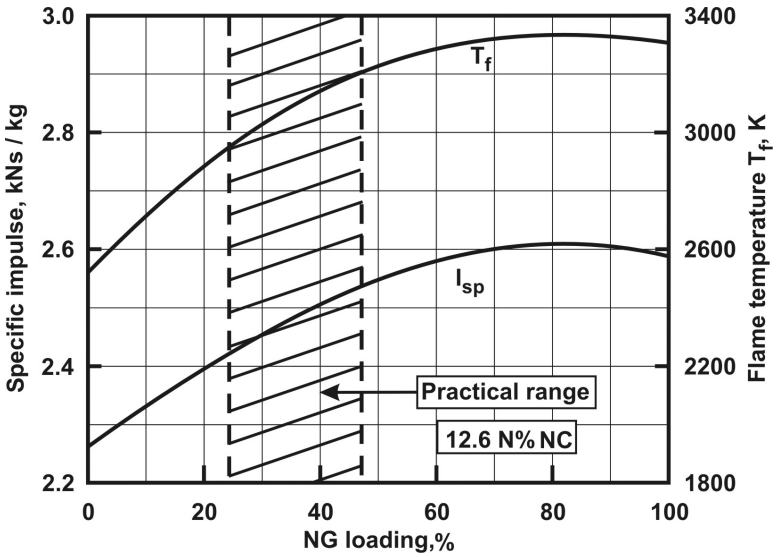

Figure 7.4: Flame temperature (T_f) and Specific impulse (I_{sp}) for a double base propellant with NG loading

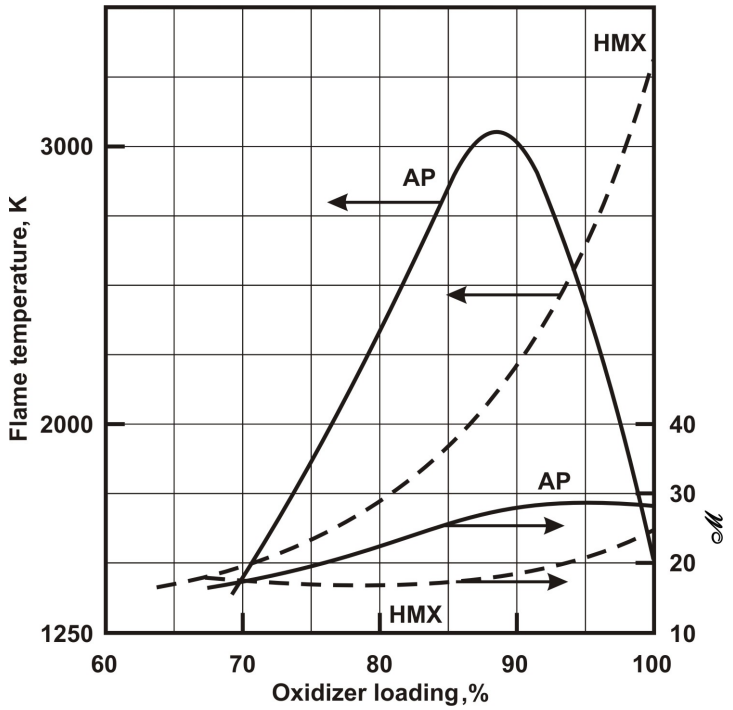

Figure 7.5: T_f and $\mathscr{M}$ for composite propellants based on AP and HMX vs. solid loading

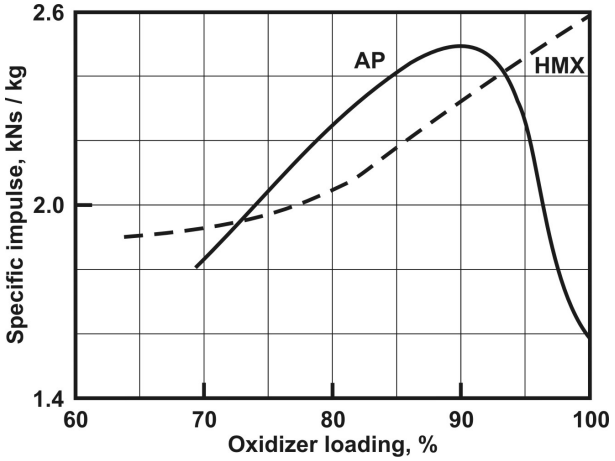

Figure 7.6: Specific impulse of AP and HMX based composite propellants vs. solid loading

NG in a DB propellant. In the case of CP, the peak in I_{sp} occurs around 90 % AP in the propellant. Introduction of aluminum increases the flame temperature by 10 % with change in molecular weight marginal so that I_{sp} goes up by 5 %. CMDB propellants show an increase compared to the performance of DB propellants to the level of CP or in some cases, slightly better. The more important reason for the emergence of CMDB propellants is the fact that by using RDX/HMX it is possible to equal the performance of CP with little smoke in the exhaust.

7.6.8 Linear Regression Rates or Burn Rates

Since solid propellants carry both fuel and oxidizer components, they burn by themselves – in an inert atmosphere or an atmosphere of their products of combustion. The most important geometric feature of their combustion is that *they burn normal to the local surface*. This means a plane surface will regress in a planar manner. A circular grain burning from inside will burn as circular surfaces of increasing diameter. Equally well, if a solid cylindrical grain is instantly ignited all over the outer surface, it will burn into cylinders of smaller diameter. The rate at which the regression occurs is called the burn rate (the word regression rate also includes cases where the process is endothermic. In these cases, the regression occurs because of heat input from elsewhere – from a gaseous flame, from a laser heating source, etc). The burn rate depends on several variables – the composition of the propellant, the static pressure over the surface, the initial temperature of the solid, and the lateral velocity of gases over the propellant. Since the burn rate is being discussed for a specific propellant, one needs to determine the influence of static pressure ($p_{c,s}$), initial temperature (T_{in}), lateral velocity of gases (V_g) on the

burn rate ($\dot{r}$). The effect of lateral velocity is also termed as erosive burning effect.

Experiments are conducted in an apparatus called Strand Burner to determine $\dot{r}$ vs. $p_{c,s}$, T_{in}, and a special set of rocket motors to evaluate the effect of V_g. Typical parameter ranges are $\dot{r}$ = 0.1 to 50 mm/s, $p_{c,s}$ = 1 to 200 atm, and T_{in} = - 40 to + 50 °C and V_g up to 1.0 km/s, but more usually, 500 m/s. A strand burner consists of a chamber that can be pressurized to the levels required and help maintain the pressure even during the burning of the strand. This is achieved by holding a large volume chamber connected to the test cell containing the burning strand. The strand is a propellant typically 10 mm dia or 10 mm square about 100 mm long suitably inhibited and held in a ceramic frame and attachments to initiate ignition. The burn rate is assessed by one of the several means. Wires pierced into the strand at equal distances (say 30 mm each, three wires) can be connected to an electrical timer circuit that operates in a manner in which burn up of one wire will initiate one or two timers and the the burn up of the following wires will stop them. The length burnt divided by the time taken will give the burn rate. This was adopted in the early periods. In later times, optical measurement techniques by photographing the burning strand through a window, acoustic measuring technique to detect the beginning and end point of burn of a given length and other techniques have been developed. Most data when set out on a log-log plot show a line indicating a behavior $\dot{r} = ap_{c,s}^n$, where n is the pressure index of burn rate, and a the burn rate at 1 atm. (taking the units of $p_{c,s}$ in atm.). Similarly, to extract the dependence on initial temperature, the strands are conditioned at the appropriate temperature for five to eight hours and taken out from the temperature conditioning chests just before use in the strand burner. The long duration of conditioning is required to ensure uniformity of the strand temperature because of the low thermal conductivity of the propellant. The reason for using immediately after removing from the chest is to ensure that the heat pick up from the ambient does not alter the temperature. The burn rate variation is expressed by

$$\dot{r}/\dot{r}_{T_o} = exp[\sigma_T(T_{in} - T_o)] \tag{7.9}$$

where σ_T is called the temperature sensitivity coefficient and T_{in} is the initial temperature of the propellant. The above equation can be recast as

$$\sigma_T = \frac{d\ln\dot{r}}{dT} \sim \frac{2}{(\dot{r}_2 + \dot{r}_1)} \frac{(\dot{r}_2 - \dot{r}_1)}{(T_{in,2} - T_{in,1})} \tag{7.10}$$

The most common behavior of the propellants is captured in Table 7.14.

Specific impulse of a propellant affected by the adiabatic flame temperature and the average molecular weight of the gases is controlled by the equilibrium behavior of the chemical system. *As different from this behavior, the burn rate behavior shown in Table 7.14 is a "rate phenomenon" and so controlled by chemical kinetics and molecular diffusion*. Thus, introducing *small quantities of chemical*

Table 7.14: Burn rate behavior with pressure and initial temperature of solid propellants, $\dot{r} = a_{70}[p_{c,s}/70]^n$, IO = Fe_2O_3, CC = $CuCr_2O_4$, 44NC = 44 % NC

	Material	a_{70} mm /s (atm)^n	n -	σ_T % / K
1	AP	7.9	0.77	0.20
2	HMX	10.0	0.93	0.20
3	DB1 (44NC + 43NG + 11DEP + 2EC)	7.0	0.72	0.56
4	DB2 (56NC + 40NG + 4DEP)	10.0	0.58	0.34
5	DB3 (50NC + 37NG + 13DEP)	7.3	0.82	0.62
6	CP1 (80AP + 20HTPB)	7.5	0.38	0.25
7	CP2 (68AP + 18 Al + 14 HTPB)	6.7	0.42	0.32
8	CP2 + 0.25 IO -0.25 AP	8.3	0.49	0.34
9	CP2 + 0.50 IO -0.50 AP	8.9	0.51	0.36
10	CP2 + 1.00 IO -1.00 AP	9.8	0.54	0.37
11	CP2 + 2.00 IO -2.00 AP	10.3	0.55	0.38
12	CP2 + 0.25 CC -0.25 AP	12.0	0.43	0.26
13	CP2 + 3.00 CC -3.00 AP (CP2′)	15.0	0.44	0.28
14	CP3 (80HMX + 29HTPB)	1.9	0.64	0.55
15	CMDB1 (DB1 with 30AP)	15.0	0.40	0.54
16	CMDB2 (DB1 with 30HMX)	6.5	0.83	0.54

compounds, identified in Table 7.4 as burn rate modifiers, can leave *the specific impulse virtually unaltered* while *changing the burn rate behavior substantially*. Even so, increasing the energy content of the propellant by suitably proportioning the oxidizer and the fuel increases the burn rate. DB2 which is a higher energy propellant has a higher burn rate compared to DB1 and DB3. This effect is not due to "burn rate modifier" effect.

In constructing the Table 7.14, the data presented are the burn rate at 70 atm and the pressure index and temperature sensitivity around this condition. In looking for "goodness" of propellants, burn rate at a standard pressure (a_{70} in the Table 7.14) is to match with a specific value required by the designer, the pressure index must be very low, and temperature sensitivity low. Low pressure index is desired to enhance stability of motor operation (see Chapter 9) and low temperature sensitivity is desired to ensure minimal deviation in performance with ambient temperature variation (since several tactical rocket motors are deployed in open areas).

The choice of the reference condition for indicating the burn rate is at high pressure (a_{70}) because most propulsion systems operate at high pressures and therefore, the behavior at high pressure is more relevant. This is particularly so since some propellants have varying index with pressure (see Figure 7.7) and

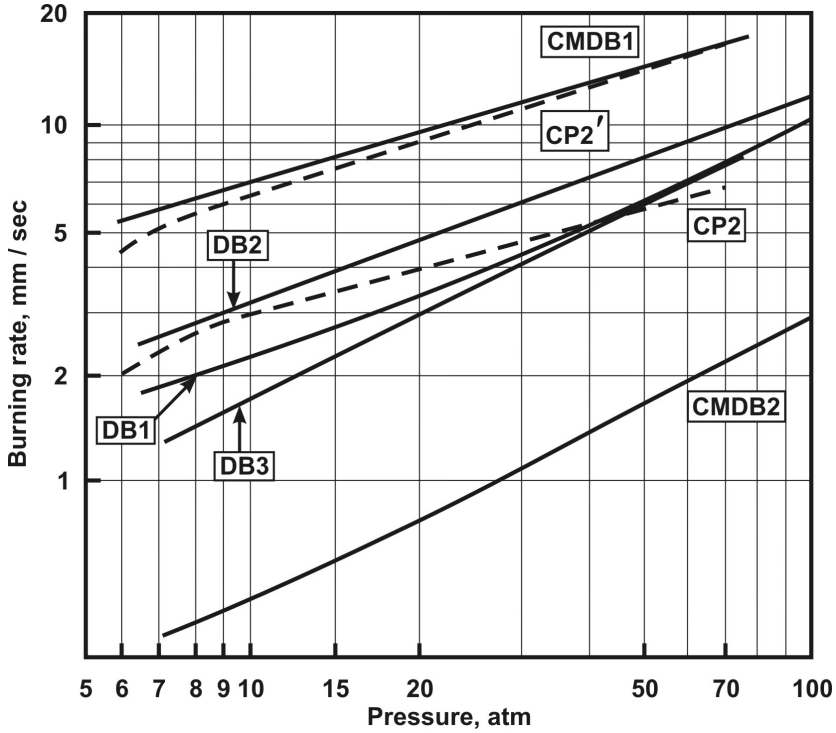

Figure 7.7: Burning rate vs pressure for the candidate propellants of Table 7.14

what matters is the index at higher pressures. It can be noted that monopropellants like AP and HMX burn with relatively high index – close to unity (see Table 7.14). This will be discussed subsequently. DB propellants have higher pressure indices compared to composite propellants for reasons similar to monopropellants. The temperature sensitivity of the burn rate is also generally higher with DB propellants. In fact it is correlated to pressure index, though in a weak way. In the case of composite modified propellants, use of AP reduces the pressure index, but the use of HMX to increase the specific impulse, increases the pressure index substantially.

The modification to burn rate behavior through additives as seen in the Table 7.14 is a small subset of a whole range of possibilities. An effect called platonizing in which the burn rate does not vary with pressure normally over a restricted range of pressures can be created using additives. This is particularly prominent in the case of DB propellants. In select propellants, the burn rate decreases over a range of pressures. These propellants are unusual and used after a careful assessment. This is because the use of exotic compounds may, some times, result in meeting desired requirements well. But the exotic compounds are usually very reactive and this might lead to reactivity even on storage and hence, result in

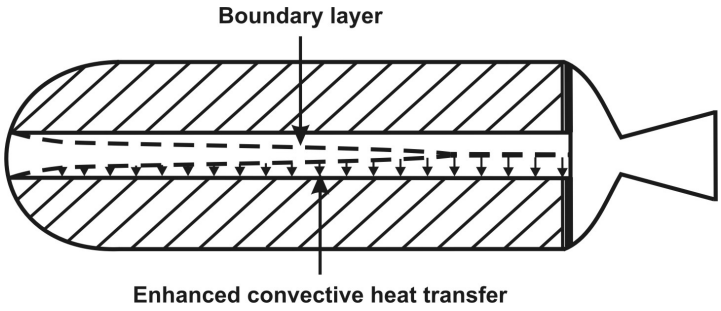

Figure 7.8: Schematic of a highly loaded solid rocket motor experiencing large mass flux in the port leading to larger heat flux to the surface and enhanced burn rate (erosive burning)

performance degradation in a period shorter than desired.

7.6.9 Erosive Burning Effect

As indicated earlier, erosive burning effect is the effect of the flow of hot burning gases past the propellant on the linear burn rate. This is present in propellant geometries with a port through which the hot gases flow from the head end to the nozzle end. In highly loaded propellants (implying that the port cross sectional area is comparable to the nozzle throat area), the mass flux of the hot gases moving past the burning surface is large (see Figure 7.8). This is simple to see if we note that in a rocket motor the mass flux is the largest at the throat and by making the port size comparable to the throat cross section, the flux will be comparable to that at the throat. Under these conditions, the convective flux to the surface of the propellant is enhanced. This will cause enhanced burn rate. The burn rate of a propellant is stated as $\dot{r}/\dot{r}_{ne} = F(\rho_g V_g, others)$, where $\dot{r}_{ne}$ is the non-erosive burn rate composed of pressure and initial temperature effects described earlier. Experimental data have been obtained by several kinds of apparatus. In one of the techniques, the propellant is instrumented with fine wire probes embedded into the propellant at several axial locations. The fine wires are electrically activated so that when they break, a signal is registered. As the propellant burns through, these fine wires burn up giving indication to the arrival of the flame at this point. By acquiring data from a large number of locations over the web and the length, along with the chamber pressure at the head and aft ends, one can extract the basic parameters governing the erosive burning phenomenon. To process the burn rate data, one needs to create a gas dynamic model of the flow through the port. This gives the mass, momentum and energy flux at each axial location (see Williams Barrere and Huang, [27]). The flow through the port is one of continuous mass, momentum and energy addition into the port. This leads to a reduction in stagnation and static pressures through the port (see Rayleigh process discussed

in section 4.6.2). This consequently leads to the drop of the non-erosive part of the burn rate. The enhanced mass flux implies increase in the local Reynolds number of the flow. This implies a reduction in heat transfer film thickness and enhanced heat transfer to the propellant with consequent enhancement in the burn rate.

Experiments have also been conducted with two-dimensional motors supplied by hot gas from separate gas generators. In one early study, tablets of test propellants were fixed in the test section and their burn rate obtained. In later studies, the test section is equipped with transparent window and data on web vs. time over the entire length has been obtained by using high speed photography over the burn duration. The photographs are analyzed to obtain the burn rate data. These are combined with the analysis described above to extract the basic data on erosive burning. Two general observations made in these studies are that the (i) enhancement in burn rate is observed only after a minimal velocity/mass flux, and (ii) enhancement is higher with a slower burning propellant (non-erosive burn rate). The data obtained over a broad range of conditions were correlated in terms of Mach number, mass flux, and pressure. In recent times (Mukunda and Paul, [57]), it was recognized that all the effects are condensed into a single g parameter defined by

$$g = [\rho_g V_g / \rho_p \dot{r}_{ne}](Re_0/1000)^{-0.125} \tag{7.11}$$

where $Re_0 = \rho_p \dot{r}_{ne} d_0/\mu$, and d_0 is the local port diameter. Figure 7.9 shows the non-dimensional plot with data from more than dozen sources. These data appear well correlated by the curve on the figure even though there is fair amount of scatter. The scatter in the data is in part related to the measurement techniques and in addition, there are differences in the results from different sources on the same propellant. The curve is represented by the equation

$$\frac{\dot{r}}{\dot{r}_{ne}} = 1 + 0.023[g^{0.8} - g_{th}^{0.8}]\mathscr{H}(g - g_{th}), \quad g_{th} = 35.0 \tag{7.12}$$

It can be noted that the idea of threshold mass flux is preserved in the correlation and the second observation concerning enhanced erosion for lower non-erosive burning rate is automatically imbedded in the parameter g; decrease in $\dot{r}_{ne}$ implies increase in g. This correlation has been tested for its predictive quality in highly loaded motors and found satisfactory. It can, therefore, be used in design with confidence.

7.7 Ignition Composition

Pyrotechnic mixtures are classically used as ignition ingredients. The choice of the ingredients is made to (a) generate sufficiently high flow rate of high temperature gases and (b) generate hot particulate matter so that the particle impingement

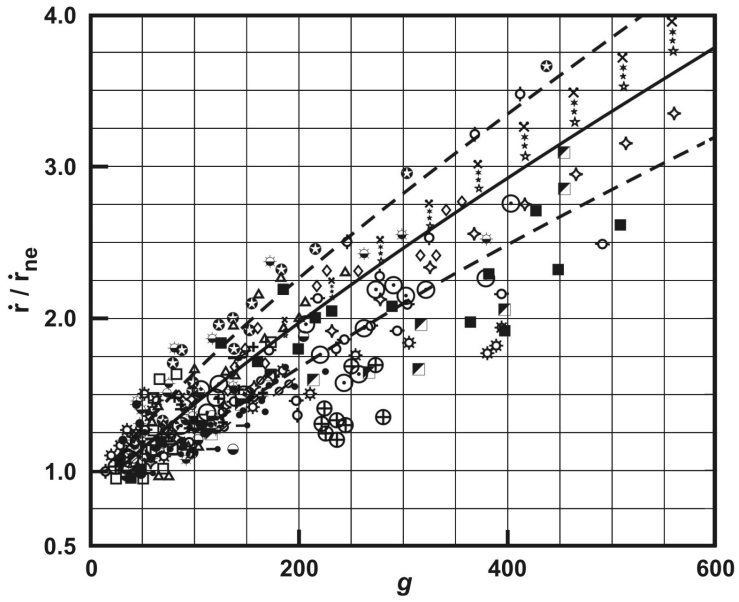

Figure 7.9: The plot of the ratio of burn rate with erosive burning to that without erosive burning with non-dimensional parameter g

on the solid propellant will cause a number of local hot ignition spots. The choice and the arrangement must also ensure long term safe storage and insensitivity to random electrical and other disturbances. Conventional black powder is composed of 75 % of potassium nitrate, 15 % charcoal and 10 % of sulphur with an average density of 900 to 1100 kg/m^3 after they are granulated. Typical grain sizes used are about 1 – 3 mm. Generally, 1 kg of black powder gives 0.4 kg gases and 0.6 kg particulate matter. This composition is sensitive to moisture. In later times a variety of compositions have been developed. They are all based on a combination of a binder, a metal powder and oxidizer much like the composition of the main motor. There is greater freedom in the choice of the ingredients, because, one is not attempting to optimize the specific impulse, but a combination of temperature, fraction of hot particulate matter and gas generation rate. The common ingredients used are: metal powders like aluminum, magnesium, titanium, boron, zirconium and the oxidizing agents are: potassium nitrate, AP, potassium perchlorate amongst others. One can use the fuels and oxidizers in any combination. One also uses binders to make granules, pellets and cast blocks. One of the requirements of compositions for igniters is that the mix must burn fast, typically at 15

to 30 mm/s. In these cases, one uses the metal powder between 20 to 40 % with very fine oxidizer, typically AP of 50 – 60 % and some burn rate accelerators ($\sim$ 1 – 2 %) along with 5 to 10 % of binder.

Small rocket motors use pellets in a basket made of metal or fiber reinforced plastic, with holes all around. Larger ones can use a chamber filled with pellets and a nozzle at the exit. This is used in intermediate size tactical motors. Very large motors use pyrogen system. This is a small rocket motor within a large rocket motor. The igniter motor itself has another ignition assembly. The exit of such a motor can have several jets located at different angles to enable the hot igniter jets to impinge on the propellant surface at different locations. One of the key elements of the ignition train is called a squib. It receives an electric current of suitable magnitude, transfers the energy to a primer or heat sensitive explosive. Typical compounds are Mercuric fulminate or Lead azide. Other details of the ignition system are discussed in Chapter 9.

7.8 Fuels and Oxidizers for Liquid Rockets

Liquid propellants are classified in several ways: (a) Monopropellants and Bipropellants. Amongst bipropellants, the classification is , (i) Hypergolic (self-igniting) or non-Hypergolic, and (ii) Storable or Cryogenic. Much research and development has gone into the choice of the propellants over the last six decades and in the early stages, many propellant combinations were tried out. However, only some combinations have remained in use for long time till recent times. These are the subject of consideration here.

7.8.1 Monopropellants

Monopropellants by definition are those liquids that have both oxidizer and fuel elements in their molecular structure and/or are in an unstable state that on initiation – catalytically or thermally, they decompose exothermically to gases. Two monopropellants that have been used for a long time are, hydrogen peroxide (H_2O_2), belonging to the first category and Hydrazine (N_2H_4), belonging to the second category. Hydrogen peroxide was used in early space missions, like Mercury, but abandoned later due to problems of thermal sensitivity in storage and handling in favor of hydrazine. When hydrazine is sprayed over a noble metal catalyst, it decomposes exothermically. The development of the catalyst has taken place in many countries like the USA, France, Germany and India. The only catalyst favored by satellite designers (who have the need to build control thrusters based on Hydrazine that need to operate for more than a hundred thousand cycles and for as long as seven to ten years in space) is the one made by Shell com-

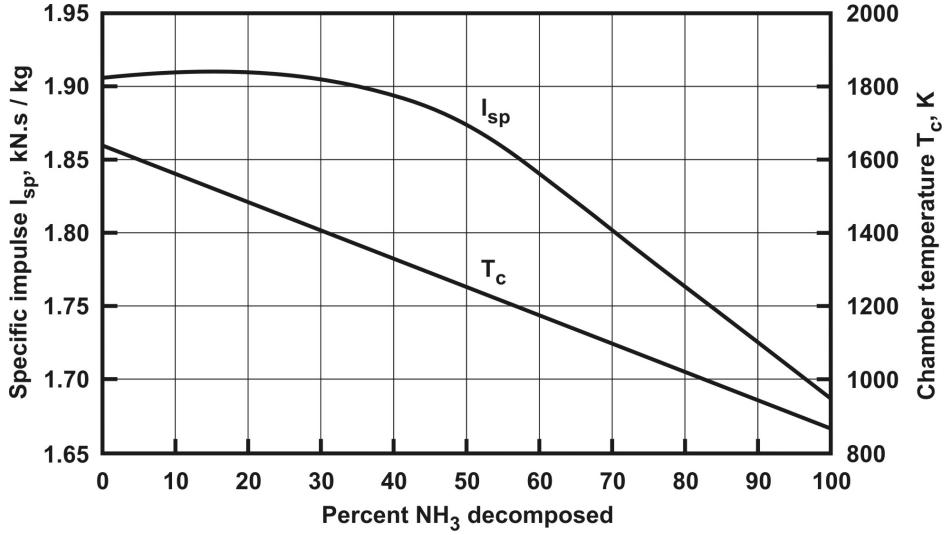

Figure 7.10: The specific impulse and the adiabatic temperature as a function of % Ammonia decomposed

pany, USA. This catalyst is based on porous alumina particles – 2 to 10 mm size on which iridium coating is provided by chemical vapor deposition or other techniques. These are extensively used in the thrusters – 3 mm dia to 20 mm dia to generate thrust of 1 N to 50 N. Its decomposition is characterized by the following chemical equation.

$$\mathrm{N_2H_4} \rightarrow \alpha_\mathrm{d}\mathrm{NH_3} + (1 - \frac{\alpha_\mathrm{d}}{2})\mathrm{N_2} + (2 - \frac{3\alpha_\mathrm{d}}{2})\mathrm{H_2} \tag{7.13}$$

If α_d = 4/3 implying that the products are NH_3 and N_2 only, the heat liberated leads to flame temperature of 1649 K. If dissociation goes to equilibrium implying that N_2 and H_2 are the only products, then the flame temperature is only 867 K. Since the residence time in the thruster is about 3 to 5 ms, and NH_3 decomposes slowly, the performance of a monopropellant thruster is governed by the fraction α_d in the chemical equation (7.13). Figure 7.10 shows the specific impulse and adiabatic flame temperature as a function of Ammonia decomposed (note that α_d = (4/3) [1 - fraction decomposed]). One can notice that at 20 to 40 % Ammonia decomposition, one gets the best performance of I_{sp} = 1900 N.s/kg. Hydrazine can also be used as a fuel in bipropellant rockets; it has been used in 50:50 proportion with unsymmetrical dimethyl hydrazine (UDMH).

7.8.2 Bipropellants

A brief description of the propellants can be found in section 1.14. The oxidizers available are

(a) WFNA (White fuming nitric acid – 98 % HNO_3 + 0.5 % NO_2 + rest water), (b) RFNA (Red fuming nitric acid – 82 % HNO_3 + 15 % NO_2 + rest water), (c) NTO (Nitrogen dioxide, N_2O_4), (d) MON (Mixed oxides of nitrogen – NO with NTO in different proportions), all of which are considered "earth storable", and (e) LOX (Liquid Oxygen, O_2) is a cryogenic oxidizer requiring thermal insulation.

The oxidizers (a) to (d) all can be hypergolic with a number of fuels, implying that they are self-igniting and therefore the rocket engines do not need any ignition system.

The fuels used are

(i) Xylidine, Triethyl amine [$(C_2H_5)_3N$] and mixtures, (ii) MMH (Monomethyl hydrazine, CH_3 $NH.NH_2$), (iii) UDMH [$(CH_3)_2NNH_2$] and mixtures with hydrazine, (iv) Kerosene (RP series similar to JP series in air breathing engines), all of which are earth storable and the liquids in (i) and (ii) are hypergolic with the oxidizers (a) to (d). Kerosene is not hypergolic with any of the oxidizers noted above. (v) LH_2 (Liquid hydrogen,) is a cryogenic fuel. It is not hypergolic with LOX with which alone it is used.

RFNA is very corrosive. One strategy adopted is to passivate it by dissolving about 0.5 to 0.8 % of hydrofluoric acid (HF) so that this very reactive compound reacts with the surface and forms a thin coating of a fluoride compound preventing further corrosive action. Such a RFNA is termed IRFNA – implying Inhibited RFNA.

Thus, the propellant combinations can be

(i) Xylidine/Triethyl amine (also called g-fuel) with IRFNA, (ii) UDMH with IRFNA, (iii) UDMH with NTO, and (iv) MMH with NTO (these are storable hypergolic systems), (v) Kerosene with LOX (semi-cryogenic, non-hypergolic system) and (vi) LH_2 with LOX (full cryogenic system). These are perhaps the most used combinations.

Some thermodynamic properties of these liquids are presented in Table 7.15 and 7.16. The boiling point characterizes the storability of the propellant. As can be noted excepting LO_2 and LH_2, other liquids have a boiling point at atmospheric temperature or much above. The lone exception of nitrogen tetroxide whose boiling point is 21°C is stored under pressure and/or by maintaining the temperature below 15°C. This characteristic prevents its use in prepackaged storable propulsion systems for missile use. Only IRFNA can be used for such applications. While the fuels triethyl amine and xylidine were being used in the early developments

Table 7.15: Properties of selected liquid propellants, (TEA = Triethyl amine, ρ_p = Density, BP = Boiling point, $\mathscr{L}$ = Latent heat of vaporization, T_{cr} and p_{cr} are the critical temperature and pressure)

Propellant	Formula	ρ_p kg/m^3	BP °C	$\mathscr{L}$ MJ/kg	T_{cr} °C	p_{cr} atm.
Fuels						
TEA	$C_6H_{15}N$	600	89	0.54	262	30
Xylidine	$C_8H_{11}N$	750	213-226	0.38	441	40
Hydrazine	N_2H_4	1010	113	1.40	380	145
MMH	CH_3NHNH_2	900	87	0.68	275	78
UDMH	$C_2H_8N_2$	790	63	0.58	249	60
RP 1	$CH_{1.95}$	800	170-260	0.2 - 0.3	414	21
Oxidizers						
IRFNA	Mixture	1540	65	1.10	225	55
NTO	N_2O_4	1450	21	0.41	158	100
LH_2	H_2	70	- 253	0.45	- 240	13
LOX	O_2	1140	- 183	0.22	- 119	49

of rocket engines in Germany (in the World war II period) and this reached the former USSR and was used in the surface-to-air missiles they developed, the specific impulse of this system (typically 2.25 to 2.3 kN s/kg) is easily exceeded by high energy solid composite propellants developed in the last thirty years. Military demand for little operational attention to the missile hardware and as well as instant readiness without having to fill up the propellants has generally resulted in favoring solid propulsion systems particularly when the advantage of lower volume and weight are better promised by solid propulsion systems (due to equal or higher specific impulse and certainly higher density impulse). The RFNA - UDMH combination can still be promising for smaller tactical systems. The critical temperature and pressure are relevant since the operating pressure of the rocket engines is larger than the critical pressure in many cases. In such situations, the liquids injected into the combustion chamber could behave like a puff of gas instead of having a liquid-to-solid interface with the associated features of heat absorption due to vaporization. The heat of vaporization of many of the liquids is much smaller than of water ($\mathscr{L}$ for water = 2.3 MJ/kg). Other properties like specific heat, viscosity and conductivity influence the cooling properties of propellants. Specific heat controls the temperature rise in the liquid state. For instance, MMH is superior to Xylidiene in terms of heat absorption capacity. Of course, liquid hydrogen is the best of all the fluids in this respect.

The performance of several propellant combinations calculated using the pro-

Table 7.16: Properties of selected liquid propellants, (c_p = specific heat, μ = Viscosity in centipoise, ΔH_f = Heat of formation (at 298.16 K unless otherwise stated)

Propellant	c_p kJ/kg K	μ cP	k W/m K	σ N/m	ΔH_f MJ/kg-mole
Fuels					
TEA	2.1	0.58	0.156	0.028	-99.6
Xylidine	1.8	0.62	0.111	0.032	-90.3
Hydrazine	3.2	0.97	0.209	0.063	+50.3
MMH	3.0	0.40	0.145	0.050	+54.8
UDMH	2.7	0.75	0.156	0.045	+51.6
RP 1	1.9	0.21		0.04-0.05	-159.2
LH_2	9.3	0.01	0.065	0.002	-7.9 (at 20 K)
Oxidisers					
IRFNA	1.7	0.50	0.256	0.040	-200.7
NTO	1.5	0.42	0.628	0.071	-19.6
LOX	1.6	0.19	0.025	0.013	-12.9 (at 90 K)

gram of NASA SP-273 is presented in Table 7.17. This table shows the performance of several propellant combinations at selected mixture ratios. The choice of the propellant combinations presented in the table is made on the basis that these could be contemplated for use even today. For tactical storable combination, RFNA-UDMH stands out because of its performance – stage performance (in-flight) of 2350 N s/kg for near-optimum expansion is realisable. Replacing RFNA with NTO improves the performance clearly by about 100 N s/kg on optimum expansion basis. Its use is more appropriate for space applications where the idea of storability has a different connotation. The system is not expected to allow on-board storage except during the launch period. Further, its use in upper stages implies that one expects the performance in terms of vacuum impulse. Realised stage performance in flight for engines with high chamber pressure and higher nozzle expansion ratio than is presented here is about 3200 N s/kg. Monomethyl hydrazine got introduced into the propellant system because of its superior handling characteristics and better heat transfer characteristics than hydrazine even though its performance with NTO is slightly inferior. Of course, it cannot replace hydrazine as a monopropellant because as a monopropellant, hydrazine is superior due to the possibility of catalytic decomposition. The choice of LOX – RP1 (made in the early sixties for the F-1 engine that powered the Saturn rockets in the man-to-moon mission of the USA) was based on the combined performance-cost criterion. This combination had a high performance (the specific impulse can be seen to be larger than other storable liquids) but the lowest possible cost. Typically, the cost

ratio between NTO – UDMH and LOX – RP1 for obtaining a fixed impulse would be 50 to 100 even if allowance is made for variation in costs in different countries at different times. The cost of the development of the F 1 engine that burns about 18 tonnes of propellant for 120 s was determined to be controlled by the cost of the propellants as it was estimated that about 1000 tests of full duration equivalent would be needed before the engine was accepted as developed. The use of LOX – LH_2 as a propellant combination for upper stages was considered an inevitable choice even with the low density of this combination because any increase in the specific impulse in the upper stage would directly affect the mission payload. As can be noted from the Table 7.17, the volume based O/F (oxidizer-to-fuel) ratio is lower than the weight based O/F because the fuel density is generally lower than the oxidizer density (see Table 7.15). The average density of the propellant combination is the measure of the relative volume for the propellants.

The difference between the equilibrium specific impulse and frozen specific impulse is about 50 to 150 N s/kg and the vacuum specific impulse is 200 to 300 N s/kg more than the equilibrium value at 70 atm. pressure and optimum expansion to 1 atm. The vacuum specific impulse is the relevant quantity for operation in space. The nozzle area ratio used for constructing the table is such as to allow for a pressure ratio, p_c/p_e = 70. The specific impulse values have an increasing trend with the choice of propellants indicating to the increase in the energetics of the propellants. The average density, $\bar{\rho}_p$ is about 1200 kg/m^3 for all combinations except LOX-LH_2 combination for which the density is only about a quarter of the storable combinations. Consequently, the density impulse is also a third of those for storable combinations. Thus, for tactical and booster applications, storable combinations are preferred. For upper stages where specific impulse plays a major role, the full cryogenic combination LOX-LH_2 is preferred.

It is interesting to appreciate the role of chamber pressure on the chamber properties and the specific impulse values for various fuel-oxidant mixtures. As can be noted from Tables 7.18 and 7.19, increase in the operating pressure allows the realization of high performance – raising p_c from 30 to 100 atm increases the equilibrium optimum specific impulse by 10 to 15 % and most of it due to nozzle expansion process (the change in c^* over this pressure range is about 0.6 %). The high performance of LOX – LH_2 is due to the the very low molecular weight of the gases. Even though the chamber temperature drops by 10 %, the molecular weight drops by more than a factor of 2.

The variation in the composition of the gases at chamber conditions for two propellant combinations is shown in Table 7.20. The choice of higher O/F implies lower CO, H_2 and higher values of O, O_2, CO_2, and H_2O. The values of OH, H and NO will increase with O/F because of the realization of higher temperatures that encourage dissociation.

Table 7.17: Performance of liquid propellant combinations at p_c = 70 atm. (* = kg/m^3 for $\bar{\rho}_p$, $I_{sp,eo}$, $I_{sp,f}$ and $I_{sp,e,v}$ are the specific impulse under equilibrium and frozen optimal expansion to 1 atm and vacuum conditions respectively all in N s/kg, *** = kNs/m^3 for $\bar{\rho}_p I_{sp,eo}$)

Propellants	O/F Wt.	O/F Vol	$\bar{\rho}_p$ *	$I_{sp,eo}$ **	$I_{sp,f}$ **	$I_{sp,e,v}$ **	$\bar{\rho}_p I_{sp,eo}$ ***
RFNA - UDMH	3.35	1.72	1250	2615	2500	2842	3269
	2.92	1.50	1240	2620	2546	2832	3248
NTO - UDMH	3.06	1.67	1203	2776	2605	3028	3340
	2.61	1.42	1177	2815	2667	3053	3313
NTO - MMH	2.50	1.55	1234	2804	2638	3055	3460
	2.16	1.34	1215	2836	2698	3073	3445
LOX - RP 1	2.73	1.91	1023	2943	2764	3213	3010
	2.00	1.40	998	2862	2789	3085	2862
LOX - LH_2	6.00	0.37	359	3767	3620	4086	1352
	4.00	0.25	284	3842	3800	4131	1091

Table 7.18: Performance variation of RFNA – UDMH and NTO – UDMH at specific mixture ratio with chamber pressure with optimum expansion to 1 atm.

	RFNA – UDMH, O/F = 2.92				NTO – UDMH, O/F = 2.61			
p_c atm.	T_c K	$\mathscr{M}$ g/mole	c^* m/s	$I_{sp,eo}$ N s/kg	T_c K	$\mathscr{M}$ g/mole	c^* m/s	$I_{sp,eo}$ N s/kg
30	3012	24.1	1622	2413	3342	23.4	1668	2445
50	3048	23.6	1627	2544	3400	23.5	1722	2726
70	3070	23.6	1630	2621	3436	23.9	1728	2815
100	3094	23.6	1632	2695	3475	23.7	1733	2900
200	3135	23.7	1637	2820	3549	23.8	1743	3044

Table 7.19: Performance variation of LOX – RP1 and LOX – LH_2 at specific mixture ratios with chamber pressure with optimum expansion to 1 atm.

	LOX – RP1, O/F = 2.73				LOX – LH_2, O/F = 4.0			
p_c atm.	T_c K	$\mathscr{M}$ g/mole	c^* m/s	$I_{sp,eo}$ N s/kg	T_c K	$\mathscr{M}$ g/mole	c^* m/s	$I_{sp,eo}$ N s/kg
30	3583	23.7	1719	2524	2931	9.95	2427	3561
50	3660	24.0	1777	2840	2951	9.95	2429	3739
70	3711	24.3	1785	2943	2963	9.97	2431	3842
100	3766	24.5	1792	3044	2974	9.97	2433	3902
200	3873	24.7	1806	3219	2992	9.98	2434	4105

Table 7.20: Adiabatic composition of combustion of liquid propellants, X_i = Mole fraction, $\mathscr{M}$ in g/mole, I_{sp} in N.s/kg

	NTO – UDMH			LOX – LH_2		
O/F	3.06	2.61	1.53	8.0	6.0	4.0
T_f, K	3424	3436	2779	3610	3500	2963
X_i						
CO	0.089	0.125	0.223	-	-	-
H_2O	0.342	0.349	0.222	0.743	0.660	0.492
H_2	0.034	0.059	0.274	0.115	0.253	0.492
CO_2	0.114	0.092	0.026	-	-	-
N_2	0.294	0.289	0.249	-	-	-
OH	0.050	0.040	0.001	0.094	0.044	0.004
H	0.011	0.015	0.005	-	0.035	0.012
NO	0.020	0.012	-	-	-	-
O	0.009	0.006	-	0.014	0.004	-
O_2	0.037	0.013	-	0.034	0.004	-

7.9 Fuels and Oxidizers for Hybrid Rockets

The fuels and oxidizers for hybrid rockets are based on those meant for solid and liquid rockets. Thus, the fuels that can be used are polymeric binders and the oxidizers can be RFNA, NTO and LOX. The polymeric fuels can easily be cast into whatever form required by the same kind of process that is used for making a solid propellant. Spraying the liquid oxidizer on to the surface of the fuel block after suitable ignition process is initiated will maintain the combustion process. The reverse combination namely, solid oxidizer and liquid fuel is not chosen since the structural integrity of the block made of solid oxidizer powder is unacceptable.

One of the principal problems found in the choice of polymeric fuel-liquid oxidizer combination is that the average regression rate of the solid fuel is about 1 to 3 mm/s even with large oxidizer mass flux through the port. Even if the initial regression rate is acceptable, the regression rate will keep going down since the port mass flux keeps decreasing due to increase in port area. These imply that the aspect ratio of the fuel block (L/D, length-to-diameter ratio) to be chosen should be large and this has direct impact on the the vehicle sizing. Large L/D has problems of stability and structural integrity and is not favored. To alleviate this problem, some oxidizer loading in the fuel is considered acceptable so that the regression rate is enhanced. Typical loadings of 25 to 35 % AP in HTPB would make the "fuel block" non-self deflagrating, but have regression rates of 5 to 7 mm/s. Some of these developments have not taken place in reality because most requirements of propulsion have been taken care of by solid or liquid rocket systems.

7.10 Summary

This chapter has been devoted to the characteristics of fuels and oxidizers used in aeronautical and space vehicles or missiles. Equilibrium composition of any fuel-oxidizer combination at a fixed pressure and temperature is *dependent on the elemental composition and not on the chemical structure*. Flame temperature of the same fuel-oxidizer combination at any fixed pressure is controlled by the structure of the compounds and their enthalpy (heats of formation). Small changes in composition imply small changes in flame temperature and final composition. As different from this, characteristics like burning rate and dependence on ambient pressure and temperature, particularly in solid rocket propellants are dependent on chemical kinetics and transport properties in the gas phase and small changes in composition can imply large changes in burn rate. This sensitivity is exploited to change the properties (like burn rate) substantially by the addition of small amounts of chemical compounds while leaving thermodynamic properties (like flame temperature and specific impulse) unaltered virtually.

An important point to keep in mind is that the sensitivity of solid propellants to chemical kinetic features makes the solid propulsion system far more demanding in terms of quality control than liquid rockets or hybrid rockets; this is not adequately recognized in literature. Solid propulsion systems could be working wonderfully for many launches. But a new batch of propellants loaded into the system could generate instability. To trace back the precise components responsible for this behavior is an uphill task and the solutions are neither very elegant nor well understood so as to state that the true problem has been traced and resolved. Liquid propulsion systems seem complex with lots of plumbing, control elements, turbo pumps and thrust chamber with intricate cooling passages. Since the dynamics is controlled by fluid flow and well understood mechanical engineering, even the complex systems perform with precision, and even if they do not, the fixes are clear and much better understood.

Chapter 8

Rocket Combustion Processes

8.1 General Combustion Features

The two extremes of combustion processes are (a) premixed and (b) diffusion. Most combustion phenomena fit into one of these extremes. In premixed flames, the fuel and oxidizer elements are mixed earlier to combustion and in diffusion mode of combustion, the fuel and oxidizer diffuse into each other at the flame. The classification applies to gaseous, liquid and solid combustion processes.

Combustion of gaseous methane-air mixture, decomposition of liquid monopropellants like hydrazine, and hydrogen peroxide and combustion of solid monopropellants like AP, HMX and homogeneous solid propellant (DB propellant) all constitute combustion with premixed flame structure.

Gaseous fuel jet flames, liquid droplet vaporization and combustion in gas turbines, liquid bipropellant rockets, solid composite propellants all are totally or partially diffusion dominated in their combustion behavior.

8.1.1 Premixed Combustion

Gaseous premixed flames are characterized by the speed at which a flame travels into a fuel-oxidant mixture. This quantity is called "Burning velocity". Figure 8.1 shows the gaseous premixed flame (a) and solid propellant combustion (b). The difference between the two lies in the fact that in case (b), there are two phases – gas and solid connected by an interface and the gaseous combustion process is initiated by the volatilization of the solid fuel and oxidizer elements into the gas phase because of the heat transferred from the gaseous flame. This is represented

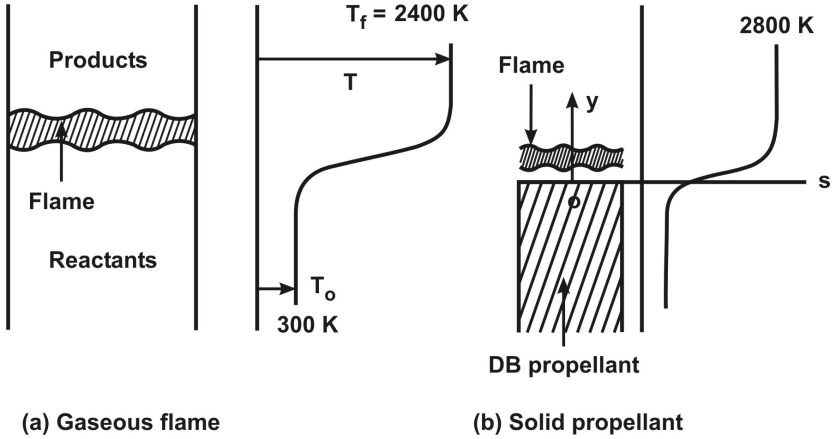

Figure 8.1: The structure of a gaseous premixed flame (a) and homogeneous solid propellant combustion (b)

by

$$q_g'' = k\frac{dT}{dy}]_{0^+} = k\frac{dT}{dy}]_{0^-} + \rho_p \dot{r} \Delta H_s \tag{8.1}$$

In the above equation the heat flux from the gas phase, q_g'' (given by the product of conductivity and the temperature gradient in the gas phase) is balanced by the sum of the heat flux in the condensed phase and the flux due to heat of phase change at the surface. If one solves the conduction equation in the condensed phase (assuming insignificant condensed phase reactivity, a fact that is generally valid excepting very close to the surface), one gets $kdT/dy]_{0^-} = \rho_p \dot{r} c_p (T_s - T_o)$ where T_s and T_o are the surface and deep bed temperatures of the propellant.

If we now rearrange the above equation we get

$$q_g'' = k\frac{dT}{dy}]_{0^+} = \rho_p \dot{r}[c_p(T_s - T_o) + \Delta H_s] \tag{8.2}$$

This equation can be turned around and stated as

$$\rho_p \dot{r} = k\frac{\frac{dT}{dy}]_{0^+}}{[c_p(T_s - T_o) + \Delta H_s]} \tag{8.3}$$

The gas phase flux can be expressed as $[dT/dy]_{0^+} \sim (T_f - T_s)/\delta_g$ where T_f is the flame temperature and δ_g is the gas phase flame thickness, a thickness over which the temperature rises from a value at the surface to that at the flame. Classical premixed flame analysis using asymptotic analysis indicates that near the flame zone, the conduction and reaction terms balance each other. This implies

$$k\frac{(T_f - T_s)}{\delta_g^2} = H_c\overline{\dot{w}'''} \tag{8.4}$$

If we invoke the heat balance $c_p(T_f - T_s) = H_c$, we can write

$$\delta_g = \sqrt{\frac{k}{c_p}\overline{\dot{w}'''}} \tag{8.5}$$

We recognize that $\overline{\dot{w}'''} \sim p^{n_r}exp(-E_g/RT_f)$, where E_g is the gas phase activation energy and n_r is the reaction order. The reaction order, n_r is 1 for monomolecular reaction or a reaction with one reactant much in excess compared to the other, 2 for all bimolecular reactions. We can write now the result as

$$\rho_p\dot{r} = \frac{c_p(T_f - T_s)}{[c_p(T_s - T_o) + \Delta H_s]}\sqrt{\frac{k}{c_p}p^{n_r}exp(-E_g/RT_f)} \tag{8.6}$$

We can represent the non-dimensional enthalpy ratio that constitutes the ratio of thermal potential in the gas phase to the heat required to maintain the thermal profile in the condensed phase including the surface heat of phase change by a transfer number, $B = c_p(T_f - T_s)/[c_p(T_s - T_o) + \Delta H_s]$. The burn rate equation can be expressed by

$$\rho_p\dot{r} = Bp^{n_r/2}exp(-E_g/2RT_f)\sqrt{\frac{k}{c_p}} \tag{8.7}$$

A more careful analysis invoking the solution of the conservation equation in the gas phase leads to

$$\rho_p\dot{r} = ln(1 + B)p^{n_r/2}exp(-E_g/2RT_f)\sqrt{\frac{k}{c_p}} \tag{8.8}$$

The two equations (8.7) and (8.8) differ in the term involving the transfer number. For small transfer number they are about the same. These equations indicate clearly that the pressure index of burn rate is $n = n_r/2$. For n_r between 1 and 2, the pressure index is between 0.5 to 1.0. If one examines the Table 7.14, the pressure indices of propellants that qualify for premixed flame structure are the range of 0.6 to 0.83. This shows that the phenomenology related to double base propellant combustion is controlled by chemical kinetics.

The dependence on initial temperature expresses itself through the transfer number, B and the variation of flame temperature with the initial temperature of the propellant. In the above equations, the surface temperature is an unknown quantity. For pure substances, the phase transition temperature has a thermodynamically defined fixed value. For more complex substances like polymers, the phase transition occurs through a decomposition process that in itself

is temperature dependent. Consequently, it is usually not an equilibrium phenomenon like vaporization. It is a rate process. This is expressed in terms of $\rho_p \dot{r} = A_s exp(-E_s/RT_s)$, called the pyrolisis rate law, where E_s is the activation energy of pyrolisis. Since there are two expressions for $\rho_p \dot{r}$, they must lead to the same result. Therefore,

$$\rho_p \dot{r} = B p^{n_r/2} exp(-E_g/2RT_f) \sqrt{\frac{k}{c_p}} = A_s exp(-E_s/RT_s) \tag{8.9}$$

One can extract the temperature sensitivity of burn rate, σ_T from the above expression, if we evaluate

$$\sigma_T = \frac{dln(\rho_p \dot{r})}{dT_o} = \frac{E_s}{RT_s^2} \frac{dT_s}{dT_o} \tag{8.10}$$

from the above equation as

$$\sigma_T = \left[\frac{\Delta H_s}{c_p} + T_s - T_o \right]^{-1} \left[1 + \frac{RT_s}{E_s} \frac{T_s}{(T_f - T_s)} - \frac{c_p T_s}{[c_p(T_s - T_o) + \Delta H_s]} \right]^{-1} \tag{8.11}$$

If we now use typical values for various parameters, c_p = 1.2 kJ/kg K, T_f = 3000 K, T_s = 700 K, T_o = 300 K, ΔH_s = 400 kJ/kg, E_s/R = 8000 K, we obtain σ_T = 0.71 % /K. This value is typical for several propellants as observed in Table 7.14. The relative role of various parameters can also be noted from the above expression. The data of one propellant on the burn rate vs. initial temperature is presented in Figure 8.2 taken from Suh et al [66]. The initial temperature dependence is σ_T = 1 % / K. This value is in the upper limit of the temperature sensitivity. The figure has another interesting feature. It can be noticed that the burn rate has a tendency to rapidly increase at around 145°C. This implies that when every part of the propellant is at this temperature, all parts of it burn up without waiting for the conduction processes to bring up the specific location to the temperature needed for combustion as will happen normally (for instance, propellant at 300 K). This temperature is the *auto-ignition temperature* of the propellant and is indicative of the reactivity of the substance.

8.1.2 Diffusive Mode Combustion

It is simple to begin by examining a gaseous jet flame – like from a Bunsen burner as in Figure 8.3 (i). We evaluate the height of the diffusion flame (h) as a prelude to obtaining the burn rate of a solid propellant in diffusion mode. The flame climbs to the height, h because the oxygen in the ambient atmosphere has to diffuse to the flame on the other side of which the fuel arrives by convection. Since the combustion process occurs at an oxidizer-to-fuel ratio corresponding to stoichiometric proportions, the ratio of oxidizer flow into the flame to the fuel flow rate must be in stoichiometric proportions (s = stoichiometric ratio). The oxidizer flow is the

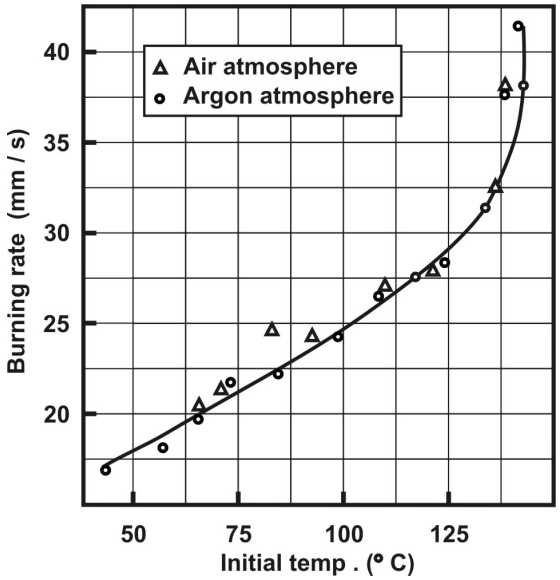

Figure 8.2: The burning rate of a homogeneous propellant with initial temperature taken from [66]

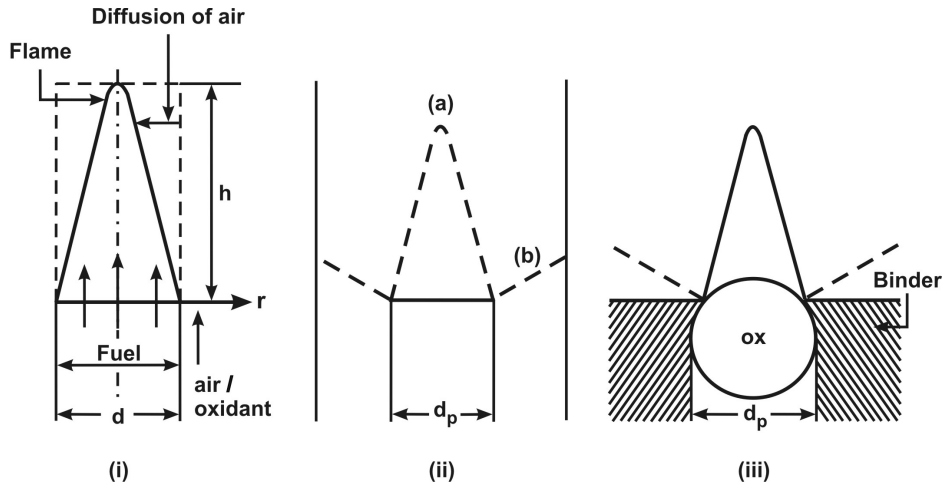

Figure 8.3: The diffusive combustion mode (i) and (ii); Equivalent solid propellant combustion system (iii)

product of the diffusion flux and the peripheral area through which this occurs. This gives $\dot{m}_{ox} = \pi dhD\rho dY_{ox}/dr$. We can combine this with the fuel flow rate to give

$$\frac{\dot{m}_{ox}}{\dot{m}_f} = s = \frac{\pi dhD\rho}{\pi(d^2/4)U_f}\frac{Y_{ox,\infty}}{(d/2)} \tag{8.12}$$

Where $\dot{m}_{ox}$ is the oxidizer mass flow rate, $\dot{m}_f$, the gaseous fuel flow rate, d is the diameter of the duct carrying the fuel gas, D is the diffusion coefficient, $Y_{ox,\infty}$ is the oxidizer mass fraction in the ambient atmosphere. This equation can be recast into

$$h = s\dot{m}_f/[2\pi Y_{ox,\infty}D\rho] \tag{8.13}$$

$$h/d = sReSc/8Y_{ox,\infty} \tag{8.14}$$

where $Re = 4\dot{m}_f/\pi d\mu$ and $Sc = \mu/D\rho$. A rigorous calculation yields the same result with the constant in the denominator of equation (8.14) changed from 8 to 48. Since the quantity $D\rho$ is independent of pressure, Equation (8.14) shows that the height of the diffusion flame is independent of pressure at fixed $\dot{m}_f$.

Figure 8.3 (ii) shows the case with the fuel flow surrounded by the flow of oxidizer. The specialty of this situation is that depending on the stochiometric ratio, an enclosed flame called over-ventilated flame may be located over the inner tube or get located in the outer tube, a mode called under-ventilated flame as shown in Figure 8.3 (ii). Now one can consider the configuration identified in Figure 8.3 (iii) in which a solid particle is surrounded by the polymerized fuel like in a composite propellant. A heat flux balance at the surface is applied without distinguishing between the fuel and the oxidizer to get equation (8.2). Now, the gradient in the gas phase is written as $dT/dy \sim (T_f - T_s)/\delta_{g,diff}$. Then $\delta_{g,diff}$ is identified with the height of the diffusion flame and hence, we can write,

$$\rho_p\dot{r}[c_p(T_s - T_o) + \Delta H_s] \sim k\frac{(T_f - T_s)}{h} \sim k\frac{(T_f - T_s)}{(s\ \dot{m}_f/2\pi Y_{ox,\infty}D\rho)} \tag{8.15}$$

We now note that $\dot{m}_f = \rho_p\dot{r}(\pi/4)d_p^2$, where d_p is the particle size of the oxidizer. We can now simplify the above equation into

$$\rho_p\dot{r} \sim \frac{k}{c_p}\ \frac{1}{d_p}\ \sqrt{8\frac{B}{s}Y_{ox,\infty}} \tag{8.16}$$

where $B = c_p(T_f - T_s)/[c_p(T_s - T_o) + \Delta H_s]$ is the transfer number. In the equation (8.16), the surface temperature, T_s and ΔH_s depend on pressure; but the dependence of ΔH_s on pressure is weak and T_s occurs both in the numerator and the denominator in a manner that the effective variation is marginal. Thus, the burn rate of the diffusion controlled combustion is independent of pressure. The burn rate is strongly dependent on the particle size. Decrease of the particle size increases the burn rate. Physically this can be understood in the following manner.

For unit cross section, a smaller particle size implies better O/F ratio locally and hence, the heat release in the gas phase and consequent heat transfer to the surface are enhanced. This leads to higher burn rate. This is in fact the case.

Composite propellants based on AP have diffusion controlled combustion and hence, show lower pressure indices compared to double base propellants. Also composite modified double base propellants with significant amount of AP will show a similar behavior. An observation of Table 7.14 shows that CMDB1 (DB1 with AP) drops the pressure index from 0.72 (for DB1) to 0.4. Composite propellants when burning at low pressures show a behavior similar to premixed propellants. The reason for such a behavior is as follows. The diffusion coefficients depend inversely on pressure and hence, the tendency for fuel and oxidizer vapors to mix faster is higher. Added to this, the reaction rates are lower at lower pressures (varying like p^2). Hence, even though the fuel and oxidizer are in "unmixed" mode, the rate processes get arranged in a manner that the flame is premixed. Thus, for composite propellants, the pressure dependence will be higher at very low pressures and lower towards higher pressures (i.e., the presssure index decreases with increase in pressure).

8.2 Combustion Mechanism of Solid Propellants

8.2.1 DB Propellants

Figure 8.4 describes the processes in the combustion of double base propellants. Double base propellants have a distinctive mode of combustion. They burn with a frothy surface with a flame located with a stand-off from the surface. The frothy surface is the one where some condensed phase reactions will take place. This zone is termed fizz zone. The zone between the surface and the flame is called dark zone. Much effort has gone into clarifying the processes that go on in various zones. In the fizz zone, the NO_2 bonds in nitro compounds (both NC and NG) break down into NO, CO, CO_2 and H_2. The conversion of NO is slow and hence, a certain residence time and distance are required before further heat release occurs. This zone constitutes the dark zone. The flame zone is one in which the exothermic heat release processes occur in significant measure. The thicknesses of the dark and flame zones vary strongly as a function of pressure, because the heat release processes are strongly reaction rate dependent and reaction rate varies strongly with pressure. Increase in pressure causes increase in burn rate. The pressure dependence of dark zone and flame thicknesses for DB1 are $\delta_{dark} \sim 0.02(70/p)^{1.5}$ mm and $\delta_{flame} \sim 0.01(70/p)^{1.3}$. Thus, when a propellant is burnt at ambient pressure the dark zone thickness is about 10 mm. Because of this property, it is possible to burn a DB propellant in a flame-less combustion mode – if a thin red hot cinder is brought into contact with the surface of a double base propellant, it will have

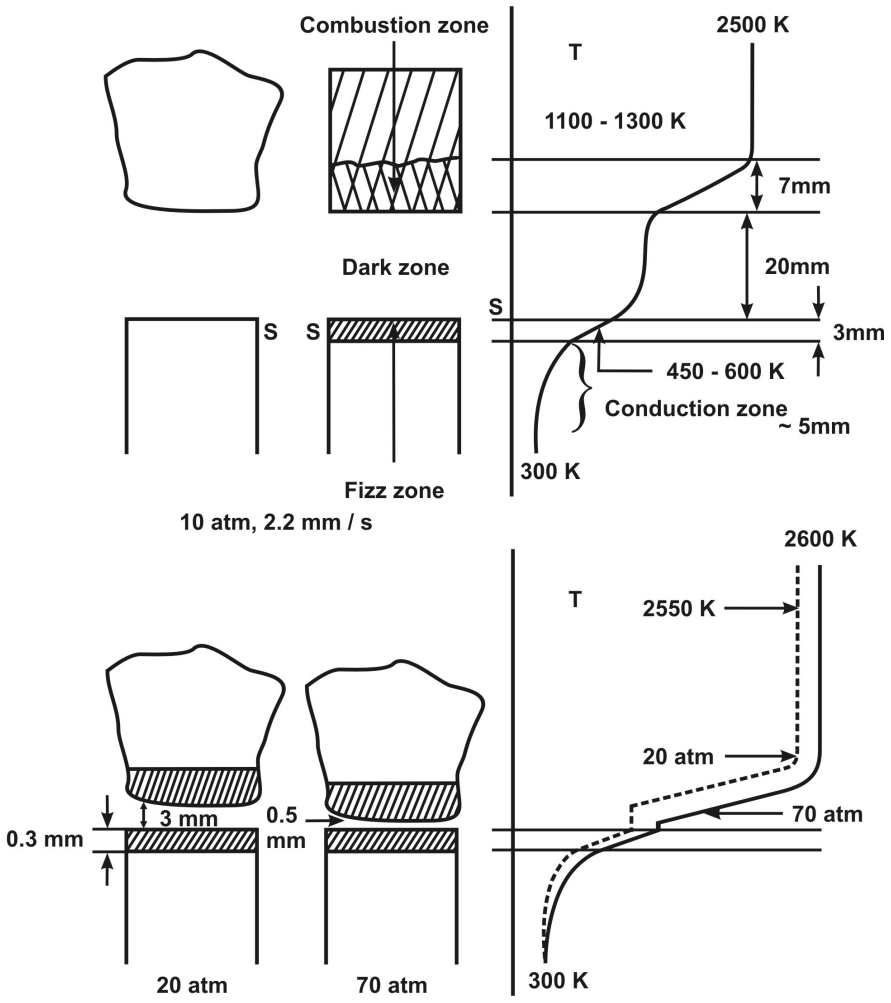

Figure 8.4: The combustion features and the temperature profiles in a double base propellant

a dancing surface combustion without a gaseous flame. It is possible to obtain a gaseous flame if one ignites the products of combustion suitably. The slow conversion processes near the surface of a burning DB propellant can be energized through the use of suitable additives. Such an addition has been found to catalyze the reactions in the fizz zone raising the heat flux into the solid and hence, increase the burn rate of the propellant. This is called super burn rate phenomenon. This effect is dominant over a pressure range and beyond this range the effective reaction cycle in the fizz zone reaches an equilibrium leading to a condition not different from the un-catalyzed propellant.

8.2.2 Composite and CMDB Propellants

Composite propellants based on AP show a combustion behavior that has been explored a great deal because of their relevance. At the simplest scale, the combustion is conceived as the burning of a single AP particle surrounded by polymeric fuel with no interaction with other particles. Even this has sufficient complexity that understanding it has been considered essential before other complexities are resolved. The single particle combustion has three minimum flame structures – a diffusion flame at the interface between the fuel and the oxidizer particle, called the *primary diffusion flame, PDF*, a *premixed flame, APF* above the oxidizer, and a *final diffusion flame, FDF* between the products of combustion of oxidizer particle and fuel vapors not participating in the primary diffusion flame. The heat transferred from each of the flames to the surface of the binder (or fuel) and the oxidizer causes the phase change from c-phase to g-phase by thermal degradation processes. The flames shown in Figure 8.3 (iii) illustrate a part of the description noted above. The primary diffusion flame can be an enclosed flame or open flame shown in dotted lines. Which one of these will occur depends on the stoichiometric ratio, s and the relative velocity from the oxidizer and the fuel surfaces. If s is large and fuel velocities are small, one gets an enclosed flame. If s is small and fuel velocity is larger, open flame will result. For axisymmetric configuration, it is possible to work out the structure of the flame.

The relative importance of the three flames with change in pressure can be qualitatively examined. For pressures below the low pressure deflagration limit (LPDL) of AP (about 20 atm at 300 K), one cannot expect self supported AP decomposition flame. Hence, the *PDF* is the most dominant one. As the pressure approaches the LPDL, the relative importance of the *FDF* and *APF* will improve. Beyond LPDL, AP decomposition process along with the *FDF* will become important. As pressure increases, the role of *FDF* will become more important. Studies on modeling have been developed along a well known approach known as BDP model (Beckstead-Derr-Price model) in solid propellant literature (see for a recent summary of the developments in this area, a paper by Cohen and Strand [47]). This approach has only been moderately successful in quantifying the importance

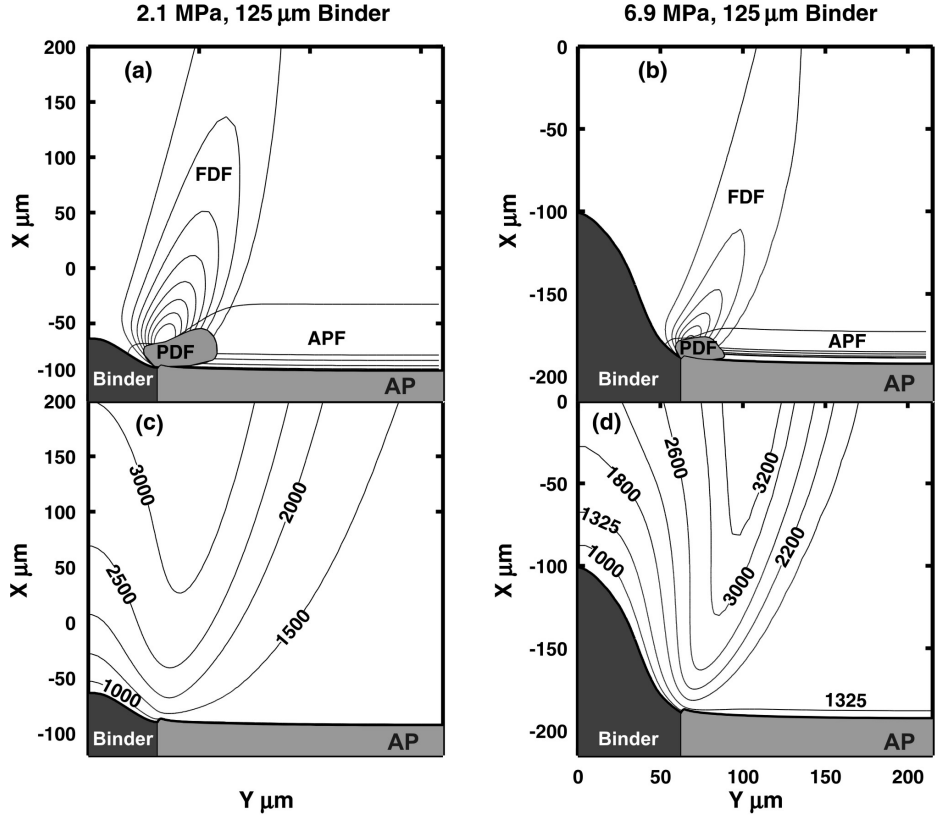

Figure 8.5: Gas Phase temperature contours (c,d) and reaction rate contours (a,b) for a pressure of 21 atm (a,c) and 69 atm (b,d) at a binder thickness of 125 μ m (half binder thickness 62.5 μ m). Position of the flames marked there off (primary diffusion flame shaded). At 21 atm (a) Final diffusion flame reaction rates 8500 (Inner Ring):1000 (Increment):500 (outer Ring) kg/m^3 s, Maximum primary diffusion flame reaction rate: 13000 kg/m^3 s and Maximum AP decomposition flame reaction rate :3.5 $\times 10^5 kg/m^3$ s.At 69 atm (b) Final diffusion flame reaction rates 5000 (Inner Ring):10000 (Increment):65000 (outer ring) kg/m^3 s, Maximum primary diffusion flame reaction rate:13000 kg/m^3 s and Maximum AP decomposition flame reaction: 3 $\times 10^6 kg/m^3$ s.

of processes in solid propellant combustion.

To understand the basic processes at a finer detail, studies on two-dimensional sandwiches have been carried out by several researchers. Figure 8.5 from a recent study by Ramakrishna et al [63] indicates the relative importance of the reaction rates of a burning sandwich at pressures of 21 and 69 atm. The behavior shown here is from calculations replicating many aspects of the combustion behavior of AP and AP-Polymer sandwiches quite satisfactorily.

One can use the mechanistic approach to predict the combustion behavior of say, ammonium nitrate – polymer propellants. Ammonium nitrate is a lower energy oxidizer compared to AP (it is not also a monopropellant – implying it does not burn by itself). One would expect lower burn rate compared to AP-Polymer propellants due to the low energetic character. Typically, the burn rate at 70 atm is about 2 mm/s with n = 0.6. The low burn rate implies a large flame thickness. This allows greater possibility of the mixing of the fuel and oxidizer elements and the combustion behavior approaches a premixed behavior. If this were not so, one would obtain a very low pressure index because the combustion behavior should be diffusion dominated (without the premixed flame associated with the self-deflagration character of AP).

The role of aluminum in the burn rate behavior needs to be understood. It has been determined that aluminum does not influence the burn rate at small fractions – of a few percent. At high loadings of 15 to 18 %, there is slight reduction in burn rate. The reason for the weak influence on burn rate is due to the fact that aluminum powder is quickly oxidized on the surface leading to the formation of aluminum oxide that melts only at high temperature – 2700 K. Hence, aluminum will act as an inert till it moves away from the surface of the propellant into the combustion zone where the aluminum oxide coating melts allowing the core aluminum to be oxidized. This heat release occurs far downstream and does not influence the heat transfer to the surface, excepting by radiation. These radiational effects are not significant for relatively small motors and corresponding propellant sizes and that is why the propellant burn rate gets reduced by the addition of aluminum. The reduction of burn rate at large loadings of aluminum arises from the replacement of reactive solid by relatively "passive" material (in terms of burn rate) to substantive extent. In large rocket motors, the radiational contribution partly offsets the reduction due to aluminum loading. Though from the burn rate view point, aluminum seems to have no role, it is worth repeating that its addition chiefly arises from the substantial contribution to the spoecific impulse that its addition causes.

The role of burn rate modifiers also needs explanation. The variety of burn rate modifiers is so much, and the effects are so particular to the chemical structure and dependent on the pressure range, that generalizations would not be possible. However, based on several studies it is inferred that the catalyst (a) does not affect the sub-surface activity and (b) but affects the reactions in the gas phase, more particularly the decomposition of perchloric acid that is generated consequent upon the decomposition of AP into $HClO_4$ and NH_3 [62]. An examination of Table 7.14 shows that with the addition of Ferric oxide (IO in the table), the pressure exponent n increases from 0.42 (at catalyst fraction = 0, row 7 in the table) to 0.54 (at catalyst fraction of 2 %, row 11). This is indicative of the gas phase reaction order increasing and hence, gas phase chemistry getting directly affected.

HMX based composite propellants function with a structure differing in many aspects compared to AP based CP. The observed flame structure shows a visible flame that stands off at a distance from the surface somewhat similar to the DB propellants with the zone (between the surface and the visible flame) decreasing with increase in pressure. HMX (or in fact RDX) is slightly fuel rich with a high flame temperature (see Table 7.6). Hence, the role of binder in a CP made of HMX or the rest of the substances in a CMDB made with HMX would be *to act as a coolant*. Consequently, the burn rate decreases. This is clearly noted in Table 7.14. Also, the diffusional effects so dominant in an AP based CP reducing the pressure index cannot be expected in HMX propellants as these effects do not control the heat transfer rates. As pressure increases, the reducing flame thickness with the high flame temperature of HMX monopropellant, will control the heat transfer. Hence, the burn rate index of any high energy propellant made of HMX will not depart much from that for the monopropellant (note that n(HMX) = 0.93, and n (HMX based CMDB) = 0.83, see Table 7.14). Combustion mechanisms have been discussed in some detail by Kubota [17]

8.3 Combustion Mechanism in Liquid Rockets

The mechanisms of combustion for monopropellants, hypergolic bipropellants and non-hypergolic propellants are all different.

8.3.1 Monopropellants

The requirement in the case of monopropellant is that the liquid spray should impinge on the catalytic bed at ambient temperature, typically, 25 °C and undergo decomposition. In some instances, the facility to heat the thrust chamber to 100 to 300 °C before the liquid spray is allowed to impinge on the catalyst bed, has been deployed. The catalyst bed itself consists of alumina particles with high internal surface area coated with iridium, largely (as indicated earlier in sections 1.14 and 7.8.1). The molecular process of decomposition is complex. When liquid hydrazine is injected into the chamber, it flows through the interstices between the catalyst particles. The capillary effect of the fine pores draws in the liquid. The liquid vaporizes inside and in contact with active catalyst sites decomposes to ammonia, hydrogen and nitrogen. During this period, the liquid would be continuing to move into the pore because of capillary pressure and gas pressure is getting built up due to the decomposition process. There comes a time when the internal gas pressure exceeds the capillary pressure and the gas expels the liquid and comes out into the chamber. Since the pressures (due to capillary effect) are large, the pressure at which the gas comes out is also large and the ignition process leads to rise in chamber pressure. Since the fine pores experience large pressures, there will be

inevitable effect on the structural integrity of the material. Slowly, over a period of time with the increase in the number of start and shutdown cycles, the sudden expulsion process leads to the creation of fissures and break up of the particle. This attrition limits the number of cycles of pulsing demanded from the thruster. Not only does the start-up have peaks in pressure due to the accumulation of the fluid and sudden pressure rise after a certain delay, the impulse bit that the thruster is designed to provide will also degrade. Increased life of the thruster can be obtained by heating the thruster to higher temperatures. The thrusters, the fluid line and the storage vessel are heated using on-board electric power (from the solar photovoltaic modules) to different levels of temperature. The storage vessel can be maintained at 25 °C, the line at 35 to 40 °C and the thruster between 100 – 300 °C. Use of higher temperatures will reduce the pressure levels inside the pores and hence, the structural integrity of the catalyst bed improves providing much longer life. The catalyst bed on Voyager spacecraft is maintained at 200 °C and is qualified for four hundred thousand cycles.

The arrangement of the particle sizes in the bed is also important. The rate of reaction is dependent on the surface area of the catalytic material. This implies one should use fine particulate material with high internal surface area. The limitation, of course, is that the pressure drop through the bed will be larger. Also, as the extent of use in pulse mode increases, there will be attrition of the particulate material and some of it will be washed out through the nozzle. Accounting for these features, the bed consists of fine particulate material in the first part, coarse particles in the next part so as to optimize the surface area available and also allow for some attrition without loss in performance. The bed thickness controls the decomposition of Ammonia and thus, the performance.

8.3.2 Hypergolic and Other Propellants

In the case of hypergolic propellants, the mechanism is composed of liquid phase exothermic reaction that leads to energetic gas phase species that react further exothermically to generate gases at high temperature. The exothermic liquid phase reaction is central to the avoidance of a separate ignition system. A parameter that characterizes the time it requires for the propellants to generate burnt gases from liquid state at start-up is called the ignition delay. Typical values for most hypergolic systems are 5 to 10 ms. If this delay is larger, the liquid pumped into the rocket combustion chamber will accumulate in reasonable quantities and then suddenly get converted to high temperature gas leading to high chamber pressure rise with undesirable peaks. This is particularly important in restartable systems. Take for example the Lunar Assistance Module used by astronauts to land on the surface and then take off for the return journey. The rocket engine must have smooth start-up even at the conditions of hard vacuum.

The ignition delay is best determined by using a micro-rocket motor with transparent windows. The propellants are injected into the combustion chamber by an injection system typically, an impinging jet. The phenomenon inside the chamber is tracked by using a high speed motion picture camera. The typical parameters that are varied in such an experiment are: (a) relative flow rates, (b) injection advance – oxidizer or fuel lead into the chamber and (c) initial pressure. Flow rates close to those that lead to the highest flame temperature would help smoother ignition. Injection advance is an unavoidable feature of engineering nature. It will be difficult to ensure simultaneity. Fuel lead in the case of some fuels can cause an initial fuel rich mixture in some parts of the chamber and some of the fuel rich mixtures can be explosive in nature. If these are formed and then full ignition takes place, the explosive mixture may actually detonate. The classical example is the case of Agena rocket engine using IRFNA/UDMH. An explosion that resulted due to a restart was traced later to the fuel lead in the start-up sequence. Generally, in hypergolic systems (IRFNA or NTO is the oxidizer) oxidizer lead is recommended. Typically, this could vary between 30 to 100 ms with ramped flow rate change. The ambient pressure has a significant influence. For the first start-up of an engine even at altitude, it is possible to provide a nozzle closure near the throat or downstream so that the chamber pressure is maintained at a desired pressure, say, 1 atm during the flight of the vehicle up to the time ignition is initiated. However, for a second ignition that would be demanded in some missions, the start-up occurs at conditions of hard vacuum. The ignition process involves gas phase reactions and these depend on pressure strongly (typically like p^2). Hence, decrease in pressure implies reduced reaction rates and hence, longer ignition delays. Longer ignition delays imply sharp pressure rise to values higher than the equilibrium pressure leading to "hard start".

While the use of additives to reduce the ignition delay was contemplated in the early stages of rocket engine development when the fuels used were not as reactive, most of the hypergolic combinations contemplated in later times (discussed in section 7.8.2) have been so reactive that ignition related problems have been overcome.

There are commonalities and differences between the combustion process in hypergolic propellants and non-hypergolic systems – IRFNA, NTO with UDMH or Aerozine (an equi-volume mixture of hydrazine and UDMH) belonging to the former class and LOX – RP1 and LOX – LH_2 belonging to the second category. The commonalities are that (a) the hot gas mixture is found in the entire chamber due to complex incompressible fluid flow physics, (b) drop atomization takes place close to the injector, (c) gas phase reactions are very fast due to high chamber pressures, and (c) *drop vaporization is the rate limiting step*. The differences arise because of possible liquid phase reactions in the case of hypergolic systems, something absent in other cases; consequently, the heat release rates for hypergolic systems tend to be higher compared to other systems.

The drop density will be very high close to the injector and this density decreases as one goes downstream. The drops have a high momentum close to the injector and hence, entrain the gas with them. Downstream, the gas velocity takes over the liquid drop velocity and hence, the liquid drops create drag to the flow. The drop diameter continues to decrease till it completely vaporizes. The drop vaporization process has been discussed already in section 6.3.3 in connection with the combustion dynamics of a gas turbine combustor. Restated, the expression for the vaporization time, t_v is given by

$$t_v = \frac{\rho_l \ d_0^2}{8(k_g/c_p) ln(1+B_c)} \tag{8.17}$$

where d_0 is the drop diameter, ρ_l is the liquid density, k_g and c_p are the gas phase thermal conductivity and specific heat and B_c is the Transfer number. The differences between the processes that occur in a gas turbine and a rocket combustion chamber are several (see Table 8.1). As can be noticed, there are some features that are more favorable for rocket engine compared to gas turbine engines, like more reactive fluids, higher peak temperatures and pressures, but unfavorable features like spray density that is one order higher than in a gas turbine engine. Further, the presence of the recirculation zone in a gas turbine combustor allows the use of the simple expression (8.17) for estimating the residence time requirements. In the case of a rocket engine, the liquid drops move with the gas all through till the end of the combustor by which time it is expected that very little has remained un-vaporized. The multi-phase flow features in which the drops moving at 40 to 100 m/s in the early stages will cause drag to the gaseous flow and subsequently accelerate to the same conditions as the gaseous stream are important in the case of rocket engine. In the case of a gas turbine engine, part of the combustor is devoted to bringing down the gas temperature to turbine inlet conditions and hence, the combustion process is expected to be completed in a volume smaller than the complete combustor volume. In the case of rocket engine, the volume – diameter and length – are chosen to achieve as much of vaporization as possible since this feature limits the combustion efficiency. While gas turbine combustors operate at high pressures at take off and supersonic flight conditions, there are several conditions where they operate at relatively low pressures. In the case of rocket engines, however, the operating pressure is always high. The peak temperatures are also much higher. One can therefore expect the vaporization rates to be higher compared to gas turbine engines. If we introduce typical values into the terms on the right hand side of equation (8.17), we get $t_v = 25 \times 10^4 \ d_0^2$, with d_0 in m and t_v in seconds. A typical 100 micron droplet will require about 2.5 ms to vaporise. The length required for combustion can be estimated by $L = U_{mean} t_v$. The gas velocity will increase from the injector to the exit because more and more of high density liquid is being vaporized and burnt up to high temperature gases. The velocity at the throat of the thrust chamber is typically about 1000 m/s. The velocity at the entry to the nozzle could be between 600 to 800 m/s. Hence, the

Table 8.1: Differences in the drop vaporization processes between a gas turbine and a rocket engine

Feature	Gas turbine combustor	Liquid rocket combustor
Liquid flow rate	2.5 kg/s (max)	600 kg/s (max)
Drop sizes	20 – 60 μm	20 to 150 μm
Flow rate/Area	30 – 40 kg/m^2s	400 to 1000 kg/m^2s
Dilute spray?	Yes	Far more dense
Recirculation zone	Yes, significant	Very little
Chamber pressure	5 – 40 atm	50 – 200 atm
Peak temperature	2300 K	3300 K

mean velocity could be 300 to 400 m/s. With a mean velocity of 400 m/s, L = 1.0 m. If the drop diameter becomes 75μ m, L = 0.6 m. Typical values of $L \sim 0.8$ m. Thus, it is important to control the mean size of the drops to ensure complete evaporation with a reasonable choice of the combustor length. More details on the combustion chamber will be presented in section (10.3).

8.4 Combustion Mechanism of Hybrid Rockets

Figure 1.20 shows the details of a hybrid rocket motor. The oxidizer is typically IRFNA, NTO or LOX. The fuel block in the case of storable oxidizers will be a special solid that could be hypergolic with these oxidizers or could be a non-hypergolic plastic like polyethylene, polybutadiene or a similar substance. With LOX, any of these fuels would be satisfactory. One needs a separate system to start the ignition process. The flow of the oxidizer past the surface creates a boundary layer and the combustion process occurs as a consequence of turbulent diffusion of the vaporized fuel fragments and the oxidizer into the flame interface. The heat transfer from the flame vaporizes the fuel. The mechanism is identical to the erosive burning phenomenon in solid propellants (see Figure 7.8); the difference lies in the nature of the condensed phase. In the present case, it is a non-reactive solid and in the case of solid propellant, it is reactive solid. The non-reactive solid cannot burn by itself and this gives significant advantage in terms of safety of operations. The linear regression rate of the fuel is governed by the oxidizer flux through the port and is represented by $\rho_p \dot{r}_{hyd} = a_{hyd} G^m$ where G is the local mass flux through the port (flow rate per unit port area). Considerable research has been done to determine the values of a and m. The theory of turbulent heat transfer with fuels in which large molecular weight fragments of the basic polymeric material come off from the surface has been worked out (see Paul et al, [60]) and has been shown to compare with experimental results. The correlation provided in this work is rather

complex and it is useful to express the result in simpler terms: it is expressed as $\dot{r}_{hyd} = 0.75[G_{ox}/100]^{0.5}$ mm/s, where G_{ox} is expressed in kg/m$^2 s$ for LOX – styrene-butadiene rubber system. For a 10 tonne thrust engine with a specific impulse of 2500 N s/kg and an O/F of 2.0, the oxidizer flux works out at 1200 $kg/m^2 s$ at a cross section of 0.2 m^2 port area. The initial regression rate works out as 2.6 mm/s, a figure about a third of what one would expect in a solid rocket for similar applications. This implies that the grain geometry has to have a very high surface area for the same port area. These are the aspects that would need to be taken care in design. As a matter of comparison, if one considers a large solid rocket motor of 4.5 MN thrust capability (like PS 1, see Table 9.7), the mass flow rate is about 1400 kg/s at a cross sectional area of 0.7 m^2 amounting to a total mass flux of 2000 $kg/m^2 s$. Equivalently, this implies an oxidizer mass flux of 1330 $kg/m^2 s$ at an O/F of 2. This implies a regression rate of 2.75 mm/s. The solid propellant burn rate for PS 1 is 9 mm/s. If one were to design a rocket motor for the same thrust, the burning area needs to be raised by a factor of 3. This calls for a grain design that would need multiple ports or in part, addition of an active ingredient like AP to an extent required to raise the burn rate but allowing the propellant itself to remain largely a fuel.

8.5 Comparative Analysis of the Combustion Features

The mass production rate of the various propulsion systems can be set out as

$$\dot{m} = \rho_p A_b a p_c^n \quad \text{(solids)} \tag{8.18}$$

$$\dot{m} = \dot{m}_{ox} + \dot{m}_f \quad \text{(liquids)} \tag{8.19}$$

$$\dot{m} = \dot{m}_{ox} + \rho_p A_b a_{hyd} G_{ox}^{0.5} \quad \text{(hybrids)} \tag{8.20}$$

In the case of liquids and hybrid rocket engines, the propellant flow rates ($\dot{m}_{ox}$ and $\dot{m}_f$) are controlled by an injection pressure (or manifold pressure, $p_{manifold}$), chamber pressure, p_c and injector geometry. Typically, the liquid flow rate is given by

$$\dot{m}_{ox,\,f} = c_d A_{inj} \sqrt{2(p_{manifold} - p_c)\rho_l} \tag{8.21}$$

where c_d is the discharge coefficient, typically 0.3 to 0.7, A_{inj} is the injector cross sectional area and ρ_l is the density of the liquid.

The mass generation rate increases with p_c in the case of solid rocket engine, but decreases for liquids and also for hybrids since the oxidizer fraction of the total flow is significant (about 65 %). Hence, the question of stability arises in solid rocket engines and limits the pressure index to 1. It does not arise in liquid or hybrid rockets; they are statically stable. The reason is evident from Figure 8.6.

As can be noticed, the mass generation rate decreases with increase in pressure and any positive perturbation on the chamber pressure is opposed by larger

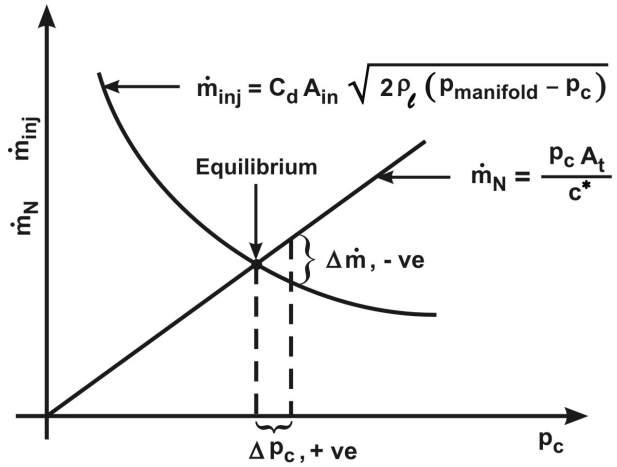

Figure 8.6: The plot of mass injection rate and nozzle flow rate with chamber pressure

nozzle flow rate ensuring return to the equilibrium operating point. There are issues of dynamic stability – coupling between (a) energy release processes in the combustion chamber and (b) feed system leading to low frequency instability and (c) with chamber acoustics leading to high frequency instability that need to be tackled; these are the subjects of discussion in chapter 11.

Solid propellant combustion process is significantly chemistry-controlled; diffusional effects are definitely present, but play a modulatorythe speed at which the flame travels into a fuel-oxidant mixture role. Hence, pressure plays a key role.

Liquid and hybrid propellant combustion processes are diffusion limited, in the former, through liquid vaporization process and in the latter, through boundary layer combustion process. Hence, pressure plays an indirect and less important role. In the case of liquid propellant combustion, pressure affects the boiling point and heat of vaporization. The chamber conditions may be beyond the critical properties of the propellant and in such cases, the lack of a phase boundary may need to be accounted for in the conversion process. There are also arguments that what matters is the possible non-exceedance of the partial pressure of the propellant in the vapor phase beyond critical value, even if the total pressure is more than the critical pressure. In any case, it is the diffusion dominated phenomenon and therefore, the reduced importance of the chamber pressure. The principal effect is that the distance for completing the combustion process is weakly dependent on pressure in the practical range of pressures.

Diffusion limitedness of the combustion in hybrid rockets modulates the influence of pressure. Increase in pressure helps increase the mass flux through the

port and hence, the regression rate. But any possible structural deformity like a crack or a blow hole has little influence on the pressure-time curve unlike in a solid rocket. This is because the fuel gasification process is controlled by heat transfer from the gas phase and any parts of the crack that are farther removed from the flame will also receive less heat from the flame and will regress less. Thus, over some time the opened-up blow hole will get smoothened and any small deviations will reduce with the time of operation.

8.6 Summary

This chapter has been devoted to discussing the mechanistic behavior of rocket propellant combustion. Two classes of fundamental behavior are identified – premixed and diffusion. The premixed character is strongly dependent on chemistry as the principal controlling mechanism, even though diffusive processes modulate the combustion process. The highly diffusive hydrogen can alter the combustion process in a LOX – LH_2 system. The ignition behavior of all systems – gaseous, liquid or solid depends on the exothermic chemistry to achieve combustion and hence, chemical rate processes control the ignition phenomena. Premixed character of combustion implies strong pressure and ambient temperature dependence. The premixed character governs the combustion processes in solid propellants as well as solid and liquid monopropellants. Diffusive processes show little dependence on pressure. Hence, at high pressures where diffusion controls the burn rate, the pressure index is brought down from what is observed at low pressures. Diffusion process also affects the liquid propellant combustion behavior, though weakly. The dependence on pressure arises in liquid rocket systems from the consideration that the operating pressure exceeds the critical pressure of the propellants. In bipropellant liquid rockets, vaporization is the rate limiting feature.

As a general maxim in science, it is generally understood that if the controlling mechanisms of a process are clear, one would have the ability to control them. In the case of liquid propellants, controlling the vaporization process is somewhat straight forward – varying the pressure drop across the injector (given the propellant combination that is usually fixed from considerations of specific impulse). In the case of processes controlled by chemical kinetics like solid propellant combustion, the processes are so complex that even if an understanding of the essential aspects of the behavior is present, controlling the precise outcome by a certain input is most difficult. Substantial efforts to unravel the mechanistic behavior have been made and they have paid rich dividends; however, the variety of behavior is so vast that capturing all of it is nearly impossible. The general impression of a solid rocket engine being simple is to be significantly moderated by these fundamental considerations.

Several books provide the information on the relevance of fundamentals of combustion to rocket propulsion. These are by Williams [35], and Mukunda [32].

Chapter 9

Solid Rocket Engine

9.1 General Features

The operation of any rocket motor depends on the mass balance between the gaseous mass generation and exhausting rates. This is stated by

$$\frac{dm_g}{dt} = \dot{m}_{production} - \dot{m}_{nozzleflow} \tag{9.1}$$

This states that the chamber gas mass filling rate is the difference between the rate of production of gas and its flow out of the chamber through the nozzle. The mass production rate of a solid rocket is given by $\rho_p \dot{r} A_b$, where, A_b is the burning surface area. The burn rate $\dot{r}$ is dependent on the local chamber static pressure, $p_{c,s}$, the initial temperature, T_{in} and the local lateral mass flux, all of which are discussed in Chapter 7. The nozzle flow rate is obtained from the choked flow analysis presented in Chapter 4 as equation (4.31) stated as $\dot{m} = p_{c,t} A_{th}/c^*$. It must be noted that the nozzle flow rate depends on the chamber stagnation pressure at the entry to the nozzle and the burn rate depends on the local static pressure. The pressure variation in many rocket motors that are not highly loaded is small enough to let one assume $p_{c,s} = p_{c,t}$. This is true with a large number of applications. In fact, we use p_c as the symbol for the chamber pressure instead of $p_{c,s}$ or $p_{c,t}$. Further the burn rate is represented by $\dot{r} = a p_c^n$, where a represents $a_{70}/(70)^n$ including the initial temperature effect unless explicitly stated. Thus, the chamber mass conservation equation becomes

$$\frac{dm_g}{dt} = \rho_p A_b a p_c^n - \frac{p_c A_t}{c^*} \tag{9.2}$$

where $m_g = p_c \mathscr{V}_c / R T_c$ with $\mathscr{V}_c$ as the chamber free volume and $A_t = A_{th}$, the throat area.

If the mass flow rate generated equals the mass outflow through the nozzle, we get dm_g/dt = 0 and therefore solve the algebraic relation for p_c as

$$p_c = p_{c,eqm} = \left[\rho_p \frac{A_b}{A_t} c^* a\right]^{1/(1-n)} \tag{9.3}$$

This equation states that if a rocket motor is set up with a propellant surface area, A_b and nozzle throat area, A_t with the propellant properties of a given c^*, a and n, the equilibrium chamber pressure, $p_{c,eqm}$ is given as above. For a given composition, ρ_p, c^*, a and n will be fixed values and the design parameters are A_b and A_t. The burning area, A_b is dependent on the grain geometry (discussed in section 9.2).

The thrust of the rocket engine given by $F = c_F p_c A_t$ in terms of other variables can be expressed as

$$F = [\rho_p A_b c^* a]^{1/(1-n)} A_t^{-n/(1-n)} \tag{9.4}$$

These equations, appearing simple though, contain very important information concerning motor operation. If one considers a double base propellant or a HMX based composite propellant, the pressure index n is high $\sim$ 0.6 to 0.8 (see Table 7.14). The exponent $1/(1-n)$ will be 2.5 to 5. This is so large that small deviations in any of the parameters – A_b, A_t, a or c^* will have very significant, sometimes disastrous consequences to the operation of the rocket motor. For instance, if there is a minor crack in the propellant increasing the effective surface area by 1 %, the chamber pressure will increase by 2.5 to 5 %. Thus, a propellant with high n and small structural deficiencies could lead to unintended pressure rise and if such a pressure rise is beyond limits, could lead to motor blow-up. The throat of a solid rocket that uses materials like graphite or carbon-carbon composite will erode with time of operation. Typically, the throat diameter remains constant for a duration in which the temperature of the backup material increases to levels where the erosion mechanisms come into play. Typically, the erosion rate is 0.05 to 0.2 mm/s depending on the material and the gas phase mass flux past the surface (it is useful to recall the mechanism of erosive burning; here too, convective heat transfer affects the erosion rate). Thus, in large motors with throat diameter of 500 to 700 mm, erosion rate of 0.15 mm/s for a typical 100 s burn time implies a throat area variation of 8 to 12 %.

The true implications of the temperature sensitivity can be understood by examining the role of a in the equation (9.4). We express the temperature dependence by $a = a_{T_o} exp[-\sigma_{T_o}(T_{in} - T_o)]$, where a_{T_o} is the burn rate at an initial temperature, T_o. The dependence on T_o can then be expressed by

$$p_c = [\rho_p \frac{A_b}{A_t} c^* a_{T_o}]^{1/(1-n)} \exp[-\sigma_{T_o}(T_{in} - T_o)/(1-n)] \tag{9.5}$$

$$F = [\rho_p A_b c^* a_{T_o}]^{1/(1-n)} A_t^{-n/(1-n)} \exp[-\sigma_{T_o}(T_{in} - T_o)/(1-n)] \tag{9.6}$$

It is first important to examine the excursions in atmospheric temperature. Typical daily variations could be about 10 to 15 °C. However, seasonal variations can go from – 30 to + 50 °C. A temperature sensitivity of 0.5 %/K implies that 5 % variation on a daily basis and 40 % variation on a seasonal basis. The implications on chamber pressure and thrust even on a daily basis are significant and may become unacceptable on a seasonal basis. While emphasizing the criticality of the initial temperature effect, one moderating influence that must be borne in mind is that all propellants have low conductivity. Hence, even though ambient temperature varies, there will be weak effects on the core temperature due to size and low conductivity unless the system is soaked at the given condition for a long enough time, typically 24 to 72 hours. In order to estimate the influence of the parameters, one calculates the fractional change of thrust and chamber pressure with propellant burn area, nozzle throat area and initial temperature. These are expressed in terms of differentials as in the following equations.

$$\frac{dp_c}{p_c} = \frac{dF}{F} = \frac{1}{(1-n)} \frac{dA_b}{A_b} \tag{9.7}$$

$$\frac{dp_c}{p_c} = -\frac{1}{(1-n)} \frac{dA_t}{A_t} \quad \text{Or} \tag{9.8}$$

$$\frac{dp_c}{p_c} = \frac{1}{(1-n)} \frac{dK_n}{K_n} \quad [K_n = \frac{A_b}{A_t}] \tag{9.9}$$

$$\frac{dp_c}{p_c} = \frac{dF}{F} = \frac{\sigma_{T_o}}{(1-n)} \Delta T_{in} \tag{9.10}$$

$$\frac{dF}{F} = -\frac{n}{(1-n)} \frac{dA_t}{A_t} \tag{9.11}$$

For practical values of n, and σ_T, the influence of variations in burning area, throat area and initial temperature on the changes in chamber pressure and thrust are presented in Table 9.1. Any increase in chamber pressure is synonymous with change in burn rate according to $d\dot{r}/\dot{r} = n dp_c/p_c$. This implies a change in burn rate and also burn time with increase in burn rate implying reduction in burn time and vice versa. In constructing this table, it must be noted that only small variations around a nominal point are considered. If the variations are large the basic equations (9.5 and 9.6) need to be used to calculate the changes. The very significant variations in chamber pressure and thrust due to larger n are very clear from this table. The coupled effects of even 10°C change on the thrust and chamber pressure can be very significant. Double base propellants with larger

Table 9.1: The effects of burning area, Throat area and initial temperature variation on chamber pressure and thrust

Parameter For		dp_c/p_c %	dF/F %	$d\dot{r}/\dot{r}$ %	dt_b/t_b %
dA_b/A_b = + 1 %	n = 0.2	1.25	1.25	0.25	-0.25
	n = 0.7	3.33	3.33	2.33	-2.33
dA_t/A_t = + 1 %	n = 0.2	- 1.25	- 0.25	- 0.25	+0.25
	n = 0.7	- 3.33	- 2.33	- 2.33	+2.33
ΔT_{in} = + 10 °C	n = 0.2	2.50	2.50	0.50	-0.50
σ_T = 0.2 %	n = 0.7	6.60	6.60	4.60	-4.60
ΔT_{in} = + 10 °C	n = 0.2	10.0	10.0	2.00	-2.00
σ_T = 0.8 %	n = 0.7	26.6	26.6	18.60	-18.60

value of $\sigma_T \sim 0.8$ % and larger $n \sim 0.7$ show up 26 % variation in chamber pressure and thrust. These are unacceptable for operation in many tactical missions. One strategy that is adopted would be to change the throat area when the ambient temperature changes consistently for a minimum period of time. Figure 9.1 shows a central plug that can be moved backward and forward to control the throat area. In summer, when the initial temperature is large, the throat area is increased. Equation (9.6) can be manipulated to show that such an area variation must follow $A_t \propto exp[\sigma_T(T_{in} - T_o)/n]$ to ensure constant pressure and thrust. While it may be too difficult to completely offset the temperature effect, the influence may be restricted by changing the area by the scheme indicated here. In some cases, particularly short range missiles, the entire system is maintained in air conditioned environment with both the temperature and humidity control.

9.1.1 Stability of Motor Operation

The mass balance equation (9.2) can be rewritten by invoking the equation of state as

$$\frac{d(\rho_c \mathscr{V}_c)}{dt} = \mathscr{V}_c \frac{d(p_c/RT_c)}{dt} + \rho_c \frac{d(\mathscr{V}_c)}{dt} = \rho_p A_b a p_c^n - \frac{p_c A_t}{c^*} \tag{9.12}$$

where ρ_c is the density of the gases in the chamber = p_c/RT_c. If we take $d\mathscr{V}_c/dt = A_b\dot{r}$ = $A_b a p_c^n$, we can write the above equation as

$$\frac{\mathscr{V}_c}{RT_c}\frac{dp_c}{dt} = (\rho_p - \rho_c)A_b a p_c^n - \frac{p_c A_t}{c^*} \tag{9.13}$$

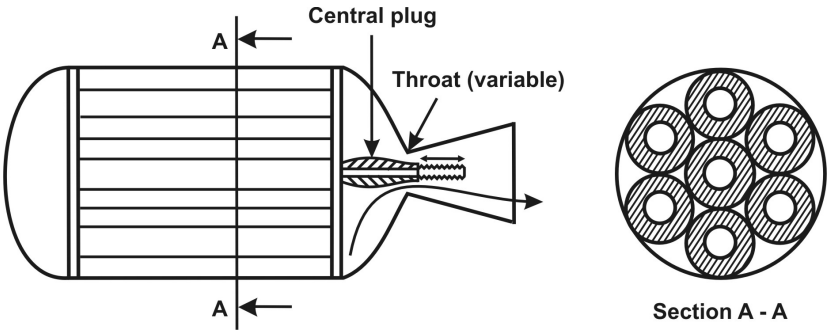

Figure 9.1: A rocket motor for tactical applications with facility for varying the throat. Notice that by moving the object back and forth using the central screw, one can vary the minimum cross section of the fluid passage and thus, control A_t

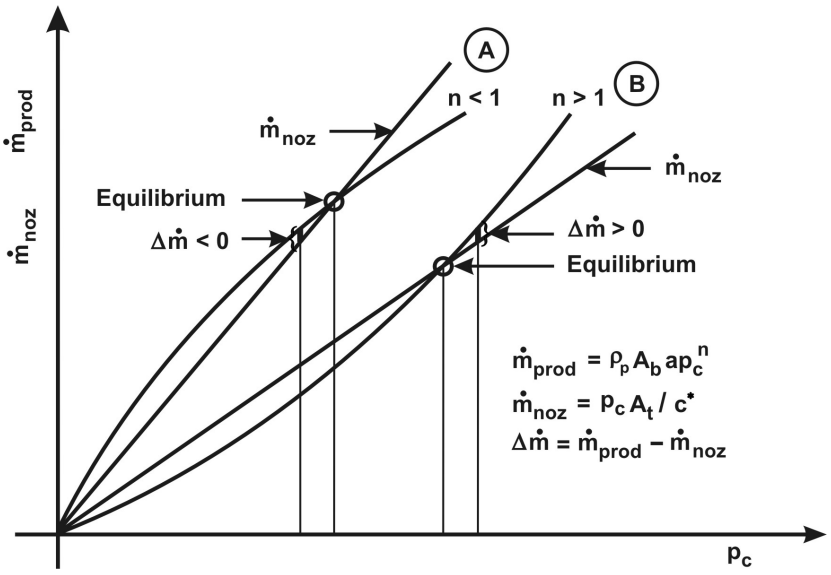

Figure 9.2: Stability diagram for a solid rocket motor on a plot of mass production rate and nozzle out flow rate with p_c

The magnitude of ρ_c can be worked out taking typical parameters as p_c = 100 atm, T_f = 3000 K, and $\mathscr{M}$ = 26 as 12.5 kg/m^3. Its spread in practical situations is 8 to 15 kg/m^3. When compared with ρ_p = 1600 to 1750 kg/m^3, it is 0.5 to 1 %. hence, the equation can be simplified into

$$\frac{\mathscr{V}_c}{RT_c}\frac{dp_c}{dt} = \rho_p A_b a p_c^n - \frac{p_c A_t}{c^*} \tag{9.14}$$

The question of stability is posed thus – It is known that at equilibrium, the right hand side is 0. At this condition, if a momentary change in parameters takes place through A_b, A_t, or c^*, would there be a tendency for the motor operation to return to equilibrium or move away from it. This can be analyzed by plotting the variation of both the terms on the right hand side as a function of p_c. Figure 9.2 shows the details. We consider the case of the pressure exponent, $n > 1$ and $n < 1$ as two important cases, since this parameter decides the rate of change of mass generated with respect to nozzle outflow rate when pressure is perturbed. For $n < 1$, the curve droops (see A in Figure 9.2) and for $n > 1$, it sharply rises as indicated by B in the figure. Now consider a slight decrease in p_c through one of the several parameters. For the case $n < 1$, this leads to a situation where the mass production rate is larger than the mass flow rate through the nozzle. Hence, there is a tendency for pressure to increase. This implies that the operation is stable. This argument holds good even if there is an increase in pressure. The mass flow rate through the nozzle is slightly higher than the mass generation rate and hence, pressure drops. For the case of $n > 1$, when pressure rises as indicated in B, the effect is that the production rate is larger than mass outflow rate and hence, there is a tendency for pressure to rise further. This tendency leads to explosion. Hence, the stability criterion is that $n < 1$. If the term involving ρ_c is taken into account in the first term on the right hand side of equation 9.14, this condition becomes $n < 1/(1 - \rho_c/\rho_p)$. This implies that the critical limit is pushed to a value slightly in excess of 1. For most motor operations, the recommendation is to stay much below n =1. This is the reason why low values of n are preferred for the propellant.

9.1.2 Transients

Equation (9.14) can be expressed in a non-dimensional form. We note the equilibrium pressure, $p_{c,eqm}$ is given by setting the right hand side to 0 as in equation (9.3). We invoke $\overline{p}_c = p_c/p_{c,eqm}$ to get

$$\frac{\mathscr{V}_c}{RT_c}\frac{d\overline{p}_c}{dt} = \frac{A_t}{c^*}(\overline{p}_c^n - \overline{p}_c) \tag{9.15}$$

This equation can be rearranged as

$$\frac{d\overline{p}_c}{dt} = \frac{RT_c}{\mathscr{V}_c}\frac{A_t}{c^*}(\overline{p}_c^n - \overline{p}_c) \tag{9.16}$$

We use the relationship $RT_c = [c^*\Gamma(\gamma)]^2$ (see equation 4.32). We define a time scale t_c using the quantity outside the brackets on the right hand side of the equation (9.16) as

$$t_c = (\mathscr{V}_c/A_t)/(c^*\Gamma^2) = L^*/(c^*\Gamma^2) \tag{9.17}$$

where L^* is the ratio of the free gaseous volume of the combustion chamber up to the throat to the throat area and t_c signifies the residence time of a fluid in a rocket motor. By further defining a non-dimensional time scale $\bar{t}$ by $\bar{t} = t/t_c$, we can restate the mass balance equation by

$$\frac{d\overline{p}_c}{d\bar{t}} = (\overline{p}_c^n - \overline{p}_c) \tag{9.18}$$

Integration can be carried out from the initial time ($t = 0$) to the time to reach equilibrium pressure. It is necessary to note that the propellant ignition process involves separate ignition composition with a certain mass and energy. For the present purpose, it is sufficient to note that time = 0 corresponds to the completion of the ignition process during which period (that lasts 10 ms to 50 ms depending on the size of the rocket motor), the chamber pressure achieved is the ignition pressure, $p_{c,ign}$ (ignition transients need to be separately considered and will be discussed subsequently). The integration from $\bar{t}$ = 0 ($\overline{p}_c$ = $p_{c,ign}$) yields

$$\bar{t} = \int_{\overline{p}_{c,ign}}^{\overline{p}_c} \frac{dz}{(z^n - z)} \tag{9.19}$$

This can be explicitly put down as

$$\bar{t} = ln \left[\frac{1 - \overline{p}_{c,ign}{}^{(1-n)}}{1 - \overline{p}_c{}^{(1-n)}} \right] \tag{9.20}$$

This indicates that the time for p_c to approach $p_{c,eqm}$ is infinity in the logarithmic way. In actuality if one takes approach to 95 % $p_{c,eqm}$, the time taken will be a realistic representation.

The quantity L^* in the equation (9.17) has relevance in motor operation. It occurs both in solid and liquid rockets. Typical values of L^* in small solid motors is about 0.8 to 1.5 m and in large boosters could be as high as 40 m. It increases from a minimum value at start and reaches a maximum at the end. Its significance in solid rockets is related to low frequency instability like chuffing that occurs in low chamber pressure motors and during start-up if the ignition energy is inadequate.

Typical value of t_c is 1.5 to 2 ms in small motors and 20 to 40 ms in large motors. Its significance is related to achieving of complete combustion in rocket engines. Aluminum oxidation to aluminum oxide takes the longest time, typically about 5 to 20 ms. Since the residence time (that is about 2 to 5 times t_c) exceeds this magnitude, the combustion efficiency achieved in large rocket motors is close to 99 % with realized specific impulse efficiency exceeding 93 %, the loss of 7 % being due to a combination of chemical kinetics, two phase and wall frictional losses.

When the propellant is burnt up completely, A_b = 0 and hence, the pressure is controlled by the nozzle flow rate alone. In this case, $\overline{p}_c = exp(-\overline{t})$. Thus, the time required for the fall in pressure from equilibrium level would be t_c.

9.2 Geometric Aspects of Solid Propellants

From equation (9.3), it is clear that $p_{c,eqm} \sim A_b^{1/1-n}$ and hence, the pressure variation is a strong function of the burning area A_b. Figure 9.3 indicates the three simple geometries indicative of the broad burning behavior of propellants. If A_b is constant as in an end burning grain [Figure 9.3 (a)], pressure will be constant. Such a characteristic is called "neutral" burning characteristic. If a cylindrical grain that burns from inside is considered [Figure 9.3 (b)], the burning area increases with time till the outer surface is reached and hence, the pressure keeps increasing with time. This configuration is termed "progressive" burning. If a cylindrical grain burning only from outside is considered [Figure 9.3 (c)], then the burning area decreases with the time of burning and hence, pressure decreases with time. Such an arrangement is termed "regressive" burning. These are the fundamental geometric features that will be exhibited by any choice of geometric configuration of the propellant. In fact, even in one propellant geometry one could have a combination of neutral and progressive, neutral and regressive, or regressive and progressive modes of combustion.

End burning configuration shown in Figure 9.3 (a) is a standard geometry for certain applications In this configuration, the burning area is limited by the motor diameter, since the grain diameter is the [motor inner diameter – twice the insulation and inhibition thickness]. This configuration is used in situations where a

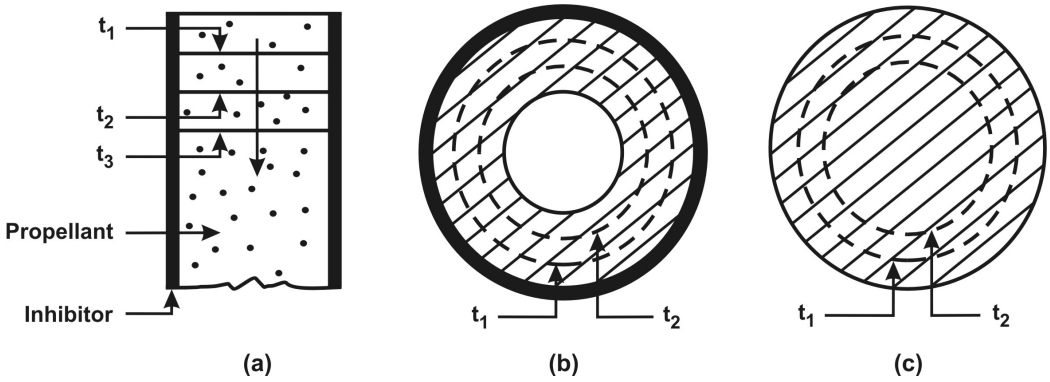

Figure 9.3: The end burning grain (a), the circular internal burning grain (b) and an outside-to-inside burning cylindrical grain (c)

small thrust is required for a long time. Such a condition in missile propulsion is called "sustain" mode of operation. As different from this condition, a "boost" mode in which high thrust for short duration occurs is demanded in the first stage of missile flight during which period, the missile accelerates to high speeds, generally higher than the speed of the target it is supposed to chase. After this condition, a period of "sustain" mode is needed to ensure that the guidance system tracks the target and reaches it to neutralize it. To obtain high thrust, one needs to have larger A_b. This is obtained from internal-external burning or internal burning geometry.

Figure 9.4 shows the variety of geometries used for such applications. They can be classified into (a) side burning two-dimensional configurations and (b) three-dimensional configurations. A side inhibited hollow cylinder burning radially both from inside and outside represents a neutral burning configuration. Allowing the sides also to burn is a three dimensional configuration with regressive characteristic. For a long tube, the three-dimensional effect is small. A rod-in-a-cylinder burning along radial direction alone or including the sides is another alternative to obtain even higher surface area with enhanced regressivity. If an inside burning cylinder is used, the initial burning area is $\pi d_{in} L$, where d_{in} and L are the initial diameter and length respectively. In many situations one would need an area much larger than can be provided within this length. Higher surface area is obtained by wrinkling the internal surface like a star, wagon wheel or a similar geometry shown in Figure 9.4. This enhances the perimeter three to four fold and hence, the area as well. This is why a star or wagon wheel burning geometry is extensively used.

In select missile applications, to match the high loading density and the length-to-diameter ratio, one uses three-dimensional geometries like slotted tube (a tube that has slots over a part of the length) cone-in-a-cylinder (conocyl) or fin-in-a-cylinder (finocyl), spherical motor with internal slots, all of which are shown in Figure 9.5.

In order to understand how the burning area varies when the propellant burns, we examine two cases – an inside burning square and a star. Figure 9.6 shows the two configurations. It is first recognized that every propellant burns along a local normal. Therefore, the segment AB of the square port will become $A'B'$ with no change in the length and each corner will evolve into a quarter of a circle – like point A becoming $A'A''$, etc. The latter occurs because, the corner point has to move equal radial distance and this leads to a part of a circle. This regression y will occur at a rate $\dot{r} = dy/dt$. The increase in burning area per unit depth is 2 πy. This is the maximum change in the perimeter that would be possible in a two-dimensional configuration as any burning surface will ultimately become circular as time advances. The evolution of a pointed star as combustion proceeds is shown in Figure 9.6. The surface generated by the segment AB will evolve into

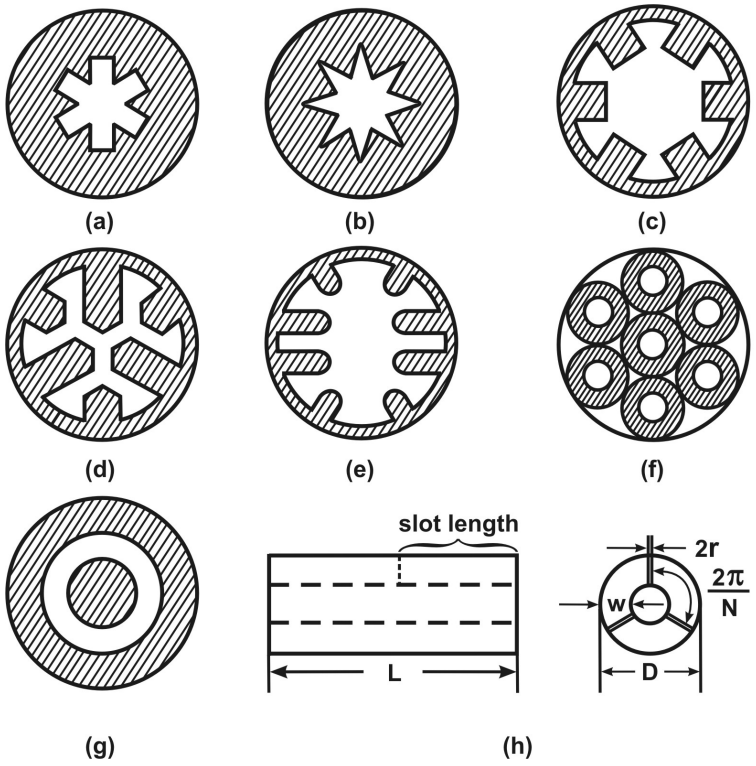

Figure 9.4: Different geometries used for rocket grains (a) Star-square, (b) Star, (c, d) Wagon wheel, (e) Dendrite, (f) All side burning tubes, (g) Rod-in-a-shell, (h) Slotted tube

$A''A'B'$. Since this segment is repeated $2n_{star}$ times, where n_{star} is the number of star points, it is sufficient to examine the behavior of $(1/2n)^{th}$ segment of the configuration. Figure 9.7 shows such a segment. There are two geometric parameters controlling the geometry – n, the number of star points and θ, the angle between the star segments at the star point. It is seen from the figure that segment $A'C$ = Δ_+ is created after combustion of a web to the extent y and the segment AB has reduced by $DB = \Delta_-$ to CB'. The sum $\Delta_+ + \Delta_-$ constitutes the net increase in the perimeter which multiplied by the depth and $2n$ will give the increase in burning area of the grain. We need to obtain the increments in burning length now. We first obtain the different angles that depend on π/n, and $\theta/2$ that control the geometry. These are indicated in the Figure 9.7. From these we get

$$\Delta_+ = A'C = (\frac{\pi}{2} + \frac{\pi}{n} - \frac{\theta}{2})y \tag{9.21}$$

$$\Delta_- = DB = ycot\frac{\theta}{2} \tag{9.22}$$

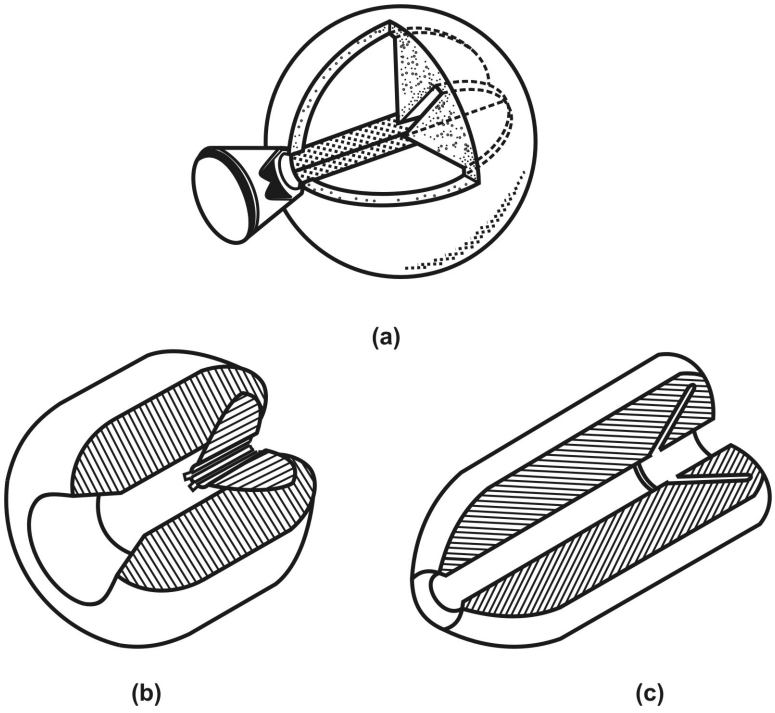

Figure 9.5: The spherical (a), Fin-in-a-cylinder or Finocyl (b) and Cone-in-a-cylinder (Conocyl) three dimensional configurations

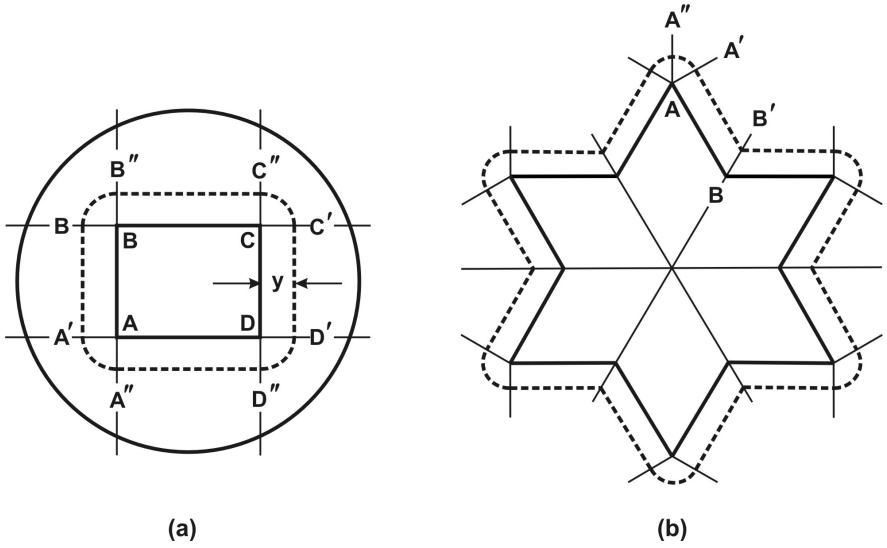

Figure 9.6: A circular grain with a square port and a star burning configuration

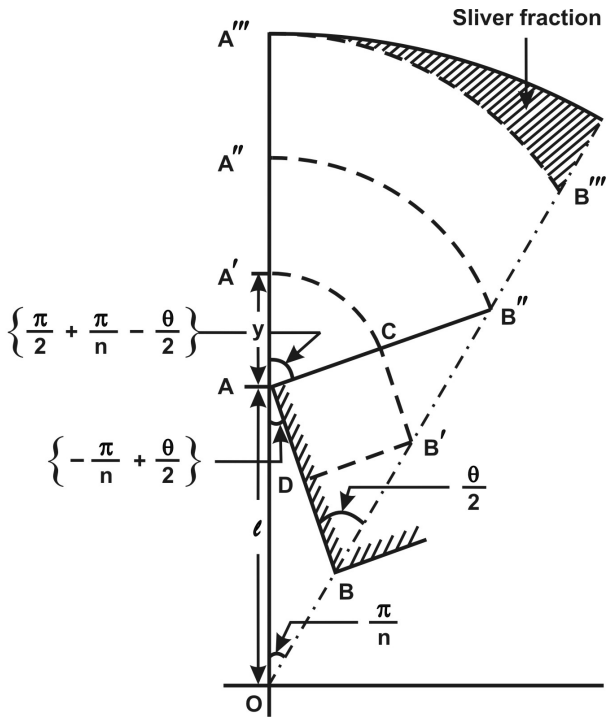

Figure 9.7: A typical star segment showing the different phases of burning

Table 9.2: Star angle for neutral burning vs. No. of star points

n	5	6	7	8	9	10	11	12
$\theta_{n,neutral}$	62.2	67.0	71.1	74.6	77.7	80.4	82.8	85.0

The progressivity of combustion is proportional to $(\Delta_+ + \Delta_-)$. If this sum is 0, one has neutrality. This leads to

$$\Delta_+ + \Delta_- = [\frac{\pi}{2} + \frac{\pi}{n} - \frac{\theta}{2} + cot\frac{\theta}{2}] = 0 \tag{9.23}$$

This transcendental equation is solved to obtain $\theta(n)$ denoted by $\theta_{n,neutral}$. Since $(\Delta_+ + \Delta_-)$ becomes negative for $\theta > \theta_{n,neutral}$, one gets regressive combustion mode for this choice of θ. For $\theta < \theta_{n,neutral}$, combustion will become progressive. Thus, through the choice of suitable θ, one can obtain all the three modes of combustion. Table 9.2 indicates the values for different values of n.

The control on the neutrality and regressivity will last as long as there is a segment that decreases with web burnt. It can be seen from Figure 9.7 that when point B'' is reached, the segment contributing to decrease in area will be com-

pletely burnt up. Beyond this point, the burning area *will only increase*. This increase will go on till the point A''' is reached. This constitutes the outer wall – could be the beginning of insulation/inhibition segment. At this time, the combustion surface is $A'''B'''$. Till this point, the combustion area is in progressive mode from the point the possibility of the three modes (implying neutral, progressive and regressive) is lost (Point B''). On reaching $A'''B'''$, the burning area begins to fall sharply. This wall layer is called sliver fraction. In several motor operations, it will not burn due to sudden decrease of pressure to much lower values that occur due to reduction in the burning area, particularly when propellants with large pressure index are used. One of the objectives of grain design is to reduce the sliver fraction. If the propellant burns to longer web thickness in the regime beyond B'', the shape of the profile will be closer to the outer circle and the sliver fraction will be lower even though the burning area keeps increasing. This behavior is simply due to the fact that a circle drawn with O as the center and A as the center (see Figure 9.7) become close to each other at radius large compared to the distance OA. The question of sliver fraction is important for rocket motors using case bonded double base propellants as in tactical motor applications. For cartridge loaded systems, the grain geometry will be such that the propellant will burn up from all sides or at least radially from outside as well as inside. In this case, it is possible that some propellant fragments may remain unburnt due to small changes in burn rates locally and this cannot be dealt with by geometric changes. In launch vehicles, the lower stages are generally large size motors with reasonable loading. This implies that the propellant outer radius will be larger compared to the distance between the centers discussed above. In rocket motors used for upper stages (that operate at high altitudes) using composite propellants with low pressure index, say < 0.4, the motor will continue to cause efflux of gases from the insulating material and propellant remaining unburnt due to the heat stored in them after the combustion of the major portion of the propellant. This maintains chamber pressures that are low but much higher than the ambient (that is under hard vacuum). This implies that all the propellant will burn up and the issue of sliver fraction is not a vital aspect.

Two-dimensional geometries involving star, wagon wheel and other simple designs can be analyzed analytically for the perimeter and the port area as a function of the web burnt. The results will invariably be in the form of trigonometric functions for the different phases of combustion (initial part for which one can get neutral, regressive or progressive modes) and a later phase which is always progressive. Figure 9.8 shows the plot of the perimeter and Figure 9.9 shows the port area and the sliver area for the case of $n = 6$. Depending on the web chosen, one can obtain both the quantities. To aid design, figures like these are generated for a variety of geometric parameters.

Three-dimensional geometries are the slotted tube, conocyl, finocyl, spherical motor with internal slots at various orientations like in Figure 9.5 and other sim-

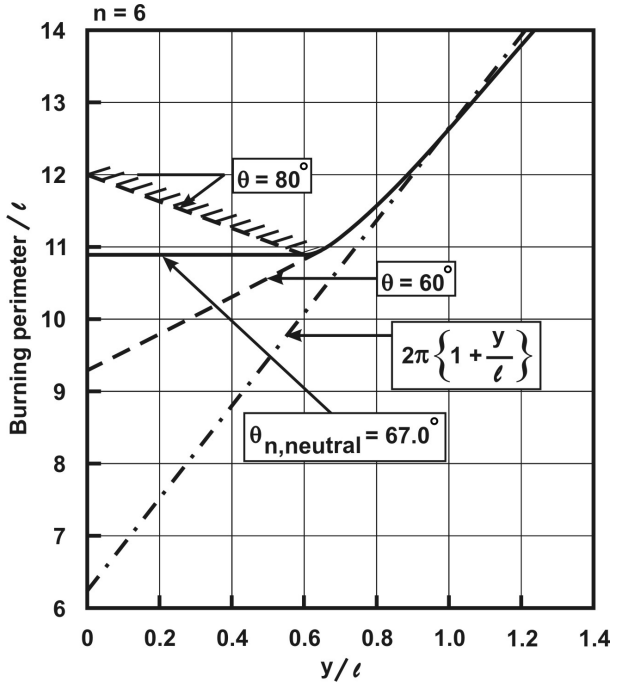

Figure 9.8: The normalized perimeter with burnt distance

ilar configurations that can be conceived. It must be understood that while conceiving these geometries is simple, to ensure that they can be realized in practice through a meaningful casting procedure is not trivial. Calculation of the burning area with web requires computer based strategies. One such strategy involves covering the surface with a large number of points in an appropriate coordinate system and allowing each point to regress a certain distance along the local normal and identifying the collection of such points as a new surface. This process is continued until some portions are completely consumed and the points disappear. Even such a procedure takes a long time for computation. It is suggested that standard contour plot routines can be used gainfully in computing the surface and port areas.

9.2.1 Choice of Neutral and Other Configurations

When grain design is performed in practice, one can obtain neutral burning behavior over a certain web burnt region for applications involving the various configurations discussed above. The extent of neutrality of these geometries is presented in Table 9.3.

It is often stated that neutral burning propellant configuration would be a pre-

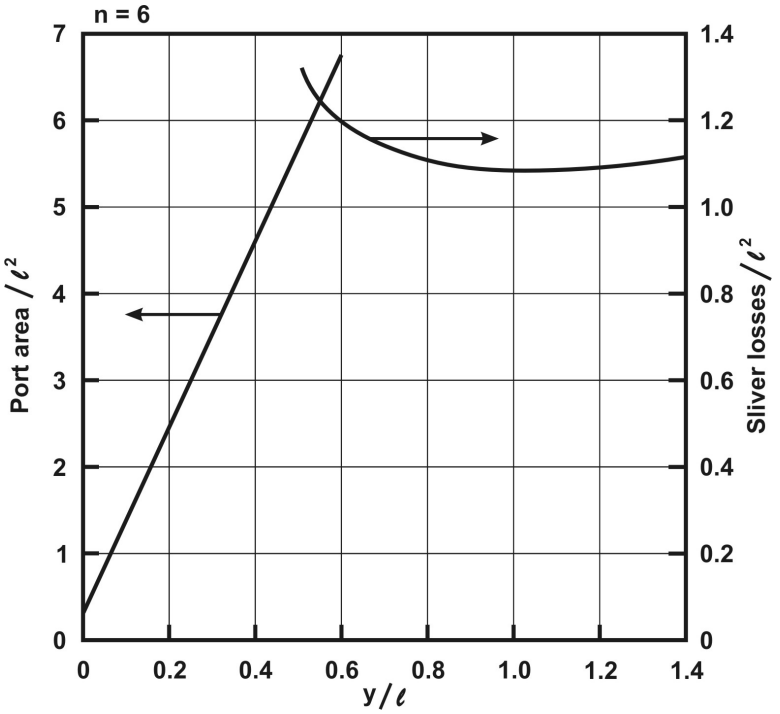

Figure 9.9: The normalized port area and sliver area as a function of burnt distance

Table 9.3: Grain configurations and extent of possible neutral web burn

Configuration	Neutral web fraction, %
End burning	100
Int-ext-side burning	30 – 60
Slotted tube	50 – 90
Rod and shell	30 – 50
Star	30 – 60
Wagon wheel	10 – 30
Conocyl	50 – 90
Finocyl	70 – 90
Spherical	70 – 80

Table 9.4: Longitudinal and lateral acceleration range of various vehicles

Application	Features of motor	Number of g
Tactical	Free standing grain $t_b \sim 10s$	up to 15 at start 20 at burn-out
Strategic missile	Case bonded grain $t_b \sim 100s$	1.5 at start 4 at burn-out
Launch vehicle First stage	Case bonded grain $t_b \sim 50s$	1.3 at start 4 at burn-out
Launch vehicle Upper stages	Case bonded grain $t_b \sim 50s$	2 at start 3 at burn-out

ferred configuration since the pressure-time variation shows a constant pressure. This feature must be interpreted in conjunction with design of the rocket motor for flight operating conditions. In reality, maintaining structural integrity of the rocket motor casing as well as the propellant is connected to the choice of the burning configuration. To understand the forces on the motor and the propellant, one must appreciate the flight acceleration profile.

Most rocket motors experience acceleration during the flight, both longitudinal and lateral. Typical values are presented in Table 9.4. While all large size motors, particularly the motors for launch vehicles use case bonded grains, the motors for tactical military applications use cartridge loading (free standing grains). The acceleration of the first stage of large strategic or space vehicles is usually low at start to keep the acceleration that increases till burn-out within limits. In the upper stages, the thrust demanded is lower and hence, the changes in acceleration between that at start and propellant burn-out will not be large. Starting acceleration of space launch vehicles is smaller than for military vehicles because of the freedom in the time of launch of space vehicles something that cannot be allowed for military applications (the reason is that early flight path can be affected considerably due to wind speeds and higher vehicle acceleration reduces the wind effects).

In case bonded grains, with motors where the acceleration loads are not significant, near constant pressure inside the motor has the advantage of keeping the structural efficiency high because the material strength is used optimally. To explain this point further, if we take a progressive grain configuration, the chamber pressures will increase continuously during the burn duration. The rocket motor casing has to be designed for it to withstand the peak operating pressure as per standard design codes. Such a motor will reside at pressures lower than the design most of the time and yet will have larger casing thickness and weight. Equally, a

largely regressive grain will cause similar issues. In motors that are accelerating significantly with reasonable structural loads on the propellant – casing interface, a mildly regressive grain could be beneficial. Thus, one needs to combine the structural efficiency with structural integrity to arrive at an optimal solution.

If one sets down what one desires from a propellant-propulsion system, they are (a) high propellant loading, (b) near neutral burning, (c) low total weight, and (d) low sliver losses. The high propellant loading will help accommodate the propellant inside a smaller envelop (diameter) so that the vehicle weight is brought down. This leads to a design with the port area comparable to the throat area. In such a situation, there will be erosive burning effects and substantial stagnation pressure difference between the head and aft end. This will cause additional compressive forces on the grain. Coupled with lateral acceleration, it could lead to structural failure of the propellant. In motor development, there have been many cases of this nature when high propellant loading density has been sought. Hence, there arises a need to restrict the loading density. The other aspects (b), (c) and (d) have been discussed earlier. Thus, propellant design will need to be a compromise amongst various desirable features. Large motors have settled down to the propellant design with an "M" curve for pressure-time, in which the pressure has two peaks, one at the early time and another towards the tail end. The key aspect in these and other similar designs is to ensure that the ratio of the peak pressure to the mean pressure is not large, since it is this ratio that decides the structural efficiency of the casing.

9.3 Rocket Motor Operation

When the ignition system of a loaded rocket motor is started up, the motor fires and the pressure measured by a transducer mounted on the head end will appear as shown in Figure 9.10. The first part of the pressure rise is due to the combination of igniter mass burn up and the mass of burnt gas generated from the combustion of the ignited propellant surface. Typically, about 30 % pressure rise is contributed by the igniter mass and subsequent pressure rise is due to the propellant itself. Usually, there will be a pressure peak at the end of this rise and the pressure drops to equilibrium value that can remain constant, increase or decrease depending on the burning area variation with time till a moment when the propellant has burnt up. Since all the propellant will not burn up simultaneously, there is a rate of pressure drop associated with the burn of the last fragments. It may also happen that some pieces that are still burning could be thrown out of the rocket motor through the nozzle since these burning masses move through the fluid towards the nozzle during the course of the burn-up. The pressure finally drops down to the ambient pressure after the burn-up of the propellant.

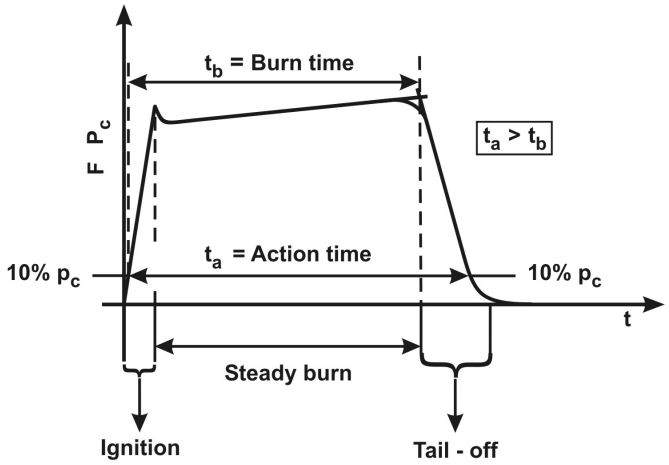

Figure 9.10: A typical chamber pressure vs time trace with identification of burn time and action time

There are two times associated with the pressure-time trace – burning time, t_b and action time, t_c. Burning time is the time from 10 % maximum pressure point to the point of drop-off of pressure located by the intersection of two lines tangential to the curve along the edge of the drooping curve (see Figure 9.10). Action time is the time between the 10 % maximum pressure at the point of pressure rise to a similar point along the pressure decay line. Action time is always more than the burning time. For small sliver non-erosive burn profile, the two times will differ by no more than 2 %. For highly loaded propellant configuration, and/or those with large sliver loss, the two will differ by as much as 4 to 6 %. This is illustrated in Figure 9.11 (a) and (b). While the ignition peak drops off fast in the case of a motor with no erosive burning, the peak drops off slowly when erosive burning is significant. Also, the tail-off is much slower since the burning profile would have caused some portions to be consumed when the significant pressure drop begins. The actual shape of the burning profile in both cases (with and without erosive burning) is shown in Figure 9.11 (a). The nozzle end portions affected by large convective heat transfer burn up at a faster rate compared to the head end segments leading to an axially non-uniform profile variation in comparison to the non-erosive case where the combustion is uniform.

While designing rocket motors whether progressively or regressively burning, one uses the equilibrium relation (9.3) to obtain p_c vs. t in the following manner. Given a geometric configuration, one can calculate A_b vs. y. From equation (9.3) one can get p_c vs y since at every y, one knows A_b. By using $dy/dt = \dot{r} = ap_c^n$ one can integrate for t in terms of y as

$$t = \int_0^y \frac{dz}{ap_c^n} \tag{9.24}$$

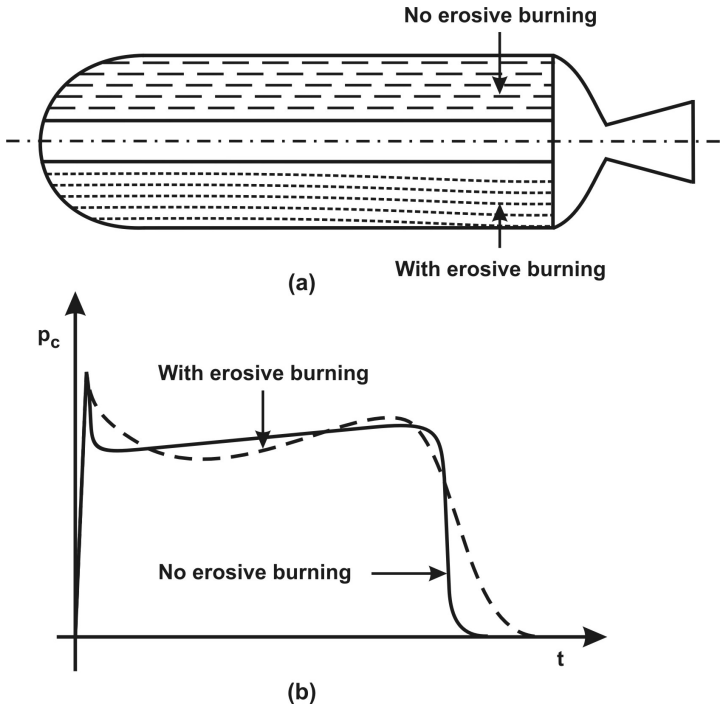

Figure 9.11: The effects of erosive burning on p_c vs. t curve

where the value of p_c at every z (or y) is obtained from the equilibrium relation noted earlier. Thus, one obtains p_c vs. t. With progressive mode of operation, since p_c will vary significantly with time, a question that may arise is: Would the use of equilibrium relation ignoring the unsteady term be justified under these circumstances? To answer this, one should compute the ratio of the left hand side term to one of the terms on the right hand side of equation (9.14) and examine the magnitude. If this ratio is large, one cannot ignore the left hand side term. Thus, we calculate

$$R_{lr} = \frac{\mathscr{V}_c}{RT_c}\frac{dp_c}{dt}/(\rho_p A_b \dot{r}) \tag{9.25}$$

By noting that $dp_c/dt = dp_c/dy \times dy/dt = \dot{r}dp_c/dy$ we can recast the above relation as

$$R_{lr} = \frac{\mathscr{V}_c}{RT_c}\frac{dp_c}{dy}\dot{r}/(\rho_p A_b \dot{r}) \tag{9.26}$$

Now we use the equilibrium relation for p_c and obtain dp_c/dy as

$$\frac{1}{p_c}\frac{dp_c}{dy} = \frac{1}{(1-n)}\frac{1}{A_b}\frac{dA_b}{dy} \tag{9.27}$$

We make use of the equation of state $1/RT_c = \rho_c/p_c$. With some algebra, we get

$$R_{lr} = \frac{1}{(1-n)} \frac{\rho_c}{\rho_p} \frac{\mathscr{V}_c}{A_b} \frac{1}{A_b} \frac{dA_b}{dy} \tag{9.28}$$

To get an estimate of the ratio R_{lr}, we make use of a hollow circular cylinder burning from inside as it represents the asymptotic profile in the burning profile of a propellant with any internally burning two-dimensional geometry. In this case, $A_b = \pi d_p L$ and $dA_b/dy = 2\pi L$ where L is the length of the grain and d_p is the port diameter. $\mathscr{V}_c = \pi d_p^2 L/4$. If we substitute these into the above equation, we get

$$R_{lr} = \frac{1}{2(1-n)} \frac{\rho_c}{\rho_p} \tag{9.29}$$

The magnitude of ρ_c/ρ_p was estimated as 0.005 – 0.01 [see the discussion following equation (9.13)]. For $n = 0.7$, the order of magnitude of R_{lr} is therefore 0.01 – 0.015. Thus, even for the highest pressure rise rate, the unsteady filling term dm_g/dt constitutes about 1.5 %. That is why equilibrium estimation of chamber pressure is quite accurate. Of course, this condition will not be obeyed during the starting transient and the tail-off. Under these conditions, one needs to account for the chamber gas mass filling term on the left hand side.

9.4 Ignition System and Process

Igniters have several components. The first component is an initiator. This transfers the energy to the main charge through a thermo-chemical process. Many variants of initiation systems have been built to help safe and sure operation. The initiation systems are electrical, mechanical shock wave, laser or semiconductor bridge.

The electrical system could be hot wire initiator or exploding bridge wire initiator. The hot wire initiator has been used for a long time and is a work horse even now. The first component of this is a squib. Figure 9.12 shows the elements of a squib. This is a bridge wire of nichrome that gets heated on the passage of an electric current. There is a no-fire current, an all-fire current and a recommended fire current. Typically these are 0.1, 1, and 0.5 amps respectively. Around the squib is placed the primer. As soon as the bridge wire gets red hot, the primer material (mercuric fulminate or lead azide) will explode. These together weigh 50 mg – 1 g and will burn up in less than 5 ms. This energy is picked up by a transfer charge, a booster charge and a main charge in sequence. The transfer charge consists of 0.5 to 5 g of powder or granules (1 – 3 mm size). Since material is in powder form, it picks up the energy from the squib fast enough and holds the fire for about 5 to 10 ms before the booster charge takes over. The essential character of booster

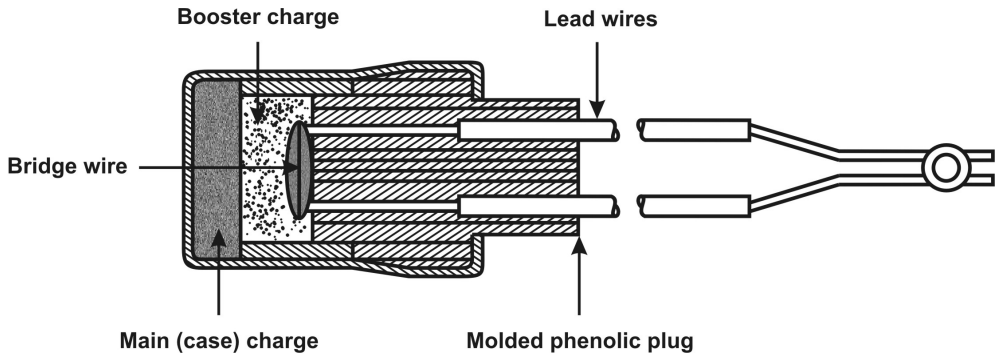

Figure 9.12: Details of a squib used in pyrotechnic igniters, adapted from ref. [22]

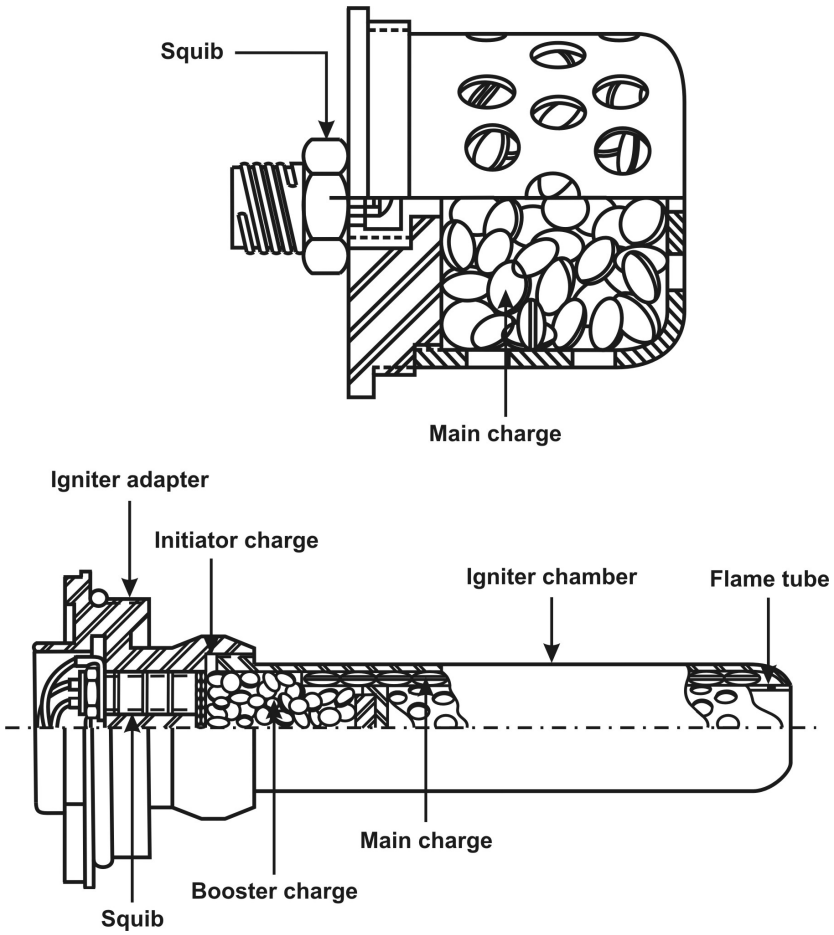

Figure 9.13: Two types of igniters – Basket igniters and Jet flame igniters, adapted from ref. [22]

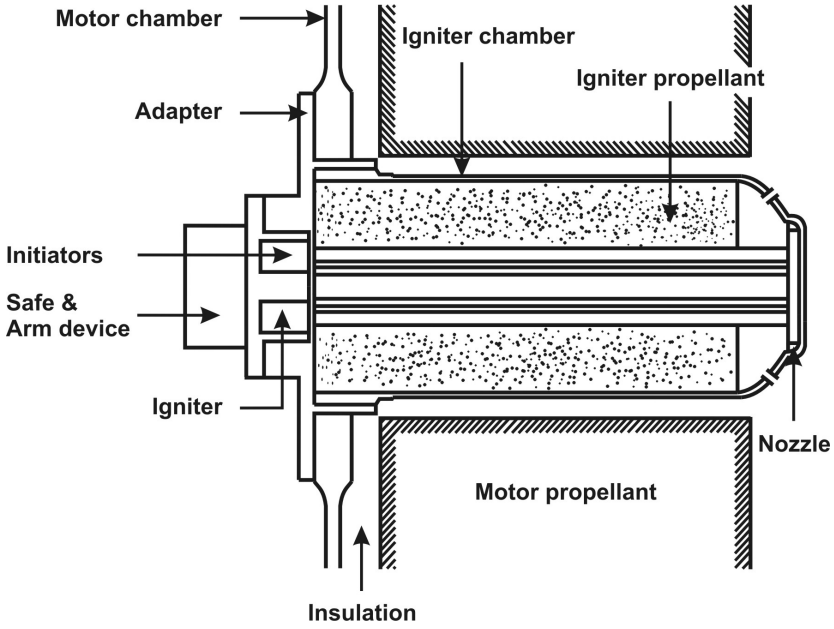

Figure 9.14: The pyrogen igniter system with safe-arm facility

charge and the main charge is about the same – both are made of pellets of size – 5 to 10 mm size. Their weight is dictated by the motor free volume and the pressure that is intended to be built up – typically between 30 to 40 % of the equilibrium pressure (just at the end of the ignition transient). Figure 9.13 and 9.14 show the details of three classes of igniters – basket, jet and pyrogen. The basket igniter is the simplest and used in many small motor applications. It is robust even though it is heavy. Its operation allows smooth pressure rise. For larger size motors, one adopts the jet igniter assembly. As can be noted from the Figure 9.13 (b), a jet effect is caused towards the end of the igniter assembly. It would also be possible to provide jets in several directions to reach all parts of the burning surface. The pyrogen ignition system shown in Figure 9.14 is a small rocket motor with the grain composition meant for igniters as discussed in section 7.7. This itself has an ignition system usually more elaborate than squib-transfer-booster-main charge strategy. This is because the igniter is used in large motors. The exit of this pyrogen motor can also have multiple holes for the hot particle laden jets to issue and cause a number of hot spot ignition points. The dynamics of ignition of large motors is controlled by the fluid flow processes.

The exploding bridge wire initiator uses gold/platinum wires with low resistance that are subject to high voltage so that in times of the order of 5 to 10 μs, the initiation is obtained. The high explosives used are not the primary explosives; the explosives used here are RDX or PETN (pentaerythritol tetranitrate). They

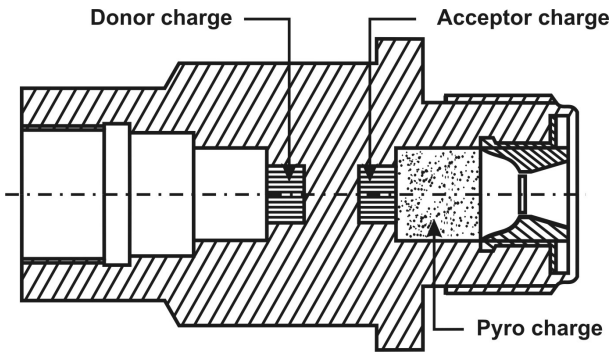

Figure 9.15: The schematic of a Through-Bulkhead Initiator

are "more safe" since they are not sensitive to stray currents or disturbances. The high voltage supply system implies heavier insulation and hence, larger weight penalties. The mechanical shock wave kind is called a Through-Bulkhead Initiator (TBI); it is shown in Figure 9.15.

A steel structure of the kind shown in the figure carries a donor and acceptor explosive charge. The donor charge is exploded usually with flexible detonating fuse in about a microsecond. The shockwave from the donor charge is transmitted through the metal body into the acceptor charge that ignites the pyro-charge. The gases from the pyro-charge can ignite the propellant in the pyrogen igniter assembly. This system is combined with safe/arm devices in duplicate to provide for redundancy. The safe position isolates the firing lines from the initiators carried in the safe/arm device and also mis-align the explosive train until "arm" is energized.

The laser device consists of a laser firing system, a communicating fiber-optic line through a sealed optical window into the explosive material. Short wave length laser beams ($\sim 0.3\ \mu m$) cause initiation of the explosive by bond breaking and long wave length beams ($\sim 1\ \mu m$) cause local heating that can be enhanced by using better heat absorbing materials like carbon. These systems awaiting exploitation are considered "highly safe" because they are tolerant to a number of incidents like electrostatic discharge and radio frequency disturbances.

The semi-conductor bridge type consists of a doped poly-silicon layer formed on a silicon substrate on a metallic surface acting as a conductor of electricity. A current pulse through the system causes the bridge to burst into a bright plasma discharge in microseconds transferring energy to the main charge. This is also tolerant to disturbances like the laser device.

All solid rocket motor systems using any one of the initiators and main charge pyrotechnic compositions in pellets-in-a-basket or pyrogen motor need to fulfill

certain requirements on the pressure-time behavior. These are

(1) The time delay between the ignition pulse (electric command) and 10 % pressure rise point as well as time interval between 10 % to 90 % pressure rise should be within a specified limit (typically 30 to 100 ms depending on the motor size). These have effect on the exit nozzle operation (severely over-expanded for the period before the exit pressure exceeds 30 % of the ambient pressure) leading to unsteadiness in thrust.

(2) The pressure rise rate (dp_c/dt) should not be so high as to cause shock loads on the propellant affecting its structural integrity.

(3) Minimization of hardware weight and volume particularly in small tactical motors since the inert mass can become significant fraction of the total mass of the motor.

The key feature of the igniter, namely, the weight of the main charge (w_{ign}) is obtained from the requirement that it should have some solids fraction (sf) and the hot gaseous component attain a certain chamber pressure inside the motor (the entire free volume of the chamber, usually taken up to the throat).

$$w_{ign} = \frac{1}{(1-sf)} \frac{p_{c,ign} \mathcal{V}_c}{(RT_c)_{ign}} \tag{9.30}$$

where $p_{c,ign}$ is the chamber pressure at the end of the ignition phase, V_c is the free volume of the combustion chamber, sf, R_{ign} and $T_{c,ign}$ are the solids fraction, the gas constant and flame temperature of the products of combustion. This equation is simply the equation of state for the gaseous fraction of the products at the end of the ignition phase. In the case of black powder, the molecular weight of the products of combustion is about 35 and the flame temperature 2600 K. The more energetic composition using Boron (28.5 %), Potassium Nitrate (69.0 %) and Poly ethyl cellulose (2.5 %) gives products at T_c = 3535 K with composition involving liquid boron (36 %) and gaseous products as follows (by volume): BO = 0.140, N_2 = 0.103, KBO_2 = 0.125, B_2O_2 = 0.055, CO = 0.055, HBO = 0.035, H_2 = 0.017, H = 0.012 and B_2O_3 = 0.01. In this case sf = 0.36.

Equation (9.30) is satisfactory for motors that are not long. In case of large motors (that are usually long – 20 to 40 m), the free volume is large (20 to 40 m^3), one needs to consider the aero-thermo-chemical dynamics to enable predict the pressure – time curve. Data on several tactical motors as well as large motors used for strategic or launch vehicle applications are shown in Table 9.5. It can be seen from this table, tactical motors use a igniter weight-to-free volume ratio of about 7 – 8 kg/m^3 (excepting for tactical motor T-2, in which case, the propellant is stated to be a fuel rich solid propellant difficult to ignite and so, larger igniter weight is needed to cause a smooth ignition). In the case of large motors, the igniter weight used is much smaller in proportion to the free volume. This is due to the fact that

Table 9.5: Igniter data for some vehicles, (C_1 = 28.5 B, 69 KNO_3, 2.5 Polyethyl cellulose, C_2 = 14 HTPB, 84 AP, 2 Al); T -1 to T-4 = Tactical motor 1 – 4; L1 = Large tactical motor, L2 = PSLV, India, L3 = Space shuttle solid rocket booster, USA

System	T-1	T -2	T -3	T - 4	L1	L2	L3
F, kN	6.0	20.0	21.0	100.0	700	4860	13820
V_c, l or m^3	0.95 l	2.0 l	6.8 l	35.0 l	1.76 m^3	29 m^3	40 m^3
w_{ign}, g or kg	6 g	70 g	55 g	300 g	3.3 kg	25 kg	56 kg
Comp.	C_1	C_1	C_1	C_1	C_2	C_2	C_2
w_{ign}/V_c, kg/m^3	7.0	35.0	8.1	8.6	1.87	0.82	1.4

the process of ignition in large motors has more aspects to raising the pressure of the free volume. The total ignition process can be split into ignition of all of the propellant surface that actually calls for a flame spreading process from the head end to the aft end and the chamber filling process in which the gas has to fill in entire free volume to equilibrium values. The ignition of all segments occurs by a flame spreading process. For a 35 m long motor, if we take that the flame spread occurs in 400 ms, the spread rate amounts to 90 m/s. This spread rate is not uniform. It starts off at about 10 m/s in the early ignition time and accelerates to 150 m/s towards the propellant end segment. One of the key features would be the time for which igniter has to keep firing. In the case of Polar Satellite Launch Vehicle (PSLV, India) and Space Shuttle - Solid Rocket Booster (SS-SRB, USA), the igniter firing time is about 600 ms. Attempts to bring this down to 300 ms to increase the pressure rise rate of the motor are in progress in advanced versions of these systems.

9.5 Extinction and Thrust Termination

Strategic vehicles like IRBM and ICBM are designed for a wide horizontal range to enable a class of targets be accessible to a set of vehicles. The launch involves the setting of parameters for the payload to be launched at a specific point in space or on earth or under water with a specific velocity (including the vector) so that subsequent ballistic path will lead the warhead to the target. Great accuracies of the position and velocity are required to ensure little errors in reaching the target (low Circular Error Probability, as the usual terminology treats it). Since the same vehicle will need to be positioned at different locations in space depending on the distance of the target from the launch point, it is essential to have a strategy to terminate the thrust of the vehicle at a point close to the location at which the ballistic trajectory begins. The strategy used to terminate the thrust is the process of extinction of the burning propellant caused by sharp de-pressurization. At

any point of burn, $p_c \sim (A_b/A_t)^{1/(1-n)}$ as obtained from equation (9.3). The strategy for causing extinction lies in suddenly increasing A_t so that the equilibrium pressure is brought down. This is usually accomplished by the use of explosive cord around a cross section that is designed for opening up when required. Typical duration over which this occurs is about 0.6 to 1 ms. The sudden drop in pressure leads to the gaseous flame over the propellant to move away - rather, the flame thickness increases. This causes the temperature gradient over the propellant to drop, reduce the heat transfer to the propellant, reduce the surface temperature, decrease the gas production rate. The process could stabilize at a new condition of burn and a certain chamber pressure if the sharpness of the transient is not large enough. Experimental studies have shown that if the chamber pressure drop rate is such that *the time taken for it to drop to half its value is less than about 3 ms*, the propellant will not reignite, but simply quench. From this point onwards, the chamber pressure falls off exponentially with the characteristic time being $t_c = (\mathscr{V}_c/A_t)/(c^*\Gamma^2)$, where the A_t is the new enhanced value contributing to reduction in t_c. There are other methods of extinguishing a burning propellant, like injection of water/inert gas, but the most commonly adopted technique is the de-pressurization strategy. In practice, the area ratio is so chosen that the chamber pressure falls below 0.2 - 0.3 atm. from the operating pressure - 40 to 60 atm. such that the half pressure fall occurs in less than 4 ms so that the possibility of re-ignition is totally eliminated. Whenever the pressure transient brings down the pressure, there may result oscillatory combustion called “chuffing”. In this mode of combustion, there are periods of burning at low pressure interrupted by extinction. In the period when extinction is experienced, the propellant that has some residual heat in it and additional heat pumped into it from the cylinder walls, can suddenly burst into combustion with the generation of a large mass of gas that then goes through the nozzle leading to a sudden pressure rise. Depending on the conditions, this process may repeat itself. This is the reason for bringing down the pressure to less than 0.2 atm. so that no possibility of re-ignition or chuffing takes place.

9.6 Thermal Protection Systems

Thermal protection systems are required for all parts of the rocket motor. It is not the high temperature alone that matters, but also the intense convective flux due to the flow of the hot gases past the surface. In cases where internal burning propellant configuration is adopted, the area of the outer wall exposed to the hot gases is limited to some portions of the head end and some at the nozzle end. In case end burning configuration is adopted, the wall segment will get continuously exposed during motor burn. This causes heat transfer to the wall due to the flow of gases. Apart from these conditions, the hot gases will flow through the nozzle

at much higher flux than in the motor itself. In fact, as will be clear in later paragraphs, the mass flux is the largest at the throat and the heat flux also will be the highest. The heat transfer between the hot gases and the wall is estimated by noting that the transfer process is controlled by a turbulent boundary layer. The heat transfer rate is obtained from

$$Nu = 0.023 Re^{0.8} \tag{9.31}$$

with $Nu = h_g D_l/k$, $Re = \rho V_g D_l/\mu$, where Nu = Nusselt number, Re = local Reynolds number, h_g is the heat transfer coefficient, D_l = local diameter of the nozzle, k, μ are the free stream thermal conductivity and viscosity of the gas, ρV_g is the mass flux, the product of the density and the velocity of the gas. The heat flux is obtained from $\dot{q}'' = h_g(T_{c,t} - T_w)$ where $T_{c,t}$ is the stagnation temperature of the fluid and T_w is wall static temperature. For a given rocket motor, with a fixed flow rate through the nozzle, the Reynolds number can be expressed as

$$Re_t = \frac{\dot{m} D_l}{(\mu \pi D_l^2/4)} = \frac{4\dot{m}}{\pi D_l \mu} \tag{9.32}$$

Now, the variation of h along the axial distance defined by the local diameter, D_l can be obtained by

$$h_g = 0.023 k \left[\frac{4\dot{m}}{\pi \mu}\right]^{0.8} \frac{1}{D_l^{1.8}} \tag{9.33}$$

The heat transfer coefficient (and the heat transfer) increases from the entry to the nozzle to the throat at which location D_l attains the lowest value through the cross section (= D_t), and decreases beyond the throat up to the nozzle exit.

For a nozzle of polar satellite launch vehicle booster, we estimate the heat flux at the throat: $\dot{m}$ = 1400 kg/s, $D_l = D_t$ = 0.8 m, $\mu = 6 \times 10^{-5}$ kg/m s, Re = 3.7 $\times 10^7$. At this value, Nu = 2.6 $\times 10^4$ and h_g = 5.2 kW/m^2 K. Typical distribution of the heat transfer coefficient for one of the motors is shown in Figure 9.16. The approach presented here is modified to include some subsidiary effects like boundary layer growth up the entry to the nozzle and acceleration effects through the nozzle. The above expression can be used to understand the influence of chamber pressure also. In rocket chamber design, the chamber pressure is a parameter chosen by the designer. For the same mass flow through the nozzle, the choice of increased chamber pressure implies reduced throat dimension to obtain a predefined thrust. By rearranging the terms of the equation (9.33), we can express the heat flux in terms of individual parameters as,

$$h_g = 0.023 k [\frac{\pi}{4}]^{0.1} \dot{m}^{-0.1} \mu^{-0.8} p_c^{0.9} c^{*-0.9} \tag{9.34}$$

It is clear from the above equation that the heat flux varies as $p_c^{0.9}$.

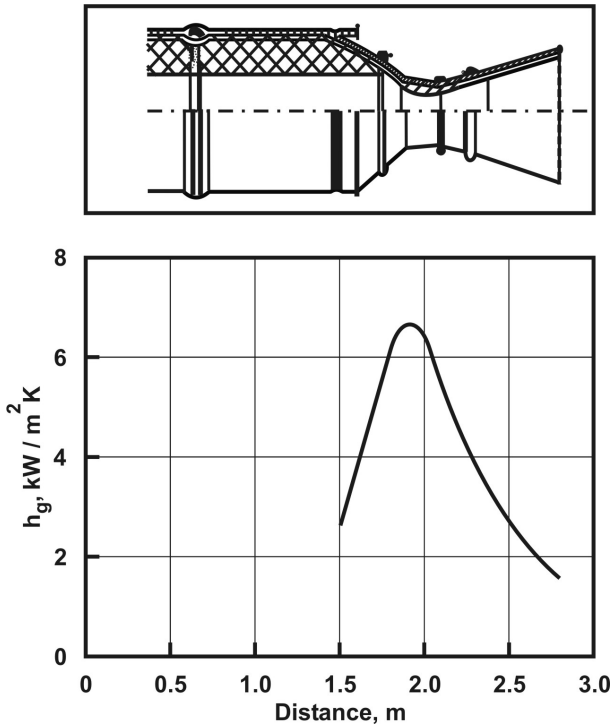

Figure 9.16: The distribution of heat transfer coefficient with nozzle length for a large motor

There is another way of presenting the above equation. This expresses the result in terms of thrust and chamber pressure. This gives

$$h_g = 0.023k[\frac{\pi}{4}]^{0.1}F^{-0.1}\mu^{-0.8}p_c^{0.9}c^{*-0.8} \tag{9.35}$$

By introducing values to quantities that are unlikely to vary much in rocket engines, one can write

$$h_g = 0.0043c_p\frac{p_c^{0.9}}{c^{*0.8}F^{0.1}} \tag{9.36}$$

The intriguing dependence on c^* can be understood to imply that if c^* increases at the same p_c, throat area increases and hence, the heat flux gets reduced. So also can one explain inverse weak dependence on the thrust. The total heat flux received at any point on the surface of the rocket motor also includes that due to radiation from gases and particulate matter. The gases that contribute to radiation are those that are infrared sensitive, namely, carbon dioxide and water vapor. The total magnitude of radiant flux is about 10 – 30 % of the convective flux. The flux in gas phase is dependent on the average beam length of radiation that passes through a layer of gas with certain partial pressure of the absorbing gas. The radiant flux is derived from the classical expression

$$\dot{q}''_{rad} = \epsilon_w \sigma_r [\epsilon_g T_c^4 - \alpha_g T_s^4] \tag{9.37}$$

where ϵ_w, ϵ_g, and α_g refer to the emissivity of the wall and the gas and absorptivity of the gas, respectively and σ_r is the radiation constant (= 5.67×10^{-8} W/m^2 K^4).

After taking into account the radiant properties, an approximate expression has been obtained as (see reference [12])

$$\dot{q}''_{CO_2} = 12.8(p_{CO_2} L_e)^{1/3} [(\frac{T_c}{1000})^{3.5} - (\frac{T_w}{1000})^{3.5}] \tag{9.38}$$

$$\dot{q}''_{H_2O} = 4.1 p_{H_2O}^{0.8} L_e^{0.6} [(\frac{T_c}{1000})^{3} - (\frac{T_w}{1000})^{3}] \tag{9.39}$$

It must be noted that p_{CO_2} and p_{H_2O} are the partial pressures of carbon dioxide and water vapor in atm. and L_e is the mean beam length chosen between 0.65 to 0.9 D_l in m, and the heat flux in kW/m^2. For the high energy solid propellant (CP2 from Tables 7.7 and 7.8) the mole fractions of CO_2 and H_2O are given by 0.009 and 0.087 respectively. At a chamber pressure of 50 atm., these mole fractions translate to p_{CO_2} = 0.45 atm. and p_{H_2O} = 4.35 atm. respectively. Taking the beam length as 0.7 D_l with D_l = the motor diameter (2.8 m), L_e = 2.0 m. With T_c = 3381 K and $T_w \sim 2000$ K, we get $\dot{q}''_{CO_2}$ = 737 kW/m^2 and $\dot{q}''_{H_2O}$ = 620 kW/m^2. The total radiant flux will be 1357 kW/m^2. This constitutes about 16 % of the total flux. If we divide this flux by $(T_c - T_w)$ = 1381 K, we get $h_{g,rad}$ = 0.94 kW/m^2 K.

A simpler way to calculate the heat transfer from the gas phase to the surface by radiation when the gas phase involves particulate matter that may include metal oxides and carbon particles, is to use equation (9.37) with experimental information on the emissivity. Measurements have shown $\epsilon_g = 1.35 - 0.33(T_c/1000)$ for a temperature range of $3600 > T_c > 2000$ K. For the data indicated in the earlier paragraph, with $\epsilon_w = 0.9$, $\alpha_g = \epsilon_g$, the estimate of the radiant flux is 1310 kW/m^2. This value includes all aspects of radiation unlike the previous result that depends only on the gaseous radiation component. If the two values are within 20 % of each other, it should be considered satisfactory.

9.6.1 Materials for Thermal Protection

From the earlier discussion, it is clear that different parts of the nozzle experience different degree of heat flux, the throat region being the most critical one. It should also be noted that (a) the high temperature gases contain gases that could react with wall material, like water vapor and carbon dioxide with carbon, if carbon or graphite is used and contribute to regression of the wall surface and (b) the products contain metal oxides that travel at high speeds, some of them too large to follow the gas and thus, impinge at high velocities on the wall surface. This could

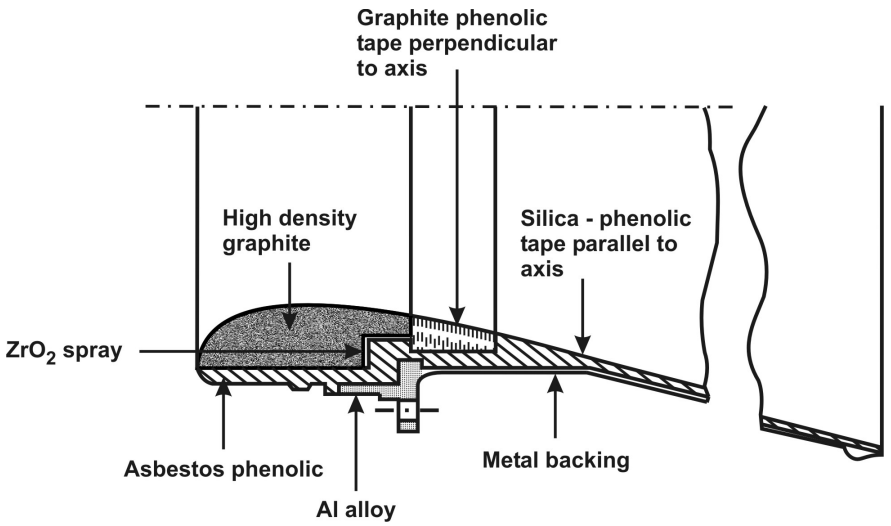

Figure 9.17: Details of the flexible segment of the flex-nozzle

cause deposition on the surface as seen some times and mechanical removal of the wall material in other times. The choice of materials should be such as to stand up to such conditions. It is desirable that the dimensions of the nozzle, throat in particular do not change during the operation, for otherwise the chamber pressure will continue to drop due to this effect. Most of these materials do erode or "ablate". The ablation rate is kept low by the choice of the material. Typical materials used are metals like Tungsten, high density graphite, or composite ceramic materials. The composite materials used are asbestos-phenolic, silica-phenolic, carbon-phenolic, and carbon-carbon cloth in the increasing order of severity in use. Throat region has either high density graphite or carbon-carbon cloth. The back up for this could be asbestos-phenolic composite. The downstream regions of the nozzle could be made of silica-phenolic material. The composite material based structures are produced by weaving the fibers in a predetermined geometric arrangement after being coated with the phenolic resin on to a mandrel. The block is then cured at high pressure (5 to 7 atms) and temperature (200 – 250 °C) in an autoclave for 15 to 30 hours depending on the size of the system and the curing cycle employed. The final mechanical properties are strongly dependent on the approach chosen to make the blocks. Figure 9.17 shows the elements of a large nozzle that utilizes a variety of high temperature materials in a single assembly. This arrangement is typical for large motor application. The properties of materials used for thermal protection are presented in Table 9.6. The table is revealing. It is useful to note that thermal conductivity (k) controls the temperature gradient across a thickness at steady state and thermal diffusivity ($k/\rho_p c_p$) controls the time it takes to reach a certain temperature under a flux. It can be seen

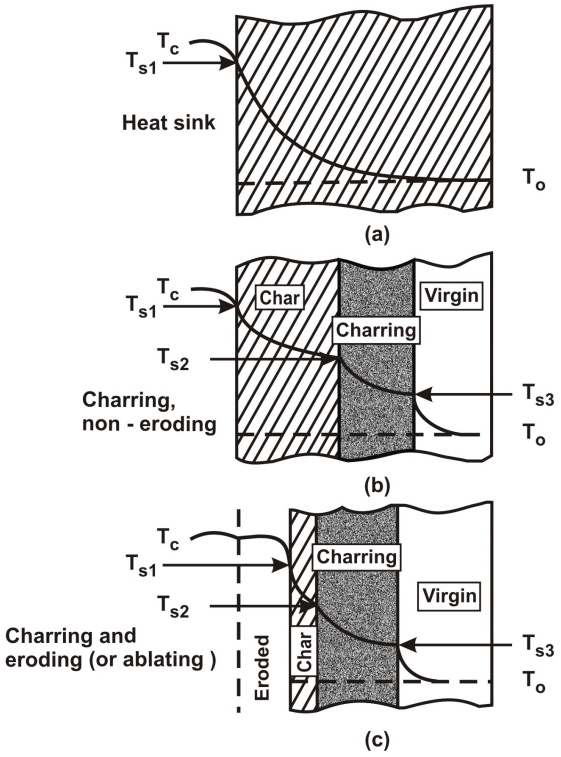

Figure 9.18: Temperature profiles through heat sink, charring and ablating materials, adapted from ref.[22]

that graphite and other composites act in different ways. In the case of graphite, thermal conduction is the only process. In the case of charring materials, heat is absorbed locally by decomposition of the resinous components keeping down the peak temperature. The temperature profile is also affected by the heat absorption process. In the case of charring and ablating materials, surface material is continuously pealed off after thermochemical degradation. By choosing materials that absorb a lot of heat per unit mass, it is possible to keep down the degradation rate. Figure 9.18 shows the temperature profile through various classes of materials. The three categories indicated in the figure are in the increasing order of heat extracting capability. All the composites belong to this category.

In the case of graphite or heat sink class of materials (including tungsten that is often contemplated for this purpose), shown in Figure 9.18 (a), the surface temperature, T_s will keep increasing till it reaches a value close to T_c. If one solves the thermal problem for a block of material subject to heat flux with a heat transfer coefficient h_g on one side and with adiabatic conditions at the other, the solution to the one-dimensional conduction problem leads to a result in which the surface tem-

Table 9.6: Thermal and mechanical properties of materials for thermal protection; Si = Silica, Ph = Phenolic, C = Carbon, * = along grain/across grain

Property	Graphite	Si-Ph	C-Ph	C-C
ρ_p, kg/m^3	1840	1780	1450	1450
c_p, kJ/kg K	0.71	1.01	0.84	1.31
k, W/m K	130.0	0.35	0.66	31.0/13.8*
$\alpha = k/\rho_p c_p$, mm$^2/s$	100.0	0.20	0.54	16/7
UTS, MPa	14.2	88.4	50	90/5*

perature and the heat penetration distance both will keep increasing with time. If one wishes to obtain non-dimensionalization time scale, it can be formed from the gas phase heat transfer coefficient (h_g), thermal diffusivity (α), and thermal conductivity (k) in the following manner - $t_{con} = c_0 k^2/h_g^2\alpha$. The depth of penetration in non-dimensional form is obtained from defining a depth at which the temperature attains a specified value. Thus, one can define a depth $\xi_w = x_w/2\sqrt{\alpha t_{con}}$, where x_w is the position from the surface into the solid at which $\tau_w = (T - T_0)/(T_c - T_0)$ attains a specified value. For c_0 = 1.0, the non-dimensional temperature τ_w is 0.58 and ξ_w = 1.52. For c_0 = 4 and 9, τ_w = 0.83, 0.9 and ξ_w = 1.75, 1.8.

If we take some typical values – α = 16 mm^2/s, k = 31 W/m K, h_g = 4.5 kW/m^{2}K, the above relations show that the surface temperature reaches a value very close to adiabatic gas temperature (τ_w = 0.9) in about 9 ms. Hence, the heat sink material should have a melting point above the adiabatic flame temperature. The depth of heat penetration, x_w is 1.6 mm which is small. Since the thermal profile propagates as $x_w \sim 3.6\sqrt{\alpha t}$, the thickness of the material required is 144 mm for a 100 s burn duration. Providing such a thickness at throat with reducing thickness on either side of the throat is a reasonable solution to handling thermal protection issues in a solid rocket motor.

9.7 Thrust Vector Control

Thrust vector control is needed for several flight vehicles. Aerodynamic control is usually the preferred option for operations within the atmosphere where it is feasible. Tactical missiles using booster-sustainer motors prefer to do boosting without control and restrict control operations to the sustainer mode during which mode, the axial forces on the vehicle are much lower. Very small tactical systems use vanes in the exhaust of the engine to cause forces that could be used for pitch (up and down) and yaw (left and right) control. Launch vehicles/strategic missiles are usually launched vertically and the early stages of flight (till the first ten to fifteen seconds or so at which stage, speeds up to M = 0.5 are reached) could be

affected by lateral winds.

Figure 9.19 shows a launch vehicle (PSLV) designed and built in India. It has a core motor and six strap-on motors of lower thrust. This arrangement of a single large thrust motor at the core and smaller thrust motors on the periphery is chosen to benefit from the available motors and minimise the size of a very large thrust motor that has to be developed anyway. The outer motors have a nozzle that is canted radially outwards. The thrust vector from all the motors is expected to meet on the axis of the vehicle. Inevitably, there will be mis-alignments in the thrust vector both in terms of direction and magnitude. This will cause forces on the vehicle that can take it away from the intended trajectory. To overcome this problem, one needs a thrust vector control system. Such large vehicles use side injection thrust vector control (SITVC) approach shown in the Figure 9.19 or gimballing nozzle section of the motor shown in Figure 9.25. In SITVC, one can introduce a piece of ceramic/graphite or a jet of fluid laterally into the flow at a location in the expanding portion of the nozzle. This injection can be at a specific number of locations to enable a specific vector to be obtained. The principle of the approach is shown in Figure 9.20. The jet that is injected with sufficient momentum ($\rho_j V_j^2$) compared to the momentum of the gas ($\rho_g V_g^2$) of a paraboloidal shape that is normal near the wall. This shock causes a large pressure gradient on the boundary layer. Under this strong negative pressure gradient, there will be an upstream separation bubble. The jet itself will break up into droplets and bend over and the droplets vaporize and create a region of vapor behind the oblique shock. The pressure distribution in the azimuthal direction will be asymmetric. A part of the wall region will experience higher pressure and hence, a lateral force will be created. Of course, another component of the force is the momentum of the jet itself. For small flow rates of the injectant, the side force will linearly increase and the axial thrust does not suffer any decrease because the decrease due to the formation of the oblique shock is partly or more than compensated by the additional flow of fluid through the nozzle. Many liquids are proposed as an injectant. Since the liquid is to be carried in tanks and the tanks themselves need to be pressurized to cause the flow through the system, it has been found useful to use a high density fluid. Strontium perchlorate (30 %) solution in water has been used as the injectant. In this case, experiments have shown that the ratio of the side force to axial thrust is about a third to half of the ratio of the injectant flow rate to the main flow rate. Design of such systems is based on a number of subsidiary experiments and a statistical assessment of misalignments and wind effects. The liquid that one carries is usually more than demanded by the worst case scenario since its presence will be mission critical. The optimization of the amount to be carried is dependent on the accuracies achieved in all the manufacturing processes.

Consequently, a more elegant system, namely the use of flexible nozzle (flex-nozzle) has come into play. In the last two decades, many countries have developed

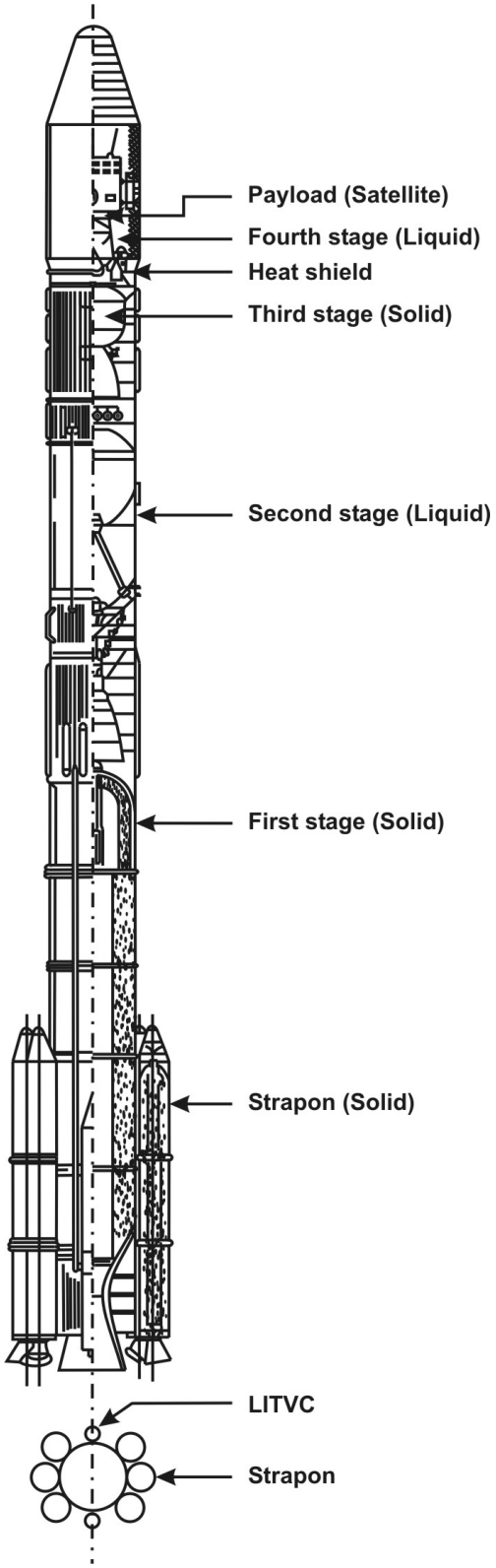

Figure 9.19: The assembly of a Polar Satellite Launch Vehicle

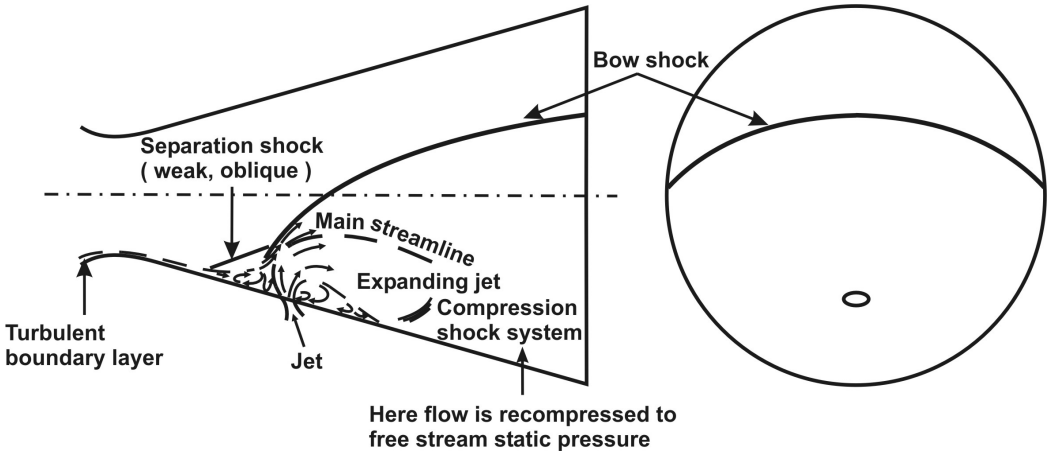

Figure 9.20: The fluid dynamics of liquid injection thrust vector control system used in large motors

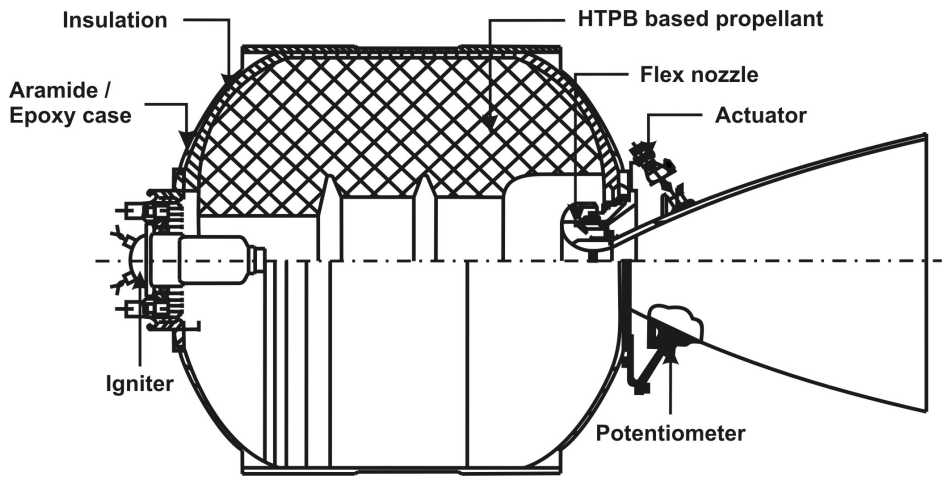

Figure 9.21: A motor with flexible nozzle

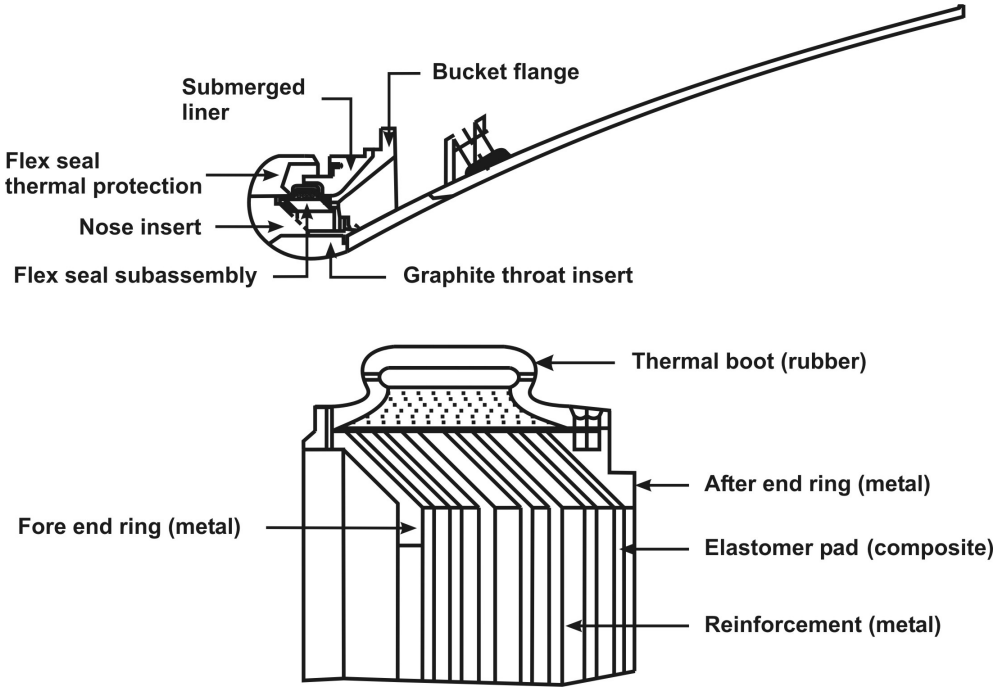

Figure 9.22: The details of a flexible nozzle; the critical component is the flexible element made of ply of metal sheets and silica phenolic composite

the flex-nozzles even on large motors. Figures 9.21 and 9.22 show the details of the flexible nozzle developed for the third stage of PSLV vehicle.

As can be noted, the nozzle is submerged in the rocket chamber. The flow from the most forward part of the propellant has to turn around the submerged section of the nozzle before passing through the nozzle. Flexibility of the nozzle is obtained through the use of a number of high temperature composite sheathing joined with one another in a manner that they can move with respect to each other. A pneumatic/hydraulic actuator located in a position that provides for high mechanical advantage can rotate the nozzle by the required amount. Typically, rotation of 4 to 7° is considered reasonable. The development of flex-nozzles is controlled by the components of composites that need to have the appropriate flexibility at high temperature. Most large motors have flex-nozzles as clear from Table 9.7.

9.8 Performance Losses

It has been brought out in section 4.4 that the two typical nozzle shapes in use are the conical and contour. The divergence losses are about 2.5 to 3 % in the

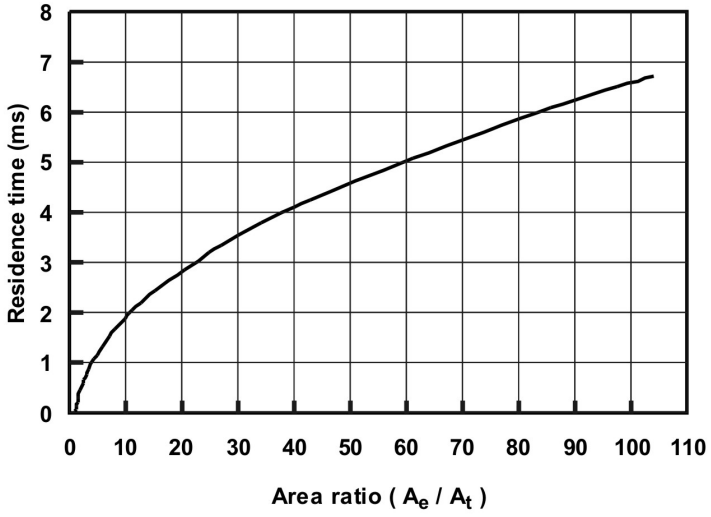

Figure 9.23: The variation of flow time with nozzle area ratio

conical nozzle and are higher than those in contour nozzles (about 1.5 to 2 %). Two phase flows due to aluminum oxide particulate matter flowing with the gas cause additional loss. The loss is a strong function of the particle size and observed particle sizes are in the range of 0.1 to 10 μm. The cause for the loss is the velocity and thermal lag with respect to gas, something that becomes larger with larger sizes of the particle. A simple formalism will bring out the essential parameters. Assuming that all the particles are spherical in shape, the momentum balance on an accelerating/decelerating particle of diameter d_p is given by

$$m_p dV_p/dt = 3\pi d_p \mu_g (V_g - V_p) \tag{9.40}$$

where the right hand side constitutes the Stokes drag on the particle. When the particle velocity,V_p equals the gas velocity, V_g, there is no further acceleration. The time required for velocity equilibration can be constructed from the above relationship as $t_{veql} = m_p/3\pi d_p \mu_g$. The flow time, t_f is the ratio of the length of the nozzle to the mean velocity of the flow. It can be represented by $t_f = \int_0^{L_n} dx/V_g$ where L_n is the length of the nozzle, x is the axial coordinate. Its variation with area ratio of a nozzle is shown in Figure 9.23. The increase in the flow time increases sharply in the early stages. For area ratios of 10, the flow time is less than 2 ms. One can now form a non-dimensional lag parameter, $L_p = t_f/t_{veql}$ which when simplified leads to

$$L_p = \frac{t_f}{t_{veql}} = \frac{18 L_n \mu_g}{V_g \rho_p d_p^2} \tag{9.41}$$

With typical values of $t_f \sim 1$ ms, μ_g = 10 $\times 10^{-5}$ kg/ms, $\rho_p = 3000\ kg/m^3$, $d_p = 2\ \mu m$, one obtains L_p = 1000. For $d_p = 10\ \mu m$, one obtains L_p = 40. It is generally known that for particle sizes of about 1 μm (L_p = 4000), the two phase effects are marginal because, the particles virtually follow the gas flow. At $L_p \sim 40$, the loss in specific impulse can be as large as 25 %. In reality, there is a particle size distribution and the Sauter mean diameter (surface average mean diameter) is what matters. Typical loss because of two phase flow effects has been determined as 4 – 5 %. In addition there are boundary layer losses, chemical kinetic effects all amounting to an additional 1 – 2 %. Thus, the total losses will amount to 7 – 9 %. The overall specific impulse will therefore turn out to be 91 to 93 % of the equilibrium value. This is in fact the specific impulse efficiency.

9.9 Features of Rocket Motors

The characteristics of some large motors built across the world are shown in Table 9.7. Figures 9.24 and 9.25 show the schematic of large size motor configurations and the principal performance data. The igniter is at the head end in both cases (pyrogen igniter, see section 9.4), the cross section of the motor in Figure 9.24 is a star at the head end and cylindrical downstream. This motor is built on "segmented motor" design concept. This implies that several motor segments are built separately, but put together in a sequence through a tongue and lip joint depicted with a separate mark in the figure. This joint usually used in many vehicles including the space shuttle booster, is the one that gave problems in the flight of Challenger in 1984, because of an unusual low temperature soak. An O – ring seal became brittle at the low temperature, cracked due to brittleness and allowed high pressure high temperature gases to leak out. The jet hit the liquid propellant tanks, opened it up allowing the entire liquid propellants to be expelled and burn within the atmosphere leading finally to the death of the astronauts. The solution was found by changing the material of the O – ring and also the design of the joint. In the second case – Figure 9.25, the grain is entirely of a star shape. The nozzle is of fixed geometry in the former case and is a flexible one in the latter case. The nozzle segment is joined to the motor assembly through a flexible joint that allows the rotation of the nozzle. The hydraulic actuator fixed with reference to the motor can move the nozzle on either side, typically by $\pm\ 5^\circ$. The performance data on pressure-time behavior at various propellant temperatures is also shown in the figure. These data get into a mission analysis in which it is verified if all the objectives of the mission are fulfilled with the thrust-time variation arising out of initial temperature. If there is a compromise on mission objectives, the subject has to be further examined by the propellant designer and other options of the propellant choice and the geometry need exploration.

Figure 9.26 shows the configurations of boost-sustain arrangement of a tactical

Table 9.7: Characteristics of some large solid rocket motors (FN = Flex-nozzle, Mass fraction = ratio of the propellant weight to the total motor weight, * = This mass is for the earlier version; Reevaluation of insulation has allowed propellant loading to go up to 138 tonnes)

Country	USA	USA	USA	ESA	Japan	India
Motor designation	RSRM	ASRM	SRMU	P-230	M V	PS 1
Case diameter, m	3.71	3.81	3.81	3.0	2.5	2.8
Length, m	38.44	38.44	34.13	27.0	14.1	20.3
Prop. binder	PBAN	HTPB	HTPB	HTPB	HTPB	HTPB
Thrust control	FN	FN	FN	FN	FN	SITVC
Burn duration, s	123.4	135.0	140.0	130.0	51.0	100.0
Max. thrust, MN	13.82	14.24	-	6.0	-	4.86
I_{sp}, kN.s/kg	2.62	-	2.61	2.66	2.71	2.57
Prop. mass, tonnes	502.3	547.1	312.2	236.5	70.0	127.0*
Mass fraction	0.880	0.896	0.890	0.893	0.888	0.870

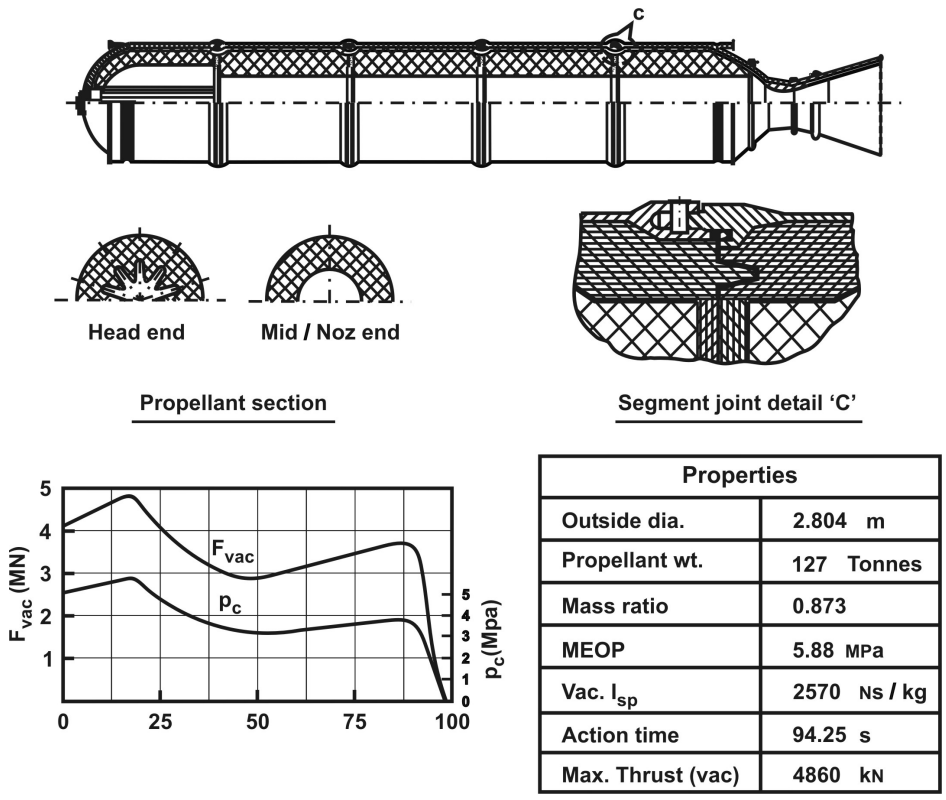

Figure 9.24: A large size motor for space applications with its geometry and performance

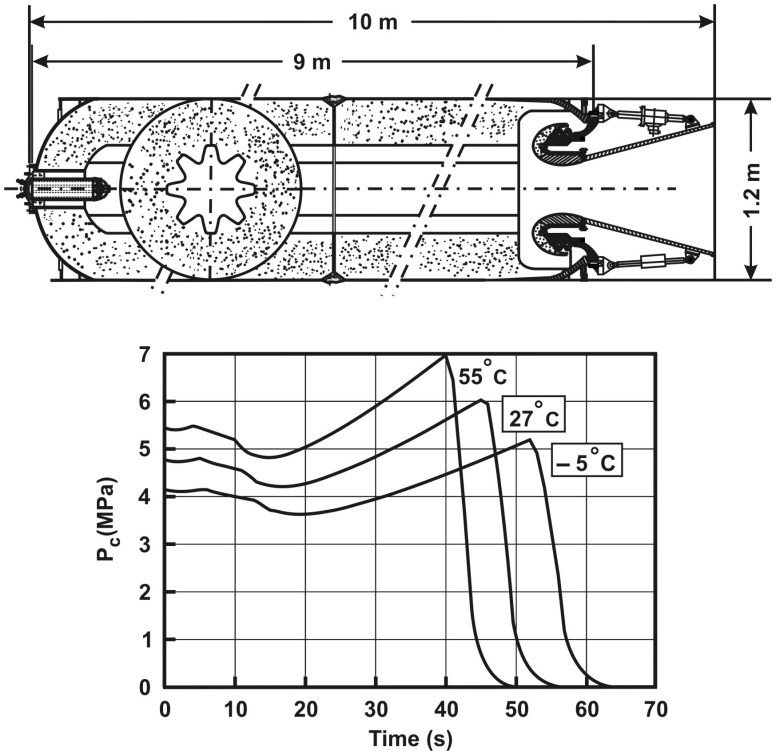

Figure 9.25: A tactical rocket motor with the pressure time curves as a function of initial temperature. The hydraulic system attached to the nozzle allows gimballing of the nozzle and hence, thrust vector control

propulsion system. Demand of compactness has resulted in the use of four canted nozzles that are scarfed – nozzle end is cut in a manner that expansion is not symmetrically completed along the nozzle axis. This geometry is constructed so that all the elements are within the overall envelop of the vehicle (for otherwise, the drag of the projecting segment is very large). This makes the thrust vector non-axial with respect to the specific nozzle. The changed vector is only a few degrees away from the vehicle axis and does not influence the performance significantly. The sustainer shows another classical motor configuration. The chamber with the propellant and the nozzle is connected by a long central duct. This is to facilitate locating other control hardware and missile components around the central tube. The gases pass through the tube called the blast tube under supersonic conditions. This leads to substantive stagnation pressure loss. This is considered inevitable and accepted since the arrangements of components is otherwise not possible. Such problems are typical of small tactical missile systems as they are volume limited applications. As will also be pointed out later, it is in such applications that solid propellants score significantly over liquid propulsion systems.

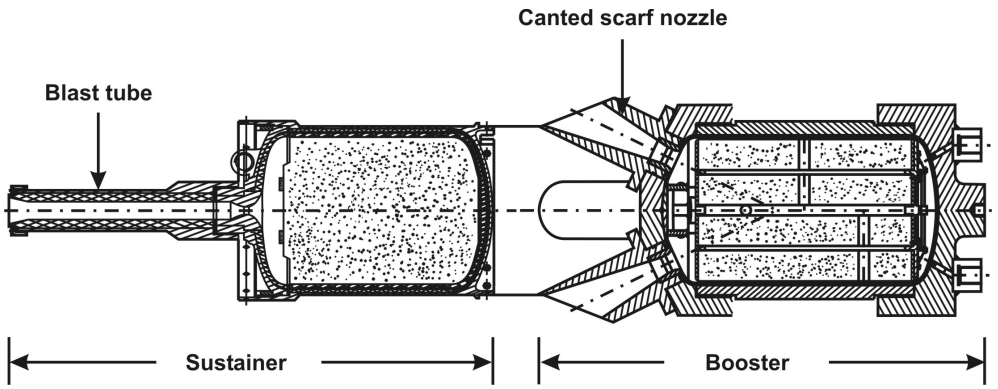

Figure 9.26: A tactical solid rocket motor with booster-sustainer combination

9.10 Design of Solid Rockets

The mission analysis team provides the specifications for the design of the propulsion system. Such a specification may include (a) total impulse, (b) burn time, and a maximum weight and volume of the envelop. The volume may also be provided in terms of diameter limitation. Such specifications are laid down in the back drop of similar developments elsewhere or what may be capable of being achieved with additional developments in propellants as well as casing materials. There may be three broad classifications – (i) large booster for strategic systems, (ii) small boosters and (iii) sustainers for tactical motors. If one wishes to have a small thrust and long burn duration, end burning configuration is the choice. The thrust range that can be obtained is limited by the burn rate that can be achieved – typically 10 to 25 mm/s. The design for higher burn rate may need to include active burn rate modifiers that could degrade the storage life of the system. If this is not desired, then the variations possible in the propulsion system design are small. The booster systems that work for 2 to 20 s can have a variety of design options in terms of burn rate and propellant grain geometry. The aim in the design would be to obtain a high propellant loading. The use of highly loaded two-dimensional radial burning configurations calls for a strip-wise analysis of the burning of the propellant described below. Large motors can use two- or three-dimensional configurations for optimizing the loading as well as a pressure time curve that preserves the structural efficiency of the design. In these cases also a strip-wise analysis may be needed.

The strip-wise analysis requires that the propellant be treated as a large number of strips from the head end to the aft end. The initial surface area and the mass flow through the port are calculated from the head end to the aft end through the various strips. In doing this calculation, it is essential to take into account the gas

dynamics of the flow – the loss in stagnation pressure due to heat addition must be accounted for. After this, the propellant is allowed to regress by an amount $\Delta y = \dot{r} \times \Delta t$, where Δy and Δt are the increments in web burnt and the time step chosen. This regression must be along a local normal. The new geometry is then subject to the above calculation procedure. This is in the stagnation pressure between the head and nozzle ends. If this is large, there will be performance loss. Hence, one may need to rework the configuration to ensure that the performance loss due to high loading is not larger than the benefit that may be obtained by increasing the loading.

9.11 Summary

This chapter has discussed the internal ballistics of solid rocket propulsion system. Propellant characteristics like burn rate depend on pressure and temperature and these control the design of the propulsion system. Achieving the desired features of a mission calls for providing specifications to the propulsion system designer that would usually be difficult to meet with and an iterative consultative process is needed before the propellant of specific ballistic and structural features is engineered and then the configuration designed to meet with the requirements. It is appropriate to conclude that most technologies needed to build solid rocket motors have achieved maturity and any further developments that may take place would possibly be incremental in character and would add to alternatives.

Several earlier books that can be consulted on this subject are: Barrere et al [12], Williams et al [27], Timnat [26], Sutton [25], and Hill and Peterson [31].

Chapter 10

Liquid Rocket Engine

Every liquid rocket engine has a fuel storage with (i) a feed system and a thrust chamber consisting of (ii) a combustion chamber and (iii) a nozzle. Since the combustion chamber pressures have to be large, the feed system pressures should be larger. To drive the fluids into the chamber, one can use a gaseous pressurant held at very high pressures in light weight pressure bottles and drive the fluids stored in tanks through valves into the combustion chamber through (iv) a carefully designed injection system. Since in large impulse delivering bipropellant systems, the weight of the tanks will be large due to the high pressures involved, it is possible to reduce the weight of the system by storing the propellants at low pressures (3 – 6 atm), but increasing the pressure using (v) turbo pumps and delivering the high pressure fluids to the thrust chamber. The turbines associated with the pumps need to be run; these need (vi) gas generators that may use separate high pressure combustion systems or other variants. While hypergolic propellants do not need any ignition system, the non-hypergolic fluids need a separate (vii) ignition system. While the discussion in section 1.14 has provided an overview, the details of the above elements is the subject of discussion of the present chapter.

Liquid rocket engines can be expected to deliver a variety of thrust – time profiles. Figure 10.1 shows the several possibilities. One can expect to get constant thrust for a certain duration. This is typical of most booster engines. One can obtain variable thrust from the engine. Throttleable engines are used in aircraft like applications (like X-15 aircraft powered by a LOX – Ammonia liquid rocket engine) or in missions where accurate trajectory control is demanded (like lunar descent engines). One can expect restartability from liquid engines. This is particularly valuable in orbit change maneuvers for which one needs to determine the effects of commands periodically to optimize the use of the propellants as well as ensure the position of the satellite during the orbit change maneuver. Pulsing is a capability expected of thrusters mounted on satellites. Since only small changes are required to manage the station keeping task, small forces are applied and the

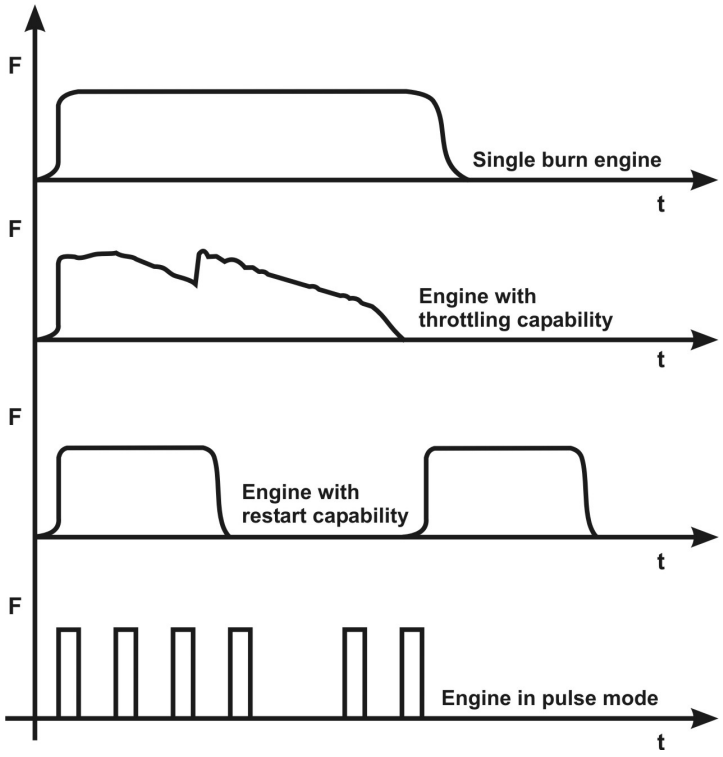

Figure 10.1: Various thrust – time profiles with liquid rocket engines

effects observed before further commands are considered. Thus, there is a whole range of possibilities from liquid rocket engines that cannot be expected from solid rocket motors.

10.1 Monopropellant Thruster

Monopropellant engines use a pressure fed system. A very high pressure bottle ($\sim$ 350 – 500 atm.) carrying helium (chosen because of its inertness and low molecular weight) will deliver the gas through pressure regulators to the propellant tank. The liquid then flows through electro-mechanical valves into a plenum from which it gets sprayed into the combustion chamber through injectors. These thrusters are used on satellites for on-orbit control and station keeping. The thrust level itself is between 1 to 10 N. Hydrazine is a typical propellant. Typical operating chamber pressures are between 7 to 9 atm. The storage tank pressures are 15 to 20 atm. The pressure drop across the injector is 7 to 10 atm. The thrust demanded will be some times in steady mode, but most of the time in pulse mode. The specific impulse values achieved are 2300 N s/kg in steady mode and 2000 N s/kg in pulse

mode. If we combine this data with the thrust demanded, the liquid flow rate required is 0.5 to 5 g/s or 1.8 to 18 kg/hr. The low flow rates are carried by ducting that could be as small as 0.2 to 0.5 mm. These impose critical requirement on the cleanliness of the propellant as well as the components. This is the reason why the entire operations of thruster assembly and integration with the satellite takes place in a technically qualified clean room. Some important issues in a monopropellant thruster system are (a) propellant acquisition and (b) cold start and (c) thruster design for performance that includes life of the thruster.

10.1.1 Propellant Acquisition

Satellites work at near 0 – g conditions. Also, there will be accelerations caused by internal operations and by solar pressure on parts of the satellites. These are typically in the range of 0.1 to 100 μg. These can cause the propellant to move about inside the tank with the pressurizing gas and the propellant located inside in a way that when thrust is demanded of the system, the propellant is unavailable for being drawn by the engine. Only gas may come through to the thruster. This could be catastrophic. Therefore, positive expulsion devices have been developed. These devices are designed so that they permit liquid flow to occur on demand under any orientation of the spacecraft and whatever be the accelerations that they may be subject to. Further, they must aid in extracting as much of the fluid as possible from the tanks. This is defined by expulsion efficiency (η_{expul}). Use of bellows, flexible diaphragms and bladders made of propellant compatible polymeric material constitute a possible solution. Polytetrafluoroethylene and special rubbers have been contemplated and used in early development period. Figure 10.2 shows the arrangements. The propellant is separated from the pressurant (pressurizing gas) by a diaphragm. Pressure applied on one side of the diaphragm is adequate to expel the fluid into the piping that carries the fluid to the thruster. Since (a) the use of polymeric materials implied ensuring flexibility and structural integrity over long periods of time – of the order of seven to ten years – something that was considered difficult, (b) expulsion efficiencies were limited to about 97 % and it was desired to raise to 99 % or better, and (c) alternatives to seek a system that could be lower in weight, passive propellant acquisition device using surface tension of the propellant has been developed.

Contact angle

The fundamental principle of surface tension device is related to the wettability of a fluid with a surface. For a liquid to be in equilibrium with a solid surface, the surface tension forces at the solid-liquid-vapor interface must balance along the

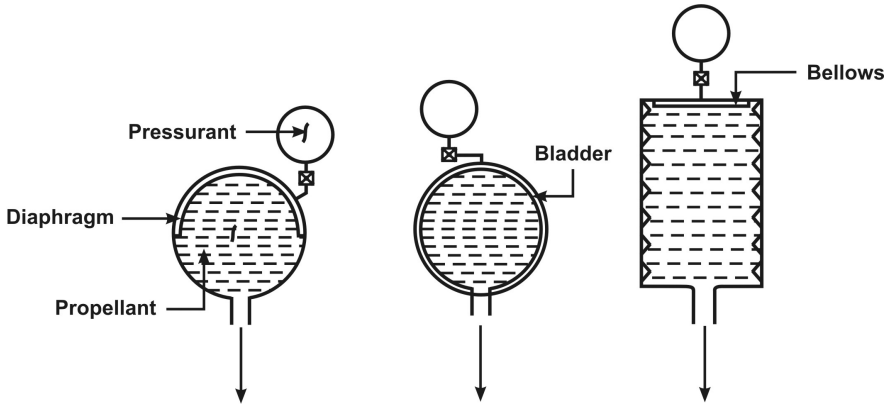

Figure 10.2: Three positive expulsion devices based on diaphragms, bladders and bellows

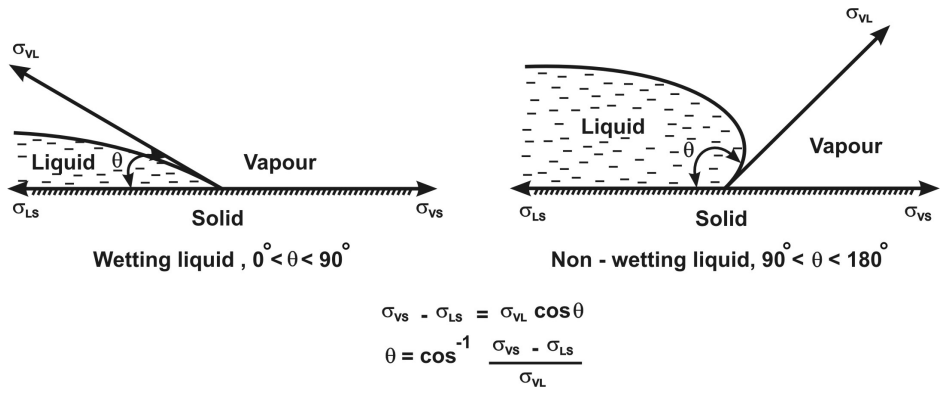

Figure 10.3: The contact angle at the surface on which liquid rests with associated forces

solid surface. The contact angle θ_c is given by

$$\theta_c = cos^{-1}[\frac{\sigma_{vs} - \sigma_{ls}}{\sigma_{vl}}] \tag{10.1}$$

where σ_{vs}, σ_{ls}, and σ_{vl} are the surface tensions of the vapor – solid, liquid – solid and vapor – liquid interfaces respectively. For all 0 < $(\sigma_{vs} - \sigma_{ls})/\sigma_{vl}$ < 1, 0 <θ_c < $\pi/2$, the liquid is called wetting liquid (see Figure 10.3).

For other values of surface tension that allow θ_c to take values between $\pi/2$ and π, the liquid does not wet the surface (simplest example is of mercury). The contact angle is independent of gravity since it depends on the values of surface tension. Surface treatment or impurities in the liquid can alter the values of surface tension.

Bubble pressure

When a porous barrier separates the liquid and gas, a curved interface is formed at the edge of the pores due to surface tension such that the interface can resist gas pressure attempting to break through the liquid region. The interface can stand a pressure differential, ΔP_{st} given by

$$\Delta P_{st} = \sigma \left[\frac{1}{R_1} + \frac{1}{R_2} \right] \tag{10.2}$$

where $\sigma = \sigma_{ls} - \sigma_{vs}$ and R_1 and R_2 are the principal radii of curvature of the interface. For circular pores, R_1 = R_2 = R. Thus, $\Delta P_{st} = 2\sigma/R$. This pressure differential is called the bubble pressure.

Bond and Weber numbers

The ratio of force due to acceleration of the system to surface tension (capillary) force is called the Bond number, B_0 defined by

$$B_0 = \frac{\rho_l R^3 a}{\sigma R} = \frac{\rho_l R^2 a}{\sigma} \tag{10.3}$$

where a is the acceleration imposed on the system. R represents here the bubble size. Smaller the Bond number, larger is the influence of surface tension effects. For a given fluid, one can reduce the Bond number by reducing the pore size. For an acceleration, a = 1 milli g = 0.01 $m/s^2 \sim$ 0.001 m/s^2, ρ_l = 1000 kg/m^3, σ = 0.063 N/m (for hydrazine) and a pore radius of 5 mm = 0.005 m, one gets B_0 = 0.004. This is clearly the regime where surface tension effects are dominant. The recommendation on Bond number is to keep it below 0.04 (see J. F. McCarthy, 1968, ref. [18]) to ensure the dominance of surface tension. This implies that the same pore structure can allow larger acceleration of 0.01 g.

The ratio of inertial forces to surface tension forces is the Weber number, We defined by

$$We = \frac{\rho_l V^2 R}{\sigma} \tag{10.4}$$

where V is the local velocity. Low values of the Weber number are desired to ensure that liquid flow does not break the surface (it is useful to note that for atomization, one desires high values of Weber number). For typical values noted earlier and V = 0.01 m/s, one gets We = 0.8. This value is considered low enough for locating a stable film. The stability of liquid films is presented on a $We - B_0$ plot as shown in Figure 10.4. The design of surface tension based devices belongs to the left bottom quadrant on this figure. Some basic aspects of zero – g problems have been discussed by McCarthy, Jr [18].

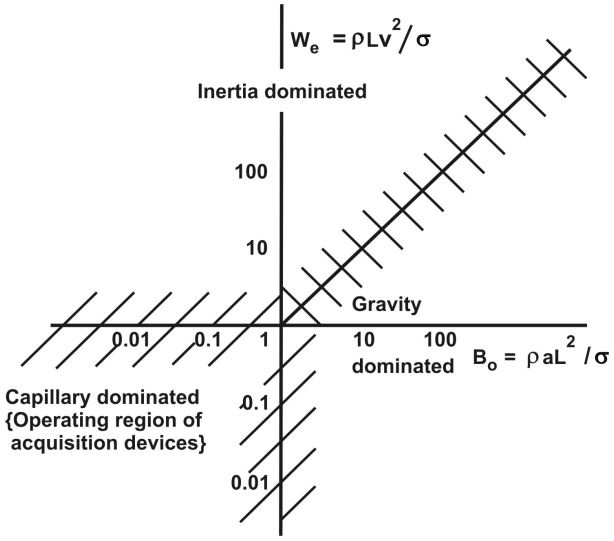

Figure 10.4: A Weber number – Bond number based plot containing the regimes of operation

10.1.2 The Acquisition Device

The key question of acquiring the propellants at start/restart after experiencing zero – (or more accurately, micro – g) for providing a pulse/long duration burn would need to be dealt with. The simple approach found adequate is the providing of a sump below the tank (called catch tank) that has a surface tension element above it so that some amount of propellant is always found in this zone. Any start command drains the propellant from this volume so that the necessary thrust is generated from the thruster. In this period, propellant settles in a direction opposite to the direction of the acceleration force. This propellant comes into contact with the surface tension element inside the container and is drawn through it into the sump. There will be entrapment of gas bubbles in this process. There must be a facility to separate the gas bubbles and allow them to join the space above the liquid (technically called ullage) containing the gas. Figures 10.5 and 10.6 show the details of the tank and the elements of the propellant acquisition system. The tank has its interior filled with the capillary element made of screen mesh along the wall and in the central zone arranged in ways depending on the possibilities of accelerations created in the mission. The arrangements can be extensive becoming a complete communication device, but should be limited by the needs of the mission as extra hardware will add to the weight.

The central conical segments can be as tall as the height of the container or limited to a certain height. The outer structure with wire mesh creates a hold up inside the container. The inner mesh structure helps as gas arrester screen. When

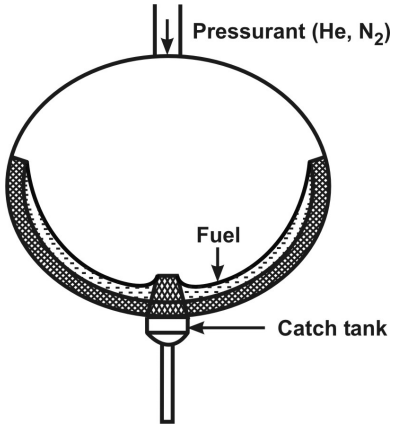

Figure 10.5: The tank with a 0-g propellant acquisition device

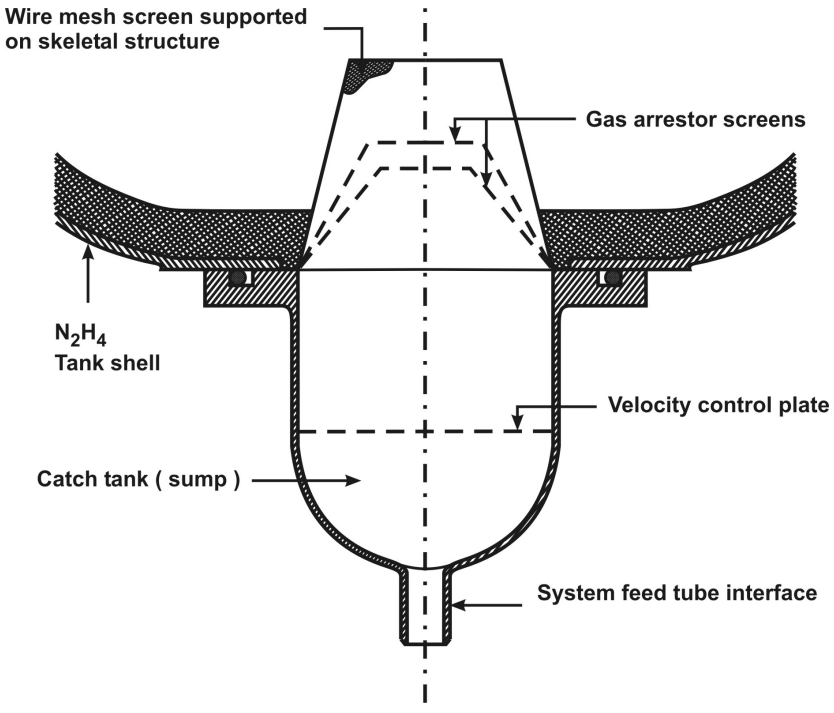

Figure 10.6: Details of the propellent acquisition section

the thruster fires, the liquid and the gas bubbles located variously will move and intersect the central structure. At this stage, the gas and liquid may enter into the zone within the outer screen. The bubbles are prevented from proceeding through the inner screen through the choice of the size of the pores. Since 0 – g environment encourages bubbles to join together to form larger size bubbles, they will move in the direction of the outer screen and get expelled.

In order to obtain a high expulsion efficiency, it is necessary that the gas break-through be prevented till the last stage. After the liquid depletes to the level of the sump, the final arrangement is a porous plate that prevents the break-through of the gas into the liquid. All the elements put together will make it possible to have acquisition-on-demand and expulsion of 99 %.

10.1.3 System Schematic and Pulsing Performance

A general schematic was set out in Figure 1.17. Since monopropellant systems are used on board spacecraft for an expected life of 7 – 10 years without any possibility of access for repair (as the altitudes are a 1000 km or 36000 km), the system design must be fault tolerant to an extraordinary level. Amongst the approaches chosen for this purpose, some are as follows. A thrust chamber valve failure leading to leakage or open status being held despite "close" command, can be handled by having two valves used in series. Thrust chamber valve refusing to open even when commanded can be overcome by having a duplicate system (with two sets of engines connected to two storage containers). By connecting the two storage tanks, a failure of either propellant system can be handled. Other problem areas include the freezing of hydrazine. Since the freezing point of hydrazine is 2°C, and any freezing can lead to line rupture because hydrazine shrinks on freezing, heaters are provided around the storage tanks, plumbing and thrusters so that the temperature is not allowed to go below about 25°C. In recent times, in order to ensure that the life of the catalyst bed is large, the thruster and the elements leading to it are also heated to different temperatures. As discussed in section 8.3.1, these temperatures can be between 100 – 300°C. Figure 10.7 shows schematically these features. Instrumentation is also duplicated and arranged in a manner that if there is a fault in one, the data from the other can be used to cross check and only the qualified data set is used.

The start-up of the system calls for filling the tanks including the plumbing till the thrust chamber valves. This has impingement on the safety of the operations. Generally, this approach is adopted in most satellite operations. The pressurizing gas is also to be filled into pressurant tanks. Usually, the pressurant used is helium. An alternate is nitrogen. The mass of helium required to perform the pressurization is much lower than for nitrogen (due to $\mathscr{M}_{He}/\mathscr{M}_{N_2} \sim (1/7)$. The problem with helium is that the prevention of its leakage is far more difficult due

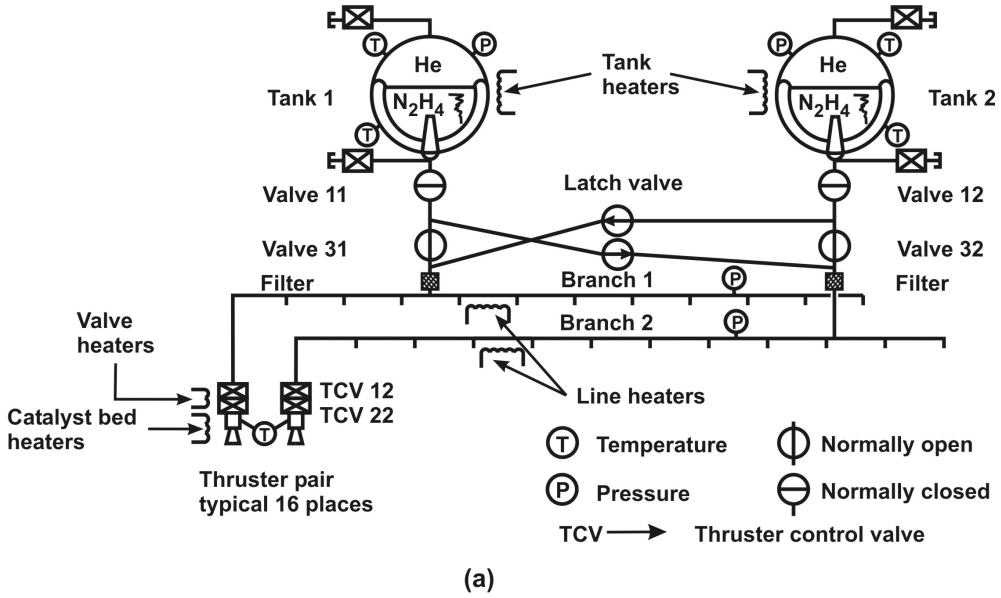

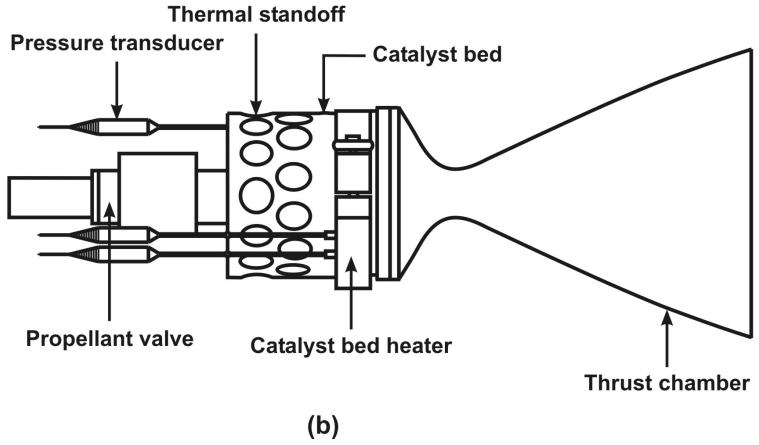

Figure 10.7: The arrangement of the total monopropellant system also showing the thruster with its heating arrangement, adapted from ref. [14]

Table 10.1: Features of monopropellant systems (Dgm = Diaphragm, Cplry = capillary)

Satellite	Year	Thruster	Hydrazine kg	Tank	PMD
SROSS 1	1987	6 x 1 N	5.6	1 x10 l	Dgm
IRS 1A	1988	16 x 1 N	80.0	4 x 30 l	Dgm
IRS 1C	1988	16 x 1 N	84.0	4 x 30 l	Dgm
IRS 1B	1991	16 x 1 N	80.0	4 x 30 l	Dgm
IRS P2	1994	16 x 1 N	80.0	4 x 30 l	Dgm
IRS P3	1996	16 x 1 N	84.0	4 x 30 l	2 Dgm, 2 Cplry
IRS 1D	1997	16 x 1 N	84.0	4 x 30 l	Cplry
IRS P4	1999	16 x 1 N	84.0	4 x 30 l	Cplry
IRS P6	2003	16 x 1 N 4 x 11N	150.0	1 x 390 l	Cplry

to its low molecular size. Despite this problem, its use is so advantageous that methods of jointing are arranged to reduce the problem substantially. The general approach is to weld most joints except the locations of control elements. The gas tank used for pressurization is sized by the requirement of whether the operation has to be regulated for the full life or pressure keeps decaying from start by loading the tank containing the liquid with gas as well at a fixed pressure. As the propellant gets consumed, the gas in the tank will expand to lower pressure. This method is called “blow down”.

A term known as blow down ratio is employed in describing this feature. This is simply the ratio of initial-to-final pressure. If the propellant draw-down is fast, the pressure may fall adiabatically since there is not much time for heat exchange. In such cases, the chamber pressure may fall below the value that would get attained when the system is allowed to equilibrate to a temperature of 25 °C because the adiabatic fall in pressure will reduce the temperature below the ambient value. However, if the draw-down is slow, it is possible that the pressure fall may take place isothermally. This fall in the tank pressure leads to thrust decay. The reason why the approach of blow-down is contemplated is that it is very simple and therefore reliable. Typical blow-down ratios are 3 – 4. The features of several monopropellant systems are summarized in Tables 10.1 and 10.2. The initial thrust varies from about 1 N to a few kilo-Newtons. Most systems till the eighties used nitrogen as the pressurant. Helium has been used in more recent times when the leakage prevention technology was mastered. As can be noted, most systems before the eighties depended on diaphragm for positive expulsion. The spin system introduces a centrifugal force and enables locating the propellant in desirable places for acquisition. Surface tension devices (or capillary devices) are the post-eighties development.

The detailed specifications of a monopropellant thruster can be seen in Table

Table 10.2: Features of monopropellant and bipropellant systems (Mar4 = Mariner4, Lndst = Landsat, Pionr = Pioneer, INST = INSAT, Pr. mode = Pressurization mode, Reg. = Regulated, Bldr = Bladder, Bldn = Blow-down, Dgm = Diaphragm, Cplry = capillary)

Aspect	Mar4	Lndst	Pionr	INST2A	INST3C	INST3E
Launch year	1964	1972	1978	1992	2002	2003
Mono/Biprop	Mono-	Mono-	Mono-	Bi-	Bi-	Biprop
No. thrusters	1	3	7	16, 1	8, 8, 1	8, 8, 1
No. Tanks	1	1	2	3	2	2
F, N	220	4.4	6.6	22, 440	22, 10, 440	22, 10, 440
Pressurant	N_2	N_2	He	He	He	He
Pr. mode	Reg.	Bldn	Bldn	Reg.	Reg.	Reg.
Bldn ratio	1	3.3	1.8			
PMD	Bldr	Dgm	spin	Cplry	Cplry	Cplry
Prop. mass, kg	9.8	30.4	39.2	998	1527	1592

2.9. These include details like (a) thrust repeatability, (b) steady state I_{sp}, (c) I_{sp} degradation over the life, (d) the minimum impulse bit, (e) impulse bit repeatability, (f) rise time to 90 % thrust under steady mode and pulse mode, (g) decay to 10 % thrust in steady and pulse mode, (h) roughness measured as a root mean square value of the fluctuations about the mean, (i) life in million pulses in steady as well pulse mode, (j) space life in years. There are also requirements for qualifying the systems for vibration and shock to ensure that the system performs as expected after going through the launch vehicle environment before becoming operational.

Pulsing performance is an important requirement of monopropellant thrusters. Demand on pulses can be for as short as 20 ms. It could also pulse at 1 s duration. The short duration of the impulse bit requires valves with ultra-fast response, typically 1 – 3 ms open-and-shutdown times mounted just on the thruster to reduce the flow time. The thrusters need to be heated to ensure quick reaction in decomposition and also long life (as indicated in section 8.3.1).

10.2 Bipropellant Engines

Bipropellant liquid engines have been used for spacecraft and launch vehicle control as well as launch vehicle main propulsion. They can be pressure fed or turbopump fed. Pressure fed engines are used for low total impulse or when very high reliability is called for and adopt low chamber pressures, typically less than about 10 atm. A discussion of the essentials can be found in Chapter 1.14. The full stage of one of the liquid engines called Vikas used as the second stage of the PSLV vehicle (Figure 9.19 shows the assembly of various stages of the vehicle) is shown in Figure 10.8. It is useful to appreciate the various elements of such a vehicle. At

the bottom is the thrust chamber. The thermal management of the thrust chamber makes use of high temperature metals and film cooling (see section 10.4.1 for more details); the throat section has a throat made of high temperature composite material (see sections 10.4.3 and 9.6.1). The turbopump assembly is located over the thrust chamber. The liquid propellants flow from the tanks to the turbo pumps. One can notice an element termed "POGO corrector" in the fluid path line. This is introduced to tackle the propulsion-structure interaction problem (see section 11.5). The upper portion consists of the fuel and oxidizer tanks and pressurization systems. It is useful to appreciate that the tanks themselves will constitute the outer surface of the vehicle. The anti-slosh baffles on both the tanks are placed to ensure that the oscillations in liquid surface that may be induced because of the flight dynamics of the vehicle is brought down to acceptable levels. The thrust frame transfers the force created by the thrust chamber to the vehicle.

In order to understand the various aspects of the design of such a system and others, it is useful to examine a few of the engines built in different countries over the last six decades. Table 10.3 provides the principal data. Several other details of these systems are presented in succeeding sections. As can be seen from the Table 10.3, excepting for Agena which was built in the early fifties, most other engines have chamber pressures above 50 atms. The O/F could vary for the same propellant combination. For instance, Titan II uses different O/F values for stage I and II. It depends on the optimization of the vehicle mass, that is more favorably inclined to the choice of denser propellants. Such features are true of LOX – LH_2 systems also. The realized specific impulse values are in the expected range with SSME engine showing the highest specific impulse. The CUS engine that belongs to the same family of topping cycle engines as SSME (the exhaust from the turbine also passes through the combustion chamber) has a lower specific impulse due to the choice of lower chamber pressure that prevents a large area ratio to be obtained. The realized specific impulse values in flight are affected by mixture ratio variations. While most engines have a mixture ratio controller (like the Vikas engine having a $\pm$ 2% accuracy controller) that maintains the same mixture ratio irrespective of the variation in flight altitude, any deviation in this value will imply that one of the propellants will remain un-utilized. This brings down the total impulse provided by the system. Hence, the derived specific impulse will be lower than the instantaneous specific impulse. Such features could occur in solid rockets as well due to sliver fraction not burning due to fast decay in the chamber pressure. However, the issues are not serious since the solid propellant is in a hot environment (as can be expected in large combustion chambers) and pressures are such that the chamber dynamics continues to be isolated from the ambient due to outside pressure being very low; the propellant will burn up even though the contribution to thrust will be low. In the case of liquid propellants, though, *the unburned propellants contribute to inert mass*.

Table 10.4 contains the data of cryo-engines built in several countries over

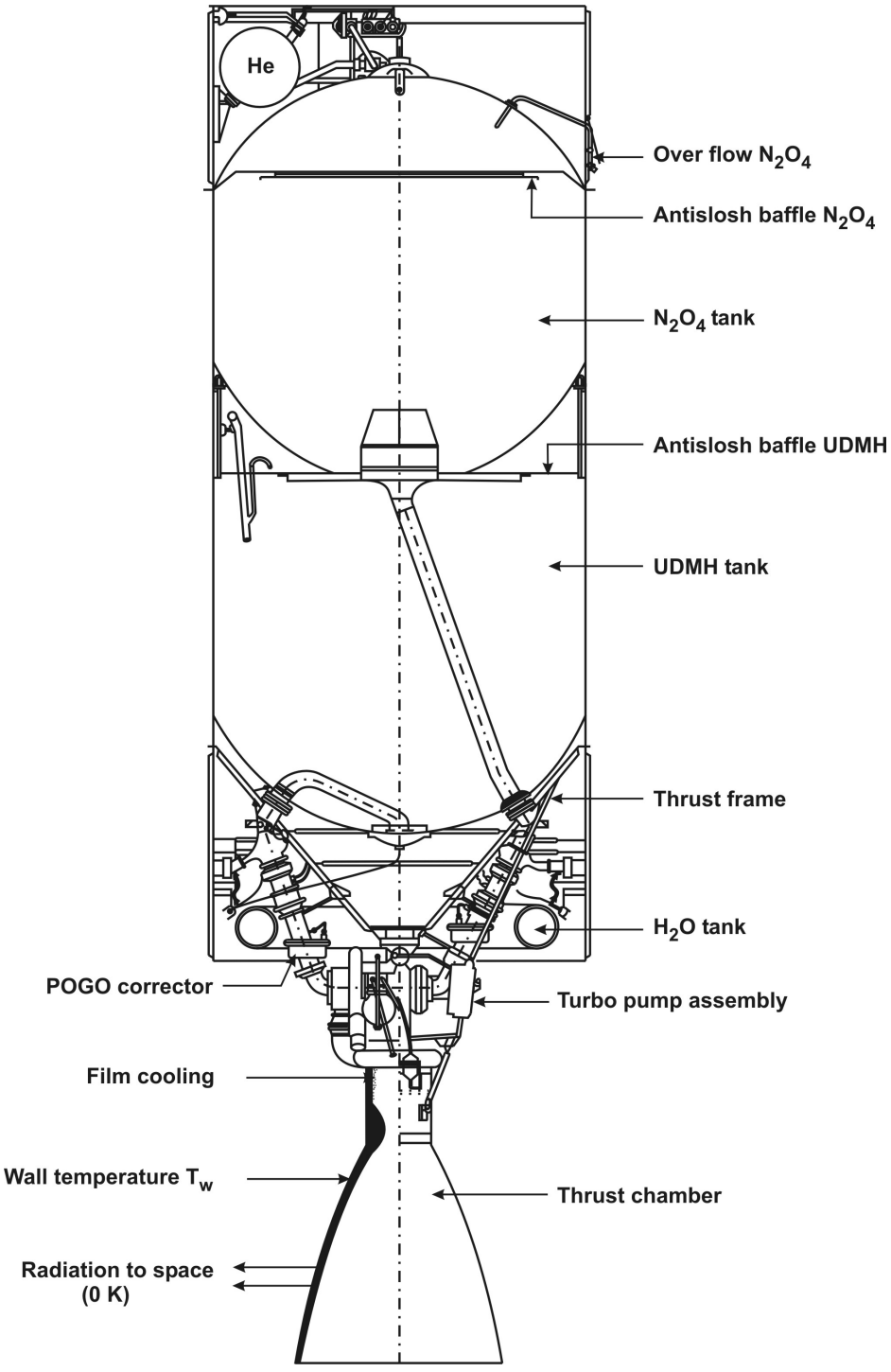

Figure 10.8: The Vikas engine based second stage of PSLV vehicle developed by ISRO

Table 10.3: Characteristics of major liquid rocket engines; * = N s/kg, F-1, J-2 – Saturn mission, TII – Titan II, SI – Stage I, VikasU – Uprated Indian version of Viking engine of Ariane vehicle, CUS - Cryogenic upper stage – Russian design modified in India, SSME - Space shuttle main engine; SSOME = Space shuttle orbital maneuvering engine; v = vacuum exit condition

	Engine	Props.	F kN	p_c atm.	$\dot{m}$ kg/s	A_e/A_t	O/F	I_{sp} *
1.	F 1	LOX	6860	76.3	1846.1		2.37	2.61
		RP1			778.0			
2.	J 2	LOX	1034	53.5	209.0	27.5	5.50	4.19
		LH_2			38.0			
3.	Agena	RFNA	70,v	34.7	17.8		2.57	2.85
		UDMH			6.9			
4.	TII/SI	NTO	952	56.5	250.0	8.0	2.01	2.54
		A-50			124.5			
5.	TII/SII	NTO	446,v	57.4	94.1	49.2	1.80	3.05
	A-50			52.2				
6.	VikasU	NTO	823,v	58.5	173.8	31	1.70	2.94
		UDMH			102.3			
		H_2 O			3.8			
7.	CUS	LOX	71,v	56.5	14.0	199	6.09	4.48
		LH_2			2.3			
8.	SSME	LOX	2160	222.0	407.0	40	6.01	4.55
		LH_2			67.7			
9.	Apollo	NTO	47,v	10.3	9.5	53	1.60	3.05
	LEMDE	A-50			5.9			
10.	SSOME	NTO	27,v	8.7	5.0	55	1.65	3.34
		MMH			3.1			
11.	RD253	NTO	1720	150	384.0	26.2	2.67	3.20
		UDMH			144.0			

Table 10.4: Comparison of modern cryogenic engines; * = kN, ** = kN s/kg, *** = N/kg

Engine	J2	RL10	SSME	HM7	HM 60	CUS	LE 5
Country	USA	USA	USA	France	France	Russia	Japan
F, vac, *	1034	67	2160	62.7	1025	71	103
$\dot{m}$, kg/s	247.0	15.8	474.7	14.4	241.6	16.3	23.1
O/F	5.5	5.0	6.0	4.8	5.1	6.0	5.5
$I_{sp,v}$ **	4.25	4.44	4.55	4.46	4.30	4.48	4.30
p_c, atm.	53.5	27.3	222.0	35.5	101.0	56.5	37.0
A_e/A_t	27.5	57.0	77.5	82.5	106.0	199.0	140.0
L, m	3.4	1.8	4.2	1.9	2.9	2.1	2.6
t_b, s	470	450	520	731	500	741	370
Wt., kg	1542	132	3065	155	1100	435	255
F/wt., ***	677.0	507.6	704.7	404.5	931.0	163.2	404.0

several decades. The O/F used varies between 4.8 and 6.0. The choice of p_c varies between 35.5 and 222 atm. The exit-to-throat area ratio varies from 27.5 to 199. The motor length that depends on the choice of the chamber pressure and exit-to-throat area ratio varies from 1.8 to 4.2 m. The thrust to dry weight ratio is an indication of the level of technology – SSME and HM 60 engines have a very high value – 705 to 930 N/kg. The CUS engine has a lower value than LE5 engine that works on gas generator cycle. RD 253 Russian engine, a staged combustion cycle based engine (see section 10.2.6) based on storable propellant combination (see Table 10.3, row 11) has a thrust to dry weight ratio of 1380 N/kg, perhaps the highest for any engine.

10.2.1 Injectors and Injection Head

Injector is a part of the thrust chamber. Its design allows the combustion system to have (a) stable combustion with (b) high combustion efficiency in (c) a short distance by keeping the (d) combustion chamber temperature within limits.

Many geometries have been developed by different designers in the USA, Russia, France, Germany and other countries. Most combustion chambers use axial injection – the axis of the combustion chamber is normal to the injector head. There are radial injectors like in Viking engine developed by France (adopted as Vikas engine in India) where the injection process occurs radially inwards from the head end of the combustion chamber and the fluid then turns around and flows out of the nozzle. Amongst the injector geometries, one can choose a straight hole injection or swirl injector. Straight hole injectors can be (a) showerhead, (b) impinging jet or (c) coaxial injection design. In the case of swirl or coaxial injec-

Table 10.5: Features of injectors (TII/SI = Titan II/Stage I; HFI = High frequency instability)

Element	Advantages and Disadvantages	Application
Showerhead	Good for film cooling; Poor atomization; requires larger combustion volume	X 15
Like doublet	Good mixing and more stable combustion; no blow-apart; Simple to manifold; could be sensitive to mixture ratio differences; More mixing space than unlike impingement	F 1, H 1 TII/SI Atlas SI
Unlike doublet	Very good mixing; Faster combustion; Simple to manifold; Extensively studied; Wall compatibility issue; Subject to blow-apart with hypergolic propellants; Prone to instability (HFI)	LAMAE Delta
Unlike Triplet	A great advantage is that mixture ratio differences do not affect the change of momentum vector	Agena Apollo LEMDE
Unlike quadlet	Advantages as above; but not easy to manifold	TII/SII
Swirl burner	Good mixing and faster combustion, good for small thrust; wall compatibility issue	SA2 of Russia
Concentric tube with swirl	Moderate mixing with low pressure drop, but difficult to fabricate with small gaps	

tors, the strategy is to produce a large number of identical elements called burners, select from them elements that are within acceptable limits and fit them on to a head that has suitable manifolds. In the impinging jet design, one has the choice of like-impingement (implying fuel-on-fuel or oxidizer-on-oxidizer impingement) or unlike-impingement (implying fuel-on-oxidizer impingement). The geometries used for impingement can be doublet, triplet, quadlet or other variations. Further, in a triplet, one can use a two oxidizer jet streams impinging on a central fuel jet or the other way. Similarly, one could have variations in the quadlet design. Some broad features of the design are presented in Table 10.5. Showerhead design was quickly left behind because of poor combustion efficiency. Both like- and unlike-impingement designs, particularly as doublets, are used extensively.

One of the disadvantages of doublets is that even if the injector holes are accurately and well machined, the resultant angle of the momentum vector, β_{inj} seen in Figure 10.9 given by

$$\tan \beta_{inj} = \frac{\dot{m}_f V_f sin\alpha_f - \dot{m}_o V_o sin\alpha_o}{\dot{m}_f V_f cos\alpha_f + \dot{m}_o V_o cos\alpha_o} \tag{10.5}$$

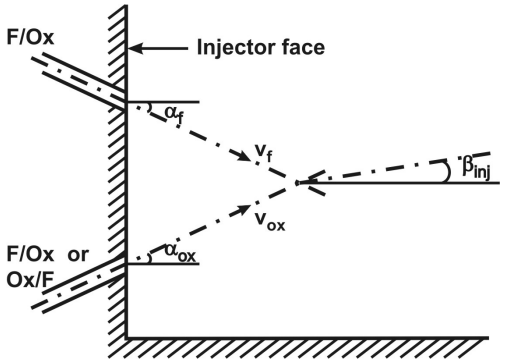

Figure 10.9: The impingement geometry - the resultant angle at which the spray is oriented depends on the momentum of the impinging jets

will get altered if there is mixture ratio variation, since this will alter the flow rates and velocities. It is clear from Figure 10.9 that increase in the velocity V_f or decrease in V_{ox} will reduce β_{inj} and vice versa. This problem is overcome in the triplet design (see Figure 10.10, case (d) corresponding to unlike triplet) in which the central fuel jet (say) surrounded by two oxidizer jets alter similarly even if there is mixture ratio variation and the resultant jet angle will remain unaffected [42]. The like-impingement design scores over the unlike-impingement in producing a more tolerant design towards instability (HFI). This is largely because it generates a broader combustion profile than the unlike-impingement, more particularly with hypergolic combinations. In fact, *if the orifice diameter is increased, the droplet size distribution will tend to be more coarse and the heat release distribution broader*. Making the orifice diameter smaller will atomize the liquid to finer sizes and this leads to sharper combustion profile that is more prone to HFI. The higher order elements like quadlets or pentads are also used, but depend more on the designer's choice. Swirl burners are a specialty of Russians and they have used it in a 30 kN class engine. This design cannot be easily scaled up for very large thrust engines because the frontal area required to fit them is unavailable in such engines. The frontal area is better used by impinging jet designs. Coaxial injectors are specially used for cryogenic propellants (LOX/LH_2). In these injectors hydrogen gets injected after it has passed through the wall of the thrust chamber for cooling purposes. It is injected as a gas. LOX, on the other hand, gets injected as a liquid.

Figure 10.10 shows the several injectors discussed in the Table 10.5. There can be several variations even in the arrangement of the injection holes on the injector head. Three of them are shown in Figure 10.11. The thrust chamber performance in terms of c^* and stability of operation are dependent on the injection arrangement. Injection arrangement (iii) in Figure 10.11 is known to be more

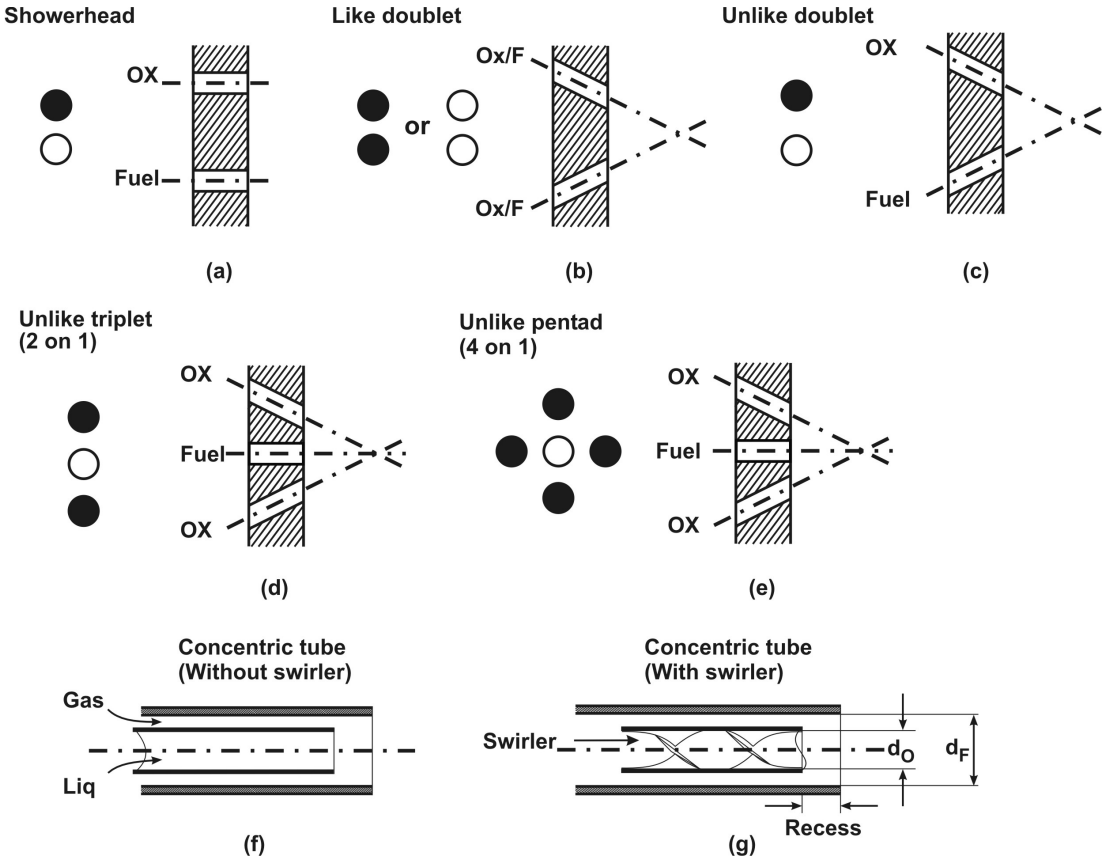

Figure 10.10: Different types of straight hole injectors - shower head, doublets, triplets, quadlets, like and the unlike impingement strategies

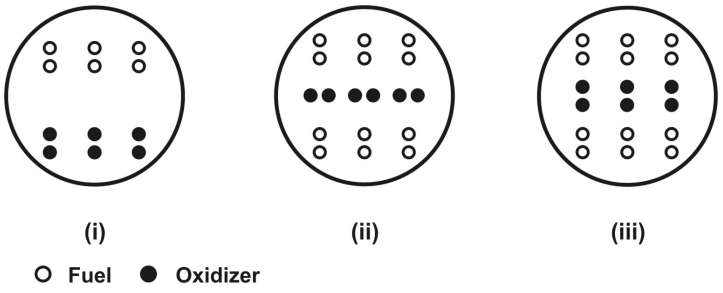

Figure 10.11: The arrangement of injector hole distribution on an injector plate

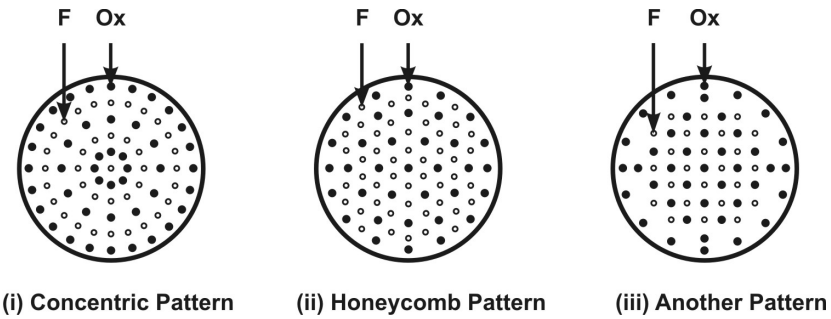

Figure 10.12: Some injector hole distributions on the injection head

stable than (ii), but would need 10 % larger L^* (= $\mathscr{V}_c/A_t$) to obtain the same c^*; with the arrangement shown in (i) increasing the velocity for the same throughput gives higher c^* at lower L^*, but the stability rating is lower. In the case of Viking engine used on Ariane vehicle (with radial injector, like impingement arrangement), the high frequency instability that was found late in the program (in fact, in the fourth flight) was overcome by making the injection holes coarse and pressure drop lower (hence, injection velocity lower) so that the combustion is more broadly distributed. This change led to a drop in c^* by 1 % since the rest of the thrust chamber was unchanged. Figure 10.12 shows a few more design alternatives. The manifolding of the fuel and oxidizer is another complex task. To illustrate the principles, Figure 10.13 presents a cross sectional view of the manner in which the fuel and oxidizer are separately manifolded before being injected into the chamber.

To determine the influence of injector hole distribution, one measures by a simple apparatus the amount of oxidizer and fuel distributed downstream of the injector. At various axial distances one creates a bank of distributed radially tubes that will collect the liquids intercepted by them. By rotating the tube bank, one can obtain an azimuthal distribution. The information obtained from this experiment is two-fold. One can obtain (a) if the mass flux distribution of the fluids is concentrated over some segments and (b) the oxidizer-to-fuel ratio over the cross section. The mass flux distribution of selected geometries is illustrated in Figure 10.15. One can notice that the liquid mass is distributed in a flat region when the two injectors are symmetrically arranged (this is easily possible with like injection). What happens is that the jets coalesce after impingement into a sheet that spreads outwards while simultaneously becoming thin. When the sheet is sufficiently thin, the intrinsic jet instabilities aided by aerodynamic shear tear the sheet into ligaments which further break down into droplets. The droplets can impinge on each other and can result in further break-up or merger leading to larger droplets. The atomization process is dependent on the injection velocities. *Typical velocities of injection vary between 35 to 45 m/s.* These correspond to 6 to 10 atm.

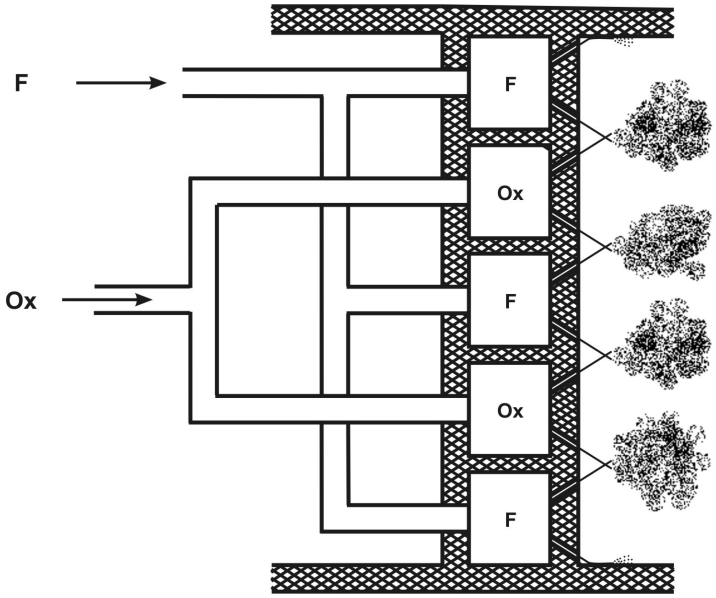

Figure 10.13: The cross section of the injection head showing the manifolding

in terms of pressure drop across the injector. *Typical orifice diameters vary from 1 to 7 mm*.

The velocity of the fluid in the plenum (that is expected to have low velocity), the nature of orifice entry and the (l/d) of the injector have a significant influence on the repeatable performance from the combustion system. The manifold must be arranged to have relatively low velocity so that the fluid distribution to the upstream zone of the injector is relatively uniform. The entry can be sharp-edged, chamfered or smooth rounded. For the purpose of fabrication, one classifies the injector heads as accessible, semi-blind or blind. If it is possible to do the welding of the injector plate after drilling holes, then it is taken that both sides of the injector plate are accessible and one can use the strategy of a smooth rounded entry with a l/d of 4 - 5 so that jet exit from a sharp-edged exit is stable. Use of smaller $l/d \sim 2$ - 3 sometimes leads to irreproducible performance and needs care in the choice of distribution of the holes; J 2 engine has dealt with these issues successfully. However, sharp-edged orifices are more common. They have the advantage of defined vena-contracta and good flow distribution provided the l/d is kept above 4 (typically, 5 is found acceptable). The presence of burr due to machining can pose serious problems that need to be addressed; electro-polishing is a strategy adopted to deal with this problem. The “semi-blind” orifices in which there is access only from a side and the “blind” orifices in which there is no access to the inlet side of the orifices pose varying degrees of problems in orifice production control. In any engine, it is possible that some parts belong to “accessible” type

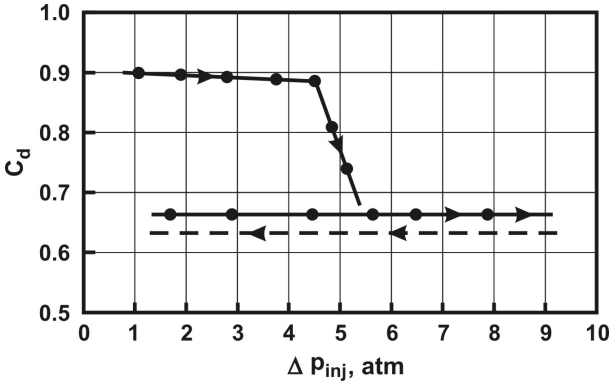

Figure 10.14: The variation of injector hole discharge coefficient with pressure drop across the injector showing the hysterisis effect – two values of c_d for the same pressure drop depending on the approach to this condition

and others semi-blind or blind. The only solution available is to allow for variation in the pressure drop across the latter class in the design itself. These become serious in larger engines that have orifices as large as 4 to 7 mm and it is difficult to provide for reasonable l/d for the orifice. In these cases the typical l/d chosen is about 2 – 3.

The flow through a straight hole is characterized by

$$\dot{m} = \rho_l A_{inj} V_{inj} = c_d A_{inj} \sqrt{2\rho_l \Delta p} \tag{10.6}$$

where $\dot{m}$ is the mass flow rate through the injector element, A_{inj} is the injector cross sectional area, Δp is the pressure drop across the injector (equal to the difference between the pressure in the manifold and that in the combustion chamber), ρ_l is the density of the liquid. This equation is the same as (8.21). It is simply derived from Bernoulli's equation. The velocity through the injector is given by $\rho_l V_{inj}^2/2 = \Delta p = (p_{manifold} - p_c)$ where the dynamic head is related to the pressure difference across the injector. The manifold pressure is taken as being close to stagnation conditions. The injector pressure drop is chosen to lead to injector velocities of 35 to 45 m/s for storable liquids and in the case of cryogenic propellants, hydrogen gas velocity of 100 to 120 m/s. In the above equation, c_d is called the coefficient of discharge and accounts for frictional effects in straight hole injectors and includes the energy going into the tangential motion for swirl injectors. Its typical value of 0.6 to 0.7 for straight hole injectors and 0.3 to 0.5 for swirl injectors. The geometrical features of the injector head discussed in the earlier paragraph reflect themselves in terms of a value for c_d that could be influenced by the the pressure drop across the injector itself.

Figure 10.14 shows the plot of c_d as a function of the Δp across the injector. One can notice the hysterisis effect . There are two values of c_d at a fixed pressure drop

and what value gets selected depends on the approach to the condition. Excursions in pressure drops could occur if the design pressure drop is in the range of two values of c_d. The reason for the two values is that the flow behavior at the entrance to the injector could have separated flow, partially attached flow and/or stream misdirection. The general recommendation is to avoid the range of pressure drops where two solutions are noticed; to choose a higher pressure drop to ensure robust fluid dynamical behavior. For variable thrust engines, it is important to keep in mind that the Δp_{inj} be above a critical value even at the lowest thrust rating. Recent advances in computational fluid dynamics could be used very effectively to understand the distribution of fluids in injector manifolds and through the holes where needed.

10.2.2 Drop Size Distribution

The drop size distribution is a function of the diameter of the orifice, the pressure drop (or the jet velocity) and the chamber pressure. Smaller the orifice diameter, larger the jet velocity, larger the chamber pressure, better would be the atomization. Many of the effects are highly nonlinear. The two non-dimensional numbers that control the drop size distribution are: (a) Jet Reynolds number = Re_j = $\rho_l V_j d_j/\mu_j$ and (b) the Weber number = $We_j = \rho_l V_j^2 d_j/\sigma_j$, where V_j and d_j are the jet velocity and diameter, μ_j, σ_j are the viscosity and surface tension of the jet fluid. Since more than one fluid is involved, one would expect the resultant drop size to be expressed as

$$\frac{d_{smd}}{d_j} = F(Re_f, Re_{ox}, We_f, We_{ox}) \sim 5Re^{-0.15}We^{0.2} \tag{10.7}$$

The equation does not show any suffix (fuel/oxidizer) on the Reynolds and Weber numbers. The question of how the drop size distribution gets affected if the velocities of one of the propellants is changed does not seem to have been addressed. Therefore, the dependence can be taken as valid in a qualitative sense. In the above equation, d_{smd} is the Sauter mean diameter and the coefficient and the exponents are drawn from the work of Mugale (AIChEJ, v. 6, 1960, p. 3). Both Reynolds number and Weber number are in the range of 10^5 – 10^6 and 10^5 respectively. For Re = We = 10^5, one obtains d_{smd} = 0.09 d_j. For a 1 mm orifice diameter, one gets d_{smd} = 90 microns. This is a typical value. From a range of experiments conducted with simulated propellants, it has been determined that if the orifice diameter is 1 mm, Δp_{inj} is 6 atm., chamber pressure is 50 atm., the expected mean droplet diameter (SMD – Sauter mean diameter) would be 80 microns. Any increase in orifice diameter will tend to increase the drop diameter at the same station, but can reduce with distance due to collisions with many droplets in the dense droplet atmosphere. An interesting feature observed in the experiments is that if the pressure of the gaseous medium is higher as is usually the

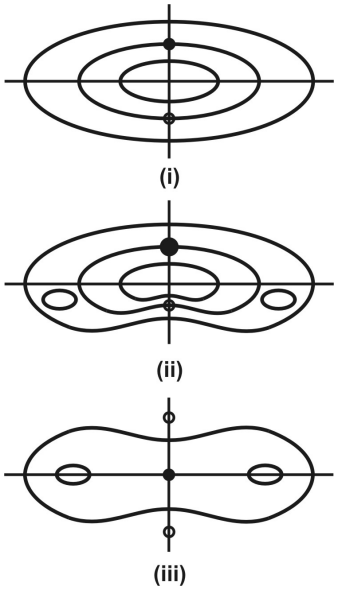

Figure 10.15: The mass flux contours downstream of the injector holes; the reason for the flat distribution is the fact that impinging jets coalesce into a sheet broadens while simultaneously becoming thinner and then breaks down into droplets

case with rocket engines, the atomisation process is enhanced significantly due to higher aerodynamic resistance of the ambience. The behavior appears to be quite complex. Fine orifice based injectors (at fixed pressure drop) show an increasing tendency for the mean drop size with increase in the chamber pressure – asymptoting to about 100 microns at 20 atm. Orifices with diameter more than 2 mm show a decreasing tendency of mean drop size from about 300 microns at ambient pressure to about 200 microns at 30 atm. [12]. These peculiar features are related to the droplet collision dynamics. Fine droplets can coalesce when they collide and large droplets can break down to a number of small droplets when they collide with other droplets. These processes are only qualitatively understood and need to be explored through modeling approaches.

The injector types used on several engines is presented in Table 10.6; this table has interesting information on them.

The number of injector holes to be drilled on an injector head is so large (thousands) that this particular action is complex and time consuming. It could be a schedule affecting activity in development or realization. The injector orifices can be as small as 0.73 mm and as large as 7.1 mm. The thrust per element is calculated by counting an "element" as an oxidizer-fuel group. For instance in a doublet, one oxidizer hole with one fuel hole would constitute an element. In a quadlet like for Titan II/stage II system, three oxidizer injectors with one fuel injector will con-

Table 10.6: Characteristics of injectors of major liquid rocket engines; Elmt Type = Element type, Dbt = Doublet, Co-l = Coaxial, Tpt = Triplet, Qdt = Quadlet, IP dia = Injector plate diameter, F-1, J-2 - Saturn mission, TII – Titan II, SI – Stage I, Vikas – Indian version of Vikas engine of Ariane vehicle, CUS – Cryogenic upper stage – Russian design modified in India, SSME – Space shuttle main engine; (v) = vacuum exit condition; F/El = Thrust per element, $\eta_{c^*} = c^*$ efficiency = ratio of actual to theoretical c^*

	Engine	Props.	F kN	$\dot{m}$ kg/s	Elmt Type	IP dia mm	No. Ele.	d_{inj} mm	F/El kN/El	Δp_{inj} atm	η_{c^*} %
1.	F 1	LOX	6860	1846.1	Like	996	714	6.1	9.8		93.8
		RP1		778.0	Dbt		702	7.1			
2.	J 2	LOX	1034	209.0	Coal	470	614	4.6	1.7		98.6
		LH_2		38.0				0.43			
3.	Agena	RFNA	70	17.8	Tpt	274	88	2.8	0.9		95.7
		UDMH		6.9			176	1.2			
4.	TII/SI	NTO	952	250.0	Like	554	568	1.2	1.8		97.2
		A-50		124.5	Dbt		516	0.73			
5.	TII/SII	NTO	446	94.1	Qdt	368	1319	0.9,1.3	0.5	10.0	97.4
		A-50		52.2			818	0.74		10.0	
6.	VikasU	NTO	823	173.8	Like	500	432	4.3	1.9	8.2	96.5
		UDMH		102.3	Dbt		432	2.9		11.9	
7.	CUS	LOX	71	14.0	Co-l	200	109	4.6	0.6	20.8	99.2
		LH_2		2.3						7.9	
8.	SSME	LOX	2323	407.0	Co-l	452	600	4.8	5.1		99.6
		LH_2		67.7				1.65			
9.	Apollo	NTO		9.5	Tpt	288	55	1.96	0.8	2.6	97.2
	LEMDE	A-50	47	5.9	FOF		110	1.24		2.6	
10.	SS	NTO	27	5.0	Like	206	136	0.81	0.2	3.8	97.5
	OME	MMH		3.1	Dbt		136	0.71		4.1	
11.	RD253	NTO	1720	384.0		430					
		UDMH		144.0							

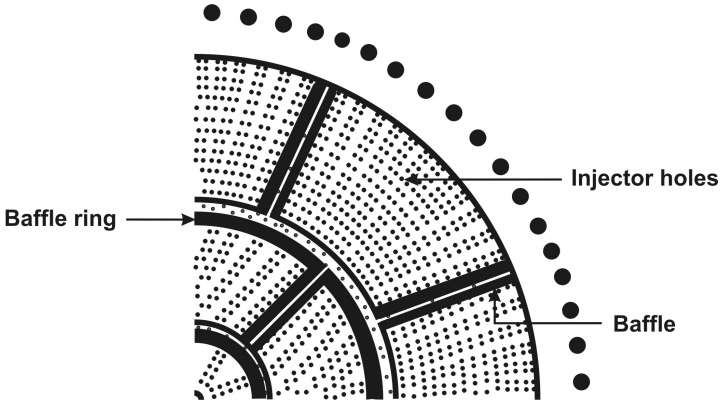

Figure 10.16: The baffles - radial and circumferantial - on a F1 engine injector, from [28]

stitute an element. From the Table 10.6 it can be seen that the Agena engine or Titan II/ Stage II suffer from a low thrust per unit element. The SSME engine appears to score over J 2 engine in respect of this parameter (5.1 against 1.7).

Figure 10.16 shows the F 1 injector head. As can be noticed there are radial and circumferential baffles as a part of the injector. These are used to overcome the high frequency instability (HFI) problem on the engine. The injectors can also be designed to allow for acoustic cavities at the outer boundary to enable absorption of acoustic energy to help stabilize the combustion process. The outer ring of holes in most injectors is arranged so as to inject the fuel on to the wall. This provides "film cooling" of the wall. This is a standard feature that is used in every engine since it helps provide a cooler environment near the wall. Even if other cooling techniques are used, all of them combine them with film cooling.

Figure 10.17 shows the arrangements for radial injector of Vikas engine whose cross section is shown in Figure 10.18.

The asymmetry in the left and right hand sides is by design. The geometry is arranged such that the oxidizer, NTO enters from the holes indicated to the right and the fuel enters from the holes indicated to the left. The channels connecting the oxidizer holes to the top dome are separated from the volute that brings in the fuel to the appropriate segments. In the case of cryo-engines or those storable engines using swirl injectors, one uses what are termed "burners". Individual elements that qualify in water calibration tests as belonging to acceptable values of flow per element at rated pressure drop (implying a value of c_d) are selected and welded on to the flat injector plates at the designated holes. Typical distribution is shown in Figure 10.19.

Injectors used in small thrust engines will have small number of elements. Only a single impinging jet system is found adequate to pass the flow. Minimiz-

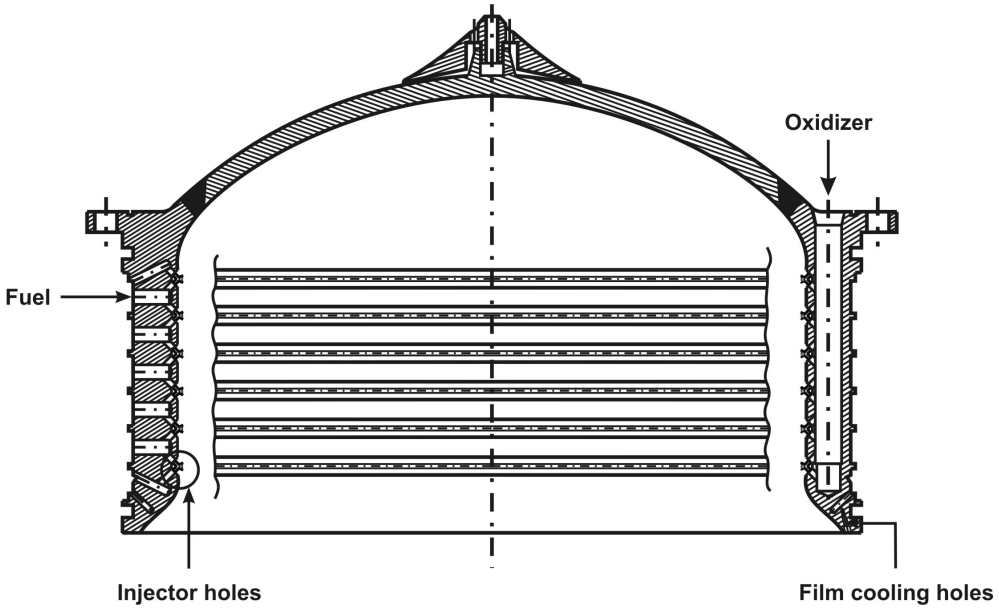

Figure 10.17: The injection head of Vikas engine

ing the deviations in O/F is very difficult. One of the concepts that has been tried for a range of thrust levels and for engines needing variable thrust is the coaxial injector design. Figure 10.19 shows the schematic of the injection system. In this design, one of the propellants flows through an annulus with small spacing and is impinged by radially issuing thin sheets. Together a conical sheet is formed. The conical sheet then breaks down into fine droplets of fuel and oxidizer for further reactions to take place. The injectors used for gas generators follow the same principles as for the main injectors. The difference between the two classes of injectors lies in the O/F ratio. In the main combustion chamber, one uses a mixture ratio that optimizes on the specific impulse; the O/F does not deviate from stoichiometry very much. The peak temperatures are about 3300 K. In the case of gas generators, the O/F used is far into fuel rich condition. Hence, the injector sizes would be different and the arrangement of the holes has to made such that some zones enjoy a high enough O/F for sustained combustion process while others are arranged so as to allow the richer fluid to vaporize and mix with the high temperature gases. Table 10.7 shows some features of the injectors for gas generators.

Typical values of various parameters for the gas generator are presented in Table 10.8. This shows the oxidizer to fuel ratio is much on the rich side when compared to the main combustion chamber. Also, the residence time required to complete the reaction process in the gas generator is larger – typically 6 to 10 ms excepting for LOX – LH_2 systems. In the main combustor as well as gas genera-

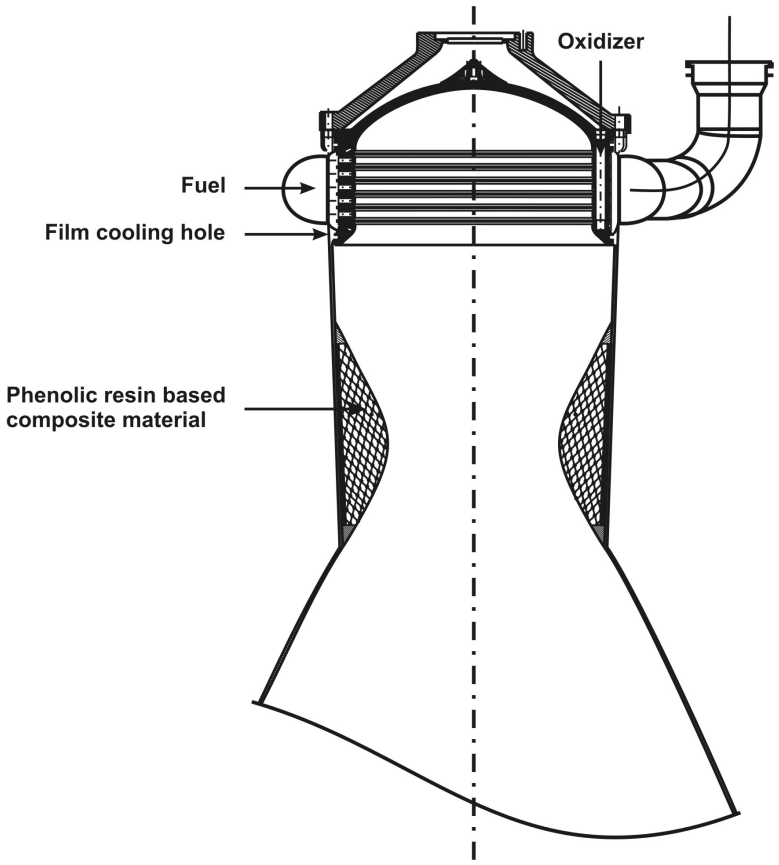

Figure 10.18: The Vikas engine with the thrust chamber and the injection head

Table 10.7: Design features of injectors for gas generators (Special = Hydrogen jet into which oxygen jets are injected; TII = Titan II, SI = Stage I, SII = Stage II, CUS = Cryogenic upper stage)

Engine	Propellants	Injector	Flow path	Igniter
F 1	LOX - RP1	Doublet	Reverse	Pyro
M 1	LOX - RP1	Coaxial	Axial	Pyro
J 2	LOX - LH_2	Poppet	Axial	Spark
Agena	RFNA - UDMH	Doublet	Axial	Hypergolic
TII/SI	NTO - A-50	Doublet	Axial	Hypergolic
TII/SII	NTO - A-50	Doublet	Axial	Hypergolic
VikasU	NTO - UDMH	Doublet	Axial	Hypergolic
CUS	LOX - $\mathrm{LH_2}$	Special	Axial	Pyro

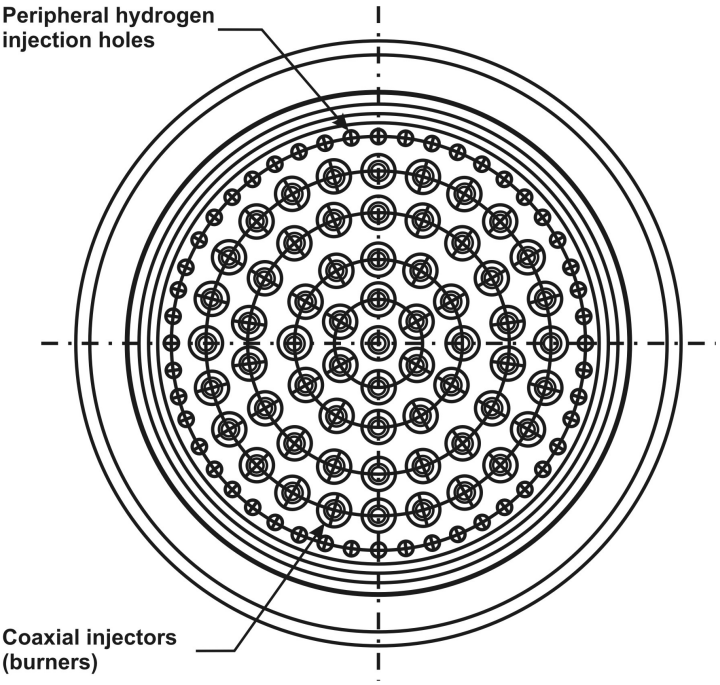

Figure 10.19: The injector face of a LOX-LH_2 injection head; All are coaxial type. The outer most injection holes are for hydrogen to help film cooling

Table 10.8: Design features of gas generators for turbines (T_{gg} and p_{gg} = Gas generator temperature and pressure, P_T = Power of the turbine); (W) refers to water injection

	Engine	$\dot{m}$ kg/s	O/F	T_{gg} K	$p_{c,gg}$ atm	t_{res} ms	P_T MW
1.	F 1	77.2		1060	70.0	5.0	41.0
2.	J 2	3.3		920	44.7	0.3	7.7
3.	Agena	0.7		1030	3.3	4.3	0.3
4.	TII/SI			1180	38.0	3.7	3.7
5.	TII/SII	2.6		1170	34.0	2.3	1.6
6.	VikasU	1.9+0.75 + 3.76 (w)	2.53	870	38.0	2.0	3.1
7.	CUS	3.2	0.57	915	81.3	1.0	8.0
8.	SSME, Ox			870	360.0		20.4
	SSME, F		0.37	1030	350.0		57.0

tors, the O/F distribution across the section will not be uniform. Due to the need to provide for a cooler region near the walls, fuel jets are injected such that they move along the wall as a thin sheet with little break up and vaporize due to the heat transferred from the core combustion products. Due to this reason, other regions have an O/F to compensate for the film cooling. Even here, it is possible that different regions have different O/F due to the fact that the jet impingement process brings about different O/F values over the regions around the injection orifices. If one measures the O/F distribution across the section at different stations downstream of the injector plate, one finds the distribution does not change over the axial distance. This feature seems to be preserved even in a hot flow. *Thus, the mean O/F values of different stream tubes remain the same as they move through the combustion chamber*. This is because the temperatures and velocities of different stream tubes are different and the mixing rates are low due to differential density effects; the distances traversed in the combustor are insufficient to mix them. Hence, a stream tube analysis is made the basis of a procedure to predict the overall performance of a rocket engine allowing for changes in O/F as the streams flow through the combustion chamber and the nozzle. The cooler zone near the walls is also preserved over the distance, even though the mean temperature keeps increasing as it flows out towards the exit. Typical exit temperatures could reach 1200 – 1400 K when the core exit temperatures are about 2000 K. Figure 10.20 shows the injector head for a typical gas generator. One can notice the manifolding that is done on the injector head.

10.2.3 Gas Generators for Turbo-Pumps

Gas generators are always run off-stoichiometry due to the limits on the temperatures acceptable to the turbine. This implies that the system can run fuel or oxidizer rich. Oxidizer rich operation is avoided for the simple reason that with most oxidizers, hot oxidizer rich gas could oxidize away the wall or turbine material at higher temperatures. If any ablative is used as a wall material, it would also get oxidized very easily. Operating the system on fuel rich condition avoids these problems. It is true that the mechanism of vaporization and decomposition of the fuel has remained elusive due to the complexity of fluid-chemistry interactions; but employing intuitive approach based on general principles and substantive testing have provided enough base for the realization of successful systems. The O/F at which the gas generators are expected to operate is 0.5 to 0.7 for storable mixtures and 0.6 to 0.8 for LOX-LH_2 system. To ensure smooth ignition and combustion, it is necessary that a part of the injection system works at much higher O/F and the excess fuel introduced through orifices be atomized to fine droplets so that they vaporize and mix with the hotter gases to bring the temperature to the design value. The high temperature gases move faster due to lower density and the rest of the fluid maintains a lower velocity with weak mixing, a point discussed above.

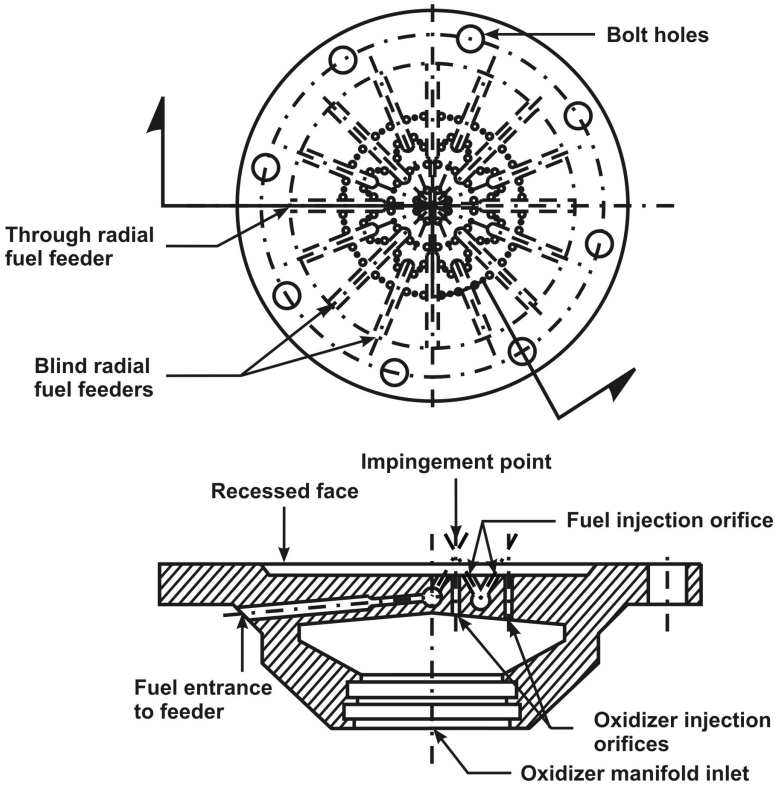

Figure 10.20: Injector head for a gas generator combustion system, drawn from ref. [38]

This stratification causes hot streaks of fluid to impinge on parts of the combustion chamber and also on the turbine. To overcome this problem, additional mixing elements are introduced and the fluid path is made more complex so that both classes of fluid have enough space and time to mix as well as possible. Typical residence time for gas generators is between 3 to 5 ms (see Table 10.8) in the combustion chamber and the time will be 10 to 15 ms if one includes the path to the turbine. Another way of expressing this would be in terms of a parameter L^* introduced already in solid rocket engines (see section 9.17). This quantity is typically 3 to 4 m for gas generators. For main combustion chambers, it would be 0.8 to 1.2 m.

Figure 10.21 shows three designs that have been used in actual systems - (a) the design with a central tube arrangement with its larger pressure drop does not allow the gases to go out of the combustion chamber until mixing is substantial, and (b) a design with a convergent mixer and a bend to ensure better mixing and (c) a design in which the O/F is not much below stoichiometry and the burnt gases are mixed with water spray to reduce the temperature of gases. The tri-fluid combination calls for an additional tank having water and its pressurization system. This approach is more complex and has been used in Viking engine (Vikas

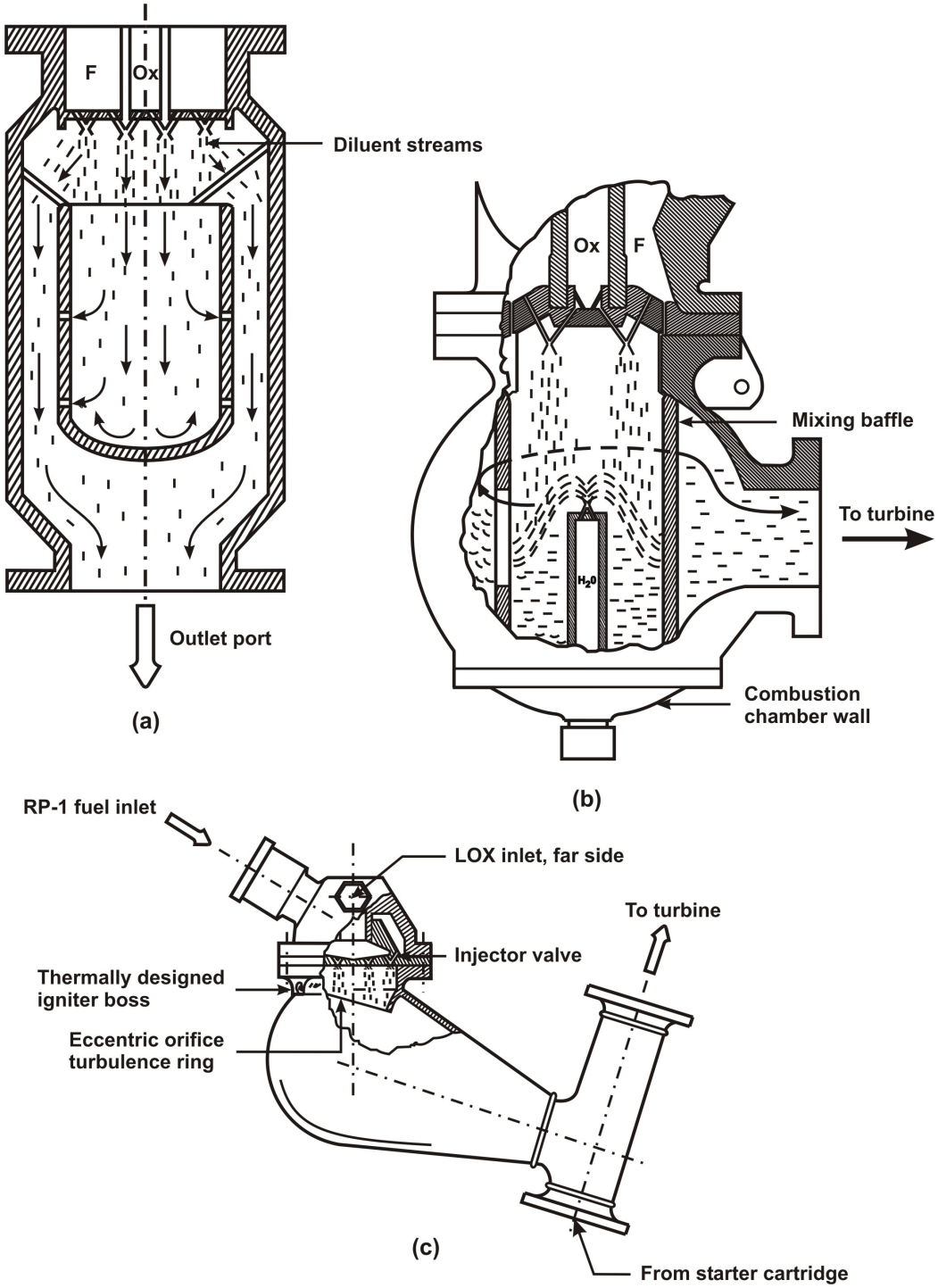

Figure 10.21: Types of gas generator arrangement with (a) an internal can type for enhancing mixing, (b) a tri-propellant system with NTO - UDMH and water, and (c) a turbulence generator and a curved mixing device for a semi-cryogenic system

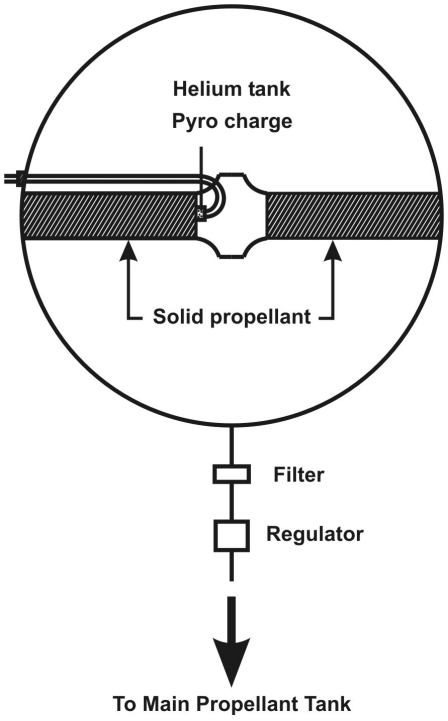

Figure 10.22: The high pressure gas bottle with Helium gas with additional energy input from a solid propellant

engine of Indian adaptation). The designs (a) and (b) have been used in F 1 and J 2 vehicles. Table 10.8 contains the details of gas generators used on several vehicles.

10.2.4 Pressurization Systems

The simplest of the pressurization systems is the inert gas drawn from a high pressure storage. This has been presented in all the schematics of the feed systems. There are many variants possible. The key aspects on which the system quality is based are: system weight, volume, propellant compatibility and system complexity. The first variant is to heat up the helium by passing it around the thrust chamber. This reduces the weight and volume of the helium storage system by 40 %. One could use a solid propellant gas generator feeding into helium tank, heating the helium inside the tank to appropriate levels. With respect to the cold helium case, this option reduces the weight to 30 % and volume to 8 %.

Figure 10.22 shows schematically the arrangement. Other variants include the tapping of the gas from the two gas generators meant for the turbine, diluting them with helium and using the oxidizer rich gas for the oxidizer tank and fuel

rich gas in the fuel tank. The reduction in weight and volume compared to cold helium case is about the same as in the earlier case even though the complexity of the system is higher. One could use the hydrogen from the regenerative heating passage at an appropriate location (in terms of temperature) as the pressurizing fluid in the hydrogen tank.

10.2.5 Turbopumps in Feed Systems

Turbopump assemblies form a complex part of the liquid rocket engine. The sub-assemblies consist of gas generator, turbine/s and pumps. Amongst these, the gas generator has already been discussed as an independent element since it is a combustion system. Other elements are rotating components. There are several ways of arranging the fluid circuit involving the above elements. Some of these are variants that can be considered as designers' choice – in fact, one could use any equivalent schematic. However, some relate to technology advancement and imply significant improvement in the overall performance. We examine first the various possibilities and then each of these elements in detail.

10.2.6 Schematics of Turbopump-Gas Generator Systems

Figure 10.23 shows the four standard schematics that have been used in most engines. The first one uses a separate monopropellant tank that derives a pressurant from the main pressure source but branched off into another line with a suitable pressure regulator (from 350 to 50 atm.). This monopropellant is sprayed into the gas generator that would have been started up with solid propellant cartridge starter. The monopropellant decomposes exothermically and the hot gases drive the turbine to deliver the power for the pumps. The exhaust from the turbine passes through a separate nozzle into the ambient. This ensures that the turbine operating conditions do not change with altitude.

In the second approach, the start-up can be done with solid propellant cartridge starter. A part of the liquid propellants pumped into the thrust chamber is drawn at required flow rates into the gas generator. The combustion process in the gas generator provides the gas at high pressure to drive the turbine. In this approach, no separate monopropellant and associated arrangements are required. The technique is called bootstrap technique since the same propellants are drawn for running the gas generator.

In the third approach, that is particularly suitable for liquid hydrogen because it remains undecomposed as it passes through the regenerative cooling system and gets heated to temperatures to enable extraction of energy, liquid hydrogen that is pumped into the regeneratively cooled chamber gets heated and then a suitable

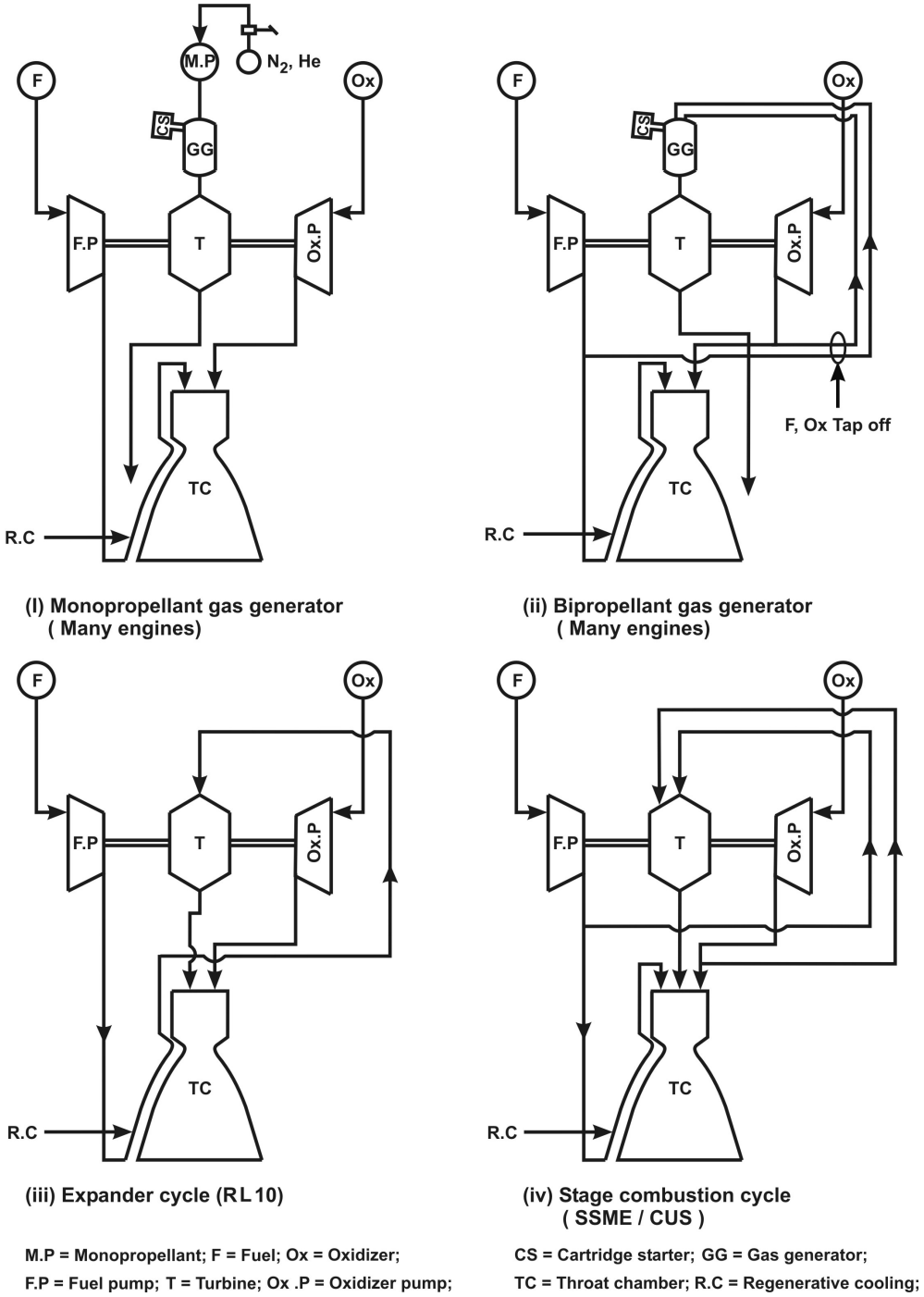

Figure 10.23: Different types of arrangements for powering the turbines (a) Monopropellant type, (b) Bipropellant type (bootstrap arrangement), (c) Expander cycle and (d) Staged combustion cycle

part of the gas is drawn to run the turbine; the gas then passes into the main combustion chamber. Since the pressure at the exit of the turbine must be around the chamber pressure, the turbine inlet pressure equal to the gas generator pressure will need to be very high to enable extraction of work from the turbine. This implies that hydrogen pump outlet pressure must be very high in this approach or the chamber pressure must be low. This method is called expander cycle followed in RL 10 engine where the combustion chamber pressure is 27.3 atm.

The fourth approach combines parts of the second and third strategies. The oxidizer and the fuel are drawn into gas generator that runs the turbine and the turbine exhaust enters the main combustion chamber. In the case of SSME engine, several additional features were introduced. The fuel and oxidizer pump outlet flows are tapped into two separate gas generators that power two separate turbines. These turbines run two separate pumps. The peak pressure in this system is 550 atm for a chamber pressure of 222 atm.

Figure 10.24 shows several classical arrangements that have been used in several systems. The system (a) positions the fuel and oxidizer pumps back-to-back with the turbine operated on the same shaft. The back-to-back arrangement helps reduce the axial thrust of the pumps (F 1 engine). Arrangement (b) has a turbine running at high speed and through a gearing system the fuel and oxidizer pumps can be run at different optimum speeds. In case (c), there are dual pump-turbines and the hot gas runs the turbines in series. This option is used in J 2 engine. The choice of pressure ratios and the rpm of the two systems is made optimally. In case (d), the turbine is located between the pumps (SA 2 Russian engine). This is a common arrangement. It works well for propellants with similar densities (like LOX – RP1). Case (e) is a variant of (b). The pumps run on the same shaft at a speed different from the turbine speed; this is called offset turbine. Another variation is (f) used in SSME engine. It has great flexibility for optimizing the off-design operation due to the independence in the selection of operating parameters for both the turbopumps.

In all these strategies, the pump delivery pressure is set higher than required and it is dropped across a tunable resistance (during qualification testing) so that the engines have specified characteristics downstream.

10.2.7 Choices of Turbines and Pumps

Turbines and pumps can be centrifugal or axial, and single or multistage. In turbines, one could have impulse or reaction, velocity compounded or pressure compounded. It is desirable to appreciate some general considerations for the choice of the options. Axial turbines are more efficient in the range of use, can be multistaged easily; also for the same choice of the turbine tip velocity-to-gas velocity, axial flow turbines are lighter [41]. Consequently, the design of turbines for rocket

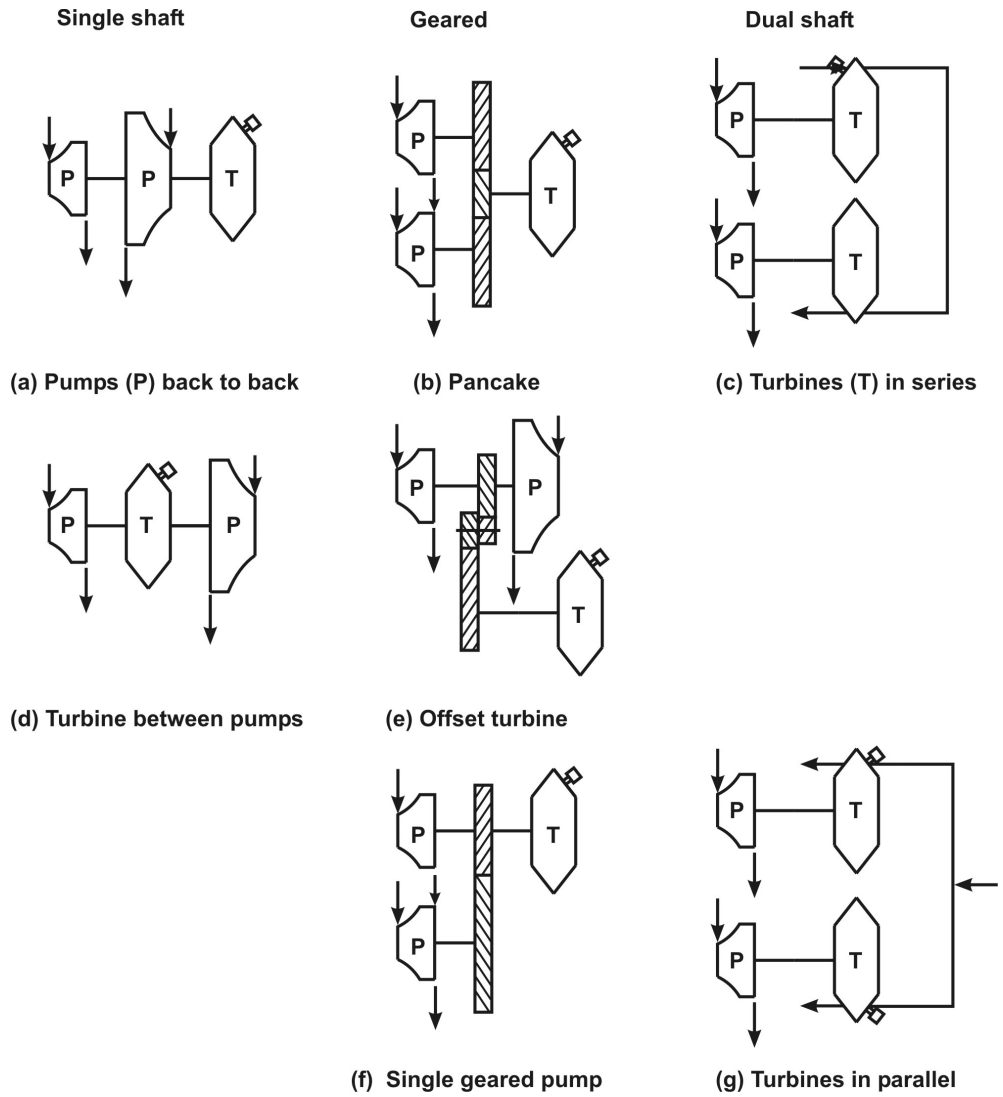

Figure 10.24: Various pump drive arrangements

engines are of the axial nature. In smaller engines, a single nozzle connected to the gas generator expands the flow to high velocity and this jet impinges on the rotor blades to transfer the momentum to the rotor. This is a partial admission single stage impulse turbine [Figure 10.25 (a)]. If all the momentum is not absorbed in a single rotor assembly, a second stator assembly simply directs the velocity vector appropriate to a second rotor assembly and the energy extracted, such a system is called velocity compounded turbine [Figure 10.25 (b)]. It is also possible to do pressure compounding. Multiple nozzles are used to drop the pressure in stages and use rotors for extracting work from the high speed stream [Figure 10.25 (c)].

Figure 10.25 shows the plots containing velocity and pressure variation through stages describing the above features. Whether one should use impulse or reaction stage, what the number of stages should be, whether they should be velocity or pressure compounded depends on the velocity ratio V_{ml}/C_0, where V_{ml} is the mean line velocity of the turbine and C_0 is the velocity of the jet impinging on the rotor blades.

Figure 10.26 shows the plot of the efficiency with velocity ratio for a typical set of options. Multiple stage operations offer better efficiency at the same velocity ratio. Reaction stage offers high efficiency at high velocity ratio. Table 10.9 shows the details of the choice for various systems. As can be noticed from this table, most turbines are impulse type. Most large engines use full admission flow excepting Agena engine that used partial admission, implying admission of the hot gases over a fraction of the periphery due to low flow rates – a single nozzle is used to create the high velocity stream to impinge on the rotor. The turbine inlet temperatures are between 700 and 1200 K. The gas generator pressures and the pressure ratio dictate the number of stages or whether it should be compounded.

Figure 10.27 shows the cross section of a typical full admission two stage axial turbine.

The power output from the turbine is given by

$$P_T = \dot{m}_T c_{p,T} T_{c,T} \eta_T \left[1 - {\pi_T}^{(\gamma-1)/\gamma}\right] \tag{10.8}$$

As to what the design power level should be, is given by the power demanded by the pumps and this balance is given by

$$P_T = \frac{1}{\eta_{mech}} \left[\frac{\dot{m}_f(\Delta p_f/\rho_f)}{\eta_{p,f}} + \frac{\dot{m}_{ox}(\Delta p_{ox}/\rho_{ox})}{\eta_{p,ox}}\right] \tag{10.9}$$

where η_{mech} is the mechanical efficiency of power transfer, $\eta_{p,f}$ and $\eta_{p,ox}$ refer to the pump efficiencies of the fuel and oxidizer pumps. Typical values of the turbine and pump efficiencies are presented in Table 10.10. In the early developments like Agena, the efficiencies were small. The efficiencies of modern systems have been substantially higher.

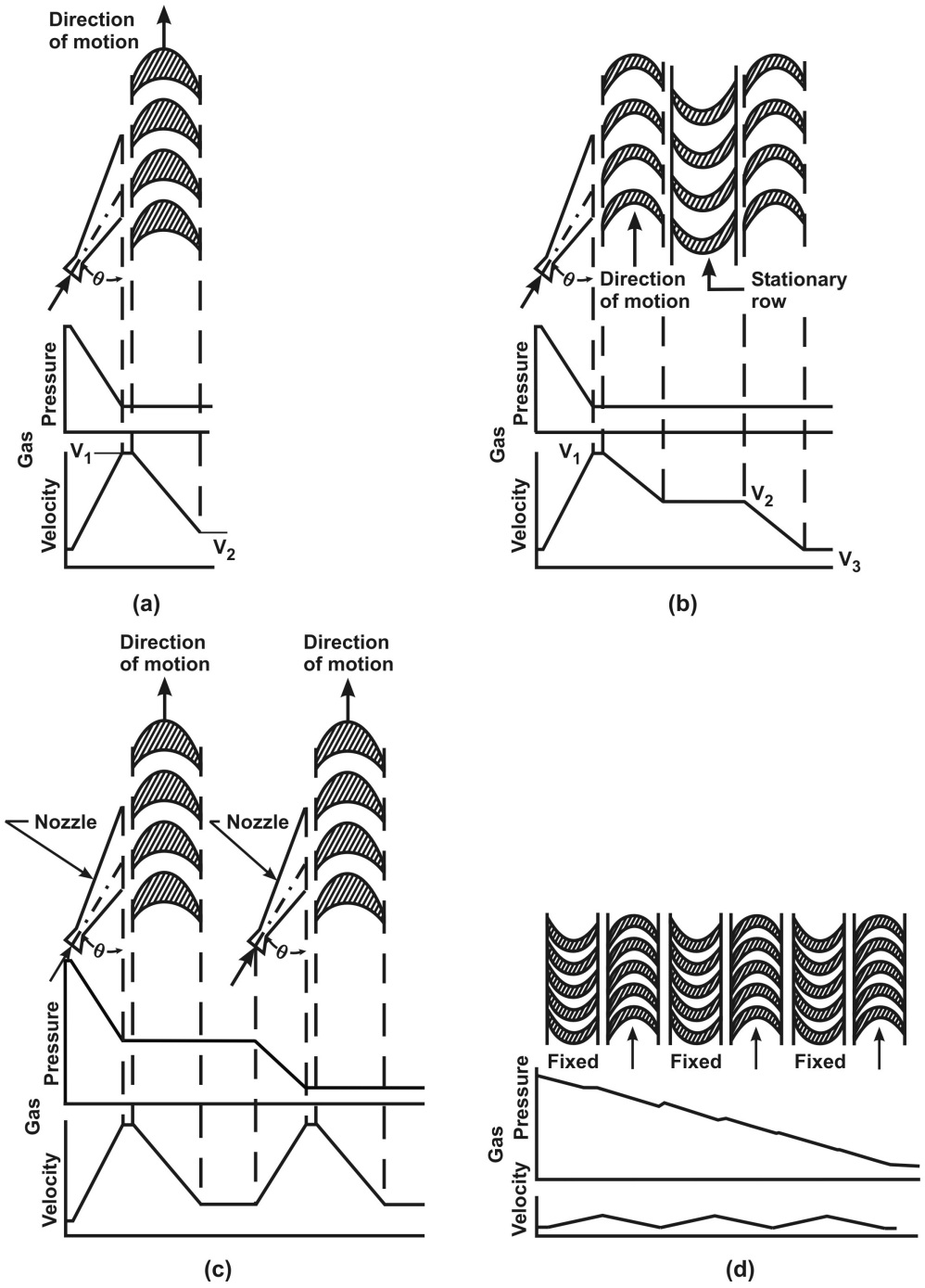

Figure 10.25: Mean velocity and pressure variations through the stages in turbines; (a) partial admission single stage turbine, (b) a two stage velocity componded design, (c) a two stage pressure compounded design, (d) a multistage partial reaction design

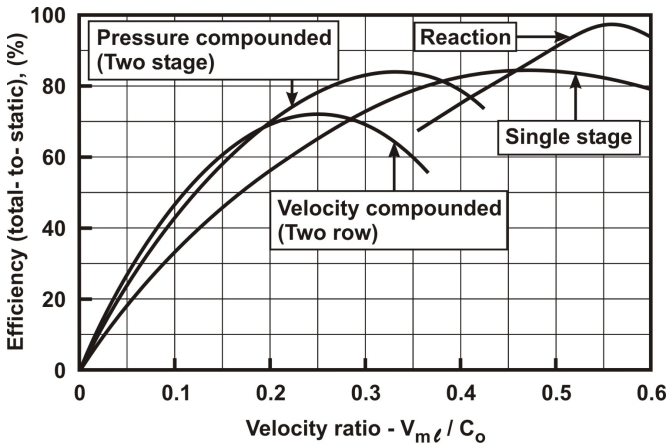

Figure 10.26: The efficiency of a turbine with different design options

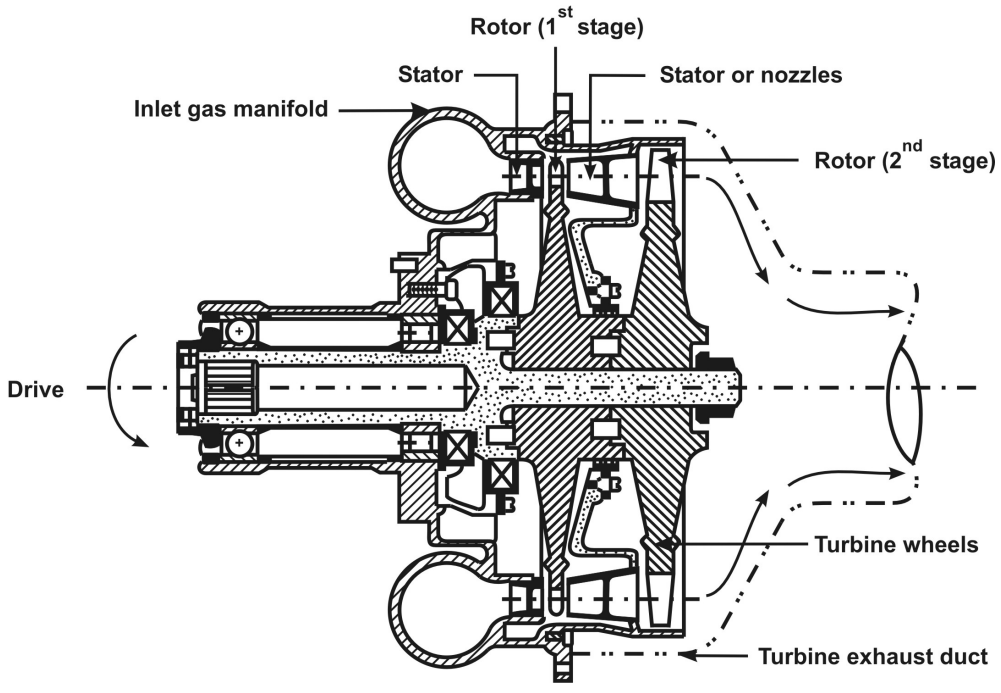

Figure 10.27: An axial turbine assembly with details

Table 10.9: Features of Turbines (No. St. = Number of stages, 2vs = two row velocity compounded, i,pa = impulse partial admission, pc = pressure compounded, rean = reaction, p_c = turbine inlet pressure = gas generator pressure, $1/\pi_t$ = pressure ratio across the turbine, V_{ml} = velocity at the rotor mean line)

	Engine	Props.	No. St.	Type	$T_{c,T}$ K	$p_{c,T}$ atm	$1/\pi_t$	$\dot{m}_T$ kg/s	rpm	V_{ml} m/s
1.	F 1	LOX	1	2vc	1060	62.5	16.4	78.1	5488	256
		RP1							5488	
2.	J 2	LOX	1	2vc	680	6.1	2.5	2.3	8753	180
		LH_2	1	2vc	920	44.7	7.3	3.2	27130	451
3.	Agena	RFNA	1	i,pa	1030	32.6	37.7	0.6	24800	260
		UDMH								
4.	TII/SI	NTO	2	pc	1180	30.1	17.8	5.8	24000	299
		A-50								
5.	TII/SII	NTO	2	pc	1170	29.2	29.0	2.5	23700	294
		A-50								
6.	VikasU	NTO			870	36.0	17.1	6.3	10000	
		UDMH							10000	
7.	CUS	LOX	1		915	81.3	1.3	3.2	42710	360
		LH_2	2						42710	
8.	SSME	LOX	2	rean	870	400	1.6	28.8	31000	415
	SSME	LH_2	2	rean	1030	396	1.6	72.3	37400	506

Table 10.10: Features of Turbines - contd, η_T and η_p = Efficiencies of turbine and pumps

	Engine	Arrangement	P_T MW	Wt. kg	P_T/Wt kW/kg	η_T %	η_p %
1.	F 1	Single shaft Turbine on end	41.0	1429	28.7	60.5	44.6
2.	J 2, Ox	Dual Turbopump	1.76	138	12.7	48.4	37.4
	J 2, F	Series Turbines	5.94	167	35.5	60.1	44.9
3.	Agena	Geared Turbine and pumps	0.26	28	9.5	41.0	20.0
4.	TII/SI	As above	3.86	220	17.6	56.0	38.1
5.	TII/SII	Geared NTO pump	1.58	116	13.6	53.0	36.3
6.	VikasM	Single shaft	2.39		71.0	52.0	40.5
7.	CUS	Central Turbine	1.01	47	21.5		
8.	SSME, Ox	Separate	20.43	252	82.2	73.0	56.5
	SSME, F	systems	57.00	318	178.6	79.0	58.5

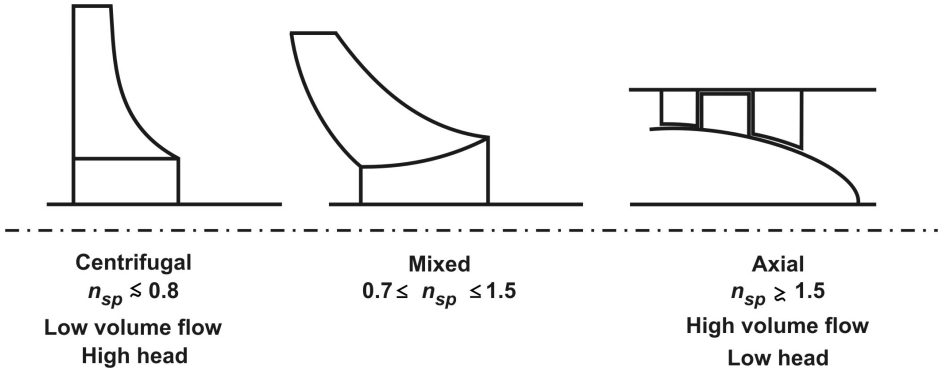

Figure 10.28: Different impeller types (a) Centrifugal, (b) Mixed and (c) Axial type

With respect to pumps, one has the choice between centrifugal, mixed or axial flow types. Centrifugal type is the choice for low flow rate and high head; axial type is meant for high volume flow rate and lower head. Figure 10.28 shows the broad geometric features of these types. These features are best analyzed by examining the dependence of the related parameters. The fact that the pumps are designed to raise the pressure of the fluids at specific flow rates efficiently can be expressed in terms of connected quantities as below.

$$\Delta p_p = \rho g \Delta H = F(\mathrm{rpm}, \dot{\mathrm{m}}_\mathrm{p}, \rho_\mathrm{p}, \mathrm{d_p}, \mu_\mathrm{p}, \mathrm{geometry}) \tag{10.10}$$

$$\eta_p = F(\mathrm{rpm}, \dot{\mathrm{m}}_\mathrm{p}, \rho_\mathrm{p}, \mathrm{d_p}, \mu_\mathrm{p}, \mathrm{geometry}) \tag{10.11}$$

where Δp_p is the pressure developed by the pump, ΔH is the head developed in m, d_p is the impeller diameter, and η_p = pump efficiency. The pump output is a strong function of the the rotational speed (rpm) and the pump impeller diameter. These quantities can be related by

$$\frac{\Delta p}{\rho_p \omega^2 d_p^2} = F\left[\frac{\omega\sqrt{\dot{Q}}}{(g\Delta H)^{(3/4)}}, \frac{d_p (g\Delta H)^{(1/4)}}{\sqrt{\dot{Q}}}\right] = F[n_{sp}, d_{sp}] \tag{10.12}$$

where ω is the rotational speed in radians per second, d_p in m, $\dot{Q}$ is the liquid flow rate in m^3/s, ΔH is the pump head in m. The left hand side is the non-dimensional pressure head. The right hand side has two non-dimensional terms representing speed and impeller diameter. They are termed *specific speed,* n_{sp} and *specific diameter,* d_{sp} as identified in equation 10.12. In most traditional literature, specific speed is treated in dimensional terms more as an engineering practice prevalent for over two hundred years. As can be verified, the quantities in the expression (10.12) are dimensionless.

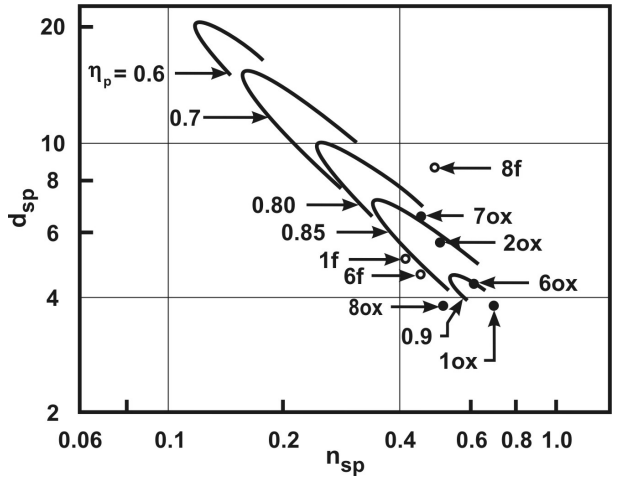

Figure 10.29: The plot of specific diameter vs. specific speed with data on pumps on several engines (η_p = pump efficiency). The notation 1f, 1ox, etc refer to the engines identified as numbers in Tables 10.11 and 10.12 and f (fuel pump) and ox (oxidizer pump)

Research conducted to determine the dependence of the pump performance as a function of various design features has resulted in plots shown in Figure 10.29 for centrifugal pumps. The best choice of parameters must result in the values of n_{sp} and d_{sp} in the regime shown by the curves of constant efficiency for various geometric parameters. The regime of good operation is restricted to a narrow range of d_{sp} - n_{sp} values. The plot shows that higher efficiency designs are obtained at larger values of n_{sp} and smaller values of d_{sp}. The values of these quantities obtained from the data of actual systems [41] are also set out as numbers identifying the systems in the first column of Table 10.11. These data points are found spread around the plot. Yet there are three significant aspects. The CUS engine design is a good example of a compromise. Since this staged engine design requires very high head for hydrogen due to its low density, the choice should have been a design with different speeds for LOX and LH_2. However, it was decided by the designers to set the pumps on the same shaft. If the speed is so high as to optimize the hydrogen pump design, then, the oxygen pump would need to have such small impeller making it difficult to realize the hardware with accuracy; also, the design would demand dealing with enhanced cavitation problem. The problem was solved by choosing a speed such that even LOX impeller would have reasonable size and hydrogen pump would have a two-stage centrifugal pump. An additional feature was to use two separate low pressure pumps and deliver the fluids to the main pumps at a minimum pressure to help avoid cavitation. In the case of SSME turbo-pump design, the pump-turbine system for the fuel was made separate from that of the oxidizer.

Table 10.11: Features of Turbo-pumps ($\dot{Q}$ = Volumetric flow rate, ΔH = Head developed by the pump, C = Centrifugal, M = Mixed, A = Axial, d_p = Pump impeller diameter, n_{sp} = Specific speed, d_{sp} = Specific diameter, * = calculations are made apportioning the head developed equally amongst the stages)

	Engine	Props.	Type	$\dot{Q}$ lit/s	ΔH m	rpm	d_p m	n_{sp} -	d_{sp} -
1.	F 1	LOX	C	1620	944	5488	0.49	0.774	3.8
		RP1	C	970	1575	5488	0.60	0.410	5.5
2.	J 2	LOX	C	180	666	8753	0.27	0.534	5.7
		LH_2	A	540	11582	27130	0.16	0.337	4.0
3.	Agena	RFNA	C	11.3	414	25390			
		UDMH	C	8.8	643	14410			
4.	TII/SI	NTO	C	170.3	530	8380			
		A-50	C	137.5	1031	9210			
5.	TII/SII	NTO	M	63.7	522	8405	0.21	0.367	7.0
		A-50	M	57.0	909	23685	0.19	0.644	7.7
6.	VikasM	NTO	C	120.0	500	10000	0.19	0.619	4.6
		UDMH	C	129.5	832	10000	0.21	0.438	4.9
		H_2O	C	3.8	720	10000			
7.	CUS	LOX	C	12.3	1205	42710	0.07	0.435	6.6
		LH_2	A,2	32.8	15980	42710	0.16	0.172^*	14.8^*
8.	SSME	LOX	C	452.3	2938	31000	0.34	0.493	3.5
		LH_2	C,3	1025.3	59100	37400	0.42	0.433^*	8.7^*

Table 10.12: Features of Turbo-pumps – continued ($\dot{Q}$ = Volumetric flow rate)

	Engine	Props.	Head m	rpm	$NPSH_{min}$ m	n_{ssp}
1.	F 1	LOX	944.0	5488	20.0	13.9
		RP1	1575.0	5488	21.3	10.3
2.	J 2	LOX	666.0	8753	5.5	19.5
		LH_2	11582.0	27130	22.9	35.9
3.	Agena	RFNA	414.5	25390	13.6	
		UDMH	643.1	14410	10.4	
4.	TII/SI	NTO	530.3	8380	13.4	
		A-50	1030.5	9210	13.1	
5.	TII/SII	NTO	522.1	8405	9.1	7.6
		A-50	908.6	23685	30.5	8.2
6.	VikasM	NTO	500.0	10000	18.6	7.3
		UDMH	831.6	10000	22.8	6.5
		H_2O	720.0	10000	10.0	
7.	CUS	LOX	1205.0	42710	21.0	9.1
		LH_2	15980.0	42710	10.0	43.4
8.	SSME	LOX	2938.0	31000	3.0	86.3
		LH_2	59100.0	37400	3.0	534.7

10.2.8 Cavitation and Inducers

The propellants flow from the tanks that are set at some pressure (typically, 3 to 5 atm.) through valves and plumbing into inlet of pumps. The pumps rotate at high speed and therefore, accelerate the fluids to high velocities first; the fluid then is decelerated in diffuser section to recover the pressure head. *The acceleration of the fluids can reduce the static pressure in some sections to levels below the vapor pressure of the fluid*. This causes the fluid to release bubbles. The bubbles move into high pressure area and suddenly implode into liquid form. This action that occurs close to the impellers in very short durations of time, creates very sharp pressure pulses leading to shock waves. This process called *cavitation* with sudden local pressure fluctuations at micro levels, could damage the hardware by local pitting and cracking. This is considered serious from the stand point of hardware damage with applications that involve hundreds of thousands of hours of steady operation as required of these pumps. In the case of rocket engine applications, the fluctuating pressure field is transmitted to the outlet and is therefore, operationally unacceptable. In order to define quantities concerning this problem, a quantity called net positive suction head ($NPSH$) is defined. It is $NPSH = [(p_{stag} - p_v)_{pump\ inlet}]/\rho_l g$ where two terms on the right hand side are the

stagnation pressure of the fluid at the inlet and the vapor pressure. One can now form a non-dimensional parameter, suction specific speed (n_{ssp}) as

$$n_{ssp} = \frac{\omega\sqrt{\dot{Q}}}{(gNPSH)^{(3/4)}} \tag{10.13}$$

The cavitational characteristics of a pump are sensitively dependent on the geometry of the pump and to ensure cavitation free operation, pumps are test run at different suction pressures at the rated rpm (above and below this value as well) to obtain the possible behavior of the pump. The suction head at which the delivery pressure drops by 2 % below the rated value at the rated speed is considered for calculating the net positive suction head. It is this value that is set out in Table 10.12. From this value, one can calculate n_{ssp}. It can be noted that the value of suction specific speed, n_{ssp} is at least one order higher than the steady operating specific speed (shown in Table 10.11), as it should be.

For any given pump, it is possible to operate it without any cavitational problem by increasing the tank pressure suitably so that the $NPSH$ is adequately provided for. Any increase in tank pressure will imply increase in tank weight due to increased wall thickness. If one were to reduce the tank pressure from this consideration, one would lower the inlet stagnation pressure close to vapor pressure with inevitable problems of cavitation. Ways to avoid cavitation in pumps under these circumstances would be (a) to introduce an ejector before the suction with a small part of the high pressure fluid from the outlet being used to raise the pressure of the fluid in the suction area, or (b) use an inducer section with the pump or (c) two separate pumps in series, with the first set with a low pressure ratio. In option (a), the momentum derived from a small part of the high pressure fluid in the delivery is used to increase the static pressure of the fluid from the tanks. Option (b) is somewhat more universally adopted, one in which the use of an "axial" pump section attached to the impeller ensures increase in static pressure to a level acceptable to the main pump section. Option (c) can be thought of as a more complex variant of option (b).

Figures 10.30 and 10.31 show the pump cross section indicating the presence of the inducer section in the entry zone for both centrifugal and axial pumps. These sketches also show other details of the pumps that are classical in pump design.

Figure 10.32 shows the sectional views of an inducer. It is important to notice that the swirl angle provided is such that at the speed at which the pump is running, the fluid sees a small angle of attack at the entry. This is the key to ensuring that velocity and static pressure changes in the fluid occur gradually till the build up of pressure (that occurs due to the transfer of momentum from the vanes of the inducer) allows the fluid to accelerate in the main pump section without cavitation. In some cases, the inducer section can be so substantial (like in SSME engine where the pressure increase demanded of the main pump is very

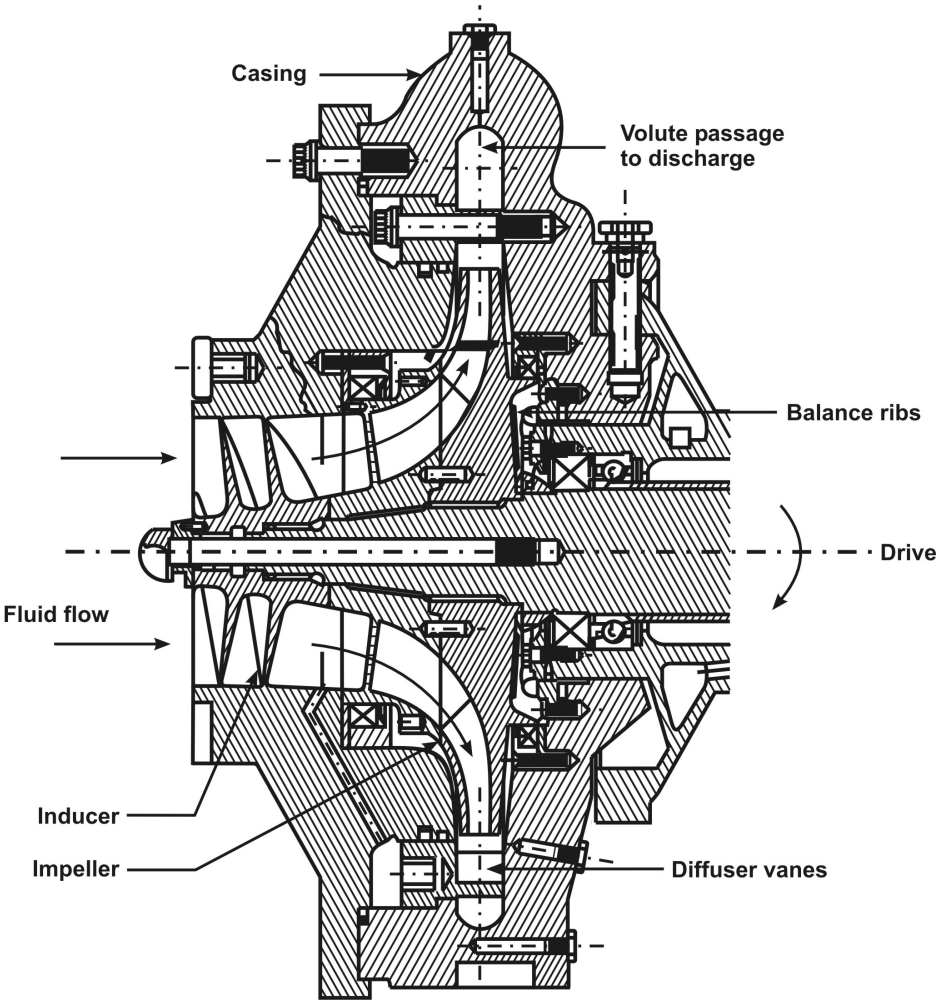

Figure 10.30: A typical centrifugal pump with its details

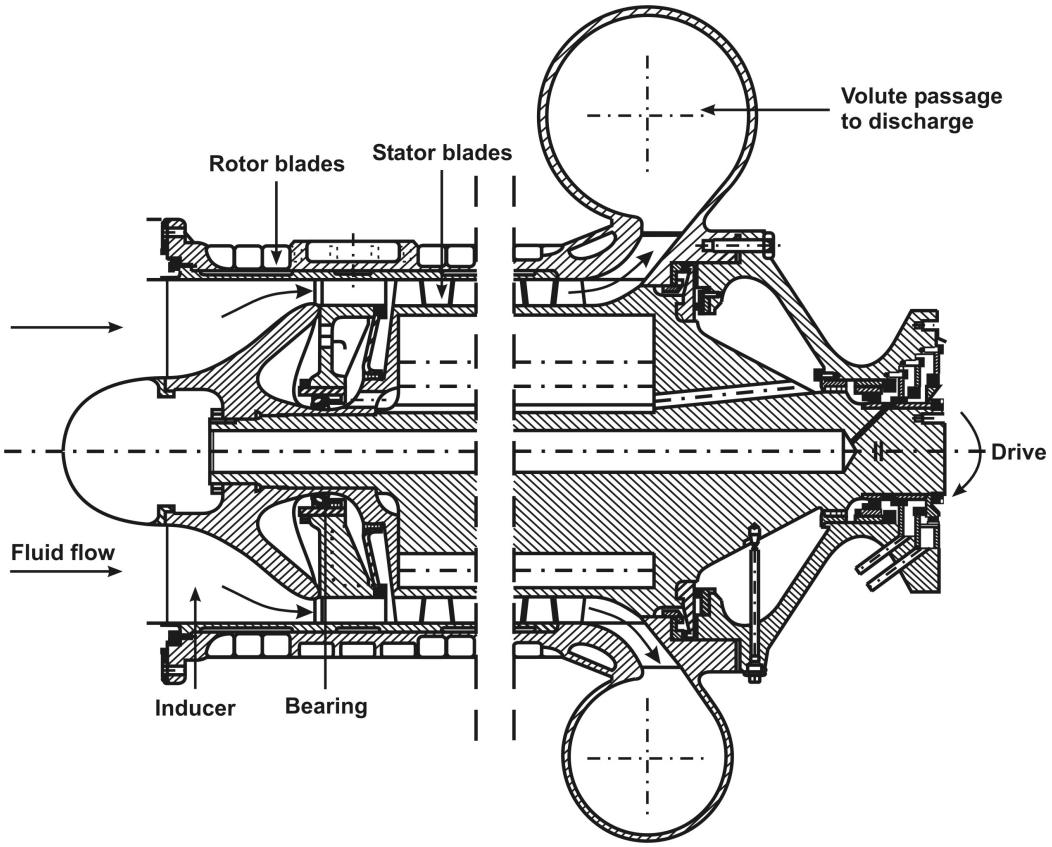

Figure 10.31: A typical axial flow pump assembly with details

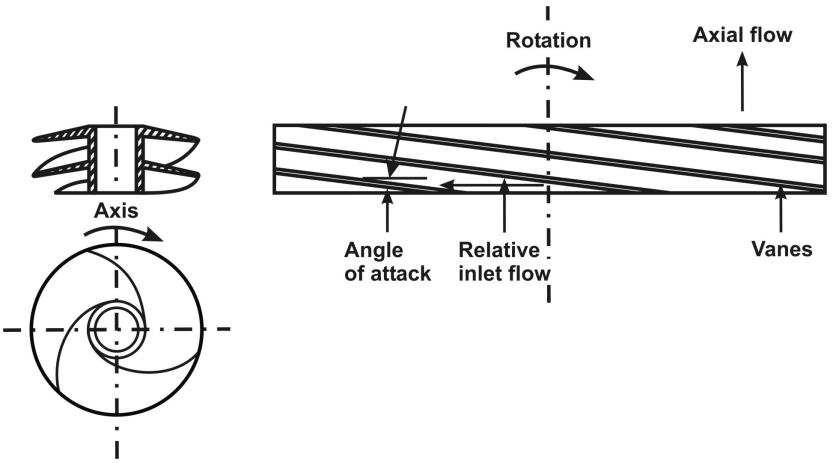

Figure 10.32: Schematic of a typical inducer

large) that it is worthwhile having a separate lower pressure turbo pump for the purpose.

Figure 10.33 shows the full turbopump assembly of the uprated-Vikas engine (VikasU in the Tables 10.3 onwards). This uprating was carried out at Liquid Propulsion System Center, Trivandrum (of ISRO family).

In multiple-stage designs, the essential fluid dynamic feature is to take the fluid from the exit of one pump to another as shown in Figure 10.34. An important aspect in handling cavitational issues in cryogenic fluids is an advantage they provide in operation compared to storable propellants. The cryogenic propellants operate at temperatures that are not far below the boiling points. When cavitation begins due to fluid dynamic effects that reduce the static pressure below the vapor pressure, the local temperature also drops since the heat for vaporization is drawn from the liquid. This reduces the permissible vapor pressure for operations. Stated differently, the $NPSH$ chosen for operations for liquid hydrogen and liquid oxygen can be a third and half of the values chosen for storable liquids. This feature is consistent with the values indicated in Table 10.12 even though many factors including the design of the impeller are relevant to the choice of $NPSH$.

10.3 Thrust Chamber Sizing

Thrust chambers are sized to ensure complete combustion. The physics of the combustion process constitutes vaporization limited phenomenon aided by convective heat transfer (discussed in section 8.3.2). This controls the volume and the length of the combustion chamber and is characterized by $L* = \mathscr{V}_c/A_t$.

Figure 10.35 shows the variation of the combustor shapes possible. They are controlled by the ratio A_c/A_t where A_c is the combustion chamber cross sectional area and A_t, the throat area. Reducing the ratio reduces the total surface area to be cooled but increases the stagnation pressure losses because of high velocities in a region with heat addition. Increasing the ratio reduces the mean velocities in the chamber and also the stagnation pressure losses up to the entrance to the nozzle. One cannot, however, change the geometry this way arbitrarily since the droplet trajectories will need a minimum residence period and hence, a corresponding length. Thus, the practical range is between A_c/A_t = 1 – 3 for main combustion chambers. From the point of view of combustion chamber cooling, it is advantageous to use lower values of A_c/A_t since the surface-to-volume ratio varies as d_c^{-1} (d_c is the combustion chamber diameter) even though the stagnation pressure loss penalty is to be paid. The value of the chamber-to-throat area ratio for the cryo engines RL 10, SSME and HM 60 are 2.95, 2.96 and 2.99 respectively. The value of L^* used in all these motors varies between 0.8 - 1.0 m. For the above three engines, it is 0.98, 0.8 and 0.85 m respectively. Even for the same propellants,

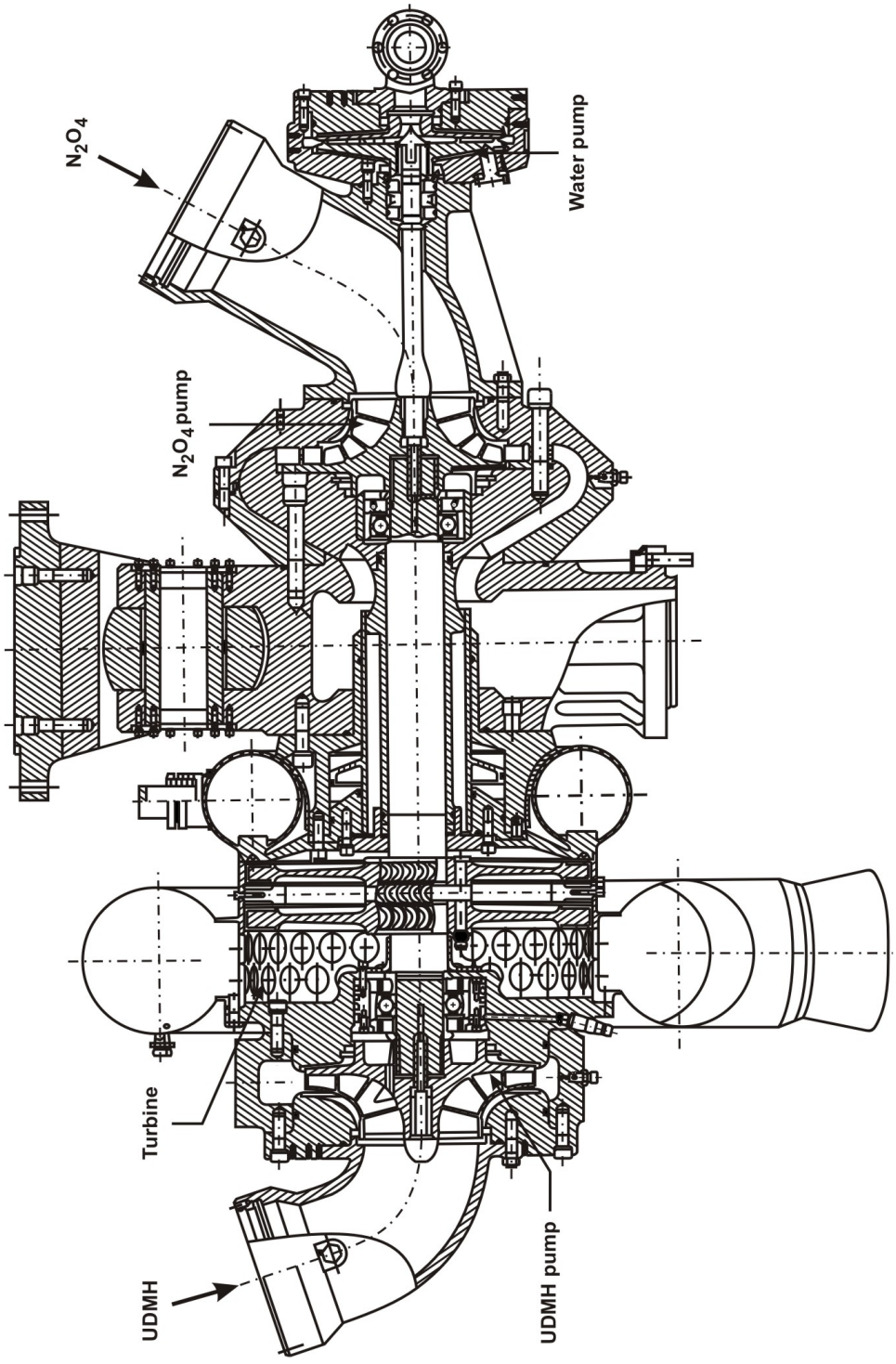

Figure 10.33: Turbopump assembly of the uprated Vikas engine

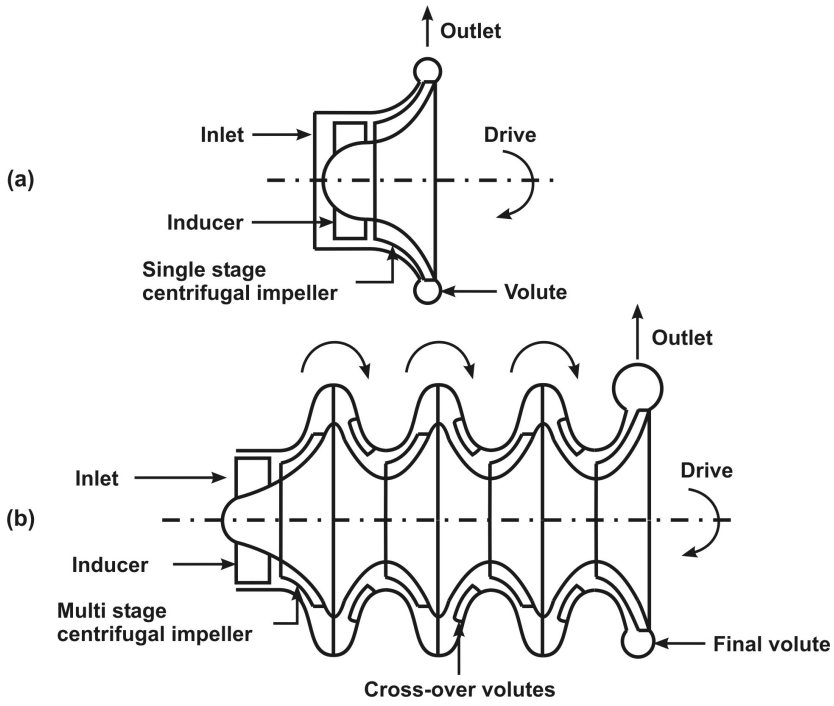

Figure 10.34: Schematic of a single stage and multi-stage centrifugal pump showing the fluid path

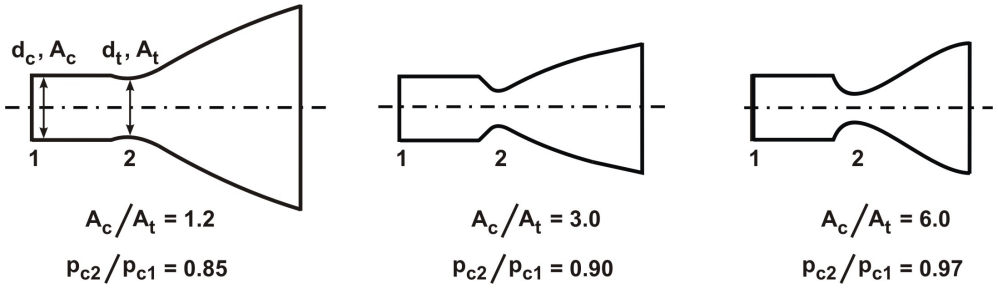

Figure 10.35: Comparison of combustion chambers with different combustor-to-throat area ratios

Table 10.13: Chamber dimensions for some vehicles, L_c = combustion chamber length from injector face up to throat

	Engine	F kN	d_c mm	L_c mm	d_t mm	A_c/A_t	Film cooling % fuel flow
1.	F 1	6860	996				
2.	J 2	1034	470				
3.	Agena	70	274				
4.	TII/SI	952	554	1070	387	2.04	14.5
5.	TII/SII	446	368	970	232	2.51	16.0
6.	VikasU	823	500	600	306	2.67	12.7
7.	CUS	71	200	300	90	5.00	
8.	SSME	2323	452		261	2.96	
9.	LEMDE	47	288	670	182	2.51	8.7
10.	SSOME	27	206	760	147	2.00	0.0
11.	RD253	1720	430		279	1.54	

the value chosen depends on the coarseness of the injector drop size distribution, more coarse it is, larger will be L^* in the above range. The combustion efficiency in terms of ${c^*}_{exp}/{c^*}_{th}$ obtained from experiments is presented in Table 10.6. It can be noticed that the combustion efficiency is very high for cryogenic engines (J2, SSME and CUS) but degrades with the choice of higher thrust per element to 93 – 95 %. Typical chamber dimensions for select vehicles are shown in Table 10.13.

10.4 Thrust Chamber Cooling

Thrust chamber needs to be cooled because the temperature of the gases is high and the flow velocities are large, both of which contribute to high heat fluxes. Combustion chamber protection is somewhat additional to what one would do for thermal protection in solid rockets. The fact that liquids are available for cooling the walls of the chamber will be used to transfer the heat to the liquid that gets fed back to the combustion chamber unlike in a solid rocket. Several techniques that are used for cooling are (a) film cooling, (b) heat sink and radiative cooling, (c) ablative cooling, and (d) regenerative cooling. One usually combines film cooling with other techniques as it provides the much needed support for thermal protection in all the cases. Efficient use of other techniques helps reduce the amount of film coolant required and hence, optimize on the realized specific impulse.

One of the general issues for dealing with thermal protection is the heat flux estimate. Liquid rocket engines function over a wide range of thrust levels, burn times and in modes like multiple burns, unlike solid rockets. Very small thrusters

experience low Reynolds numbers and therefore, can be expected to experience laminar flow. Experiments have suggested [43] that below a $Re_t < 2 \times 10^5$ (where Re_t is the Reynolds number at the throat) laminar flow correlation terms of Nusselt number given by

$$Nu = 0.15 {Re_t}^{0.5} \tag{10.14}$$

is used for making heat transfer estimates. For $Re_t > 1.5 \times 10^5$, the correlation given by equation (9.31) in section 9.6 restated below

$$Nu = 0.023 Re^{0.8} \tag{10.15}$$

can be used for calculating the heat transfer coefficients for turbulent flows.

10.4.1 Film Cooling

Film cooling has been addressed already while discussing injection head and injectors. The outer most set of injection holes is arranged in a manner that the jets impinge on the wall, usually in a tangential direction. The injection is like showerhead and is intended to move along the wall as a jet. Typical injection holes of diameter 0.2 to 0.5 mm with spacing of 5 to 10 mm have been used. The jet hits the wall and thins out, merges with the liquid from the neighboring jets in a manner that a thin uniform sheet moves along the wall. The gases in the neighborhood of liquid transfer heat to it causing vaporization. The vapors move along in stream tubes close to the wall. It is important to note that even though turbulence levels in the injector zone are large – typically 15 to 25 %, the degree of mixing noted between the different streams that can be traced back to the groups of injectors is small. Measurements of temperature profiles at the nozzle end show that significant peaks and valleys can be related to the adiabatic temperatures expected from groups of injector segments with different O/F values. They seem to retain the broad O/F distribution found near the injectors. This is traced to the issue that different stream tubes with different O/F values have different temperatures and move at different velocities. This stratification reduces the mixing rate. It is because of this feature that cool wall layers remain relatively cool compared to the core and help bring down the wall heat transfer. In cryo-engines, gaseous hydrogen is injected and provides the necessary blanket of a cooler gas sheathing downstream. Table 10.14 shows the film coolant used along with major coolant used for regenerative cooling. The fraction of the fuel flow going into film cooling is seen in Table 10.13 for some engines. Figures 10.17 and 10.18 show the location of film cooling holes on Vikas engine.

Table 10.14: Regeneratively cooled chambers with film coolants; all film coolant is introduced through injector orifices aligned at small angles to the wall

Engine	Propellants	Regenerative coolant	Film Coolant
F 1	LOX – RP 1	RP 1	RP 1
J 2	LOX – LH_2	Gas H_2	Gas H_2
Agena	IRFNA – UDMH	IRFNA	UDMH
TII	NTO – A-50	A-50	A-50
CUS	LOX – LH_2	Gas H_2	Gas H_2

10.4.2 Heat Sink and Radiation Cooling

Heat sink technique implies that all the heat transferred by the hot gases is stored in the thrust chamber hardware. Since the heat flux values are large, this technique of storing the heat can work for a few seconds of burn time only. Usually, the high temperature materials used will be capable of storing the heat by attaining a high temperature. Wall temperatures go up to 1500 to 1700 K. They will transfer the heat to space by radiation from the outer surface. Figure 10.8 shows the schematic of the cooling scheme on the thrust chamber described as a part of the stage. In the case of space thrusters used in apogee-perigee module, PAM or Apogee Kick module, AKM (see 2.8) that adopt this cooling technique normally, the choice of the material for the thrust chamber and the extent of film cooling are used for the thermal management of the thruster. Use of this technique has limitations in terms of thrust and chamber pressures because as these parameters increase, they result in higher Reynolds numbers and therefore, higher heat flux. Higher heat flux implies higher wall temperatures and material related problems. The practical rule is that these are used for engines with thrust levels less than 100 kN and pressure levels less than 10 atm. Since the thruster is attached to a satellite, the satellite body also receives heat from the thruster and one needs to provide necessary thermal shields to provide enough thermal isolation to the satellite body. They can also be used in the downstream portion of the nozzle where the gas phase heat flux values are small.

Radiation cooled chambers are designed with storable hypergolic propellants, typically NTO – Hydrazine, Aerozine or MMH combination. The chamber materials used are Molybdenum, Columbium with Silicide coating to provide oxidative resistance or (90 % Tantalum + 10 % Tungsten) with aluminide coating with additional coating of pyrochrome for emissivity control. By increasing the outer wall emissivity to as high as 0.7 – 0.85, it is possible to reduce the wall temperatures significantly. The coatings are obtained by dipping the hardware into a solution to enable the coating material to be acquired on the surface and then the hardware

Table 10.15: Thermal data of some materials for heat sink and radiation cooling, * = Values at 20°C

Material	ρ_m kg/m^3	k_m W/m K	c_p kJ/kg K	α_m mm^2/s
Copper	8950	386	0.38	112.3
Graphite	2200	120	0.71	76.8
Graphite FRP	1400	30	0.32	67.0
5% Cr steel	7890	40	0.41	12.3
Columbium	8860	40	0.26	26.6
Molybdenum	10214	120	0.25	47.0
Tungsten	19350	160	0.13	63.6

is fired in a high temperature furnace so that the material gets bonded to the surface. Typical coating thicknesses obtained by this technique are 100 to 300 μm. It is also possible to provide the coating by plasma spray coating techniques. The mechanical integrity with this technique appears to be inferior to the one obtained by dipping technique.The physical and thermal properties of some of these materials are presented in Table 10.15. It is possible to analyze the radiation method of cooling by a simple approach. The steady thermal balance of the body of the thruster is given by,

$$\dot{q}'' = h_g(T_g - T_{g,w}) = h_m(T_{g,w} - T_w) = \sigma_r \epsilon (T_w^4 - T_\infty^4) \tag{10.16}$$

where h_g and h_m are the gas phase and wall material heat transfer coefficient, T_g, $T_{g,w}$, T_w and T_∞ are the temperatures of the hot gas, wall on the gas side, outer wall and ambient condition. σ_r and ϵ are the radiation constant (= 5.67×10^{-8} W/m^2 K^4) and emissivity of the outer surface. The equation states that the heat flux from the gas phase to the wall is passed through the wall by conduction to the outer surface from where it is transferred by radiation to the ambient (or deep space as is more usual with these thrusters). In the above equation, h_g is estimated by equations (10.15) and (10.14) depending on the assessment of the nature of flow, $h_m = k_m/t_m$ is the ratio of thermal conductivity of the wall material to the wall thickness. All quantities excepting $T_{g,w}$ and T_w are known and these two are obtained by solving the two equations. The first set leads to

$$T_{g,w} = \frac{(h_g T_g + h_m T_w)}{(h_g + h_m)} \tag{10.17}$$

Introducing this into the second of the heat balance equations, we get

$$T_w = T_g - \left[\frac{1}{h_g} + \frac{1}{h_m}\right] \sigma_r \epsilon (T_w^4 - T_\infty^4) \tag{10.18}$$

This transcendental equation can be solved for T_w.

For T_g = 2500 K, h_g = 500 W/m^2K, t_m = 5 mm, the heat transfer coefficient is obtained as h_m = 0.200 (kW/m K) / 0.005 (m) = 40 kW/m^2 K, and with T_∞ = 0 K (deep space), ϵ = 0.8, one gets,

$$T_w = 2500 - 90.7[T_w/1000]^4 \tag{10.19}$$

A simple iterative solution gives the value of T_w = 1715 K. This value may be unacceptably high for operational reasons. If this value is to be brought down, one needs to reduce the gas phase heat flux through a larger film coolant flow or the choice of this cooling system restricted to larger expansion ratio regions of the nozzle where the heat flux values can be expected to be lower. Suppose h_g is brought down to 250 W/m^2K keeping other quantities same, we get the balance equation as $T_w = 2500 - 181.4[T_w/1000]^4$ whose solution gives T_w = 1523 K. This may be an acceptable temperature for columbium like material. Alternately, if the film coolant was set such that the value of T_g is limited to 2000 K, one would be able to accept the higher gas phase heat transfer coefficient as in the earlier case. From this example, it is clear how critical the design issues can be. Once the temperatures are kept within limits, the thrust chamber has no operational time limits. Radiation cooled chambers (with appropriate film cooling) have functioned for longer than one hour either continuously or on multiple-burn mode.

10.4.3 Ablative Cooling

Most of the discussion presented in section 9.6.1 is relevant to liquid rockets as well. Ablative technique can handle a more hostile environment since the heat flux is significantly offset by the ablation of the material. The environment is made more benign by ensuring barrier film cooling by the fuel. Even so, the burn time is limited to the thickness provided and the mean ablation rate. Its use is normally restricted to small thrust engines and for relatively small burn durations. An important exception is the Vikas engine (uprated version of the Viking engine of French design) that uses a large ablative throat with film cooling support. This engine has been able to function at p_c = 70 atm. for a burn duration of 180 s.

10.4.4 Regenerative Cooling

The principal method of cooling used for large thrust engines and also those that burn for a long time particularly on a single continuous burn mode is the regenerative method of cooling. In this method one of the liquid propellants is passed through the thrust chamber walls so that the heat flux from the gases can be absorbed by the liquid keeping the walls relatively cool. The critical issues for design are: (a) the maximum flow rates are fixed, and (b) the liquid coolant properties

are to be accepted as native to the propellant and yet one should design the system for as high a chamber pressure as possible. The design of the regeneratively cooling system is closely interlinked to the injector and the volume/surface area of the thrust chamber. By designing the outer most injector holes appropriately, it is possible to provide a fuel rich environment as brought out in the section 10.2.1 on injectors. The volume-to-surface area plays an important role in optimized designs as discussed in section 10.3.

The wall cooling design is principally controlled by the heat flux distribution over the chamber surface. The heat flux distribution is calculated along the lines described in section 9.6. The heat transfer coefficient is the common feature between the various cooling techniques. The heat flux itself differs from heat sink, ablative and regenerative cooling techniques because the wall temperatures are significantly different. For an identical gas phase thermal environment, the peak wall temperature may approach 1700 K, 1300 K and 1100 K in the three techniques respectively. In the case of regenerative cooling, the wall thickness is kept small (so that the wall heat transfer coefficient is high and so the thermal resistance of the wall is small) and this allows the wall temperature to be low as the heat is carried away by the liquid. It is interesting to compare the peak heat transfer coefficients and the heat flux values for different systems. These are presented in Table 10.16 along with the values used to get these quantities.

The table is very instructive. The parameters listed in the table are obtained from actual data where available or estimated from separate calculation. All the parameters used in the calculations are indicated. Radiative flux is calculated from equations (9.38 and 9.39). The partial pressures are obtained from the chamber pressure and the mole fractions of H_2O and CO_2 from the equilibrium composition. One can notice that the peak heat transfer coefficient varies significantly over the engines. The most significant parameter contributing to this is the chamber pressure. SSME engine stands out specially in comparison to others because of its ability to generate the thrust from a small frame (notice that the SSME engine has a throat diameter less than half of F1 engine and therefore, quarter in area, yet producing a third of the thrust). The heat absorbed by the regenerative cooling system is also stupendous. For F1 and SSME engines, it works out to 327 and 286 MWth. The peak heat flux of SSME engine is vastly higher than in any of the other engines. The thermal management of the thrust chamber is a substantial achievement of the technology.

Different fabricational techniques are used for the chamber to allow for regenerative cooling. These are (a) a cylindrical sheet of suitable thickness shaped as a nozzle, is rolled first and long and fine holes are drilled along the wall, (b) tubular construction in which shaped tubes are arranged around in the form of circular chamber and welded or brazed, and two thin-walled cylindrical annular chambers are constructed and joined by corrugations through brazing, and (d) helical wire

Table 10.16: Comparison of peak heat transfer coefficients and flux values for different rocket engines ΔT_{clnt} = Increase in temperature of the coolant

The engine	NTO – MMH thruster	F-1 engine	SSME engine	PS 1 solid rocket motor
Thrust, kN	0.4	6860	2160	4500
p_c, atm	10	76.3	222	60
D_t, m	0.016	0.59	0.24	0.8
$\dot{m}$, kg/s	0.133	2624.1	474.7	1400
μ, kg/m s, $\times 10^{-5}$	5.0	5.0	5.0	6.0
Re_t, $\times 10^5$	2.1	1130.0	500.0	370.0
Nu	416	63710	33200	26100
k, W/mK	0.1	0.12	0.16	0.18
h_g, kW/m^2K	2.6	13.0	22.1	5.9
T_g, K	2500	2800	2600	3500
$T_{w,g}$, K	1000	1000	1000	1600
ΔT_g, K	1500	1800	1600	1900
$\dot{q}''_{conv}$, MW/m^2	3.9	23.4	35.6	11.2
p_{CO_2}, atm	0.7	10.3	-	0.50
p_{CO_2}, atm	3.5	24.5	146.0	5.0
$L_{e,rad}$, m	0.035	0.7	0.2	2.5
$\dot{q}''_{CO_2}$, MW/m^2	0.13	1.13	-	1.1
$\dot{q}''_{H_2O}$, MW/m^2	0.03	1.11	5.2	1.1
$\dot{q}''_{total}$, MW/m^2	4.06	25.66	40.8	13.4
h_g, MW/m^2	2.7	14.2	25.5	7.1
ΔT_{clnt}, K	75	140	254	-

wrap between the outer and the inner shells. The construction techniques for the four methods are shown in Figure 10.36. Electrochemical milling process is also used for the construction of copper based combustion chambers.

The manifold for the entry of the coolant is usually located towards the nozzle exit and the heated liquid is taken out of the passages at the head end to deliver it to the injector head. The cooling liquid entry manifold is not always at the nozzle exit plane. A part of the liquid, perhaps at a lower flow rate is drawn off towards the nozzle exit plane and returned to a point downstream in the fluid flow path. The point at which such a bifurcation is performed depends on the heat transfer calculations made section-wise along the path of the fluid. While it is normal to expect that the liquid flows once from the nozzle end to the head end, in specific cases, the liquid may be passed twice (called 2-pass) to ensure better heat extraction. Table 10.17 provides the data on the regenerative cooling design used on several engines. As can be noted, all the techniques described above have been used in various engines. Typical wall thickness varies between 0.46 to 1.2 mm. In large area ratio engines that are started up at sea level or low altitudes but have to operate in near vacuum conditions over a large part of the burn time, it turns out that the starting transients create a very low pressure in the nozzle and the difference between the ambient pressure that is higher and the inside may cause buckling of the chamber. To prevent this from happening, the outer shell is reinforced so that its buckling strength is adequate to meet with the starting transients. The method by which reinforcement is provided is also shown in the last column of Table 10.17. The materials used and the wall thickness chosen can be noted from the Table 10.17.

10.4.5 The Heat Transfer Process

The physics that makes the design of the regenerative cooling possible is related to liquid phase convective heat transfer that involves nucleate and film boiling processes. Figure 10.37 illustrates the principles involved in the heat transfer process. At small levels of heat flux, the liquid flowing inside the passage will absorb the heat by convective process – creation of a thin liquid boundary layer through which the heat is transferred and absorbed by the liquid. If the heat flux keeps increasing, the absorption of the heat occurs linearly as $\dot{q}'' = h_l(T_{w,l} - T_l)$, where h_l is the liquid side convective heat transfer coefficient, $T_{w,l}$ is the wall temperature on the liquid side and T_l is the liquid temperature. For the same flow conditions, as flux is increased, the liquid side wall temperature will increase. Correlations have been developed to enable calculations of the heat transferred to the liquid flowing in the passages.

$$h_l = 0.023 \frac{k_l}{d_l} Re_l^{0.8} Pr_l^{1/3} \tag{10.20}$$

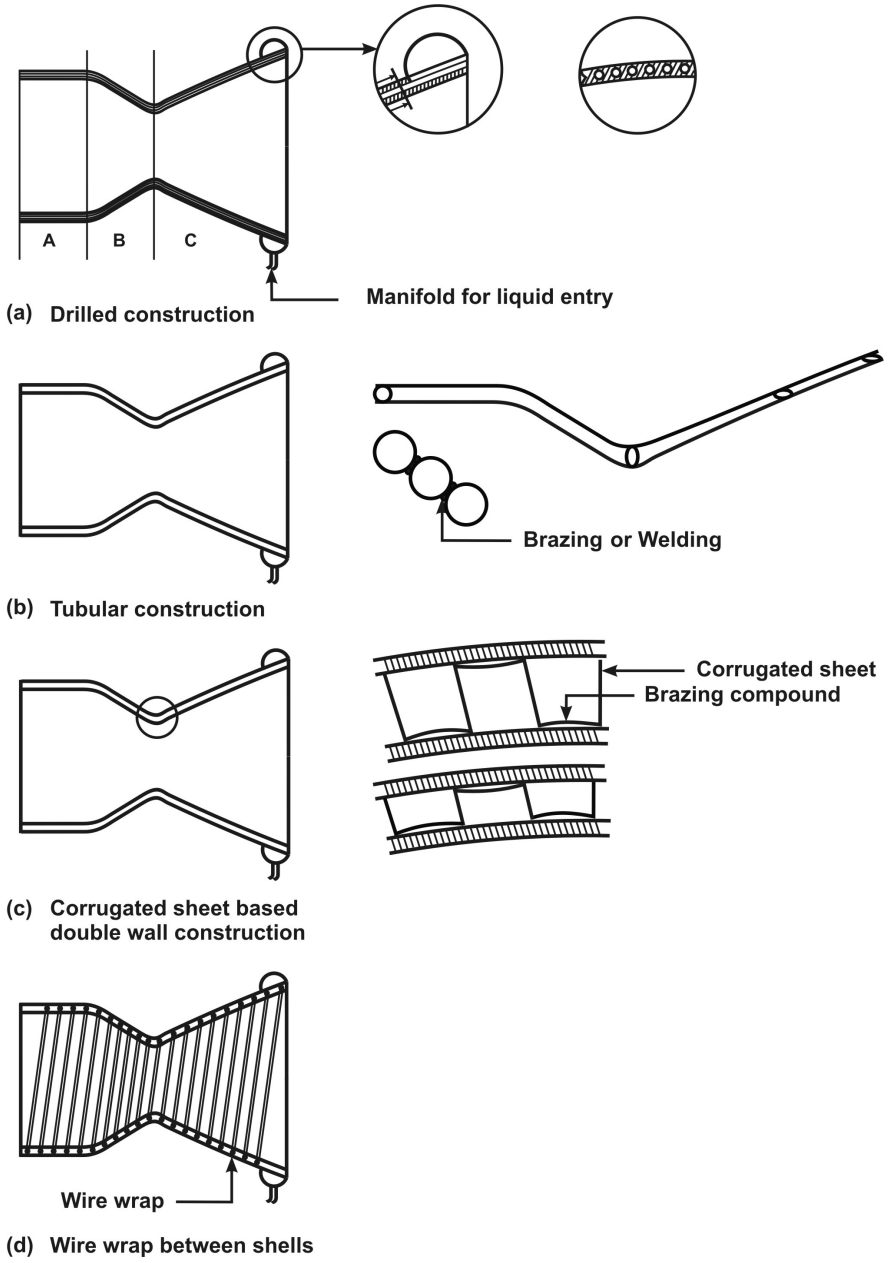

Figure 10.36: Methods of construction of thrust chambers - (a) drilled construction, (b) tubular construction, (c) corrugated sheet between shells and (d) wire-wrap between shells

Table 10.17: Characteristics of major liquid rocket engines; (C) = Coolant, 2 p = two pass, 1 1/2 p = one-and-a-half pass; 1 bifn = one bifurcation, g-fuel = equal volume mixture of xylidine and triethylamine

Engine	Props.	O/F	Cooling design	Material th, mm	Reinforcement
Agena	RFNA (C) UDMH	2.57	Drilled holes 1 1/2-pass	6061 T6 Al, 1.2	Integral wall
F 1	LOX RP1 (C)	2.37	Brazed tubes 2-p, 1 bifn	Inconel X. 0.46	Brazed shell
J 2	LOX LH_2 (C)	5.50	Brazed tubes 1 1/2-p	CRES 347, 0.48	Brazed shell
TII/SI	NTO A-50 (C)	2.01	Brazed tubes 2-p, 1bifn	CRES 347, 0.85	Wirewrap
TII/SII	NTO A-50 (C)	1.80	Brazed tubes 2-p, 1bifn	CRES 347, 0.76	Wirewrap None
SA2/SII	RFNA (C) g-fuel	3.3	Corrugated twin-shell	CRES, 1.2	
AKM	NTO MMH (C)	1.6	Wire-wrap	SS321 1.2	
CUS	LOX LH_2 (C)	6.09			
SSME	LOX LH_2 (C)	6.01			

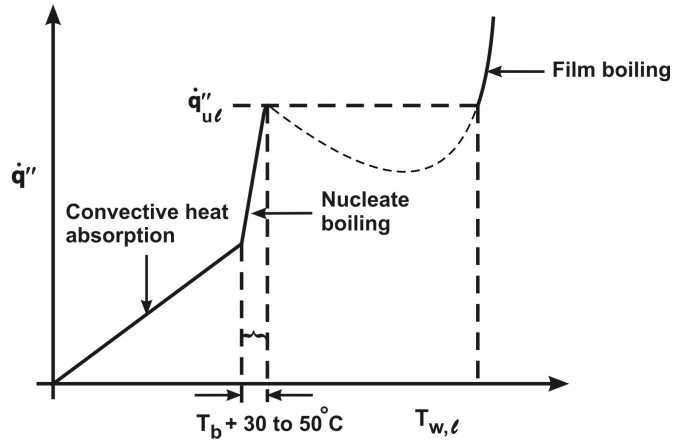

Figure 10.37: Plot of heat flux absorbed by a liquid with liquid side wall temperature

where h_l is the liquid side heat transfer coefficient, k_l and d_l are the liquid conductivity and tube diameter or an equivalent hydraulic diameter of the passage with bounding walls, $Re_l = \rho_l U_l d_l/\mu_l$ and $Pr_l = \mu_l c_{p,l}/k_l$ are the Reynolds number and the Prandtl number of the fluid, all estimated at ($T_{w,l} + T_l$ /2). U_l is the speed of the fluid in the passage.

As the flux approaches a condition that makes the wall temperature approach the boiling point, small vapor bubbles are formed on the surface, leave the surface and enter the fluid and condense, transferring the heat. This heat transfer process is called nucleate boiling. The wall temperature may exceed the saturation temperature by 30 to 50°C. In this process, the heat absorbed by the flowing liquid increases dramatically as the number of bubbles being formed and leaving the surface increases. Beyond a point, the heat flux is large enough to sustain a vapor film over the metal surface. The entire heat flux needs to be transferred through the thin vapor film and this causes the liquid side wall temperature to rise sharply – so sharply that the jump can be of the order of 400 to 600 °C.

Figure 10.38 describes the process pictorially and the heat flux relationship with the wall temperature is shown in Figure 10.37.

The key point of the design is to extend the heat extraction process such that at the highest heat flux region, one can make use of the nucleate boiling feature and raise the heat flux that can be absorbed by the liquid. This critical heat flux data is known reasonably well for RP1, Aerozine (A-50), and RFNA and not very well defined for LH_2. Fortunately, the specific heat of absorption does not vary much for hydrogen transitioning from liquid to gas and the absence of this data is not very critical. Typical limiting values of liquid side wall temperature are 730 K for RP1, 590 K for A-50, and 630 K for RFNA. Hence, the liquid flow rates need

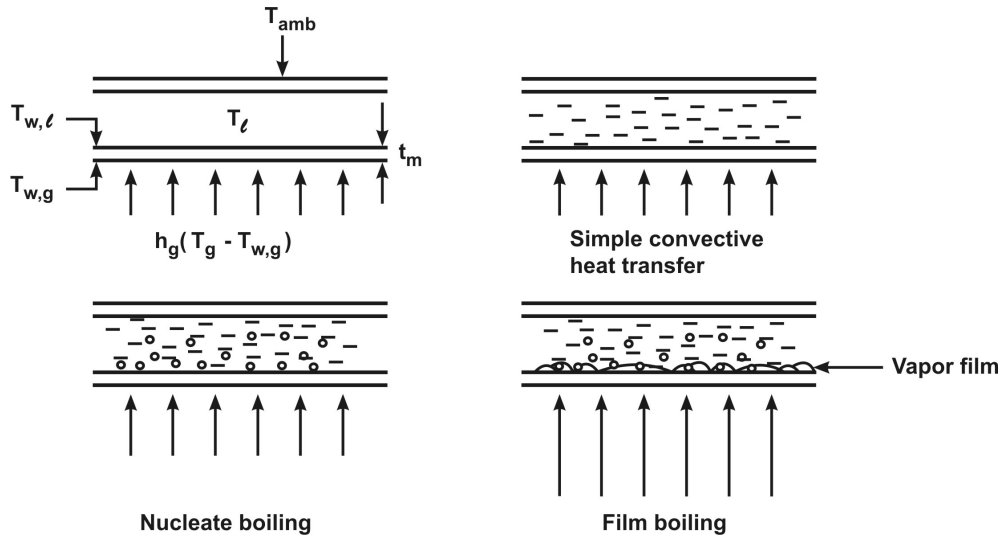

Figure 10.38: Pictorial presentation of differnt boiling regimes

to be set at such levels that the convective heat extraction process keeps the wall temperature around the limiting values.

The choice of the chamber pressure imposes certain physical characteristics on the regenerative cooling design. The engine chamber pressure (and therefore, the pressure of the liquid) is higher than the critical pressure in several cases – for example, kerosene with a critical pressure of 21 atm. is used in F 1 engine cooling at pressures in excess of 75 atms. In this case, if the liquid picks up heat to cross the full boiling range, the liquid may enter supercritical operational regime. Also, in the case of kerosene, the decomposition process will generate soot that deposits on the wall unless it is very smooth. Experience has suggested that the deposit flakes away at high velocities in the cooling channel. In the case of liquid hydrogen, the vaporization process occurs in the channel, many times even before the throat area is reached. If this happens, the heat transfer process occurs with gaseous hydrogen. One can describe the regimes of operation on a pressure – temperature diagram as in Figure 10.39.

In regime A, the coolant enters the coolant jacket as a sub-cooled liquid (temperature below the boiling point at the local pressure). The wall temperature rises, but the liquid temperature is below the critical value. This is typical of what happens in Titan II engines as well as SA 2 engine (Russian design). In regime B, the coolant enters as a liquid above the critical pressure. This is the condition in F 1 engine. In regime C, the coolant enters under super critical conditions and is quickly converted to gas. Regime C is typical of J 2, SSME and CUS engines (see Table 10.14). These aspects are set out in Table 10.18 along with some additional

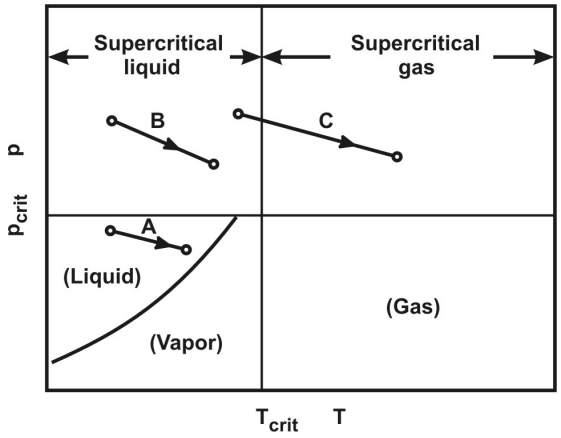

Figure 10.39: Different cooling strategies on a pressure - temperature diagram

Table 10.18: Heat transfer behavior of liquid coolants, (T_{cr} and p_{cr} are the critical temperature and pressure; H.t.r = Heat transfer regime; Liq. Vel = Liquid velocity)

Propellant	T_{cr} °C	p_{cr} atm.	H.t.r Fig. 10.39	Liq. vel m/s	$h_l/h_{l,ref}$
Fuels					
TEA	262	30	A	20 – 30	
Hydrazine	380	145	A	30 – 40	4
MMH	275	78	A	20 – 30	4
UDMH	249	60	A, B	10 – 30	3
RP 1	414	21	B	10 – 20	1
LH_2	– 240	13	C	90 – 200	10
Oxidizers					
IRFNA	225	55	A		4
NTO	158	100	A	15 – 20	3

features. The liquid velocities are typically 20 to 40 m/s except for hydrogen for which it is large. This is because the coolant is already in gaseous state. The heat transfer coefficient that the system can accept has been set out indirectly with reference to kerosene (RP 1). One can notice that the cooling capability of several other fluids is much better than of kerosene.

10.4.6 Analysis of the Heat Transfer Process

We treat the heat transfer process as one-dimensional across the section, a feature considered accurate for describing the heat transfer process, as the metal walls are thin and the heat transfer process is rapid. The heat balance across any section is given by

$$\dot{q}'' = h_g(T_g - T_{w,g}) = h_m(T_{w,g} - T_{w,l}) = h_l(T_{w,l} - T_l) \tag{10.21}$$

The balance should be taken forward to the heat transfer to the outer metal wall from which place the heat is lost to the ambient. In reality, this heat loss is very small and ignored. It is assumed that all the heat is transferred to the liquid. The two equations for $T_{w,g}$ and $T_{w,l}$ can be solved and one obtains

$$T_{w,g} = \left[(\frac{1}{h_m} + \frac{1}{h_l})T_g + \frac{1}{h_g}T_l\right] / \left[\frac{1}{h_g} + \frac{1}{h_m} + \frac{1}{h_l}\right] \tag{10.22}$$

$$T_{w,l} = \left[\frac{1}{h_l}T_g + (\frac{1}{h_g} + \frac{1}{h_m})T_l\right] / \left[\frac{1}{h_g} + \frac{1}{h_m} + \frac{1}{h_l}\right] \tag{10.23}$$

The heat transfer analysis of the regeneratively cooled chamber is carried out along the fluid path as it moves from the nozzle end to the head end in 1 or 2-pass with a bifurcation or otherwise section by section. The variation of h_g throughout the chamber is known from the equation (10.15) as well any radiant heat transfer that would be required to be estimated. At the point at which the fluid enters the chamber, T_l is known. The heat flux integrated over the inner surface of cylindrical segment of the chamber gives the heat flow into the liquid. This is utilized to strike a heat balance such as

$$\dot{m}c_{p,l}[T_l(x + dx) - T_l(x)] = \dot{q}''_g \times dA_s \tag{10.24}$$

where x and $x + dx$ refer to the axial sections along the fluid path and dA_s refers to the surface area of the wall section between x and $x + dx$ that has received the heat flux $\dot{q}''_g$. This balance will give $T_l(x + dx)$, the liquid temperature at the next station. This process is repeated till the entire path up to the head end is covered. It must be noted that the liquid velocities and the geometry of the coolant passage can change with axial distance and this should be kept track of in the calculations. The most critical area for the heat transfer is the throat region. In this region it is necessary to check if the heat flux is below, at or above the nucleate boiling regime. Should it cross the nucleate boiling regime, the passage dimension can be controlled so that the convective transfer process brings it below the peak of the nucleate boiling regime. It is to be noted that nucleation process is complex and can depend on the smoothness of the surface as well. Hence, experiments on scaled chambers as well as the full chamber are unavoidable before the design becomes acceptable.

Table 10.19: Features of cooling systems for various applications (Opn. time = Operational time, H. sink = Heat sink, Res.Th = Residual thrust, Ltd. = Limited, CL + Coating life, Wt. = Weight, Ign. problem = Ignition problem)

	H. sink	Ablative	Film	Radiative	Regenerative
Opn. time	Ltd.	< 20 min	No limit	an hour	No limit
Limit on p_c	Ltd.	Ltd.	No limit	< 10 atm	No limit
Vac. Opn	OK	Res.Th.	Res. Th.	Ltd. (CL)	Ign. problem
Restarts	OK	OK	OK	OK	Trapped coolant
Throttling	OK	OK	Ltd.	OK	Limited
Pulsing	OK	Res.Th	Ltd.	OK	Not possible
Penalties	Wt.	Wt.	I_{sp}	Wt.	Pressure drop

10.5 Comparison of Cooling Systems

A comparison of cooling systems for various applications is presented in Table 10.19. As can be noted from the table, each technique has its advantages and disadvantages. For high thrust long burn duration applications, there is no escape from regenerative cooling technique. In some cases, it is possible that regenerative cooling is marginal in terms of safety. To add to safety margin, one can use several strategies. One can increase the film cooling fraction; this entails specific impulse losses due to a fraction of the fluid going out of the nozzle at lower temperatures. If this is unacceptable, one can restrict the area cooled by the liquid and the downstream section that experiences lower heat flux can be cooled by ablative technique, if radiative cooling is considered unacceptable. Otherwise, it is possible to split a part into ablative cooling and another part into radiative cooling. By such strategies, one can achieve cooling without adding to the weight penalties.

For restart applications, regenerative cooling is used in a limited way. This is because the trapped propellant could decompose and deposit unwanted solids in the fluid path adding to pressure drop or even blockage of the flow. The demand on throttling has several implications. Reduced thrust calls for reduced flow rates of propellants. The simplest way of accommodating this would be to reduce the manifold pressure. The chamber pressure drops in proportion to the drop in manifold pressure. This assumes that the atomization process remains unaltered. If the atomization process becomes coarser, combustion efficiency drops and specific impulse efficiency also drops. To preserve the atomization process, it is possible to reduce the injector area while maintaining the manifold pressure. The alteration of the geometry is somewhat complex and pintle injector design allows for such a process (see Figure 10.40). For throttling, the dependence on film cooling needs to be minimized since the reduction in flow rate has more adverse effect on thermal safety of parts of the chamber deprived of the film coolant.

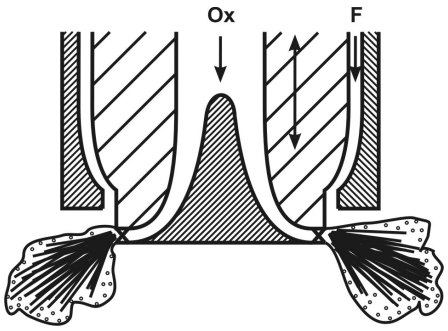

Figure 10.40: The schematic of a Pintle injector - coaxial injector design for storable propellants

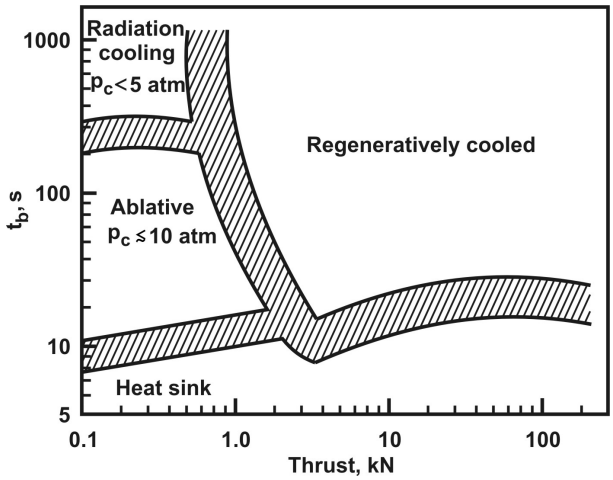

Figure 10.41: Regimes of use of different cooling techniques from [48]

Figure 10.40 shows the cross section of a pintle injector that has been used for variable thrust applications for nominal thrust ratings of 4 to 40 kN thrust level. The specialty of this injector design developed by M/s TRW systems, USA has been shown to be dynamically stable over the entire range of thrust levels without any stabilization device.

For pulsing, the sharp cut of thrust pulse is compromised in the case of ablative cooling since a part of the heat stored in the ablative will cause release of gases and this will produce residual thrust. Regenerative cooling system is unsuited to pulsing because the amount of propellant stored in the cooling passages will to vaporize or decompose and generate residual thrust. Figure 10.41 drawn from Coulbert [48] displays on a burn time (t_b) vs. thrust plot, the various regimes of cooling normally deployed in liquid rocket engines.

10.6 Ignition System

Hypergolic propellants like those based on IRFNA and NTO, and g – fuel, UDMH and Aerozine do not need an ignition system. What is important is to arrange the arrival of the propellants with appropriate timing – oxidizer lead mostly. Propellants based on liquid oxygen namely, LOX - RP1 and LOX - LH_2 require an ignition system. The design of the systems will need to account for single start or multiple start. Both spark ignition in and pyrotechnic ignition systems have been developed. In the case of spark ignition systems, the propellants, particularly those that can easily be vaporized (like LOX – LH_2 system) are brought into a small chamber from which the gases enter the main combustion chamber. The spark system generates spark with energy of 0.1 to 0.2 J and the flow of hot gases is maintained throughout the operational period till shut down. Restart will begin the same way. However, there are issues of heat soak back into various components that need to be dealt with. In the case of pyrotechnic system, for instance, the CUS engine has an ignition system that has variants - for a single start and multi-start option. In the case of the single start option, the ignition system operates for 7 s. In the case of two-start option, there is a facility of four igniters with the gases flowing from that system that is initiated but not affecting other igniters with the back flow from the main combustion chamber positively prevented thermally as well as pneumatically. The device has passages with diaphragm based arrangement that is much stronger in one direction compared to the other.

10.7 Clustering Engines

History of development of vehicles in any nation has shown a trend towards larger and larger size engines. There are also time schedules to achieve a certain objective – bring to readiness a missile for deployment or launch a new satellite. These impose constraints on development. Two approaches towards obtaining a larger thrust would be (a) to build a higher thrust engine ab-initio so that all the new features developed till then would be incorporated into the new design or (b) build a cluster of engines integrated into a stage. In the cluster design, it need not be taken that the entire engine frame is accepted into the new configuration. One can conceive of clustered thrust chambers being fed from a larger turbopump assembly. The famous one-and-a-half stage arrangement of Atlas vehicle in which two outer engines are jettisoned with the core engine providing thrust for much longer time is a variant in this class. In case (b), it is understood that the tankage and pressurization system are altered and the necessary plumbing to the cluster arrangement is provided for newly. Of course, there are issues of control and this is cared for by gimballing specific engines in appropriate directions to generate the necessary control force. Such a conceptualization allows the project objectives to

be achieved in shorter time frame. But development groups keep working to create newer fronts to conquer and this allows for larger engines or more efficient engines to be built. To achieve the objectives of Saturn mission, clustering of 8 LOX – RP1 engines for S-I mission and 5 F-1 engines for S - V mission (Apollo mission) were adopted. The Agni missile uses two SA 2 engines that are gimballed in such a manner that full thrust vectoring is possible.

10.8 Propulsion System Option Comparison

The discussion so far in this chapter is concerned with monopropellant thrusters and bipropellant pressure fed and turbopump fed engines. A simpler system that has not been discussed refers to cold gas thrusters in which the stored cold gas is the "propellant". It is introduced into a thrust chamber and passage through the nozzle produces thrust. Since the effective stagnation temperature is low ($\sim$ 300 – 350 K), the value of c^* also will be low, (and also the specific impulse). The reason it is used is that the system is very simple and as long as the demand on the total impulse is low, the system size and weight will be optimal. The optimality of the weight of the system will be an important criterion in making the choice of the system. The single performance parameter that controls the choice is the total impulse that the propulsion system has to deliver – for, the total impulse divided by the specific impulse will give the weight of the propellant to be carried. This divided by the density (separated into fuel and oxidizer as per the chosen O/F for bipropellants) will give the volume of the propellants. Multiplied by a factor more than 1 (typically, 1.03 to 1.07) will provide the tank volume. The 3 to 7 % referred to here is the ullage space above the propellants occupied by the pressurant gas. The tank has to maintain a pressure to drive the fluid through valves, plumbing into the thrust chamber directly or through turbopumps. This value is typically 20 to 40 atm for pressure fed systems and 3 to 5 atm for turbopump fed systems. If the total impulse delivered by the propulsion system is large, so will the tank volume be and the tank weight will be substantial if the pressures that it has to withstand is larger. Thus, the additional weight of the pressure fed system in comparison to turbopump fed system is partly balanced by the weight of turobopump assembly. If one computes the weight of the system using classical engineering practices, one can draw a plot of the system weight as a function of total delivered impulse.

This is shown in Figure 10.42. It is clear from this figure that cold gas system is excellent for very low total impulse, and as demand on impulse increases, monopropellant system takes over; this is taken over by pressure fed bipropellant system and for large impulse values, turbopump system is always optimal. Such an understanding has to be tempered by other demands like restarts, throttling and pulsing. Table 10.20 shows the broad features of all propulsion systems including solid propellant systems. The table is self-explanatory.

Table 10.20: Comparison of characteristics of various types of propulsion systems (Ra = radiation cooling, F = film cooling, Re = Regenerative cooling, Ab = ablative cooling, Hs = heat sink; reqd. = required)

	Cold gas	Monoprop	Pr. Biprop	TP Biprop	Solid
Thrust range	50 – 100 mN	0.5 N – 3 kN	0.4 – 100 kN	20 kN – 10 MN	0.1 kN – 10 MN
Impulse range, kN s	< 3 – 5	3 – 400	200 – 10^4	600 – 10^6	0.2 – 10^6
Operational time	20 ms – 100 s	20 ms – 1 hr	100 s – 1 hr	500 s	140 s
I_{sp}, kN s/kg	500	2200	3000	4560	2800
ρ_{mean}, kg/m^3	40 – 350	1000	1300	300 – 1300	1600 – 1750
Cooling method	not reqd.	Ra	F + Ra	Re + F + Ab,Ra	Hs + Ab
Restart	Yes	Yes	Yes	Yes	No
Throttling	No	Yes	Yes	Yes	No
Pulsing	No	Yes	Yes	No	No

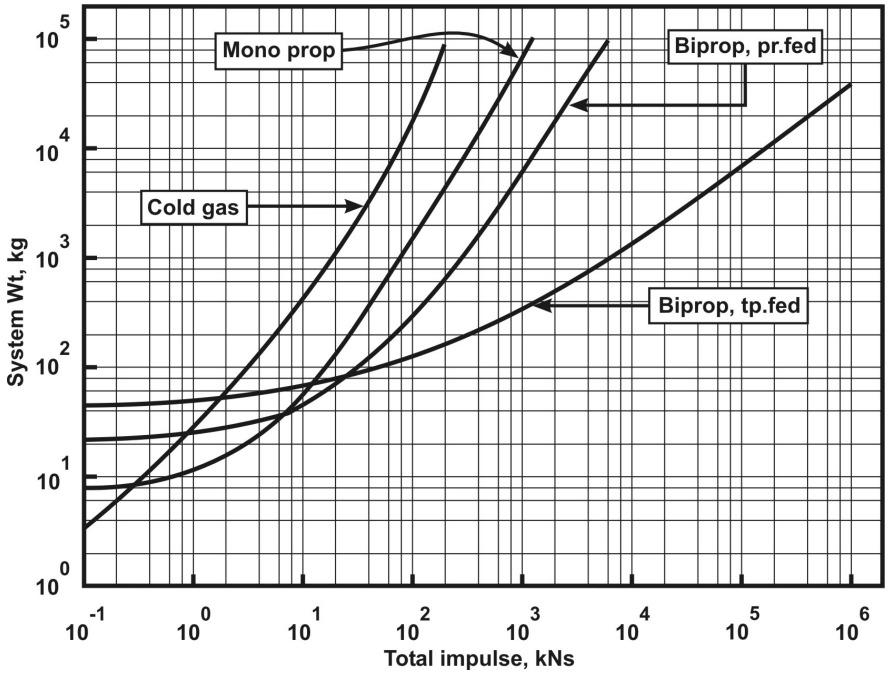

Figure 10.42: The dry weight of systems as a function of total impulse delivered by the propulsion system

10.9 Comparison of Gas Turbines and Liquid Rocket Engines

The compressors for gas turbine class engines have compressible fluids; even so, a majority of the fluid flow behavior is covered by incompressible flows. Rocket engine turbo-pumps work only in incompressible mode as liquids can be treated as incompressible with accuracy. Issues of to-be-avoided regimes like surge that are found in compressors are also found in pumps.

As an example, the stall regime of the axial flow turbo pump of J2 engine is shown in Figure 10.43. This diagram is similar to Figure 6.22.

The principal features of combustor, namely, allowing the residence time for all the aspects of combustion process to be completed are similar in both cases (like drop vaporization, mixing and reaction). In the former case, the combustion process is less intense compared to rocket engines because (a) the fluids are less reactive (compare kerosene and air in gas turbine engines with kerosene and oxygen in liquid rockets) and (b) operative pressure regime is less favorable (compare combustor pressures of 4 – 5 atm. of gas turbine engines with a minimum of 50 atm for rocket engines). This has implications on the problem of acoustics induced

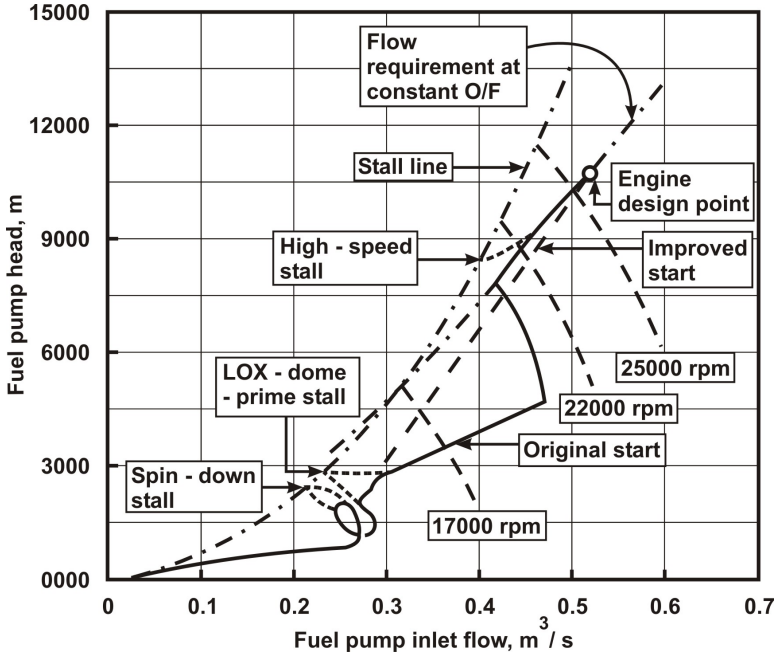

Figure 10.43: The stall characteristics of Mark 15 pump used on J2 engine drawn from the ref. [44]

instabilities that are far more serious in rocket engines than in gas turbine engines.

The turbine section is far more demanding in the case of gas turbine engines than in rocket engines. The design must ensure smooth rotation of the rotor assembly with little leakage even after a large number of hot-to-cold changes, and preserve the performance for long operating hours (several thousands of hours). The maximum that the turbine of a rocket engine has to endure is about ten hours (only in the case of a reusable vehicle like Space shuttle). The procedures used for the design of turbines for gas turbines are directly relevant and applicable to turbines for turbopumps.

The demand for compactness is present in both. But the effects of small errors in the case of rocket engines can be far more catastrophic because the fluids used are far more reactive. The disasters of the challenger space shuttle are a case in point.

10.10 Summary

This chapter has been devoted to the study of liquid rocket engines – both monopropellant and bipropellant. These are composed of several elements – pressurization system, tankage, turbines, pumps, injector, combustion chamber and nozzle. Aspects of design and analysis involve fluid flow behavior at ambient temperatures as well as temperatures much below and above the ambient, with and without chemical reaction. Understanding the operational behavior calls for a greater appreciation of fluid dynamics than chemical kinetics, though some aspects like ignition are controlled by kinetics. Most powerful engines across the world have been built in the USA and Russia (in fact, former USSR). These were built with considerable intuitive understanding and substantial test experience on elements as well as integrated systems. This chapter provides a description of a wide variety of the systems and their analysis.

A number of books address the aspects discussed in this chapter – Barrere et al [12], Sutton, [25], Timnat [26], Penner [19], Bollinger et al [13], Huzel and Huang, [16], and Brown [14]. The NASA special publications, NASA SP 8081 [38], NASA SP 8087 [39], NASA SP 8089 [42], NASA SP 8107 [41], NASA SP 8113 [40], NASA SP 8124 [43], and NASA SP 8125 [44] contain data on many elements of a rocket engine and these have been used in this chapter. The data from these sources are not necessarily identical. Variations seen are due to reporting at various times during which period developments would have taken place.

Chapter 11

Combustion Instability

11.1 General

Combustion instability is an irregular pressure fluctuation in the pressure-time trace of an engine. This pressure fluctuation can be in the acoustic range or below this range. It can occur in air-breathing engines or rocket engines, both solid and liquid (limited understanding of hybrid rocket engines shows that they do not experience any serious instability problems). A second way of classifying the instability is to separate them in the frequency range. Instabilities below about 100 Hz are termed low frequency instability (LFI). Fluctuations in the frequency range of 100 to 500 Hz or thereabouts are termed intermediate frequency instability (IFI). Fluctuations in a frequency range beyond this value are termed high frequency instability (HFI). In air-breathing engines, the after-burner has been known to be beset with instability problems largely of HFI kind. Solid rockets that use high energy solid propellants involving Aluminum loading do not usually experience any instability. Even so, some tactical motors based on composite propellants and others based on double base propellants experience instability problems. Liquid rockets experience the whole range of instabilities. There are two participating elements in liquid rockets – feed system and thrust chamber. The coupling can result in instabilities. These usually belong to the class of LFI because the wave length involved is large (acoustic speed/frequency $\sim$ 1000 m/s / (20 to 100) Hz = 50 to 10 m), in fact much larger than the combustion chamber size. When this occurs, one hears a chug – chug sound and the instability is termed *chugging*. In the other extreme, if one takes HFI, the frequencies involved are typically 1 – 3 kHz. In this case, the wave length involved is much smaller than the feed system length scale. The feed system is unable to respond to these high frequency fluctuations. Hence, the entire dynamics is restricted to the combustion chamber. Since the frequency is in the acoustic range, acoustic field can be conceived to be

responsible for the phenomenon. In fact, the length scales can be so small that it could be expected that the pressure fluctuations in different parts of the combustion chamber would have phase differences and this is indeed found true. When a rocket engine is tested, if one hears a high frequency sound – screeching, it is usually inferred that the combustion chamber has suffered a HFI. What more, it is usually feared that the chamber would be damaged and the hardware lost. These observations have been repeatedly seen in developmental programs of various engines, and HFI is dreaded amongst the developers of large liquid rocket engines. In fact, while acoustic instabilities are feared generally in all combustor developments, it is not as virulent in after-burners that use an anti-screech device or solid rockets that depend on the presence of metal oxide particulate matter to dampen the fluctuations. It is instructive to examine two classic historical examples of instability.

Early in the development of larger thrust rocket engines, the presence of instability was noticed, much less from good instrumentation than tell-tale signs of destruction in tests. Since the true dimensions of the problem were not assessed, a statistical view of instability was taken. It was taken that if the engine suffered only a few instabilities in a large number of tests, one could take it that the engine is stable to a large extent. Setting a limit for this, any engine that was within this threshold was accepted for flights. The engines used for the Atlas vehicle were qualified for operation in this mode; these resulted in catastrophic failure of the first flight. This caused a complete change of perception and it was decided that every engine accepted for flight must be dynamically stable – any perturbation introduced into a steadily operating engine should die down in a specific time. This concept was refined over a period of time and methods of stabilizing otherwise unstable engines were found and then not only would the engine be proved stable, but a margin of stability could be extracted from the tests and presented for qualification and possible acceptance. The concepts of stability rating (as it was called) were refined and documented (NASA SP 194, [52]).

In the late 1970's, the French were involved in the development of a satellite launch vehicle termed, Ariane. This vehicle used the "Viking" whose several details are presented in the previous chapter. The engine used a radial injector described in Figures 10.17 and 10.18. The entire development took place without a firm consideration of qualifying the engine for stability. While the first three flights were successful, the fourth flight was lost because of HFI problems. This led to a major injector modification program involving a large number of injectors and tests and finally an injector was selected that generated a coarser distribution of droplets leading to a more graded heat release allowing for a larger margin of safety from problems of HFI. Subsequent flights have been successful indicating that the margins of stability have been adeqaute.

A form of instability that is related to propulsion system-structure interaction

Table 11.1: Typical parametric dependences of low frequency instability

Parameter variation	Effect on frequency	Effect on amplitude
L^* from 2 m to 4 m	from 100 to 70 Hz	decreases
p_c from 10 to 20 atm	from 50 to 100 Hz	decreases by 4-5
Δp_{inj} from 2 to 5 atm	from 20 to 30 Hz	Stability recovered
O/F from lean to rich	Little effect	affected

called POGO has been observed in rocket engines used on large vehicles. This instability is a low frequency oscillation – typically in the range of a few to tens of Hz known to affect the motion of the vehicle, particularly at times close to burn out that would need to be overcome.

11.2 Low Frequency Instability in Liquid Engines

The low frequency instability is a result of phase differences between the feed system response to the combustion chamber pressure oscillation. It is not deadly, but needs to be cured. A large number of experimental and control system based modeling studies were performed in the early sixties to understand parametric dependences. It was observed that the amplitude of the oscillation would be large at low pressures and the amplitude would come down with increase in chamber pressure. Even in high pressure engines, the starting transients involve a certain amount of oscillatory behavior that dies down when the steady pressure is built up. The dependence of the frequency and amplitude of oscillations on various parameters, found from various experments, is set out in Table 11.1. Many experimental aspects are described in reference [12]

Combustion efficiency decreases by as much as 20 % if LFI is present. A standard method of overcoming the instability would be to increase the pressure drop across the injector. This isolates the fluctuations in the chamber from the feed system. The time lag between the propellant flow into the combustion chamber and the conversion to hot gas, is a parameter that characterizes the phase difference between the feed system response and chamber pressure oscillation. This parameter is used to model the instability behavior. While such an analysis to be presented here explains the phenomenon, it is not easily possible to control the time lag. Increase in pressure drop across the injector can be related to better atomization and hence, altering the time lag into a favorable condition. The analysis starts with the mass balance equation of the combustion chamber.

$$\frac{dm_{cc}}{dt} = \dot{m}_p - \dot{m}_{noz} \tag{11.1}$$

We recognize that m_{cc} = mass of the gas in the combustion chamber = $p_c v_c / RT_c$, $\dot{m}_{noz} = p_c A_t / c^*$. We now treat the aspect related to the response of the system by invoking $\dot{m}_{gas} = \dot{m}_p(t - \tau)$ where τ is the response time of the system composed of fluid acceleration and delivery as well as ignition. The liquid mass flow rate $\dot{m}_p$ is given by

$$\dot{m}_p = c_d A_{inj} \sqrt{2\rho_l (p_{inj} - p_c)} \tag{11.2}$$

If we now set $p_c = \bar{p}_c(1 + \phi)$ and $\dot{m}_p = \bar{\dot{m}}_p(1 + \psi)$, where the quantities with bar are steady and ϕ and ψ are perturbations in pressure and mass flow rate. Substitution and simplification results in

$$\frac{d\phi}{dt} + \frac{\phi}{t_c} = -\frac{P}{t_c}\phi(t - \tau) \tag{11.3}$$

where $P = \bar{p}_c / 2\Delta\bar{p}_c$, $t_c = L^*/c^*\Gamma^2$ (equation 9.17). In addition, treatment of equation (11.2) using perturbation variables leads to

$$\psi = -P\phi \tag{11.4}$$

To determine the linear stability of the equation, one can substitute

$$\phi = \exp(\lambda + i\omega)t \tag{11.5}$$

and introduce it into equation (11.3) and separate into real and imaginary parts as

$$\lambda + \frac{1}{t_c} + \frac{P}{t_c} e^{-\lambda\tau} cos\omega\tau = 0 \tag{11.6}$$

$$\omega - \frac{P}{t_c} e^{-\lambda\tau} sin\omega\tau = 0 \tag{11.7}$$

We can examine the condition for stability for which $\lambda < 0$. Neutral stability is obtained for $\lambda = 0$. From these, one can obtain a criterion for stability as

$$\frac{\tau}{t_c} \leq \frac{1}{\sqrt{P^2 - 1}} [\pi - tan^{-1}\sqrt{P^2 - 1}] \tag{11.8}$$

This equation states that for a certain delay time (τ) as a multiple of the characteristic time of the combustor (t_c), the behavior of P, the ratio of the chamber pressure to the pressure drop across the injector will be according to the above equation - it turns out that $P < P_{crit}$ for stability. This implies that increase in $\Delta\bar{p}_{inj}$ helps stability. This is also consistent with the experimental results. Table 11.2 presents the results from equation (11.8). The above analysis includes the effects of $L^*, p_c, \text{ and } \Delta p_{inj}$. Including the effect of O/F calls for a two-fluid treatment. Also, it is possible to include the effects of resistance, inductance and capacitance of the fluid circuit as as other finer details of the response of pressure regulator. These can be found in NASA SP 194 [52] and several references found therein.

Table 11.2: Results of stability in terms of τ/t_c vs P_{crit}, the critical value of P below which there is stability

τ/t_c	P_{crit}
1.2	2.00
2.0	1.49
2.5	1.36
3.5	1.32
4.0	1.08

A recent experience of this kind of instability might be instructive. A cryo-engine that was known to be free of instabilities otherwise, was undergoing ground tests and these tests showed oscillatory pressure-time trace with frequencies of 130 to 140 Hz and amplitude of fluctuations as much as 15 %. Alterations were made to bring the system as close to the original configuration sequentially test after test. This led ultimately to a pressure transducer fitment on the H_2 line that had a short line to isolate the low temperatures from the transducer. This had a compliance that caused the resonant behavior. Elimination of this compliance permitted smooth operation of the engine.

11.3 High Frequency Instability (HFI)

High frequency instability is a combustion chamber phenomenon linked to acoustics. While features like vortex shedding from sharp edges have been identified as possible causes, the single most important cause has been found to be the *coupling between heat release rate fluctuations and acoustic field*. In the case of liquid rocket engines, this implies that the flow rates into the combustion chamber remain unaffected during the period when the engine experiences the instability. This is because the feed system does not have the ability to respond to the fluctuations. The amplification process leads to changes in chamber pressures that could be comparable to the mean chamber pressure and local heat flux that can be several orders larger than the mean. Both these can lead to destruction of the hardware. The acoustic field inside the thrust chamber can be affected by the flow processes in addition to heat release. However, the geometry of the thrust chamber leads to an acoustic field with well defined natural frequencies and modes. The natural frequencies can be the first, second and higher harmonics and the modes are longitudinal, radial and transverse. The modes can be standing or propagating and could be coupled – a coupling between the longitudinal and tangential modes leads to a spiral mode.

The first thing to do would be to solve the acoustic equations for the combustion

chamber geometry and determine the natural frequencies for various modes. The acoustic propagation is governed by

$$\frac{\partial^2 p'}{\partial t^2} = a^2 \nabla^2 p' \tag{11.9}$$

where a is the acoustic speed, typically 1000 to 1500 m/s in the combustion chamber because the static temperatures are about 3000 to 3500 K, molecular weights about 12 to 26 and γ, 1.15 to 1.2. The coordinates chosen are x, the axial direction normal to the injector face and along the axis of the thrust chamber, varying from 0 to L, r, the radial coordinate varying from 0 to $d_c/2$, θ, the tangential angular coordinate from 0 to 2π. The independent variable, p' is the pressure perturbation whose distribution is related to sound propagation. In the case of solid rocket motor, the port region of the grain that is usually cylindrical in shape constitutes the outer boundary. In the case of liquid rocket engine, the combustion chamber is treated as a cylinder of diameter d_c, and boundary conditions applied are that the pressure anti-node occurs at all boundaries – the pressure gradient normal to the surface must be 0. This is not difficult to appreciate for the injector face and the cylindrical walls. The acoustic velocities must be 0 and hence, pressure perturbation must be an extremum. It is not so clear how this condition is appropriate at the exit – throat region of the nozzle. It turns out that the nozzle open end also appears "closed" to the acoustic field. This is because the flow with strong gradients at the throat reflects longitudinal waves to an extent that treating it as closed is considered a very good approximation [24]. For other transversal modes, it is clear that it appears as a closed end. Even though this implies that natural frequencies can be calculated in this manner, there could be loss of energy through the nozzle end and it is calculated as a response function or admittance function. The solution to the acoustic problem can be set out by using the separation of variables technique; the axial and tangential modes have simple harmonic functions (sine and cosine). The radial variation is obtained in terms of Bessel functions. The final result can be expressed as

$$p' = \exp\left[i(\omega_{mnq} t + n\theta + q\pi \frac{x}{L})\right] J_n(\pi \alpha_{mn} \frac{2r}{d_c}) \tag{11.10}$$

Where $J_n(arg)$ is the Bessel's function of the first kind. The wave numbers m, n and q refer to the different modes, and as a part of the solution, ω_{mnq} is given by

$$\omega_{mnq} = \frac{\pi a}{2} \sqrt{\left[\frac{2\alpha_{mn}}{d_c}\right]^2 + \left[\frac{q}{L}\right]^2} \tag{11.11}$$

For only lateral modes, q = 0, and the above equation leads to ω_{mnq} = ω_{mn0} = $\pi \alpha_{mn} a/d_c$. The values of the α_{mn} are presented in the Table 11.3.

The values of the constants for higher modes are listed in NASA SP 8113 [40]. If we take the first tangential mode, the pressure fluctuation can be expressed by

$$p' = \exp\left[3.68 \frac{a}{d_c} it + i\theta\right] J_1(3.68 \frac{r}{d_c}) \tag{11.12}$$

Table 11.3: The values of α_{mn} for some modes; $\alpha_{mn} = n/\pi$ for $n \gg 1$; $\alpha_{mn} = m + n/2 + 1/4$ for $m \gg 1$, $m > n$

Mode	m	n	α_{mn}
First Tangential	0	1	0.586
Second Tangential	0	2	0.972
First Radial	1	0	1.22
Third Tangential	0	3	1.34
Fourth tangential	0	4	1.69
First Combined	1	1	1.70

Table 11.4: The longitudinal, and tangential natural frequencies for a few cases, $f_{1L} = a/2L$, $f_{1T} = 0.586a/d_c$, $f_{2T} = 0.972a/d_c$

L	d_c	f_{1L}	f_{1T}	f_{2T}
m	m	kHz	kHz	kHz
0.5	0.5	1.0	1.17	1.94
1.0	0.5	0.5	1.17	1.94
10.0	1.0	0.05	0.59	0.97

For the first radial mode it becomes

$$p' = \exp\left[7.66\frac{a}{d_c}it\right]J_0(7.66\frac{r}{d_c}) \tag{11.13}$$

For longitudinal mode only, we set $m = n = 0$, to get $\omega_{00q} = \pi aq/2L$.

Figure 11.1 shows the behavior of acoustic pressure and velocity fluctuations for various modes. The first longitudinal mode through every quarter of a period is shown at the bottom left. It is seen that the pressure anti-node and the velocity node occur at the ends. Velocity fluctuation reaches the peak when the pressure fluctuation is at the minimum. The first and second tangential as well as radial modes are described at the top of the Figure 11.1, and the corresponding radial variations of the normalized radial and tangential velocities on the right side.

For products of combustion of solid propellants and storable hypergolic propellants as well as LOX – RP1 systems, $a \sim 1000m/s$. The 1L, 1T and 2T mode frequencies calculated from the equation 11.11 are presented in Table 11.4. Since in solid rockets, $L/d_c >> 1$ (could be as large as 5 to 20), the longitudinal mode frequency will be much lower than the tangential modes (and also radial modes as can be inferred from Table 11.3). In liquid rockets, L/d_c is about 1.2 to 4 and the role played by lateral modes is far more important.

The motors for which instabilities have been observed are listed in Table 11.5.

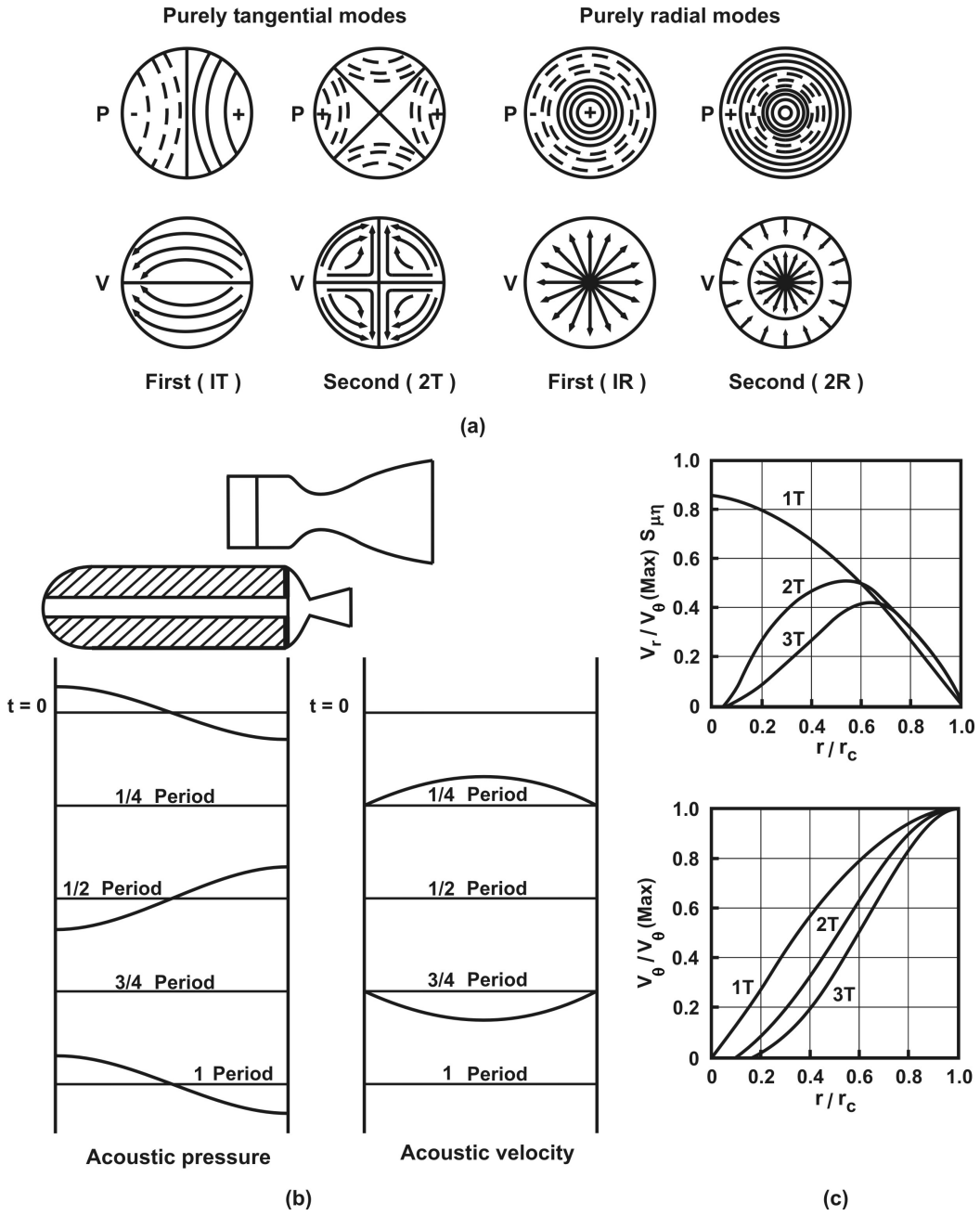

Figure 11.1: The longitudinal, radial and tangential modes of acoustic pressure and velocity fluctuations as well as variation in space drawn from [52] and [65]

Table 11.5: Features of instabilities observed on various liquid rocket engines; * = unstable without ac oustic absorber

Engine	Props.	Injector	Chamber dia, m	Dominant Instability
F 1	LOX RP1	Like doublet	0.99	1T 0.5 kHz
J 2	LOX LH_2	Coaxial		1T 1.8 kHz
P & W AGENA	NTO Aerozine	Triplet		1T, 3.2 kHz 1T-1L, 2.5 kHz
Rocketdyne LMA, unbaffled*	NTO Aerozine	Unlike doublet		1T 3.3 kHz
Rocketdyne LMA, baffled*	NTO Aerozine	Unlike doublet		1R, 3T 7 kHz
XRL booster	RFNA UDMH	Unlike doublet		Feed system Coupled, 1.3kHz
Aerojet LMA	NTO Aerozine	Triplet		1T, 3.5 kHz + 2T, 5.7 kHz
SSME	LOX H_2 (gas)	Coaxial	0.45	

It can be noted that 1T mode is found most commonly, 2T and 1L modes become comparable in engines with the length of the combustion chamber comparable to the diameter. Also, the lower range of frequencies that cause instability are more virulent in amplitudes compared to higher modes. In fact, one general principle used is that as long as all the frequencies less than about 5 kHz are damped, one may be reasonably sure of not encountering instability problems. However, no principles are without exceptions. One, some times, finds a virulent instability at 9 kHz as well.

The primary cause for instability is located in the processes occurring in the heat release zones. This inevitably links the processes to the injector since the injection process controls the heat release rate. It also appears necessary to consider processes special to storable hypergolic, semi-cryogenic and full cryogenic propellants separately.

Storable hypergolic propellants that use unlike-impingement encounter what is known as popping phenomenon. This phenomenon involves several aspects – (a) periodic separation of impinging jets because of condensed phase hypergolic

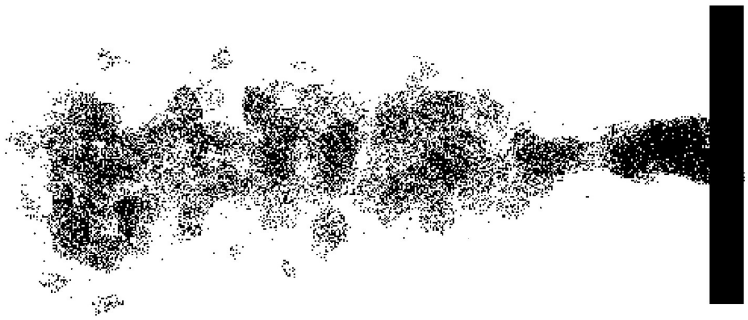

Figure 11.2: The clumping of atomized fluid from an injector called Klystron effect

reactions between oxidizer and the fuel, and (b) the formation of tiny ligaments of a mix of the fuel and the oxidizer that react in the condensed phase when the reactants are reasonably cold (300 K) with the formation of reactive intermediates and suddenly burst into an explosive flame with a "pop".

Resurging is another form of instability partly attributed to the dynamics of film cooling. It is hypothesized that the flow of the film coolant is affected by the main chamber gas dynamics such that it is periodically pealed off and this burns up leading to pressure rises. The popping that was found on F1 engine and similar engines (with non-hypergolic propellants) has been argued to be also due to operating pressures being beyond the critical pressures. It has been argued that the liquid temperature would be below the critical temperature when the liquid enters the chamber and as it heats up it crosses the critical condition and this leads to combustion phenomena related to loss of phase between the liquid and vapor. The problem of F1 engine was solved by a redesign of the film coolant thickness. Resurging is also claimed to be related to what is known as "Klystron effect" (see NASA SP194, [52]) in which the atomization process leads to clumping of propellant droplets. Reaction of these masses leads to sudden pressure rise that can trigger short duration pressure fluctuations. Consequently, there is a continuous series of pressure peaks showing up as HFI.

Figure 11.2 shows the injector spray indicating the clumping of fluid along the jet outflow.

In storable hypergolic propellant combinations, a number of causes like reac-

tive stream separation, film coolant related issues, the hysterisis effect of injectors (discussed with reference to Figure 10.14) can all contribute to the problems of instability to varying degrees.

For LOX – RP1 propellant combination, particularly with like-impingement, the processes involved in causing instabilities would be the coupling between the atomization, vaporization and heat release processes with the local flow field. With the liquid coming out of the injector face at velocities of 20 to 40 m/s through the injector orifices, there will be entrainment of gas around. This reduces the local pressure. To fill this region, gas from downstream will pass through the cloud of droplets and enter. Depending on the path that the gas takes, it is possible that the hot gas moves in. The motion of this gas creates a velocity parallel to the surface and a heat distribution close to the injector face affecting the local processes. The heat release distribution affected by these processes could be significant with in 100 to 150 mm from the face of the injector. This zone is very sensitive to acoustic oscillations. If the coupling between the heat release and pressure fluctuations leads to favorable phase relationship, one has instability. If the heat release rate is slow as might happen if the drop size distribution is coarse, the acoustic fluctuations will receive less phase locked energy and the high density drop distribution will provide a damping of oscillations. The relative energy balance of wave packet propagating through the complex medium will decide whether the wave will amplify or decay.

LOX – LH_2 engines have problems of instability whose causes are different from the above. The injection system that is used in most engines is the coaxial type (the injector head is shown in Figure 10.19). A cross section of one of the injectors is shown in Figure 11.3.

There are a number of parameters of the injector geometry. Apart from the diameter of the injection holes, the recess and the divergent inner section and the possibility of using swirl on the oxygen flow are additional features. Experimental and early developmental studies revealed no instabilities and it was only much later when liquid hydrogen at lower initial temperature ($\sim$ 50 to 100 K) was injected into the combustion chamber that instabilities were detected. It was then discovered that instability was strongly connected to the temperature of hydrogen. Experiments conducted with hydrogen temperature ramping from a higher value to lower values indicated precisely the temperature at which instability would begin. Typically, hydrogen injection temperatures in excess of 100 K are found to favor stability under most practical operating conditions. This is confirmed by data presented in Figure 11.4 (a) where it is seen that the stability is dependent on the chamber-to-throat area ratio with smaller values needing higher temperatures for stability. In this figure, it appears that stability is favored even at hydrogen temperatures of 60 K.

Another key parameter influencing the combustion process is the injection ve-

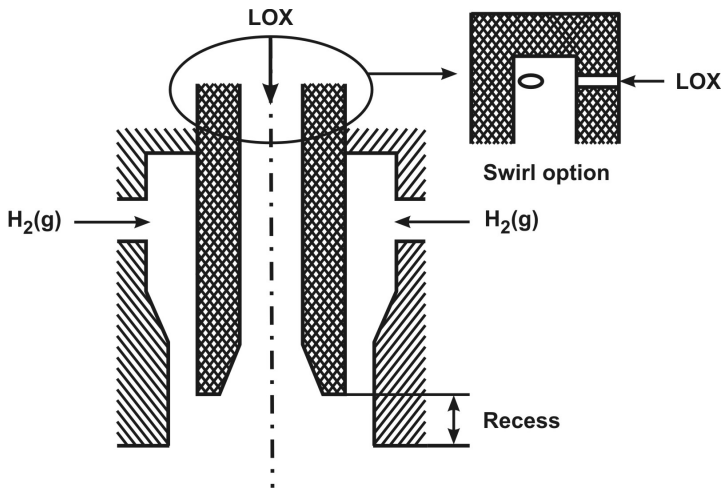

Figure 11.3: The cross section of a typical coaxial injector with swirl or straight oxidizer injection

locity ratio between gaseous hydrogen and liquid oxygen. The results of experimental studies (see NASA SP 194) [52] shown in Figure 11.4 (b) indicate that if the velocity ratio is kept at values in excess of 12, the engine should be stable, particularly when the O/F chosen is 6 or thereabouts. Other studies of the stability on chamber pressure and hydrogen injector pressure drop have shown weak effects or contradictory trends. Even though the stabilizing effects of higher hydrogen injection temperature are known for over forty years, *there has been no clear and simple explanation*. Amongst several explanations indicated, one that seems to fit several observations is the influence of entropy wave from mixture ratio variations reflected from the throat region (page 20, NASA SP 194). This is a weak mode that fits with the general observation that the instabilities in cryo systems are not as damaging as in storable or semi-cryo systems and the temperature effect. Lowering the temperature in a fixed thrust chamber allows oxidizer-fuel ratio variations to remain up to the throat and lead to instability. Fundamental work in this area is needed to clarify the true causes of instability even though motivation seems limited because successful engines have been built and can be built even now based on the foundation of earlier work.

11.3.1 Solutions to HFI in Liquid Rocket Engines

Instability can be eliminated by reducing the intensity of combustion or providing damping devices to absorb the oscillations or both. There are four methods adopted to eliminate the instabilities. These are: (a) reduce the pressure drop across the injector and increase the diameter of the injection holes to pass the same mass flow

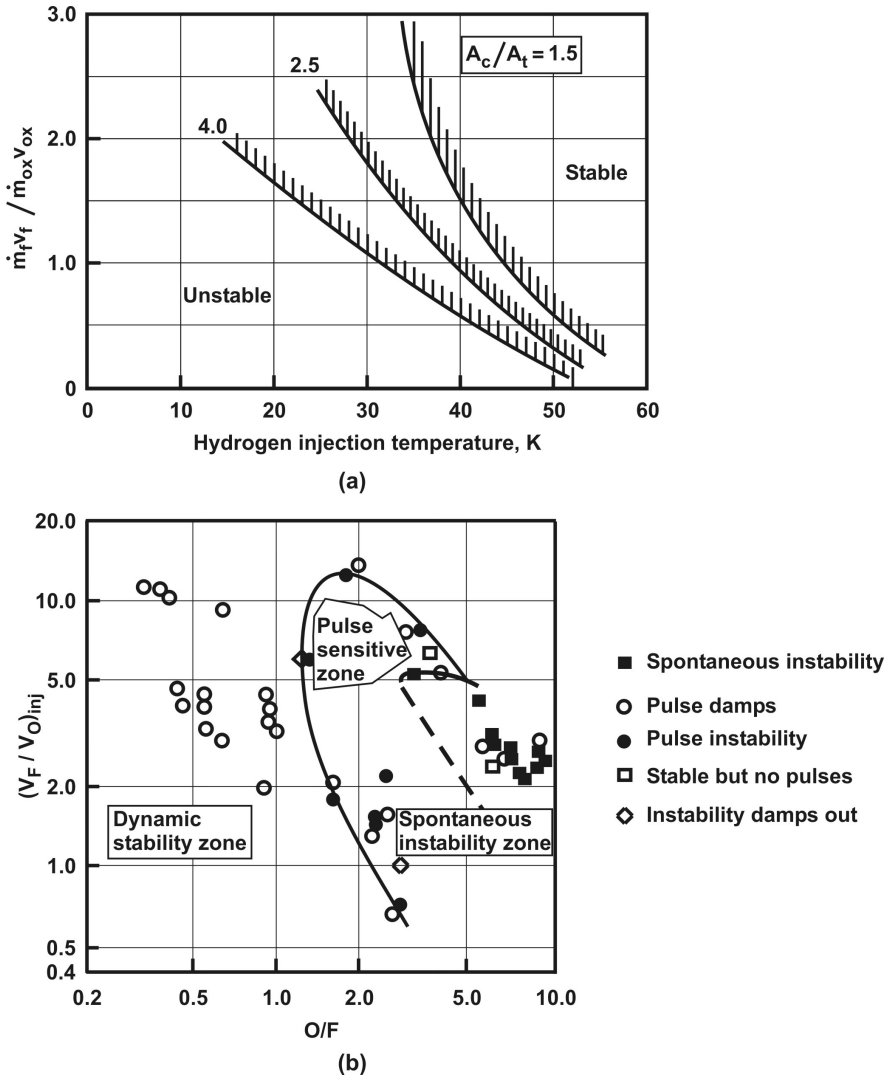

Figure 11.4: a. The oxidizer-to-fuel momentum ratio with hydrogen injection temperature showing the stable zones, b. The fuel-to-oxidizer velocity ratio with O/F showing the zones of stability drawn from ref. [52]

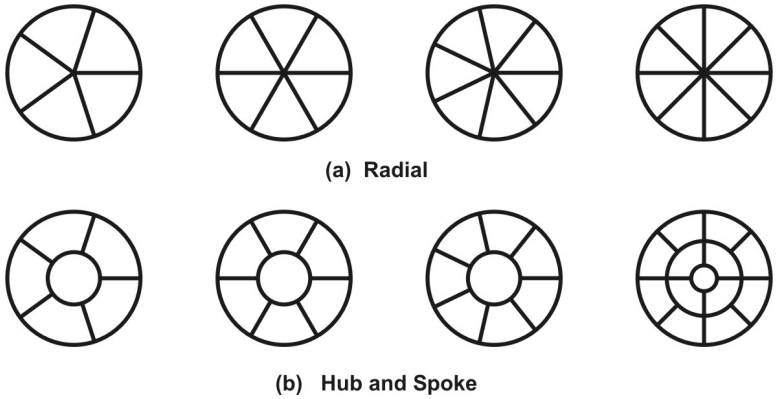

Figure 11.5: Some typical radial blade and hub-and-spoke baffle designs

rate, so that the injection velocity gets reduced and the atomization process takes longer distance to complete, (b) provide baffles at the injector head so that destructive mode is dampened and any possible higher mode that may get excited cannot derive so much energy from the mean flow to sustain the oscillations, (c) provide acoustic damping devices at the head end or over the chamber so that oscillations are damped and (d) provide ablative liners so that acoustic damping improves. Of these techniques, technique (a) belongs to the category of reducing the combustion intensity and techniques (b) to (d) belong to the category of providing for damping of the destructive mode. The use of baffles is very effective against tangential and radial modes. By providing a certain number of radial blades of sufficient depth (along the combustion chamber), the transverse acoustic motions are interrupted. The velocity fluctuations have to be zero along several points in the azimuthal direction at locations where the baffles are present. The depth of the baffles must be chosen so as to cover the peak heat release area. To eliminate radial modes, a circular baffle may be created along with radial blades so that the standing waves may be interrupted. There are several possible designs of baffles. Figure 11.5 shows the possibilities.

A typical baffle design used in Titan II stage I engine is shown in Figure 11.6. The blades of the baffle arrangement need to be cooled since they need to survive the harsh thermal environment. A typical arrangement presented in Figure 11.7 shows the strategy for cooling the baffles.

Based on a large number of experimental studies, some guidelines have been developed for the choice of the number of baffles as well as the depth. A two-bladed baffle can eliminate a spinning tangential mode. A three bladed design damps the 1T and 2T modes. An aperiodically arranged four-bladed baffle can help damp 2T mode. A five bladed design will be helpful in providing damping up to four modes. The blades must be of sufficient depth to cause the damping. The

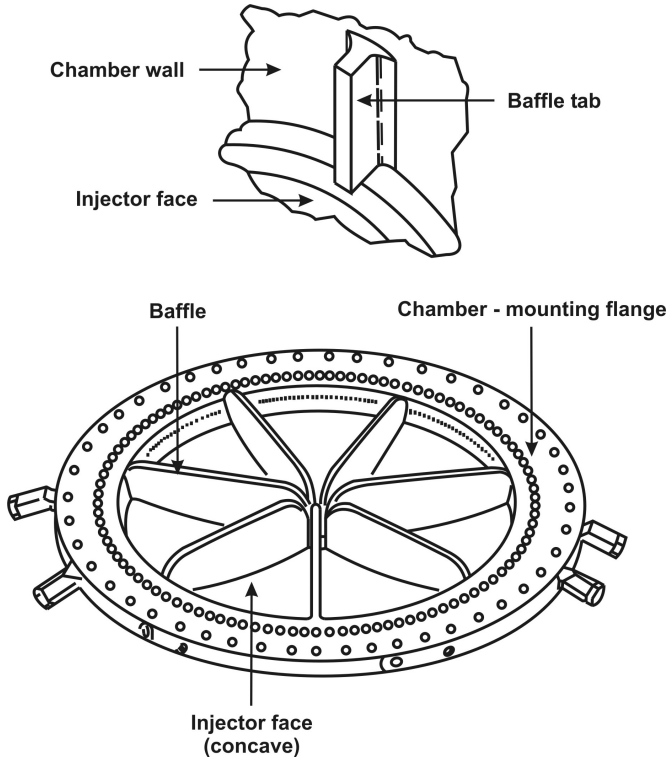

Figure 11.6: Baffle design used on Titan vehicle, drwn from ref. [43]

blade depth be 15 to 30 % of the chamber diameter with the lower sizes for large diameter engines is usually considered adequate. Russian designs (see Rubinsky in ref. [21]) use combustible felt ribs around the cylindrical combustion chamber even in production engines. This makes sense only if the instability occurs early in the operational duration as was assessed to be the case with one of the engines (RD 0110 engine with LOX – RP1 propellants).

Acoustic resonators and cavities are included in the combustion chamber to act as damping devices. Figure 11.8 shows both Helmholtz oscillator and quarter-wave damping device along with the dimensions. The frequencies are given by

$$f_{hc} = \frac{a}{2\pi}\sqrt{\frac{\pi d^2/4}{V(l+0.85d)}} \quad \text{(Helmholtz oscillator)} \tag{11.14}$$

$$f_{qwo} = \frac{a}{4(L+0.85d)} \quad \text{(Quarterwave oscillator)} \tag{11.15}$$

where f_{hc} and f_{qwo} are the frequencies of Helmholtz oscillator and quarter wave oscillator, d is the orifice diameter, L is the orifice length and V is the volume of

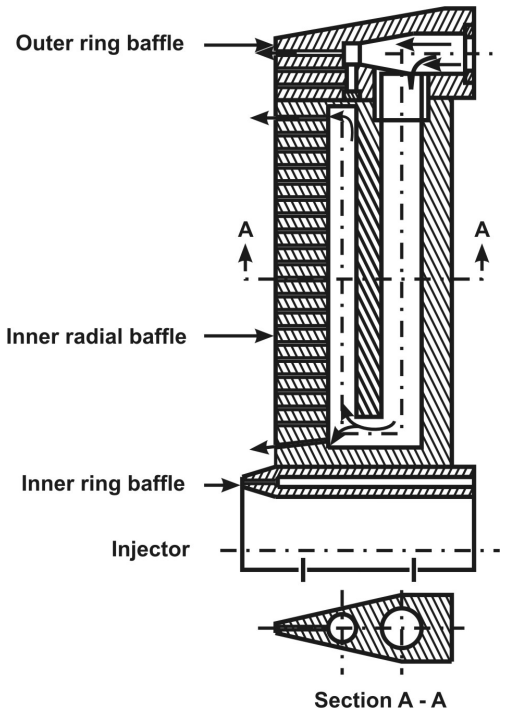

Figure 11.7: The arrangements made for cooling the baffles; notice the passages for leading the propellant that should act as a coolant, drawn from ref. [43]

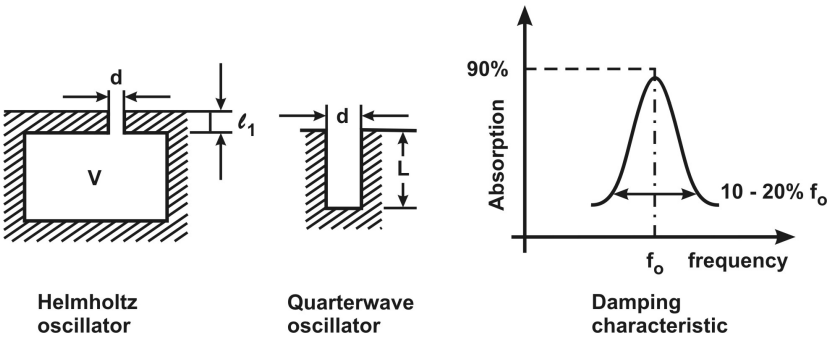

Figure 11.8: Acoustic absorption concepts

the oscillator. Typical values like $d = 3mm$, $L = 10mm$, $V = 500mm^2$, $a = 1000m/s$ lead to f_{hc} = 5.3 kHz and f_{qwo} = 20 kHz. The damping of the oscillations occurs around the resonant frequency within $\pm$ 10 %, the peak going up to 90 %. These are provided usually in a zone between the chamber wall and the injector head. Several rocket engines – Apollo LEM descent, Space shuttle PRCS Space shuttle pump OME have all used cavities for stabilizing the engine. A pintle injector design that has been used in the above engines (see Figure 10.40) has been shown to be dynamically stable over the entire range of applications. It has been suggested that the primary heat release occurs in a zone midway between the axis and the wall and this zone has the least destabilizing tendency. The most critical zones, namely the axis and the wall region do not experience the high heat releases and hence, help the stability of combustion. No special stabilization devices have been used in this class of engines.

11.4 Intermediate Frequency Instability (IFI)

IFI is a result of coupling between the feed system and the combustion chamber. The feed system excitation can cause the flow rate into the combustion chamber to be affected in a manner that could sensitize the high frequency instability in the chamber. This is particularly so with injection systems that are sensitive to changes in the velocity of injection – like impingement with doublets, a feature that has been brought out in section 10.2.1. Changing the compliance of the feed system – usually making it stiffer - helps ensuring decoupling between the feed system and the combustion chamber.

11.4.1 Analytical Tools for Studying Instability

The two principal approaches possible are the linear and non-linear stability analysis. Any non-linear processes grow out of linear oscillatory behavior. A system that is linearly stable can have a wide range of stability unless the system is subject to a strong pulse. Most system designs account for the internal growth of oscillations and these inherent instabilities pass through the linear range before non-linear processes take over. It has always been found useful (even though the simplicity argument is more easily put forth) to analyze the linear processes and if one allows for a reasonable margin of stability in reality, it is considered reassuring that the behavior of the system will remain stable.

Most stability analyses - Time lag approach, Priem- Heidmann approach, and Dykemma analysis address parts of the instability behavior and have been shown by Culick to be equivalent to a certain degree (see pp. 226 - 231 of ref [52] for a lucid exposition of a comparative assessment of these models). Deeper understanding

of these analyses and their implications could be obtained from a study of NASA SP194 [52] and more recent work in this area in a book published by AIAA [20].

11.4.2 Stability Rating

One of the key aspects of rocket engine development is related to establishing that the engine is stable on the test stand before being used on a flight. Dynamic stability consideration requires that the engine be triggered with a substantive disturbance and expect it to recover from this disturbance within a short time. Normally this is done by introducing an explosive charge that is triggered after the engine has traversed the initial transient and reached a steady operating condition. This causes a pressure peak that should die down in a few microseconds to a few milliseconds depending on the size of the charge introduced and the mode and the frequency that is intended for examination. The subject of stability rating is very specialized and readers can examine NASA SP 194 [52].

11.5 POGO Instability

The instabilities – LFI, IFI and HFI discussed earlier are for the engine and the stage in a multi-stage vehicle. They assume no interaction with other stages of the vehicle. A given liquid rocket engine-stage combine can be used in different vehicles as a first stage, or as an upper stage. When the stage is a part of other stages and operating, the liquid stage experiences g – loads because of vehicle acceleration and in addition, the structural flexibility of other stages along with the operating liquid stage can excite certain low frequencies leading to propellant flow modulation and therefore resulting in a propulsion system instability. This coupled mode between the structure and propulsion system is called POGO. It is essentially a flight related problem. The instability is not encountered in early stages of the operation of liquid stage since the structural rigidity is adequate. As the liquid stage continues to operate, the liquid propellant is depleting and this brings down the structural rigidity of the vehicle continuously since the propellant mass that was adding to the rigidity is reducing. The principal mode has been found to be the longitudinal mode. This causes the structural frequency (it is simple to recall $f \sim \sqrt{SSs/m}$ with SSs representing the spring stiffness and m, the mass) to drop down and under certain conditions can get coupled to the engine operation. It has been found on Titan II vehicle with instability frequency of 10 to 13 Hz and in Thor/Agena flights at frequencies of 17 to 21 Hz [64]. It is usually not of destructive nature. There could be undesirable vibrations in the payload compartment. The principal procedure to overcome this instability is to vary the compliance in the feed system appropriately.

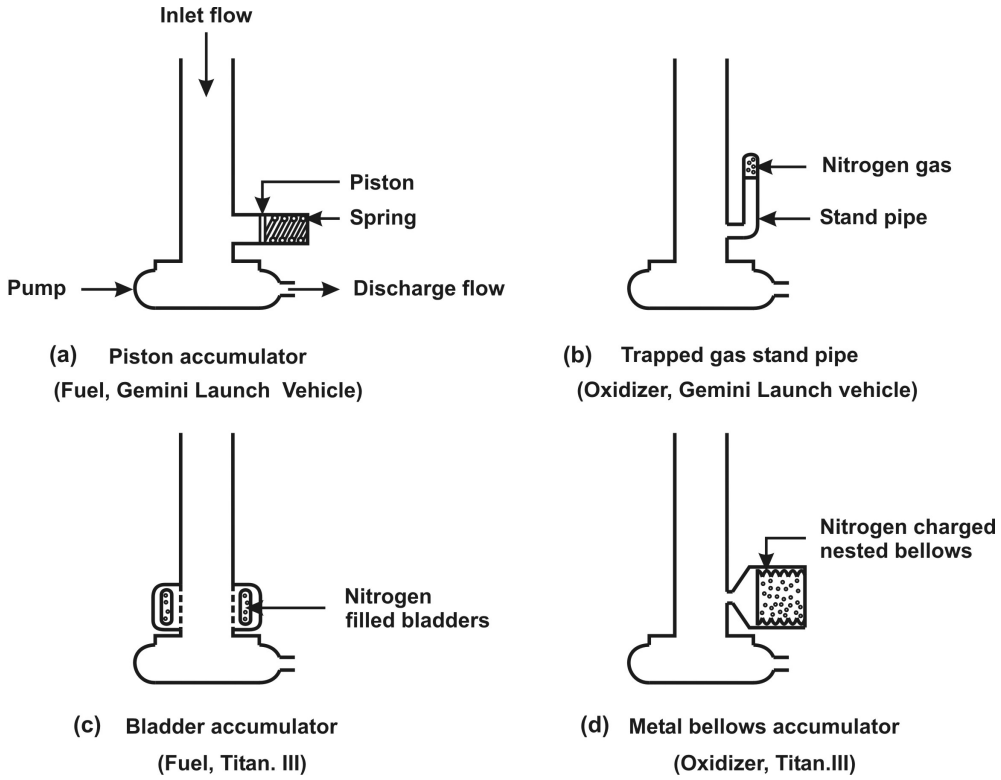

Figure 11.9: Pogo instability correction devices used on some vehicles

Some methods of varying the compliance are shown in Figure 11.9. In each of the cases, the device responds by absorbing the pressure fluctuations in the suction piping caused by the instability. The crucial point is that the frequency tuning is important. Otherwise, the pogo device may induce instability. These passive devices called POGO correctors have been found adequate for stable operation of the engines identified in the figure. The location of a POGO corrector used on PSLV engine is shown in Figure 10.8. Detailed calculations based on the vehicle structural modeling as well as the propulsion system modeling for both structural aspects as well as propulsion aspects showed that the vehicle is sensitive to POGO beyond 95 s and most critical at 140 s at a frequency of 27.5 Hz. The corrector that has been designed to provide minimum stability margin at the most critical condition.

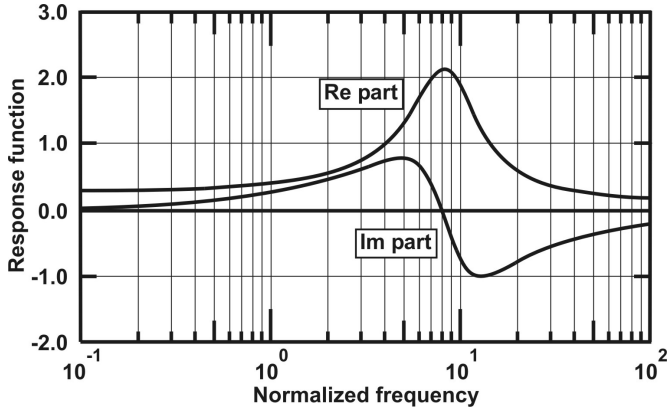

Figure 11.10: The plot of the response function with normalized frequency

11.6 HFI in Solid Rocket Motors

The high frequency instability in solid rockets involves issues similar to the ones discussed for liquid rocket engines but also has several other physical features. The general approach has been to estimate energy amplifying and absorbing elements. This is done by expecting that the pressure fluctuation varies as $\exp(\alpha_{pp}t)$ where the constant α_{pp} is determined for different processes for a specific mode. The value of α_{pp} is positive for processes like the response of the burning surface for pressure or velocity fluctuations, the former called pressure coupling and the latter velocity coupling. The particulate matter in the product gases coming from the metal in the propellant, the response of the nozzle to fluctuations, and the sudden expansion of the flow from the propellant section to the intermediate dump zone ahead of the nozzle will all contribute to negative values of α_{pp}. These values will change during the burning since the propellant geometry is also varying during this period. The sum of the constants of all the processes will determine if the combustion process will be stable. If the net value of α_{pp} is positive, then the system will be linearly unstable. In this case, there will be amplification of the disturbance and could grow to large levels with non-linear interactions. This could lead to sustained oscillations over a certain period of time and could also decay.

11.6.1 Growth Rates and Response Function

The effect of acoustic fluctuations on the burn rate arising out of pressure fluctuations is termed pressure coupling. Since $\dot{r} = ap_c^n$, the response function given by $(d\dot{r}/\dot{r})(dp_c/p_c)$ = $(\dot{r}'/\dot{r})/(p_c'/p_c)$ in the limit of zero frequency is n. If one treats the problem of determining the response function by modeling the combustion process

with a coupling between the gas phase and the condensed phase, one obtains the result in which the response function will have both real and imaginary parts. The result can be expressed in terms of a non-dimensional frequency, $\omega\alpha_c/\dot{r}^2$ where ω is the frequency, α_c is the condensed phase diffusivity and $\dot{r}$ is the steady burn rate. The dependence of mean pressure is involved in $\dot{r}$. A typical plot of the response function with dimensionless frequency defined above is shown in Figure 11.10. The real and imaginary parts can be seen in the figure. One can notice that there is a peak in the response function. The dimensionless frequency of 0.9 for which one gets peak response that is more than four times the steady response. The frequency corresponds to about 0.8 to 1.2 kHz the variation being largely due to pressure (or steady burn rate). The response function can be expressed by

$$\frac{\dot{r}'}{\dot{r}} = Real(R_p^r + iR_p^i)\frac{p_c'}{p_c} \tag{11.16}$$

One can write the dependence of the response of the burn rate to lateral velocity fluctuations (essentially same as erosive effect, but then of a fluctuating velocity field) as

$$\frac{\dot{r}'}{\dot{r}} = Real(R_v^r + iR_v^i)\frac{V'}{\bar{a}} \tag{11.17}$$

where $\bar{a}$ is the mean acoustic speed used as the normalizing quantity for velocity fluctuations V'. Since p_c'/p_c is real, equation (11.16) reduces to

$$\frac{\dot{r}'}{\dot{r}} = R_p^r\frac{p_c'}{p_c} \tag{11.18}$$

Since acoustic velocity is out of phase with pressure fluctuations by $\pi/2$, velocity fluctuations can be taken as imaginary, we can write the expression for velocity coupled response function as

$$\frac{\dot{r}'}{\dot{r}} = R_v^i\frac{V'}{\bar{a}} \tag{11.19}$$

Both these quantities are experimentally determined by using a laboratory apparatus called T – Burner. The burner can be designed to extract pressure coupled mode as well as velocity coupled mode by locating the propellants appropriately.

Figure 11.11 shows the two configurations of arranging the propellant for obtaining the pressure coupled and velocity coupled modes and a typical pressure-time trace. The growth factor can be extracted by examining the variation of the envolop of the pressure-time trace. While there are no other alternatives for determining the growth factor for propellants, the results from this approach are not considered highly reliable since intrinsically the result is very sensitive to the propellant composition. Also, the process of measurement has to be handled very carefully since the dimensions of the apparatus are small and getting repeatable results is not-so-easy a task.

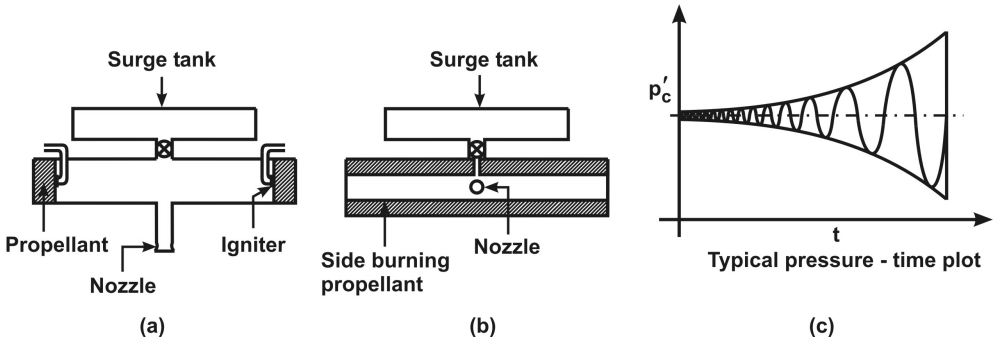

Figure 11.11: Two configurations of a T – burner and a typical pressure time trace of the oscillatory part of the pressure. Configuration (a) is used to evaluate the pressure coupled mode and configuration (b) is used to evaluate velocity coupled mode

The relationship between the growth factor and the response function is obtained from analysis as

$$\alpha_{pp} = \frac{\gamma \rho_p \bar{\dot{r}}}{2\rho_g} \frac{A_b}{\forall} R_p^r \tag{11.20}$$

where ρ_g is the gas phase mean density, R_p^r is the response function for pressure fluctuations and γ is the ratio of specific heats. One can compute the growth factor for other elements of a rocket engine (see Culick, [65]) using several modeling assumptions and put them together into the following relation for longitudinal mode (found most often in solid rockets).

$$\alpha_{net} = \alpha_{pp} + \alpha_{noz} + \alpha_{fltu} + \alpha_{particle} \tag{11.21}$$

$$= \frac{\gamma \rho_p \bar{\dot{r}}}{2\rho_g} \left[R_p^r - \frac{(\gamma+2)}{\gamma} \right] - \omega F_{Al} \left[\frac{\omega \tau_v}{1+\omega^2 \tau_v^2} + 0.27 \frac{1.6\omega\tau_v}{1+2.56\omega^2\tau_v^2} \right] \tag{11.22}$$

where α_{pp}, α_{noz}, α_{fltu}, $\alpha_{particle}$ are the growth factors for the propellant, nozzle, flow turning and the particulate matter and F_{Al} is the fraction of aluminum in the propellant (typically 0.15 to 0.17), τ_v is the velocity equilibration time for particulate matter given by

$$\tau_v = \frac{\rho_{Al_2O_3} \sigma^2}{18 \mu_g} \tag{11.23}$$

In arriving at the above equations, values typical of high energy solid propellants have been used. The growth factor will be positive without the particulate damping. This value is about 2.7 and this magnitude of the response function is obtained for most propellants (as can be noted from Figure 11.10).

Hence, particulate damping is central to the stability of solid rocket propellants. In some propellants that use a smaller aluminum loading, of a few percent, there is the problem of instability.

11.7 Summary

This chapter has dealt with the subject of combustion instability in propulsion systems. Many systems - afterburners of turbojets, ramjets, medium energy solid rockets and cryogenic propellant based and storable propellant based liquid rocket engines face the high frequency instability problem with the relative intensity of the problem increasing in the order of systems identified. This is largely because of the intensity of combustion vis-a-vis acoustic oscillatory modes. Afterburners and ramjet combustors work at 2 - 5 atm with kerosene and air as the fuel and oxidizer. Medium energy solid rockets use double base propellants or composite propellants with little aluminum (to avoid primary smoke coming from metal oxide particles) and operate at high pressures, typically 50 to 100 atm. The cryo engines use LOX – LH_2 propellants and the combustion mode is of gaseous fuel at high velocity combusting with liquid oxidizer droplets – largely in diffusion mode. Storable hypergolic or non-hypergolic propellants using impinging jet system generate a sharp to not-so-sharp energy profile with distance depending on the atomization characteristics. These combustion processes occur at pressures between 50 to 100 atm. If we recognize that heat release rates vary as the square of the chamber pressure, the intensity of combustion process can be seen to be increasing along the path of devices just described. It is this basic feature that leads to the problems noticed in these systems. The solutions, likewise, are tailor-made for each of these devices.

Most afterburners and ramjets use a screech preventing perforated cylindrical sheathing inside the combustor to act largely as Helmholtz oscillator. In solid rocket motors, one introduces damping devices like metal rods or lateral holes in propellants to break the structure of standing waves (usually longitudinal in these cases). In liquid rocket engines, one introduces baffles on the injector face or on the walls, in addition to acoustic absorbers to deal with different levels of instability. Analytical approaches to describe instability are complex; linear approaches themselves need to allow for a wide variety of processes that have to be accounted for. Computational procedures in uncovering instability mechanisms need to be developed for greater robustness. Motivation for this is dwindling because successful designs have been developed through intuitive effort and more designs are not being looked for in aerospace vehicle programs.

Appendix A

Atmospheric Data

The properties of a standard atmosphere are derived from simple considerations. The pressure gradient is caused by the weight of air above a certain location. Thus,

$$\frac{dp_o}{dh} = -\rho g \tag{A.1}$$

Now the equation of state, $\rho = p_o/RT_o$ is used to replace the density. Experimentally, it is known that atmospheric temperature decreases linearly with height. This is given by $T_o = T_{o,ref}(1 - L_{ar}h)$ where $T_{o,ref}$ is the reference temperature, say 288.16 K, and L_{ar} is the lapse rate - rate at which temperature decreases with height measured as 6.51 K /km up to a height of 11 km, *the tropopause*. The above equation can be recast as

$$\frac{dp_o}{p_o} = -\frac{g}{R}\frac{dh}{dT_o}\frac{dT_o}{T_o} \tag{A.2}$$

which can be integrated to lead to

$$\frac{p_o}{p_{o,ref}} = \left[\frac{T_o}{T_{o,ref}}\right]^{g/(RL_{ar})} \tag{A.3}$$

If we now introduce the values, g = 9.81 m/s^2, R = 287.0 m^2/s^2 K, L_{ar} = 0.00651 K/m, we get

$$\frac{p_o}{p_{o,ref}} = \left[\frac{T_o}{T_{o,ref}}\right]^{5.256} \tag{A.4}$$

One can deduce density after pressure is obtained. The data are listed below in Table A.1. From 11 km onwards, the temperature is constant up to an altitude of 25 km. The equation (A.1) can be used to obtain the pressure from 11 to 25 km from the following equation.

$$p_o = p_{o,11km} exp[-1.735(h/11 - 1)] \tag{A.5}$$

where h is in km. These data are also presented in Table A.1

Table A.1: The properties of international standard atmosphere, p_o, T_o, ρ_o = static pressure, temperature and density, 1 atm. = 101.325 kPa

Altitude km	p_o atm.	T_o K	ρ_o kg/m^3	a$_o$ m/s
0.0	1.000	288.16	1.225	340.3
1.0	0.887	281.65	1.112	336.4
2.0	0.785	275.15	1.007	332.5
3.0	0.692	268.66	0.909	328.6
4.0	0.608	262.17	0.819	324.6
5.0	0.533	255.68	0.736	320.5
6.0	0.466	249.19	0.660	316.4
7.0	0.406	242.70	0.590	312.3
8.0	0.352	236.21	0.526	308.1
9.0	0.304	229.73	0.467	303.8
10.0	0.261	223.25	0.413	299.5
11.0	0.224	216.77	0.365	295.1
12.0	0.191	216.65	0.312	295.1
13.0	0.164	216.65	0.267	295.1
14.0	0.140	216.65	0.228	295.1
15.0	0.120	216.65	0.195	295.1
16.0	0.102	216.65	0.166	295.1
17.0	0.087	216.65	0.142	295.1
18.0	0.075	216.65	0.121	295.1
19.0	0.064	216.65	0.104	295.1
20.0	0.054	216.65	0.089	295.1

References

Books on Aeronautical Propulsion

[1] Nicholas Cumpsty. *Jet Propulsion*. Cambridge University Press, The Edinburgh Building, Cambridge CB2 2RU, United Kingdom, first edition, 1997. A Simple guide to the aerodynamic and thermodynamic design and performance of jet engines.

[2] J. W. Frzard. The british aerospace harrier - case study in aircraft design. AIAA Professional Study Series, 1978.

[3] D. W Harvey. The combustion system for the olympus concorde engine. In E. R. Norster, editor, *Combustion and Heat transfer in gas turbine systems*, volume II of *Cranfield international sysmposium series*, pages 3 – 20. Pergamon Press, 1971.

[4] T. C. Herman. *Gas turbine engineering*. MacMillan Press Ltd., 1981.

[5] J. L. Kerrebrock. *Aircraft Engines and Gas Turbines*. The MIT Press, second edition edition, 1992.

[6] Michael J. Kroes and Thomas W. Wild. *Aircraft Powerplants*. Glencoe Aviation Technology. Glencoe Division of Macmillan / McGraw- Hill School Publishing Company, McGraw- Hill Book Co.- Singapore, seventh international edition, 1994.

[7] Jack D. Mattingly. *Elements of Gas Turbine Propulsion*. Mechanical Engineering Series. McGraw - Hill, Inc., 60 Tuas Basin Link, Singapore 638775, mcgraw - hill international edition, 1996.

[8] Barnes W. McCormick. *Aerodynamics, Aeronautics, and Flight Mechanics*. John Wiley and Sons, Inc, New York, United States of America, second edition, 1995.

[9] E. R. Norster. *Combustion and Heat Transfer in Gas Turbine Systems*, volume Two of *Cranfield International Symposium*. Pergamon Press, Pergamon

Press Ltd., Headington Hill Hall, Oxford, first edition, 1971. Proceedings of an International Propulsion Symposium held at the College of Aeronautics, Cranfield, April 1969.

[10] Gordon C. Oates. *Aerothermodynamics of Aircraft Engine Components*, volume Second of *AIAA Education Series*. American Institute of Aeronautics and Astronautics, Inc, 1633 Broadway, New York, N. Y. 10019, 1985.

[11] Gordon C. Oates. *Aircraft Propulsion Systems Technology and Design*, volume Third of *AIAA Education Series*. American Institute of Aeronautics and Astronautics, Inc, 370 L' Enfant Promenade, SW, Washington, DC 20024 - 2518, 1989.

Books on Aerospace Propulsion

[12] M. Barrere, A. Jaumotte, B. J. Veubeke, and J. Vandenkerckhove. *Rocket Propulsion*. Elsevier Publishing Company, english edition of la propulsion par fuses edition, 1960.

[13] L. E. Bollinger, M. Goldsmith, and A. W. Jr. Lemmon. *Liquid Rockets and Propellants*, volume Second of *American Rocket Society*. Academic Press Inc, Academic Press Inc, 111 Fifth Avanue, New York 3, N .Y., 1960.

[14] C. D. Brown. *Spacecraft Propulsion*. AIAA Education Series. American Institute of Aeronautics and Astronautics, Inc, 370 L' Enfant Promenade, SW, Washington, DC 20024 - 2518, first, second printing edition, 1996.

[15] P. Chandrasekharan. Manufacture of heterogeneous solid propellants. In S. R. Krishnan, S. Chakravarthy and S. K. Athithan, editors, *Propellants and Explosives Technology*, volume Propellants and Explosives Technology, chapter 4, pages 77 – 124. Allied Publishers Ltd, 1998.

[16] D. K. Huzel and D. H. Huang. *Design of Liquid Propellant Rocket Engines*. National Aeronautics And Space Administration, Washington, D. C., USA, second edition, 1971.

[17] N. Kubota. *Propellants and Explosives*. WILEY - VCH GmbH, WILEY - VCH GmbH, Weinheim, Germany, first edition, 2002. Thermochemical Aspects of Combustion.

[18] J. F McCarthy Jr. Zero g propulsion problems. In W. H. T. Loh, editor, *Jet, Rocket, Nuclear, Ion and Electric Propulsion, Theory and Design*. Springer Verlag, 1968.

[19] S. S. Penner and J Ducarme. *The Chemistry of Propellants*. Pergamon Press, Pergamon Press Ltd, Headington Hill Hall, Oxford, 4 & 5 Fitzroy Square, London W.1, 1960.

[20] R. J. Priem and K. I. Breisaher. Calculations of combustion response profiles and oscillations. In V. Yang and W. (Editors) Anderson, editors, *Liquid rocket engine combustion instability*, volume 169 of *Progress in Astronautics and Aeronautics*, chapter 17, pages 89 – 112. AIAA Inc, 1995.

[21] V. R. Rubinsky. Combustion instability in the rd - 0110 engine. In V. Yang and W. (Editors) Anderson, editors, *Liquid rocket engine combustion instability*, volume 169 of *Progress in Astronautics and Aeronautics*, chapter 4, pages 89 – 112. AIAA Inc, 1995.

[22] M. Shorr and A. J. Zaerhinger. *Solid Rocket Technology*. John Wiley and Sons, Inc, 1967.

[23] R. Steinberger and P. D. Drechsel. Manufacture of cast double base propellants. In *Propellants Manufacture, Hazards and Testing*, volume 88 of *Advances in Chemistry Series*, pages 1 – 28. American Chemical Society, 1969.

[24] Jannaf Combustion Subcommittee. *Combustion Instability in Solid Rocket Motors*, volume Two. Chemical Propulsion Information Agency, The Johns Hopkins University Applied Physics laboratory, John Hopkins road, Laurel , Maryland 20810, January 1981. A guide for Motor Designers.

[25] G. P. Sutton. *Rocket Propulsion Elements*. John Wiley & Sons, Inc., New York, United States of America, sixth edition, May 1992.

[26] Y. M. Timnat. *Advanced Chemical Rocket Propulsion*. Academic Press Inc, Academic Press Limited, 24/28 Oval Road, London NW 1, 1987.

[27] F. A. Williams, M. Barrere, and N. C. Huang. Fundamental aspects of solid propellant rockets. *AGARDograph 116*, 1969.

[28] V. Yang and W. (Editors) Anderson, editors. *Liquid rocket engine combustion instability*, volume 169 of *Progress in Astronautics and Aeronautics*. AIAA Inc, 1995.

Books on Aeronautical and Aerospace Propulsion

[29] Janes all the world's aircraft. Janes Yearbooks, 1977.

[30] D. M. Desoutter. *Aircraft and Missiles - What They Are, What They Do and How They Work*. Faber and Faber Ltd, 1959.

[31] Philip G. Hill and Carl R. Peterson. *Mechanics and Thermodynamics of Propulsion*. Addison Wesley Longman, second edition, 1999.

[32] H. S. Mukunda. *Understanding combustion*. McMillan India, second printing edition, 1994.

[33] J. Seddon and E. L. Goldsmith. *Intake Aerodynamics*. Collins Professional and Technical Books, 1985.

[34] D. G. Shepherd. *Aerospace Propulsion*. American Elsevier Pub. Co., Inc, 1972.

[35] F. A. Williams. *Fundamentals of Combustion Theory*. Addison Wesley, second edition, 1992.

[36] M. J. Zucrow. *Aircraft and Missile Propulsion - Vol. I, Thermodynamics and fluid Flow in applications and propulsion engines*. John Wesley and Sons, Inc, London, 1958.

References from Journal and Reports

[37] Anon. Supersonic combustion tests in an 8000 fps air stream. *Report 6064, Marquardt Corporation, California*, 1964.

[38] Anon. *Liquid Propellant Gas Generators*. NASA SP - 8081. National Aeronautics and Space Administration, Washinton, D. C. 20546, March 1972.

[39] Anon. *Liquid Rocket Engine Fluid - Cooled Combustion Chambers*. NASA SP - 8087. National Aeronautics and Space Administration, Washinton, D. C. 20546, 1972.

[40] Anon. *Liquid rocket engine combustion stabilization devices*. NASA SP - 8113. National Aeronautics and Space Administration, Washinton, D. C. 20546, August 1974.

[41] Anon. *Turbopump Systems for Liquid Rocket Engines*. NASA SP - 8107. National Aeronautics and Space Administration, Washinton, D. C. 20546, August 1974.

[42] Anon. *Liquid Rocket Engine Injectors*. NASA SP - 8089. National Aeronautics and Space Administration, Washinton, D. C. 20546, March 1976.

[43] Anon. *Liquid Rocket Engine Self - Cooled Combustion Chambers*. NASA SP - 8124. National Aeronautics and Space Administration, Washinton, D. C. 20546, September 1977.

[44] Anon. *Liquid Rocket Engine Axial - Flow Turbopumps*. NASA SP - 8125. National Aeronautics and Space Administration, Washinton, D. C. 20546, April 1978.

[45] Several authors. A century of aerospace propulsion and power technologies. *Journal of Propulsion and Power*, 19(6), 2003.

[46] V. Avrashkov, S. Baranovsky, and S. V. Levin. In *AIAA Second International Aerospace Planes Conference*, 1990.

[47] N. S. Cohen and L. D. Strand. An improved model for the combustion of ap composite propellants. *AIAA Journal*, 20:1739 – 1746, 1982.

[48] C. D. Coulbert. Selecting cooling techniques for liquid rockets for spacecraft. *J. Spacecraft and Rockets*, pages 121 – 139, 1964.

[49] Frignac et al. Economies of fleet performance. *Aeronautics and Astronautics*, pages 28 – 35, June 1980.

[50] S. Gordon and B. J McBride. *Computer Program for Calculation of Complex Chemical Equilibrium compositions, Rocket Performance, Incident and Reflected Shocks, and Chapman - Jouguet Detonations*. NASA SP - 273. National Aeronautics and Space Administration, Washinton, D. C. 20546, 1971.

[51] C. Gruenig, V. Avrashkov, and F. Mayinger. Self-ignition and supersonic reaction of pylon-injected hydrogen fuel. *J. Propulsion Power*, 16:35 – 40, 2000.

[52] D. T. Harrje and F. H. Reardon, editors. *Liquid Propellant Rocket engine combustion instability*, NASA SP 194. National Aeronautics and Space Administration, 1972.

[53] T. Kanda, T. Hiaraiwa, T. Mitani, S. Tomioka, and N. Chinzei. Mach 6 testing of a scramjet engine model. *J. Propulsion and Power*, 4:543 – 551, 1997.

[54] F. E. Marble, E. E. Hendricks, and E. E. Zukoski. Progress towards shock enhancement of supersonic combustion processes. *AIAA-87-1880, 23rd AIAA/ASME/ASEE Joint Propulsion conference*, 1987.

[55] R. Marguet, C. Ecary, and P. Cazin. Studies and tests on rocket ramjects for missile propulsion. In *Proccedings of ISABE IV*, pages 297 – 306, 1979.

[56] T. Mitani, N. Chinzei, and Kanda T. Reaction and mixing-controlled combustion in scramjet engines. *J. Propulsion and Power*, 16:308 – 313, 2000.

[57] H. S. Mukunda and P. J. Paul. Universal behavior in erosive burning of solid propellants. *Combustion and Flame*, 109:224 – 236, 1997.

[58] M. G. Owens, S. Tehranian, C. Segal, and V. Vinogradov. Flame holding configurations for kerosene combustion in a mach 1.8 airflow. *Jornal of Propulsion and Power*, 14(4), 1998.

[59] D. Papamoschou and A. Roshko. The compressible turbulent shear layer. *J. Fluid Mechanics*, 197:453 – 477, 1988.

[60] P. J. Paul, H. S. Mukunda, and V. K. Jain. Regression rate in boundary layer combustion. In *Proceedings of the 19th symposium (international) on combustion*, 1982.

[61] P. Payne. Supersonic combustion of liquid kerosene. *AFOSR - 2682 - 74*, 1975.

[62] C. U. Pittman Jr. Location of the action of burning rate catalysts in composite propellant combustion. *AIAA Jl.*, 7, 1969.

[63] P. A. Ramakrishna. *Computational studies on sandwich propellants*. Indian Institute of Science, Bangalore, 2003.

[64] S Rubin. Longitudinal instability of liquid rocket due to propulsion feed back (pogo). *Journal of Spacecraft and rockets*, 3(8):1188 – 1195, 1966.

[65] Jannaf Combustion subcommittee. *Combustion instability in solid rocket motors*. CPIA Publication 290, 1981.

[66] N. P. Suh, C. L. Tsai, C.L. Thomson, Jr, and J. S. Moore. Ignition and surface temperature of double base propellants at low pressure, i thermocouple measurements. *AIAA Journal*, 8:1314 – 1321, 1970.

[67] S. Tomioka, A. Murakami, K. Kudo, and T. Mitani. Combustion tests of a staged supersonic combustor with a strut. *J. Propulsion Power*, 17:293 – 300, 2001.

[68] A. Yu, B. Li, C. Chang, and Sung. Investigation of kerosene combustion characteristics with pilot hydrogen in model supersonic combustors. *J. Propulsion Power*, pages 1263 – 1272, 2001.

Index

Ablative cooling, 401, 405
Ablative materials, 339
Acoustic frequencies and mode shapes, 427
Acoustic resonator, 437
Acoustic speed, 82
Afterburner, 9, 137, 209
Air blast atomizer, 199, 200
Air intake, 157
Air–turbo rockets, 44
Air-to-air missiles, 58
Aircraft nozzles, 237
Ammonia, 301
Analysis of combustor, 201
Annular combustor, 8
Apogee Kick module, 59
Axial compressor, 5, 184

Baffles for acoustic damping, 434
Bellows, 353
Bipropellant combustion mechanism, 301
Bipropellant liquid engines, 361
Bipropellants, 279
Bladders, 353
Blow down, 360
Bond number, 355
Boost, 59
Bubble pressure, 355
Burn rate of SP, 273
Buzz in intakes, 171
Bypass ratio, 150

Can-annular combustor, 8
Capillary device, 360
Capillary effect, 300
Case bonded grain, 259, 270, 324
Catch tank, 356
Centrifugal compressor, 5, 176
Characteristic velocity, 90
Charring materials, 339
Chemical pollution, 56
Chemical reaction rates, 202
Chemical reaction time, 202
Choked nozzle, 88, 128
Chuffing, 334
Chugging, 423
Civilian aircraft, 49
Coaxial injectors, 367
Combustion chamber, 8
Combustion instability, 423
Combustion properties of solid propellants, 266
Combustion system, 192
Combustor cooling, 199
Combustor geometry, 195
Comparison of rockets, 305
Composite Propellant manufacture, 260
Compressor characteristics, 180
Compressor-Turbine matching, 234
Concorde air intake, 172
contact angle, 354
Convergent nozzles, 237
Convergent-divergent nozzle, 237
Cooling of gas turbine combustor, 198
Cryogenic, 280

Damkohler number, 204
DB propellant manufacture, 259
Degree of reaction, 225

Density impulse, 284
Design of solid rocket motor, 348
Diffusive combustion mode, 292
Double base propellants, 33
Drop size distribution, 372
Drop vaporization time, 202
Ducted rockets, 43
Dump diffuser, 198

Equilibrium calculations, 245
Equilibrium specific impulse, 284
Equlibrium constants, 246
Erosive burning effect, 273, 276
Erosive burning effects, 327
Exploding bridge wire initiator, 331
Expulsion efficiency, 353
expulsion efficiency, 358
External intakes, 167

F-15A aircraft, 163
F-16 aircraft, 163
Film cooling, 402
Flame stabilization, 211
Flat rating, 136
Flex nozzles, 344
Free standing grain, 259, 270, 324
Frozen specific impulse, 284
Fuels for gas turbines, 244
Fuels for ramjets, 244

Gas generator, 379
Gas turbine combustor, 192
Graphite for TPS, 340
Growth rates, 442

Heat sink, 339, 401, 403
Heats of formation, 249
Helicopters, 51
Heterogeneous propellants, 253
Homogeneous propellants, 33
Homogeneous SP, 252
Hybrid engines, 42
Hybrid propellant combustion mechanism, 304
Hybrid rocket engines, 41
Hydrazine, 35
Hypergolic, 279, 281
Hypergolic propellants, 301
Hypersonic flight, 28
Hysterisis in injectors, 371

Igniter composition, 279
Igniter data for vehicles, 333
Igniters, 33
Ignition system, 328
Ignition transients in SP, 314
Inhibitors, 266
Initial modulus of SP, 270
Initial temperature sensitivity, 310
Injector, 365
Insulators, 266
Intake starting, 170
Integral ram rocket, 219
Integral ram rockets, 43, 60
Intermediate Frequency instability, 439
Internal compression intake, 167

JT - 9D engine, 207

Life of components, 53
like-impingement, 367
Liner cooling in combustors, 198
Liquid hydrogen, 281
Liquid propellant rockets, 35
Liquid propellants, 279
Liquid rocket engine, 351
Loading parameter, 205
Low frequency instability, 425
LOX, 281

Mass flux distribution, 369
Materials for thermal protection, 338
Mechanical properties of SP, 270
Mechanism of LP combustion, 300
Mechanism of SP Combustion, 295
Mig-21 aircraft, 163
Military aircraft, 49
Missile air intakes, 165

Mixed compression intake, 167
MMH, 281
MON, 281
Monopropellant, 352
monopropellant, 300
Monopropellant combustion mechanism, 300
Monopropellants, 279, 280
Multi-spool compressor, 187

Neutral combustion mode, 318
Noise pollution, 55
Non-air breathing engines, 30
Non-destructive testing of SP, 269
Nozzle flow, 85
Nozzle shape, 96
NTO, 281

Olympus 593 engine, 207
Optimum expansion, 123
Over-expansion, 102
Overall efficiency, 76

Particle damping, 442
Performance losses, 345
Performance parameters, 56
Performance with inefficiencies, 143
Pitot intake, 161
POGO instability, 440
Polar satellite launch vehicle, 333
Polymers for SP, 258
Positive expulsion, 353
Positive expulsion device, 36
Premixed combustion, 289
Pressure coupling, 442
Pressure fed engine, 36
Progressive combustion mode, 318
Propellant acquisition device, 356
Propellant geometry, 316
Propellants for hybrid rockets, 287
Properties of JP fuels, 245
Properties of LP, 283
Propulsion system assembly, 347
Propulsive efficiency, 73
Pulsejet, 23
Pulsing performance, 361
Pyrogen igniter, 331
Pyrotechnic igniters, 279

Radiant flux in solid rockets, 337
Radiation cooling, 401, 403
Ramjet combustor, 209
Ramjets, 19
Rayleigh process, 105
Reaction turbine, 225
Reciprocating engine, 2
Regenerative cooling, 401, 405
Regressive combustion mode, 318
Response function, 442
Reverse flow combustor, 8, 195
RFNA, 281
Rocasin rubber, 261
Rocket motor features, 346
Rocket thrust equation, 310

Sauter Mean Diameter, 199, 202
Scramjet fuels, 251
Scramjets, 24, 212
Screeching, 424
Shell 405 catalyst, 280, 300
Showerhead, 366
Sliver fraction, 321
Solid loading density, 325
Solid Propellant (SP) compositions, 263
Solid propellant rockets, 31
Solid rocket fuels, 252
Solid rocket motor instability, 441
Solid rocket oxidizers, 252
Sounding rockets, 57
SP combustion geometry, 318
SP extinction, 333
Specific fuel consumption, 7
Specific fuel consumption (sfc), 3
Specific impulse, 7, 32, 90, 134, 139
Specifications, 52
Stability of SP operation, 313
Stability rating, 440

Stage loading, 225
Staging, 65
Stagnation conditions, 84
Starting of intakes, 170
Starting systems, 29
Static thrust, 126
Step-by-step procedure, 147
Storable, 280
Straight flow combustor, 195
surface tension, 353
Surface tension device, 36
Surface-to-air missiles, 58
Sustain, 59
Swirl atomizer, 199, 200

Tactical rocket motor, 347
Temperature-entropy diagram, 83
Thermal efficiency, 76
Thermal protection systems for SP, 334
Through-bulkhead initiator, 331
Thrust augmentation, 12, 142
Thrust chamber, 398
Thrust per unit flow rate, 134
Thrust termination, 333
Thrust vector control, 341
Thruster
    monopropellant, 352
Tri-ethyl amine, 281
Triethylamine, 35
Turbine, 221
Turbine cooling, 231
Turbofan, 148
Turbojet, 3
Turbojet with afterburner, 137
Turboprop, 14
Turbopump fed system, 37
Turbulent mixing time, 202
Two/Three spools, 13

UDMH, 35, 281
Ullage, 37, 356, 418
Ultimate Tensile strength of SP, 270
Under-expansion, 102
Unlike-impingement, 367

Vacuum casting of SP, 262
Vacuum specific impulse, 284
Valveless pulse jets, 24
Velocity coupling, 442
Vortex controlled diffuser, 198

Water-methanol, 12
Weber number, 355
Wetting liquid, 354

Xylidine, 35, 281